

A Thesis Submitted for the Degree of PhD at the University of Warwick

Permanent WRAP URL:

<http://wrap.warwick.ac.uk/93856>

Copyright and reuse:

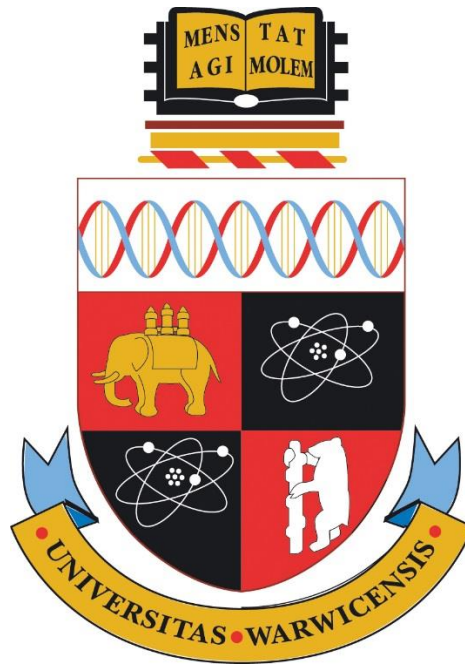
This thesis is made available online and is protected by original copyright.

Please scroll down to view the document itself.

Please refer to the repository record for this item for information to help you to cite it.

Our policy information is available from the repository home page.

For more information, please contact the WRAP Team at: wrap@warwick.ac.uk



Development of a Handheld Breath Analyser for the Monitoring of Energy Expenditure

Timothy A. Vincent

School of Engineering

University of Warwick

Thesis submitted to the
University of Warwick for the degree of
Doctor of Philosophy
May 2017

Contents

Summary	xxvi
1 Metabolism	2
1.1 Project Aims	5
1.2 Components of Energy Expenditure	6
1.2.1 Physiological and Environmental Factors.....	7
1.2.2 Physical Activity	9
1.2.3 Effect of Eating	10
1.3 Weight Management	13
1.4 Psychological Guidance	15
1.4.1 Metabolic Rate and Condition of Patient.....	18
1.4.2 Energy Requirements of Intensive Care Patients.....	18
1.5 Conclusions	23
1.6 References	24
2 Calorimetry	34
2.1 Direct Calorimetry.....	35
2.2 Indirect Calorimetry	37
2.2.1 Respiratory Room	38
2.2.2 Nitrogen Measurement for Assessment of Protein Metabolism	47
2.2.3 Error Introduced without Nitrogen Measurement.....	51
2.3 Breath Sample Acquisition.....	53
2.3.1 Alveoli Gas	53
2.3.2 Mouthpiece and Face Mask Breath Sampling	61
2.4 Metabolic Rate Measurement in a Free Living Environment	65
2.4.1 Doubly Labelled Water	65
2.4.2 Mathematical Equations.....	67

2.4.3	Heart Rate Monitoring	68
2.4.4	Activity Monitoring	70
2.5	Motivation for Developing Portable Breath Analyser	74
2.6	References	75
3	Gas Sensor Specification	87
3.1	Sensitivity Analysis	91
3.2	Oxygen Gas Sensors	96
3.2.1	Ambient Temperature Electrochemical Sensors	96
3.2.2	Zirconia Oxide Sensors	99
3.2.3	Paramagnetic Sensors	100
3.2.4	Resistive Oxygen Sensors	101
3.3	Carbon Dioxide Gas Sensors	103
3.3.1	Electrochemical CO ₂ Sensors	104
3.3.2	NDIR Gas Sensors	105
3.4	VOC Sensors	111
3.4.1	Metal Oxide Sensors	114
3.4.1.1	Operation of MOX Sensors	115
3.4.1.2	Metal Oxide Sensor Coatings	116
3.4.1.3	MOX sensors Measurement Principle	119
3.4.1.4	MOX sensors for breath analysis	121
3.5	Commercial Sensors	122
3.5.1	Oxygen Sensor	122
3.5.2	Flow Sensor	123
3.5.3	Temperature and Relative Humidity Sensor	124
3.5.4	VOC MOX Sensor	125
3.6	Conclusions	125
3.7	References	126

4	Mainstream Sampling	140
4.1	Chamber Design	141
4.2	Methodology - Bench Gas Rig Experiments.....	143
4.2.1	Classification Experiments	144
4.2.2	Sensor Data Preparation for Model Input	146
4.2.3	Model Training and Testing Vectors	147
4.2.4	Partial Least Squares (PLS)	148
4.3	Gas Rig Classification Experimentation	150
4.3.1	Experimental Results for Gas Rig Classification.....	152
4.3.2	Verification of CO ₂ Sensor Performance.....	155
4.4	VOC Sensor Measurements	158
4.5	Conclusions	161
4.6	References	164
5	Carbon Dioxide Breath Sensing	167
5.1	NDIR Emitter Drive Signal.....	168
5.1.1	Emitter DC Drive	169
5.1.2	Emitter AC Drive	172
5.2	Experimental Results.....	182
5.2.1	Lock-In Amplifier 80 mm Path Length	183
5.2.2	Lock-In Amplifier Path Length Optimisation.....	184
5.3	Digital Filtering	189
5.4	Linearity of Response.....	191
5.5	Conclusions	195
5.6	References	197
6	Control and Acquisition Software.....	201
6.1	Bench Gas Rig Control Software	201
6.1.1	Data Acquisition.....	204

6.1.2	Heater and Emitter Control	207
6.1.3	Furnace Control.....	208
6.1.4	MFC Module.....	210
6.2	Microcontroller Data Acquisition	212
6.2.1	Sample Rate	214
6.2.2	Communication Link	217
6.3	LabVIEW Breath Analyser Interface	218
6.4	Android Application for Breath Analyser	219
6.4.1	Application for USB Microcontroller Link.....	220
6.4.2	Application for Bluetooth Communication with Breath Analyser	222
6.5	Conclusions	225
6.6	References	227
7	Side-Stream Sampling	229
7.1	Side-Stream Chamber.....	230
7.1.1	Design of Sensor Housing.....	230
7.1.2	Flow Modelling.....	231
7.1.3	Construction of Chamber	233
7.1.4	VOC Sensor Holder	234
7.1.5	Main-stream and Side-stream Sensor Systems	235
7.2	Oxygen Sensor Response	235
7.2.1	Flow Dependence.....	237
7.2.2	Temperature Dependence.....	240
7.2.3	Humidity Dependence.....	241
7.2.4	Governing Equations of O ₂ Sensor Reaction.....	243
7.2.5	Design Considerations	248
7.3	Side-stream Gas Bench Rig Experiments	250
7.4	Side-stream Laboratory Breath Tests	253

7.5	Conclusions	258
7.6	References	262
8	Resting Energy Expenditure Measurements.....	265
8.1	Resting EE Experiment Methodology.....	265
8.1.1	Commercial Sensors in Comparative Side-Stream Unit.....	266
8.1.2	Measurement Protocol	267
8.1.3	Collection of Data	268
8.1.4	Subjects	269
8.2	Experimental Results.....	270
8.2.1	Measured Gas Concentrations and Sensor Response.....	270
8.2.2	Sensor Performance and Comparison to Respiratory Chambers	273
8.2.3	Energy Expenditure Measurements	278
8.2.4	Harris-Benedict BMR	281
8.3	Smartphone EE Measurement	283
8.4	Conclusions	287
8.5	References	289
9	Project Conclusions	292
9.1	Human Energy Expenditure	292
9.2	Portable EE Measurements	293
9.3	Achievements	294
9.4	Further Work	297
9.4.1	MOX VOC Sensor	297
9.4.1.1	MOX Hotplate Temperature	297
9.4.1.2	MOX Sensor Coating	299
9.4.1.3	NO ₂ Experimental Results.....	300
9.4.1.4	Acetone Experimental Measurement	307
9.4.1.5	Response Processing	309

9.4.2	O ₂ and CO ₂ Sensors	311
9.4.3	Software	312
9.4.4	Experimental	313
9.5	Concluding Remarks	315
9.6	References	316
10	Appendices.....	320
10.1	Appendix A – Published Work	320
10.1.1	A.1 - Development of a handheld side-stream breath analyser for point of care metabolic rate measurement	320
10.1.2	A.2 - A low cost MEMS based NDIR system for the monitoring of carbon dioxide in breath analysis at ppm levels	328
10.2	Appendix B – Ethics Approval for Laboratory Breath Testing	339
10.2.1	B.1 - BSREC Application Form	339
10.2.2	B.2 - BSREC Protocol	344
10.2.3	B.3 - BSREC Participant Information Leaflet	350
10.2.4	B.4 - BSREC Participant Consent Form.....	354
10.2.5	B.5 - BSREC Participant Recruitment Email Template	355
10.2.6	B.6 - BSREC Recruitment Advert for Research Webpage.....	356
10.2.7	B.7- BSREC Full Approval Letter	357
10.3	Appendix C – Gas Testing Rig LabVIEW Software	358
10.3.1	C.1 - Gas Rig Data Logging Flow Chart	358
10.3.2	C.2 - Gas Rig Data Logging Code	359
10.3.3	C.3 - Gas Rig Mass Flow Controller Operation Flow Chart.....	363
10.4	Appendix D – Microcontroller code for Acquiring Sensor Signals	367
10.5	Appendix E – Handheld Breath Analyser Data Logging LabVIEW Software 368	
10.6	Appendix F – Android code for Data Analysis from Hand-Held Unit	369

List of Figures

Num.	Caption	Page
1.1	Resting Metabolic Rate from 1 year of age to 75+ years of age, in terms of body surface area.	7
1.2	a) Total daily EE increased after a single bout of SIT. Closed and open circles indicate individual responses and group mean respectively; b) Mean EE found from the group during the sedentary day compared to the SIT period.	10
1.3	EE and physical activity measured under conditions of two and three meals per day. Arrows indicate meal times.	11
1.4	RMR increases above normal baseline for patients with conditions such as: (a) Head trauma; (b) Sepsis; (c) 20 % burns; (d) 65 % burns and (e) Severe burns. Injury occurred at 0 weeks and metabolic rate was measured at intervals during the recovery period.	21
2.1	Schematic diagram showing chamber for direct calorimetry measurements.	36
2.2	Indirect calorimetry chamber basic layout. Typical size 2.0 x 2.5 x 3.0 m (18,000 L volume excluding furniture). Subjects can remain in the chamber for several days. Toilet, bed, step (for exercise), desk and chair are fitted inside the chamber.	38
2.3	Diagram of ventilated hood apparatus, used for measurement of EE in seated or supine positions.	44
2.4	Photograph of MedGem portable breath analyser.	46
2.5	Photographs of Breezing® calorimeter and associated apparatus.	47
2.6	Illustration of human respiratory system, showing the alveoli in the lungs and the gas exchange into the blood.	53
2.7	Three phases of exhalation shown by concentration of CO ₂ sample on from a breath. Exhaled tidal volume shown for an adult male, taken from a series of exhalations recorded in a laboratory environment during initial testing of prototype breath analyser.	54
2.8	Drawing of the operation of the Bio-VOC, where sample is collected and stored in tube for transportation or direct connection to analyser.	58

Num.	Caption	Page
2.9	Schematic of the breath sampling system with major components identified.	60
2.10	Inhalation and exhalation phases of breathing separated by the flow direction.	60
2.11	The area of the face where a mask or nose clip is worn is sensitive to an applied force, a) areas of skin supplied by the three major trigeminal nerve divisions [105]; b) Tactile detection threshold of areas on the face compared to the index finger (weights in milligrams).	63
2.12	Photograph of Sensewear armband and accompanying computer software.	72
3.1	Relationship between the lung volume, airflow, esophageal pressure and alveolar pressure for an adult human male (normal tidal breath at a rate of 12 breaths per min).	90
3.2	Histograms to show the sensor relative sensitivity required for 1 % EE calculation for O ₂ and CO ₂ ; a) and b) with three respiratory rates; c) and d) with fixed respiratory rate.	95
3.3	Schematic of low temperature electrochemical O ₂ sensor.	97
3.4	Principle of zirconia oxygen sensor.	100
3.5	Zirconia based flange mounted O ₂ sensor from SST Sensing.	100
3.6	Paramagnetic O ₂ sensor diagram.	101
3.7	a) SEM photograph of Nanosized particles of SnO ₂ deposited by a mechanochemical reaction; b) BFT with 0.3 tantalum content photographed with SEM after sintering.	101
3.8	Resistive O ₂ sensor based on SOI device, a) Structure of micro-hotplate; b) Sensor resistance measured with O ₂ concentrations in the range of 1 to 16 %.	103
3.9	Alphasense CO ₂ -D1 electrochemical gas sensor (detection range 0.5 to 90 % CO ₂).	104
3.10	Basic principles of NDIR sensing in four stages.	105
3.11	Absorbance of IR radiation by water, CO ₂ , CO and acetone.	106

Num.	Caption	Page
3.12	SEM photograph of the hexagonal plasmonic structure on NDIR emitter designed for enhanced transmission at 4.26 μm (hole diameter and spacing labelled).	107
3.13	a) Emissivity of plasmonic structures from 3.5 to 5 μm , top panel pitch fixed at 2.8 μm and radii varied between 350 and 1150 nm, lower panel radii kept constant at 800 nm and pitch varied between 2.3 and 2.9 μm ; b) Map of the surface normal emissivity at 4.26 μm wavelength, dots and crosses indicate radii and pitches respectively.	108
3.14	Commercial NDIR sensor, 20 mm diameter sensor offers CO ₂ detection up to 100 %, given the range of models available.	109
3.15	a) Cross-sectional drawing of a commercial pyroelectric detector (LME-302 from InfraTec [105]); b) Photograph of a commercial thermopile detector (ST150 from Dexter Research Centre [106]) mounted on the same TO-5 package with filter cap.	109
3.16	Physical model of the conductive mechanism when a semiconductor sensor is exposed to a) air and b) CO, with corresponding band model, from [144]. Models of electron transfer between grains are shown for c) a double Schottky barrier model and d) for a tunnelling model.	115
3.17	Sensitivity profiles of common materials used for MOX sensors.	116
3.18	Typical configuration of semiconductor thick film gas sensor. Photographs of the micro hotplate of size 1 mm \times 1 mm, a) The	117
3.19	MEMS device with coating on a resistive sensor and b) mounted on TO5 header for use in a gas sensing chamber.	120
3.20	Simplified MOX sensor schematic, with heater current drive capability and readout circuitry (non-inverting amplifier or buffer).	121
3.21	a) Photograph of a City Technology O ₂ sensor; b) Drawing of an Alphasense O2G2 sensor.	123
3.22	Photograph of Sensirion SFM3000 flow sensor.	124
3.23	Photograph of a GE ChipCap2 Temperature and RH Sensor.	124

Num.	Caption	Page
3.24	Photograph of a miniature commercial MOX sensor from SGX SensorTech (MICS-4514). Dual sensors for oxidising and reducing gas detection.	125
4.1	CO ₂ sampling techniques for mechanically ventilated patients, a) mainstream and b) side-stream.	140
4.2	Block diagram of mainstream breath analyser function.	141
4.3	Photograph of mainstream chamber configured to test on bench gas rig.	142
4.4	Fluid flow model of mainstream chamber with 1 SLPM flow inlet.	142
4.5	a) Sensor output observed during preliminary tests; b) ideal step response change in gas concentration to produce sensor output.	144
4.6	3D plot to show the desired test gas sensor model area.	145
4.7	a) Model block diagram displaying the input and output data; b) Desired output plot to compare predicted and actual measurements.	146
4.8	Schematic representation of PLS algorithm. Left graphic shows factor decomposition is used to obtain scores t common to X and Y that reflects their covariance. Plot on right shows regression is applied to relate t to each of the response variances y_m via regression coefficient b^*_m .	150
4.9	Raw sensor outputs from pulsing experiments, over a duration of 70 minutes.	151
4.10	Section of test patterns used to generate the PLS regression model of the O ₂ and CO ₂ sensors converted to percentage concentrations.	151
4.11	Normalised data for O ₂ , CO ₂ and RH sensors shown for the 70 minute repetition.	152
4.12	a) First 20 s window from the O ₂ sensor showing raw sensor output, bi-exponential fitted curve and step change in O ₂ concentration; b) First 20 s window from the CO ₂ sensor response to a step gas concentration change, with raw, fitted curve and input step change plotted.	153

Num.	Caption	Page
4.13	a) Model output for O ₂ sensor including 95 % CI calculations to assess performance, demonstrating that the sensor is operating close to the desired target 0.52 % accuracy; b) Model output for the CO ₂ sensor, target relative accuracy of 1.20 %, 70 % CI demonstrates poor performance.	154
4.14	Comparison between the SprintIR and the IR3107 gas sensors for 1 minute pulses of CO ₂ in the range of 0 to 4 %.	156
4.15	Bi-Exponential models fitted to 20 s output window of a) Affordable commercial SprintIR sensor and b) Relatively expensive commercial Hummingbird sensor.	157
4.16	a) Components shown inside FIS SB-500-12 sensor for CO detection; b) Equivalent circuit shown for the device, typically 2.8 Ω heater resistance at room temperature and 4.5 kΩ to 40 kΩ sensor resistance in the presence of 100 ppm CO.	159
4.17	FIS CO sensor output when exposed to pulses of CO (0, 10, 20, 50, 100, 150 ppm) for five consecutive pulses of 1 minute each.	160
4.18	Model output from CO sensor data, showing predicted vs actual concentration for 50:50 split of training and test data.	161
5.1	a) SOI emitter, provided by Cambridge CMOS Sensors, with 0.28 mm ² heating area; b) Emitter mounted on a TO46 header for fitting into the NDIR system; c) Heimann commercial thermopile also mounted on a TO46 header.	168
5.2	The temperature that a IR heater produces compared to the transistor drive voltage.	169
5.3	Photograph of the holder for the gold or aluminium tube (12 mm IR path length).	170
5.4	Prototype CO ₂ sensor compared against two commercial reference devices with IR path a) of gold plated tube and b) of aluminium tube.	170
5.5	Functional block diagram of NDIR sensor system with lock-in amplifier.	174
5.6	Simplified circuit schematic of NDIR lock-in system, showing initial amplification stage, lock-in IC chip and final filtering process.	175

Num.	Caption	Page
5.7	Operation of lock-in amplifier. Raw thermopile output (a) is compared to a reference sinusoid (from signal generator) with lock-in amplifier (b) and then the output is filtered (c).	175
5.8	Absorption coefficient for CO ₂ across the wavelength range of 4 to 5 μm .	177
5.9	Model curve fitted to find the coefficients for power losses due to conduction and convection.	179
5.10	Measured hotplate resistance compared to ΔT .	180
5.11	a) Input sinusoid to the model, demonstrated over a 1 s period; b) Output from the model, showing ΔT over a period of 1s, the waveform is no longer perfectly sinusoidal.	180
5.12	a) FFT plot comparing the CO ₂ detector data and model output waveform; b) Corresponding plot on logarithmic scale.	181
5.13	Block diagram of digital filtering process used to recover the response to CO ₂ presence from the noisy detector signal.	182
5.14	Photograph of the 80 mm Aluminium bench top chamber showing the PCBs for the IR emitter and thermopile detector.	182
5.15	Photograph of the adjustable path length design of the IR emitter and detector housing. 40 mm aluminium tube is fitted with 20 mm tube as shown.	183
5.16	Sensor outputs (relative to baseline of synthetic air with 80 mm path length showing detection of CO ₂ in the range of 50 ppm to 2.5 %, (a) with dry gases and (b) in a constant environment of 25 % relative humidity.	184
5.17	Response of the sensor to CO ₂ concentrations in the range of 0.5 % to 5 % with a 40 mm IR path length.	185
5.18	Comparison between 10, 20 and 40 mm path lengths for CO ₂ detection in the range of 0.5 to 5 %.	186
5.19	Time series data for 40 mm path length in 25 % RH conditions. CO ₂ varied from 0.5 % to 5% with constant 0.5 SLPM flow.	187
5.20	Data from 10, 20 and 40 mm path lengths summarised for 25 % RH conditions.	188

Num.	Caption	Page
5.21	Data recorded at 50 % RH for path lengths of 10, 20 and 40 mm.	189
5.22	Raw amplified thermopile output from the CO ₂ sensor system with concentrations shown in the table from 500 ppm to 10 ppm.	190
5.23	a) FFT filtering operation on the raw amplified thermopile signal produces b) FFT peak extraction data showing noise reduced output.	190
5.24	Measurements of CO ₂ between 0.5 % and 5 % with a 5 Hz drive signal and 1 minute steps per concentration input.	191
5.25	Thermopile raw output voltage compared to path lengths of 10, 20 and 40 mm across CO ₂ gas concentrations from 0.5 to 5 %.	192
5.26	Modified Beer-Lambert law equation plotted against output data for 10 mm IR path length (50 % RH) for CO ₂ concentration from 0 % to 5 %.	194
5.27	Modified Beer-Lambert law equation (3.2) plotted against output data for 80 mm IR path length for the FFT digital filtering method with concentrations of CO ₂ from 0 to 500 ppm.	195
6.1	Photograph of gas testing rig in laboratory.	202
6.2	Block diagram of gas rig.	202
6.3	Screen-print of LabVIEW interface for gas rig control and layout diagram showing options in each sub-section of the interface.	204
6.4	Screen-print of the data logging interface with graphs to show both prototype and commercial sensor outputs. The layout shown is of the control screen.	205
6.5	Photograph of a BME280 chip mounted on a circuit board. The interface board converts the sensor output to serial communication which is then converted to the USB inside the connector shown.	207
6.6	NI DAQ Analogue output system, for the IR emitter and MOX heater control.	208
6.7	Photograph of the Memmert Furnace; temperature controlled environment from 5 °c above ambient to ~ 300 °c.	209
6.8	LabVIEW VI for basic programming of MFCs, a) One value sent to the controllers with manual button push; b) Table of flow values, rows written automatically to the flow controllers after a given time.	211

Num.	Caption	Page
6.9	Screen print of an automated gas flow calculation (upper right table) given input of the desired gas concentrations (upper left table). The lower diagram indicates the function of each section of the VI.	212
6.10	Photograph of PJRC Teensy 3.2 microcontroller with micro USB port.	213
6.11	Effect of aliasing on a 2 Hz analogue sinusoidal waveform over a 4 s period, sampled at a) 16 Hz, b) 8 Hz, c) 5 Hz and d) 2.5 Hz. The original waveform is shown as solid line, dots indicate the sampling points and the dashed line shows the curve reproduced by linear interpolation.	216
6.12	Screen print of LabVIEW VI showing data acquired from a breath analyser using a USB link with a microcontroller. Example breathing for a 1 minute period is shown.	219
6.13	Screen prints from the Android USB wired data logging application, a) Breath data are recorded and graphed in real time; b) Basic data analysis performed post-logging, showing the data recorded for the O ₂ sensor during one experiment.	221
6.14	Photograph of a smartphone connected to breath analyser via a Bluetooth connection used for taking breath EE measurements and recording data.	223
7.1	Diagram showing layout of side-stream chamber. Mainstream and side-stream flow paths identified for directions of inhalation and exhalation.	231
7.2	Flow simulated through the chamber for the peak flow rate of a resting exhalation.	232
7.3	Manufactured chamber for the hand-held breath analyser, constructed from POM.	233
7.4	NDIR holder for POM chamber, a) Sketch in Solidworks; b) Photograph of 3D printed part.	234
7.5	VOC sensor holder add-on module to the chamber, a) Sketch in Solidworks; b) 3D printed part with the VOC sensor on TO46 header inserted. Interface circuit board attached.	234

Num.	Caption	Page
7.6	Photograph of the aluminium chamber to house O ₂ sensors for the experiments, with a temperature and humidity sensor fitted to measure environmental conditions.	237
7.7	Drawing of the aluminium chamber in Solidworks, showing construction of the gas tubing and the location of the sensor mounting.	237
7.8	Response of two O ₂ sensors to step a change in O ₂ concentration at flow rates of 2, 1, 0.5 and 0.25 SLPM.	238
7.9	Comparison of two MOX-20 O ₂ sensors, a) Voltage output at varying flow rates (O ₂ concentration as specified); b) t_{90} response time for the sensor to recover to baseline from 10.45 % O ₂ ; c) t_{90} response time for the sensor to reach final value for 10.45 % O ₂ from a baseline of 20.9 % O ₂ .	239
7.10	Response from two oxygen sensors for a change in environmental temperature, a) Voltage output from the devices; b) Response time for the devices to turn 'on' to a step concentration change from 20.9 % to 10.45 % O ₂ and 'turn off' for the opposite increase in O ₂ concentration.	241
7.11	Response from the 12 month old and new O ₂ sensors to a change in humidity condition, a) Voltage output from the sensors; b) Response time for the sensors to turn 'on' to a step decrease in O ₂ concentration (20.9 % to 10.45 %) and to turn 'off' for a step in O ₂ of opposite direction.	242
7.12	Flow diagram to show the side-stream system to be modelled.	244
7.13	RC Circuit diagram for the side-stream system.	244
7.14	Model fit created within Berkeley Madonna compared against O ₂ sensor data for an exhalation.	246
7.15	Subject breathing through the side-stream device, output from the O ₂ and CO ₂ sensors.	247
7.16	Scaled (0 to 1) responses from the O ₂ and CO ₂ sensors for an exhalation, with fitted delay model outputs.	248

Num.	Caption	Page
7.17	Photograph of the breath analyser with sensors for flow, temperature, humidity, CO ₂ and O ₂ .	250
7.18	O ₂ sensor calibrated with 3 gas concentrations.	251
7.19	CO ₂ sensor calibrated with 4 gas concentrations.	252
7.20	Oxygen sensor calibration procedure, a) Calibration line calculated for raw voltage data; b) Calibration equation applied to the raw sensor voltage output.	252
7.21	Carbon dioxide sensor calibration procedure, a) Calibration curve calculated for raw sensor voltage data; b) Calibration equation applied to raw sensor output.	253
7.22	Photographs of the hand-held analyser when used, a) With wired connection to Smartphone; b) With wireless Bluetooth connection.	254
7.23	Subject breaths through the breath analyser for period of 1 minute, a) At a breathing rate of 6 cycles per minute; b) At a rate of 10 cycles per minute.	255
7.24	Side-stream analyser tested with subject exhaling at 10 breaths per minute, 90 s data shown, a) Comparison of the prototype NDIR sensor against a commercial device (Hummingbird IR3107); b) Corresponding O ₂ sensor output.	257
8.1	Photograph of hand-held breath analyser, installed in a robust enclosure for monitoring of EE inside respiratory chambers. Battery power available for portable measurements.	266
8.2	Photograph of additional side-stream analyser, consisting of commercial sensors for comparison against the prototype hand-held breath analyser.	267
8.3	Output data plots for one subject for the duration of the 3 hour experiment for a) The O ₂ concentration measured (MOX-20 sensor) and b) The CO ₂ concentration measured (prototype NDIR sensor).	271

Num.	Caption	Page
8.4	Sensor data for a 3 min period when the subject was breathing through a hand-held analyser, a) O ₂ and CO ₂ sensor data (MOX-20 and prototype NDIR sensor respectively); b) Flow sensor data (SFM3000 sensor) with tidal volume; c) Temperature and RH sensor data (ChipCap2 sensor).	272
8.5	Simplified block diagram showing the data processing stages from calculating human EE from the raw data collected from the O ₂ , CO ₂ and flow sensors.	274
8.6	Subject data comparison between the hand-held analysers and respiratory rooms, a) O ₂ consumed by one female subject; b) Corresponding CO ₂ produced; c) O ₂ consumed by one male subject; d) Corresponding CO ₂ produced.	275
8.7	Data collected from 10 subjects with hand-held analysers, respiratory rooms and analysers with commercial sensors, a) O ₂ consumed and b) CO ₂ produced.	277
8.8	EE calculated for 10 subjects using HH devices, RR systems and the CS analyser.	278
8.9	EE measured with HH instrument in relation to a) Subject age and gender; b) Subject BMI, age and gender.	280
8.10	EE measured on HH instrument compared to calculated BMR using HB equation.	281
8.11	Block diagram for operation of the hand-held measurement device with a smartphone application.	284
8.12	Concentrations of O ₂ and CO ₂ recorded over a 1 minute period for a) One subject with a respiratory rate of 10 breaths per minute; b) Second subject with a respiratory rate of 8 breaths per minute.	284
8.13	Screen prints from Android smartphone showing the companion EE measurement application for the hand-held analyser, a) Data logging screen; b) EE measurements performed over a 1 minute period.	285

Num.	Caption	Page
8.14	EE recorded over a 6 hour period for one subject. Measurements taken at 1 hr intervals during an office-based day. One period of activity shown between the vertical time lines and the meal time is indicated with arrow.	286
9.1	a) Average sensor response time as a function of temperature for 50 ppb of NO ₂ in 50 % RH diluted with synthetic air; b) Corresponding response and recovery times in the same conditions.	298
9.2	SEM photograph of surface deposition of WO ₃ material onto the sensor surface at 250x magnification. Coating manufactured and deposited courtesy of Dr. B. Urasinska-Wojcik, University of Warwick.	300
9.3	Response of the sensor to NO ₂ in dry conditions, a) plotted as a function of time and b) sensitivity against concentration.	302
9.4	Sensors tested in 25 % RH conditions, a) response time plot shown and b) sensitivity.	302
9.5	Sensor tested in 50 % RH conditions, a) response time plot shown and b) sensitivity.	303
9.6	SEM micrograph of WO ₃ film sensor by Su and Peng, fabricated by one-pot polyol process.	305
9.7	Sensor tested in Acetone 100 to 300 ppm, with a) Normalised resistance plot and b) Response plot.	308
9.8	a) Resistance response plot for the prototype sensor to concentrations of NO ₂ and CO; b) Differentiated initial responses to each gas concentration.	310
9.9	A single breath sampled through three analysers, a) O ₂ sensor response; b) CO ₂ sensor response.	314
C.1	Screen print of interface screen layout preparation code.	359
C.2	Screen print of acquisition of data from USB unit to front panel display.	359
C.3	Screen print of saving data to file with column labels.	360

Num.	Caption	Page
C.4	Screen print of control software for Memmert Oven used in the gas testing rig. Temperature values set in a table can be sent to the oven after the passage of a set period of time, to enable step changes in the environment of the gas sensor chamber (inside the oven).	361
C.5	Screen print of code to output various waveform shapes from a file or from set parameters to the analogue output from a USB unit (National Instruments Data Acquisition Unit). The code allows for a sinusoid, square wave or DC voltage to be applied to the analogue output. A file can be loaded with custom points (voltages) and a time period (s) which will be output through the analogue port. The loop is executed at a fixed rate (1 kHz) to ensure accurate frequency generation.	362
C.6	Screen print of code to send flow values to MFCs on gas testing rig. Sub-VI is used to calculate flow rates from desired gas concentrations.	365
C.7	Screen print of sub-VI code to calculate flow rates for MFCs, given a desired gas concentration and the concentration available from the gas cylinders.	366
D.1	Screen print of a section of the microcontroller code written to acquire the signals from the sensors in the hand-held unit.	367
E.1	Screen print of LabVIEW code for recording data from the Teensy microcontroller for the handheld analysers.	368
F.1	Screen print of Android layout designer in Android Studio, with the graph elements on the main-screen of the application selected.	369
F.2	Screen print of code section showing data being received from a serial link and being stored in a buffer.	370
F.3	Screen print of code section to calculate the amplitude of a sinusoidal signal.	371
F.4	Screen print of code used to display the EE calculated from a 1 minute breath sample.	372

List of Tables

Num.	Caption	Page
1.1	List of associated health risks with obesity.	3
1.2	Disease effect on metabolic rate measured across a range of subjects.	22
2.1	Characteristics of volunteers trialled in respiratory chambers by Ravussin.	40
2.2	Urinary nitrogen loss rate following injury or illness.	50
2.3	Stress level compared to urinary nitrogen (g/day).	50
2.4	Subject information for observing chamber performance.	51
2.5	Summary of urine nitrogen content for subjects and error introduced to EE calculation.	52
3.1	Gases found in exhaled breath and concentration range compared to air.	87
3.2	Conditions found on exhaled breath compared to ambient air conditions.	88
3.3	Subject data metabolic rate error and required sensor sensitivity (varying respiratory rate between 6 and 30 breaths per minute).	93
3.4	Subject data metabolic rate error and required sensor sensitivity (constant respiratory rate of 10 breaths per minute).	94
3.5	General comparisons between NDIR and Electrochemical CO ₂ sensor principles.	103
3.6	List of available VOC detection methods for a portable analyser.	113
3.7	List of example gases and VOCs found in exhaled breath and their diagnostic purpose.	114
4.1	Experiments performed to model the output from the sensor.	145
4.2	Normalisation process required for each sensor.	147
4.3	Response times calculated for the turn-on phase for both commercial CO ₂ devices.	157
6.1	List of microcontroller devices and specifications used in this work.	214
7.1	Experimental parameters for comparison of O ₂ sensors.	236
7.2	Component values estimated using Berkeley Madonna.	246
8.1	List of sensors included in the respective breath analysers.	268

Num.	Caption	Page
8.2	Summary of the EE data from the 10 subjects compared to the reference standard of the RR measurement.	282
9.1	Gas Concentration steps of NO ₂ tested with the MOX sensor.	301
9.2	Gas Concentration steps of Acetone tested with the MOX sensor.	308

Acknowledgements

I would like to express my thanks to my supervisor Prof. Julian Gardner, for granting me the opportunity to research in this field of breath analysis and gas sensors and for all his support during my time at the University. I would also like to thank Prof. Adrian Wilson (Department of Physics, University of Warwick and Human Metabolism Research Unit, University Hospital Coventry and Warwickshire), Dr. Michael Chappell (School of Engineering, University of Warwick) and Dr. John Hattersley (HMRU, University Hospital Coventry and Warwickshire). Together with Prof. Gardner, their tireless assistance and guidance has helped me overcome the challenges that were presented during this work.

I would also like to thank my colleagues at the Microsensors and Bioelectronics Laboratory (MBL) within the School of Engineering at the University of Warwick. I extend special thanks to my partner Farah Villa-Lopez from the MBL group, for her understanding and patience throughout this work. Without her limitless support and time to help to bounce ideas, this work would not have been completed.

I am grateful to the School of Engineering and University Hospitals Coventry and Warwickshire NHS Trust for their financial support during this work. I would like to acknowledge Cambridge CMOS Sensors, Cambridge, U.K. for providing the CMOS devices used in this research. I am grateful to Dr. Barbara Urasinska-Wojcik for the development of the metal oxide sensors used in this work and the deposition of sensor coatings.

I would like to extend my thanks to all the members of the School of Engineering technical support team that have helped with the construction of the sensor systems developed in this work. In particular I am very grateful to Mr. Francis Courtney and Mr. Ian Griffith for their patience and help with construction of the mechanical and electronic components, respectively, needed to complete this work.

Declaration

This thesis is submitted to the University of Warwick in support of my application to the degree of Doctor of Philosophy. It has been composed by myself and has not been submitted in any previous application for any degree. Parts of this thesis have been submitted to conferences and published in journal papers as outlined below in chronological order.

Published Journal Papers and Book Sections

Copies of the first two articles from this list are shown in Appendix A.

- **T.A. Vincent**, A. Wilson, J.G. Hattersley, M.J. Chappell, J.W. Gardner, Development of a handheld side-stream breath analyser for point of care metabolic rate measurement, in: *Lect. Notes Comput. Sci. (Including Subser. Lect. Notes Artif. Intell. Lect. Notes Bioinformatics)*, Cham, Switzerland, 2016: pp. 13–21. doi:10.1007/978-3-319-31744-1_2.
- **T.A. Vincent**, J.W. Gardner, A low cost MEMS based NDIR system for the monitoring of carbon dioxide in breath analysis at ppm levels, *Sensors Actuators B Chem.* 236 (2016) 954–964. doi:10.1016/j.snb.2016.04.016.
- J.W. Gardner, **T.A. Vincent**, Electronic noses for well-being: Breath analysis and energy expenditure, *Sensors.* 16 (2016) 947–966. doi:10.3390/s16070947.
- B. Urasinska-Wojcik, **T.A. Vincent**, M.F. Chowdhury, J.W. Gardner, Ultrasensitive WO₃ gas sensors for NO₂ detection in air and low oxygen environment, *Sensors Actuators, B Chem.* 239 (2017) 1051–1059. doi:10.1016/j.snb.2016.08.080.

Conference Presentations

- **T.A. Vincent**, J.W. Gardner, J.G. Hattersley, A. Wilson, M.J. Chappell, Environmental Monitoring of Human Body Odours, in: *COST Action TD1105 - New Sens. Technol. Air-Pollution Control Environ. Sustain.*, 2013: p. 71.
- **T.A. Vincent**, A. Wilson, J.G. Hattersley, M.J. Chappell, J.W. Gardner, Design and Modelling of a Portable Breath Analyser for Metabolic Rate Measurement, in: *Procedia Eng.*, 2014, pp: 668–671. doi:10.1016/j.proeng.2014.11.576.

- **T.A. Vincent**, A. Wilson, J.G. Hattersley, M.J. Chappell, J.W. Gardner, Design and Development of a Portable Side-Stream Metabolic Rate Breath Analyser, in: *PGBiomed 2015 Proc.*, 2015: pp. 12–13.
- **T.A. Vincent**, A. Wilson, J.G. Hattersley, M.J. Chappell, J.W. Gardner, Design and modelling of a handheld side-stream breath sampling system for metabolic rate analysis., in: *Int. Symp. Olfaction Electron. Nose*, 2015: pp. 198–202.
- J.W. Gardner, G. Wei, **T.A. Vincent**, K. Volans, P. Tremlett, T. Wotherspoon, et al., A gas sensor system for harsh environment applications, in: *Procedia Eng.*, 2015: pp. 275–278. doi:10.1016/j.proeng.2015.08.608.
- **T.A. Vincent**, B. Urasinska-Wojcik, J.W. Gardner, Development of a Low-cost NDIR System for ppm Detection of Carbon Dioxide in Exhaled Breath Analysis, in: *Procedia Eng.*, 2015: pp. 388–391. doi:10.1016/j.proeng.2015.08.648.
- B. Urasinska-Wojcik, **T.A. Vincent**, J.W. Gardner, H₂S sensing properties of WO₃ based gas sensor, in: *Procedia Eng.*, 2016, In Press.
- **T.A. Vincent**, J.W. Gardner, M.J. Chappell, J.G. Hattersley, A. Wilson, Measurement of energy expenditure on a smartphone using a handheld breath analyser, in: *Procedia Eng.*, 2016, In Press.

Summary

Metabolic rate is not routinely assessed in healthcare for the general population, nor is it a measure commonly recorded for in-patients (incorrect feeding can slow post-operation recovery rate). For the general community, this lack of knowledge prevents the accurate determination of calorific need and is a factor contributing towards the onset of an overweight and an increasingly obese population. In the UK alone, obesity costs the National Health Service a staggering £5 billion annually. In this thesis a novel low-cost hand-held breath analyser is presented in order to measure human energy expenditure (EE). A unique optical CO₂ sensor was developed, capable of sampling exhaled breath with a fast response time ~1 s and resilience to a humidity range of ~30 % to near saturated. The device was tested in a laboratory gas testing rig and a detection limit of ~25 ppm CO₂ was measured. A low power metal oxide sensor (~100 mW) was developed to detect volatile organic compounds (VOCs) in the breath, for disease detection and investigation of the variation of inter-individual metabolism processes. The device was sensitive to acetone (100 to 300 ppm, which is a biomarker for type-I diabetes). Other VOCs, such as NO₂ were tested (10 to 250 ppb). Further work includes investigating the inter-individual variance of metabolism processes, for which the metal oxide sensor would be well-suited. Software was developed to operate the gas testing rig and acquire sensor output data in real-time. An application was written for smartphones to enable EE measurements with the breath analyser, outside of a laboratory environment. Three hand-held analysers were constructed and tested with a trial of 10 subjects. A counterpart (benchmark) unit with medical grade commercial sensors (cost of ~£2500) and hospital respiratory rooms (reference) were included in the trial. The newly developed analysers improved upon the performance of the benchmark system (average EE measurement error +2.4 % compared to +7.9 %). The affordable device offered far greater accuracy than the traditional method often used by practitioners (predictive equations, error +41.4%). It is proposed a set of periodic (hourly) breath measurements could be used to determine daily EE. The EE analyser and associated low-cost sensors developed in this work offer a potential solution to halt the growing cost of an obese population and provide point-of-care health management.

Abbreviations

Abbreviation	
ADC	Analogue-to-Digital Converter
BMI	Body Mass Index (kg m^{-2})
BMR	Basal Metabolic Rate
CI	Confidence Interval
CMOS	Complementary Metal-Oxide-Semiconductor
COPD	Chronic Pulmonary Disease
COSHH	Control of Substances Hazardous to Health
CSV	Comma-Separated-Value
DAQ	Data Acquisition
DIT	Diet Induced Thermogenesis
DLW	Doubly Labelled Water
EE	Energy Expenditure
EMF	Electromotive Force
EN	Enteral Nutrition
FEM	Finite Element Modelling
FFM	Fat-Free Mass
FFT	Fast-Fourier Transform
HAPI	HITRAN Programming Interface
HITRAN	High-Resolution Transmission Molecular Absorption
HB	Harris-Benedict
HR	Heart Rate
HMRU	Human Metabolism Research Unit (University Hospital Coventry)
ICU	Intensive Care Unit
I.D	Internal Diameter
IR	Infrared
LCD	Low Calorie Diet
MEMS	Micro-Electro-Mechanical Systems
MFC	Mass Flow Controller
MFM	Mass Flow Meter
MLR	Multiple Linear Regression

Abbreviation

MOX	Metal Oxide
MR	Metabolic Rate
NHS	National Health Service (UK)
NDIR	Non-dispersive Infrared
PA	Physical Activity
PCR	Principle Component Regression
PID	Proportional-Integral-Derivative
POM	Polyoxymethylene (Polyacetal)
ppm/ppb	Parts Per Million/Billion
RH	Relative Humidity
RMR	Resting Metabolic Rate
RQ	Respiratory Quotient
RTIL	Room Temperature Ionic Liquid
SEM	Scanning Electron Microscope
SIT	Sprint Interval Training
SLPM	Standard Litres Per Minute
SOI	Silicon-On-Insulator
SPI	Serial Peripheral Interface
SPN	Supplementary Parental Nutrition
SSoW	Safe System of Work
STD	Standard Deviation
TEF	Thermal Effect of Food
TO	Transistor Outline
TUN	Total Urinary Nitrogen
UHCW	University Hospitals Coventry and Warwickshire NHS Trust
UN	Urinary Nitrogen
USB	Universal Serial Bus
UUN	Urinary Urea Nitrogen
VI	Virtual Instruments
VISA	Virtual Instrument Software Architecture
VLCD	Very Low Calorie Diet
VOC	Volatile Organic Compound

Chemical Formulae

Formula	
Ag	Silver
CO	Carbon Monoxide
CO ₂	Carbon Dioxide
CO (NH ₂) ₂	Urea
H ₂	Hydrogen
H ₂ O	Water
Ln ₂ O ₃	Lanthanide sesquioxide
N	Nitrogen
N ₂	Nitrogen Gas
NO	Nitric Oxide
NO ₂	Nitrogen Dioxide
O ₂	Oxygen
POM	Polyoxymethylene
Pt	Platinum
SnO ₂	Tin Oxide
TiO ₂	Titanium Dioxide
WO ₃	Tungsten Oxide

CHAPTER I

Human Metabolism

Preface

The study of human metabolism has progressed extensively since the latter part of the 20th century and although the components of energy expenditure are now well defined their variance with human daily routine is less well understood. Globally, the trend towards an obese population is becoming increasingly widespread, putting substantial additional pressure on health services worldwide. The array of diseases associated with an overweight population is swallowing healthcare resources and when accrued with absence rates, costing the global economy billions every year. The cause of the overwhelming surge towards an overweight population is usually placed on changes in lifestyle and diet, the quality of which greatly effects human energy balance. Today, we are made more aware of the calorific content of our food, and the importance of exercise towards a healthy lifestyle. The unknown factor in the energy balance equation, between energy intake and energy consumed, is the energy we need as individuals. In this chapter the components of energy expenditure are discussed and the need for the routine measurement of patient energy expenditure.

1 Metabolism

Our lifestyles are continuously evolving and with the turn of each year it seems a new gadget is released to supposedly make our lives easier both at home and at work [1]. These labour saving technologies have contributed to a reduction in manual tasks and consequently our daily activities have become less active (with a reduction in daily exercise) and more sedentary [2,3]. A behavioural shift in society has led to an increased reliance on cars as a means of transport [4]. In England, 6 % of car journeys in 2014 were less than 1 mile (50 % less than 5 miles) [5]. It has been reported that the reason for 21 % of short car journeys were made for convenience or to save time [6]. In 2014 cars, vans and taxis were used for 654 billion passenger kilometres, double the values recorded in 1972 [7].

In simple terms, to maintain a healthy weight calorific intake must equal the energy required over the course of a day. In a sedentary seated position, the human body burns fewer calories, than intensive manual work, or even standing [8]. The consumption of sugary foods and alcoholic beverages has increased in the UK [9]. Nutritional information is now commonplace on packaging, although consumers are not motivated to review the labels [10]. A diet with high calorific content (when a diet exceeds 120 % daily calorific requirement [11], particularly high fat and sugar content) combined with a reduction in energy requirements in our daily activities has seemingly contributed to an increase in an overweight population.

European regulations introduced in December 2011 (and mandatory from December 2016) made nutritional labelling compulsory for any pre-packed products [12]. For consumers aware of their diet, this information can offer a means of calculating their calorific intake but accurately determining the amount of calories a person consumes is still not a trivial task.

The missing information in the energy balance to maintain a healthy weight is the amount of calories burnt by the human body. Many simple methods have been proposed to determine energy requirements, for example predictive equations or activity monitoring, however accurate determination during everyday life is challenging. As discussed in the following chapter, each of the methods has fundamental flaws, which negates their routine use in clinical practice and none are

suitable for use by the general public. It is the need for an accurate method of determining energy expenditure (EE) of a human in a free-living environment that motivated this project, namely to develop a hand-held unit to monitor EE through breath analysis.

In the UK, the National Health Service (NHS) spends an estimated £15.4 billion every year on treatments related to an overweight population [13]. It is suggested that obesity is one of the top three global social burdens, and in the UK this has an annual economic impact of £51 billion [14]. It is estimated 23.9 % of females and 22.1 % of males are obese (body mass index ≥ 30) in the UK [15]. Table 1.1 lists possible comorbidities of obesity. Premature deaths are also associated with obesity, where only tobacco smoking carries a greater risk [16]. The risk of mortality increases as BMI increases (although a BMI outside the lower limit of the 20-25 kg/m² range also increases the risk). Additionally, a fluctuation in body weight can also cause premature death and increase the risk of chronic diseases [16].

Table 1.1 – List of associated health risks with obesity.

Associated Disease	Risk	Ref
Cancer	Increased risk of reproductive cancers (breast, uterus, cervix, prostate).	[17]
Cardiovascular	Elevated risk of heart attack and stroke.	[16]
Diabetes	Overweight people twice as likely to develop type 2 diabetes. Itself, type 2 diabetes is major cause of early death, heart disease, kidney disease and blindness.	[17]
Gallbladder Disease	Related to obesity, probability of contracting disease increases with weight gain. Gallstones are associated with fast weight loss.	[18]
Gout	Uric acid in the blood causes gout, when stone or crystal masses are deposited in joints.	[17]
Gut	Changes in gut hormone secretion and changes in gut microflora.	[18]
Hypertension	Overweight people more likely to have high blood pressure.	[16]

Associated Disease	Risk	Ref
Osteoarthritis	Extra weight on joints can increase the risk. Pressure on joints wears away protective cartilage.	[16]
Pulmonary	Abnormal function possible in obese patients. Can cause obstructive sleep apnea.	[17]
Psychosocial	Can cause eating disorders, poor self-esteem and depression.	[18]

A general underestimation of energy intake and an overestimation of the calories expended during exercise or while sedentary has been reported [19]. Knowledge of energy expenditure for the general population is a key element in avoiding unintentional overeating and to achieve energy balance [20]. There are no routine checks prescribed to advise on the EE of an individual. The current generation of indirect calorimeters is acknowledged to be expensive devices and the measurements taken using these devices are time-consuming and require a well-trained team [21,22]. In the UK, the NHS recommend that to maintain a healthy weight, daily calorie intake should not exceed 2,500 kcal for men and 2,000 kcal for women [13,23].

Knowledge of energy requirements is greatly beneficial for healthy individuals, but for the care of patients in intensive care units (ICUs) could be considered essential. However in a collection of around 8000 ICU cases only 0.8 % used indirect calorimetry to determine energy requirements [24]. The lack of accurate calorific knowledge costs lives in ICUs and the introduction of routine calorific requirement measurement could dramatically improve patient care and survival rates.

The energy requirements of a patient in intensive care can vary depending on their underlying illness. Comparing patients with the same condition, metabolic requirements depend on the stage of the illness and its severity [25,26]. Therefore it is difficult to adapt equations to suit ICU patients, with many factors estimated by the practitioner.

Malnutrition, where the patient is underfed, has been found to increase the length of stay in an ICU and also increases the risk of complications (particularly infections) [27]. One study even reported an increased mortality rate for patients who had an energy deficit of >1200 kcal/day over a 2 week period [28]. Feeding a patient in an

ICU with excess nutrition can also endanger life, where overfeeding has been associated with hypercapnia, re-feeding syndrome and immune dysfunction [29,30]. It has been reported 71 % of critically ill patients were overestimated in a study of 34 patients when compared against indirect calorimetry [29]. It was noted that the preferred method of monitoring energy requirements was indirect calorimetry, although this is not always feasible.

1.1 Project Aims

A handheld breath analyser will be developed for this project. This section summarises the target specification for the prototype unit. The motivation for developing a hand-held unit is discussed in section 2.7, following a discussion of the currently available EE measurement techniques.

- Develop a device capable of measuring human EE.
 - The device developed during the project should contain the necessary sensors to measure human EE. It should work on a breath-by-breath basis and be able to perform measurements quickly, over a period of a few minutes.
- Build a robust and affordable unit suitable for widespread adoption.
 - The unit needs to be portable and robust but still affordable. To enable use in the general community, it must use components able to withstand being transported yet while remaining low cost, miniature and accurate. Infrequent calibration required (if at all), that is simple and does not require specialist equipment.
- Create an easy to use means of calculating EE with the analyser.
 - The device should be robust and simple to use, without requiring the assistance of a clinician. A reliable yet intuitive means of measuring EE should be developed (software to perform calculations, for example a smartphone application). The device should be able to measure EE with only infrequent calibration. The sensors need to be reusable and not require maintenance or replacing in-between breath measurements.

- The device should measure a 1 % change in EE.
 - To be of use in clinical practice the device must be capable of measuring a 1 % change in EE (discussed in section 3.1). Briefly, a 1 % tolerance is required to monitor the changes in components of total EE, of particular interest is the effect of eating on metabolism. The device must be able to accurately measure EE and allow reproducible results.
- Verified against clinically proven method of EE measurement.
 - To validate the EE measurements performed with the developed prototype breath analyser against a renowned measurement technique. The portable unit will be verified with subjects in respiratory rooms.
- Expandable measurement system for research devices.
 - Allow extra sensors to be added to the system to expand the capabilities of the device for breath analysis. Volatile organic compound sensors could be included to allow further analysis of breath contents.

1.2 Components of Energy Expenditure

Metabolic rate for human beings is the amount of energy expended by the body over a given period of time, the aggregate of all the energy expending chemical processes taking place. In a free-living environment the energy required by a human can be divided into four components. The majority of daily EE (60 to 70 %) is consumed by basal metabolic rate, the minimum amount of energy required to sustain life [31]. Approximately 25 % of the daily EE is attributed to purposeful physical activity, 7 % to non-exercise activity (e.g. fidgeting) and the remaining 8 % to thermal effect of food (TEF). Knowledge of these components and their variance can aid design of a protocol to reproducibly measure EE. Resting metabolic rate (RMR) is measured in a seated or supine position, and is the energy required by the body to maintain normal body functions at rest (the subject should be awake but not perform any activity and should have fasted beforehand).

1.2.1 Physiological and Environmental Factors

Metabolic rate is usually higher in males compared to females. Additionally, RMR decreases with age [32]. Fig. 1.1 shows the rapid decrease in RMR during childhood. Male RMR is higher than for a female across the age range shown (1 to 75+ years). RMR is usually measured in the morning, after a 12 hour fasting period [33]. No strenuous activity should have been performed before the test (nor any physical activity for the duration of the test). All psychological and physical factors that cause excitement must be eliminated [34].

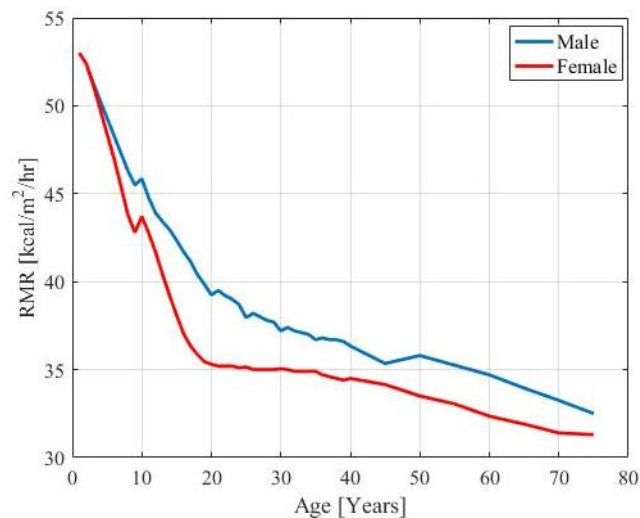


Fig. 1.1 – Resting Metabolic Rate from 1 year of age to 75+ years of age, in terms of body surface area. Data from [32,35].

The rapid decrease in RMR from the age of 3 can be explained by changes in body composition through growth. Normally the RMR decreases by 1-2 % per decade, however the uneven growth of organs and changes in body composition cause a peak for over 10 years starting from 3 years of age [33]. Growing children (for example teenagers) need to consume a higher amount of calories per day than older adults [36]. Body composition has an effect on RMR. As the body ages, muscle mass tends to decline. At rest, muscle tissue uses more energy than fat tissue. Intrinsically, the body composition of a female, with a higher fat to muscle mass ratio (specifically essential fat) means a males have a higher RMR at every age [37]. Muscle mass can be improved through exercise, although typically only accounts for 25 % of basal oxygen (O_2) consumption (compared to vital organ tissue, which accounts for around 60 %) [38].

In terms of body weight, under normal circumstances around 5 to 6 % of total body weight can be attributed to the weight of the brain, liver, heart and kidney, compared to around 30 to 40 % attributable to muscle mass [39]. It has been estimated that the organ cells account for more than 60 % of RMR [39]. It has been reported that age related reduction in fat-free mass (FFM, muscle mass) is responsible for the decline in RMR during adult life [40]. Lazzer et al. in a study of 8,780 subjects showed that gender was a significant determinant of RMR in obese children and adolescents, but not obese adults [40]. In children and adolescents gender remained significant after adjustment for body weight and FFM. Around 80 % of inter-individual variability in RMR is accounted for by FFM, fat mass (FM), age and gender [41]. The majority, 75 %, is FFM with around 5 % accounting for the other covariates.

Hormone levels also have an effect on MR. Thyroid hormone increases MR, where a total loss of thyroid secretion may decrease MR by as much as 40 to 60 % of normal level [34]. When the gland secretes maximal amounts of thyroxin the MR can rise by as much as 50 to 100 %. Notably, the gland adapts to different climates, secreting a higher amount of thyroxin in colder climates and a lower amount in warmer climates. Thyroxin increases the rates of the chemical reactions taking place in many cells, thus a higher level of thyroxin causes a higher MR. Comparing people living in arctic conditions to those in tropical conditions, RMR of people living in colder climates could be higher than those in hotter climates by perhaps 5 to 20 % [42]. In hotter climates, exercise causes a higher elevation in metabolic load compared to thermoneutral environments (~5 %). Three factors can directly produce an increased thermogenic effect namely: Elevated core temperature; additional energy required for sweat gland activity and altered circulatory dynamics. Shivering thermogenesis refers to a person shivering to generate heat, which can cause RMR to triple. This effect is particularly visible in cold stress during exercise, such as the subject being immersed in cold water.

The calorific intake required for male individuals is well known to be larger than comparative females [34]. Male sex hormones have a far greater effect on MR than female sex hormones; testosterone can increase MR by 10 to 15 %, whereas female sex hormones may only increase RMR by a relatively insignificant amount [34]. The larger effect of male hormones on MR is due to the hormones anabolic effect in increased skeletal muscle mass. Growth hormones can also cause a rise in MR, for the

same reason, by stimulating cellular metabolism. Adults with growth hormone deficiency can attend replacement therapy sessions, with recombinant growth hormones which increase RMR by about 20 %. Taking a view of the population in general, women have lower energy intake and lower average daily MR due to lower body mass, fat-free mass and a higher percentage of body fat [43]. RMR in females does vary on a daily basis as hormones that regulate the menstruation oscillation [36].

1.2.2 Physical Activity

The need for an active lifestyle, along with a balanced diet, to maintain or lose weight is clear when considering 25 % of daily EE is attributed to physical activity (PA). Increasing PA levels is often recommended for weightless patients to lose weight, to compensate for the decrease in RMR associated with weight loss. Furthermore, in general the amount of energy required to complete a set activity is proportional to weight. Thus the same level of activity requires less energy after weight loss [44]. It has been reported that bariatric surgery (with 50 kg weight loss) can cause a decrease in RMR of 573 kcal/day[44].

A study by DeLany et al. found subjects achieved body weight loss by a prescriptive energy deficit of between 500 and 1000 kcal/day [44]. A weight loss of 7 % was targeted. The study emphasised the difficulties in adhering to diet plan, where it was noted not all participants followed the guide [44]. The target goals were made deliberately ambitious, to encourage weight loss and more daily PA. It was discovered that although some subjects were the most active, and lost the most weight, this group had the greatest drop in RMR. The participants were divided into two groups, one prescribed only a diet plan and the other prescribed both a diet plan and exercise regime. This study cannot be seen as representative for the general population, due to the high proportion of female participants (87 %) and restricted age group (mean age 47.8 years, \pm 6.4 years). The effect of PA as a tool to minimise the drop in total daily EE and EE due to PA was masked, by the non-adherence to the PA prescription by both groups in the study.

Exercise has been shown to affect MR for several hours beyond the duration of the activity [45]. Knab reported subjects displayed an increased metabolic rate for 14 hours after a 45 minute bout of cycling, when measured in a metabolic chamber [46]. The data from 10 subjects demonstrated that during the exercise period, EE increased

by an average of 514 kcal. Over the following 14 hours a total of 190 kcal was expended above comparative measurements taken the previous day, where the subjects were sedentary. After approximately 14 hours the EE measured returned to the baseline level, set by previous days inside the chambers.

Sevits et al. studied the effect of a single bout of sprint interval training (SIT) on the daily EE of 12 adult males inside respiratory chambers [47]. The SIT consisted of five sprints on a cycle ergometer, with recovery time in-between (total period of ~30 minutes). An increased level of EE was recorded for 4 hours after SIT and an increased daily EE of 225 kcal was calculated, shown in Fig. 1.2 a). Sevits et al. further explored the influence of SIT on 24 hour metabolism, by use of respiratory data to quantify changes in substrate oxidation. It was found that minute by minute respiratory exchange values, shown in Fig. 1.2 b), were increased only for a four hour period.

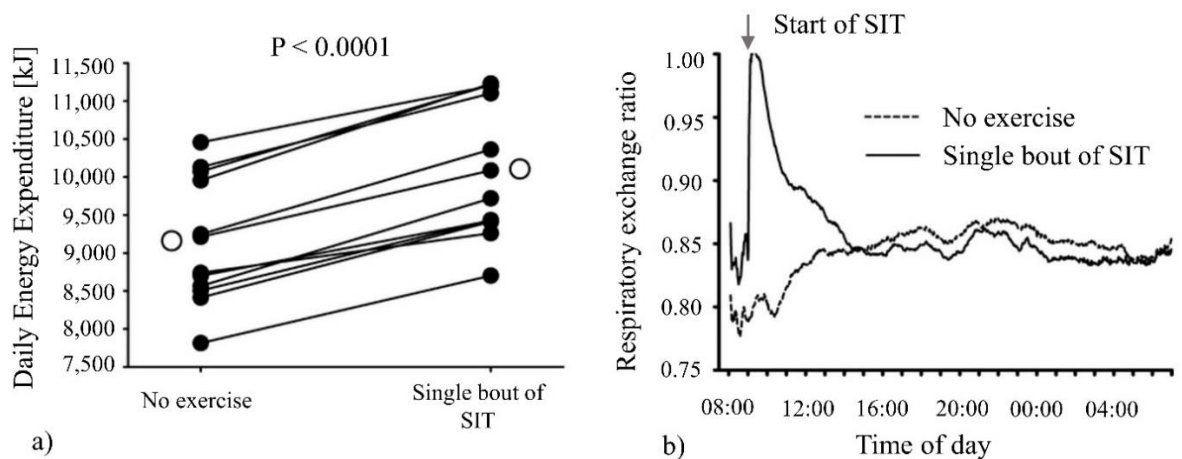


Fig. 1.2 – a) Total daily EE increased after a single bout of SIT. Closed and open circles indicate individual responses and group mean respectively; b) Mean EE found from the group during the sedentary day compared to the SIT period. Adapted from [47].

1.2.3 Effect of Eating

The TEF (or DIT, Diet Induced Thermogenesis) component of EE varies by person, and is one of the more difficult methodological barriers to the study of energy balance in humans [43]. Diet variation can influence TEF by as much as 15 % (for a healthy subject ~10 % is expected). Oxygen consumption has been reported to rise after a meal and is lowest in the morning and at night [48]. O_2 consumption has also been shown to correlate with body fat, body surface area and body weight. The ratio between CO_2 produced and O_2 consumed is also dependent on such factors. The energy content of

the food most determines the TEF, followed by the protein factor. Food high in fat content reduces the thermal effect of food. Food with a high protein or high alcohol content contributes significantly to a higher TEF. An example of the effect of TEF is shown in Fig. 1.3, where subjects were inside a calorimetry chamber for two days and randomly assigned a meal condition each day; either two meals or three meals per day [49].

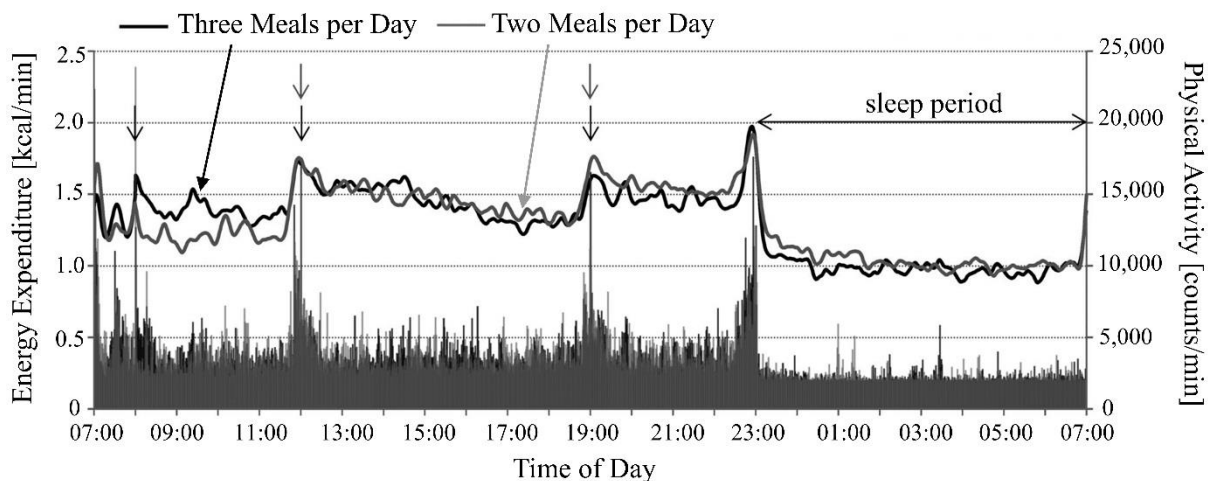


Fig. 1.3 – EE and physical activity measured under conditions of two and three meals per day. Arrows indicate meal times; adapted from [49].

The meal sizes and calorific content of food given to subjects in metabolic studies can vary. Indeed in free living, meals vary both in content and periodicity. This perhaps provides reasons for the uncertainty regarding the length of time DIT has an effect on the MR of a subject. In one study DIT had an effect on the EE of subjects for up to 10 hours after the last meal [43]. In other studies it has been estimated that the effect lasts for up to 15 hours subsequent to eating (fat consumption can have an effect that lasts for 8 hours) [50,51]. It may not be necessary to measure for such a long period to obtain an estimate for the DIT of a meal. In one study 3 hours were sufficient to nearly completely assess a <1500 kJ (360 kcal) meal given to subjects, and it was found the same period provided sufficient time to observe the DIT of larger meals for MR analysis [52]. In terms of a 3 meal feeding protocol, it has been shown that DIT has an effect on total EE from breakfast until 8 hours after the final meal (in the evening) [53]. In a study by Westerterp, DIT was visible on the EE from subjects between breakfast and lunch (4 hour period) and from lunch until evening meal (5 hour period) [53].

The content of the diet of an individual naturally effects their energy intake. The institute of Medicine of the National Academies (U.S.) recommends a diet that contains: 45 to 65 % kcal from carbohydrates; 10 to 35 % kcal from proteins and 20 to 35 % kcal from total fat [54]. The recommendation extends to advise minimal intake of saturated fat, trans fat and dietary cholesterol. The suggested diet content is consistent with the advice from other organisations. It is noted by Kennedy et al. that individuals at risk of diabetes may be the major beneficiaries of a diet intervention that is both effective and easy to tolerate, given that being overweight or obese is the major modifiable risk factor for Type 2 diabetes [55].

The available energy for metabolism from each gram of protein, fat and carbohydrate is 4.0, 8.9 and 4.0 kcal/g, respectively [56]. The available energy from each macronutrient for combustion is 5.65, 9.40 and 4.10 kcal/g respectively, not all of which is available to the body. Nitrogen is excreted from the body in the form of urea, which represents some of the energy not available to the body (it is formed in the breakdown of protein and amino acids). It arises as amino acids are not completely oxidised in the body [57]. The digestion time of each macronutrient varies and is also dependent on the overall content of a meal. Carbohydrates affects DIT for a period of around 2 hours post consumption.

Combining food types can slow digestion. The following full digestion times (to exit the stomach) are reported for the following types of food: water 10 minutes (10 minutes), juice 15 to 30 minutes (15 to 30 minute), fruit 30 to 60 minutes (2 to 3 hours), proteins 2 to 3 hours (12 hours), carbohydrates 3 to 4 hours (6 to 8 hours) and fats 3 to 4 hours (12 hours) [58,59]. There are two distinct types of digestion; acid digestion for proteins and alkaline digestion for carbohydrates (fats are a special case, and leave the stomach largely unchanged) [60]. The content of meals therefore has an effect on the digestion effort and time, thus varying the energy required to digest the food. In addition to the characteristics of meals given to subjects (size, composition and timing), TEF is affected by physiological factors, thus measurements are difficult to reproduce. Factors such as age of the subject, genetic background and physical fitness further increase variation between studies. The methodological variance in metabolic studies (type of calorimetry/measurement equipment used, environmental factors and duration of the test) also hinders reproducibility [61].

In a free living environment there is no restriction on an individual for any activity after a meal. The requirement to remain inside a respiratory room restricts the subject to limited activity and to avoid disturbing the measurement system the subject must remain in a fixed position. It has been reported that postprandial exercise (such as walking or any other form of light endurance exercise) increases gastric emptying [62], and this increase reduces blood glucose (an important risk factor for Type 2 diabetes) [63,64]. However, the effect of light exercise after eating is not fully understood. A study by DiPietro et al. noted EE was not significantly different between days when exercise was enforced after meals and control days when the subject rested [64].

1.3 Weight Management

Metabolism studies have focused on the health issues caused by an overweight population for a considerable period. A study performed in 2001 reported 55 % of adults in the United States were overweight or obese [65]. This proportion is increasing, in 2015 it was reported around 70 % of adults were categorised as overweight or obese [66]. An overweight population is more susceptible to diseases affecting the heart as well as diabetes and cancer [65]. Research into technologies to help encourage an active lifestyle and promote awareness of the consequences of an unhealthy daily routine are well-established. Sedentary behaviour is suggested to be one of the underlying causes of the weight gain seen in the population over the last two decades. In the daily life of the general population, an increase in the proportion of time spent sitting or lying decreases the amount of energy expended [67]. Eating snacks and convenience food could also be attributed to slow, but consistent, weight gain. It is estimated that weight gain can be started by consuming just 100 kcal/day above daily energy requirements [68]. Although metabolic rate increases with weight, consistently consuming 100 kcal/day above the daily energy needed will lead to a steady weight gain.

Concurrently to lose weight it is necessary to consume less calories than the daily EE requirements. To induce weight loss, studies have previously requested obese participants to reduce their calorie intake to between 1000 to 1500 kcal/day [65,69,70]. Behaviour is a major factor towards obtaining an energy balance [71]. Changes to dietary habits and exercise are the most effective behavioural characteristics in order to achieve weight loss [65]. It has been found that subjects are usually unable to adapt

to sudden changes in exercise habits, but over a longer period, guided exercise plans can motivate subjects to exercise more frequently.

Development of a handheld device to monitor EE is proposed, in part, to motivate users into making the necessary lifestyle changes to lose and then maintain weight within healthy bounds. Motivation is noted as a possible important element in losing weight [72]. The process of standardised and routine EE measurements is part of the motivation required to lose weight, as well as the continual monitoring of EE during a weight loss plan to ensure the subject remains focused on long term calorie intake and exercise regimes.

Weight measurements can only provide short term motivation, as rapid weight loss can also be associated with greater weight regain over, for example, a 12 month period [72]. Dropout rates from diet groups can be used as crude, but realistic, measures of the willingness of subjects to remain on diet plans. In one study three groups were compared: a VLCD (very low calorie diet), LCD low calorie diet and a restricted normal food group [72]. Dropout rates over a one year period were lower for the most effective weight loss group, VLCD (18 %), compared to the LCD group (23 %) and a normal-food group (26 %).

In the literature, there is much disagreement about the ability to maintain high levels of weight loss [73–75]. While it has been reported that while VLCDs offer greater initial weight loss, there is also an increased risk of regaining weight over a longer period [71]. VLCDs are arbitrarily defined, although commonly diets of <800 kcal/day [71] or <500 kcal/day [72] or diets that provide ~50 % of the predicted resting EE for an individual are classified as VLCDs. Similarly, no fixed calorie intake is used to define a LCD, however diets with calorific intakes below 1200 kcal/day are usually referred to as LCDs [71,72].

The term LCD is also used to denote the prescriptive nature of a diet, rather than just when a subject merely attempts to reduce their calorific intake without a designated guideline. A review by Tsai et al. summarises follow-up assessments from VLCDs from 1 to 5 years after their completion [73]. The report suggest VLCDs should not be prescribed except in a few select cases. VLCDs were not recommended to induce losses of between 15 % and 25 % of initial weight. It was found that patients were rarely able to maintain weight loss even under the best of circumstances. In some

extreme cases, VLCDs have led to death, thus in the US such programmes must be managed by a physician [72]. This intense dieting regime cannot be recommended as a weight loss method for the general overweight population.

1.4 Psychological Guidance

The need for a subject to be motivated in order to remain committed to a lifestyle change is clear, although suitable methods to maintain this motivation over a period of years are difficult to prescribe. The type of food consumed, amount of calories and frequency of meals/snacks are often decided by a psychological craving. This craving can be a reason for the failure to comply to a LCD. In one study it was noted the popular cravings for male obese patients were pizza and French fries, and for women cravings were for cake and doughnuts [76]. Commercial weight loss programmes usually include weekly or bi-weekly meetings to facilitate behavioural changes. Such treatment sessions appear to help motivate subjects to lose weight [77]. In a review of 11 studies, it was reported that on average, patients lost an extra 1.47 kg (across various length trials), compared to control groups [74]. The need for continued persuasion to stay dedicated to a treatment plan is noted by Perri et al. [78], where individuals on a 40 week plan achieved a far greater weight loss than those on a similar 20 week venture.

Food restrictions and dieting will increase appetite and the feeling of hunger [76]. The motivation required to overcome these feelings is perhaps lacking in patients who stray from reduced calorie treatment plans. In part, hormone levels can play a factor on levels of metabolism and the ability to avoid over eating. In particular, leptin (a protein hormone), produced by fat tissue, is suggested to give the brain a rough indication of the body's fat mass (in order to regulate appetite and metabolism) [79]. The reduction in resting metabolism associated with weight loss can cause a plateau in weight. A theory was proposed by Johannsen et al., that combining exercise with a weight loss programme could help maintain fat free mass in subjects and thereby prevent a dramatic slowing of resting metabolism [75]. The study found that vigorous exercise (90 min/day of circuit training and/or aerobic training) was not sufficient to prevent fat free mass from decreasing.

Further studies are required to identify the underlying mechanisms governing leptin concentrations [80]. It has been reported that leptin injections can help maintain fat

free mass, which in turn helped subjects in one study maintain higher levels of total EE [80]. However other studies report inconclusive findings, where the effects on EE cannot be categorically proven to relate to leptin concentration, where it is perhaps just a central effect [81,82]. In cases where subjects have a leptin deficiency, replenishing leptin has been shown to aid treatment plans for overweight subjects. In one study it was noted participants easily lost bodyweight when leptin levels were supplemented to normal levels [82]. A striking effect of leptin administration was reported by Rosenbaum et al. [80], where the increased hormone level caused an rise in total EE on a small sample size of 4 patients. The study has limited credibility however, with a small number of participants and lack of thorough daily EE measurement over the trial period. The behavioural effect discussed above could prove a more reliable method for weight loss (i.e. willpower), where control subjects lost a similar amount of weight in the study [80].

In the case of many metabolism studies, children are less well reported due to the legal constraints. Childhood is a crucial period for establishing eating habits for later life, although risk calculations suggest that less than half of adult obesity can be attributed to childhood obesity [83]. However, when also including those children who are overweight, some reports suggest that up to 80 % of overweight adolescents will become obese adults [84]. Obesity in childhood and adolescence can have severe consequences for adulthood and youth, such as type 2 diabetes and cardiovascular diseases [85]. There have also been reports of an increased risk of several cancers, for example: colon, thyroid, gallbladder, oesophageal and breast [86]. From a young age (6 to 10 years) children already associate obesity with laziness and sloppiness and tend to incorporate a cultural preference for thinness [87].

The psychological impact of childhood obesity cannot be ignored. Table 1.1 lists depression and poor self-esteem as illnesses which can be caused by obesity. Preference tests have demonstrated that 10 to 11 year old children prefer friends with other children with a wide variety of handicaps (wheelchair user, crutches user, facial disfigurement etc.) rather than those who are overweight [88]. Overweight children are ranked lowest with those with whom they would like to be friends [88]. It has been reported that child body mass index (BMI) scores are highly correlated with parent BMI scores. In one study it was found that 23.2 % of obese parents have an obese child, and 35.1 % of overweight parents have an overweight child [89]. A reduction in

adult obesity could help decrease the cycle of obese families. One report notes that children are least likely to “grow out of” obesity when it is more severe, and when they have at least one obese parent [90].

In the short term, the consequences of childhood obesity can also include: asthma, chronic inflammation, type 1 (and 2) diabetes, orthopaedic abnormalities and liver disease. In the long term it is reported that adults (who were obese as a child or as an adolescent) can have persistence of obesity, arthritis and premature mortality [90]. In England the prevalence of obesity in children aged 11 to 15 years has increased over the last two decades. Jaarsveld et al. reported upon the trend, with data for BMI records sourced from the Clinical Practice Research Datalink database (containing about 7 % of UK family practices) [91]. In 1994, the prevalence of obesity in boys was 28.1 % and 29.3 % for girls aged between 11 and 15 years. In 2013 comparative data showed the prevalence for both genders had increased to 37.8 % and 36.6 % for boys and girls respectively, of the same age range.

To prevent the onset of obesity in children, it was found that parents and school teachers need to help enforce a better lifestyle. Benefits were seen on an obesity prevention trial, where subjects reduced television viewing hours but increased physical activity and provided a balanced diet (with increased fruit and vegetable intake) [92,93]. The trial, conducted over two school years, included 1295 school children. The outcomes were that the school based changes were found to be sustainable and cost effective, girls were found to be at reduced risk of becoming obese and there was remission of existing obesity.

The largest intervention effects were seen for African American girls, where obesity prevalence was significantly reduced. However, no differences were found for boys [92]. However, a further article notes that eating disorders are 10 times more common in girls than boys [93]. The intervention programme was noted to reduce disordered weight control behaviours. In particular, it has been shown that treatment can be performed as a family, where children benefit from simple lifestyle changes such as a reduction in sedentary activities as a family, an increase in physical activity (for example walking to school) and by introducing a balanced nutritional diet (without snacking in-between meals) [90,92].

1.4.1 Metabolic Rate and Condition of Patient

Disease in the ICU can make estimating metabolic requirements difficult for patients. Similarly, diseases contracted by the general population can also have a profound effect on metabolic rate (most notably for multi-organ system failure). For instance, fever increases the chemical reactions in the body by an average of 120 % for each 10 °C rise in temperature (it is estimated every 1 °C rise in body core temperature causes RMR to rise by approximately 13 % [94]).

Sleep decreases metabolic rate (a deficit in the range of 10-15 % below normal), due to decrease tone of the skeletal musculature and decreased activity of the central nervous system [34]. Similarly, malnutrition decreases metabolic rate, but by a higher factor of up to 20 to 30 % (it is presumed malnutrition causes paucity of food substance in cells [34]).

Disease often has an effect on the EE of a subject. EE is increased in disease states due to abnormal protein metabolism, the breakdown of fatty acids, tissue degradation and the production of humoral and inflammatory mediators [95]. A slight change in EE for non-hospitalised subjects can occur with infections such as influenza [95]. A significant change in EE is usual for acutely ill patients. Long et al. list the percentage increase in resting metabolic expenditure for six categories of patient following injury or illness [96], namely elective surgery 23.9 %, skeletal trauma 32.2 %, blunt trauma 36.6 %, trauma with steroids 60.8 %, sepsis 79.2 % and burns 131.7 %.

Further examples are given in Table 1.2. The increase in nutritional requirement can be difficult to quantify with predictive equations, particularly due to the great dependence on the condition of the individual patient. Patients with severe burn injuries, are discussed with great concern in the literature [96,97]. In ICUs staff have little choice but to use predictive equations to prescribe feeding to patients, although energy requirements cannot be precisely predicted. In particular, it is recommended that RMR of thermally injured patients should be measured, due to the likelihood of a variable hypermetabolic state during recovery [97].

1.4.2 Energy Requirements of Intensive Care Patients

The extreme outcomes of incorrectly feeding mechanically ventilated ICU patients were observed by Bartlett et al. [98]. The group of 57 patients at risk of multiple organ dysfunction, with average stays of 18 days in the ICU, were fed on regimes based on

the estimation of calorific and nitrogen requirements. Out of 14 patients that developed a cumulative negative caloric balance (that was at discharge more than 10,000 kcal) 12 died (86%). Another 3 patients developed a 10,000 kcal deficit, but this was reversed by increasing the calorific intake (only one died). A cumulative caloric balance of between 0 and -10,000 kcal was found in 28 patients (including the 3 above), of which 11 died. 15 patients developed a positive cumulative non-protein caloric balance, of which 4 died. Multiple organ dysfunction occurred more often in patients with large caloric deficits, however the link was inconclusive. From the total group of 57 patients, 27 died (47 %).

Mault et al. concluded that large negative energy balance in critically ill patients was associated with longer ventilator and ICU days [99]. Positive energy balance was associated with better outcomes, but the author stated that nutritional support should still be determined by daily indirect calorimetry for a critically ill population. The impact of malnourishment or over-nourishment can be severe with respect to patient recovery. The use of indirect calorimetry to accurately determine energy requirements could help reduce the time that a patient needs to spend in intensive care and further their recovery.

As demonstrated in the study by Bartlett et al. above, patients in ICU are often subjected to malnutrition and underfeeding [27]. It has been suggested that feeding is given a low priority compared to other ICU treatments. Possibly due to a lack of specific education, particularly of the staff who are in closest contact with patients in relation to feeding [100]. It has been noted as important to feed the patient adequately and where necessary, start artificial nutrition early (within the first 24 hours after admission). Delays in starting artificial nutrition increase the risks associated with under-feeding and significantly increase mortality rates [101]. Maintaining energy balance and avoiding over-feeding are equally as important, where energy supply, in excess of energy needs, is associated with the increased rate of complications [102].

Both the quantity of energy required by a patient and the timing of its delivery is influential in the progression of patient recovery. In some cases, enteral nutrition (EN) is not sufficient to meet the energy requirement of a patient [103]. Supplementary parenteral nutrition (SPN) was shown to help meet energy needs of patients in intensive care by Heidegger, without compromised glycaemic control or increased

insulin needs. For the subjects prescribed SPN, it was administered to patients from day 4 to day 8 of their stay in the ICU. The energy needs of patients were tested by indirect calorimetry after 3 days in intensive care. The target of 100 % energy balance was met precisely in the SPN group. The SPN prescription was carefully monitored and did not lead to over-feeding (by comparison, on average, the EN group reached around 75 % of the energy target). Over-feeding would be indicated by excess carbon dioxide (CO₂), which did not occur in any of the SPN patients. No adverse effects attributed to hyperglycaemia occurred in the SPN group, which the authors note could be the reason why the SPN group spent less time on mechanical ventilators than the control group (prescribed EN alone). The study concludes the adequate feeding in that SPN group led to faster weaning from the mechanical ventilators.

It is noted by Singer et al. that immune and healing function can be reduced when under-feeding occurs, due to the promotion of protein catabolism, needed to fuel obligatory glucose requirements [102]. Singer et al. also note that EN should cover the needs of most patients under the care of a competent team and SPN is not required, unless patients fail to tolerate EN. The importance of indirect calorimetry in understanding the energy needs of a patient is endorsed by many studies, although its availability is insufficient to permit routine use in many ICUs [22,102–104]. Comparative studies of various metabolic analysers are published with the intent of increasing the use of calorimetry in clinical practice. However, in some cases newly available instruments need rigorous testing before being recommended for clinical use [105]. The delays in verifying the capability of a device and the outlay required to purchase expensive equipment hinders the use of breath analysers in clinical care.

A fixed value for calorific need (based on body weight) is used to determine feeding prescriptions for many patients in ICUs [106], although this practice is widely condemned for providing inaccurate results [107]. The calorific need of ICU patients is likely to vary depending on their recovery stage. In severe conditions the recovery stage can stretch into months, and often beyond their stay in intensive care. Fig. 1.4 shows five examples of metabolic rate variance for different conditions. Chioléro et al. reported the prolonged metabolic response for patients with head injuries lasted 2 to 4 weeks (measured through indirect calorimetry) [108]. It was noted that the effect was usually associated with a marked resistance to nutritional support (which can complicate the outcome) and a raised heart rate. Chioléro et al. found that prescribing

doses of propranolol reduced the hyper-metabolism in a study with 12 patients (resting heart rate decreased). The report concluded that agitation in ICU patients contributed to their elevated RMR.

In order for patients' recovery to progress, their energy needs must be met by sufficient feeding. The amount of feeding required is not constant, and the trend for energy requirements is dependent on the type and severity of the illness. It is estimated that around 20 % of patients will not tolerate early enteral feeding (and in most cases, patients cannot tolerate more than 2.5 litres per day) [109]. This can make it difficult to feed patients sufficiently and careful monitoring of blood glucose is required when attempting to meet spikes in calorific need over a period of several days.

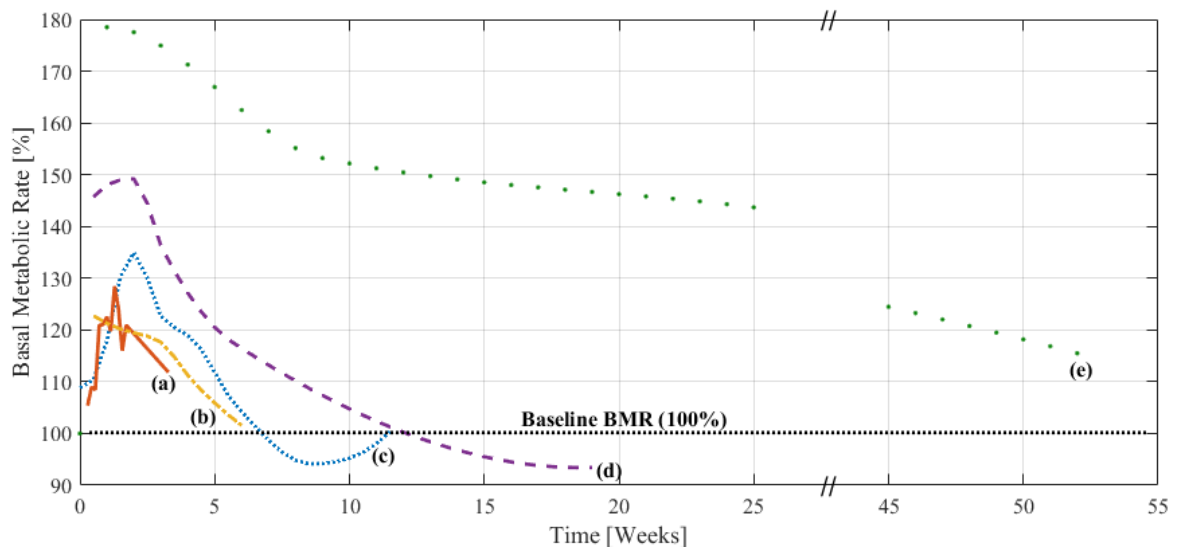


Fig. 1.4 – RMR increases above normal baseline for patients with conditions such as: (a) Head trauma [110]; (b) Sepsis [111]; (c) 20 % burns [112]; (d) 65 % burns [113] and (e) Severe burns [114]. Injury occurred at 0 weeks and metabolic rate was measured at intervals during the recovery period.

The examples shown in Fig. 1.4 demonstrate the peak in the energy requirement can occur approximately 1-2 weeks after contracting the condition. In the trauma cases shown, the energy requirement is increased over the baseline requirement prior to admission to the ICU. The EE values shown are from patients that make a recovery after a period in intensive care. Not all patients recover from such chronic conditions; non-survivors are characterised by a drop in RMR before death [115]. The notable decrease can occur a significant time after recovery has begun (range from 2 weeks to 9 weeks after ICU admission). Table 1.2 lists a number of acute diseases with the approximate change in RMR they cause.

Long term starvation can reduce EE by up to 30 to 40 % [94]. Reduced energy expenditure can occur with any disease that decreases oral intake and that involves cachexia. Malnutrition is a global problem, most prevalent in South-East Asia [116]. However, it is recognised that a large number of adult patients admitted into British and Irish hospitals have a BMI of $< 20 \text{ kg/m}^2$ (10 to 40 % compared to 4- 5 % in the population) [116]. Undernutrition is often untreated in hospital in-patients and outpatients. It is noted that the aggressive over-feeding of malnourished individuals, especially those recovering from disease, can cause sudden death from re-feeding syndrome [117]. There is still uncertainty about prescribing optimal feeding strategies and energy targets for ICU patients with pre-existing malnutrition [105]. During the first week's stay of a patient in intensive care, lower energy targets may be suitable. Regardless of feeding strategy, it is necessary to calculate the EE for an individual, before an energy plan can be set.

Table 1.2 – Disease effect on metabolic rate measured across a range of subjects.

Disease	Metabolic Rate Adjustment
Mild Starvation [118]	<-15 %
Partial Starvation [117]	0 to -10 %
Elective/uncomplicated surgery [119]	0 %
Burns 10 % (1 st month)	
Single Fracture (1 st Week)	0 to +10 %
Inflammatory bowel disease	
Mild infection [117]	
Infection/Persistent fever (per °c) [119]	+10 to +15 %
Burns between 10 to 25 % (1 st month)	+10 to +30 %
Multiple long bone fractures [117]	
Major operation/surgical procedures [119]	+20 to +40 %
Sepsis [120]	+25 to +45 %
Severe trauma [119]	+20 to +50 %
Major infection [118]	< 60 %
Severe burns (25 to 90 %) [121]	+140 to +180 %

As previously discussed, the tools available to most clinicians are prediction equations or past experience. The reliance on estimation assumptions regarding the condition of

the patient hinder the accurate calculation of energy needs. Indirect calorimetry measurements would ideally be performed (to determine the individual need of a specific patient), but often the limited adoption of such equipment has restricted the use of this method.

1.5 Conclusions

In order to stem the rising trend towards an obese population, steps must be taken to provide an understanding of the risks associated with being overweight and the balanced diet and lifestyle required to maintain a healthy weight. The components of EE (particularly TEF) make calculating total daily EE challenging, with a large variance possible between inter-individual preferences.

The occupations of the adult populations in countries such as the U.K. have become more sedentary, especially since the development of many predictive equations used to determine calorific requirements. There is a need for new methods of calculating energy need, given the variety of lifestyles and body compositions seen in the population today. The lack of availability of precision medical instruments is somewhat to blame for the weight gains seen in the general population.

In the case of intensive care, where diseases and injuries can vary metabolic rate by up to 180 %, indirect calorimetry provides an accurate means of assessing energy requirements. The mortality rates presented in various patient groups (e.g. 47 % in one case) demonstrates the need for metabolic assessment without the reliance of estimation techniques.

In the next chapter, indirect calorimetry and other methods of measuring EE are discussed with their uses in the general population and clinical care.

1.6 References

- [1] M. Snooks, *Health Psychology: Biological, Psychological, and Sociocultural Perspectives*, Jones & Bartlett Learning, Sudbury, U.S., 2009.
- [2] P.C. Hallal, L.B. Andersen, F.C. Bull, R. Guthold, W. Haskell, U. Ekelund, et al., Global physical activity levels: Surveillance progress, pitfalls, and prospects, *Lancet*. 380 (2012) 247–257. doi:10.1016/S0140-6736(12)60646-1.
- [3] L. Straker, S.E. Mathiassen, Increased physical work loads in modern work--a necessity for better health and performance?, *Ergonomics*. 52 (2009) 1215–25. doi:10.1080/00140130903039101.
- [4] D. Ogilvie, M. Egan, V. Hamilton, M. Petticrew, Promoting walking and cycling as an alternative to using cars: systematic review, *BMJ*. 329 (2004) 763. doi:10.1136/bmj.38216.714560.55.
- [5] Department for Transport, Road Use Statistics Great Britain 2016, (2016) 28. https://www.gov.uk/government/uploads/system/uploads/attachment_data/file/514912/road-use-statistics.pdf (accessed June 22, 2016).
- [6] R.L. Mackett, Why do people use their cars for short trips?, *Transportation (Amst)*. 30 (2003) 329–349. doi:10.1023/A:1023987812020.
- [7] Department for Transport, Transport Statistics Great Britain: 2015, Dep. Transp. (2015) 2. doi:ISBN: 9780115530951.
- [8] G.J. Welk, J.J. McClain, J.C. Eisenmann, E.E. Wickel, Field validation of the MTI Actigraph and BodyMedia armband monitor using the IDEEA monitor, *Obesity (Silver Spring)*. 15 (2007) 918–28. doi:10.1038/oby.2007.624.
- [9] S.W. Ng, C. Ni Mhurchu, S.A. Jebb, B.M. Popkin, Patterns and trends of beverage consumption among children and adults in Great Britain, 1986-2009., *Br. J. Nutr.* 108 (2012) 536–51. doi:10.1017/S0007114511006465.
- [10] K.G. Grunert, L. Fernández-Celemín, J.M. Wills, S. Storcksdieck Genannt Bonsmann, L. Nureeva, Use and understanding of nutrition information on food labels in six European countries., *Z. Gesundh. Wiss.* 18 (2010) 261–277. doi:10.1007/s10389-009-0307-0.
- [11] W. Harris, *Examination Paediatrics*, Elsevier, Chatswood, Australia, 2011.
- [12] S. Storcksdieck Genannt Bonsmann, J.M. Wills, Nutrition Labeling to Prevent Obesity: Reviewing the Evidence from Europe., *Curr. Obes. Rep.* 1 (2012) 134–140. doi:10.1007/s13679-012-0020-0.
- [13] B. Collins, S. Capewell, M. O’Flaherty, H. Timpson, A. Razzaq, S. Cheater, et al., Modelling the Health Impact of an English Sugary Drinks Duty at National and Local Levels, *PLoS One*. 10 (2015) e0130770. doi:10.1371/journal.pone.0130770.
- [14] R. Dobbs, C. Sawers, F. Thompson, J. Manyika, J.R. Woetzel, P. Child, et al., Overcoming obesity: An initial economic analysis, *McKinsey Reports*. (2014). http://www.mckinsey.com/insights/economic_studies/how_the_world_could_better_fight_obesity (accessed May 20, 2015).

-
- [15] C. Pérez Rodrigo, Current mapping of obesity., *Nutr. Hosp.* 28 Suppl 5 (2013) 21–31. doi:10.3305/nh.2013.28.sup5.6915.
- [16] E. Whitney, S.R. Rolfes, *Understanding Nutrition*, Cengage Learning, Belmont, U.S., 2007.
- [17] P. Insel, D. Ross, M. Bernstein, K. McMahon, *Discovering Nutrition*, Jones & Bartlett Publishers, Burlington, U.S., 2015.
- [18] V. Ionut, R.N. Bergman, The Disease of Obesity, in: A. Youdim (Ed.), *Clin. Guid. to Treat. Obes.*, Springer New York, New York, U.S., 2015: p. 7. doi:10.1007/978-1-4939-2146-1.
- [19] C.L. Harris, V.A. George, Dietary restraint influences accuracies in estimating energy expenditure and energy intake among physically inactive males., *Am. J. Mens. Health.* 4 (2010) 33–40. doi:10.1177/1557988308327052.
- [20] B. Wansink, P. Chandon, Slim by design: Redirecting the accidental drivers of mindless overeating, *J. Consum. Psychol.* 24 (2014) 413–431. doi:10.1016/j.jcps.2014.03.006.
- [21] S. Graf, V.L. Karsegard, V. Viatte, C.P. Heidegger, Y. Fleury, C. Pichard, et al., Evaluation of three indirect calorimetry devices in mechanically ventilated patients: which device compares best with the Deltatrac II? A prospective observational study., *Clin. Nutr.* 34 (2015) 60–5. doi:10.1016/j.clnu.2014.01.008.
- [22] M.L. Rousing, M.H. Hahn-Pedersen, S. Andreassen, U. Pielmeier, J.-C. Preiser, Energy expenditure in critically ill patients estimated by population-based equations, indirect calorimetry and CO₂-based indirect calorimetry., *Ann. Intensive Care.* 6 (2016) 16. doi:10.1186/s13613-016-0118-8.
- [23] NHS, What should my daily intake of calories be? - Health questions - NHS Choices, NHS Choices. (2013) 2014. <http://www.nhs.uk/chq/pages/1126.aspx?categoryid=51> (accessed April 30, 2014).
- [24] P. Singer, J. Singer, Clinical Guide for the Use of Metabolic Carts: Indirect Calorimetry--No Longer the Orphan of Energy Estimation, *Nutr. Clin. Pract.* 31 (2016) 30–38. doi:10.1177/0884533615622536.
- [25] P. Singer, M. Hiesmayr, G. Biolo, T.W. Felbinger, M.M. Berger, C. Goeters, et al., Pragmatic approach to nutrition in the ICU: expert opinion regarding which calorie protein target., *Clin. Nutr.* 33 (2014) 246–51. doi:10.1016/j.clnu.2013.12.004.
- [26] S. V. Desai, S.A. McClave, T.W. Rice, Nutrition in the ICU, *Chest.* 145 (2014) 1148–1157. doi:10.1378/chest.13-1158.
- [27] S. Villet, R.L. Chioloro, M.D. Bollmann, J.-P. Revelly, M.-C. Cayeux R N, J. Delarue, et al., Negative impact of hypocaloric feeding and energy balance on clinical outcome in ICU patients., *Clin. Nutr.* 24 (2005) 502–9. doi:10.1016/j.clnu.2005.03.006.
- [28] C. Faisy, N. Lerolle, F. Dachraoui, J.-F. Savard, I. Abboud, J.-M. Tadie, et al., Impact of energy deficit calculated by a predictive method on outcome in

- medical patients requiring prolonged acute mechanical ventilation., *Br. J. Nutr.* 101 (2009) 1079–87. doi:10.1017/S0007114508055669.
- [29] A. Pirat, A.M. Tucker, K. a Taylor, R. Jinnah, C.G. Finch, T.D. Canada, et al., Comparison of measured versus predicted energy requirements in critically ill cancer patients., *Respir. Care.* 54 (2009) 487–94.
- [30] J. Preiser, A.R. van Zanten, M.M. Berger, G. Biolo, M.P. Casaer, G.S. Doig, et al., Metabolic and nutritional support of critically ill patients: consensus and controversies, *Crit. Care.* 19 (2015) 1–11. doi:10.1186/s13054-015-0737-8.
- [31] E.T. Poehlman, A review: exercise and its influence on resting energy metabolism in man., *Med. Sci. Sports Exerc.* 21 (1989) 515–525.
- [32] W.M. Boothby, Basal Metabolism: Man, in: W.S. Spector (Ed.), *Handb. Biol. Data*, Saunders, 1956: p. 259.
- [33] B. Caballero, P. Finglas, F. Toldra, *Encyclopedia of Food and Health*, Academic Press, Burlington, U.S., 2015.
- [34] J.E. Hall, A.C. Guyton, *Guyton and Hall Textbook of Medical Physiology*, 12th Ed., Saunders/Elsevier, Philadelphia, U.S., 2011.
- [35] A. Fleisch, Basal metabolism standard and its determination with the “metabocalculator,” *Helv. Med. Acta.* 18 (1951) 23–44.
- [36] E.S. Rawson, S.L. Volpe, *Nutrition for Elite Athletes*, CRC Press, Boca Raton, U.S., 2015.
- [37] W.H. Carpenter, E.T. Poehlman, M. O Connell, M.I. Goran, W.P. Krijnen, K. Sullivan, et al., Influence of body composition and resting metabolic rate on variation in total energy expenditure: A meta-analysis, *Am. J. Clin. Nutr.* 61 (1995) 4. doi:http://dx.doi.org/10.1108/17506200710779521.
- [38] S.S. Gropper, J.L. Smith, *Advanced Nutrition and Human Metabolism*, Cengage Learning, Belmont, U.S., 2012.
- [39] M.A. Holliday, Metabolic rate and organ size during growth from infancy to maturity and during late gestation and early infancy., *Pediatrics.* 47 (1971) Suppl 2:169+.
- [40] S. Lazzer, G. Bedogni, C.L. Lafortuna, N. Marazzi, C. Busti, R. Galli, et al., Relationship between basal metabolic rate, gender, age, and body composition in 8,780 white obese subjects., *Obesity (Silver Spring).* 18 (2010) 71–78. doi:10.1038/oby.2009.162.
- [41] A. Walker, J.B. Watkins, C. Duggan, W.A. Walker, C. Duggan, J.B. Watkins, *Nutrition in pediatrics: basic science and clinical application*, 3rd Ed., B.C. Decker, Hamilton, Canada, 2003.
- [42] V.L. Katch, W.D. McArdle, F.I. Katch, *Essentials of Exercise Physiology*, 4th Ed., Wolters Kluwer/Lippincott Williams & Wilkins Health, 2011.
- [43] M. Tarnopolsky, *Gender Differences in Metabolism: Practical and Nutritional Implications*, CRC Press, 1998.
- [44] J.P. Delany, D.E. Kelley, K.C. Hames, J.M. Jakicic, B.H. Goodpaster, Effect of

- physical activity on weight loss, energy expenditure, and energy intake during diet induced weight loss., *Obesity* (Silver Spring). 22 (2014) 363–70. doi:10.1002/oby.20525.
- [45] B. Brehm, Elevation of Metabolic Rate Following Exercise, *Sport. Med.* 6 (1988) 72–78. doi:10.2165/00007256-198806020-00002.
- [46] A.M. Knab, R.A. Shanely, K.D. Corbin, F. Jin, W. Sha, D.C. Nieman, A 45-minute vigorous exercise bout increases metabolic rate for 14 hours, *Med. Sci. Sport. Exerc.* 43 (2011) 1643–1648. doi:10.1249/MSS.0b013e3182118891.
- [47] K.J. Sevits, E.L. Melanson, T. Swibas, S.E. Binns, A.L. Klochak, M.C. Lonac, et al., Total daily energy expenditure is increased following a single bout of sprint interval training, *Physiol. Rep.* 1 (2013) e00131. doi:10.1002/phy2.131.
- [48] G. Bray, M. Schwartz, R. Rozin, J. Lister, Relationships between oxygen consumption and body composition of obese patients., *Metabolism.* 19 (1970) 418–29. doi:10.1016/0026-0495(70)90093-4.
- [49] H. Ogata, F. Kobayashi, M. Hibi, S. Tanaka, K. Tokuyama, A novel approach to calculating the thermic effect of food in a metabolic chamber., *Physiol. Rep.* 4 (2016) e12717. doi:10.14814/phy2.12717.
- [50] E. Ravussin, S. Lillioja, T.E. Anderson, L. Christin, C. Bogardus, Determinants of 24-hour energy expenditure in man. Methods and results using a respiratory chamber., *J. Clin. Invest.* 78 (1986) 1568–78. doi:10.1172/JCI112749.
- [51] E. Ravussin, B. Burnand, Y. Schutz, E. Jéquier, Twenty-four-hour energy expenditure and resting metabolic rate in obese, moderately obese, and control subjects., *Am. J. Clin. Nutr.* 35 (1982) 566–73.
- [52] J.A. Weststrate, Resting metabolic rate and diet-induced thermogenesis: a methodological reappraisal., *Am. J. Clin. Nutr.* 58 (1993) 592–601.
- [53] K.R. Westerterp, Diet induced thermogenesis., *Nutr. Metab. (Lond).* 1 (2004) 5. doi:10.1186/1743-7075-1-5.
- [54] A.E. Griel, E.H. Ruder, P.M. Kris-Etherton, The Changing Roles of Dietary Carbohydrates: From Simple to Complex, *Arterioscler. Thromb. Vasc. Biol.* 26 (2006) 1958–1965. doi:10.1161/01.ATV.0000233384.97125.bd.
- [55] R.L. Kennedy, K. Chokkalingam, H.R. Farshchi, Nutrition in patients with Type 2 diabetes: are low-carbohydrate diets effective, safe or desirable?, *Diabet. Med.* 22 (2005) 821–832. doi:10.1111/j.1464-5491.2005.01594.x.
- [56] A.C. Buchholz, D.A. Schoeller, Is a calorie a calorie?, *Am. J. Clin. Nutr.* 79 (2004) 899S–906S.
- [57] T. Sanders, P. Emery, C. Forces, C.F. Definition, P. Energy, *Molecular Basis Of Human Nutrition*, CRC Press, New York, U.S., 2003.
- [58] R. DeLuz, J. Hester, D. Reverand, T. Up, Y. Vetabolism, *1 Pound a Day: The Martha’s Vineyard Diet Detox and Plan for a Lifetime of Healthy Eating*, Gallery Books, New York, U.S., 2014.
- [59] L. Taylor, *The Book*, Ednil Publishing, Kent, U.K., 2013.

-
- [60] R.A.S. Hemat, *Principles of Orthomolecularism*, Urotext, London, U.K., 2004.
- [61] P.A. Tataranni, D.E. Larson, S. Snitker, E. Ravussin, Thermic effect of food in humans: methods and results from use of a respiratory chamber., *Am. J. Clin. Nutr.* 61 (1995) 1013–9.
- [62] A. Franke, H. Harder, A.K. Orth, S. Zitzmann, M. V Singer, Postprandial walking but not consumption of alcoholic digestifs or espresso accelerates gastric emptying in healthy volunteers., *J. Gastrointestin. Liver Dis.* 17 (2008) 27–31.
- [63] A.T. Høstmark, G.S. Ekeland, A.C. Beckstrøm, H.D. Meen, Postprandial light physical activity blunts the blood glucose increase., *Prev. Med. (Baltim).* 42 (2006) 369–71. doi:10.1016/j.ypmed.2005.10.001.
- [64] L. DiPietro, A. Gribok, M.S. Stevens, L.F. Hamm, W. Rumpler, Three 15-min bouts of moderate postmeal walking significantly improves 24-h glycemic control in older people at risk for impaired glucose tolerance., *Diabetes Care.* 36 (2013) 3262–8. doi:10.2337/dc13-0084.
- [65] J.M. Jakicic, K. Clark, E. Coleman, J.E. Donnelly, J. Foreyt, E. Melanson, et al., American College of Sports Medicine position stand. Appropriate intervention strategies for weight loss and prevention of weight regain for adults., *Med. Sci. Sports Exerc.* 33 (2001) 2145–56.
- [66] S.A. Tsai, N. Lv, L. Xiao, J. Ma, Gender Differences in Weight-Related Attitudes and Behaviors Among Overweight and Obese Adults in the United States., *Am. J. Mens. Health.* (2015) 1557988314567223-. doi:10.1177/1557988314567223.
- [67] J.L. Miles-Chan, D. Sarafian, J.P. Montani, Y. Schutz, A.G. Dulloo, Sitting comfortably versus lying down: is there really a difference in energy expenditure?, *Clin. Nutr.* 33 (2014) 175–8. doi:10.1016/j.clnu.2013.11.009.
- [68] J.O. Hill, J.C. Peters, H.R. Wyatt, Using the energy gap to address obesity: a commentary., *J. Am. Diet. Assoc.* 109 (2009) 1848–53. doi:10.1016/j.jada.2009.08.007.
- [69] R.W. Jeffery, R.R. Wing, Long-term effects of interventions for weight loss using food provision and monetary incentives., *J. Consult. Clin. Psychol.* 63 (1995) 793–6.
- [70] J.M. Jakicic, C. Winters, R.R. Wing, W. Lang, Effects of Intermittent Exercise and on Adherence , Weight Loss , and Fitness in Overweight Women, *JAMA.* 282 (1999) 1554–1560. doi:10.1001/jama.282.16.1554.
- [71] K. Johansson, M. Neovius, E. Hemmingsson, Effects of anti-obesity drugs, diet, and exercise on weight-loss maintenance after a very-low-calorie diet or low-calorie diet: a systematic review and meta-analysis of randomized controlled trials., *Am. J. Clin. Nutr.* 99 (2014) 14–23. doi:10.3945/ajcn.113.070052.
- [72] E. Hemmingsson, K. Johansson, J. Eriksson, J. Sundström, M. Neovius, C. Marcus, et al., Weight loss and dropout during a commercial weight-loss program including a very-low-calorie diet, a low-calorie diet, or restricted normal food: observational cohort study., *Am. J. Clin. Nutr.* 96 (2012) 953–61.

doi:10.3945/ajcn.112.038265.

- [73] A.G. Tsai, T.A. Wadden, The evolution of very-low-calorie diets: an update and meta-analysis., *Obesity*. 14 (2006) 1283–93. doi:10.1038/oby.2006.146.
- [74] M.J. Armstrong, T.A. Mottershead, P.E. Ronksley, R.J. Sigal, T.S. Campbell, B.R. Hemmelgarn, Motivational interviewing to improve weight loss in overweight and/or obese patients: a systematic review and meta-analysis of randomized controlled trials., *Obes. Rev.* 12 (2011) 709–23. doi:10.1111/j.1467-789X.2011.00892.x.
- [75] D.L. Johannsen, N.D. Knuth, R. Huizenga, J.C. Rood, E. Ravussin, K.D. Hall, Metabolic slowing with massive weight loss despite preservation of fat-free mass., *J. Clin. Endocrinol. Metab.* 97 (2012) 2489–96. doi:10.1210/jc.2012-1444.
- [76] C.K. Martin, D. Rosenbaum, H. Han, P.J. Geiselman, H.R. Wyatt, J.O. Hill, et al., Change in food cravings, food preferences, and appetite during a low-carbohydrate and low-fat diet., *Obesity (Silver Spring)*. 19 (2011) 1963–70. doi:10.1038/oby.2011.62.
- [77] J.S. Brar, R. Ganguli, G. Pandina, I. Turkoz, S. Berry, R. Mahmoud, Effects of behavioral therapy on weight loss in overweight and obese patients with schizophrenia or schizoaffective disorder., *J. Clin. Psychiatry*. 66 (2005) 205–12.
- [78] M.G. Perri, A.M. Nezu, E.T. Patti, K.L. McCann, Effect of length of treatment on weight loss., *J. Consult. Clin. Psychol.* 57 (1989) 450–2.
- [79] R. Sell, M.D., M. Rothenberg, C. Chapman, *Dictionary of Medical Terms*, 6th Ed., Barron's Educational Series, n.d.
- [80] M. Rosenbaum, E.M. Murphy, S.B. Heymsfield, D.E. Matthews, R.L. Leibel, T. Journal, et al., Low Dose Leptin Administration Reverses Effects of Sustained Weight-Reduction on Energy Expenditure and Circulating Concentrations of Thyroid Hormones, *J. Clin. Endocrinol. Metab.* 87 (2013) 2391–2394.
- [81] V. Lecoultre, E. Ravussin, L.M. Redman, The fall in leptin concentration is a major determinant of the metabolic adaptation induced by caloric restriction independently of the changes in leptin circadian rhythms., *J. Clin. Endocrinol. Metab.* 96 (2011) E1512-6. doi:10.1210/jc.2011-1286.
- [82] J.E. Galgani, F.L. Greenway, S. Caglayan, M.-L. Wong, J. Licinio, E. Ravussin, Leptin replacement prevents weight loss-induced metabolic adaptation in congenital leptin-deficient patients., *J. Clin. Endocrinol. Metab.* 95 (2010) 851–5. doi:10.1210/jc.2009-1739.
- [83] M.K. Serdula, D. Ivery, R.J.J. Coates, D.S.S. Freedman, D.F.F. Williamson, T. Byers, Do obese children become obese adults? A review of the literature., *Prev. Med. (Baltim)*. 22 (1993) 167–77. doi:10.1006/pmed.1993.1014.
- [84] S.R. Daniels, D.K. Arnett, R.H. Eckel, S.S. Gidding, L.L. Hayman, S. Kumanyika, et al., Overweight in Children and Adolescents: Pathophysiology, Consequences, Prevention, and Treatment, *Circulation*. 111 (2005) 1999–2012.

doi:10.1161/01.CIR.0000161369.71722.10.

- [85] F.M. Biro, M. Wien, Childhood obesity and adult morbidities, *Am. J. Clin. Nutr.* 91 (2010) 1499S–1505S. doi:10.3945/ajcn.2010.28701B.
- [86] W.H. Dietz, Health consequences of obesity in youth: childhood predictors of adult disease., *Pediatrics.* 101 (1998) 518–25. doi:10.2307/2089861.
- [87] J. Robert Staffieri, A Study of Social Stereotype of Body Image in Children, *J. Pers. Soc. Psychol.* 7 (1967) 101–104.
- [88] S.A. Richardson, N. Goodman, A.H. Hastorf, S.M. Dornbusch, Cultural Uniformity in Reaction to Physical Disabilities, *Am. Sociol. Rev.* 26 (1961) 241–247. doi:10.2307/2089861.
- [89] B.E. Saelens, J.F. Sallis, L.D. Frank, S.C. Couch, C. Zhou, T. Colburn, et al., Obesogenic Neighborhood Environments, Child and Parent Obesity: The Neighborhood Impact on Kids Study, *Am. J. Prev. Med.* 42 (2012) e57–e64. doi:10.1016/j.amepre.2012.02.008.
- [90] J.J.J. Reilly, D. Wilson, Childhood obesity, *BMJ.* 333 (2006) 1207–1210. doi:10.1136/bmj.39048.503750.BE.
- [91] C.H.M. van Jaarsveld, M.C. Gulliford, Childhood obesity trends from primary care electronic health records in England between 1994 and 2013: population-based cohort study, *Arch. Dis. Child.* 100 (2015) 214–219. doi:10.1136/archdischild-2014-307151.
- [92] S.L. Gortmaker, K. Peterson, J. Wiecha, A.M. Sobol, S. Dixit, M.K. Fox, et al., Reducing Obesity via a School-Based Interdisciplinary Intervention Among Youth, *Arch. Pediatr. Adolesc. Med.* 153 (1999) 409. doi:10.1001/archpedi.153.4.409.
- [93] S.B. Austin, A.E. Field, J. Wiecha, K.E. Peterson, S.L. Gortmaker, The Impact of a School-Based Obesity Prevention Trial on Disordered Weight-Control Behaviors in Early Adolescent Girls, *Arch. Pediatr. Adolesc. Med.* 159 (2005) 225. doi:10.1001/archpedi.159.3.225.
- [94] S.A. McClave, H.L. Snider, Use of indirect calorimetry in clinical nutrition, *Nutr. Clin. Pract.* 7 (1992) 207–221. doi:10.1177/0115426592007005207.
- [95] R.J. Nelson, Seasonal immune function and sickness responses, *Trends Immunol.* 25 (2004) 187–192. doi:10.1016/j.it.2004.02.001.
- [96] C.L. Long, N. Schaffel, J.W. Geiger, W.R. Schiller, W.S. Blakemore, Metabolic Response to Injury and Illness: Estimation of Energy and Protein Needs from Indirect Calorimetry and Nitrogen Balance, *JPEN. J. Parenter. Enteral Nutr.* 3 (1979) 28. doi:10.1177/014860717900300609.
- [97] R. Dickerson, J. Gervasio, M. Riley, J. Murrell, W. Hickerson, K. Kudsk, et al., Accuracy of predictive methods to estimate resting energy expenditure of thermally-injured patients, *J. Parenter. Enter. Nutr.* 26 (2002) 17–29. doi:10.1177/014860710202600117.
- [98] R.H. Bartlett, R.E. Dechert, J.R. Mault, S.K. Ferguson, A.M. Kaiser, E.E. Erlandson, Measurement of metabolism in multiple organ failure., *Surgery.* 92

(1982) 771–9.

- [99] J.R. Mault, I. Iga, L.M. Keith, R. Dewitt, K. Fuka-, Y. Wu, et al., Energy Balance and Outcome in Critically-ill Patients: Results of a Multi-Center, Prospective, Randomized Trial by the ICU Nutrition Study Group, in: 24th Clin. Congr. Abstr. J. Parenter. Enter. Nutr., 2000: p. S4. doi:10.1177/014860710002400111.
- [100] A.M. Beck, U.N. Balknas, P. Fürst, K. Hasunen, L. Jones, U. Keller, et al., Food and nutritional care in hospitals: how to prevent undernutrition--report and guidelines from the Council of Europe., *Clin. Nutr.* 20 (2001) 455–60. doi:10.1054/clnu.2001.0494.
- [101] T. Grau, A. Bonet, M. Rubio, D. Mateo, M. Farré, J.A. Acosta, et al., Liver dysfunction associated with artificial nutrition in critically ill patients., *Crit. Care.* 11 (2007) R10. doi:10.1186/cc5670.
- [102] P. Singer, G.S. Doig, C. Pichard, The truth about nutrition in the ICU., *Intensive Care Med.* 40 (2014) 252–5. doi:10.1007/s00134-013-3162-y.
- [103] C.P. Heidegger, M.M. Berger, S. Graf, W. Zingg, P. Darmon, M.C. Costanza, et al., Optimisation of energy provision with supplemental parenteral nutrition in critically ill patients: a randomised controlled clinical trial, *Lancet.* 381 (2013) 385–393. doi:10.1016/S0140-6736(12)61351-8.
- [104] M.F. Picolo, A.F. Lago, M.G. Meneguetti, E.A. Nicolini, A. Basile-Filho, A.A. Nunes, et al., Harris-Benedict Equation and Resting Energy Expenditure Estimates in Critically Ill Ventilator Patients, *Am. J. Crit. Care.* 25 (2016) e21–e29. doi:10.4037/ajcc2016758.
- [105] M.S. Rehal, E. Fiskaare, I. Tjäder, Å. Norberg, O. Rooyackers, J. Wernerman, Measuring energy expenditure in the intensive care unit: a comparison of indirect calorimetry by E-sCOVX and Quark RMR with Deltatrac II in mechanically ventilated critically ill patients., *Crit. Care.* 20 (2016) 54. doi:10.1186/s13054-016-1232-6.
- [106] L.S. Brandi, R. Bertolini, M. Calafà, L. Severino Brandi, Indirect calorimetry in critically ill patients: Clinical applications and practical advice, *Nutrition.* 13 (1997) 349–358. doi:http://dx.doi.org/10.1016/S0899-9007(97)00074-9.
- [107] V. Fraipont, J.-C. Preiser, Energy Estimation and Measurement in Critically Ill Patients, *J. Parenter. Enter. Nutr.* 37 (2013) 705–713. doi:10.1177/0148607113505868.
- [108] R.L. Chioloro, E. Breitenstein, D. Thorin, L. Christin, N. de Tribolet, J. Freeman, et al., Effects of propranolol on resting metabolic rate after severe head injury, *Crit. Care Med.* 17 (1989) 328–34.
- [109] G.L. Clifton, C.S. Robertson, R.G. Grossman, S. Hodge, R. Foltz, C. Garza, The metabolic response to severe head injury, *J. Neurosurg.* 60 (1984) 687–96. doi:10.3171/jns.1984.60.4.0687.
- [110] F. Hammarqvist, Nutrition in head trauma patients; Traumatic brain injury – case discussion of nutritional, caring and ethical aspects, in: *ESPEN Congr. Gothenbg.*, 2011.

-
- [111] L.D. Plank, A.B. Connolly, G.L. Hill, Sequential changes in the metabolic response in severely septic patients during the first 23 days after the onset of peritonitis., *Ann. Surg.* 228 (1998) 146–58.
- [112] R.G. Clark, Caloric requirements after operation, *Proc. Nutr. Soc.* 30 (1971) 158–165. doi:10.1079/PNS19710028.
- [113] O. Cope, G.L. Nardi, M. Quijano, R.L. Rovit, J.B. Stanbury, A. Wight, Metabolic rate and thyroid function following acute thermal trauma in man., *Ann. Surg.* 137 (1953) 165–74.
- [114] D.W. Hart, S.E. Wolf, R. Mlcak, D.L. Chinkes, P.I. Ramzy, M.K. Obeng, et al., Persistence of muscle catabolism after severe burn., *Surgery.* 128 (2000) 312–9. doi:10.1067/msy.2000.108059.
- [115] D.W. Hart, S.E. Wolf, D.N. Herndon, D.L. Chinkes, S.O. Lal, M.K. Obeng, et al., Energy expenditure and caloric balance after burn: increased feeding leads to fat rather than lean mass accretion., *Ann. Surg.* 235 (2002) 152–61.
- [116] M. Elia, Hunger Disease, *Clin. Nutr.* 19 (2000) 379–386. doi:10.1054/clnu.2000.0157.
- [117] M. Elia, Insights into energy requirements in disease, *Public Health Nutr.* 8 (2005) 1037–1052. doi:10.1079/PHN2005795.
- [118] M.M. Rothkopf, M.J. Nusbaum, R.D.N.C. Lisa P. Haverstick, *Metabolic Medicine and Surgery*, Taylor & Francis, Boca Raton, U.S., 2014.
- [119] R. Chioléro, J.-P. Revely, L. Tappy, Energy metabolism in sepsis and injury, *Nutrition.* 13 (1997) 45–51. doi:10.1016/S0899-9007(97)83043-2.
- [120] C.L. Long, Energy balance and carbohydrate in infection and sepsis, *Am. J. Clin. Nutr.* 30 (1977) 1301–1310.
- [121] D.N. Herndon, R.G. Tompkins, Support of the metabolic response to burn injury, *Lancet.* 363 (2004) 1895–1902. doi:10.1016/S0140-6736(04)16360-5.

CHAPTER II

Metabolic Rate Measurement

Preface

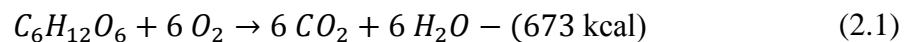
The components that comprise human metabolic rate, discussed in Chapter I, imply a level of variation that cannot be neglected but which can only somewhat be predicted by routine to a certain level. The methods available to determine energy expenditure are discussed in this chapter, and the need for a portable analyser for use with the wider population established. Calorimetry, the measure of heat energy, is one method used to determine human energy expenditure. Indirect calorimetry, where exhaled gas is analysed to determine energy consumed, is reported as the gold standard for metabolic rate measurement. However, to assess certain aspects of daily living, subjects must remain inside respiratory rooms, which restrict daily living activities and is not practical for the general population. It is the need for a quick, portable and affordable means to perform indirect calorimetry that motivated this project to develop a low cost handheld calorimeter. This chapter summarises the current devices available for energy expenditure measurement and state of the art developments.

2 Calorimetry

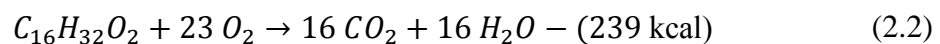
The amount of energy expended by a human can be measured by calorimetry and estimated by a number of methods such as physical activity or heart rate. For clinical use, the usual techniques for measuring EE are based on calorimetry. For healthy subjects, applications on many devices (such as smartphones, smartwatches or smart bands) provide basic measures of energy burnt each day using certain parameters (e.g. height, age, gender and weight) combined with data collected from activity sensors. As discussed in the section 1.2, the thermal effect of food contributes a significant part to daily EE and thus cannot be neglected. Furthermore, disease and medical operations can affect metabolic rate, which would not necessarily be shown by activity monitoring.

For discussion of metabolism processes and EE calculations it is common to refer to the ratio of CO₂ produced to O₂ consumed as the respiratory quotient (RQ). The inter-individual variance of RQ is discussed in section 2.2.1.1.

Nutrients, consumed in meals and via feeding, allow the production of energy through oxidation. The energy produced corresponds to EE, for example, a molecule of glucose oxidises to produce 673 kcal of energy (shown in equation 2.1) [1]. The carbohydrate example demonstrates a RQ of 1.0. The heat equivalent of O₂ for carbohydrate is 5.047 kcal/L [2].



The oxidation of a fat (for example, palmitic acid, shown in equation 2.2) requires more O₂ to be consumed [3]. As proportionally less CO₂ is produced, the RQ for the fatty acid is 0.68 [2]. The lower (non-protein) RQ for fat corresponds to a lower equivalent calorific value of O₂ (4.686 kcal/L) [2]. The oxidation process for palmitic acid consumes 239 kcal of energy.



The reaction to oxidise protein is not as straightforward as the examples for carbohydrates and fat. Proteins are not completely oxidised, and some oxygen, nitrogen and nitrogen from the protein molecules are used to form urea, CO(NH₂)₂ [4]. The process for albumin is shown in equation 2.3. The RQ for albumin is 0.82,

which cannot be directly compared with the RQs for carbohydrate or fat (equation 2.3 demonstrates the complex process of metabolising protein, compared to fat or carbohydrate) [2]. It is estimated the heat equivalent of O₂ for protein is 4.656 kcal/L [5].



Calorimetry, the process of measuring the amount of heat produced during chemical reactions, can be used to measure the oxidation reactions in human beings. The process of measuring heat expended from a subject is called direct calorimetry. Alternatively, indirect calorimetry estimates the heat produced by measuring the volumes of oxygen consumed (VO₂) and carbon dioxide produced (VCO₂) by a subject during aerobic (oxygen consuming) metabolism [6].

2.1 Direct Calorimetry

All energy consumed is eventually released as heat (after performing work). To perform direct calorimetry with a human subject, a sophisticated insulated room is required in which the subject can reside for a period of time, and which allows the measurement of heat expended [7]. Usually the change in temperature is measured via water or air circulating in the walls of the chamber. The method can produce accurate results, but is complex and therefore usually limited to research or validation of other EE measurement techniques [1]. Also, it is not suitable for portable applications, nor for patients requiring regular treatment (as subjects must be isolated inside the room).

The first direct calorimetry experiments were performed on animals, by French chemist Antoine Lavoisier [8]. Heat expended was calculated from the water produced by ice melting from the body heat of an animal. Importantly, Lavoisier discovered there was a relationship between the O₂ consumed and CO₂ produced, energy expenditure and heat production (i.e. indirect calorimetry).

Direct calorimetry experiments, inside room-sized chambers (e.g. shown in Fig. 2.1), can be performed over a 24 hour period or longer, with usually a 10 to 12 hour fasting prior to entering the room [9]. Atwater et al. described a calorimeter for measurement of human EE, where volunteers occupied the chamber for between 1 and 13 days [10]. Over a 12 year period, 22 experiments were performed. Dauncey et al. further developed the principles described by Atwater, taking advantage of computerised data

logging to allow a greater number of experiments to be performed over a short time frame (60 experiments in 18 months) [11].

The constructed chamber was designed to perform both direct and indirect EE measurements. The design used 24 thermocouples to measure the temperature in the chamber, with CO₂ and O₂ analysers for expired gas measurement. In a comparative study between direct and indirect calorimetry, 24 hour measurements were made on 8 adult subjects [12]. Each subject was tested 3 times; overall a mean difference of 1.2 % was found between the two estimates of 24 hour EE. In later work by Dauncey et al., only indirect calorimeter measurements were performed [13].

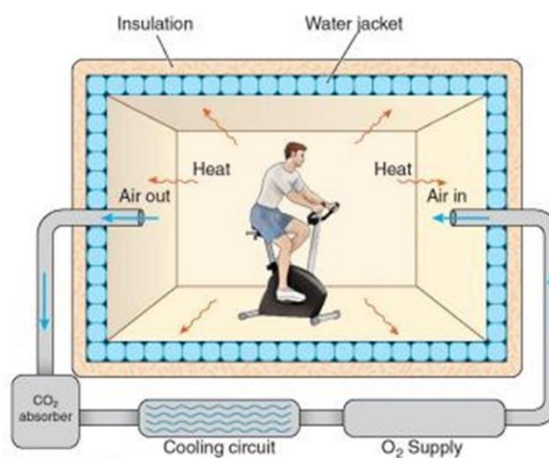


Fig. 2.1 - Schematic diagram showing chamber for direct calorimetry measurements [14].

The majority of wearable devices for EE measurement use activity sensors to estimate EE. The 'Lifechek' is a wearable armband (worn on the upper arm) designed to measure all four components of heat flux [15]. The device has not featured greatly in the literature since its introduction around one decade ago, although the device uniquely specified as performing direct calorimetry compared to breath analysers which use indirect calorimetry. It is assumed it has been superseded by other devices, more reliant on other sensors, such as accelerometers and heart rate monitoring. One study notes that studies investigating the contribution of the heat flux components to EE have yet to be performed [15]. No follow up studies involving the 'LifeChek' device have been published.

2.2 Indirect Calorimetry

Indirect calorimetry has become the gold standard for assessing EE in clinical care settings, exercise physiology and nutritional research facilities [16], and is often used as a benchmark to verify the performance of experimental techniques for metabolic rate assessment. The equations (2.1) to (2.3) demonstrate how EE can be calculated for each macronutrient. The EE for a person given breath samples with known $\dot{V}O_2$ and $\dot{V}CO_2$ can be calculated using the Weir equation [17]. The abbreviated Weir equation is shown in equation (2.4), neglecting the term for urinary nitrogen, as shown in equation (2.5). The possible errors introduced by using the abbreviated form of the equation are discussed in section 2.2.2.

$$\text{Total EE [kcal]} = 3.9 \dot{V}O_2 - 1.1 \dot{V}CO_2 \quad (2.4)$$

$$\text{Total EE [kcal]} = 3.9 \dot{V}O_2 - 1.1 \dot{V}CO_2 - 2.2 UN \quad (2.5)$$

The derivation of the terms in equation (2.5) is briefly described below, as reported by Weir [17]. For digestion of food, a given volume of O_2 will be required for metabolising, which can be divided into x , y and z for the metabolism of carbohydrates, proteins and fats respectively. Therefore the volume of O_2 consumed is given in equation (2.6). Given the RQs, discussed in section 2, an equation for the volume of CO_2 produced can be written (2.7). The total energy produced can be written as the sum of the energies from carbohydrates, fats and proteins, as shown in (2.8).

$$\text{Litres } O_2 \text{ consumed, } V = x + y + z \quad (2.6)$$

$$\text{Litres } CO_2 \text{ consumed, } RV = x + 0.82y + 0.68z \quad (2.7)$$

$$\text{Energy produced, } K = 5.047x + 4.656y + 4.686z \quad (2.8)$$

The equations (2.6) to (2.8) can be solved simultaneously. The reduced equation can be written in the form (2.9).

$$K = 3.94 V + 1.107 RV - 0.365y \quad (2.9)$$

The final unknown, y , represents the correction factor for the error introduced in the equation through incomplete protein metabolism. It has been reported that 1 g of urinary nitrogen signifies that 5.94 L of O_2 have been consumed (RQ of 0.801, 4.76 L of CO_2 produced, 26.5 kcal produced) [18]. The final term in (2.9) can be calculated, by substituting the volume of O_2 consumed ($0.365 \times 5.94 = 2.2$ kg cal /g urinary nitrogen), as shown in (2.5).

2.2.1 Respiratory Room

Whole body calorimeters are often used for EE measurement, where inhaled and exhaled gases can be monitored continually, without requiring the subject to wear a mask or mouthpiece (for example, the subject is able to eat without hindrance). Air is pumped into the chamber (ambient) and gas concentrations compared to the air extracted from the chamber. Fig. 2.2 demonstrates a simplified layout of such a room. Inside the chamber, a bed allows subjects to remain comfortable at night, and a TV/computer permits daily activities similar to normal daily routine for an office worker.

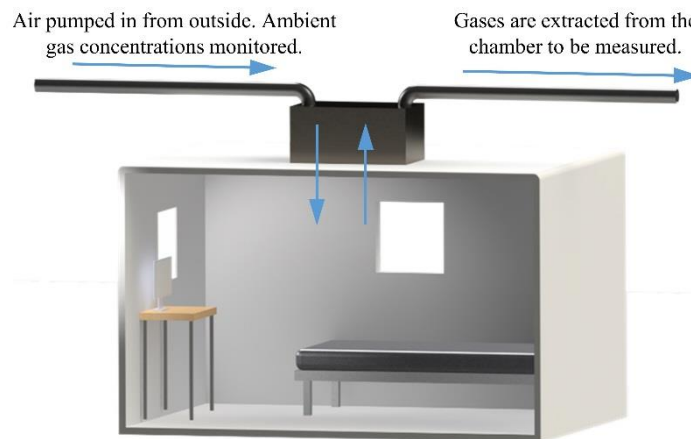


Fig. 2.2 – Indirect calorimetry chamber basic layout. Typical size $2.0 \times 2.5 \times 3.0$ m (18,000 L volume excluding furniture). Subjects can remain in the chamber for several days. Toilet, bed, step (for exercise), desk and chair are fitted inside the chamber.

A breath sample allows for instantaneous values of EE to be calculated. To determine total daily EE for the subject (inclusive of all normal daily activities), breath samples need to be taken throughout a 24 hour period. It is reported in some cases, that a per minute value for EE can be calculated and multiplied by a factor to determine daily EE [19]. In theory this technique avoids the need of a 24 hour breath measurement,

but care should be taken to account for the variance in EE throughout a normal day (as discussed in the previous chapter). A shorter measurement period has been trialled with some ICU patients [20]. The changes in RMR caused by some diseases in intensive care cause considerably more variance than daily activities. Patients in need of such care are unlikely to have a comparative daily routine to a healthy subject.

Indirect calorimetry is often performed in a respiratory room for a 24 hour period. Again the disadvantages of this approach include the subject being constrained to a small room for that period without being able to receive medical treatment. Furthermore, the chambers can be slow to respond to a change in metabolic rate, due to the large volume of the room into which the subject is breathing. The exhaled gases are greatly diluted considering the large volume of the room, thus large averaging times are needed to get accurate results.

Calorimeters that sample breath directly, for example through a mask, mouthpiece or hood, are of great interest in the research field. Ventilated hood measurements are often used for shorter periods of time (30 to 60 minutes), while the subject is in a comfortable position. These shorter measurements can be used to determine RMR, which can be useful in recommending calorific intake, although it does not provide the detailed information available from longer experiments.

The respiratory chamber provides a reasonably comfortable, but controlled environment for a subject to reside. The rooms are usually well insulated and pressurised with control over temperature and humidity. Ravussin et al. reported on the measurement of daily EE of 177 subjects [21], of which the components of EE were studied for 118 subjects. The subjects were not allowed to perform any vigorous exercise (although spontaneous physical activity was assessed).

A wrist band was used to measure movement, before a radar system (using the Doppler principle) was later installed to allow precise and non-invasive measurement of activity in the chamber. Ravussin et al. recruited volunteers with a wide range of body weights and compositions. The volunteers, when admitted to the study, were determined to be in good health (apart from having diabetes and obesity) and none were taking any medication. The characteristics were summarised as shown in Table 2.1.

Table 2.1 – Characteristics of volunteers trialled in chambers by Ravussin et al [21].

Subject Characteristic	Study Population Mean	Range
Age	27 years	18 to 65 years
Weight	96.9 kg	41.3 to 178.1 kg
Body Fat	32 %	3 to 50 %
Fat Free Mass	64.2 kg	34.0 to 105.9 kg
Energy Intake	2360 kcal/day	1,610 to 3,615 kcal/day

For the subjects whose activity levels were measured by the radar system, the energy intake was on average 2,330 kcal/day (range 1,610 to 3,515) compared to an energy expenditure of 2,275 kcal/day (range 1,371 to 3,485). As the subjects remained inside the chamber for a full 24 hour period, assessment of daily EE and sleeping metabolic rate could be performed. It was found that the daytime energy expenditure was on average 1.78 kcal/min (range 1.06 to 2.69) and the sleeping metabolic rate was 1.12 kcal/min (range 0.70 to 1.87). It was noted that spontaneous physical activity occurred for 8.7 % of the waking time (range 3.9 to 16.6 %) and accounted for 41 kcal/day (range 16 to 78). It was noted that the physical activity component would be far greater in a free-living environment. The TEF was calculated as contributing on average 165 kcal/day, around 7 % of the ingested calories.

Ravussin et al. proved the hypothesis that a universal fixed energy requirement for all individuals is not a viable solution. Additionally, the proportion of daily energy burned attributed to each component of EE varied between the study participants. The variation in energy needed for each activity (e.g. sleeping, resting, sitting etc.) supports the findings of Durnin et al., where a large variation in the components of EE between subjects was noted [22].

Ravussin et al. concluded that 24 hour measurements of EE were necessary in order to calculate the individual values of the four components of EE [21]. This finding could be questioned, due to the large volume of the chamber, with a response time measured of at least 3 minutes. A single 24 hour measurement would not allow the variation of TEF to be investigated after the consumption of a variety of meals. The reproducibility of the 24 hour measurements was verified however, with 12 of the study group spending a second 24 hour period in the respiratory room (at least 1 week

following their first participation). The variance between the first and second trials was in the range of 0.2 to 9.0 % (coefficient of variance was 2.4 %).

TEF measurements inside respiratory chambers have been described as “not ideal” by Tataranni et al., due to poor reproducibility [23]. A standard method for precise and accurate measurement of the TEF without a reference fasting experiment has yet to be established. Westerterp later reported on the use of a ventilated hood to measure TEF, and was able to successfully identify the effect of the content of various meals from total EE [24].

Tataranni et al. compared subjects in two conditions, first fasting (without breakfast) and second after having breakfast (which could be considered a standard method of finding TEF). Tataranni et al. suggested that the difference between the EE values for the two conditions would be due to the TEF. Ogata et al. proposed an original means of determining TEF in a respiratory chamber, and compared it to two existing alternatives [25], which attempt to estimate TEF from a single experiment (without the need for a reference experiment). Measuring TEF from one experiment alone would be advantageous, not only because a second experiment itself can lead to EE variance (as shown by Ravussin et al.), but also the cost, time and inconvenience associated with such measurements.

Ogata developed a method of extracting the TEF component from total EE by subtraction of a baseline EE (which included spontaneous activity). The two alternative techniques were suggested by Schutz et al. and Westerterp et al. Schutz assumed the RMR was the same before and during a meal, then calculates the TEF from the increase in total EE after eating [26]. Westerterp et al. modifies the method suggested by Schutz et al.; sleep metabolic rate (SMR) is subtracted from the total EE, opposed to RMR in the original formula [27]. Ogata et al. subtracts EE due to non-exercise activity from total EE. This activity component is calculated from linear regression on integrated physical activity [25].

The newly developed equation proposed by Ogata et al. was tested on 7 male subjects. Their mean age was 24.7 years (± 2.9 years S.D), mean height 1.78 m (± 7.3 cm) and mean weight 73.6 kg (± 12.1 kg). The subjects stayed in the respiratory rooms for 33 hours. Exercise was not permitted, and the subjects were asked to spend the majority

of their time in a seated position. The meals given to the subjects were adjusted for energy requirements for Japanese adults. The method suggested by Tataranni et al. for determining TEF was only applicable to breakfast (i.e. the study was repeated twice, once with two meals and once with three meals). For the study with three meals, breakfast contained 689 ± 121 kcal, lunch 761 ± 115 kcal and dinner 741 ± 130 kcal. For the two meal condition, breakfast contained 0 kcal, lunch 1105 ± 172 kcal and dinner 1085 ± 184 kcal. The total calorific consumption per day was 2190 ± 354 kcal consisting of 17 % protein, 21 % fat and 62 % carbohydrate.

The TEF calculated by each method is expressed as a percentage of the calorific content of each meal. The change in EE between the two meal and three meal conditions was $5.4 \% \pm 3.5 \%$ of the breakfast meal. Using the method proposed by Schutz et al. (using RMR) the TEF was calculated as of $-0.6 \% \pm 6.8 \%$. The RMR was defined as the average EE before breakfast time. This method was noted to have produced incorrect results for some subjects, due to negative EE values (which are not possible due to the definition of TEF). The TEF was found to equal $9.8 \% \pm 5.7 \%$ using the modified Schutz et al. method (taking a baseline SMR during a 5 hour period of sleeping time). Using the formula proposed by Ogata et al. the TEF was calculated as $4.1 \% \pm 2.5 \%$. This value was closest to the value found by taking the difference between the two and three meal conditions.

Ogata et al. concluded that the newly developed method of determining TEF was closest to the standard defined by Tataranni et al. (and did not produce any negative results). It should be noted the study would need refining (to test women and a larger sample size). The lunch given in the 2 meal experiment was larger than the 3 meal condition. However, using the new formula, the TEF for lunch was found to equal $5.7 \% \pm 3.6 \%$ and $5.1 \% \pm 1.8 \%$ for the two meal and three meal experiments respectively. This is unexpected, as the three meal lunch had lower calorific content. However, it was noted that the dinner TEF was larger in both cases (corresponding to a larger meal). The article shows the difficulty of calculating TEF and highlights the variance of TEF due to size and content of meals.

2.2.1.1 Portable Devices

The need for a portable breath analyser to quickly assess the metabolic rate of a subject without being confined to a whole body calorimeter has already been recognised, with

the development of several portable devices for EE assessment. The adoption of many of the devices discussed below is often slow. The devices are often unproven or expensive, which limits their use in a clinical environment. Semi-portable units, mounted on wheeled trolleys, are used in the clinical and exercise physiology environments. The inconvenience of their bulky size and expensive cost usually prevents their use for bedside care. The development of sensor technology has only recently progressed to a stage where miniature sensors (of suitable size for a mobile application) are becoming affordable and reliable (although still often limited to use in research).

A ventilated hood, shown in Fig. 2.3, offers a portable method of sampling the EE of a subject without the need for a mask or mouthpiece [28]. The ventilated hood method was devised to allow the energy requirements of critically ill patients to be measured and for the metabolic rate of subjects to be measured without any psychological effects of needing to breathe through a mouthpiece or mask. Spencer et al. developed an experimental ventilated hood calorimeter to measure the EE in both acutely ill and normal subjects [28]. The system was designed to accurately determine average values of tidal volume, minute ventilation, respiratory rate, O₂ consumption and CO₂ production. The study did not elaborate further into EE calculations, but noted the average values determined by the device over relatively long periods (30-120 minutes, excluding first 10 minutes) appeared to closely approximate average values of measurements taken over longer periods. The canopy system used a rigid plastic box which needed explanation to the subjects, to describe the purpose of the system. The subjects also took a period of time to get used to being inside the box, but Spencer et al. reported that once they had become accustomed to the unit, most subjects slept during portions of the experiment. Sleeping metabolic rate is lower than RMR (RMR is a 1.05 factor greater [29]).

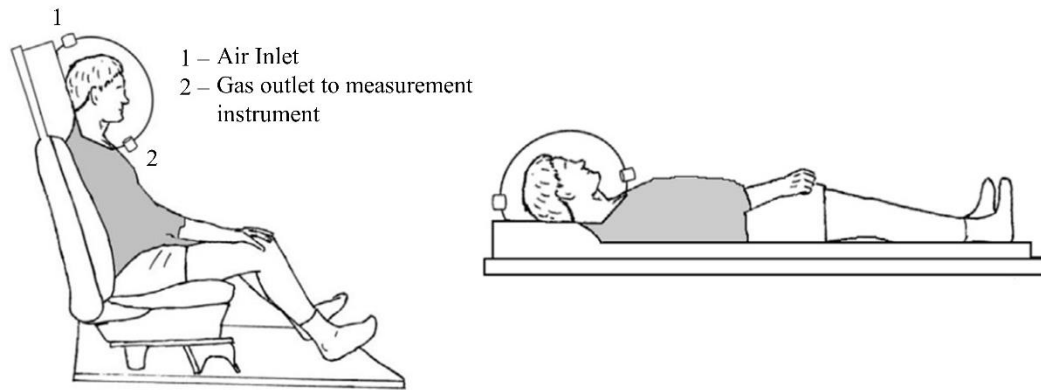


Fig. 2.3 – Diagram of ventilated hood apparatus, used for measurement of EE in seated (left) or supine (right) positions. From [30].

Ventilated hood systems are often used as a benchmark for verifying the functionality of research indirect calorimeters, where the metabolic rate of a subject can be determined over a shorter period than within a respiratory room, and without the need for the subject to go inside a chamber. The measurements can be performed, for example, in the ward or when the subject is seated, but do not usually last for long periods of time and therefore only provide a snapshot of EE. Leff et al. proposed daily EE could be calculated based on extrapolated hourly measurements between 8:00am and 4:00pm, but used a face mask rather than a hood [31]. Leff et al. found averaging the 3 middle RMRs produced the most reliable results. A similar pattern was observed for the second test day. The overall trend showed improved reliability (RMR measurements overall dropped by 2 % on average, perhaps as subjects became accustomed to the equipment).

The experiments reported by Leff et al. concluded that the most reliable method for serial measurement of RMR is to discard the first value and average the following 2 or 3 results. Average RMRs did not show significant change throughout the experiments. The article notes the importance of metabolic rate measurement for hospital patients in order for their energy and nutritional needs to be met. Both O_2 and CO_2 were analysed immediately, by a custom developed sensor system connected to the sampling system (infrared CO_2 sensor and paramagnetic O_2 sensor). It was discovered that RMR could be reproduced on different days with “very close” agreement between the study days [31]. The initial measurements demonstrated large variability, which was attributed to the time necessary for the patients to become accustomed to breathing through the analyser.

Miles-Chan et al. reported on a study of 19 participants, where EE measurement was performed in two positions, lying down and sitting comfortably [30]. For the trial, a ventilated hood was used (Deltatrac II), as it was suggested that experiments using mouthpieces/nose-clips could over or under-estimate EE. The mean age of the subjects was 24 (range 21-30) years and a mean BMI of 23 (range 18.1 to 27.9). The study found no significant change in RMR if the subject is seated or lying down (measurements taken after a 12 hour fast). Heart rate was found to be significantly higher (7 beats per minute), although breathing rate was the same in both positions.

Five of the original study participants volunteered to repeat the experiment on three different days. No differences between supine and sitting EE were observed on any day. Subjects can wear ventilated hoods immediately after eating, in order to monitor MR variation. However a baseline measurement can take 30 minutes to obtain [32]. This duration is necessary for the subject to become accustomed to the hood, and also for the gases inside the hood to become stable and a valid representation of exhaled breath.

The MedGem (Microlife Medical Home Solutions, U.S.) device, a handheld portable indirect calorimetry device, was developed for clinical use to determine EE. The BodyGem (also Microlife Medical Home Solutions, U.S.), shown in Fig. 2.4, is a unit with identical functionality, accuracy and reliability as the MedGem, but aimed for the consumer market. Anderson tested the accuracy of the MedGem device for producing resting EE against two methods; predictive equation (Harris-Benedict) and “traditional indirect calorimetry” (ventilated hood measurement, V_{max} 29N) [33]. The MedGem device is fundamentally flawed, in assuming a constant respiratory quotient of 0.85. As discussed in the previous chapter, this can vary according to energy source or body composition. The assumption of constant RQ neglects the need to measure both O_2 and CO_2 (only O_2 is measured). A RQ value of 0.85 is a source of error during EE calculations and could bias the device to certain study groups. For example, a mean RQ of 0.85 was reported for a study of 58 non-obese women by Marra [34]. However, the range of RQ values was between 0.74 and 0.96, with no relation to age, weight, BMI or RMR.



Fig. 2.4 – Photograph of BodyGem portable breath analyser [35].

To test if the MedGem device could serve as an alternative to a ventilated hood Anderson et al. tested 88 subjects aged 35 to 64 years (mean 51.7 years) [33]. The subjects were all overweight, with a mean BMI of 31.8 kg/m^2 ($\text{SD} \pm 4.2$). According to the protocol for the study, the subjects would breathe while holding the MedGem device or wearing the ventilated hood in a randomised order for 20 minutes each. The device overestimated RMR by 7 % on average. The Harris-Benedict equation (section 2.6.2) overestimated RMR by <1 %, and it was described as “remarkably consistent” [33]. It can be concluded that in this study, the HB equation performed well when considering an obese population. The results cannot be used to verify the accuracy of the HB equation for subjects with ‘normal’ BMI (range 18 to 25 kg/m^2). In general, subjects with a lower BMI will have a lower EE. In a survey conducted after the EE measurements and subjects preferred the traditional ventilated hood mechanism for EE measurement (61 % of male and female). It was suggested that this could be because of the position in which subjects were asked to perform the experiments (lying down under canopy for hood measurements, and sitting holding the device). On a five point scale, the energy assessment data was rated between 1 (“very helpful”) and 3 (“helpful”) by all of the subjects.

A mobile indirect calorimeter, Breezing® (Breezing Co., U.S.), was reported as measuring O_2 consumed and CO_2 produced using a disposable single-use colorimetric cartridge [36]. The device (shown in Fig. 2.5) focused on a consumer market, where EE could be viewed on a smartphone (using a Bluetooth connection). The device was

compared to the Douglas bag technique. Gases were collected in a bag and later tested against reference O₂ and CO₂ sensors. The mobile device was released to consumers in 2015, and has not been available for a sufficient period of time to become prominent in the literature. External comparative studies against a range of subject groups are not yet present. In the study presented by the creators (Xian et al.) [37], 12 subjects (7 male) aged between 21 and 33 volunteered for the study. The daily EE was calculated by the new device in the range of 1500 to 4000 kcal/day. All readings were within 10 % of those found using the Douglas bag method. The device uses a mouthpiece and nose-clip to obtain breath samples from subjects. The device is available for purchase online; the starter pack (\$350) includes 5 disposable (once-use) sensor cartridges (further packs of 5 can be purchased for \$25) [38].

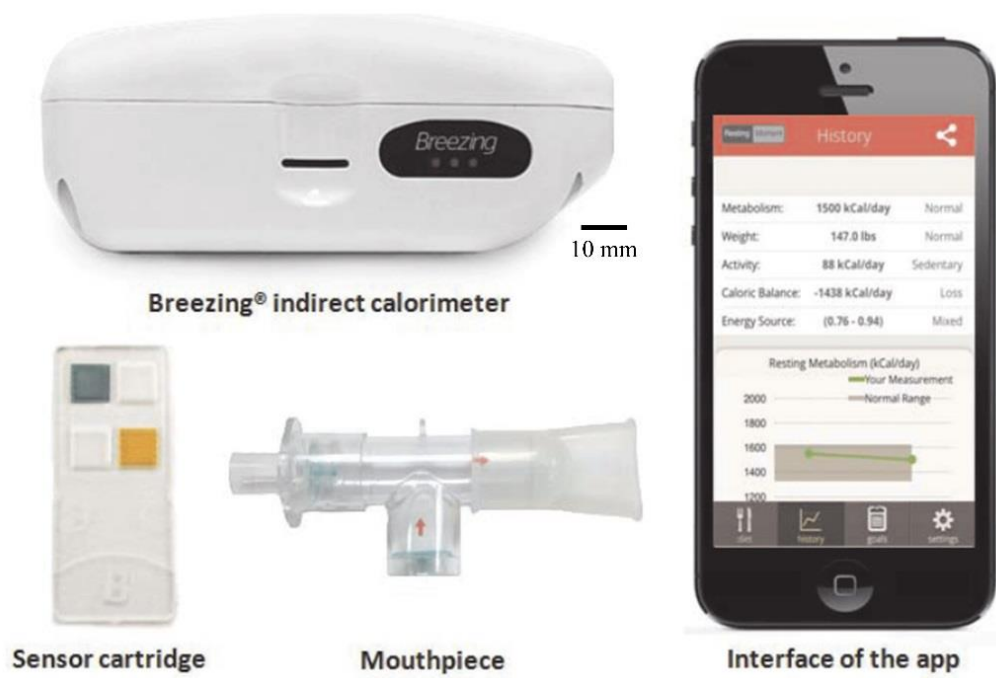


Fig. 2.5 – Photographs of Breezing® calorimeter and associated apparatus [37].

2.2.2 Nitrogen Measurement for Assessment of Protein Metabolism

The Weir equation is often abbreviated to the form shown in equation (2.4) where the end product of EE from the nitrogen component of protein metabolism is discarded. In some studies that measure EE via indirect calorimetry, the nitrogen content excreted through urea is recorded via urinary nitrogen (UN) measurements [39]. Sampling of UN does require collection of a urine sample, thus is usually performed with longer calorimetric measurements (for instance, 24 hour experiments). Equation 2.5 shows the relationship between total EE and UN (measured in grams) [17]. It has been

reported measurement of RMR is “acceptable” without the need for UN measurements, as only a minor error (as low as 2 %) is incurred for healthy subjects [40]. Therefore the abbreviated version of the Weir equation is often used [41].

The effect of protein metabolism is “commonly ignored” when estimating metabolic rates [17]. Protein metabolism is never static [8], it is continuously varying. Indirect nutritional status can be assessed through protein metabolism (as in the human body only protein is composed of nitrogen) which can be obtained through a method of measuring nitrogen excretion [42]. It is reported that nitrogen balance can be used as a means to examine metabolic stress. For a typical well-nourished adult, the expected rate of nitrogen excretion is about 12 g/day [43–45].

Healthy adults are expected to be in a state of “nitrogen equilibrium”; i.e. the nitrogen intake equals nitrogen excretion (and the amount of protein in their diet is sufficient to maintain and repair tissue) [46]. Nitrogen balance can be estimated from urinary urea excretion, which constitutes about 93 % of the total urinary loss [42]. The nitrogen losses over a day can be estimated with ‘reasonable accuracy’ by adding a factor for non-urinary nitrogen (in most cases no more than 4 g/day). It has been suggested that 0.5 g/day of nitrogen is excreted through the skin.

Nitrogen balance is often seen as an indicator of overall body health. In the case of critically ill patients, where dietary requirements are estimated, careful attention should be paid to under- or over-feeding of protein [47]. Diseases that affect the liver or kidney can affect the amount of nitrogen lost through urea, and therefore balance determination can be fraught with error and adjustments need to be made accordingly. The level of total urinary nitrogen (TUN) contained in the urea can vary across individuals; values in the range of 80 to 90 % are expected [48]. Konstantinides et al. reported urinary urea nitrogen (UUN) is too insensitive for calculating nitrogen balance [48].

In the original paper by Weir, in which the relationship between volumes of O₂ consumed and CO₂ produced was first linked to EE, it is noted that correcting for protein metabolism exactly is impossible [17]. A standard correction factor was applied to the formula, assuming protein accounts for around 12.5 % of the total calories that a patient produces. It is acknowledged that surveys performed around the

time of the article suggest that 10 to 15 % of calories are taken in the form of protein. Boyd reported patients produced heat from proteins at an average rate of 12.65 % (14 subjects) [49]. If protein metabolism was assumed as fixed at a rate of 13 %, the error in omitting urinary nitrogen would be around 1 % [49]. A 1 % error is supported by the Weir *p* factor (total calorie production due to protein correction factor), which equals 0.125 [50]. The MedGem portable calorimeter assumes a rate of 16 % [51]. This assumption is unlikely to be viable, due to the lower range reported from studies above (10 to 15 %) [49–51].

In many EE experiments the UN measurement is discarded, due to measurement difficulties or the assumption that its contribution is negligible. It is reported that the average error without nitrogen measurements is <2 % [41,52–55]. It has been reported that the measurement of UN is tedious, and its omission only adds a small error to the measurements of EE [54]. Bursztein et al. reports on 300 UUN measurements taken from 180 critically ill patients [54]. The mean and standard deviation of EE were reported as: 1685 ±597 kcal/day (with UN) and 1669 ±602 kcal/day (without), giving a difference of 27 ±14 kcal/day. On average, the error was <2 %, with a range of between 0 and 3 %.

Many clinicians find UN measurements difficult to perform for all patients and often the term is neglected [53]. The contribution of UN is greater in some cases for critically ill patients, however it is noted by Simonson and DeFronzo that incorrect measurement of UUN (or the failure to perform tests correctly) could result in a larger error in the calculation of EE [56]. The urea pool size can vary, thus short term UUN measurements may not be sufficient.

The balance of nitrogen in a human body (and consequently protein) can be estimated by comparing the nitrogen intake to the sum of the sources of nitrogen excretion (urine, faeces, skin, hair and body fluids) [46]. For example, in the case of growing children, pregnant women or people recovering from a protein deficiency or illness, a positive nitrogen balance is expected (i.e. the body is adding protein, thus nitrogen intake exceeds nitrogen excretion). For the case of individuals who are starving, on an extreme weight-loss diet or who suffer from a severe illness/fever, a negative nitrogen balance would be predicted. Negative balances are also expected for other diseases such as hyperparathyroidism (patients have an increased metabolic rate) [57].

The nitrogen balance for obese or critically ill patients is of particular interest, as TUN may vary by a significant amount compared to healthy subjects. Byrne et al. performed an experiment to investigate the changes in resting and walking EE of obese pregnant women. In this study, it was assumed that the urinary nitrogen excretion rate was negligible [58]. However, the expected nitrogen balance could vary in pregnant women as well as in obese subjects. It is stated by Byrne et al. that for weight gain to occur, daily calorie intake must exceed daily EE, therefore it should be noted that over-feeding can have a significant increase in nitrogen balance. A 3.0 g/day positive nitrogen balance was reported by Bandini and Young, when obese and non-obese subjects were subjected to over-feeding [59]. Over-feeding has an effect on TUN and should ideally be considered. A range of diseases (Table 2.2) has been shown to increase the TUN measured compared to the control value (for a healthy subject).

Table 2.2 – Urinary nitrogen loss rate following injury or illness, from [60–62].

Loss of urinary nitrogen (g/kg/day), mean value \pm standard error (where available)						
Skeletal Trauma	Blunt Trauma	Trauma w/ Steroids	Open Wound	Moderate Burn <30%	Large Burn >30%	Normal
0.317 \pm 0.27	0.322 \pm 0.055	0.338 \pm 0.106	0.12	0.17 \pm 0.025	0.36 \pm 0.037	0.085 \pm 0.002

UN losses are not usually dictated by an illness itself, but are perhaps a consequence of a change in metabolism. The stress levels of the patient increases the concomitant protein catabolism which results in an increase in TUN. Stress can present between 60 and 90 % of the nitrogen expelled through urine [63]. Examples of stress level (caused by associated clinical condition) are shown in Table 2.3. It should be noted that spinal cord injuries invalidate UUN measurement, due to disused muscle wasting.

Table 2.3 – Stress level compared to urinary nitrogen (g/day), from [63,64].

Level of Stress	Clinical Condition	Urinary Nitrogen (g/day)
Ideal Condition	-	3 to 5
Non-Stressed	Starvation	5 to 8
Mild Stress	Elective Surgery	5 to 12
Moderate Stress	Trauma	10 to 18
Severe Stress	Sepsis	>18

Nitrogen balance is calculated using equation (2.10), where 4 g is added for non-urea loss [63].

$$\text{Nitrogen Balance [grams]} = \frac{\text{protein intake}}{6.25} - ([\text{nitrogen in UUN}] + 4) \quad (2.10)$$

The error when excluding nitrogen in calculations for EE for in- and out-patients has been reported as lying in the range of 1 to 2 %, the error for critically ill patients is <4 % [65,66] (an error of 100 % in calculation would yield the same error) [67]. Often these approximations exclude minority groups, such as infants, children and the elderly. For example, Hamamoto et al. compares energy balance in infants born from HIV seropositive mothers infected and non-infected [68]. Nitrogen balance for non-infected infants is around 0.2 ± 0.3 g/kg/day (with an average weight of 7.01 kg and average RMR of 51.8 kcal/kg/day). It was found that infected patients had a lower nitrogen balance, but higher RMR (0.2 ± 0.1 g/kg/day and 68.0 kcal/kg/day respectively).

2.2.3 Error Introduced without Nitrogen Measurement

The metabolic rate data from six subjects were kindly provided by the University Hospital Coventry and Warwickshire NHS Trust. The subjects were all tested in the chambers at the hospital for a period of at least 24 hours. The physical characteristics of the subjects are shown in Table 2.4. All ethnicity of all the subjects was white Caucasian. The total tidal volume of each subject was estimated from their mass (factor of 7.7 ml/kg).

Table 2.4 – Subject information for observing chamber performance.

Subject ID (Test Date)	Weight [kg]	Tidal Volume [ml]	Age [years]	Gender
MF58 (25/07/12)	61.8	~476	45	F
MF57 (19/09/12)	71.9	~554	26	F
S243 (13/11/13)	87.3	~672	21	M
S253 (13/11/13)	72.2	~556	22	M
Stan1 (25/11/13)	71.4	~71.4	40	M
Stan2 (25/11/13)	86.0	~662	51	M

Urine was collected from the subjects at least once per study (ideally samples would be separated by 12 hours, however this was not always possible). The urine was analysed and creatinine and urine (in moles per litre) determined. This was converted into nitrogen content per sample. The rate of nitrogen oxidation is assumed to be 90 % constant. The amount of nitrogen oxidised is divided by the sample period to find the nitrogen oxidised per minute. EE was calculated using both the full Weir equation (2.5) and the abbreviated version (2.4). The comparison shown in Table 2.5 was taken from average values of EE calculated across the duration of the experiment (all values correct to 3dp).

Table 2.5 – Summary of urine nitrogen content for subjects and error introduced to EE calculation.

Subject	Urine Volume (L)	Total Urinary N (g)	Nox (g/min)	EE without N (kcal/min)	EE with N (kcal/min)	Error (%)
MF58	4.114	9.241	0.0143	1.263	1.232	2.475
	1.974	5.701	0.009	1.271	1.240	1.853
MF57	6.399	12.040	0.009	1.400	1.380	1.489
	0.475	6.497	0.010	1.883	1.861	1.261
S243	1.923	8.889	0.014	2.230	2.199	1.467
	1.44	8.108	0.013	1.751	1.722	1.755
S253	0.061	0.374	0.001	1.671	1.669	0.111
	2.289	9.841	0.015	1.984	1.951	1.794
	1.418	12.358	0.019	1.413	1.372	3.047
Stan1	1.974	5.701	0.005	1.416	1.405	0.841
	3.351	11.115	0.010	1.547	1.524	1.572
Stan2	1.249	13.815	0.013	1.418	1.390	2.009
	1.496	9.808	0.009	1.490	1.471	1.428

The average error due to the omission of nitrogen from the Weir equation was 1.62 % (range 0.1 to 2.48 %). This is well within the range of 1 to 2 % expected for healthy subjects. This error is low compared to the possible error introduced from low accuracy gas sensors.

2.3 Breath Sample Acquisition

The initial content of an exhalation contains air from the physiological dead space (large airways etc.). This air is not useful for EE assessment. The air of interest comes from alveoli inside the lungs, which are the ‘sacks’ in which gas exchange with the blood perfusing them occurs (shown in Fig. 2.6). It is important that the gas concentrations from this part of the exhalation cycle are sampled. The gas at the start of the exhalation is a mixture of inspired (ambient) gas, which dilutes the exhaled gases from the lungs. The capturing of the end part of an exhalation is discussed and also the method of sampling breath. For the measurement of resting EE, the breathing pattern of the subject cannot be disturbed by the apparatus (discomfort in sampling could cause EE to increase). The techniques to allow exhaled gas to be sampled are discussed below.

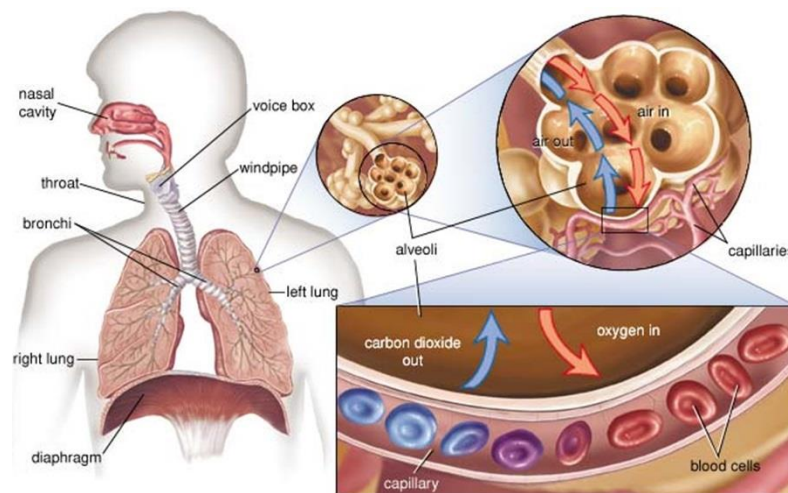


Fig. 2.6 – Illustration of human respiratory system, showing the alveoli in the lungs and the gas exchange into the blood [69].

2.3.1 Alveoli Gas

The three stages of exhalation are shown in Fig. 2.7, as defined by Miekisch [70]. The gas sampled in the initial Phase I contains only gas from the airways, and thus only ambient levels of CO_2 are detected. Phase II contains a mixture of ambient and exhaled gas. The gas from inside the lungs mixes with the remaining gas inside the airways (from inhaling previously). This ‘mixed expiratory sampling’ period (Phases I and II) is the initial part of exhaling and the gases play little part in the gas exchange component of the respiratory system [71]. The gas of interest for Volatile Organic Compound (VOC) detection and measuring of the O_2 and CO_2 levels for EE

assessment are found in Phase III of an exhalation [72]. This portion of breath is likely to come from the alveoli inside the lungs. The graphical monitoring of the level of CO₂ on breath is termed capnography, and is a convenient clinical procedure used to monitor the dynamics of breathing [73].

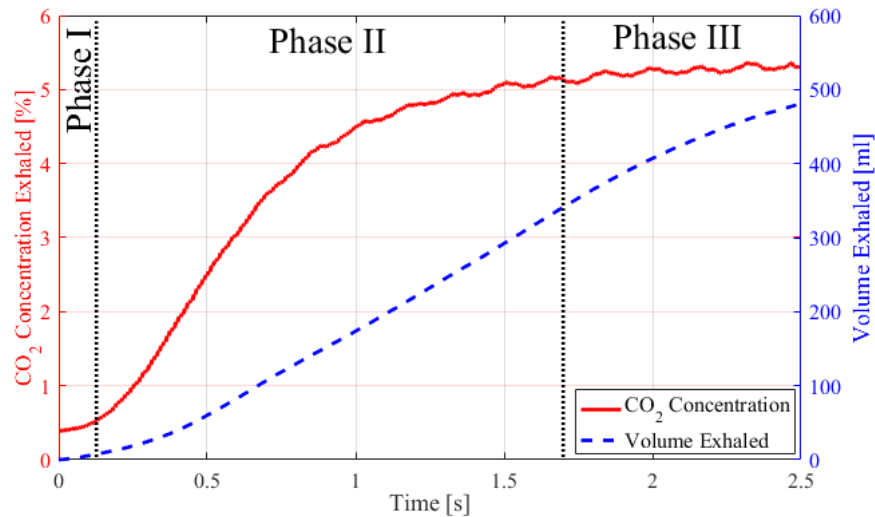


Fig. 2.7 – Three phases of exhalation shown by concentration of CO₂ sample on from a breath. Exhaled tidal volume shown for an adult male, taken from a series of exhalations recorded in a laboratory environment during initial testing of prototype breath analyser.

The accuracy of EE measured via indirect calorimetry (breath analysis, calculated through the Weir equation 2.4) is reliant upon the accurate measurement of the concentration of particularly O₂ (and CO₂) on breath. The mixing between exhaled gas from the lungs and ambient (inhaled) air causes a dilution of the compounds of interest. The concentration of CO₂ inhaled is likely to be around 0.035 % compared to between 4 and 5 % found on exhaled alveoli breath [74]. The gas plateau, seen at the end of the expiratory segment, they are close to equilibrium with pulmonary circulation of blood, thus providing a reflection of the gas exchanges occurring inside the lungs [75,76] (e.g. of volatile substances in the blood [77]). The end expired section of breath (alveoli gas sampling) provides the least contaminated samples from breath and the purest air [70]; it is also the most consistent part to sample, and therefore the easiest to reproduce [78].

2.3.1.1 Volatile Organic Compounds

VOCs are used as biomarkers for respiratory diseases, for example it has been reported VOC sensors can provide a non-invasive method to detect lung cancer [79]. VOCs are usually found in the ~100 ppb range. One study by Turner et al. noted that acetone was found on breath in concentrations of approximately 477 ppb (average value across 30 volunteers over a 6 month period) [80]. It is reported that mixed exhaled respiratory gases contain 25 % lower concentrations of blood borne VOCs and CO₂ compared to the air sampled at the end of an exhalation [81]. Dead space gases do not contain any VOCs from the subject exhalation (only if any are found in the inhaled air) as no interchange has taken place in the lungs [82]. Gas found in the alveoli can contain 3000 VOCs [78,82], although only around 200 are likely to be present in a given sample [70,82–84]. A list of example VOCs and their diagnostic purpose is given in Table 3.7.

An ideal portable VOC analyser would be able to identify the VOCs found an exhalation in real time, without the need for bulky gas collection/storage apparatus. Gas sensors currently available are usually not capable of producing a response over the short period the exhaled gas is from the desired alveoli region (< 1s, shown in Fig. 2.7). A subject at rest would be expected to breath at a rate of between 9 and 17 breaths per minute [85]. To increase the time for the sensors to respond to the VOCs found in an exhalation, some measurement systems extract the desired portion of breath for later measurement. There are many possible techniques for identifying the exhaled gas of interest. These methods are discussed below. The methods could be considered quite invasive [86], for example if a subject must breathe pure air beforehand (to eliminate contamination from background VOCs [87]).

2.3.1.2 CO₂ Identification of End Expiratory Gas

As shown above (Fig. 2.7) the gas from the alveoli can be identified by a plateau in the exhaled CO₂ concentration. Infrared based CO₂ sensors are often used, offering sufficient resolution (i.e. to record when a plateau is reached) and fast response. No standard CO₂ concentration or gradient has been determined for detecting the gas plateau. It is reported that the quality of samples obtained can vary considerably, depending on which part of the exhalation cycle the sample is taken, and an urgent need for standardisation has been identified [88]. It is acknowledged, the wide

variation in the situations a breath analyser could be used (e.g. field, laboratory etc.) and the wide range of patients (e.g. children, adults, elderly) prevent an all encompassing procedure being defined.

A sampling method was proposed by Schubert et al., based on the output from a fast response infrared CO₂ gas sensor, tested on mechanically ventilated patients [77]. An electronically operated two way valve switched between mixed respiratory gases and alveolar gas when the concentration of CO₂ exhaled exceeded 3.5 % volume (then vice versa when the CO₂ level fell below 90 % of its peak value). A pump was used (operating at 200 ml/min) to extract the sample gas (running continuously, regardless of the valve position). A 1 L sample of alveolar gas was needed from each patient. It was reported that the 1 L sample took between 6 and 22 minutes to collect (compared to between 3 and 5 minutes for mixed sampling). The method produced “reliable” results, but it was noted the CO₂ plateau level was not reached consistently for all patient groups. Patients with obstructive lung disease or those hyperventilating would exhale a lower level of CO₂ per breath.

2.3.1.3 Volume Exhaled Identification of End Expiratory Gas

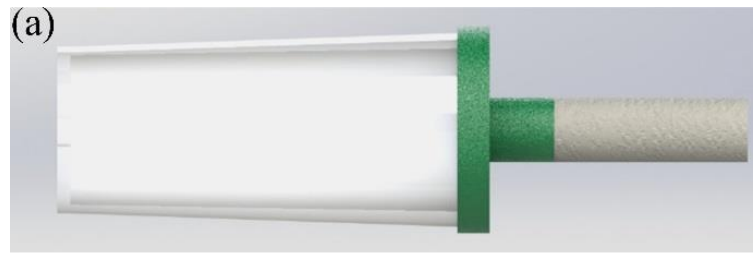
The method of sampling alveolar gas by simply taking a sample from the end of an exhalation through a long tube is often referred to as the “Haldane and Priestley” method (reported by Haldane and Priestley in 1905 [89]). A tube of approximately 4 feet length (1 inch diameter) was fitted with a mouthpiece at one end and the other end fitted with a spirometer (or left open). The ‘gas receiver’ sampling container was inserted into the exhalation tube with a tap, at a position approximately 2 to 3 inches from the mouthpiece. The subject was asked to breathe normally (while seated) for “some time”, before expiring quickly and deeply through the mouthpiece, before closing the end with their tongue. Near the end of the exhalation the tap was closed, trapping the air inside the container, for later analysis. The method was declared a success, given that the concentration of CO₂ obtained from normal breath was “practically the same” as that obtained from a very deep breath. Evidently “the sample obtained in the manner described is pure alveoli air” [89].

The approach founded by Haldane and Priestley has been developed into several portable units to allow samples of alveoli gas to be taken outside of laboratory conditions. Without reliance on electronic or complicated mechanical components,

sampling devices which capture the end volume of an exhalation can be used in extreme conditions, such as at the summit of Mount Everest, as reported by West et al. [90]. West et al. asked the subject to collect a sample in a 20 ml container. The subject needed to sit in a comfortable position and breathe normally for a few breaths, before holding their breath for a second then exhaling quickly into the container (which was sealed by a catch). A similar setup was used by Dyne et al., to collect samples from workers at a shoe manufacturing plant [91]. The system, based on the Haldane and Priestly collection method, was used successfully to obtain samples, offering a portable and simple-to-use device to monitor VOCs contained in exhaled breath from factory workers.

Commercial portable sampling systems are available, which allow exhaled breath measurements to be taken without a medical practitioner. The GaSampler (Quintron, USA) separates the first 500 ml of an exhalation into one bag (to be discarded) and samples the remaining volume of an exhalation into a second bag. The device has been used successfully in several studies [92,93], for example to detect nitric oxide on the breath of infants [94].

A similar device, the Bio-VOC (Markes International, UK) offers similar functionality, but includes a system to contain the sample in a small sorbent trap for transportation or direct measurement [95]. A sketch of the Bio-VOC is shown in Fig. 2.8, demonstrating the use of a plunger system to transfer the captured 150 ml end exhaled gas into a concentrating tube. The Bio-VOC has previously been tested in clinical diagnostic laboratories and is noted as being affordable and easy to use [96].



(a) Subject exhales through cardboard mouthpiece into container (volume ~150 ml). Last portion of exhale captured.



(b) Sample is steadily discharged into sorbent trap (x) with plunger (y). Tube is sealed using cap (z).

Fig. 2.8 – Drawing of the operation of the Bio-VOC, where sample is collected and stored in tube for transportation or direct connection to analyser. (a) shows the sample collection chamber; a plunger is used in (b) to transfer the sample into a tube for storage. Drawn using photographs from [79].

2.3.1.4 Time Based Identification

Measurement of EE from a breath sample requires breathing that is as little disturbed from normal as possible. For the sampling of VOCs however, a strict breathing routine has not been defined and instead is an aspect of interest, for example, to see how breath holding effects VOC concentration. However, a deeper exhalation after breath holding for say 10 s, means a greater volume is exhaled. Thus a system which extracts the alveolar portion of the exhalation by volume would be less effective. In such applications, the CO₂ identification method discussed above could be used, or a timing system implemented.

An example is reported by Lärstad et al., where samples are taken manually for both the dead-space air and alveolar gas (for asthma patients and healthy adults) [87]. After breath holding (for 10 or 20 s) the subject exhales for 10 s. The first 3 s are captured in one bag (150 ml volume) and the final 3 s captured in a separate bag with the (middle 4 s discarded). The method successfully distinguished the different types of gas as

desired (alveolar and dead-space). No comment was made on the suitability of the system for infants or children, nor elderly patients. The mean age in the study was 42 years (range 24 to 64 years) for the healthy group and 47 (23 to 64) years for patients with asthma.

A similar manual switching technique was demonstrated by Bikov et al., where the time to wash out the dead-space is estimated and unwanted gas discarded [97]. The wash-out time was approximated to be 1 to 2 s, based on dead-space volume, calculated as [weight (lb) added to age (years)] divided by exhalation flow (L/min). The first 3 s were discarded, to ensure that only gas from the lungs was sampled. A valve was ‘promptly’ closed at the end of each sample to avoid contamination with the ambient air. To automate the capturing mechanism, it would be necessary to detect the start time of an exhalation (and differentiate from an inhalation).

2.3.1.5 Pressure and Flow Monitoring of an Exhalation

The rate of exhalation can be tracked using a pressure sensor, for example to monitor the pressure in the upper respiratory tract and used to select portions of exhaled breath to sample. A design (Fig. 2.9) was reported by Basanta et al., where a pressure sensor was directly fitted into a Leur socket on a facemask [85]. The analogue output from the pressure sensor was read in real time via a LabVIEW program and breath-by-breath measurements were displayed. The software was able to classify exhaled breath into dead space or alveolar gas. From the output data the experimenter could select which portion to sample. The program would then use valves to direct the desired portion of an exhalation into a sample bag. Experiments were performed to compare the difference between inhaling purified air compared to ambient air. It was found the endogenous VOCs in breath were far higher and more variable when inhaling ambient air.

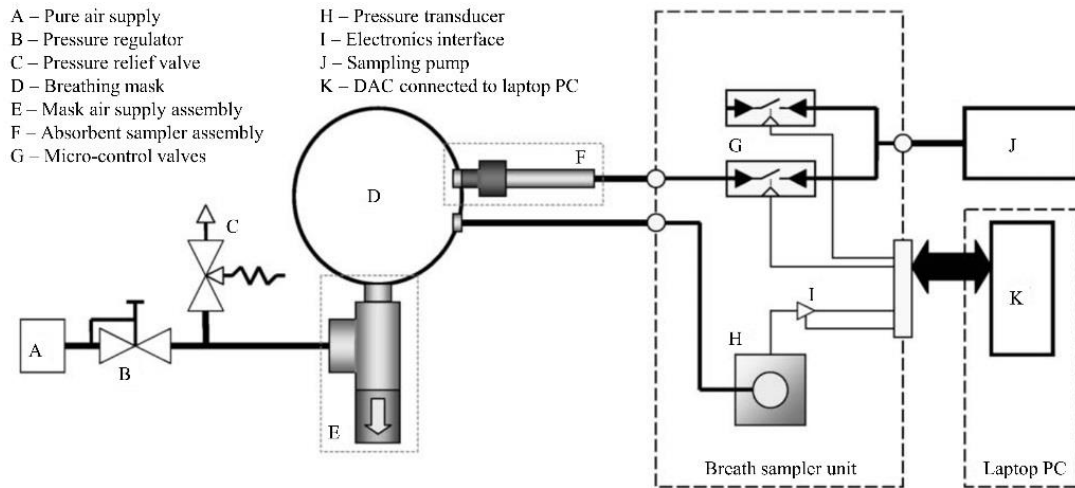


Fig. 2.9 – Schematic of the breath sampling system with major components identified. From [85].

Further information relating to the health of a subject can be determined from their exhalation flow rate and volume. Tidal volume and peak flow rates can allow the pattern and magnitude of tidal breathing to be inspected [98]. A diagram of the separation of an exhalation and inhalation by the crossing of a zero-flow line is shown in Fig. 2.10. The volume exhaled is calculated from flow measurement, the simplest method is to use the trapezium rule (integrate over time).

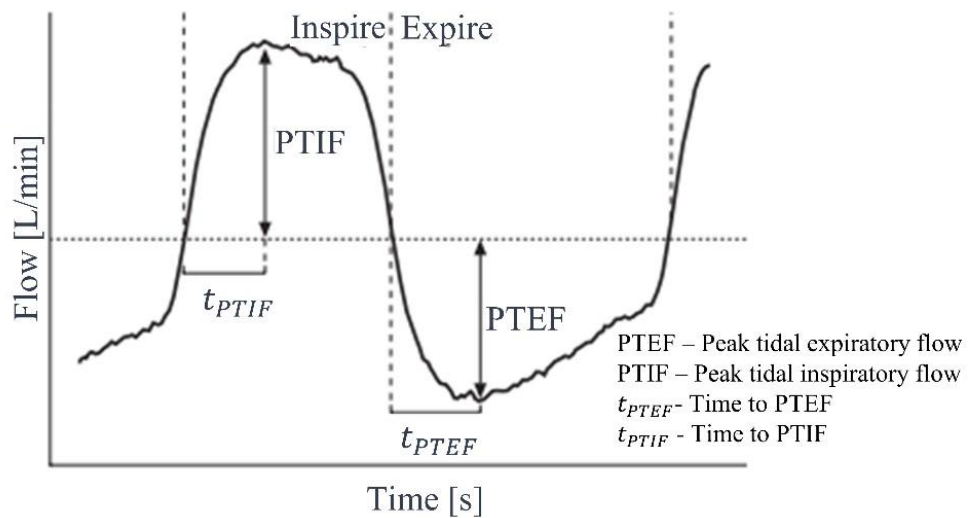


Fig. 2.10 – Inhalation and exhalation phases of breathing separated by the flow direction [98].

2.3.1.6 Exhaled Temperature and Humidity for Plateau Identification

Gas analysing equipment, such as chromatography or mass spectrometers, can often be too slow to respond to an exhalation, and unable to identify the plateau in gas

concentrations which indicate that the sampled gas is from the alveoli. Humidity is always present in exhaled breath, and can be monitored to see when the end expired gas is sampled. The level of absolute humidity is 6 % (6.2 % at 37 °c), and thus can be used as an internal standard for checking the mass spectrometer sample flow rate and reaction time [99]. One system, proposed by Herbig et al., claims to buffer the end tidal gas for a 10 s period (rather than a short period, such as 1 s) to allow time for gas sensors to respond to the sample [100]. The system relates to the Haldane Priestley method, by requesting subjects to exhale through a tube, which forms a buffer for the end tidal gas (e.g. last 40 ml). The subjects were asked to provide 1 exhalation per minute, which prevented hyperventilation and allowed time for the tube to clear, while permitting a longer period for a gas sensor response to become apparent. Humidity was used to identify the desired gas, where a threshold of 6 % absolute humidity was set by Herbig et al. [100], as also reported by Turner et al. [80]. The system was not capable of breath-by-breath sampling, although a number of breaths could be sampled over a short period.

In a similar manner to humidity, the temperature of exhaled breath tends to a plateau towards the end of a breath. Again, the temperature of an exhalation is consistent between subjects, although individual variations can be compensated for. One method of sampling alveolar gas was reported by Ljungkvist and Nordlinder, where a temperature sensor was used to monitor breath during an exhalation [101]. When the maximum temperature was reached (generally around 34.5 °C) a 100 ml gas sample was extracted. For the experiments detailed, Ljungkvist and Nordlinder used a fast temperature sensor, adapted to fit inside a commercial Mini-Wright peak flow meter. The device offered an inexpensive and easy to handle package and also low expiratory resistance. Alveoli gas was captured successfully using the temperature sensing principle. An automated gas sampler was reported by Vreman et al., again a temperature sensor was used to capture alveoli gas [102]. In this case, a heat sensitive thermistor probe was taped beneath the nostril of each subject. Once the temperature of exhalation had plateaued, a pump was activated after a 0.1 s delay. A 0.2 ml sample of breath was drawn, and confirmed as gas from the alveoli.

2.3.2 Mouthpiece and Face Mask Breath Sampling

To monitor human EE from breath measurements, ideally the breaths sampled should represent a normal breath for each subject; the subject should not need to force an

exhalation nor deliberately breathe at a slower rate than normal. The volume of O₂ and CO₂ exhaled and the rate of breathing effect the EE calculated over a given period, by the relationship shown in equation 2.4. Unfortunately, with the current gas sensor technology, in order to measure purely exhaled gas the subject needs to breathe through either a mask or a mouthpiece (with nose-clip). The effect of breathing with the addition of a mask or mouthpiece has previously been studied, as discussed in the following section.

2.3.2.1 Effect of Breath Monitoring

Breathing through a mouthpiece has been reported to increase tidal volume and decrease breathing frequency, perhaps caused by one or more of the follow three reasons: Influence of the additional dead space of the apparatus; stimulation of nasal and oral mucosa and shift of the respiratory route from the nose and mouth to just the mouth [103]. Similar findings have been discovered when sampling using a mask, where Cope et al. report that tidal volume and minute ventilation were effected [104]. It is commonly believed that the psychological load or sensor stimulation are the main culprits for the degradation in breathing rate [105]. Ventilation is normally controlled ‘automatically’, but on occasions it can be consciously controlled [106]. The contribution of each of the three effects mentioned above on breathing is a cause of disagreement in the literature.

The use of breath sampling apparatus can prevent the subject from being able to maintain a normal breathing pattern. Wearing a mask or exhaling through a mouthpiece stimulates the trigeminal receptors in the face, shown in Fig. 2.11 a), and/or oral cavity [103]. The area of the face around the mouth/nose is particularly sensitive to an applied force. Fig 2.11 b) shows the threshold of tactile detection on the face compared to the index finger.

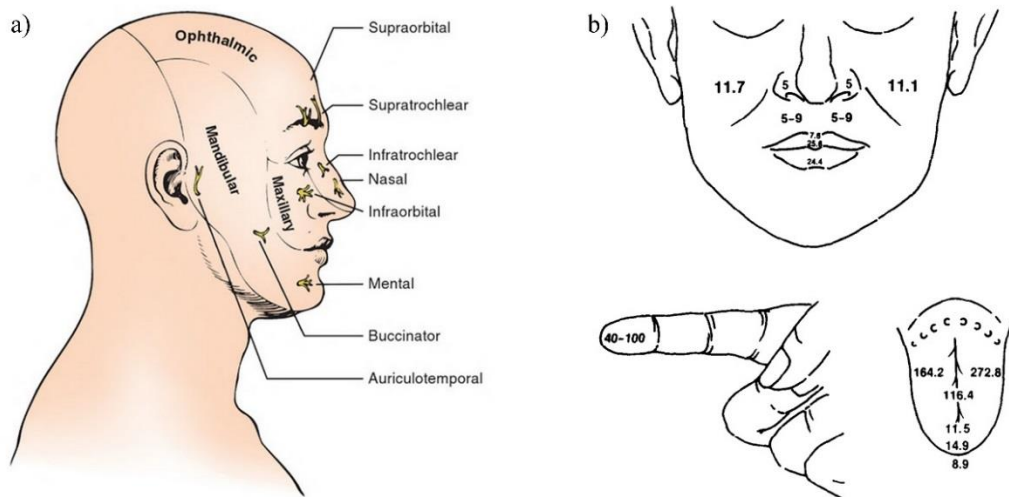


Fig. 2.11 – The area of the face where a mask or nose clip is worn is sensitive to an applied force, a) areas of skin supplied by the three major trigeminal nerve divisions [107]; b) Tactile detection threshold of areas on the face compared to the index finger (weights in milligrams) [108].

The use of a mouthpiece can stimulate the lips, gingiva and teeth [109]. Perez and Tobin noted that these stimuli had a lesser effect on the breathing pattern than changes to the respiratory route, from wearing a nose clip while breathing through a mouthpiece [110]. Contrary to Perez and Tobin, Wester and Patrick noted that the awareness of breathing being monitored is the major cause of respiratory alternations (changes in the respiratory route were said to have a less profound effect) [111]. This finding is in agreement with Shea et al. [112], where the need to control ‘behavioural and environment variables when making measurements of breathing at rest’ was highlighted. If these variables were not sufficiently controlled, there was increased risk of dramatic changes in breathing rate and tidal volume. An article by Mador and Tobin supported these statements and demonstrated that audio-visual stimulation tended to increase the variability of tidal volume, whereas mental arithmetic had no effect [113].

Gilbert et al. proposed an experiment to determine if the changes in breathing were caused by the stimulation of using a mouthpiece and nose-clip or by the dead volume in the instrument used to measure tidal volume [106]. Before the experiment, patients were left to breathe quietly for 1 hour prior to a mouthpiece and nose-clip being fitted. Electromagnetic sensors were used to unobtrusively monitor respiratory rate without the need to capture breath (by detecting chest movement). A total of 14 subjects

participated in the experiment (6 without respiratory disease and 8 with). With only the mouthpiece and nose-clip worn (without other apparatus, no dead volume added) the tidal volumes measured across the subject group increased by an average of 98 ml, and respiratory rate decreased by 25 % on average. With a pneumograph connected the tidal volume of the group increased by 124 ml/min on average and the respiratory rate fell by 6 breaths per minute. It was concluded the irritation and stimulation of the nasal mucosa was the most likely cause of depressing the respiratory frequency in humans and the fall in respiratory rate was repeated to the apparatus (mouthpiece and nose-clip). If the theory is correct, the rise in tidal volume could be a secondary effect, in response to maintaining adequate ventilation.

2.3.2.2 Automatic or Conscious Respiratory System

Automatic breathing originates in the ponto-medullary respiratory oscillator [114]. The respiratory muscles, which dictate regular breathing are controlled by a bulb-signal projection from synapses with the anterior horn cells in the cervical and thoracic spinal cord [114]. Cope et al. justify a notable respiratory effect when a mouthpiece is used, as being a sign that the control of breathing has been shifted from the automatic respiratory centres to the cerebral cortex, causing the breathing rate to alter [104]. John noted that voluntary breathing control is dependent on the functions of the cerebral cortex, while automatic ventilation is regulated by the mechanisms of the pons and medulla [115].

Further reports suggest that vagal nerve stimulation (in the nucleus of the tractus solitarius) can effect respiratory oscillations [116]. It was stated however, it is unlikely to affect the rate of breathing during normal ventilation [116]. It is noted that in affecting breathing this phenomenon has a greater effect, where vagal input becomes significant [114]. The risk of a face mask stimulating the vagal nerve has been noticed by Mostafa-Gharehbaghi et al., where it is advised face masks be fitted to infant's faces with care [117]. They should be tight enough to prevent leaks, but not apply too much pressure, else risk inducing a vagal response. The Vagus nerve is effected by breathing, regardless of whether the breathing is automatic or consciously controlled. The alternating effect of breathing on heart rate is known as 'respiratory sinus arrhythmia' [118]. The Vagus nerve innervates the heart causing a parasympathetic response in the nerve, perceived by a decrease in heart rate.

2.4 Metabolic Rate Measurement in a Free Living Environment

The need to measure metabolic rate outside of laboratory conditions has been recognised for decades and in particular for prescribing treatment for obesity and sports physiology; calculating EE for the lifestyle of a subject is important [119]. EE in free-living can be determined through a number of methods. These methods can loosely be grouped as: Doubly Labelled Water (DLW), applying relevant mathematical equations, wearable devices (for example heart rate monitoring or activity based) and portable breath analysers (discussed above). It is important to note the DLW technique and portable breath analysers measure human EE, whereas applying mathematical equations and wearable devices can only provide an estimate of EE.

2.4.1 Doubly Labelled Water

The DLW technique allows for EE determination over a much longer period of time than experiments in a respiratory chamber. Experiments can last from between 1 to 3 weeks, and allow subjects to participate in their normal free-living activities [8]. This method makes use of the known pathways for elimination of water (H_2O) from the body, which can be split into hydrogen and oxygen elimination. Both are expelled from the body as sweat, urine and respiratory water vapour. Oxygen is also eliminated as CO_2 . A more active individual will expend more energy over a set period of time than a less active person, who will consume less oxygen and produce (eliminate) less CO_2 (with a lower EE) [8]. If an isotropic label of oxygen is eliminated from the body by both CO_2 and water, an isotropic label of hydrogen would only be eliminated by water. The difference in elimination of the two labels will therefore provide a measure of the CO_2 production, and indirectly the EE of the subject [120]. The DLW method matured relatively slowly compared to other techniques. The DLW method is not without flaws, as it uses several assumptions including a constant rate of CO_2 production and constant size of body water pool throughout the measurement period [121]. Also, not all researchers use the same methods to calculate the elimination rate or mode of CO_2 conversion to EE.

Kroke et al. reported on the use of DLW to assess the validity of food-frequency questionnaires across a 2 week period [122]. The study cannot be considered comprehensive however, as although 160 subjects completed a questionnaire, only 30

were selected for comparison through the DLW method, of which 2 failed to complete the required measurements. Although a balance of men and women was selected (15 of each), all participants were aged between 40 to 67 years, and thus were not a valid representation of the wider population. The DLW EE estimates were determined by urine analysis using a mass spectrometer. The convenience of taking EE measurements was limited, as the subjects were required to keep the urine samples in controlled conditions (below -20 °c) before transporting the samples to a laboratory. The study also does not comment on the time of year/season when the measurements were taken, which has a bearing on EE. It is reported that interviews with participants allow physical activity levels to be monitored. The study concludes that energy intake was under-reported in the questionnaires.

A study by Black et al. aims to cover EE variation throughout the four seasons in a year, taking DLW measurements for 4 days in each [123]. The findings were similar to those stated by Kroke et al., where self-reporting questionnaires were found to produce under-estimates for energy intake. Meals being reported incorrectly and snacks not being recorded were blamed for the error. The study was only performed over a limited age range (middle aged and retired subjects). A large subject group was desired, however due to the expense and lack of availability of the labelled water, the study was limited to just 18 subjects. Activity levels of the subjects were self-reported, thus perhaps partly explaining the lack of agreement and EE noted by Black et al. The experiment duration did not cover a full week in each season, and therefore lacks a comprehensive energy record of weekly activities.

The DLW technique has been documented as limited to specific subject groups. For example, pregnant women, middle-aged subjects or athletes [124]. Few studies are performed on the wider population, such as children, trekking explorers or teenagers. Studies are often limited to one dose of DLW experiments per subject, thus not repeating over several months. Variable leisure activities or intermittent employment are likely to be disregarded [29]. DLW measurements only provide single measurement of EE per sample, and thus cannot be used to show how EE varies over the course of a single day, nor comparison between diurnal cycles of, for example, weekdays or weekends. A study by Wong et al. notes high reproducibility over a 4.4 year study [125]. DLW studies prior to the 1970s were only performed on small animals due to the high expense for quantities of labelled water needed for humans.

Obesity was less prevalent at the time, but is now a more persistent problem. The need for medical practitioners to determine EE has perhaps driven the increase in popularity for using DLW since the 1980s [120]. The main difference in DLW compared to the other measurement techniques of EE is the subject does not have to be compliant (e.g. animals can be tested).

2.4.2 Mathematical Equations

Clinicians routinely use predictive equations to estimate EE for patients, particularly in ICUs where indirect calorimetry is difficult to deploy [126]. Harris and Benedict devised a pair of equations (separate for men and women) to calculate daily heat production of a subject (collectively termed the HB equation) [127]. The equation related EE to measurements of height (h in cm), weight (w in kg) and age (a in years) for men (2.11) and women (2.12).

$$\text{Basal Metabolic Rate [men]} = 66.47 + 13.75 w + 5.00 h - 6.76 a \quad (2.11)$$

$$\text{Basal Metabolic Rate [women]} = 655.10 + 9.56 w + 1.845 h - 4.68 a \quad (2.12)$$

The equation, or adaptations of, are the most commonly used predicative means for estimating basal EE. It has been reported by Frankenfield et al. that the original HB equation overestimated EE systematically by 5 % and on average by 15 % [128]. The HB equation was found to apply to patients with BMIs up to 35 or 40. It is usual clinical practice to substitute ideal weight (lean body mass) when total weight exceeds ideal weight by 25 to 30 % [128].

The HB equation was also criticised by Haugen et al., stating that the equations were only designed for use with healthy patients and were not suitable for patients with complex disease processes [65]. Haugen et al. suggested RMR should be measured after a 5 hour fast, no PA or other stimulants. The presence of fever and infection can increase EE by up to 80 % compared to normal controls. Resting EE values provide critical data necessary to determine calorie intake for weight loss. Haugen et al. summaries that in obese subjects, only 38 to 64 % of resting EE values estimated using the HB equations are accurate. Furthermore, the characteristics of the subjects are dramatically different in our current population, than when the equation was proposed in 1918. Daly et al. compares the HB equation to indirect calorimetry with a sample size of 201 subjects [129]. It was found on average the equations over predicted basal EE by 12.3 % and in some extreme cases an overestimation of between 25 to 30 %

was found. Daly et al. criticised one assumption made by Harris and Benedict, that a 24 hour basal EE measurement can be predicated from a 5 to 15 minute measurement early in the morning.

Weijjs et al. conducted a validation of 18 predictive equations against indirect calorimetry results for 48 outpatients, 45 inpatients and 42 underweight patients [130]. It was found that the HB equations, acknowledged as the most evaluated, overestimated resting EE by about 4 % for obese patients and yields 1.5 % underestimated for an underweight population (actual body weight was used). An equation (including weight and height) was developed in a joint publication by the Food and Agricultural Organisation of the United Nations, the World Health Organisation and the United Nations University [131]. Weijjs et al. found the equation produced the most accurate results for adults in/out patients whereas the Mifflin St. Jeor equation (2.13 for men and 2.14 for women [132]) was considered for its relatively high percentage of in- and underweight -patients predicted well [130].

$$\text{Resting EE [men]}=9.99 \times w + 6.25 \times h - 4.92 \times a - 161 \quad (2.13)$$

$$\text{Resting EE [women]}=9.99 \times w + 6.25 \times h - 5 \times a + 5 \quad (2.14)$$

The Mifflin St. Jeor equation was also noted by Boullata et al. as performing better than the HB equation for obese (but otherwise healthy) adults [133]. Boullata et al. tested 395 subjects, with mean age of 56 years (range 16 to 92 years) and mean BMI of 24 (range 13 to 53). The HB equation was multiplied by a factor of 1.1 to obtain the most accurate results (the same factor was also applied to the Mifflin St. Jeor equation but with unfavourable results). For non-obese subjects it was found the HB equation multiplied by a factor of 1.1 produced the most accurate results (compared to indirect calorimetry measurement). Henes et al. compared the HB equation to 6 others, for use in predicting the EE of severely obese youths [134]. It was found that the HB equation had improved accuracy over other predictive equations, but only a 65 % accuracy was achieved and the equation displayed ‘noticeable errors’.

2.4.3 Heart Rate Monitoring

In all of the methods discussed thus far, none provide a solution for measuring the EE of an activity outside of a laboratory environment. In particular, Charlot et al. noted that EE during aerobic exercise is difficult to determine and field measurements are inconvenient [135]. Charlot et al. stated that accelerometers are more expensive than

heart rate (HR) monitors alone and do not represent a popular solution. An affordable solution was proposed to determine EE from affordable HR monitors. The report detailed a comparison between five existing equations used with HR monitors, and evaluates the accuracy of calculating EE prediction when parameters such as speed (via GPS) are factored into the equations.

It was found that speed monitoring greatly improved the accuracy of the EE prediction, and should be included whenever possible. The proposed equations fail to accurately predict EE in all but very specific cases. It is recorded that the coefficient of determination was 0.809 for the work developed during the study, which is more accurate than that found from the pre-existing equations (R^2 of 0.737). Moreover, Charlot et al. concede that the equation developed is only suitable for a limited age range, while running on level ground and with an intensity of between 25 and 75 % of HR reserve.

HR has been acknowledged as a useful parameter for calculating EE, but not only is careful calibration needed, but also a major problem is that not all HR variations are due to metabolic activity [136]. Spurr et al. developed a method of calculating daily EE using a HR monitor, and suggested it was a cheap alternative to the DLW technique [137]. The necessary calibration was performed based on the volume of O_2 consumed while cycling on a ergometer (the relationship between RQ and litres of O_2 consumed was used, initially developed by Lusk [138]). A critical heart rate (Flex) was found to split the relationship between HR and EE. A lower HR than the Flex cut-off value and EE was assumed to be basal; a higher HR and the calibration curves between HR and EE found from the ergometer experiments were used. The results from the initial experiments performed by Spurr et al. were not comparable to indirect calorimetry. The maximum deviation of total daily EE for individuals was in between +20 % and -15 % [137]. Additional issues were noted such as the HR electrodes becoming detached from the participants.

The Flex HR method was tested by other groups. Livingstone et al. compared the method with DLW and found that the HR technique overestimated EE by 2 ± 17.9 %, but the study other included 14 free-living adults (over a period of 15 days) [139]. Ceesay et al. compared the Flex HR to indirect calorimetry, and found that the Flex HR underestimated daily EE by on average 1.2 % (however with a large range from -

11.4 to 10.6 %) [140]. It was noted that the experiments developed by Ceesay et al. included regular exercise, which did not match the sedentary lifestyle to which the HR equations may be more suited. The findings of Blackburn and Calloway support this hypothesis, where it was noted prediction of EE from HR is unreliable in the range of 80 to 120 beats per minute [141]. Leonard similarly notes that the linear relationship between HR and EE breaks down at resting and high work levels and found the HR and EE relationship varies between individuals [142].

2.4.4 Activity Monitoring

Activity monitors attempt to provide a measure of the amount of physical activity (PA) and exertion that the wearer expends throughout daily life [143]. Modern devices use piezo-resistive or capacitive accelerometers to measure activity levels and also provide information on body position. In a review covering 25 articles and 18 accelerometers to DLW, Plasqui et al. concluded many accelerometers ‘perform badly’ in comparison [143]. Although other sensors such as HR monitors, skin temperature sensors or heat flux sensors were included in a number of experiments, their inclusion was found to decrease the accuracy of devices (compared to only measuring ‘steps’) due to poor algorithm relating the parameters to EE. The DLW technique was criticised due to only being able to give an overall EE, where as activity monitors can provide a day-by-day profile of PA. Each sensor in a multiple-sensor system can add inherent measurement error and thus the risk of technical failure can increase (in addition to potentially increasing inaccuracies). Plasqui et al. proposed that ‘activity recognition has great potential to improve the assessment of PA related health outcomes’ [143].

An intelligent device for EE and activity (IDEEA, Minisun, USA) was developed to estimate EE from 35 different postures and activities. Whybrow et al. compared the IDEEA to two experiments: 24 hour indirect calorimetry and 14 day DLW study [144]. In the study, Whybrow et al. found that not all activities could be identified, such as cycling. This activity was discounted, and it was found that EE was recorded as being 105 % of the values obtained from indirect calorimetry. The device was only able to identify 63 % of the controlled activities (e.g. lying on a bed, sitting or standing in different positions, etc.). If measured values for resting MR were input to the device (to replace the usual estimated values) for individuals, then the size of the EE overestimate was reduced, but was still noted as statistically significant.

Soric et al. studied whether the monitor was able to differentiate between lying while asleep or quiet wakefulness (in comparison to polysomnography and sleep patterns) [145]. The study concurred with the findings of Whybrow et al.; that the activity monitor showed ‘poor agreement’. The studies performed by Soric et al. were limited to laboratory based tests, with home tests required in the future. Pattern recognition has been proposed as a method of identifying activities and also data could be categorised based on previous knowledge [146]. Linear regression is a method widely adopted due to simplicity. A substantial problem is that one regression equation cannot cover all activities. A large number of equations would be required to cover all the types of activity (e.g. walking, jogging etc.), one equation would be suitable for certain activities, but severely underestimate others.

An important use for a device capable of accurate EE measurement would be in a clinical environment, perhaps in an ICU. PA would be unlikely to make a significant contribution to the EE of patients confined to bed (lying sedentary), but PA monitors would have the potential to track the progress of in- and out-patients. Examples of patients trialled with activity monitors include those diagnosed with conditions such as COPD (chronic pulmonary disease), osteoarthritis and diabetes (all in comparison with either DLW or breath analysis). Rabinovich et al. validated six activity monitors in the field (compared to the ‘gold standard’ DLW calorimetry technique), with each of 80 COPD patients wearing three or four of the six devices [147]. The study found that all of the activity monitors demonstrated a significant relationship with the activity EE compared to the DLW measurements. However, it was still suggested that the monitors should be used to assess the activities of patients in terms of the amount and/or intensity of the activity, with emphasis on the raw data, rather than relying on potentially inaccurate calculations. Of particular note is that COPD patients expend greater energy than healthy patients for a given task, due to poor mechanical efficiency. The study was limited to a small population (majority 61 of 80 patients were male, mean participant age 68 years). Furthermore, technical issues meant that 14 participants were excluded from the analysis (insufficient data recorded).

Hermann et al. studied subjects with osteoarthritis of the hip who wore a Sensewear Pro3 monitor (Fig. 2.12, Bodymedia, USA) and the data were compared against a portable indirect calorimeter [148]. Subjects with osteoarthritis, similar to COPD above, are likely to expend a greater amount of energy for a given activity, due to

functional impairment. A 2-hour protocol was implemented to simulate daily living (walking, sitting/standing, gardening). A large bias was recorded between activities (e.g. over-estimating walking activities by between 62 and 93 %, but under-estimating by -25 % when climbing stairs). The study raises concerns of using activity monitors, with problems including a large bias, which caused an overall overestimated of total EE by 72 %. Also the monitor used for the study was like a black box, so cannot easily be adapted (not dissimilar to other models). Technical problems again hindered the study, thus reducing the amount of data available for analysis.

The Sensewear armband was also tested by Machac et al., with similar findings [149]. The device was verified against DLW and mobile gas exchange calorimetry on 19 diabetic subjects. Walking on a level surface was found to be overestimated by 70 to 80 %; walking uphill was underestimated (all walking manoeuvres were performed on treadmill and not in a free-living environment). The armband was not sufficiently accurate for EE monitoring. Machac et al. stated that it would be less confusing to see steps walked instead of calculated EE, concurring with the suggestion of Rabinovich et al. [147].



Fig. 2.12 – Photograph of Sensewear armband and accompanying computer software, from [150].

The Sensewear armband was tested against 19 older adults by Mackey et al. [151]. An acceptable level of agreement was observed between the armband and measurements of total EE and EE due to activity taken by DLW and indirect calorimetry. A strength of the armband was noted as having heat-related sensors included, which helps to

assess the energy cost of non-ambulatory and low-intensity activities (that are difficult to detect with an accelerometer) which are common among older adults. Concern about the operation of the heat-flux and temperature sensors in the armband was raised by Heiermann et al. [152]; the sensors may not be beneficial to the measurements performed on older subjects, as age-related changes to the skin cause it to become thinner and drier (affecting the skin conductance measured by the device).

A study performed by Heiermann et al. assumed that the calculations performed by the software in the armband were invalid for the target study group of 49 volunteers aged 60 to 87 years. Heiermann et al. comment that resting EE error was only 1.9 % typically, compared to indirect calorimetry. It was concluded that additional studies were required to test the ability of the armband to predict EE in frail older individuals as well as in over- and under-weight older populations. A study of the Sensewear armband against the Actigraph (MTI, USA) and IDEEA by Welk et al. found that the equations used by the Sensewear device provided accurate indications of PA [119]. The tests were conducted with 30 college-aged participants in their ‘unique’ free living environment. The study was limited to a comparison between activity monitors, rather than comparing measurements against a verified calorimetry technique. The study found that the equations used in the devices were based on locomotor activities and thus were accurate for walking, but underestimated the energy cost of normal household activities by as much as 50 %. A further limitation of the study was the lack of routinely testing vigorous PA, where it was noted that only ‘one or two’ participants undertook any vigorous activity.

Moon and Butte reported on a study relating PA (vibration monitor) and HR to O₂ consumed and CO₂ produced, to meet the need for a cheaper and less intrusive means of EE assessment than expensive calorimetry techniques [153]. The relationship between O₂ consumption rates to HR is different between individuals, dependent on age, body composition and fitness. Moon and Butte found that classifying wake and sleep periods achieved an improved estimate of the volume of O₂ consumed. The range of errors in predicting day 5 awake volume of O₂ consumed was -10.6 to 4.6 % (16 % overall). Reclassifying points using HR alone, increased the mean error to 5.3 ± 8.6 %. Results confirmed the importance of calibrating O₂ consumption against HR for each individual. It was concluded that the precision of volumes of O₂ consumed and CO₂ produced improved by combining PA and HR monitoring.

2.5 Motivation for Developing Portable Breath Analyser

The motivation behind this project to develop a hand-held breath analyser is summarised below (non-exhaustive list of possible applications for the device). The summary below builds upon the aims (section 1.1) and considers the improvements required compared to the current generation of measurement equipment.

- Provide a means of determining EE for the general population to an acceptable clinical accuracy.
 - Create an accessible method of being able to determine EE, without limitations to specific study targets. Expense and complexity are barriers which hinder the use of calorimeters in medical care. A portable, affordable and simple to use device would promote the measurement of EE in general practice.
- Develop a miniature breath analyser using new sensor technology.
 - Recent developments in the sensors field offer new technology to miniaturise systems and improve performance. A breath analyser would benefit from these enhancements and demonstrate future applications for sensors.
- Promote awareness of obesity and how it can be prevented.
 - Obesity is globally becoming a major problem. Weight gain is difficult to self-diagnose and manage, and therefore can often be ignored. Being aware of the correct calorific intake during each day could help prevent the trend towards an overweight population.
- Improve upon the current generation of instruments for EE measurement.
 - At present, it is rare to find EE measurement equipment inside hospitals. The common portable units found in hospitals do not provide sufficient reliability or accuracy for clinical use.
- Investigate the components of EE and their inter-individual variance.
 - The proportion of total daily EE associated with each component varies between individuals. Meal type, frequency and content have an effect on the DIT component of daily EE. In particular this component is not well understood, and the effect of different food types could be

investigated with a device capable of quick and accurate measurement to determine slight changes in minute by minute EE.

2.6 References

- [1] B. Bissonnette, M. Functions, Pediatric Anesthesia, People's Medical Publishing House USA Limited (PMPH), Shelton, U.S., 2014.
- [2] L.M. Summerfield, Nutrition, Exercise, and Behavior: An Integrated Approach to Weight Management, 2nd Ed., Cengage Learning, Belmont, U.S., 2001.
- [3] D.A. Bender, Introduction to Nutrition and Metabolism, Fourth Edition, 4th Ed., CRC Press, Hoboken, U.S., 2007.
- [4] N. V Bhagavan, E. Metabolism, Medical Biochemistry, 4th Ed., Elsevier Science, San Diego, U.S., 2001.
- [5] G. Livesey, M. Elia, Estimation of energy expenditure, net carbohydrate utilization, and net fat oxidation and synthesis by indirect calorimetry: evaluation of errors with special reference to the detailed composition of fuels [published erratum appears in Am J Clin Nutr 1989, Am J Clin Nutr. 47 (1988) 608–628.
- [6] M.E. Shils, M. Shike, A. Tremblay, T. Proteins, Modern Nutrition in Health and Disease, Lippincott Williams & Wilkins, 2006.
- [7] M.M. Gottschlich, The Science and Practice of Nutrition Support: A Case-based Core Curriculum, Kendall Hunt, 2001.
- [8] M. Dunford, J. Doyle, Nutrition for Sport and Exercise, 2nd Ed., Cengage Learning, 2011.
- [9] R. Andersen, A.O. Questionnaire, Obesity: Etiology, Assessment, Treatment, and Prevention, Human Kinetics, 2003.
- [10] W.O. Atwater, F.G. Benedict, G.R. Libri, S. Uniti, G. Ricerca, L. La, A Respiration Calorimeter with Appliances for the Direct Determination of Oxygen, Carnegie Institution of Washington, Washington, U.S., 1905.
- [11] M.J. Dauncey, P.R. Murgatroyd, T.J. Cole, A human calorimeter for the direct and indirect measurement of 24 h energy expenditure., Br. J. Nutr. 39 (1978) 557–66. doi:10.1079/BJN19780071.
- [12] M.J. Dauncey, Metabolic effects of altering the 24 h energy intake in man, using direct and indirect calorimetry, Br. J. Nutr. 43 (1980) 257–269. doi:doi:10.1079/BJN19800089.
- [13] D. Brown, T.J. Cole, M.J. Dauncey, R.W. Marrs, P.R. Murgatroyd, Analysis of gaseous exchange in open-circuit indirect calorimetry, Med. Biol. Eng. Comput. 22 (1984) 333–338. doi:10.1093/jicru/ndm007.
- [14] W.J. Kraemer, S.J. Fleck, M.R. Deschenes, Exercise Physiology: Integrating Theory and Application, Wolters Kluwer Health/Lippincott Williams & Wilkins, Philadelphia, U.S., 2011.

-
- [15] K.Y. Chen, K.F. Janz, W. Zhu, R.J. Brychta, Redefining the roles of sensors in objective physical activity monitoring, *Med. Sci. Sports Exerc.* 44 (2012) S13-23. doi:10.1249/MSS.0b013e3182399bc8.
- [16] M. Noreik, M. Maurmann, V. Meier, I. Becker, G. Röhrig, M.C. Polidori, et al., Resting energy expenditure (REE) in an old-old population: implications for metabolic stress, *Exp. Gerontol.* 59 (2014) 47–50. doi:10.1016/j.exger.2014.06.009.
- [17] J.B. Weir, New methods for calculating metabolic rate with special reference to protein metabolism., *J. Physiol.* 109 (1949) 1–9.
- [18] C. Shilling, C. Carlston, R. Mathias, *The Physician's Guide to Diving Medicine*, Softcover, Springer US, New York, U.S., 2013.
- [19] E.E. Martinez, C.D. Smallwood, L.J. Bechard, R.J. Graham, N.M. Mehta, Metabolic assessment and individualized nutrition in children dependent on mechanical ventilation at home, *J. Pediatr.* 166 (2015) 350–357. doi:10.1016/j.jpeds.2014.09.036.
- [20] D.L. Swinamer, P.T. Phang, R.L. Jones, M. Grace, E.G. King, Twenty-four hour energy expenditure in critically ill patients, *Crit. Care Med.* 15 (1987) 637–43.
- [21] E. Ravussin, S. Lillioja, T.E. Anderson, L. Christin, C. Bogardus, Determinants of 24-hour energy expenditure in man. Methods and results using a respiratory chamber., *J. Clin. Invest.* 78 (1986) 1568–78. doi:10.1172/JCI112749.
- [22] J.V.G.A. Durnin, O.G. Edholm, D.S. Miller, J.C. Waterlow, How Much Food Does Man Require?, *Nutr. Today.* 9 (1974).
- [23] P.A. Tataranni, D.E. Larson, S. Snitker, E. Ravussin, Thermic effect of food in humans: methods and results from use of a respiratory chamber., *Am. J. Clin. Nutr.* 61 (1995) 1013–9.
- [24] K.R. Westerterp, Diet induced thermogenesis., *Nutr. Metab. (Lond).* 1 (2004) 5. doi:10.1186/1743-7075-1-5.
- [25] H. Ogata, F. Kobayashi, M. Hibi, S. Tanaka, K. Tokuyama, A novel approach to calculating the thermic effect of food in a metabolic chamber., *Physiol. Rep.* 4 (2016) e12717. doi:10.14814/phy2.12717.
- [26] Y. Schutz, T. Bessard, E. Jéquier, Diet-induced thermogenesis measured over a whole day in obese and nonobese women., *Am. J. Clin. Nutr.* 40 (1984) 542–52.
- [27] K.R. Westerterp, S.A.J. Wilson, V. Rolland, Diet induced thermogenesis measured over 24h in a respiration chamber: effect of diet composition, *Int. J. Obes.* 23 (1999) 287–292. doi:10.1038/sj.ijo.0800810.
- [28] J.L. Spencer, B.A. Zikria, J.M. Kinney, J.R. Broell, T.M. Michailoff, A.B. Lee, A system for continuous measurement of gas exchange and respiratory functions., *J. Appl. Physiol.* 33 (1972) 523–8.
- [29] A.E. Black, T.J. Cole, Within- and between-subject variation in energy expenditure measured by the doubly-labelled water technique: implications for

- validating reported dietary energy intake, *Eur. J. Clin. Nutr.* 54 (2000) 386–394. doi:10.1038/sj.ejcn.1600970.
- [30] J.L. Miles-Chan, D. Sarafian, J.P. Montani, Y. Schutz, A.G. Dulloo, Sitting comfortably versus lying down: is there really a difference in energy expenditure?, *Clin. Nutr.* 33 (2014) 175–8. doi:10.1016/j.clnu.2013.11.009.
- [31] M.L. Leff, J.O. Hill, A.A. Yates, G.A. Cotsonis, S.B. Heymsfield, Resting Metabolic Rate: Measurement Reliability, *JPEN. J. Parenter. Enteral Nutr.* 11 (1987) 354–359. doi:10.1177/0148607187011004354.
- [32] J.E. Blundell, J. Cooling, N.A. King, Differences in postprandial responses to fat and carbohydrate loads in habitual high and low fat consumers (phenotypes), *Br. J. Nutr.* 88 (2002) 125. doi:10.1079/BJN2002609.
- [33] E.J. Anderson, L.G. Sylvia, M. Lynch, L. Sonnenberg, H. Lee, D.M. Nathan, Comparison of energy assessment methods in overweight individuals., *J. Acad. Nutr. Diet.* 114 (2014) 273–8. doi:10.1016/j.jand.2013.07.008.
- [34] M. Marra, L. Scalfi, A. Covino, A.E.-D. Puente, F. Contaldo, Fasting respiratory quotient as a predictor of weight changes in non-obese women, *Int. J. Obes.* 22 (1998) 601–603. doi:10.1038/sj.ijo.0800612.
- [35] S.O. McDoniel, A Systematic Review on Use of a Handheld Indirect Calorimeter to Assess Energy Needs in Adults and Children, *Int. J. Sport Nutr. Exerc. Metab.* 17 (2010) 491–500.
- [36] D. Zhao, D. Miller, D. Shao, X. Xian, F. Tsow, R.A. Iglesias, et al., A personal device for analyzing carbon dioxide in real time and real breath: Experimental investigation and computational simulation, *Sensors Actuators B Chem.* 183 (2013) 627–635. doi:http://dx.doi.org/10.1016/j.snb.2013.03.138.
- [37] X. Xian, A. Quach, D. Bridgeman, F. Tsow, E. Forzani, N. Tao, et al., Personalized Indirect Calorimeter for Energy Expenditure (EE) Measurement, *Glob. J. Obesity, Diabetes Metab. Syndr.* 2 (2015) 4–8.
- [38] Breezing, Breezing Store, (2016). <http://store.breezing.com/> (accessed June 22, 2016).
- [39] R.S. Irwin, J.M. Rippe, *Irwin and Rippe's Intensive Care Medicine*, Lippincott Williams & Wilkins, Philadelphia, U.S., 2008.
- [40] D. Hess, N. MacIntyre, S. Mishoe, W. Galvin, *Respiratory Care: Principles and Practice*, Jones & Bartlett Learning, Sudbury, U.S., 2011.
- [41] J.W. Erdman, I.A. MacDonald, S.H. Zeisel, *Present Knowledge in Nutrition*, Wiley, Ames, U.S., 2012.
- [42] D.S. Wheeler, H.R. Wong, T.P. Shanley, *Pediatric Critical Care Medicine: Basic Science And Clinical Evidence*, Springer, 2007.
- [43] G.B. Forbes, *Human Body Composition: Growth, Aging, Nutrition, and Activity*, Springer New York, New York, U.S., 1987.
- [44] D.R. Tobergte, S. Curtis, H.C. Hemmings, P.M. Hopkins, *Foundations of Anesthesia: Basic Sciences for Clinical Practice*, Mosby Elsevier, Philadelphia,

- U.S., 2006. doi:10.1017/CBO9781107415324.004.
- [45] J.S. Garrow, W.P.T. James, *Human Nutrition and Dietetics*, 9th Ed., Churchill Livingstone, Edinburgh, U.K., 1993.
- [46] P. Insel, D. Ross, K. McMahon, M. Bernstein, *Nutrition*, Jones & Bartlett Learning, Burlington, U.S., 2010.
- [47] R.C. Schulman, J.I. Mechanick, Metabolic and nutrition support in the chronic critical illness syndrome., *Respir. Care.* 57 (2012) 958-77-8. doi:10.4187/respcare.01620.
- [48] F. Konstantinides, N. Konstantinides, J. Li, M. Myaya, F. Cerra, Urinary urea nitrogen: too insensitive for calculating nitrogen balance studies in surgical clinical nutrition, *J. Parenter. Enter. Nutr.* 15 (1991) 189-193. doi:10.1177/0148607191015002189.
- [49] W.C. Boyd, Error in Calibration of Commercial BMR Machines, *J Appl Physiol.* 6 (1954) 711-715.
- [50] J.A. McLean, G. Tobin, *Animal and Human Calorimetry*, Cambridge University Press, Cambridge, U.K., 2007.
- [51] M.M. Reeves, S. Capra, J. Bauer, P.S.W. Davies, D. Battistutta, Clinical accuracy of the MedGem indirect calorimeter for measuring resting energy expenditure in cancer patients., *Eur. J. Clin. Nutr.* 59 (2005) 603-10. doi:10.1038/sj.ejcn.1602114.
- [52] M.J. Koruda, J.L. Rombeau, Clinical studies of energy metabolism., *IEEE Eng. Med. Biol. Mag.* 5 (1986) 19-24. doi:10.1109/MEMB.1986.5006279.
- [53] L.E. MATARESE, Indirect Calorimetry, *J. Am. Diet. Assoc.* 97 (1997) S154-S160.
- [54] S. Bursztein, P. Saphar, P. Singer, D.H. Elwyn, A mathematical analysis of indirect calorimetry measurements in acutely ill patients., *Am. J. Clin. Nutr.* 50 (1989) 227-30.
- [55] R.A. Helms, D.J. Quan, *Textbook of Therapeutics: Drug and Disease Management*, Lippincott Williams & Wilkins, 2006.
- [56] D.C. Simonson, R. a DeFronzo, Indirect calorimetry: methodological and interpretative problems., *Am. J. Physiol.* 258 (1990) E399-412.
- [57] L. Cuppari, A.B. de Carvalho, C.M. Avesani, M.A. Kamimura, R.R. Dos Santos Lobão, S.A. Draibe, Increased resting energy expenditure in hemodialysis patients with severe hyperparathyroidism., *J. Am. Soc. Nephrol.* 15 (2004) 2933-9. doi:10.1097/01.ASN.0000141961.49723.BC.
- [58] N.M. Byrne, A.M. Groves, H.D. McIntyre, L.K. Callaway, Changes in resting and walking energy expenditure and walking speed during pregnancy in obese women., *Am. J. Clin. Nutr.* 94 (2011) 819-30. doi:10.3945/ajcn.110.009399.
- [59] L.G. Bandini, V.R. Young, Energy expenditure during carbohydrate in obese and nonobese adolescents, *Am. J. Physiol.* 256 (1989) 357-367.
- [60] C.L. Long, N. Schaffel, J.W. Geiger, W.R. Schiller, W.S. Blakemore,

- Metabolic Response to Injury and Illness: Estimation of Energy and Protein Needs from Indirect Calorimetry and Nitrogen Balance, *JPEN. J. Parenter. Enteral Nutr.* 3 (1979) 28. doi:10.1177/014860717900300609.
- [61] K.A. Davis, S.H. Rosenbaum, M.J. Mosier, R.L. Gamelli, *Surgical Metabolism: The Metabolic Care of the Surgical Patient*, Springer New York, New York, U.S., 2014.
- [62] Morrison's Health Care, *Manual Of Clinical Nutrition Management*, Sandy Springs, U.S., 2013.
- [63] T. Miller, *Modern Surgical Care: Physiologic Foundations and Clinical Applications*, CRC Press, New York, U.S., 2013.
- [64] F.R. Cerra, Review of branched-chain amino acid supplementation in trauma, in: *Adv. Clin. Nutr.*, Springer Netherlands, Dordrecht, 1983: pp. 51–64. doi:10.1007/978-94-011-5918-0_4.
- [65] H.A. Haugen, L.-N. Chan, F. Li, Indirect Calorimetry: A Practical Guide for Clinicians, *Nutr. Clin. Pract.* 22 (2007) 377–388. doi:10.1177/0115426507022004377.
- [66] K.M. Schlein, S.P. Coulter, Best Practices for Determining Resting Energy Expenditure in Critically Ill Adults, *Nutr. Clin. Pract.* (2013) 0884533613515002-. doi:10.1177/0884533613515002.
- [67] W.C. Wilson, C.M. Grande, D.B. Hoyt, *Trauma: Critical Care*, Taylor & Francis, New York, U.S., 2013.
- [68] L. a Hamamoto, a L. Cardoso, H.H. Marques, C. Gomes, [Energy balance in infants born from HIV seropositive mothers], *J. Pediatr. (Rio. J)*. 76 (2000) 119–24.
- [69] Britannica, Capillary, *Encycl. Br.* (2006). <https://www.britannica.com/science/capillary/images-videos> (accessed June 22, 2016).
- [70] W. Miekisch, J.K. Schubert, G.F. Noeldge-Schomburg, Diagnostic potential of breath analysis—focus on volatile organic compounds, *Clin. Chim. Acta.* 347 (2004) 25–39.
- [71] H.K. Wilson, Breath analysis. Physiological basis and sampling techniques., *Scand. J. Work. Environ. Health.* 12 (1986) 174–192. doi:10.5271/sjweh.2159.
- [72] I.W. Fellows, I.A. Macdonald, An automated method for the measurement of oxygen consumption and carbon dioxide excretion in man., *Clin. Phys. Physiol. Meas.* 6 (1985) 349–55. doi:10.1088/0143-0815/6/4/007.
- [73] K. Bhavani-Shankar, A.Y. Kumar, H.S.L. Moseley, R. Ahyee-Hallsworth, Terminology and the current limitations of time capnography: A brief review, *J. Clin. Monit.* 11 (1995) 175–182. doi:10.1007/BF01617719.
- [74] L. Wallace, T. Buckley, E. Pellizzari, S. Gordon, Breath measurements as volatile organic compound biomarkers, *Environ. Health Perspect.* 104 Suppl (1996) 861–9. doi:10.2307/3433003.

-
- [75] K.M. Dubowski, Breath analysis as a technique in clinical chemistry, *Clin. Chem.* 20 (1974) 966–972.
- [76] G.R. Kelman, Theoretical basis of alveolar sampling., *Br. J. Ind. Med.* 39 (1982) 259–64.
- [77] J.K. Schubert, K.-H. Spittler, G. Braun, K. Geiger, J. Guttman, CO₂-controlled sampling of alveolar gas in mechanically ventilated patients, *J. Appl. Physiol.* 90 (2001) 486–492.
- [78] H. Lord, Y. Yu, A. Segal, J. Pawliszyn, Breath Analysis and Monitoring by Membrane Extraction with Sorbent Interface, *Anal. Chem.* 74 (2002) 5650–5657. doi:10.1021/ac025863k.
- [79] D. Poli, P. Carbognani, M. Corradi, M. Goldoni, O. Acampa, B. Balbi, et al., Exhaled volatile organic compounds in patients with non-small cell lung cancer: cross sectional and nested short-term follow-up study., *Respir. Res.* 6 (2005) 71. doi:10.1186/1465-9921-6-71.
- [80] C. Turner, P. Španěl, D. Smith, A longitudinal study of ethanol and acetaldehyde in the exhaled breath of healthy volunteers using selected-ion flow-tube mass spectrometry, *Rapid Commun. Mass Spectrom.* 20 (2006) 61–68. doi:10.1002/rcm.2275.
- [81] W. Miekisch, S. Kischkel, A. Sawacki, T. Liebau, M. Mieth, J.K. Schubert, Impact of sampling procedures on the results of breath analysis., *J. Breath Res.* 2 (2008) 26007. doi:10.1088/1752-7155/2/2/026007.
- [82] V. Ma, H. Lord, M. Morley, J. Pawliszyn, Application of Membrane Extraction with Sorbent Interface for Breath Analysis, in: R.M. Uppu, S.N. Murthy, W.A. Pryor, N.L. Parinandi (Eds.), *Free Radicals Antioxid. Protoc. Methods Mol. Biol.* (Clifton, N.J.), Humana Press, Totowa, NJ, 2010: pp. 451–468. doi:10.1007/978-1-60327-029-8.
- [83] M.E. Dolch, L. Frey, C. Hornuss, M. Schmoelz, S. Praun, J. Villinger, et al., Molecular breath-gas analysis by online mass spectrometry in mechanically ventilated patients: a new software-based method of CO₂-controlled alveolar gas monitoring., *J. Breath Res.* 2 (2008) 37010. doi:10.1088/1752-7155/2/3/037010.
- [84] M. Phillips, Method for the Collection and Assay of Volatile Organic Compounds in Breath, *Anal. Biochem.* 247 (1997) 272–278.
- [85] M. Basanta, T. Koimtzis, D. Singh, I. Wilson, C.L.P. Thomas, An adaptive breath sampler for use with human subjects with an impaired respiratory function., *Analyst.* 132 (2007) 153–63. doi:10.1039/b608608j.
- [86] R. Hyšpler, Š. Crhová, J. Gasparič, Z. Zadák, M. Čížková, V. Balasová, Determination of isoprene in human expired breath using solid-phase microextraction and gas chromatography–mass spectrometry, *J. Chromatogr. B Biomed. Sci. Appl.* 739 (2000) 183–190.
- [87] M.A.E. Lärstad, K. Torén, B. Bake, A.-C. Olin, Determination of ethane, pentane and isoprene in exhaled air--effects of breath-holding, flow rate and purified air., *Acta Physiol. (Oxf).* 189 (2007) 87–98. doi:10.1111/j.1748-

1716.2006.01624.x.

- [88] P.O. Droz, M.P. Guillemin, Occupational exposure monitoring using breath analysis., *J. Occup. Med.* 28 (1986) 593–602.
- [89] J.S. Haldane, J.G. Priestley, The regulation of the lung-ventilation., *J. Physiol.* 32 (1905) 225–66.
- [90] J.B. West, P.H. Hackett, K.H. Maret, J.S. Milledge, J. Peters, R. M., C.J. Pizzo, et al., Pulmonary gas exchange on the summit of Mount Everest, *J. Appl. Physiol.* 55 (1983) 678–687.
- [91] D. Dyne, J. Cocker, H.K.K. Wilson, A novel device for capturing breath samples for solvent analysis., *Sci. Total Environ.* 199 (1997) 83–9.
- [92] M. Di Stefano, A. Strocchi, S. Malservisi, G. Veneto, A. Ferrieri, G.R. Corazza, Non-absorbable antibiotics for managing intestinal gas production and gas-related symptoms., *Aliment. Pharmacol. Ther.* 14 (2000) 1001–8. doi:10.1046/j.1365-2036.2000.00808.x.
- [93] A. Strocchi, C. Ellis, M.D. Levitt, Reproducibility of measurements of trace gas concentrations in expired air., *Gastroenterology.* 101 (1991) 175–9.
- [94] P.J. Franklin, S.W. Turner, R.C. Mutch, S.M. Stick, Comparison of single-breath and tidal breathing exhaled nitric oxide levels in infants, *Eur. Respir. J.* 23 (2004) 369–372. doi:10.1183/09031936.04.00084604.
- [95] J. Kwak, M. Fan, S. Harshman, C. Garrison, V. Dershem, J. Phillips, et al., Evaluation of Bio-VOC Sampler for Analysis of Volatile Organic Compoundss in Exhaled Breath, *Metabolites.* 4 (2014) 879–888. doi:10.3390/metabo4040879.
- [96] L.C.A. Amorim, Z. de L. Cardeal, Breath air analysis and its use as a biomarker in biological monitoring of occupational and environmental exposure to chemical agents, *J. Chromatogr. B.* 853 (2007) 1–9.
- [97] A. Bikov, K. Paschalaki, R. Logan-Sinclair, I. Horváth, S.A. Kharitonov, P.J. Barnes, et al., Standardised exhaled breath collection for the measurement of exhaled volatile organic compounds by proton transfer reaction mass spectrometry., *BMC Pulm. Med.* 13 (2013) 43. doi:10.1186/1471-2466-13-43.
- [98] J. Bates, G. Schmalisch, D. Filbrun, J. Stocks, Tidal breath analysis for infant pulmonary function testing. ERS/ATS Task Force on Standards for Infant Respiratory Function Testing. European Respiratory Society/American Thoracic Society, *Eur. Respir. J.* 16 (2000) 1180–1192.
- [99] P. Spaněl, D. Smith, On-line measurement of the absolute humidity of air, breath and liquid headspace samples by selected ion flow tube mass spectrometry., *Rapid Commun. Mass Spectrom.* 15 (2001) 563–9. doi:10.1002/rcm.265.
- [100] J. Herbig, T. Titzmann, J. Beauchamp, I. Kohl, A. Hansel, Buffered end-tidal (BET) sampling-a novel method for real-time breath-gas analysis., *J. Breath Res.* 2 (2008) 37008. doi:10.1088/1752-7155/2/3/037008.
- [101] G.M. Ljungkvist, R.G. Nordlinder, A field method for sampling benzene in

- end-exhaled air., *Am. Ind. Hyg. Assoc. J.* 56 (1995) 693–7. doi:10.1080/15428119591016719.
- [102] H. Vreman, D. Stevenson, W. Oh, A. Fanaroff, L. Wright, J. Lemons, et al., Semiportable electrochemical instrument for determining carbon monoxide in breath, *Clin. Chem.* 40 (1994) 1927–1933.
- [103] J.N. Han, K. Stegen, M. Cauberghe, K.P. Van de Woestijne, Influence of awareness of the recording of breathing on respiratory pattern in healthy humans., *Eur. Respir. J.* 10 (1997) 161–6.
- [104] K.A. Cope, M.T. Watson, W.M. Foster, S.S. Sehnert, T.H. Risby, Effects of ventilation on the collection of exhaled breath in humans., *J. Appl. Physiol.* 96 (2004) 1371–9. doi:10.1152/jappphysiol.01034.2003.
- [105] J. Askanazi, P.A. Silverberg, R.J. Foster, A.I. Hyman, J. Milic-Emili, J.M. Kinney, Effects of respiratory apparatus on breathing pattern, *J. Appl. Physiol.* 48 (1980) 577–580.
- [106] R. Gilbert, J.H. Auchincloss, J. Brodsky, W. Boden, Changes in tidal volume, frequency, and ventilation induced by their measurement., *J. Appl. Physiol.* 33 (1972) 252–4.
- [107] P.W. Brazis, J.C. Masdeu, J. Biller, *Localization in Clinical Neurology*, 6th Ed., Wolters Kluwer Health, Philadelphia, U.S., 2012.
- [108] E.M. Rath, G.K. Essick, Perioral somesthetic sensibility: Do the skin of the lower face and the midface exhibit comparable sensitivity?, *J. Oral Maxillofac. Surg.* 48 (1990) 1181–1190. doi:10.1016/0278-2391(90)90534-9.
- [109] J.A. Hirsch, B. Bishop, Human breathing patterns on mouthpiece or face mask during air, CO₂, or low O₂, *J. Appl. Physiol.* 53 (1982) 1281–90.
- [110] W. Perez, M.J. Tobin, Separation of factors responsible for change in breathing pattern induced by instrumentation., *J. Appl. Physiol.* 59 (1985) 1515–20.
- [111] P.J. Western, J.M. Patrick, Effects of focusing attention on breathing with and without apparatus on the face, *Respir. Physiol.* 72 (1988) 123–130. doi:10.1016/0034-5687(88)90084-9.
- [112] S.A. Shea, J. Walter, C. Pelley, K. Murphy, A. Guz, The effect of visual and auditory stimuli upon resting ventilation in man, *Respir. Physiol.* 68 (1987) 345–357. doi:10.1016/S0034-5687(87)80019-1.
- [113] M.J. Mador, M.J. Tobin, Effect of alterations in mental activity on the breathing pattern in healthy subjects., *Am. Rev. Respir. Dis.* 144 (1991) 481–7. doi:10.1164/ajrccm/144.3_Pt_1.481.
- [114] A. Guz, Brain, breathing and breathlessness, *Respir. Physiol.* 109 (1997) 197–204. doi:10.1016/S0034-5687(97)00050-9.
- [115] W. St.-John, Neurogenesis of patterns of automatic ventilatory activity, *Prog. Neurobiol.* 56 (1998) 97–117. doi:10.1016/S0301-0082(98)00031-8.
- [116] E. Ullmann, The Two Original Papers by Hering and Breuer Submitted by Hering to the K.K. Akademie Der Wissenschaften Zu Wien in 1868, in: *Ciba*

- Found. Symp. - Breath. Hering-Breuer Centen. Symp., John Wiley & Sons, Ltd., London, U.K., 1970: pp. 357–394. doi:10.1002/9780470715352.ch20.
- [117] M. Mostafa-Gharehbaghi, A. Peirovifar, B. Karimi, Comparing the Efficacy of Face Mask CPAP with Nasopharyngeal CPAP for Neonatal Transport after Delivery, *2. 15* (2013) 31–34.
- [118] M. Robin, *A Physiological Handbook for Teachers of Yogasana*, Fenestra Books, Tucson, U.S., 2002.
- [119] G.J. Welk, J.J. McClain, J.C. Eisenmann, E.E. Wickel, Field validation of the MTI Actigraph and BodyMedia armband monitor using the IDEEA monitor, *Obesity (Silver Spring). 15* (2007) 918–28. doi:10.1038/oby.2007.624.
- [120] J. Speakman, The history and theory of the doubly labeled water technique, *Am J Clin Nutr. 68* (1998) 932S–938.
- [121] M.S. Buchowski, Doubly labeled water is a validated and verified reference standard in nutrition research., *J. Nutr. 144* (2014) 573–4. doi:10.3945/jn.114.191361.
- [122] A. Kroke, K. Klipstein-Grobusch, S. Voss, J. Moseneder, F. Thielecke, R. Noack, et al., Validation of a self-administered food-frequency questionnaire administered in the European Prospective Investigation into Cancer and Nutrition (EPIC) Study: comparison of energy, protein, and macronutrient intakes estimated with the doubly labeled water, *Am. J. Clin. Nutr. 70* (1999) 439–47.
- [123] A.E. Black, S.A. Bingham, G. Johansson, W.A. Coward, Validation of dietary intakes of protein and energy against 24 hour urinary N and DLW energy expenditure in middle-aged women, retired men and post-obese subjects: comparisons with validation against presumed energy requirements, *Eur. J. Clin. Nutr. 51* (1997) 405–413. doi:10.1038/sj.ejcn.1600425.
- [124] R.J. Hill, P.S.W. Davies, The validity of self-reported energy intake as determined using the doubly labelled water technique, *Br. J. Nutr. 85* (2001) 415. doi:10.1079/BJN2000281.
- [125] W.W. Wong, S.B. Roberts, S.B. Racette, S.K. Das, L.M. Redman, J. Rochon, et al., The doubly labeled water method produces highly reproducible longitudinal results in nutrition studies., *J. Nutr. 144* (2014) 777–83. doi:10.3945/jn.113.187823.
- [126] A. Subramaniam, M. McPhee, R. Nagappan, Predicting energy expenditure in sepsis: Harris-Benedict and Schofield equations versus the Weir derivation., *Crit. Care Resusc. 14* (2012) 202–10.
- [127] J.A. Harris, F.G. Benedict, A Biometric Study of Human Basal Metabolism., *Proc. Natl. Acad. Sci. U. S. A. 4* (1918) 370–3.
- [128] D.C. Frankenfield, E.R. Muth, W.A. Rowe, The Harris-Benedict studies of human basal metabolism: history and limitations., *J. Am. Diet. Assoc. 98* (1998) 439–45. doi:10.1016/S0002-8223(98)00100-X.
- [129] J.M. Daly, S.B. Heymsfield, C. a Head, L.P. Harvey, D.W. Nixon, H. Katzeff, et al., Human energy requirements: overestimation by widely used prediction

- equation., *Am. J. Clin. Nutr.* 42 (1985) 1170–4.
- [130] P.J.M. Weijs, H.M. Kruizenga, A.E. van Dijk, B.S. van der Meij, J. a E. Langius, D.L. Knol, et al., Validation of predictive equations for resting energy expenditure in adult outpatients and inpatients., *Clin. Nutr.* 27 (2008) 150–7. doi:10.1016/j.clnu.2007.09.001.
- [131] FAO/WHO/UNU, Energy and protein requirements. Report of a joint FAO/WHO/UNU Expert Consultation., World Health Organ. Tech. Rep. Ser. 724 (1985) 1–206.
- [132] M.D. Mifflin, S.T. St Jeor, L.A. Hill, B.J. Scott, S. a Daugherty, Y.O. Koh, A new predictive equation for resting energy expenditure in healthy individuals., *Am. J. Clin. Nutr.* . 51 (1990) 241–247.
- [133] J. Boullata, J. Williams, F. Cottrell, L. Hudson, C. Compher, Accurate determination of energy needs in hospitalized patients., *J. Am. Diet. Assoc.* 107 (2007) 393–401. doi:10.1016/j.jada.2006.12.014.
- [134] S.T. Henes, D.M. Cummings, R.C. Hickner, J.A. Houmard, K.M. Kolasa, S. Lazorick, et al., Comparison of predictive equations and measured resting energy expenditure among obese youth attending a pediatric healthy weight clinic: one size does not fit all., *Nutr. Clin. Pract.* 28 (2013) 617–24. doi:10.1177/0884533613497237.
- [135] K. Charlot, J. Cornolo, R. Borne, J.V. Brugniaux, J.-P. Richalet, D. Chapelot, et al., Improvement of energy expenditure prediction from heart rate during running., *Physiol. Meas.* 35 (2014) 253–66. doi:10.1088/0967-3334/35/2/253.
- [136] J. Driskell, I. Wolinsky, *Sports Nutrition: Energy Metabolism and Exercise*, 2nd Ed., CRC Press, Boca Raton, U.S., 2007.
- [137] G.B. Spurr, A.M. Prentice, P. Murgatroyd, G. Goldberg, J.C. Reina, N. Christman, Energy expenditure from minute-by-minute heart-rate recording: comparison with indirect calorimetry, *Am J Clin Nutr.* 48 (1988) 552–559.
- [138] G. Lusk, ANIMAL CALORIMETRY. Twenty-Fourth Paper ANALYSIS OF THE OXIDATION OF MIXTURES OF CARBOHYDRATE AND FAT, *J. Biol. Chem.* 59 (1924) 41–42.
- [139] M. Livingstone, A. Prentice, W. Coward, S. Ceesay, J. Strain, P. McKenna, et al., Simultaneous measurement of free-living energy expenditure by the doubly labeled water method and heart-rate monitoring, *Am. J. Clin. Nutr.* 52 (1990) 59–65.
- [140] S.M. Ceesay, A.M. Prentice, K.C. Day, P.R. Murgatroyd, G.R. Goldberg, W. Scott, et al., The use of heart rate monitoring in the estimation of energy expenditure: a validation study using indirect whole-body calorimetry, *Br. J. Nutr.* 61 (1989) 175. doi:10.1079/BJN19890107.
- [141] M. Blackburn, D. Calloway, Heart rate and energy expenditure of pregnant and lactating women, *Am. J. Clin. Nutr.* 42 (1985) 1161–1169.
- [142] W.R. Leonard, Measuring human energy expenditure: what have we learned from the flex-heart rate method?, *Am. J. Hum. Biol.* 15 (2003) 479–89. doi:10.1002/ajhb.10187.

-
- [143] G. Plasqui, A.G. Bonomi, K.R. Westerterp, Daily physical activity assessment with accelerometers: new insights and validation studies., *Obes. Rev.* 14 (2013) 451–62. doi:10.1111/obr.12021.
- [144] S. Whybrow, P. Ritz, G.W. Horgan, R.J. Stubbs, An evaluation of the IDEEA™ activity monitor for estimating energy expenditure., *Br. J. Nutr.* 109 (2013) 173–83. doi:10.1017/S0007114512000645.
- [145] M. Soric, M. Turkalj, D. Kucic, I. Marusic, D. Plavec, M. Misigoj-Durakovic, Validation of a multi-sensor activity monitor for assessing sleep in children and adolescents., *Sleep Med.* 14 (2013) 201–5. doi:10.1016/j.sleep.2012.11.003.
- [146] D.R. Bassett, A. Rowlands, S.G. Trost, Calibration and validation of wearable monitors., *Med. Sci. Sports Exerc.* 44 (2012) S32–8. doi:10.1249/MSS.0b013e3182399cf7.
- [147] R.A. Rabinovich, Z. Louvaris, Y. Raste, D. Langer, H. Van Remoortel, S. Giavedoni, et al., Validity of physical activity monitors during daily life in patients with COPD., *Eur. Respir. J.* 42 (2013) 1205–15. doi:10.1183/09031936.00134312.
- [148] A. Hermann, M. Ried-Larsen, A.K. Jensen, R. Holst, L.B. Andersen, S. Overgaard, et al., Low validity of the Sensewear Pro3 activity monitor compared to indirect calorimetry during simulated free living in patients with osteoarthritis of the hip., *BMC Musculoskelet. Disord.* 15 (2014) 43. doi:10.1186/1471-2474-15-43.
- [149] S. Macháč, M. Procházka, J. Radvanský, K. Slabý, Validation of physical activity monitors in individuals with diabetes: energy expenditure estimation by the multisensor SenseWear Armband Pro3 and the step counter Omron HJ-720 against indirect calorimetry during walking., *Diabetes Technol. Ther.* 15 (2013) 413–8. doi:10.1089/dia.2012.0235.
- [150] A. Cranny, A. Beriain, H. Solar, G. Tartarisco, G. Pioggia, Vital Sign Sensing Technology, in: *Syst. Des. Remote Healthc.*, Springer New York, New York, U.S., 2013: p. 81.
- [151] D.C. Mackey, T.M. Manini, D.A. Schoeller, A. Koster, N.W. Glynn, B.H. Goodpaster, et al., Validation of an armband to measure daily energy expenditure in older adults., *J. Gerontol. A. Biol. Sci. Med. Sci.* 66 (2011) 1108–13. doi:10.1093/gerona/qlr101.
- [152] S. Heiermann, K. Khalaj Hedayati, M.J. Müller, M. Dittmar, Accuracy of a Portable Multisensor Body Monitor for Predicting Resting Energy Expenditure in Older People: A Comparison with Indirect Calorimetry, *Gerontology.* 57 (2011) 473–479. doi:10.1159/000322109.
- [153] J.K. Moon, N.F. Butte, Combined heart rate and activity improve estimates of oxygen consumption and carbon dioxide production rates., *J. Appl. Physiol.* 81 (1996) 1754–61.

CHAPTER III

Gas Sensors for Breath Analysis

Preface

Breath-by-breath measurement of gas concentration presents numerous challenges for traditional gas sensors. To measure the gas concentration of an exhaled breath the sensors need to respond within the short time frame of an exhalation, perhaps over less than two seconds. The high level of humidity in a breath can also affect sensor response as well as the increase in temperature from ambient to breath. The Weir equation (2.4) discussed in chapter II relates the volume of carbon dioxide produced and oxygen consumed to energy requirements. For comprehensive breath measurements of energy expenditure sensors for both gases are required. For further analysis of metabolism and health, volatile organic compounds are of interest. These compounds have been reported to aid the diagnosis of diseases. Various compounds, such as acetone, have also been linked to diabetes. Measurement or identification of an abnormal level of these compounds could present further information to help understand human metabolism. In this chapter gas sensors are discussed with focus on their use in breath analysis.

3 Gas Sensor Specification

The breath analyser to be developed must be capable of analysing gas directly sampled from human exhalation, ideally without storage or external conditioning. The gas sensors incorporated in the design must be able to measure a range of gas concentrations, as found in exhaled breath. Table 3.1 lists the approximate range of gas concentrations that the sensors must be able to detect, given the concentrations expected in ambient (inhaled) air and exhaled breath.

Table 3.1 – Gases found in exhaled breath and concentration range.

Measurand	Typical Conditions of Exhaled Breath		Typical Conditions Inhaled Air	
Oxygen	16 – 17 %	[1,2]	20.9 %	[3,4]
Carbon Dioxide	4 – 5 %	[5]	0.035 %	[6–8]
Temperature	32 – 36 °C	[9,10]	18 – 22 °C room	[11]
			UK outside average 4 to 18 °C	[12]
Relative Humidity	< 100 %	[13]	40 – 65 % room	[14]
			Extreme levels from possible from 35 to 85 %	[15,16]
Flow Velocity	6 – 7 L/min (resting)	[17–19]	N.A.	-
	< 100 L/min (exercising)			
Carbon Monoxide	0 – 40+ ppm (non-regular-smoker)	[20–22]	0 – 2 ppm	[23]
	0 – 50 ppb (normal)	[24]		
Ethanol	180+ ppm (UK driving limit)	[25]	0 – 1 ppb	[27,28]
		[26]		

The global concern with regards to air pollution has led to more interest in air quality monitoring sensors. These devices are usually unsuitable for use in breath analysers, which require a different concentration range to be detected and a fast response time is not critical. Gas sensors are not usually impervious to the conditions found in exhaled breath. For example, the elevated level of relative humidity (RH) associated with an exhalation can block the mechanisms reacting inside various types of gas sensors and suppress any response to a change in gas concentration (alternatively the gas sensor can show a high response to humidity rather than the measurand).

Furthermore, the time available for the gas sensors to respond to a change in gas concentration is much lower when measurements are taken on a breath-by-breath basis. Ideally a gas sensor unit would be able to sample and measure gas immediately after an exhalation is provided. This would enable a miniature low-cost device, where no samples need to be stored, nor any bulky system needed to divert a portion of the flow for measurement. The flow rates during an exhalation are significant compared to ambient conditions, which can further disrupt sensor performance. The variables found in exhaled breath that could disrupt sensor performance are listed in Table 3.2.

Table 3.2 – Conditions found on exhaled breath compared to ambient air conditions.

Parameter	Ambient Air Condition	Exhaled Breath Condition
Flow Rate	N.A.	~6.7 L/min average exhaling
Contaminants	Air pollutants, e.g. CO, NO or hydrocarbons	VOCs, ethanol (alcohol), CO (smokers)
Flow Quality	Atmospheric conditions (minimal)	Normally laminar (Re 1600 to 2000 [29]), potentially turbulent (Re 2697+ [30])
Pressure	Atmospheric pressure	Pressure difference from lungs and required to exhale through device
Dust and Dirt	Minimal level of dust and dirt in rooms (higher levels possible in some environments)	Particles of food, saliva and oral content could be present

The elevated temperature of exhaled breath, combined with the level of RH, can cause water droplets to condense in any container (at ambient temperature) that captures an exhalation. Although the temperature of an exhalation is slightly below body temperature, it is still likely to be above room (or ambient) temperature and thus there is a risk of condensation. The effect of temperature variation in the ambient environment is not likely to cause substantial drift (even for devices sensitive to temperature), as variance of less than 10 °C would be expected for room conditions. Room temperatures could peak at 30 °C [31]. The minimum workplace temperature is specified as 13 °C (Health and Safety Executive [32]) when physical work is involved. If the device is used outdoors, the temperature variance is pronounced between seasons (e.g. the UK average outdoor temperature is ~4 °C in January compared to 18 °C in July) but stability is not a cause for concern over short measurement periods. The body uses breath as one means of expelling water, thus it can be almost 100 % humid, compared to ambient conditions of approximately half this level, the affect of humidity variation could be prominent enough to effect sensor response. In the UK (London for example), humidity extremes could be as low as 35 % in summer [15] or as high as 85 % (or higher) in winter [16].

A typical adult has a tidal volume of 0.5 litres [33–37]. The ratio of time spent inhaling to exhaling is typically 1:3 [38]. Therefore, assuming a 6 second breath cycle (respiratory period 10 breaths per minute), the average flow rate of exhaled breath would be 6.66 L/min. This assumes the flow rate is constant throughout the exhalation phase; however an exponential decay is expected during an exhalation. The flow rate at the end of expiring (alveoli gases from previous chapter) will perhaps be a factor of 5 lower than the peak level. A graph of the exponential decrease in exhaled flow rate is shown in Fig. 3.1; the peak flow rate for an exhalation is approximately 30 L/sec.

A breath analyser system must be capable of functioning in an environment that has a lot of pollution. For example, in a city urban environment (with vehicles etc.) potential pollutants could include nitric oxide (NO), hydrocarbons and carbon monoxide (CO) [39]. It is usual for sensors to be immune to cross-sensitivity for some gases and compounds, however there is a risk of such particles poisoning the sensor or contaminating the sensor surface which could reduce the performance of the device.

In the UK, air quality bandings state a moderate level of CO is in the range of 10 to 11.5 ppm [40] (and levels are commonly between 0 to 2 ppm [23]).

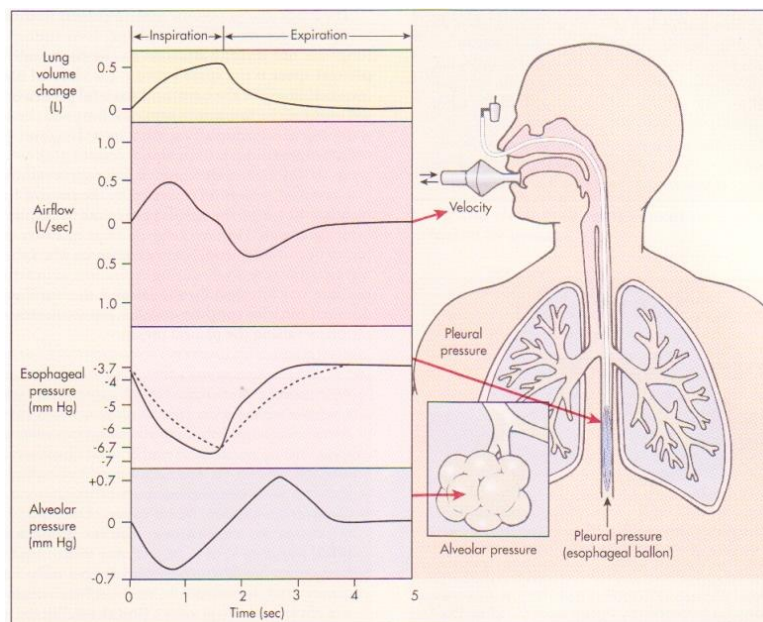


Fig. 3.1 – Relationship between the lung volume, airflow, esophageal pressure and alveolar pressure for an adult human male (normal tidal breath at a rate of 12 breaths per min) [41].

VOCs in exhaled breath are possible sources of interference for cross-sensitive devices. Behaviour such as smoking or consuming alcohol could increase the level of CO or ethanol found in exhaled breath. VOCs such as NO and acetone can indicate the presence of diseases (e.g. lung cancer), but are only present in very low concentrations [42]. Smokers increase the concentration of CO found in breath by up to 40+ ppm (from ~0 ppm for control subjects) [20,21,43]. Alcohol consumption can increase the level of ethanol in breath, from a baseline of 0 ppm to an excess of 180 ppm (the current UK driving limit) [26,44].

The flow of exhaled air from the lungs and out of the mouth or nose is usually laminar, in most conditions of calm exhaling. If air is exhaled at a fast rate (e.g. heavy breathing) the flow could become turbulent. Typically, a healthy adult breath flows through the trachea with a Reynolds (Re) number between 1600 and 2000 [29]. Zhao et al. report on simulations of exhaled levels of CO₂ through a sampling tube used to analyse breath [30]. Reynolds numbers of 2697 and 4495 were reported for flows of 6 and 10 L/min, respectively. It is generally reported a laminar flow is indicated by Re

<2300 and turbulent indicated by $Re > 4000$ (transient $2300 < Re < 4000$) [45]. While exhaling, the lungs are at a higher pressure than atmospheric (by around 2 to 3 mmHG [46]). Amitrano and Tortora report an ambient pressure of 760 mmHg with pressure in the alveoli around 762 mmHg [47]. Additionally, a pressure drop may be caused by the sensor chamber. Zhao et al. report a relatively small change was measured as a result of adding a sensor chamber [30].

In most cases clean ambient air does not contain a significant level of dirt or dust particles to damage gas sensors. In large quantities, such particles could block the sensor inlets, although the likelihood of external elements being forced into the sensor chamber is unlikely, when there is little to no flow in ambient conditions. A subject exhaling into a device has greater potential to bestow unwanted dirt in the sensor chamber, with high flow rates (in excess of 30 L per minute) possible. Exhaled breath can often contain oral content, saliva [48] or food fragments [49]. Such matter could block up either the sensors themselves or the sample tubing. The flow rate and frequency of breathing can be influenced by wearing a mask or mouthpiece/nose-clip as discussed in chapter II.

3.1 Sensitivity Analysis

The target of this project is to develop a portable breath analyser to measure a 1 % change in EE, which was chosen as tolerance acceptable for the data to be clinically useful. The abbreviated Weir equation (2.4) uses the volume of O_2 consumed and CO_2 produced to calculate EE. The aim of the work in this section is to calculate the relative accuracy to which the O_2 and CO_2 gas sensors must be able to measure their respective target gas to meet the 1 % target EE measurement.

The data from six subjects (subject information presented in Table 2.3) was obtained from the University Hospital Coventry and Warwickshire NHS Trust (respiratory room data). The data is presented in Tables 3.3 and 3.4 for the 6 subjects (6 EE readings are taken for each subject). The calculated metabolic rate shown in Table 3.3 assumes a variable breathing rate of either 10, 30 or 6 breaths per minute for normal (sitting), exercise (high exertion) and sleeping (overnight), respectively. The metabolic rate data shown in Table 3.4 assumes a constant breathing rate.

Concentrations of O₂ and CO₂ were measured in the chamber and averaged over 30 minute periods. From the minute values of O₂ and CO₂ the exhaled volumes of each gas are converted into a volume per breath. The ambient inhaled air conditions were assumed to contain 20.9 % O₂ and 0.035 % CO₂.

The measurement error in the gas concentration data from the chamber (α) can be calculated using the target metabolic rate error (1 %), the actual recorded metabolic rate and the volumes of O₂ and CO₂ exhaled (ml/min) using equation (3.1). The exhaled volumes of O₂ and CO₂ were provided from the hospital, although are not presented here.

$$\alpha = \frac{BMR_{calc} \times [Error \%]}{\{\sqrt{(3.9 \times [O_2 \text{ error per min}])^2 + (1.1 \times [CO_2 \text{ error per min}])^2}\}} \quad (3.1)$$

Using α , the absolute gas volume errors per minute can be calculated (i.e. multiply the volume of each gas inhaled/exhaled per minute by α). This can then expressed as an error per breath (from the given respiratory rate) and the error in gas concentration (from given tidal volume).

Finally, the error in the gas concentration can be compared to the gas concentration measured in exhaled breath, giving a percentage value for relative sensitivity. This is the accuracy that the sensors must perform within (when measuring inhaled and exhaled gas concentrations) to enable the metabolic rate to be calculated to within a 1 % tolerance.

The O₂ and CO₂ data in Table 3.3 show the average accuracy required by the O₂ and CO₂ sensors is 0.52 % and 1.20 % respectively (in order to measure EE to a 1 % tolerance). The data in Table 3.4 (fixed respiratory rate) show the sensors need to measure to an accuracy of 0.61 % and 1.20 % for O₂ and CO₂, respectively.

Table 3.3 – Subject data metabolic rate error and required sensor sensitivity (varying respiratory rate between 6 and 30 breaths per minute).

Subject	Value (Rate of Respiratory)	Metabolic Rate [kcal/min]	α (Error) [%]	O ₂ Relative Sensitivity [%]	CO ₂ Relative Sensitivity [%]
MF58	Min EE (6)	0.790	1.19	0.46	1.18
	Mean EE (10)	1.159	1.20	0.38	1.19
	Max EE (10)	1.355	1.20	0.47	1.19
BMI: 22.56	Sleep (6)	0.900	1.21	0.55	1.20
	Sedentary (10)	1.051	1.20	0.34	1.19
	2 nd Peak EE (10)	1.400	1.19	0.50	1.18
MF57	Min EE (6)	1.031	1.20	0.54	1.19
	Mean EE (10)	1.400	1.20	0.40	1.19
	Max EE (10)	1.928	1.20	0.64	1.19
BMI: 25.47	Sleep (6)	1.089	1.20	0.58	1.19
	Sedentary (10)	1.468	1.20	0.43	1.19
	2 nd Peak EE (10)	1.697	1.21	0.52	1.20
S243	Min EE (6)	1.299	1.21	0.56	1.20
	Mean EE (10)	1.957	1.21	0.48	1.20
	Max EE (30)	4.244	1.22	0.31	1.20
BMI: 25.79	Sleep (6)	1.417	1.21	0.64	1.20
	Sedentary (10)	1.893	1.22	0.46	1.21
	2 nd Peak EE (30)	3.987	1.22	0.29	1.20
S253	Min EE (6)	1.090	1.21	0.58	1.20
	Mean EE (10)	2.423	1.40	0.60	1.40
	Max EE (30)	5.297	1.21	0.55	1.20
BMI: 24.12	Sleep (6)	1.175	1.19	0.65	1.18
	Sedentary (10)	1.617	1.21	0.49	1.20
	2 nd Peak EE (10)	4.305	1.21	0.41	1.20
Stan 1	Min EE (6)	1.048	1.21	0.55	1.20
	Mean EE (10)	1.482	1.21	0.44	1.20
	Max EE (10)	2.622	1.20	1.08	1.20
BMI: 22.54	Sleep (6)	1.173	1.20	0.66	1.19
	Sedentary (10)	1.560	1.21	0.47	1.20
	2 nd Peak EE (10)	2.514	1.21	0.99	1.21
Stan2 BMI: 28.08	Min EE (6)	1.045	1.22	0.42	1.21
	Mean EE (10)	1.454	1.21	0.33	1.20
	Max EE (10)	2.101	1.21	0.55	1.20
	Sleep (6)	1.197	1.20	0.51	1.19
	Sedentary (10)	1.639	1.20	0.39	1.19
	2 nd Peak EE (10)	1.823	1.20	0.45	1.19

Table 3.4 - Subject data metabolic rate error and required sensor sensitivity (constant respiratory rate of 10 breaths per minute).

Subject	Value	Metabolic Rate [kcal/min]	α (Error) [%]	O ₂ Relative Sensitivity [%]	CO ₂ Relative Sensitivity [%]
MF58	Min EE	0.790	1.19	0.24	1.17
	Mean EE	1.159	1.20	0.38	1.19
	Max EE	1.355	1.20	0.47	1.19
	Sleep	0.900	1.21	0.28	1.19
	Sedentary	1.051	1.20	0.34	1.19
	2 nd Peak EE	1.400	1.19	0.50	1.18
MF57	Min EE	1.031	1.20	0.27	1.19
	Mean EE	1.400	1.20	0.40	1.19
	Max EE	1.928	1.20	0.64	1.19
	Sleep	1.089	1.20	0.29	1.18
	Sedentary	1.468	1.20	0.43	1.19
	2 nd Peak EE	1.697	1.21	0.52	1.20
S243	Min EE	1.299	1.21	0.28	1.19
	Mean EE	1.957	1.21	0.48	1.20
	Max EE	4.244	1.22	1.96	1.21
	Sleep	1.417	1.21	0.32	1.20
	Sedentary	1.893	1.22	0.46	1.21
	2 nd Peak EE	3.987	1.22	1.67	1.21
S253	Min EE	1.090	1.21	0.29	1.19
	Mean EE	2.423	1.40	0.60	1.40
	Max EE	5.297	1.21	17.50	1.21
	Sleep	1.175	1.19	0.32	1.18
	Sedentary	1.617	1.21	0.49	1.20
	2 nd Peak EE	4.305	1.21	3.83	1.21
Stan 1	Min EE	1.048	1.21	0.28	1.19
	Mean EE	1.482	1.21	0.44	1.20
	Max EE	2.622	1.20	1.08	1.20
	Sleep	1.173	1.20	0.32	1.18
	Sedentary	1.560	1.21	0.47	1.20
	2 nd Peak EE	2.514	1.21	0.99	1.21
Stan2	Min EE	1.045	1.22	0.22	1.20
	Mean EE	1.454	1.21	0.33	1.20
	Max EE	2.101	1.21	0.55	1.20
	Sleep	1.197	1.20	0.26	1.19
	Sedentary	1.639	1.20	0.39	1.19
	2 nd Peak EE	1.823	1.20	0.45	1.19

The histograms shown in Fig. 3.2 demonstrate the spread of the sensitivity data (36 samples per histogram, consisting of 6 subjects and 6 error calculations per subject). The data is taken from the sensitivity values calculated in Tables 3.3 and 3.4. The relative sensitivity is the accuracy to which the sensor must be able to measure the gas concentration.

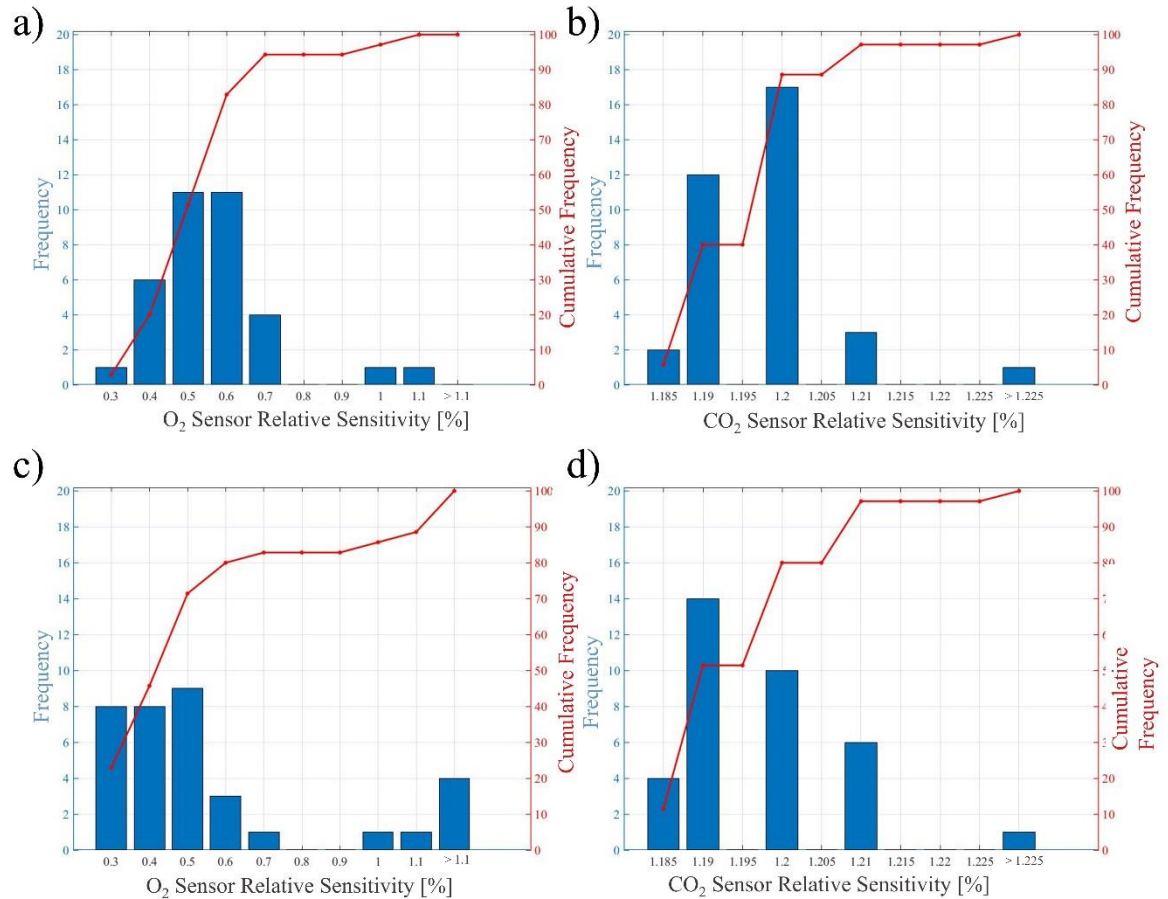


Fig. 3.2 – Histograms showing the sensor relative sensitivity required for 1 % EE calculation for O₂ and CO₂; a) and b) with three respiratory rates; c) and d) with fixed respiratory rate.

The histograms plots allow a clear overview of the required sensitivity and provide a simple means to determine the target sensor accuracy. For example, from the data shown in Fig. 3.2 a) it can be seen the O₂ sensor must have a relative accuracy of 0.5 %. There are 2 data points (which represent 2 EE calculations shown in Table 3.3) for which a sensor with an accuracy of 1 % O₂ concentration would be sufficient to calculate EE to the target 1 % accuracy. A sensor that can measure O₂ to 0.6 % accuracy would be sufficient for 18 samples. A sensor that has a 0.5 % accuracy would

be sufficient to calculate EE for 29 samples (the remaining 7 samples need a sensor of higher accuracy).

From Figs. 3.2 a) and b), when varying the respiratory rates for exercise, sleep and sedentary values, the O₂ sensor requires a relative sensitivity of lower than 0.60 % and the CO₂ sensor requires lower than 1.20 %. When a fixed respiratory rate is assumed, the O₂ and CO₂ sensitivity levels are not changed (0.60 % and 1.20% are sufficient), as shown in Figs. 3.2 c) and d).

3.2 Oxygen Gas Sensors

A number of techniques have emerged to measure O₂ concentrations, including galvanic (often referred to as low-temperature electrochemical), partial pressure, zirconia and paramagnetic [50]. As noted in Table 3.1, the O₂ content between inhaled and exhaled air varies by approximately 4 to 5 %. Sensors based on infrared (IR) principles cannot be used as O₂ is not absorbed by IR radiation [51]. Homonuclear diatomic molecules (such as O₂, N₂ etc.) cannot absorb IR radiation as they do not have the necessary dipole allowed vibrational rotational moments [52]. Diatomic molecules made up of different atoms have vibrational movement that absorbs radiation in the IR range [53].

3.2.1 Ambient Temperature Electrochemical Sensors

The principle of a galvanic cell is the generation of a current between two dissimilar electrodes due to chemical reactions occurring inside the cell [54]. The electrodes are immersed in an aqueous electrolyte (e.g. potassium hydroxide) [55], as shown in Fig. 3.3. A membrane, situated between the sample gas (for example breath or air) and the inlet to the cell, prevents unwanted molecules from entering into the sensor; only O₂ molecules can pass through the membrane. The O₂ molecules are reduced at the cathode and form (along with water and electrons) negatively charged hydroxide ions. Due to the loss of electrons, the cathode becomes positively charged. Hydroxyl ions oxidise at the anode, which yields an electrical current (in the range of nA to μ A [56]). The formation and migration of the ions between the cathode and anode is proportional to the concentration of O₂ in the sample gas [56]. Manufacturers of such sensors usually recommend that a load resistor is placed between the anode and cathode to produce a voltage output, suitable for reading with an appropriate data acquisition module.

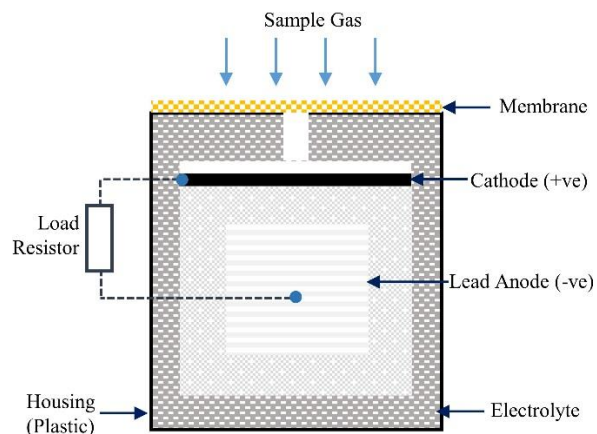


Fig. 3.3 – Schematic of low temperature electrochemical O₂ sensor [57,58].

The simple principle means galvanic cells are affordable (€10 to €20), although the bulky dimensions required to electrolyte (in sufficient quantity to allow a reasonable lifespan after considering evaporation) prevent the development of miniature devices (the smallest sensors are perhaps 20 mm in diameter). In the past 50 years the development of electrochemical devices has greatly progressed [57]. The improvement in sensor technology enables reduced instability (previously caused by excessive noise and drift). Importantly, sensitivity and selectivity have improved and increased the working life span of the devices (from a few months to two years) [59]. These sensors have the potential for use in industrial applications, with low cross-sensitivity to other common gases [60]. The devices are less attractive for applications where regular sensor replacement or for those in which the corrosive nature of the basic solution is a concern [61]. The sensors are susceptible to poisoning, by acid gas species such as hydrogen sulphide and sulphur dioxide. [55], although these are unlikely to be present in high concentrations during breath sampling. These devices can be used for portable applications (with the great advantage of low power consumption), and are not affected by movement or vibration, unlike their counterpart paramagnetic alternatives [62].

Development of electrochemical O₂ sensors for breath applications is limited, possibly due to the unusual conditions found in an exhalation listed in Table 3.2. The necessary fast response time, uncharacteristic of electrochemical sensors, is perhaps why other types of O₂ sensors are usually considered for breath-by-breath measurements, albeit at a greater expense. The research field of miniature O₂ sensors for medical

applications is strong however, for example wearable sensors for premature infants. The sensors suitable for use in clinical environments would be practical for use in a breath analyser, although the resilience to fast flow rates and response times needed for rapid changes in gas concentration might prevent their adoption.

Mitsubayashi et al. reported on a research wearable O₂ sensor for use in neonatal intensive care [63]. The flexible device was designed to monitor arterial oxygen pressure in infants to prevent premature retinopathy. The device was designed to be a comfortable replacement to the rigid cylindrical cells which were commercially available, but often caused skin rashes. The new device had a reduced risk of causing rashes (accurate measurements were only possible when the skin was heated, which increases the O₂ transmissibility from the blood to the skin). The device was constructed with a platinum (Pt) electrode and a silver (Ag) electrode patterned on a gas-permeable membranes (width 15 mm, length 50 mm, thickness 200 nm). A t_{90} response time of 11 s (to 90 % of final value) was achieved comparing ambient air to nitrogen conditions. The device was applied to the forearm of healthy male subjects, inhaling either 21 % O₂ or 60 % O₂ (for 10 minutes). The output from the sensor typically increased from ~12 μ A to ~16 μ A with a 39 % increase in supplied O₂.

A further revision of the flexible O₂ sensor was reported by Iguchi [64], which was capable of performing O₂ measurements through the conjunctiva. The device neglected the need for heating, due to the conjunctiva allowing for high gas penetration. The sensor was smaller than the previous generation (a decrease in width of up to 3 mm), but had a slower response time (with a N₂ purge 90 % response measured after 45 s). The sensor was tested with a rabbit, inhaling 21 %, 60 % and 90 % O₂ for periods of 2 minutes. Typically, the sensor output was 0.30 μ A when inhaling 21 % O₂, 0.35 μ A at 60 % O₂ and 0.38 μ A at 90 % O₂.

The restricted lifetime of amperometric sensors was noted by Xiong et al. on the specification of products from manufacturers such as Crowcom, Alphasense, Draeger and Honeywell (with associated companies, such as City Technology) [65]. Commercial examples are the O2G2 (Alphasense) and the MOX-20 (City Technology). These sensors often use a strong aqueous sulfuric acid as an electrolyte to prolong the lifespan of the devices. It was suggested that using a room temperature ionic liquid (RTIL) as an electrolyte would allow, in principle, the sensor to overcome

the issues with amperometric sensors in high temperature environments and short sensor lifetimes. A membrane-free microelectrode/array was developed with a thin layer of RTIL deposited by blotting (where the ionic liquid eliminates the need for a membrane). Long response times were cited as an issue with current commercially available sensors. With the research prototype sensors, response times of < 15 s were found. The device was tested between 10 % and 100 % O_2 , with current output demonstrating a near linear increase from ~ 10 μA to 60 μA . The principle of membrane free amperometric sensing was demonstrated, although improvements in RTIL deposition would be required to achieve reproducible measurements.

Wang et al. reported a substantial improvement with amperometric O_2 sensors with the use of newly developed RTILs as the membrane [66]. A limit of detection for O_2 as low as 0.05 % was found with a response time of 2 minutes. The prototype devices were noted to perform well over a period of several months, and offer a potential amperometric sensor for use in harsh environments and air-quality monitoring applications. Wang et al. commented the use of ionic liquids as electrolytes allow great promise for future generations of O_2 sensors to be miniaturised. At the stage of the work presented, the experimental data came only from laboratory based experiments, with no testing in real world applications. The sensor had a sensitivity of 61.6 μA per % O_2 . Gębicki et al. reviewed the application of ionic liquids for amperometric gas sensors and stated the limit of detection of sensors based on the classic Clarke cell principle could be improved with the use of ionic liquids [67]. The principle could be applied to air quality monitoring for safety applications, where detection of low ppm concentrations of gases (CO, NO etc.) would be necessary.

3.2.2 Zirconia Oxide Sensors

Zirconia probes are potentiometric oxygen sensors, most commonly used in the automotive industry (sometimes referred to as lambda sensors, where λ refers to the air fuel ratio) [68]. Although the device operates on an electrochemical principle, a potentiometric configuration is usually implemented (with voltage readout), and unlike the previously discussed devices, zirconia sensors are usually operated at high temperatures. In the case of a car exhaust, the reference electrode is exposed to atmospheric air, while the sensing electrode was exposed to exhaust gases, as shown in Fig. 3.4. At very high temperatures, zirconia is a solid state oxygen ion conductor [69]. The sensing electrode surface (usually coated in platinum) allows the oxygen to

form a reversible redox couple. The movement of oxygen ions across the zirconium oxide causes a voltage to be produced. The EMF generated is proportional to the temperature, which is usually set in the range of at least 600 to 800 °c.

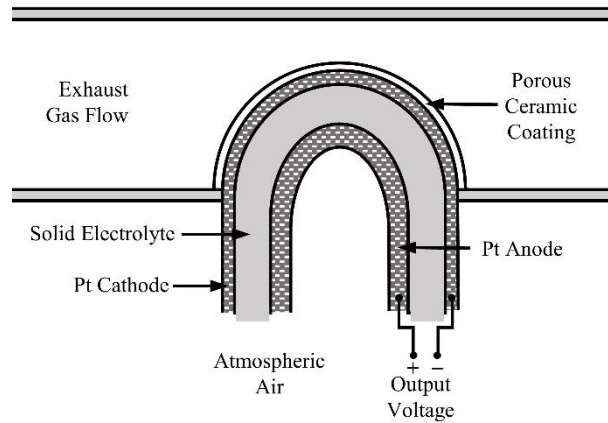


Fig. 3.4 – Principle of zirconia oxygen sensor [70,71].

An example of a commercial zirconium oxide sensor is shown in Fig. 3.5. These types of sensors, are not suitable for a portable device. Although fast response times (120 ms or lower [72]) are possible at high temperatures (in excess of 550 °c), the devices demand high power consumption (for example, 9 W at 12 to 15 V [73]), which limits their use in mobile applications. For industrial applications or the automotive industries, these problems are only a minor compromise for the durability of the devices.

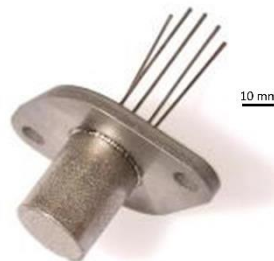


Fig. 3.5 – Zirconia based flange mounted O₂ sensor from SST Sensing [74].

3.2.3 Paramagnetic Sensors

Paramagnetic O₂ sensors are expensive, but can measure very low levels of O₂, which is the reason why they are often incorporated into calorimeters used in industry (where sensitive measurements are required) [75]. Oxygen is a highly paramagnetic gas, so is readily attracted to magnetic fields (several hundred times greater than most gases such as N₂ and helium). A small glass tube with two spheres on either end (the shape of a dumbbell) contains an inert gas (such as nitrogen) and is wrapped in a coil (shown

in Fig. 3.6) [76]. The dumbbell is suspended in a non-uniform magnetic field. When a sample cell is passed through, any O₂ molecules in the gas are attracted to the stronger magnetic field, causing the dumbbell to rotate. The degree of rotation is measured using a light source and photodiode (with an amplifier). An opposing current is applied to restore the dumbbell to its original position. The magnitude of the current is directly proportional to the partial pressure of the oxygen in the sample gas. The partial pressure of the oxygen in the sample can be displayed in terms of a percentage (with resolution as low as ±0.01 % [77], such as the O₂ readout panel shown in Fig. 3.6.

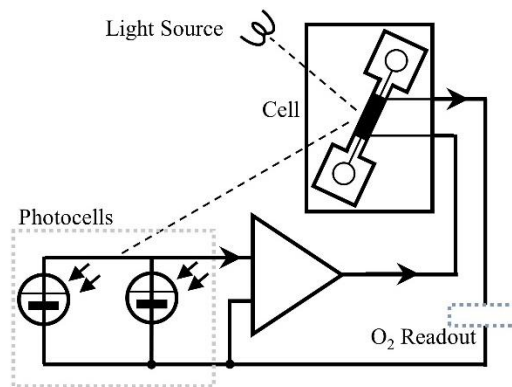


Fig. 3.6 – Paramagnetic O₂ sensor diagram [75,77].

For a breath analyser, the accuracy available from sensors using the paramagnetic principle would be appealing, although the expense of the device prevents its use in affordable equipment. The greatest problem for portable equipment is the intolerance of the devices to vibration (the dumbbell component) [78]. They are somewhat delicate and would need re-calibration if not used in a stable location. For these reasons, paramagnetic based sensors remain unsuitable for affordable or mobile breath analysers.

3.2.4 Resistive Oxygen Sensors

Metal oxide gas sensors have been available commercially for almost 50 years, and since their introduction, their performance has improved in terms of response time, sensitivity, detectable gases and compounds and power consumption. The gas sensing properties of a tin oxide sensor to O₂ were reported by Cukrov et al. [79]. Nano-sized particles of SnO₂ were used as the sensing layer, prepared by a mechanochemical reaction, a micrograph is shown in Fig. 3.7 a). The dynamic response of the thin film sensor was defined as $S(O_2) = (R_{O_2}/R_{1ppm})$. The response was found to be ~20.0 (4.5 MΩ resistance) for 10 % O₂ concentration. The response times of metal oxide

sensors limits their use in breath analysis however, as a t_{90} time of 2 to 3 minutes has been reported [79]. The sensors were noted as demonstrating extremely good stability and repeatability (baseline resistance was maintained throughout the duration of experiments, across a large concentration range).

The search for the optimal material coating for O_2 monitoring is an ongoing topic in gas sensor research, with a wide variety of applications benefiting (for example, O_2 content in exhaust fumes). $BaFe_{1-x}Ta_xO_{3-\delta}$ (BFT), a material investigated by Bektas et al. for O_2 detection, was trialled with Tantalum content (x) tested in the range of $0.2 \leq x \leq 0.7$ [80]. A scanning electron microscope (SEM) photograph of a layer of BFT30 is shown in Fig. 3.7 b). For the application of exhaust gas testing, the sensor must be insensitive to temperature variation. It was reported that BFT30 was a promising variant that permitted temperature independent monitoring of O_2 content. It was tested over a range from 1 % to 100 % O_2 . No response time of the sensors was given, however the experiments were performed over a period of hours.

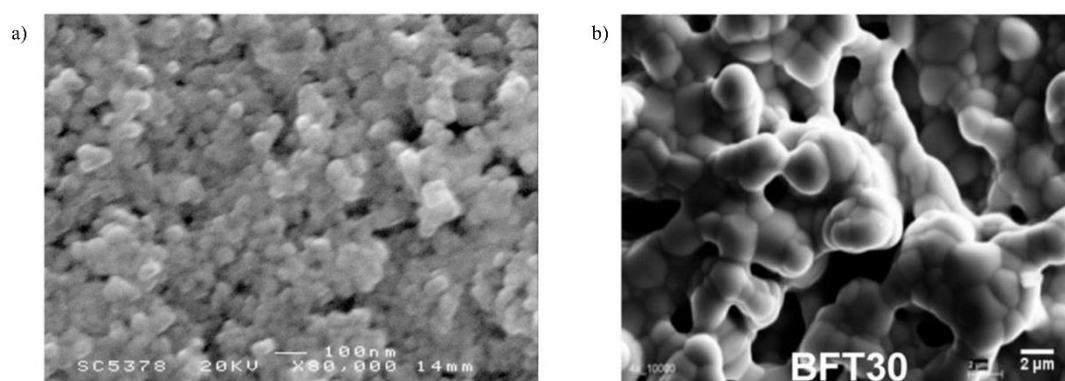


Fig 3.7 a) SEM photograph of nanosized particles of SnO_2 deposited by a mechanochemical reaction; b) BFT with 0.3 tantalum content photographed with SEM after sintering. From [80].

Resistive O_2 sensing has particular advantages when the temperature of the operating environment exceeds $60^\circ C$. A report by Cobianu et al. (Honeywell Sensors and Wireless Laboratory) note for the application of monitoring O_2 levels inside a domestic boiler [81]. Metal oxide sensors are capable of withstanding the high temperature environment and can be coated with STFO to become sensitive to oxygen (with no sensitivity to temperature variation in the range of 750 to $900^\circ C$. Fig. 3.8 a) shows the structure of the silicon on insulator (SOI) based micro-hotplate upon which the O_2 sensor is based.

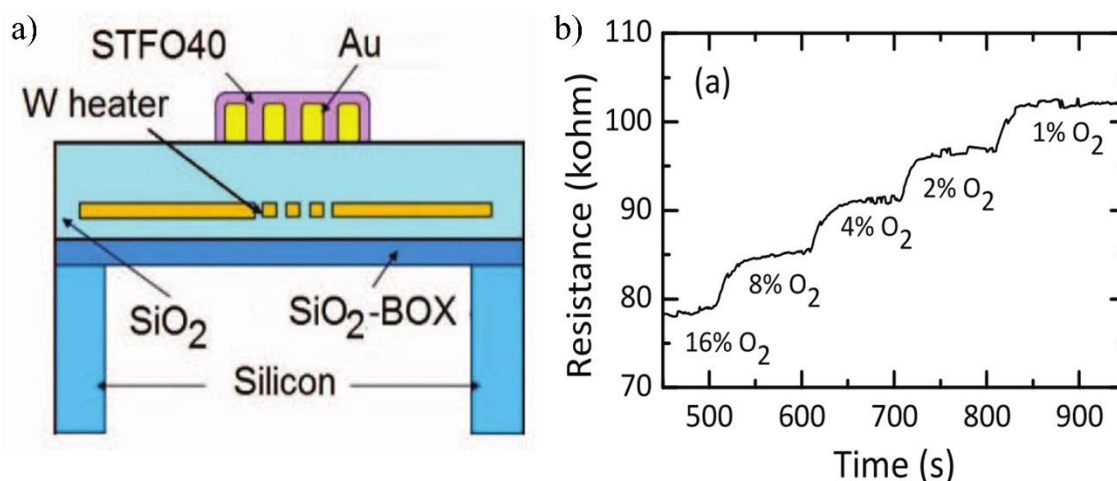


Fig. 3.8 – Resistive O₂ sensor based on SOI device, a) Structure of micro-hotplate; b) Sensor resistance measured with O₂ concentrations in the range of 1 to 16 % [81].

Cobianu et al. demonstrate the STFO coated sensor was able to measure O₂ concentrations in the range of 1 to 16 %, shown in Fig. 3.8 b). The power consumption of the sensor was 80 mW. The results were described as encouraging, although it was conceded further work was required to improve the film composition. The sensor was only tested over a short period, and further work was required to ensure its robust long-term operation and also to minimise the sensor drift over time and with relative humidity variation.

3.3 Carbon Dioxide Gas Sensors

The most commonly available CO₂ sensors are based either on an electrochemical sensing principle or on an optical absorption method, non-dispersive infrared (NDIR) [82]. The selection between the two technologies is dependent on application, where the merits of each usually contrast the other; a brief typical comparison is shown in Table 3.5.

Table 3.5 – General comparisons between NDIR and Electrochemical CO₂ sensor principles [83–86].

Parameter	NDIR CO ₂ Sensor	Electrochemical CO ₂ Sensor
Measurement Range	50 ppm to 100 % (range can be selected to improve accuracy)	400 ppm to 90 % typical (range of models available)
Response Time	<5 s typical	<2 min typical

Parameter	NDIR CO ₂ Sensor	Electrochemical CO ₂ Sensor
Power	< 100 mW	No power required
Consumption		
Warm-up Time	< 1 min	< 30 min
Cross Sensitivity	CO or humidity possible	Humidity
Response Decay	Temperature variance possible	Output decays over usage life
Lifespan	20+ years	< 1 year
Physical Size	Miniature	Small

3.3.1 Electrochemical CO₂ Sensors

The slow response time typical of an electrochemical CO₂ sensor limits its use for breath-by-breath analysis. However, the Alphasense CO₂-D1 (shown in Fig. 3.9) is noteworthy because it requires no power to operate (although the necessary signal amplification would require a power source). In terms of mobile sensor systems, a considerable space is often required for batteries. The reduction in power requirements reduces the necessary capacity of the battery; Alphasense suggest a coin-sized CR2032 battery (20 mm diameter) would give between 6 and 12 months use [84]. An example application is discussed by Bonfiglio et al., where the device was chosen to be tested in boots for use by emergency services workers [87]. The CO₂ sensor needed to be close to ground level (where, as it is heavier than air, CO₂ accumulates). The boots also contained space for energy harvesting equipment, thus a low power sensor would be beneficial.



Fig. 3.9 – Alphasense CO₂-D1 electrochemical gas sensor (detection range 0.5 to 90 % CO₂) [84].

3.3.2 NDIR Gas Sensors

A brief introduction to NDIR sensors is given here, with a full explanation of the operation of the final sensor system given in a chapter V. Unlike many of the devices discussed previously, NDIR sensors do not rely on chemical reactions to detect a gas or compound, but instead measurements are taken based on the physical absorption of IR. This process is almost instantaneous, and therefore IR sensors fundamentally offer faster response times, such as those required for breath-by-breath analysis. Measurement of IR intensity is inherently plagued with noise. The signal processing necessary to remove or compensate for the wide band noise causes much of the delay found in commercial NDIR systems.

The Beer-Lambert law relates the level of light transmitted through an absorbing medium such as gas [88]. The law, shown in eq. (3.2), can be used to calculate the reduction in intensity of IR radiation (transmitted by an emitter) from an initial value (without target gas present) I_0 to the intensity $I(c)$ received by an IR detector due to the concentration c of a particular gas [89]. The absorption index of the target gas (e.g. CO₂) at a given wavelength is denoted by k_g and the IR optical path length given by l . A simplified principle of operation is given by the stages shown in Fig. 3.10.

$$I(c, \lambda) = I_0(\lambda) e^{-k_g c l} \quad (3.2)$$

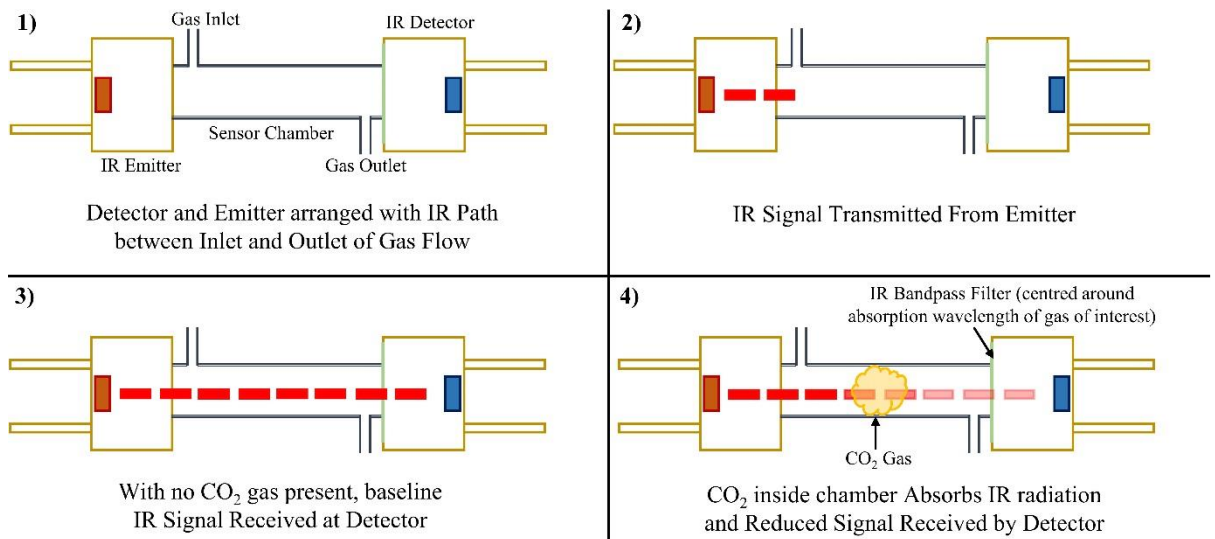


Fig. 3.10 – Basic principles of NDIR sensing in four stages.

The path length of the NDIR sensor defines the concentration of a particle element that can be detected. For example, path lengths may be as short as 10 mm (for detection

of CO₂ concentration higher than 1 %) but longer paths (e.g. 80 mm) could allow for 100 ppm or lower measurements. Improvements in optical configurations to increase the path length possible in a small area have been widely reported in the literature. The received signal (the intensity of IR radiation) decreases exponentially with the increase in path length. A shorter path length yields a higher signal output from the detector (at the expense of decreased sensitivity). Consequently a longer path produces a larger differential response to a change in gas concentration (permitting the detection of lower gas concentrations).

3.3.2.1 NDIR Emitters

The emitters included in IR systems are usually broadband and emit radiation across a spectrum of, for example, 2.5 to 12.5 μm . A sensor can be made specific to a particular gas or compound by detecting only IR absorption over a small wavelength range (perhaps 90 or 180 nm). A bandpass filter fitted into a cap covering the detector can prevent changes in IR intensity outside the range of interest from affecting the measurement. The absorption spectrum shown in Fig. 3.11 demonstrates how CO₂ absorbs IR at approximately 4.26 μm and humidity absorbs wavelengths between 2.5 and 3.5 μm .

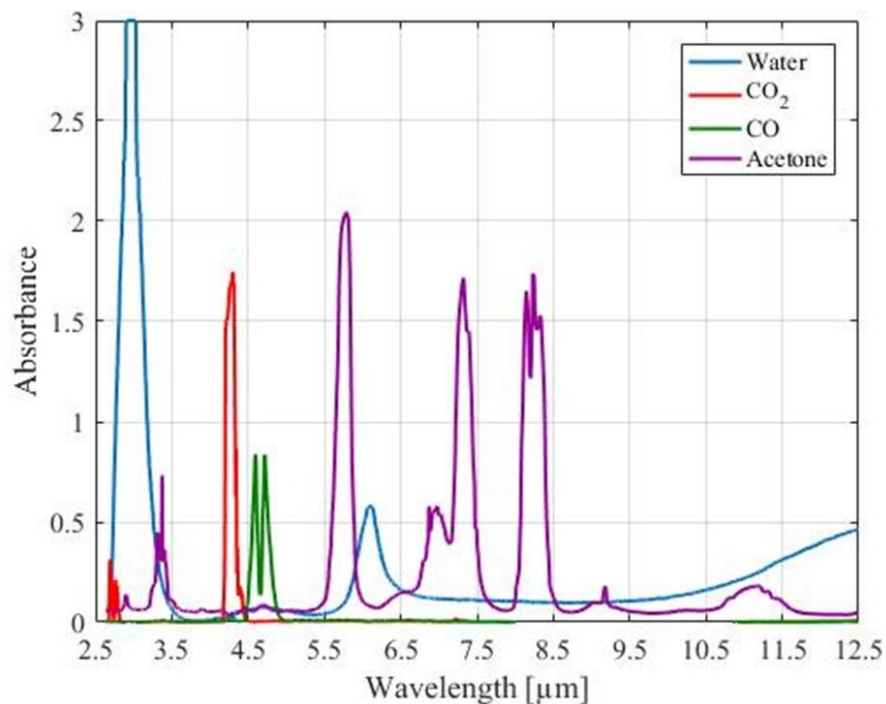


Fig. 3.11 – Absorbance of IR radiation by water, CO₂, CO and acetone [90].

The emitter in an NDIR system can be targeted for sensing of a specific gas or element by use of a subwavelength array of holes on top of the micro heater in a metal CMOS layer. Experiments have demonstrated that the array of holes enhances the IR transmission, most likely due to the generation of surface plasmons on the metal-dielectric interface [91]. An example structure is shown in Fig. 3.12, where the device with circular holes was optimised for detection of CO₂. The IR transmission enhanced at specific desired wavelengths can help avoid the interference from absorption of other elements (e.g. humidity). In general, at this stage in their development, plasmonic structures are usually integrated into the design of the IR hotplate, but in the future, they could also be included in the IR detector. This mechanism offers a potential replacement for the optical bandpass filter (usually fitted in the detector cap), which is an expensive and difficult to manufacture component.

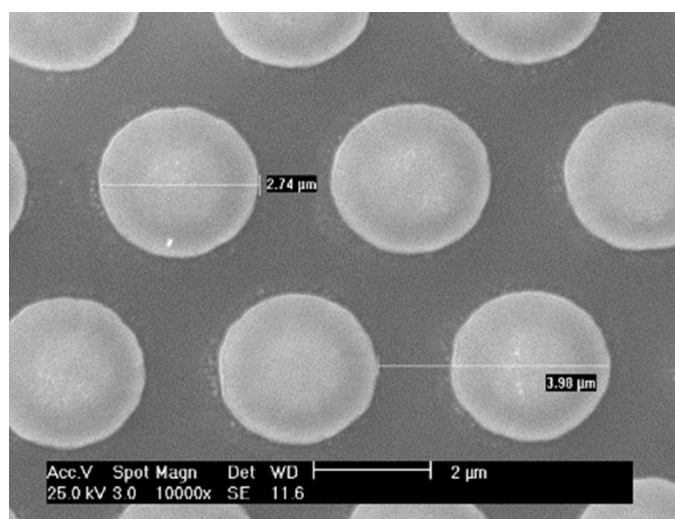


Fig. 3.12 – SEM photograph of the hexagonal plasmonic structure on NDIR emitter designed for enhanced transmission at 4.26 μm (hole diameter and spacing labelled).

There is considerable interest in the field of plasmonic structure design, where the optimum hole diameter, spacing and arrangement for specific wavelengths have yet to be determined. This is in part due to disagreement in the literature regarding the optimum configuration, but also due to manufacturing tolerances causing discrepancies between design parameters and manufactured items. A hexagonal arrangement is often chosen (triangular lattices were found to offer a narrower absorption/emission than square lattices), and can be based on a metal layer of a standard CMOS process [92]. The structure can be defined by the lattice spacing a and the hole radius r . The optimal ratio of r/a was found by Li et al. to equal 0.25 (to ensure

high emittance and narrow emission profiles) [92]. To investigate the effect of varying the structure, finite element modelling (FEM) software (such as COMSOL Multiphysics) can be used. It has been reported that r/a ratios of 0.3 and 0.35 produce the highest emissivity for some designs [93,94].

A CMOS nanoplasmonic structure is reported by Pusch et al. used to improve the performance of IR gas-sensing devices [95]. Fig. 3.13 shows the wavelength dependent emissivity with varying radii and varying pitch. The study aimed to improve emissivity at 4.26 μm (for detection of CO_2), although it was noted that detection of other gases or compounds in the wide variety of absorption fingerprints in the range of 2 to 14 μm (e.g. CO, methane, ethanol and other VOCs) could also benefit if other emissivity peaks were found. The non-plasmonic emissivity is also shown in Fig. 3.13, demonstrating the substantial improvement (almost four fold) produced by the additional plasmonic design.

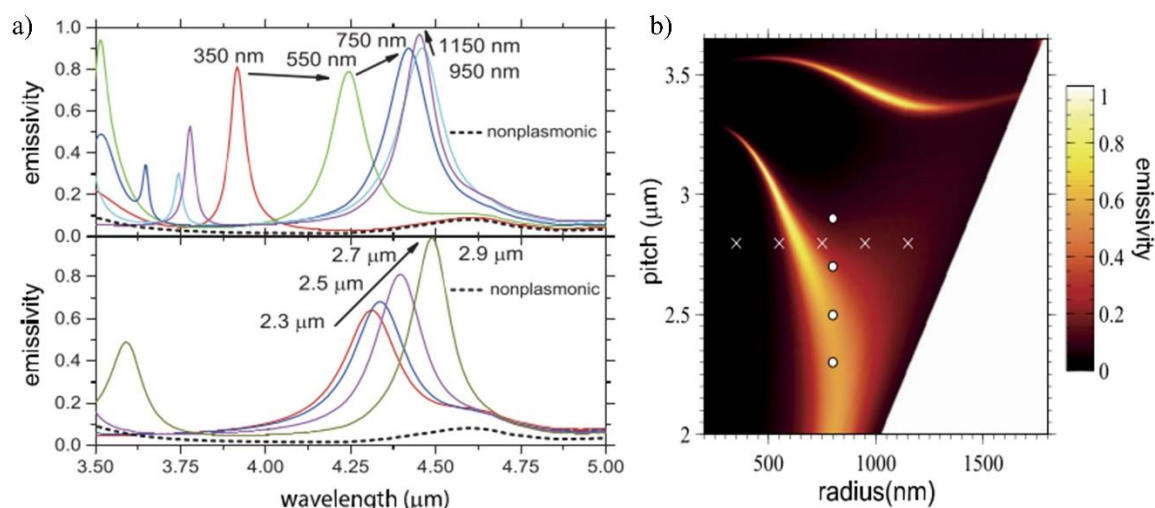


Fig. 3.13 – a) Emissivity of plasmonic structures from 3.5 to 5 μm , top panel pitch fixed at 2.8 μm and radii varied between 350 and 1150 nm, lower panel radii kept constant at 800 nm and pitch varied between 2.3 and 2.9 μm ; b) Map of the surface normal emissivity at 4.26 μm wavelength, dots and crosses indicate radii and pitches, respectively.

3.3.2.2 Commercial NDIR CO_2 Sensors

In their current generation, plasmonic devices are usually confined to use in research, with ongoing development to improve stability and emissivity range. Commercial NDIR CO_2 sensors traditionally use micro bulbs as sources of IR. Although readily

available, bulbs provide a cumbersome radiation source, compared to newer technology such as micro hotplates. In particular, SOI IR emitters have greater reliability, faster response and smaller physical dimensions [96,97]. A photograph of a typical, affordable commercial NDIR CO₂ sensor (\$150) is shown in Fig. 3.14. The device is marketed as the lowest power NDIR sensor available (35 mW on average) and requires a power supply of 3.3 V [98]. The response time is noted as adjustable, between 4 and 30 s, although the shortest response time is inadequate for breath-by-breath measurements and unsatisfactory considering the operational principle.



Fig. 3.14 – Commercial NDIR sensor, 20 mm diameter sensor offers CO₂ detection up to 100 %, given the range of models available [98].

Silicon CO₂ sensors have been studied for over a decade, however in recent years the focus of development has been on improving sensor design to enable greater sensitivity, faster response with lower power consumption [99]. An array of thermopile sensors can be used to detect multiple gases (e.g. three on a 2x2 array, with one reference channel) [100].

The design complexity of CO₂ sensors based on the radiometric thermal conductivity principle is a trade-off with the beneficial lower power consumption over traditional NDIR systems.

3.3.2.3 NDIR Detectors

Thermopile and pyroelectric detectors are the two most commonly used sensors in NDIR systems [101], which, in simple terms, are temperature sensors. Both types can be miniature, and low power. At the core of a pyroelectric detector is a slab of thermoelectric material, placed between two electrodes [102]. The slab must be poled (i.e. given a polarisation) during manufacture. When the poled detector slab is heated (i.e. by radiation) the induced polarisation and consequently the charge on the electrode, varies. To induce polarisation, there must be a changing temperature, thus the pyroelectric detector only responds to modulated (AC) or pulsed radiation (i.e. temperature levels are detected rather than temperature changes) [103]. A cross-sectional drawing of a commercial pyroelectric detector is shown in Fig. 3.15 a), with a cap integrated into the TO-5 cap (configurable bandwidth upon ordering).

The dominant source of noise varies for a pyroelectric device, dependent on the radiation frequency received by the detector. At low frequencies (up to several 10 Hz) Johnson noise (of the large necessary input load resistor, in the Meg-Ohm range) dominates [104]. At mid-range frequencies (up to 1 kHz) the dielectric loss of the pyroelectric material dominates the noise density. At higher frequencies the voltage noise (from the preamplifier) is the dominate source [105].

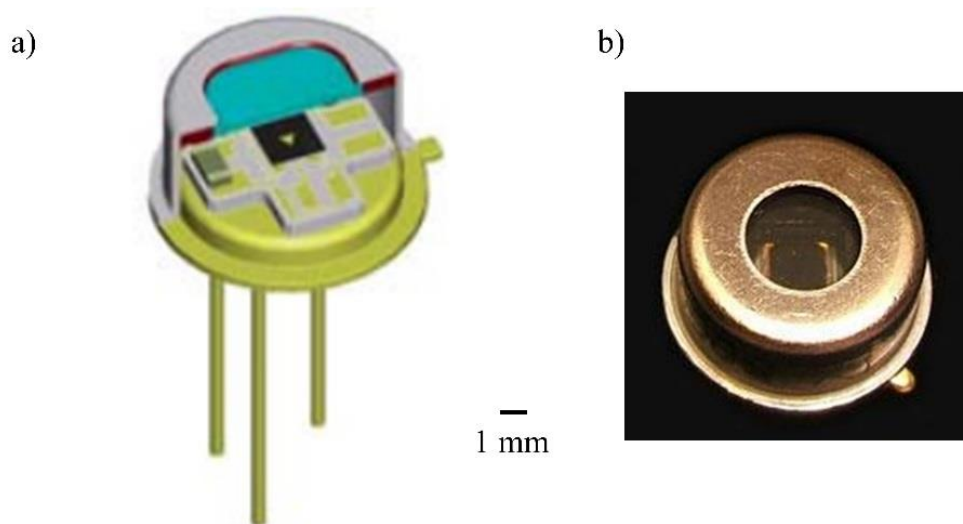


Fig. 3.15 – a) Cross-sectional drawing of a commercial pyroelectric detector (LME-302 from InfraTec [106]); b) Photograph of a commercial thermopile detector (ST150 from Dexter Research Centre [107]) mounted on the same TO-5 package with filter cap.

A thermopile is formed when a number of thermocouples are connected together in series. A temperature rise can be sensed using a thermocouple (a junction formed from dissimilar metals across which a small voltage is generated upon heating) [102]. A larger output is obtained by connecting the junctions in series (i.e. a thermopile). The equation relating the output voltage (ΔV) can be calculated using equation (3.3) from the temperature rise (ΔT), the number of thermocouples in the thermopile array (N) and the Seebeck coefficient of the junction (S). The Seebeck coefficients can be of the order $100 \mu\text{V K}^{-1}$ for materials formed from evaporated films of Bismuth and Antimony [102]. An example of a commercial thermopile detector from Dexter Research Center is shown in Fig. 3.15 b), on a TO-5 package with a bandpass filter cap for NDIR gas sensing.

$$\Delta V = NS\Delta T \quad (3.3)$$

In contrast to pyroelectric detectors, thermopile devices exhibit an inherently stable response to DC radiation. The main source of noise in thermopile systems is the summed resistance of the thermocouples [104]. Thermopiles can be designed to have response times from sub-microsecond to many seconds; 50 ms is a typical response time for an instrumentation grade device [102]. The modern thermopiles, constructed from evaporated films, are very thin and rugged. Pyroelectric detectors have a higher responsivity and are generally faster, but only operate with modulated radiation [108]. Pyroelectric detectors operate up to at least 2 kHz, whereas thermopiles are limited to around 100 Hz. Thermopiles have many advantages over pyroelectric detectors in applications where responsivity can be sacrificed; they do not suffer from the microphonic effect, are low noise and low cost [104].

3.4 VOC Sensors

Volatile organic compounds are present, in low quantities, in atmospheric air and in exhaled breath. The concentration of particular VOCs in breath can indicate the presence of various diseases. The lowest level compounds found in very low ppb concentrations can only be detected through mass-spectrometry and by recognising a fingerprint of exhaled substances. The diagnostic potential of such compounds is uncertain. A vast number, in excess of 300 [109], VOCs have been detected in exhaled breath and the key biomarkers for specific diseases (e.g. w.r.t. various types of cancer) are starting to be established, although breath tests have not been standardised for

cancer detection [110]. For this work we will concentrate on identifying compounds that can be detected with portable sensor systems. VOCs and the gas content of our exhaled breath can offer a promising means to diagnose disease and contribute to evaluating our lifestyles [111,112].

One of the most well-known uses for breath analysis is measuring the level of alcohol in the breath of drivers for law enforcement purposes. Breath analysers usually operate using one or many of three methods: the fuel cell principle, infrared spectrometry or semiconductor (MOX) devices [113]. Fuel cells are the most common in professional breath analysers, but semiconductor sensors are used in personal devices, because of their low cost and portability [114]. Here the target is to extend beyond ethanol (alcohol) detection and investigate other compounds in human breath.

There are a number of sensing methods available to detect VOCs: acoustic sensors (e.g. surface acoustic wave, thin film bulk acoustic resonator), electrochemical sensors, colorimetric sensors, metal oxide (MOX) sensors or NDIR sensors [115]. For the case of the portable analyser to be developed in this project, a MOX would be preferred, for its miniature size, ability to detect ppb levels of compounds and low power consumption. Table 3.6 shows a comparison between the available sensing methods for VOCs. Electrochemical sensors offer reliable reference devices, however their bulky size, slow response and short life-span prevent their use in a portable analyser.

As discussed above, NDIR sensors have many advantages for the detection of CO₂ against electrochemical devices, however the absorption coefficients are limited for many VOCs (although acetone is promising [116]). However, work is still ongoing to develop a stable NDIR sensor for low ppm and ppb measurements, thus in this project an NDIR sensor will be used only for detection of CO₂. Acoustic sensors were considered for use in this work, however the complexity of working at high frequency could prevent easy integration with the other sensors required for other gases (e.g. separate power supplies may be required to prevent frequency locking).

Table 3.6 – Available VOC detection methods for a portable analyser [117–120].

Sensing Method	Advantages	Disadvantages
MOX Semiconductor	<ul style="list-style-type: none"> • Mechanically robust. • Wide range of target gases possible through use of film coatings. • Highly sensitive to gases (i.e. magnitude of 10 resistance change). • Long lifetime. • Low cost. • Moderately stable (some seasonal drift). 	<ul style="list-style-type: none"> • Poor selectivity. • Susceptible to contamination. • Moderate power consumption (resistive heater required).
Electrochemical	<ul style="list-style-type: none"> • Ability to measure low ppm levels of gases (incl. toxic). • Wide range of gases can be detected. • High selectivity. • Moderate cost. 	<ul style="list-style-type: none"> • Physically bulky size (e.g. 20 mm cylindrical standard). • Contamination possible. • Limited lifetime (< 2 years). • Sensor drifts over lifespan.
Colorometric	<ul style="list-style-type: none"> • Array of sensors possible in small area (i.e. 1 x 1 mm per sensor). • Low cost. 	<ul style="list-style-type: none"> • Disposable sensors. • Scanner or camera required to digitise results. • Cross-sensitive to humidity.
Optical (NDIR)	<ul style="list-style-type: none"> • Highly selective (using filters). • Long lifetime. • Moderately sensitive (low ppm levels). • Limited to which gases can be detected (dependent on if IR is absorbed). 	<ul style="list-style-type: none"> • Path length requirement makes miniaturisation difficult. • Moderately expensive. • Can be affected by temperature or humidity changes in sample gas.

The primary function of the alveolar capillary interface, inside a human lung, is to exchange O₂ and CO₂. However, in terms of medical potential, the characteristics of each exhalation, as well as its content can highlight symptoms of diseases and provide a means of real time monitoring. Table 3.7 lists examples gases and VOCs reported in breath samples and their significance to healthcare.

Table 3.7 – List of example gases and VOCs found in exhaled breath and their diagnostic purpose.

Gas	Inhaled	Normal Exhaled	Abnormal Exhaled	Healthcare Application/Diagnosis	Ref/s
Acetone	10 – 20 ppb	300 – 900 ppb	> 1800 ppb	Diabetes	[28,121]
			16.7 – 29.3 ppm	Identification of smokers, chronic obstructive pulmonary disease (COPD)	[122–124]
Carbon Monoxide	0.25 ppm	0.5 – 2.1 ppm	1.13 ppm	Severe sepsis	[125]
			5.6 ppm	Asthmatic patients	[126]
			4.4 ppm	Hemolysis	[127]
Nitrogen Dioxide	30 – 50 ppb	< 5 ppb increase	0.5 – 1 ppm	Respiratory diseases, Asthma	[40,128,129]
			19.2 – 30 ppb	Asthma diagnosis	[130–133]
Nitric Oxide	<2 ppb	5.3 – 7.4 ppb	16.3 ppb	Seasonal rhinitis	[134]
			12.9 ppb	Experimental influenza	[135]
			2.3 – 4.7 ppb	Cystic Fibrosis	[136,137]
Hydrogen	0.5 ppm	< 5 ppm	>16-20 ppm increase	Gastrointestinal diseases (small intestinal bacteria overgrowth, carbohydrate malabsorption), diarrhoea,	[138–142]
Methane	1.7 ppm	< 1 ppm increase	>16 ppm increase	Diverticulitis, constipation, irritable bowel syndrome	[143–145]

3.4.1 Metal Oxide Sensors

Metal oxide semiconductors have been investigated for use in gas detection since the discovery that the absorption of gas into the surface of a film layer causes a significant change in electrical conduction [146,147]. The sensors are based on the principle of chemiresistance (i.e. the change in electrical conductivity or resistivity of thin films

on exposure to a target gas) [148]. Example equations to describe the operation of the device are explained below. Inflammable gases such as hydrogen and CO (and other certain toxic gases etc.) can be detected using MOX sensors; the most widely accepted explanation for this mechanism is the variation in negatively charged oxygen adsorbates [149].

3.4.1.1 Operation of MOX Sensors

The resistance of the sensor is dominated by the variation in the surface coverage of the adsorbed O_2 . For n-type semi-conducting metal oxides, the adsorbed oxygen forms a space-charge region on the surfaces of the metal oxide grains. In air, the resistance of an n-type semiconducting material is high (due to the development of a potential barrier to electronic conduction at each grain boundary). A diagram showing the operation of a gas sensor is shown in Fig. 3.16. The measurement of the sensor resistance requires only simple circuitry; a potential divider arrangement is possible, where the resistance can be calculated from the output voltage.

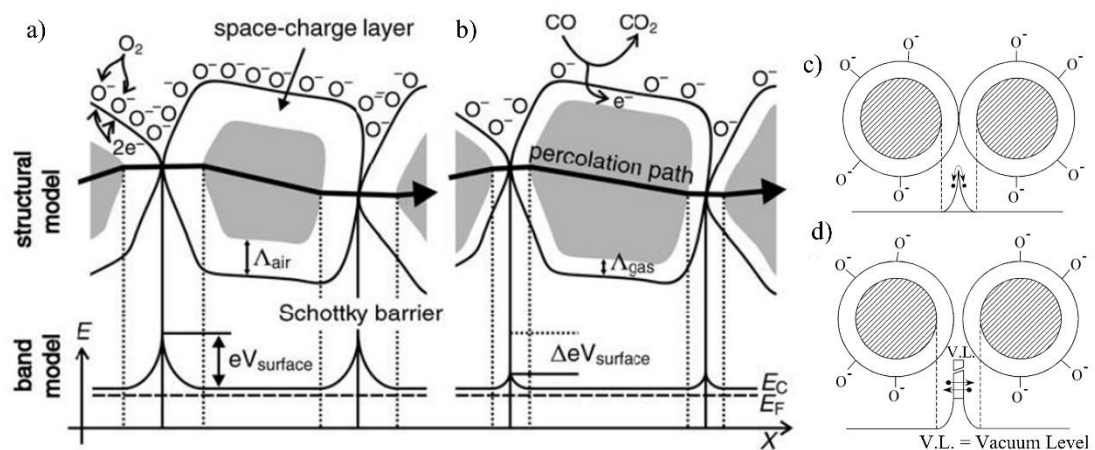


Fig. 3.16 – Physical model of the conductive mechanism when a semiconductor sensor is exposed to a) air and b) CO, with corresponding band model, from [150].

Models of electron transfer between grains are shown for c) a double Schottky barrier model and d) for a tunnelling model, from [151].

The sensor is usually heated to between 300 and 500 °c to enable reactions on the surface of the sensor to occur [149]. When exposed to a reducing gas (or gas mixture) the oxygen adsorbates on the surface are consumed by the subsequent reactions. The reactions cause the electrons trapped by the O_2 adsorbates to return to the oxide grains, leading to a decrease in the potential barrier height (shown in Fig. 3.16). This decrease in height means a decrease in resistance (a lower steady state surface coverage of the

adsorbates), which is measured as the response of the sensor to the reducing gas. Grain boundaries connect neighbouring grains in most cases, and form a potential barrier for the migration of electrons (often called the double-Schottky barrier). This barrier plays a substantial role in determining the resistance of the sensor. An enlarged view of the barrier is shown in Fig. 3.16 c).

Oxidising gases cause an opposite response to reducing gases (i.e. their presence is indicated with an increase in resistance). The negatively charged chemisorption on the grain surface of gases such as nitrogen dioxide (NO_2) or ozone (O_3) increases the surface potential barrier. In the case where grain boundaries are not formed, electrons can also be transported by tunnelling through a small gap between oxide grains [152], shown in Fig. 3.16 d).

3.4.1.2 Metal Oxide Sensor Coatings

The thin films on top of MOX sensors determine the sensitivity, operating temperature and selectivity of the device [70]. The films used on commercial devices are usually kept confidential, as this is a growing area of research, and a component of the sensor which controls its application and functionality. The sensitivity profiles of common MOX sensor coatings are shown in Fig. 3.17.

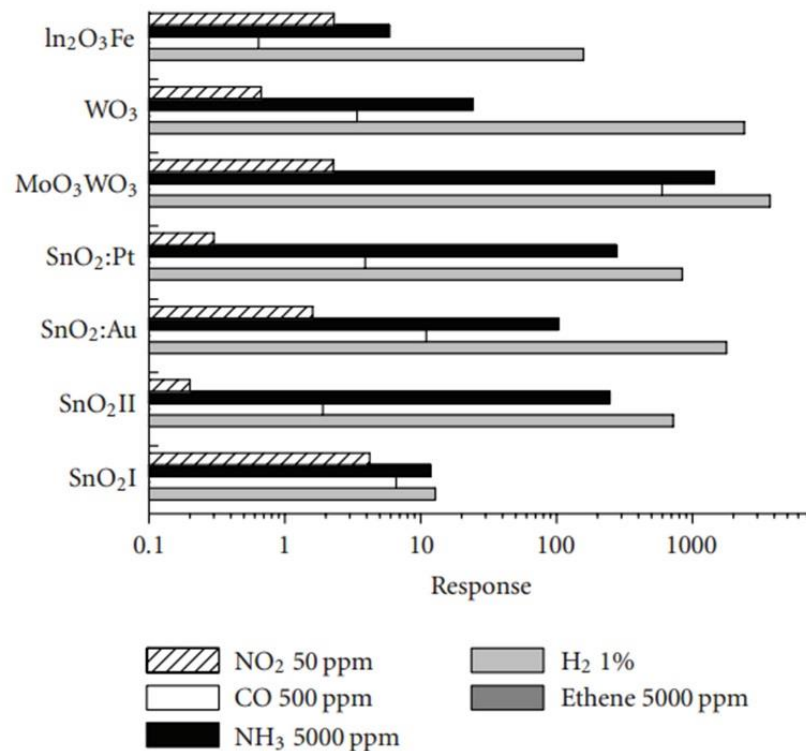


Fig. 3.17 – Sensitivity profiles of common materials used for MOX sensors [153].

Semiconductor gas sensors can be categorised as thin or thick film, which depends on how the coating is applied [154]. Thick film based sensors (Fig. 3.18) are very well established [155]. Although it is difficult to form miniature low power consumption devices, such sensors are commercially popular, compared to thin film alternatives, due to their high sensitivity at lower operating temperatures [156]. For the diagram in Fig. 3.18, C_0 represents the test gas concentration, x the distance into the film and x_0 is the film thickness.

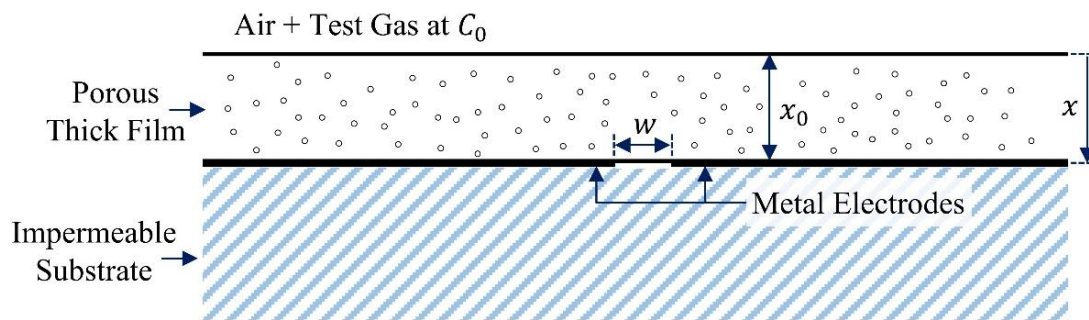


Fig. 3.18 – Typical configuration of semiconductor thick film gas sensor [157].

As the name implies, thick film devices coat the surface of a semiconductor sensor with a thick film, to which the gas must diffuse (into the porous layer) and then react to produce a response [158]. Thin film devices however, produce a response only when the gas reacts with the surface of the impermeable layer. Screen printing, inkjet printing or dip- or spray-coating are possible techniques for the fabrication of a thick film device. The device must be annealed for a period of time (e.g. 24 hours) to produce a porous polycrystalline layer. Sputter techniques are usually used to produce thin film devices, where a solid film layer is ideally created. In reality, the devices also often have a polycrystalline porous layer.

Tin oxide (SnO_2) is widely used as a base material for gas sensing, among a choice of other materials such as iron oxide and zinc oxide [147]. It is a well understood material to use and is well reported in the literature, with examples of improvements in sensitivity through adjustments of crystal structure and doping levels [159].

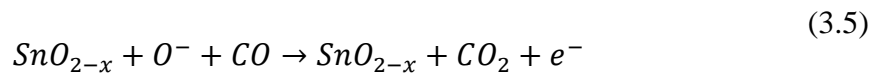
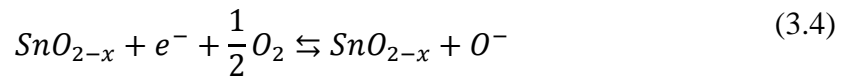
However, SnO_2 does not demonstrate an improved performance over the other sensing materials. It responds to a range of gases (e.g. CO , NO_x and O_3), meaning that although it has poor selectivity, it is a versatile material and offers reasonable sensitivity. Its versatility means it is the most widely used material in low-cost commercial devices

[160,161]. It does offer good sensitivity to NO₂ and H₂ in doping configurations with aluminium and platinum, but does not offer selectivity for a particular gas.

Lanthanide sesquioxide (Ln₂O₃) shows promising sensitivity to NO₂ however the material is difficult to process and adds complexity during manufacture [162]. Tungsten oxide (WO₃) offers a compromise between sensitivity, selectivity and stability. The response can be tuned by doping for enhanced selectivity to a particular gas.

A thick film SnO₂ gas sensor operates on the principle of a change in conductance due to the chemisorption of gas molecules into the sensor surface [147]. Adsorbed O₂ reacts with a combustible gas, which causes the conductivity to increase, as electrons are released into the conduction band. When the gas reaches the SnO₂ surface it first oxidises removing adsorbed O₂ which is then replaced by O₂ from the air (i.e. available for further oxidation).

The equation for tin oxide reaction is shown in equations (3.4) and (3.5) [163]. Equation (3.5) is valid at high temperatures compared to equation (3.4) which is for low temperature operation. It is reported, for the example of CO oxidising to CO₂, that the Langmuir adsorption isotherm holds good for physical adsorption up to 60 ppm CO (the Freundlich isotherm is followed for higher concentrations, where physical and chemical adsorption occurs) [147,157].



A number of models have been suggested to help understand the performance and mechanisms of tin oxide gas sensors. Gardner proposed a linear diffusion reaction model for the change in conductance when a sensor is exposed to a gas, equation (3.6) [146]. In this equation, G/G_0 equals the fractional conductance change, c is the fractional gas concentration change ($c = C/C_0$) and X is the fractional film thickness change ($X = x/x_0$).

$$\frac{\Delta G}{G_0} = \int_0^1 c \left[(1-X)^2 + \frac{w^2}{4x_0^2} \right]^{-1/2} dX \quad (3.6)$$

Gardner demonstrated the application of (3.6) comparing three Taguchi gas sensor output responses to 15 ppm of propanol in air [146]. It was shown that the observed response “broadly” agreed with the predicted curve. It was noted that the initial response visible in the curves may be explained by the mixing time in the chamber and also the linear model only applied at low gas concentrations, when plots of 3-60 ppm were shown.

It is believed that the negatively charged oxygen adsorbates play an important role in detecting inflammable gases. Chemisorbed oxygen (O_2^-) is the most reactive with inflammable gases in the temperature range of 300 to 500 °C [164]. In general, for an n-type semiconductor material the formation of O_2^- charges is more common and builds a space-charge region on the surfaces of the metal oxide grains. This causes an electron depleted surface layer due to electron transfer to the grain surfaces. Oxidising gases cause an n-type semiconductor sensor to increase in resistance, due to the increase in depletion region on the grain surface. The sensitivity of the device is a function of the amount of chemisorption that occurs on the surface (assuming that the surface coverage of O_2 adsorbates remains constant).

The empirical power law equation (3.7) represents the response of a semiconductor MOX sensor [154]. The law is derived by coupling the depletion theory of the semiconductor surface with the chemistry of gas adsorption and reactions [165]. The factor A_g depends of the sensing material, operating temperature and the type of gas interacting with the sensor. The concentration of the gas to which the sensor is exposed is denoted by C_g and the constant β is the exponent factor; its ideal value of 0.5 or 1 depends on the charge state of the surface oxygen species and the stoichiometry of the element reactions on the surface. This law is commonly used by researchers to express the concentration-sensitivity curves of film type nano-sensors [166].

$$S = 1 + A_g C_g^\beta \quad (3.7)$$

3.4.1.3 MOX sensors Measurement Principle

CCS Ltd (UK) design MOX sensors for gas sensing applications. The devices are based on SOI CMOS process, with the MEMS structure fabricated in a commercial foundry. A photograph of one device (CCS09C) is shown in Fig. 3.19 a) and mounted on a TO5 header in Fig. 3.19 b). The devices are supplied without a coating

(photograph shows device after coating applied). The sensors can be considered of great interest for research, as they offer an excellent base to refine coatings, drive signals and post-processing techniques. Furthermore, the devices are miniature (1x1 mm) and can be operated at low power (65 mW at 600 °C).

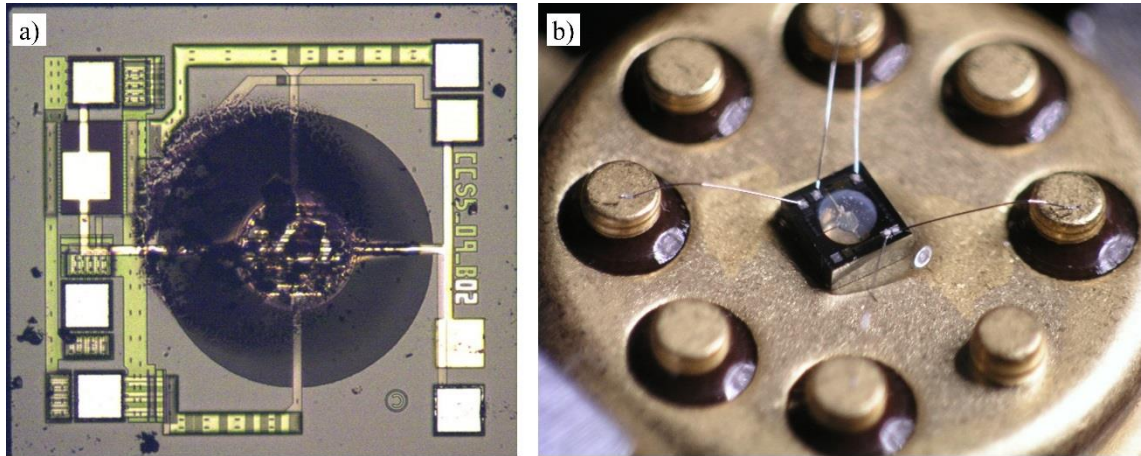


Fig. 3.19 – Photographs of the micro hotplate of size 1 mm × 1 mm, a) The MEMS device with coating on a resistive sensor and b) mounted on TO5 header for use in a gas sensing chamber.

In the membrane structure a tungsten resistive micro heater is embedded with a 5 μm thick metal oxide stack. The membrane is fabricated via a post CMOS deep reactive ion etch and both mechanically supports and thermally isolates the heater from the sidewalls. The hotplate can reach temperatures in excess of 500 °C, and heats up in 30 ms and has a cooling time of 60 ms (ambient to 500 °C and vice versa).

The variance in resistance due to the presence of a gas can be measured using the circuit shown in Fig. 3.20. A potential divider is formed between the sensor and a load resistor. In the circuit shown below, the load resistor can be adjusted through selection of a jumper pin. A potentiometer should be avoided, due to the possible noise pick-up caused by the resistor coil, and the value of the load resistor must be known exactly in order to calculate the desired sensor resistance. A non-inverting op-amp can be used to buffer the output from the potentiometer (gain of low order, e.g. 1.2).

The circuit shown allows a constant current to be applied across the heater (shown as an equivalent resistor). The drive circuitry allows a voltage to be applied, which can be in the form of an AC or DC signal. The applied voltage signal is applied across the current limiting resistor, to provide a constant current.

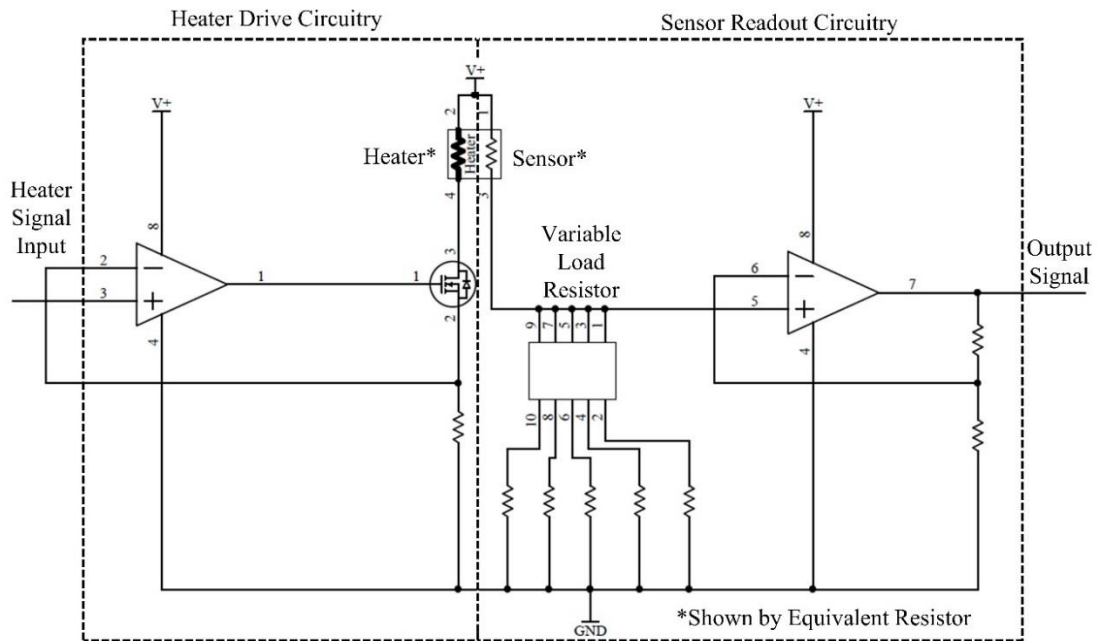


Fig. 3.20 – Simplified MOX sensor schematic, with heater current drive capability and readout circuitry (non-inverting amplifier or buffer).

3.4.1.4 MOX sensors for breath analysis

MOX sensors coated with WO_3 have been reported to have excellent sensing qualities to low ppm concentrations of NO_x (a collective term for a group of gases, usually referring to nitric oxide and nitrogen dioxide) [167,168]. The quality of ambient air is of concern for healthcare, where air pollution has been linked to respiratory diseases [169]. NO_2 and particulate matter are of particular concern in urban environments. Lung cancer and other respiratory diseases are associated with air pollution, for both smokers and non-smokers alike [170]. Ambient pollution has been reported to lead to airway inflation, which can be detected by measuring end exhaled nitric oxide [171].

The measurement of exhaled NO_x from subjects with asthma has been reported as a complement to the measurement of exhaled nitric oxide [172]. The biomarkers on exhaled breath for respiratory diseases provide a non-invasive means of testing the severity of the disease. In a study of 46 subjects (half asthma patients) a 100 % detection rate was achieved using a NO_x sensor (with a NO sensor for reference) [172]. The use of NO_x as a biomarker and replacement for NO measurements is desired in the study, to investigate the phenomena of oxidative stress (and its pathogenesis) and to ease measurements on children.

WO₃ based sensors have previously been reported to be capable of detecting acetone and hydrogen sulphide which are biomarkers for the diagnosis of diabetes and halitosis respectively. Kidney malfunction and lung cancer are also potentially diagnosable, through the detection of ammonia and toluene biomarkers, respectively [173]. Choi et al. developed a WO₃ coated sensor for the real-time monitoring of exhaling breath (100 ppb sensitivity level achieved) [173].

The mediocre response and slow recovery times (i.e. time for sensor resistance to change due to the presence of a gas of interest and the time for its return to a baseline signal after removal of the gas) limit the application of MOX sensors. Post-sensing signal processing aims to mitigate these problems. Response times are typically around 5 s, however recovery times can be as long as several minutes [174]. MOX sensors are praised as being sensitive to ppb levels of gases, but are usually cross-sensitive to humidity and have high power consumption (to raise the temperature of a heater as required for adequate sensor response) [175].

3.5 Commercial Sensors

In this project research sensors will be developed for the sensing of CO₂ (NDIR) and VOCs (MOX). However for the measurement of exhaled volume (flow sensor measures flow rate which can then be integrated) and oxygen in breath will be performed with commercial devices. Affordable commercial sensors exist for these components, from which it was assessed that performance could not be substantially improved over the duration of this work. Affordable VOC and CO₂ sensors are available for purchase, however their inadequate performance for breath sensing implied research devices were required to meet the target EE calculation accuracies for this project. Additionally, a commercial temperature and humidity sensor will be included in the breath analyser. The humidity and temperature of the sample gas passing through the sensor chamber must be monitored, to allow for compensation between the conditions found in exhaled breath and ambient air.

3.5.1 Oxygen Sensor

The City Technology (UK) MOX-20 MediceL electrochemical sensor was chosen for measurements of breath-by-breath oxygen concentration (note, not to be confused with metal oxide sensors, the model code is an abbreviation of medical oxygen). The affordable sensor was chosen for its fast response time (<750 ms specified) and stable

output ($< 10\%$ drift over a 1 year period) [176]. As commonly found with electrochemical cells, the device is bulky (with a 29.3 mm diameter cylindrical outer shell), although it is robust and will operate in humidity conditions from 0 to 99 % non-condensing. A photograph of the sensor is shown in Fig. 3.21 a). Further discussion of its performance is detailed in section 8.2. The Alphasense O2G2, Fig. 3.21 b), was used for testing in the mainstream analyser design. The lesser performance of the device led to its replacement with the MOX-20. The O2G2 is very affordable ($\sim\pounds 15$), physically smaller (20 mm diameter) and does not contain any pre-processing circuitry. Affordable electrochemical cells are widely commercially available (e.g. e2v EC410, Figaro KE-25), however the poor t_{90} times limit their use to environmental monitoring applications, instead of breath sampling.

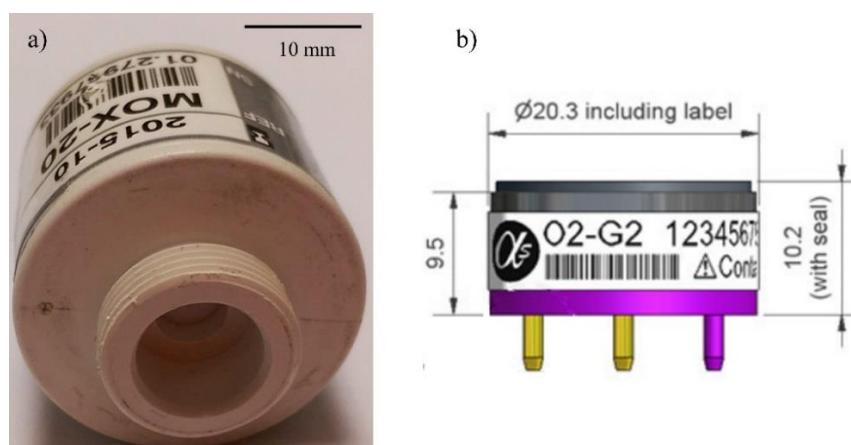


Fig. 3.21 a) Photograph of a City Technology O₂ sensor; b) Drawing of an Alphasense O2G2 sensor [177].

3.5.2 Flow Sensor

The SFM3000 commercial flow sensor (Fig. 3.22) manufactured by Sensirion (Switzerland) was selected, designed for use with ventilation medical instruments. The device offered a fast update time of 0.5 ms and an excellent flow range of ± 200 SLPM (standard litres per minute, bi-directional) [178]. The flow rate is recorded in a digital format (I^2C), which allows for easy interaction with a microcontroller. The device requires a 5 V power supply (e.g. a USB) and typical accuracy is $\pm 1.5\%$. The device has a 20 mm internal diameter main body, for direct connection to 22 mm medical respiratory tubing. The sensor is not miniature but it allows a subject to breathe through the device, with minimal effect on normal breathing pattern. Alternative commercially available devices were considered (e.g. Honeywell AWM5104VN), although the SFM3000 was selected, due to its compact size and fast response time.



Fig. 3.22 – Photograph of Sensirion SFM3000 flow sensor [178].

3.5.3 Temperature and Relative Humidity Sensor

Temperature and RH sensors are ubiquitous in gadgets, instruments and equipment. However, not many sensors offer the necessary performance (response time, resilience) to measure exhaled gas. An analogue output was preferred to avoid manufacture implemented filtering, which could slow the response of the sensor (or reduce its accuracy). The analogue output could be recorded with a microcontroller (or read using any suitable analogue to digital converter). From the available commercial devices, the GE (USA) ChipCap2 was selected, for a reasonable response time (~ 7 s) and miniature size (4 mm x 6 mm) [179]. A photograph of the chip is shown in Fig. 3.23. A Sensirion SHT21 sensor was considered, although its marginally slower response time (8s) perhaps indicates there was filtering applied in the processing stage to generate a digital output.

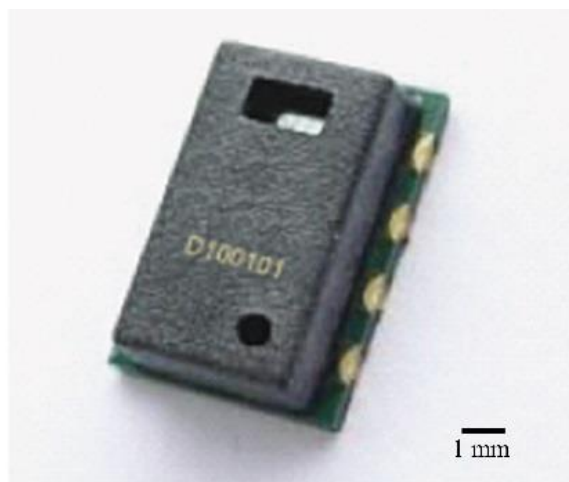


Fig. 3.23 – Photograph of a GE ChipCap2 Temperature and RH Sensor [179].

3.5.4 VOC MOX Sensor

An example of a commercial sensor from SGX SensorTech is shown in Fig. 3.24. The circuit described above could also be used with such a device. The package contains two MOX sensors, one for oxidising gases (e.g. NO₂ in the range of 0.05 – 10 ppm) and a second for reducing gases (e.g. CO in the range of 1- 10,000 ppm) [180].

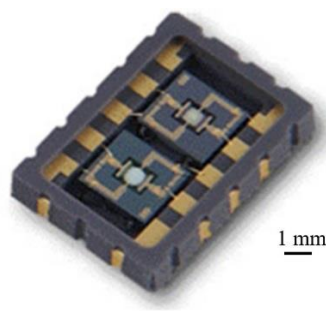


Fig. 3.24 – Photograph of a miniature commercial MOX sensor from SGX SensorTech (MICS-4514). Dual sensors for oxidising and reducing gas detection.

3.6 Conclusions

The gas sensors available both commercially and research prototypes are generally not suitable for the demands of this breath analysis project. The conditions found in exhaled breath subject the sensors to abnormal levels of humidity, temperature and flow. Furthermore, a fast response time is needed to meet the rapid changes in gas concentration between inhaling and exhaling. The abnormal levels of humidity and temperature can cause sensors to produce inaccurate responses, where the devices are responding to the polarising conditions compared to the ambient environment. It was found, in terms of VOC sensors and CO₂ sensors that research was required in order to develop devices capable of breath measurements, whereas the performance of the O₂, temperature and RH and flow sensors could not be improved upon in this project compared to the commercially available devices.

The NDIR CO₂ sensor system is a particular area of great interest, with the ability to tune a sensor to a specific wavelength (and therefore gas), lessening the need for an expensive and complex optical filter. The low power consumption of the NDIR sensor, its miniature size and fast response are attractive qualities for a portable analyser. Other gases identified as possible biomarkers for diabetics (acetone) and asthma (CO) could also be detected using similar IR setups.

3.7 References

- [1] A.H.D. Watson, *The Biology of Musical Performance and Performance-related Injury*, Scarecrow Press, Lanham, U.S., 2009.
- [2] R.W.O. Beebe, D.L. Funk, J.K. Scadden, *Fundamentals of Basic Emergency Care*, Clifton Park, U.S., 2009.
- [3] D.P. Jones, *Biomedical Sensors*, Momentum Press, New York, U.S., 2010.
- [4] C.W. Smith, R.H. Dilday, *Rice: Origin, History, Technology, and Production*, Wiley, Hoboken, U.S., 2002.
- [5] M.I. Baraton, *Sensors for Environment, Health and Security: Advanced Materials and Technologies*, Springer Netherlands, Dordrecht, Netherlands, 2009.
- [6] M.D. Joesten, J.L. Hogg, M.E. Castellion, *The World of Chemistry: Essentials*, Cengage Learning, Belmont, U.S., 2006.
- [7] A.G. Clarke, *Industrial Air Pollution Monitoring*, Springer Netherlands, Dordrecht, Netherlands, 2012.
- [8] J.Q. Koenig, *Health Effects of Ambient Air Pollution: How safe is the air we breathe?*, Springer US, Boston, U.S., 2000.
- [9] A.R. Eber, D.J. Bartell, *Attacking and Defending Drunk Drinking Tests*, James Publishing, Costa Mesa, U.S., 2007.
- [10] L. Taylor, S. Oberman, *Drunk Driving Defense*, Aspen Publishers Online, New York, U.S., 2006.
- [11] R.F. Steinert, D.F. Chang, *Cataract Surgery*, Saunders Elsevier, Philadelphia, U.S., 2009.
- [12] R. Bowden, *Countries of the World - United Kingdom*, Evans Brothers, London, U.K., 2005.
- [13] C.M. Johnson, *How Your Child Heals: An Inside Look at Common Childhood Ailments*, Rowman & Littlefield Publishers, Lanham, U.S., 2010.
- [14] D. Kilcast, P. Subramaniam, *The Stability and Shelf-life of Food*, CRC Press, Boca Raton, U.S., 2000.
- [15] R.A. Shenoi, S.S.J. Moy, L. Hollaway, *Advanced Polymer Composites for Structural Applications in Construction: Proceedings of the First International Conference, Held at Southampton University, UK, on 15-17 April 2002*, Thomas Telford, 2002.
- [16] F. Bulian, J. Graystone, *Wood Coatings: Theory and Practice*, Elsevier, Amsterdam, Netherlands, 2009.
- [17] D. Morton, N. Bagniet, G. Jones, D. Walters, *Advanced Physical Education Through Diagrams*, Oxford University Press, 2000.
- [18] J. Honeybourne, M. Hill, J. Wyse, *PE for You*, Stanley Thornes, Cheltenham, U.K., 1998.

- [19] I.P. Herman, *Physics of the Human Body*, Springer-Verlag Berlin Heidelberg, Berlin, Germany, 2007.
- [20] X.L. Wang, D.A. Scott, *Molecular Mechanisms of Tobacco-induced Diseases*, Nova Biomedical Books, New York, U.S., 2005.
- [21] S.P. Fortmann, T. Rogers, K. Vranizan, W.L. Haskell, D.S. Solomon, J.W. Farquhar, Indirect measures of cigarette use: expired-air carbon monoxide versus plasma thiocyanate, *Prev. Med. (Baltim)*. 13 (1984) 127–135. doi:[http://dx.doi.org/10.1016/0091-7435\(84\)90045-8](http://dx.doi.org/10.1016/0091-7435(84)90045-8).
- [22] L.G. Costa, L. Manzo, *Occupational Neurotoxicology*, Taylor & Francis, Boca Raton, U.S., 1998.
- [23] I. Horváth, L.E. Donnelly, A. Kiss, P. Paredi, S.A. Kharitonov, P.J. Barnes, Raised levels of exhaled carbon monoxide are associated with an increased expression of heme oxygenase-1 in airway macrophages in asthma: a new marker of oxidative stress, *Thorax*. 53 (1998) 668–672. doi:10.1136/thx.53.8.668.
- [24] Congress, *Congressional Record*, V. 146, Pt. 3, March 21, 2000 to April 4, 2000, Government Printing Office, Washington, U.S., 2000.
- [25] C. Turner, P. Španěl, D. Smith, A longitudinal study of ethanol and acetaldehyde in the exhaled breath of healthy volunteers using selected-ion flow-tube mass spectrometry, *Rapid Commun. Mass Spectrom.* 20 (2006) 61–68. doi:10.1002/rcm.2275.
- [26] B.P.J. de L. Costello, R.J. Ewen, N.M. Ratcliffe, A sensor system for monitoring the simple gases hydrogen, carbon monoxide, hydrogen sulfide, ammonia and ethanol in exhaled breath, *J. Breath Res.* 2 (2008) 37011.
- [27] A. Gasparatos, P. Stromberg, *Socioeconomic and Environmental Impacts of Biofuels: Evidence from Developing Nations*, Cambridge University Press, Cambridge, U.K., 2012.
- [28] R. Koppmann, *Volatile Organic Compounds in the Atmosphere*, Wiley, Ames, U.S., 2008.
- [29] S. Chen, M. Danao, Predictive models of ethanol concentrations in simulated exhaled breath and exhaled breath condensate under varied sampling conditions., *J. Biomed. Sci. Eng.* 2013 (2013) 788–795.
- [30] D. Zhao, D. Miller, D. Shao, X. Xian, F. Tsow, R.A. Iglesias, et al., A personal device for analyzing carbon dioxide in real time and real breath: Experimental investigation and computational simulation, *Sensors Actuators B Chem.* 183 (2013) 627–635. doi:<http://dx.doi.org/10.1016/j.snb.2013.03.138>.
- [31] M.C. do N. Nunes, *Color Atlas of Postharvest Quality of Fruits and Vegetables*, John Wiley & Sons, Ames, U.S., 2009.
- [32] Health and Safety Executive, *Workplace health, safety and welfare : Workplace (Health, Safety and Welfare) Regulations 1992 (as amended by the Quarries Miscellaneous Health and Safety Provisions Regulations 1995) : approved code of practice and guidance L24 / Health and Safety Commis, 12th Ed.*, Health and Safety Executive, Sudbury :, 1998.

-
- [33] A.C. Guyton, J.E. Hall, Textbook of Medical Physiology, 12th Ed., Elsevier Saunders, Philadelphia, U.S., 2011.
- [34] K.E. Barrett, S.M. Barman, S. Boitano, H. Brooks, Ganong's Review of Medical Physiology, 23rd Edition, 23rd Ed., Mcgraw-hill, New York, U.S., 2009.
- [35] D. Taylor, Human Physical Health, Cambridge University Press, Cambridge, U.K., 1989.
- [36] R.A. Clinchy, G.H. Egstrom, L. Fead, Jeppesen's Open Water Sport Diver Manual, Mosby-Year Book, St. Louis, U.S., 1992.
- [37] C. Shewell, Voice Work: Art and Science in Changing Voices, Wiley, Chincester, U.K., 2013.
- [38] American Academy of Orthopaedic Surgeons, Emergency Care and Transportation of the Sick and Injured, Jones & Bartlett Learning, LLC, Sudbury, U.S., 2006.
- [39] B. Daley, Air Transport and the Environment, Ashgate Publishing, Ltd., Farnham, U.K., 2012.
- [40] J. Colls, A. Tiwary, Colls, Air Pollution: Measurement, Modelling and Mitigation, Third Edition, CRC Press, London, U.K., 2009.
- [41] R.M. Berne, M.N. Levy, Principles of physiology, 3rd Ed., Mosby, St. Louis, U.S., 2000.
- [42] A.G. Dent, T.G. Sutedja, P. V Zimmerman, Exhaled breath analysis for lung cancer., *J. Thorac. Dis.* 5 (2013) S540–S550. doi:10.3978/j.issn.2072-1439.2013.08.44.
- [43] NOAA, C. Exposure, The NOAA Diving Manual: Diving for Science and Technology, Diane Publishing Company, Collingdale, U.S., 1992.
- [44] C. Turner, P. Spanel, D. Smith, A longitudinal study of ammonia, acetone and propanol in the exhaled breath of 30 subjects using selected ion flow tube mass spectrometry, SIFT-MS., *Physiol. Meas.* 27 (2006) 321–37. doi:10.1088/0967-3334/27/4/001.
- [45] A. Elersawi, World of Nanobioengineering: Potential Big Ideas for the Future, AuthorHouse, Bloomington, U.S., 2010.
- [46] E. Solomon, L. Berg, D. Martin, Biology, 9th Ed., Cengage Learning, Andover, U.K., 2010.
- [47] R. Amitrano, G. Tortora, Anatomy & Physiology Laboratory Manual, Pearson, Belmont, U.S., 2012.
- [48] D.E. Gardner, Toxicology of the Lung, Fourth Edition, 4th Ed., CRC Press, Boca Raton, U.S., 2011.
- [49] Mens Health, The Complete Book of Men's Health: The Definitive, Illustrated Guide to Healthy Living, Exercise, and Sex, Rodale, Emmaus, U.S., 2000.
- [50] B.G. Liptak, Post-Oil Energy Technology: The World's First Solar-Hydrogen

- Demonstration Power Plant, CRC Press, Boca Raton, U.S., 2008.
- [51] J.E. Shelby, Introduction to Glass Science and Technology, Royal Society of Chemistry, Cambridge, U.K., 2005.
- [52] W. Demtröder, H. Eric, E. Tsang, Atoms, Molecules and Photons: An Introduction to Atomic- Molecular- and Quantum Physics, Springer, Berlin, Germany, 2006.
- [53] J.W. Robinson, E.S. Frame, G.M. Frame, J. Melorose, R. Perroy, S. Careas, Undergraduate Instrumental Analysis, Seventh Edition, CRC Press, 2014. doi:10.1017/CBO9781107415324.004.
- [54] A.J. Bard, G. Inzelt, F. Scholz, J. Melorose, R. Perroy, S. Careas, Electrochemical Dictionary, Springer Berlin Heidelberg, Heidelberg, Germany, 2012. doi:10.1017/CBO9781107415324.004.
- [55] M. Singh, Introduction to Biomedical Instrumentation, PHI Learning Pvt. Ltd., New Delhi, India, 2010.
- [56] D.R. Thévenot, K. Toth, R.A. Durst, G.S. Wilson, Electrochemical biosensors: recommended definitions and classification, Biosens. Bioelectron. 16 (2001) 121–131. doi:10.1016/S0956-5663(01)00115-4.
- [57] B.G. Liptak, S.T. Gases, P. Ihydrafine, Instrument Engineers' Handbook, Volume One: Process Measurement and Analysis, 4th Ed., CRC Press, Boca Raton, U.S., 2003.
- [58] R.B. Northrop, Introduction to Instrumentation and Measurements, 3rd Ed., Taylor & Francis, Hoboken, U.S., 2014. doi:10.1017/CBO9781107415324.004.
- [59] J.J. Nagelhout, K.L. Plaus, Nurse Anesthesia, 5th Ed., Elsevier Health Sciences, 2013.
- [60] J.R. Cornforth, Combustion Engineering and Gas Utilisation, Taylor & Francis, Abingdon, U.K., 2014. doi:10.1017/CBO9781107415324.004.
- [61] E.A. Parr, Industrial Control Handbook, Industrial Press, Oxford, U.K., 1998.
- [62] N. McManus, Safety and Health in Confined Spaces, CRC Press, Boca Raton, U.S., 1998.
- [63] K. Mitsubayashi, Y. Wakabayashi, D. Murotomi, T. Yamada, T. Kawase, S. Iwagaki, et al., Wearable and flexible oxygen sensor for transcutaneous oxygen monitoring, Sensors Actuators B Chem. 95 (2003) 373–377. doi:10.1016/S0925-4005(03)00441-6.
- [64] S. Iguchi, K. Mitsubayashi, T. Uehara, M. Ogawa, A wearable oxygen sensor for transcutaneous blood gas monitoring at the conjunctiva, Sensors Actuators B Chem. 108 (2005) 733–737. doi:10.1016/j.snb.2004.12.099.
- [65] S.-Q. Xiong, Y. Wei, Z. Guo, X. Chen, J. Wang, J.-H. Liu, et al., Toward Membrane-Free Amperometric Gas Sensors: An Ionic Liquid–Nanoparticle Composite Approach, J. Phys. Chem. C. 115 (2011) 17471–17478. doi:10.1021/jp204309b.

- [66] Z. Wang, P. Lin, G.A. Baker, J. Stetter, X. Zeng, Ionic liquids as electrolytes for the development of a robust amperometric oxygen sensor, *Anal. Chem.* 83 (2011) 7066–7073. doi:10.1021/ac201235w.
- [67] J. Gębicki, A. Kloskowski, W. Chrzanowski, P. Stepnowski, J. Namiesnik, J. Gebicki, et al., Application of ionic liquids in amperometric gas sensors, *Crit. Rev. Anal. Chem.* 8347 (2015) 00–00. doi:10.1080/10408347.2014.989957.
- [68] K. Kendall, M. Kendall, *High-temperature Solid Oxide Fuel Cells for the 21st Century: Fundamentals, Design and Applications*, Elsevier Science, London, U.K., 2015.
- [69] T. Hübner, L. Boon-Brett, W. Buttner, P. Control, H.T. The, *Sensors for Safety and Process Control in Hydrogen Technologies*, CRC Press, Boca Raton, U.S., 2016.
- [70] D.K. Aswal, S.K. Gupta, G. Of, G.A.S. Sensor, *Science and Technology of Chemiresistor Gas Sensors*, Nova Science Publishers, New York, U.S., 2007.
- [71] R.J.D. Tilley, D.R. Tobergte, S. Curtis, *Principles and Applications of Chemical Defects*, Taylor & Francis, Cheltenham, U.K., 1998. doi:10.1017/CBO9781107415324.004.
- [72] S. Zhuiykov, *Electrochemistry of Zirconia Gas Sensors*, CRC Press, Boca Raton, U.S., 2007.
- [73] T. Mellard, *Automotive Electronic Systems*, Elsevier Science, Oxford, U.K., 2013.
- [74] SST Sensing, Zirconia Oxygen Sensors, (2011). <http://www.sstsensing.com/product/flange-mounted-oxygen-sensor> (accessed June 20, 2007).
- [75] A. McLuckie, P.O. Sensor, *Respiratory Disease and its Management*, Springer London, London, U.K., 2009.
- [76] A.R. Aitkenhead, I. Moppett, J. Thompson, N. Methods, S. Methods, Smith and Aitkenhead's *Textbook of Anaesthesia*, Elsevier Health Sciences UK, New York, U.S., 2013.
- [77] V.M. Fthenakis, J. Melorose, R. Perroy, S. Careas, *Prevention and Control of Accidental Releases of Hazardous Gases*, Wiley, New York, U.S., 1993. doi:10.1017/CBO9781107415324.004.
- [78] J.T. Joiner, *NOAA diving manual: diving for science and technology*, 4th Ed., National Oceanic and Atmospheric Administration, Office of Oceanic and Atmospheric Research, National Undersea Research Program, Office of Marine and Aviation Operations, NOAA Diving Program, Flagstaff U.S., 2001.
- [79] L. Cukrov, P. McCormick, K. Galatsis, W. Wlodarski, Gas sensing properties of nanosized tin oxide synthesised by mechanochemical processing, *Sensors Actuators B Chem.* 77 (2001) 491–495. doi:10.1016/S0925-4005(01)00751-1.
- [80] M. Bektas, D. Schönauer-Kamin, G. Hagen, A. Mergner, C. Bojer, S. Lippert, et al., $\text{BaFe}_{1-x}\text{Ta}_x\text{O}_{3-\delta}$ - A material for temperature independent resistive oxygen sensors, *Sensors Actuators, B Chem.* 190 (2014) 208–213.

doi:10.1016/j.snb.2013.07.106.

- [81] C. Cobianu, B.C. Serban, V. Avramescu, M. Brezeanu, A. Stratulat, O. Buiu, Novel materials for oxygen sensing technologies, in: 2016 Int. Semicond. Conf., 2016: pp. 17–26. doi:10.1109/SMICND.2016.7783028.
- [82] G. Tschulena, A. Lahrmann, *Sensors Applications, Sensors in Household Appliances*, John Wiley & Sons, Weinheim, Germany, 2006.
- [83] D. Li, Y. Liu, Y. Chen, *Computer and Computing Technologies in Agriculture IV: 4th IFIP TC 12 International Conference, CCTA 2010, Nanchang, China, October 22-25, 2010, Selected Papers*, Springer, 2011.
- [84] Alphasense, CO₂-D1 Carbon Dioxide Sensor Solid State, 44 (2014) 1. <http://www.alphasense.com/WEB1213/wp-content/uploads/2014/01/CO2D1.pdf> (accessed May 18, 2014).
- [85] R.J. Francey, L.P. Steele, Measuring atmospheric carbon dioxide—the calibration challenge, *Accredit. Qual. Assur.* 8 (2003) 200–204. doi:10.1007/S00769-003-0620-1.
- [86] J.G. Webster, H. Eren, *Measurement, Instrumentation, and Sensors Handbook, Second Edition: Electromagnetic, Optical, Radiation, Chemical, and Biomedical Measurement*, CRC Press, Boca Raton, U.S., 2014.
- [87] A. Bonfiglio, D. Curone, E.L. Secco, G. Magenes, A. Tognetti, Emergency and Work, in: *Wearable Monit. Syst.*, Springer US, Boston, MA, 2011: pp. 205–219. doi:10.1007/978-1-4419-7384-9_10.
- [88] J. Hodgkinson, R. Smith, W.O. Ho, J.R. Saffell, R.P. Tatam, Non-dispersive infra-red (NDIR) measurement of carbon dioxide at 4.2 μ m in a compact and optically efficient sensor, *Sensors Actuators B Chem.* 186 (2013) 580–588. doi:<http://dx.doi.org/10.1016/j.snb.2013.06.006>.
- [89] R. Frodl, T. Tille, A High-Precision NDIR CO₂ Gas Sensor for Automotive Applications, *IEEE Sens. J.* 6 (2006) 1697–1705. doi:10.1109/JSEN.2006.884440.
- [90] NIST Chemistry WebBook, (2015). <http://webbook.nist.gov/chemistry/> (accessed August 17, 2015).
- [91] R. Biswas, C.G. Ding, I. Puscasu, M. Pralle, M. McNeal, J. Daly, et al., Theory of subwavelength hole arrays coupled with photonic crystals for extraordinary thermal emission, *Phys. Rev. B - Condens. Matter Mater. Phys.* 74 (2006) 1–6. doi:10.1103/PhysRevB.74.045107.
- [92] F. Li, H. San, C. Li, Y. Li, X. Chen, MEMS-based plasmon infrared emitter with hexagonal hole arrays perforated in the Al-SiO₂-Si structure, *J. Micromechanics Microengineering.* 21 (2011) 105023. doi:10.1088/0960-1317/21/10/105023.
- [93] B.M. Wong, A.M. Morales, Enhanced photocurrent efficiency of a carbon nanotube p–n junction electromagnetically coupled to a photonic structure, *J. Phys. D. Appl. Phys.* 42 (2009) 55111. doi:10.1088/0022-3727/42/5/055111.
- [94] J. Esteve Sorribas, Study of 2-D Photonic Band Gaps for NIR applications,

- Treballs Final. Grau - Física. (2016).
- [95] A. Pusch, A. De Luca, S.S. Oh, S. Wuestner, T. Roschuk, Y. Chen, et al., A highly efficient CMOS nanoplasmonic crystal enhanced slow-wave thermal emitter improves infrared gas-sensing devices., *Sci. Rep.* 5 (2015) 17451. doi:10.1038/srep17451.
- [96] A. De Luca, M.T. Cole, A. Fasoli, S.Z. Ali, F. Udrea, W.I. Milne, Enhanced infra-red emission from sub-millimeter microelectromechanical systems micro hotplates via inkjet deposited carbon nanoparticles and fullerenes, *J. Appl. Phys.* 113 (2013) 214907. doi:10.1063/1.4809546.
- [97] J. Spannhake, O. Schulz, A. Helwig, G. Muller, T. Doll, Design, Development and Operational Concept of an Advanced MEMS IR Source for Miniaturized Gas Sensor Systems, in: *IEEE Sensors, 2005.*, IEEE, n.d.: pp. 762–765. doi:10.1109/ICSENS.2005.1597811.
- [98] GSS, H. Speed, C. Dioxide, SprintIR Datasheet, *Gas Sens. Solut.* (2016). https://www.gassensing.co.uk/media/1091/sprintir_-datasheet_gss.pdf (accessed July 1, 2016).
- [99] A. Graf, M. Arndt, M. Sauer, G. Gerlach, Review of micromachined thermopiles for infrared detection, *Meas. Sci. Technol.* 18 (2007) R59–R75. doi:10.1088/0957-0233/18/7/R01.
- [100] Q. Tan, L. Tang, M. Yang, C. Xue, W. Zhang, J. Liu, et al., Three-gas detection system with IR optical sensor based on NDIR technology, *Opt. Lasers Eng.* 74 (2015) 103–108. doi:10.1016/j.optlaseng.2015.05.007.
- [101] D.M. Considine, G.D. Considine, *Van Nostrand's Scientific Encyclopedia*, Springer US, New York, U.S., 2013.
- [102] B.L. Diffey, *O. Radiation, Radiation Measurement in Photobiology*, Elsevier Science, Burlington, U.S., 2013.
- [103] D.P. DeWitt, G.D. Nutter, D.R. Tobergte, S. Curtis, *Theory and Practice of Radiation Thermometry*, Wiley, 1988. doi:10.1017/CBO9781107415324.004.
- [104] N. Neumann, V. Banta, Comparison of Pyroelectric and Thermopile Detectors, *Proc. IRS 2013.* (2013) 139–143.
- [105] A. Rogalski, *Infrared Detectors*, 2nd Ed., CRC Press, Boca Raton, U.S., 2010.
- [106] InfraTec, LME-302 Datasheet, InfraTec. (n.d.) 1–2. <http://www.infratec.co.uk/fileadmin/media/Sensorik/pdf/LME-302.pdf> (accessed June 20, 2007).
- [107] Dexter Research Center, L. Power, G. Analysis, S. Items, D. Solutions, ST150 Technical Details, Dexter Pyroelectric Detect. (n.d.). <https://www.dexterresearch.com/?module=Page&sID=st150> (accessed June 20, 2007).
- [108] G.C.M. Meijer, A.W. Herwaarden, *Thermal Sensors*, Taylor & Francis, Bristol, UK, 1994.
- [109] G. Peng, U. Tisch, O. Adams, M. Hakim, N. Shehada, Y.Y. Broza, et al.,

- Diagnosing lung cancer in exhaled breath using gold nanoparticles., *Nat. Nanotechnol.* 4 (2009) 669–73. doi:10.1038/nano.2009.235.
- [110] A. Anton, A. Agapiou, A. Anton, A. Agapiou, Breath and sweat analysis as a tool for medical diagnostics, in: *Proc. 2014 4th Int. Conf. Wirel. Mob. Commun. Healthc. - "Transforming Healthc. Through Innov. Mob. Wirel. Technol. MOBIHEALTH 2014, 2015: pp. 250–253. doi:10.1109/MOBIHEALTH.2014.7015958.*
- [111] A. Bikov, K. Paschalaki, R. Logan-Sinclair, I. Horváth, S.A. Kharitonov, P.J. Barnes, et al., Standardised exhaled breath collection for the measurement of exhaled volatile organic compounds by proton transfer reaction mass spectrometry., *BMC Pulm. Med.* 13 (2013) 43. doi:10.1186/1471-2466-13-43.
- [112] W.-H. Cheng, W.-J. Lee, Technology development in breath microanalysis for clinical diagnosis, *J. Lab. Clin. Med.* 133 (1999) 218–228. doi:10.1016/S0022-2143(99)90077-X.
- [113] M.J. McGrath, C.N. Scanaill, *Sensor Technologies: Healthcare, Wellness and Environmental Applications*, Apress, New York, U.S., 2013.
- [114] D.M. Fahey, J.S. Miller, *Alcohol and Drugs in North America: A Historical Encyclopedia [2 volumes]: A Historical Encyclopedia*, ABC-CLIO, Santa Barbara, U.S., 2013.
- [115] P.A. Lieberzeit, F.L. Dickert, Sensor technology and its application in environmental analysis, *Anal. Bioanal. Chem.* 387 (2006) 237–247. doi:10.1007/s00216-006-0926-z.
- [116] R. Rubio, J. Santander, L. Fonseca, N. Sabaté, I. Grácia, C. Cané, et al., Non-selective NDIR array for gas detection, *Sensors Actuators B Chem.* 127 (2007) 69–73. doi:10.1016/j.snb.2007.07.003.
- [117] Z. Yunusa, M.N. Hamidon, A. Kaiser, Z. Awang, Gas sensors: A review, *Sensors and Transducers.* 168 (2014) 61–75. doi:10.13074/jent.2015.12.153163.
- [118] H.W. Jang, Y.R. Choi, Y.H. Kim, Novel Metal Oxide Gas Sensors for Mobile Devices, in: *Smart Sensors Syst.*, Springer International Publishing, New York, U.S., 2015: p. 132.
- [119] X. Liu, S. Cheng, H. Liu, S. Hu, D. Zhang, H. Ning, A Survey on Gas Sensing Technology, *Sensors.* 12 (2012) 9635–9665. doi:10.3390/s120709635.
- [120] P.J. Mazzone, J. Hammel, R. Dweik, J. Na, C. Czich, D. Laskowski, et al., Diagnosis of lung cancer by the analysis of exhaled breath with a colorimetric sensor array., *Thorax.* 62 (2007) 565–8. doi:10.1136/thx.2006.072892.
- [121] M. Righettoni, A. Tricoli, Toward portable breath acetone analysis for diabetes detection, *J. Breath Res.* 5 (2011) 37109. doi:10.1088/1752-7155/5/3/037109.
- [122] S.E. Deveci, F. Deveci, Y. Açıık, A.T. Ozan, The measurement of exhaled carbon monoxide in healthy smokers and non-smokers, *Respir. Med.* 98 (2004) 551–556. doi:10.1016/j.rmed.2003.11.018.
- [123] E.T. Middleton, A.H. Morice, *Breath Carbon Monoxide as an Indication of*

- Smoking Habit, *Chest*. 117 (2000) 758–763. doi:10.1378/chest.117.3.758.
- [124] S.E. Meredith, A. Robinson, P. Erb, C.A. Spieler, N. Klugman, P. Dutta, et al., A mobile-phone-based breath carbon monoxide meter to detect cigarette smoking., *Nicotine Tob. Res.* 16 (2014) 766–73. doi:10.1093/ntr/ntt275.
- [125] R. Zegdi, D. Perrin, M. Burdin, R. Boiteau, A. Tenaillon, Increased endogenous carbon monoxide production in severe sepsis, *Intensive Care Med.* 28 (2002) 793–796. doi:10.1007/s00134-002-1269-7.
- [126] K. Zayas, K. Sekizawa, S. Okinaga, M. Yamaya, T. Ohru, H. Sasaki, Increased carbon monoxide in exhaled air of asthmatic patients, *Am. J. Respir. Crit. Care Med.* 156 (1997) 1140–1143. doi:10.1164/ajrccm.156.4.96-08056.
- [127] A. Lal, L. Patterson, A. Goldrich, A. Marsh, Point-of-care end-tidal carbon monoxide reflects severity of hemolysis in sickle cell anemia., *Pediatr. Blood Cancer.* 62 (2015) 912–4. doi:10.1002/xbc.25447.
- [128] M. Nishimura, D. Hess, R.M. Kacmarek, R. Ritz, W.E. Hurford, Nitrogen Dioxide Production during Mechanical Ventilation with Nitric Oxide in Adults Effects of Ventilator Internal Volume, Air Versus Nitrogen Dilution, Minute Ventilation, and Inspired Oxygen Fraction, *J. Am. Soc. Anesthesiol.* 82 (1995) 1246–1254.
- [129] K. Alving, E. Weitzberg, J.M. Lundberg, Increased amount of nitric oxide in exhaled air of asthmatics., *Eur. Respir. J.* 6 (1993) 1368–70.
- [130] J.M.J.J.O.N. Lundberg, E. Weitzberg, S.L. Nordvall, R. Kuylenstierna, J.M.J.J.O.N. Lundberg, K. Alving, Primarily nasal origin of exhaled nitric oxide and absence in Kartagener’s syndrome, *Eur. Respir. J.* 7 (1994) 1501–1504. doi:10.1183/09031936.94.07081501.
- [131] N. Berkman, A. Avital, R. Breuer, E. Bardach, C. Springer, S. Godfrey, Exhaled nitric oxide in the diagnosis of asthma: comparison with bronchial provocation tests., *Thorax.* 60 (2005) 383–8. doi:10.1136/thx.2004.031104.
- [132] R.G. Stirling, S.A. Kharitonov, D. Campbell, D.S. Robinson, S.R. Durham, K.F. Chung, et al., Increase in exhaled nitric oxide levels in patients with difficult asthma and correlation with symptoms and disease severity despite treatment with oral and inhaled corticosteroids. *Asthma and Allergy Group., Thorax.* 53 (1998) 1030–4. doi:10.1136/thx.53.12.1030.
- [133] M. Pedrosa, N. Cancelliere, P. Barranco, V. López-Carrasco, S.Q.M. Quirce, Usefulness of exhaled nitric oxide for diagnosing asthma, *J Asthma.* 47 (2010) 817–821. doi:10.3109/02770903.2010.491147.
- [134] U. Martin, P. Howarth, K. BRYDEN, M. DEVOY, P. Howarth, Increased levels of exhaled nitric oxide during nasal and oral breathing in subjects with seasonal rhinitis, *J. Allergy Clin. Immunol.* 97 (1996) 768–772. doi:10.1016/S0091-6749(96)80154-0.
- [135] A.W. Murphy, T.A.E. Platts-Mills, M. Lobo, F. Hayden, Respiratory nitric oxide levels in experimental human influenza., *Chest.* 114 (1998) 452–456. doi:10.1378/chest.114.2.452.
- [136] H. Grasemann, N. KNAUER, R. BÜSCHER, K. HÜBNER, J.M.M. Drazen, F.

- Ratjen, et al., Airway nitric oxide levels in cystic fibrosis patients are related to a polymorphism in the neuronal nitric oxide synthase gene, *Am.J.Respir.Crit Care Med.* 162 (2000) 2172–2176.
- [137] I.M. Balfour-Lynn, A. Laverty, R. Dinwiddie, Reduced upper airway nitric oxide in cystic fibrosis., *Arch. Dis. Child.* 75 (1996) 319–22.
- [138] T.K. Tromp, R.-L. Shia, M. Allen, J.M. Eiler, Y.L. Yung, Potential environmental impact of a hydrogen economy on the stratosphere., *Science.* 300 (2003) 1740–2. doi:10.1126/science.1085169.
- [139] A. Eisenmann, A. Amann, M. Said, B. Datta, M. Ledochowski, Implementation and interpretation of hydrogen breath tests., *J. Breath Res.* 2 (2008) 46002. doi:10.1088/1752-7155/2/4/046002.
- [140] M. Simrén, P.-O. Stotzer, Use and abuse of hydrogen breath tests., *Gut.* 55 (2006) 297–303. doi:10.1136/gut.2005.075127.
- [141] U.C. Ghoshal, How to interpret hydrogen breath tests., *J. Neurogastroenterol. Motil.* 17 (2011) 312–7. doi:10.5056/jnm.2011.17.3.312.
- [142] D.G. Thompson, P. Binfield, A.D.E. Belder, J.O. Brien, S. Warren, M. Wilson, et al., Extra intestinal influences, *Gut.* 26 (1985) 1349–1352. doi:10.1136/gut.26.12.1349.
- [143] B.P.J. de Lacy Costello, M. Ledochowski, N.M. Ratcliffe, The importance of methane breath testing: a review., *J. Breath Res.* 7 (2013) 24001. doi:10.1088/1752-7155/7/2/024001.
- [144] M.D. Levitt, J.K. Furne, M. Kuskowski, J. Ruddy, Stability of human methanogenic flora over 35 years and a review of insights obtained from breath methane measurements., *Clin. Gastroenterol. Hepatol.* 4 (2006) 123–9. doi:10.1016/j.cgh.2005.11.006.
- [145] M. Pimental, A.G. Mayer, S. Park, E.J. Chow, A. Hasan, Y. Kong, et al., Methane Production During Lactulose Breath Test Is Associated with Gastrointestinal Disease Presentation, *Dig. Dis. Sci.* 48 (2003) 86–92.
- [146] J.W. Gardner, A diffusion-reaction model of electrical conduction in tin oxide gas sensors, *Semicond. Sci. Technol.* 4 (1999) 345.
- [147] R.K. Srivastava, P. Lal, R. Dwivedi, S.K. Srivastava, Sensing mechanism in tin oxide-based thick-film gas sensors, *Sensors Actuators B Chem.* 21 (1994) 213–218. doi:10.1016/0925-4005(94)01248-2.
- [148] P. Shankar, J.B. Rayappan, Gas sensing mechanism of metal oxides: The role of ambient atmosphere, type of semiconductor and gases - A review, *Sci. Lett.* 4 (2015) 1–18.
- [149] M.K. Ram, V.R. Bhethanabotla, *Sensors for Chemical and Biological Applications*, CRC Press, Boca Raton, U.S., 2010.
- [150] C. Wang, L. Yin, L. Zhang, D. Xiang, R. Gao, Metal Oxide Gas Sensors: Sensitivity and Influencing Factors, *Sensors.* 10 (2010) 2088–2106. doi:10.3390/s100302088.

- [151] N. Yamazoe, K. Shimano, Theory of power laws for semiconductor gas sensors, *Sensors Actuators B Chem.* 128 (2008) 566–573. doi:10.1016/j.snb.2007.07.036.
- [152] G. Eranna, *Metal Oxide Nanostructures as Gas Sensing Devices*, CRC Press, Boca Raton, U.S., 2016.
- [153] A. Helwig, G. Müller, G. Sberveglieri, M. Eickhoff, On the low-temperature response of semiconductor gas sensors, *J. Sensors.* (2009) 17. doi:10.1155/2009/620720.
- [154] J.W. Gardner, Electrical conduction in solid-state gas sensors, *Sensors and Actuators.* 18 (1989) 373–387. doi:10.1016/0250-6874(89)87043-X.
- [155] M.J. Madou, *Fundamentals of Microfabrication: The Science of Miniaturization*, 2nd Ed., CRC Press, Boca Raton, U.S., 2002.
- [156] J.F. Mcaleer, P.T. Moseley, J.O.W. Norris, D.E. Williams, O.O.X. Ora, Tin dioxide gas sensors. Part 1.—Aspects of the surface chemistry revealed by electrical conductance variations, *J. Chem. Soc. Faraday Trans. 1 Phys. Chem. Condens. Phases.* 83 (1987) 1323. doi:10.1039/f19878301323.
- [157] J.W. Gardner, A non-linear diffusion-reaction model of electrical conduction in semiconductor gas sensors, *Sensors Actuators B Chem.* 1 (1990) 166–170. doi:10.1016/0925-4005(90)80194-5.
- [158] K. Schmitt, C. Peter, J. Wöllenstein, Chromium titanium oxide-based ammonia sensors, in: M. Fleischer, M. Lehmann (Eds.), *Solid State Gas Sensors - Ind. Appl.*, Springer Berlin Heidelberg, Berlin, Heidelberg, 2012: pp. 113–135. doi:10.1007/5346_2011_8.
- [159] N. Barsan, M. Schweizer-Berberich, W. Göpel†, Fundamental and practical aspects in the design of nanoscaled SnO₂ gas sensors: a status report, *Fresenius. J. Anal. Chem.* 365 (1999) 287–304. doi:10.1007/s002160051490.
- [160] C.-C. Liu, M.A. Stuczynski, Application of silicon-based microfabrication and micromaching techniques to the development of chemical sensors, in: *Proc. Second Int. Symp. Microstruct. Microfabr. Syst.*, The Electrochemical Society, Pennington, U.S., 2001: p. 2.
- [161] A.A. Tomchenko, G.P. Harmer, B.T. Marquis, J.W. Allen, Semiconducting metal oxide sensor array for the selective detection of combustion gases, *Sensors Actuators B Chem.* 93 (2003) 126–134. doi:10.1016/S0925-4005(03)00240-5.
- [162] G. Lippert, J. Dabrowski, I. Costina, G. Lupina, M. Ratzke, P. Zaumseil, et al., Morphology and composition of selected high-k materials and their relevance to dielectric properties of thin-films, in: R. Ekwah Sah (Ed.), *Silicon Nitride, Silicon Dioxide, Emerg. Dielectr.*, 9th Ed., The Electrochemical Society, Pennington, U.S., 2007: p. 783. doi:10.1017/CBO9781107415324.004.
- [163] A. Ratna Phani, S. Manorama, V.J. Rao, Effect of additives on the response of sensors utilizing semiconducting oxide on carbon monoxide sensitivity, *Appl. Phys. Lett.* 66 (1995) 3489. doi:10.1063/1.113773.
- [164] Y. Shimizu, M. Egashira, Basic aspects and challenges of semiconductor gas

- sensors, *MRS Bull.* 24 (1999) 18–24. doi:10.1557/S0883769400052465.
- [165] L. Guo, L. Xu, Z. Xu, G. Duan, Y. Wang, H. Zhou, et al., Design and fabrication of micro-nano fusion gas sensor based on two-beam micro-hotplatform, *Microsyst. Technol.* (2016) 1–7. doi:10.1007/s00542-016-3091-0.
- [166] J. Huang, Q. Wan, Gas sensors based on semiconducting metal oxide one-dimensional nanostructures., *Sensors (Basel)*. 9 (2009) 9903–24. doi:10.3390/s91209903.
- [167] G. Sberveglieri, L. Depero, S. Groppelli, P. Nelli, WO₃ sputtered thin films for NO_x monitoring, *Sensors Actuators B Chem.* 26 (1995) 89–92. doi:10.1016/0925-4005(94)01563-W.
- [168] H. Kawasaki, T. Ueda, Y. Suda, T. Ohshima, Properties of metal doped tungsten oxide thin films for NO_x gas sensors grown by PLD method combined with sputtering process, *Sensors Actuators B Chem.* 100 (2004) 266–269. doi:10.1016/j.snb.2003.12.052.
- [169] C. Pirozzi, A. Sturrock, P. Carey, S. Whipple, H. Haymond, J. Baker, et al., Respiratory effects of particulate air pollution episodes in former smokers with and without chronic obstructive pulmonary disease: a panel study, *COPD Res. Pract.* 1 (2015) 1. doi:10.1186/s40749-015-0004-z.
- [170] M.C. Turner, D. Krewski, C.A. Pope, Y. Chen, S.M. Gapstur, M.J. Thun, Long-term ambient fine particulate matter air pollution and lung cancer in a large cohort of never-smokers., *Am. J. Respir. Crit. Care Med.* 184 (2011) 1374–81. doi:10.1164/rccm.201106-1011OC.
- [171] G. Adamkiewicz, Association between air pollution exposure and exhaled nitric oxide in an elderly population, *Thorax.* 59 (2004) 204–209. doi:10.1136/thorax.2003.006445.
- [172] N. Chérot-Kornobis, S. Hulo, J.-L. Edmé, V. de Broucker, R. Matran, A. Sobaszek, Analysis of nitrogen oxides (NO_x) in the exhaled breath condensate (EBC) of subjects with asthma as a complement to exhaled nitric oxide (FeNO) measurements: a cross-sectional study, *BMC Res. Notes.* 4 (2011) 202. doi:10.1186/1756-0500-4-202.
- [173] S.-J. Choi, F. Fuchs, R. Demadrille, B. Grévin, B.-H. Jang, S.-J. Lee, et al., Fast Responding Exhaled-Breath Sensors Using WO₃ Hemitubes Functionalized by Graphene-Based Electronic Sensitizers for Diagnosis of Diseases, *ACS Appl. Mater. Interfaces.* 6 (2014) 9061–9070. doi:10.1021/am501394r.
- [174] T. Nakamoto, *Essentials of Machine Olfaction and Taste*, Wiley, Singapore, 2016.
- [175] G. Korotcenkov, *Handbook of Gas Sensor Materials*, in: Springer New York, New York, NY, 2013: p. 331. doi:10.1007/978-1-4614-7165-3.
- [176] City Technology, MOX-20 MediceL, 2013 (n.d.). <http://www.citytech.com/PDF-Datasheets/mox20.pdf>.
- [177] Alphasense, O₂-G2 Oxygen Sensor, 44 (2013). <http://www.alphasense.com/WEB1213/wp-content/uploads/2013/07/O2G2.pdf> (accessed January 15, 2014).

-
- [178] Sensirion, Low-Pressure-Drop Flow Meter SFM3000, Sensirion. (2016). <https://www.sensirion.com/products/mass-flow-meters-for-gases/low-pressure-drop-mass-flow-meter/> (accessed August 4, 2016).
- [179] GE, ChipCap2 a Fully Calibrated Humidity and Temperature Sensor, GE MSC. (2011) 2–3. <http://www.ge-mcs.com/de/moisture-and-humidity/relative-humidity-sensors/chipcap2.html> (accessed August 4, 2016).
- [180] SGX SensorTech, Gas Sensors: Metaloxide (MICS): MICS-4514, SGX. (n.d.). <https://www.cdiweb.com/ProductDetail/MICS4514-SGX-Sensortech-Limited-formerly-e2v/333417/> (accessed July 1, 2016).

CHAPTER IV

Direct Sampling of Breath

Preface

To sample an exhalation, the most direct means of monitoring gas concentrations is to place a sensor in the mainstream exhalation airway tube (i.e. sensor placed directly in path of exhalation, without a sampling system). A breath analyser with sensors solely in a single tube, through which the user breathes, does not require a complex sampling systems to extract a portion of exhaled gas for analysis. Such devices do not require any means of extracting a sample (such as a pump or a fan), thus can reduce complexity, power consumption and noise. However, the gas sensors inside a mainstream analyser must be capable of responding to gases passing directly from an exhalation, at high flow rate and high humidity. If the sensors are located in a side-stream section, these variations (compared to ambient conditions) are less apparent. Initially, the device developed for this project used a main-stream sampling technique. In this chapter the development of the initial prototype is discussed and the pitfalls of this sampling method.

4 Mainstream Sampling

Mainstream gas analysers offer reduced power consumption, a simpler sampling system and faster response times. This method of measuring breath does not require a bulky sampling system, instead the sensors are located in a section of tubing through which the subject breaths directly. The alternative technique, side-stream sampling, takes a portion of the flow (extracted using a pump or fan) and samples the gas with sensors in a small chamber. A diagram showing the difference between main- and side-stream sampling for mechanically ventilated patients is shown in Fig. 4.1.

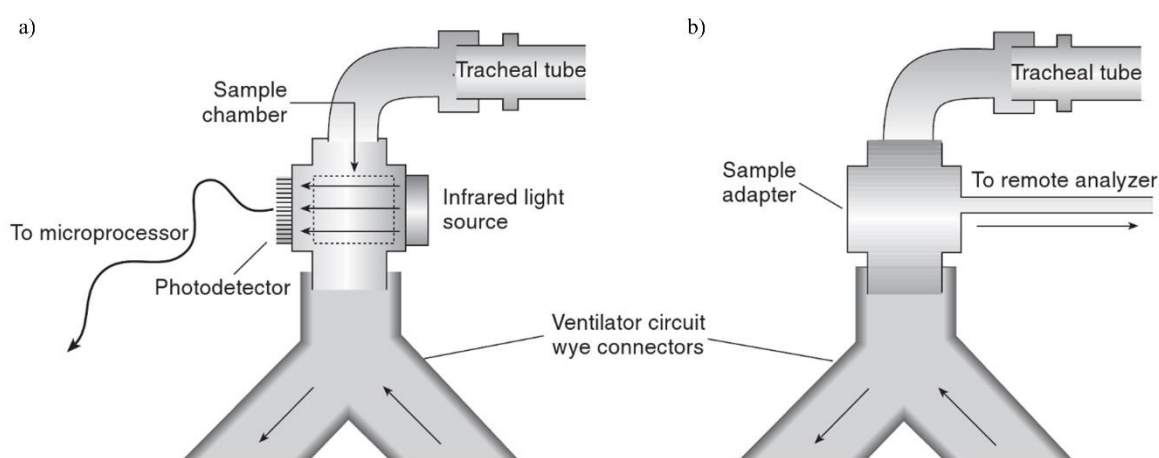


Fig. 4.1 – CO₂ sampling techniques for mechanically ventilated patients, a) mainstream and b) side-stream [1].

Mainstream sampling systems can be more bulky than side-stream designs, dependent on the mounting location of the sensors. The diameter of the sample tubing in a mainstream system is usually set to match the standard tubing size from the outlet of a mask. Metabolic rate measurements, and indeed those for CO₂ measurement of mechanically ventilated patients, require normal breathing (i.e. the measurement system should not affect the breathing pattern). Changes in tube diameter can cause the flow to become turbulent (normally exhaled flow is laminar) and restricted diameter tubing can increase breathing resistance. Standard outlet diameters from face masks and mouthpieces are usually ~20 mm. As discussed in chapter III, breathing through any apparatus can affect breathing, although the disruption can be minimised with comfortable facemasks and low resistance outlet tubing.

4.1 Chamber Design

A mainstream chamber was constructed to house multiple gas sensors for breath measurements. The device was designed to take measurements of an exhalation and report the sensor response data on a computer. At the preliminary measurement stage, only laboratory based gas rig tests were performed. The potential block diagram for the completed system is shown in Fig. 4.2. At this stage in the project development, no VOC sensor was used, although the system was designed so sensors could be added or interchanged as found necessary in the calibration process.

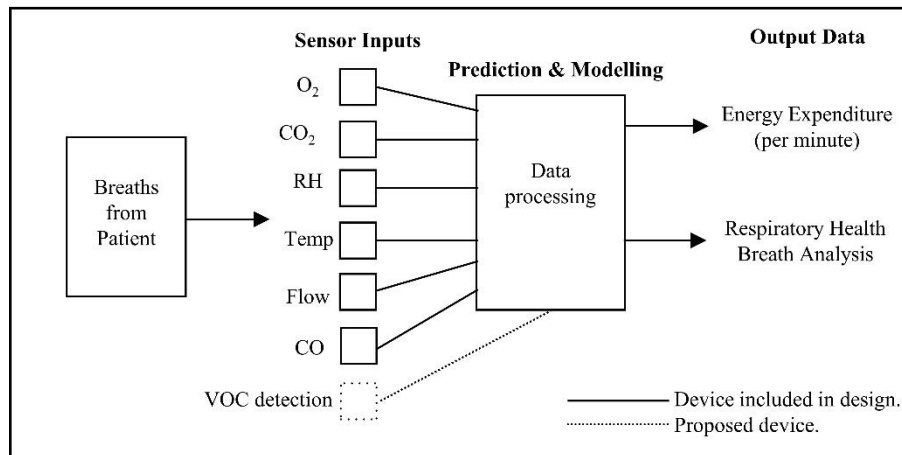


Fig. 4.2 – Block diagram of mainstream breath analyser function.

The chamber was constructed from 5 mm acrylic sheets and designed with interchangeable end plates, which enabled different inlet and outlet gas connectors to be fitted. To test and calibrate the sensors against a gas bench rig, an endplate with a 1 mm internal diameter threaded connection was fitted. For breath measurements a plate with a 20 mm I.D. was fitted (for connection to the Sensirion SFM3000 flow meter). A photograph of the chamber connected to the gas rig is shown in Fig. 4.3. As shown in the photograph, the chamber was configured to test the flow sensor, O₂ sensor (Alphasense O2G2), CO₂ sensor (Gas Sensing Solutions SprintIR), temperature and humidity sensor (GE ChipCap2) and CO sensor (Applied Sensor AS-MLC).

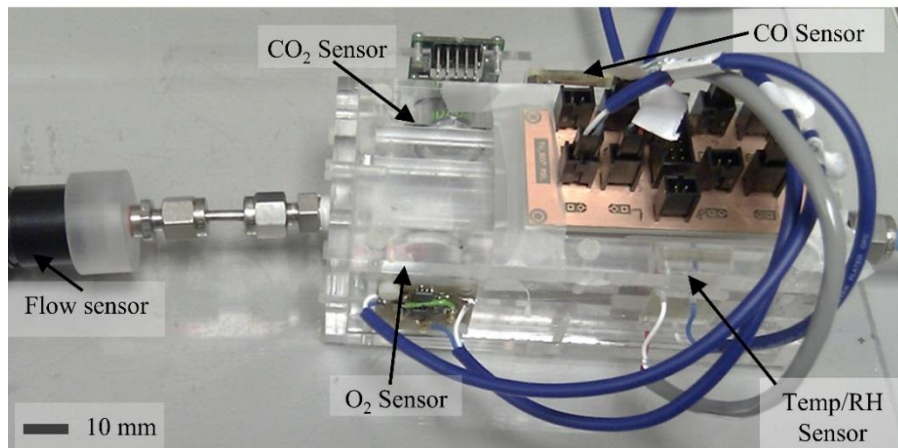


Fig. 4.3 – Photograph of mainstream chamber configured to test on bench gas rig.

The fluid flow through a model of the chamber was simulated using Solidworks 2014. The flow from the gas rig was usually configured to a total of 1 SLPM (constant, regardless of gas mixture). A screen print of the model is shown in Fig. 4.4. The model shows considerable mixing occurs inside the chamber, while the gas enters. The large chamber (126 ml) size (internal $120 \times 35 \times 30$ mm; length, width, height) means a 1 SLPM inflow will take ~ 7.5 s to fill the chamber (if ideal mixing occurs). Plug flow and ideal mixing are unlikely to occur, and the mixing time can be up to 4 times the ideal value [2]; therefore the mixing time could be up to 30 s.

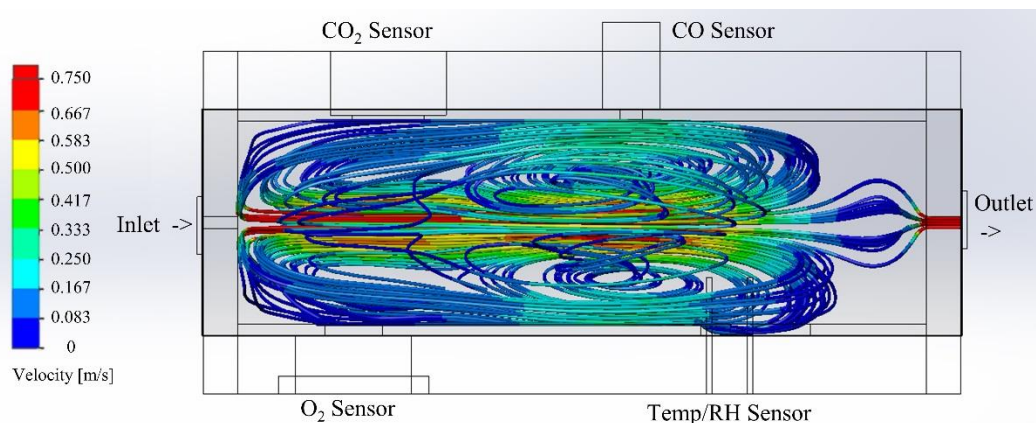


Fig. 4.4 – Fluid flow model of mainstream chamber with 1 SLPM flow inlet.

The outlet from the model was set to resemble atmospheric conditions. This was to simulate the conditions for main-stream sampling, where the outlet would not need to be connected to an exhaust. The inlet and outlet were confirmed as 5 mm diameter holes (the holes in the final unit were threaded as to allow different connectors to be attached). Inside the chamber, it was assumed each gas sensor would be fitted into the unit to allow the sensing area to fit flush to the sides of the chamber.

4.2 Methodology - Bench Gas Rig Experiments

The mainstream chamber served as a modular system, to trial affordable commercial gas sensors within a gas testing rig. The adaptable chamber permitted multiple sensors to be tested simultaneously and was able to accommodate various commercial devices for each gas of interest. The gas testing rig was used to produce gas mixtures similar to those found in exhaled breath (in terms of O₂, CO and CO₂) and importantly, high levels of humidity were also simulated. The analogue voltage outputs from the CO, O₂ and temperature and relative humidity sensors were recorded using a National Instruments (NI) USB 6341 USB data acquisition unit. The digital outputs from the CO₂ sensor and flow sensor were recorded using an Arduino Uno microcontroller. A LabVIEW (2013) virtual instrument (VI) was used to log the data from all of the sensor outputs and manage the gas flow through the sensor chamber using four Alicat MC-5SLPM mass flow controllers (MFCs).

To test if the sensors were capable of meeting the targets for EE measurement accuracy, a cross-validation model was designed in MatLab (2014) to classify the sensor outputs. From the experimental data, 50 % was used to train the model and 50 % used to test. The validation modelling computer systems are designed to predict (classify) items into a number of classes ('classification') [3]. The process is called 'learning' as it should involve choosing or adapting parameters within the model structure to perform best based on the current samples. The measurement data produced by the sensors (e.g. output voltage) potentially contain the necessary information to classify the gas (e.g. a gas concentration). The user must first specify the part of the measurement relevant to produce the desired result – i.e. a feature must be extracted from the data which should be used to separate one particular measurement from another.

The operation of gas sensors and the chamber in which they are situated (mentioned above) can affect the response characteristics. Usually the response of gas sensors exponentially tends to a final output value, although the length of this transition varies according to the type of sensor and exposure conditions. The length of the period taken to reach the final value is an issue if it is of similar order to the exposure time of the gas, i.e. for breath sampling an exhalation lasts perhaps under 3 s. The typical output envelope of a slow response gas sensor is shown in Fig. 4.5 a), compared to an ideal

response shown in Fig. 4.5 b). The real world response can be attributed to the design of the sensor chamber's mixing effect of the gases in the chamber, flow velocity and the reaction time of the sensor itself [4]. For the modelling process, a non-time dependent factor was considered, to quantify the accuracy of the sensor separately from the response time. The accuracy of the sensor is difficult to improve post-manufacture, however redesign of sensor housing to yield better response times is a simple method to improve breath analyser performance.

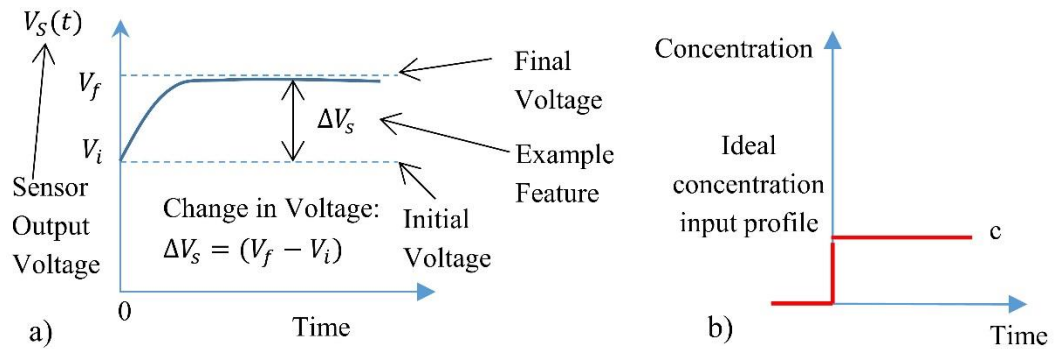


Fig. 4.5 a) Sensor output observed during preliminary tests; b) ideal step response change in gas concentration to produce sensor output.

The time-independent feature chosen to be extracted is the change in output voltage from the start of the experiment (where the device was exposed to dry, synthetic air) to the end of a gas concentration step, as denoted by ΔV_s in fig. 4.5 a). Alternative features can be extracted, such as the fractional change, $(\Delta V_F)/(V_i)$ or a log change such as $\ln(\Delta V_s)$. Baseline noise was present in all gas sensors, during preliminary testing, thus an additive feature was preferred. For a multiplicative error a ratio feature was selected (also used for removing factors such as temperature dependence). Electronic noses have often used feature extraction for signal analysis; common elements include the minimum and maximum values of each signal, the times taken to reach these values, maximum sensitivity, slope rise time or curve intervals [5–7].

4.2.1 Classification Experiments

As discussed previously, the experiments used to model the response of the sensors must expose the devices to comparable gases and conditions to those found in exhaled breath. A linear equation with four components was chosen to model the system based on the mixing of two gases and two environmental conditions (temperature and humidity). The relative humidity (RH), the amount of water vapour in the gas as ratio of the water vapour required to saturate the gas at a set temperature, was controlled

using the gas rig. The type of equations used to model the output from the sensors was of the form (4.1), where the CO₂, O₂, RH and temperature conditions are represented by the coefficients c_1 to c_4 , respectively. The 4 parameters are the partial regression coefficients to be determined. The fourth term was eliminated from the modelling experiments because temperature was kept constant.

$$y_{gas} = k_1c_1 + k_2c_2 + k_3c_3 + k_4c_4 \tag{4.1}$$

To reduce the number of experiments to a manageable task, only 1 % intervals for CO₂ and O₂ were trialled, and the RH levels were set at 0 % or 50 %. This reduced the total number of experiments required to 72, as shown in Table 4.1 (with corresponding diagram in Fig. 4.6, in terms of the concentration of each element C_i , $i = 1$ to 4). The table shows the 36 experiments performed at each humidity value (0 % and repeated for 50 % RH). For each cell in the table there were 2 results, denoted by c which were O₂ and CO₂.

O ₂ /CO ₂	0%	1%	2%	3%	4%	5%
21%	ΔV_{c00}	ΔV_{c50}
20%
19%
18%
17%
16%	ΔV_{c05}					ΔV_{c55}

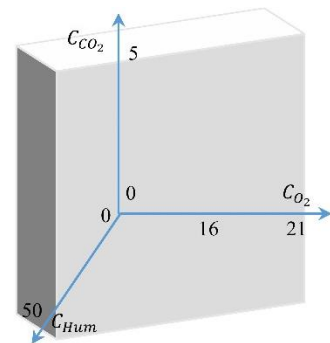


Table 4.1 – Experiments performed to model the output from the sensor.

Fig. 4.6 – 3D plot to show the desired test gas sensor model area.

The model block diagram is of the form shown in Fig. 4.7 a), where the inputs are raw sensor data and the outputs gas concentrations (or factors relating). The output from the experiments are 6 predicted values of each gas for every 1 % increment (both for 0 % and 50 % RH). A graph, similar to that shown in Fig. 4.7 b), is desired, where the test portion of the data (3 points for each concentration) are used to predict the gas level present and compared against the actual concentration. Given the predicted gas

concentrations, error bars are plotted for each test gas level and a confidence interval produced. This enables the performance of each sensor to be examined and the suitability of the sensor for this type of breath measurement to be assessed.

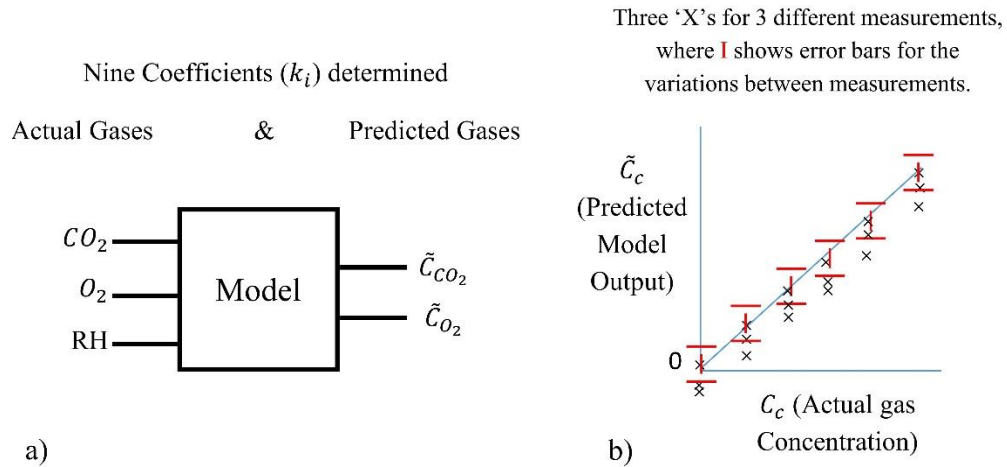


Fig. 4.7 a) Model block diagram displaying the input and output data; b) Desired output plot to compare predicted and actual measurements.

4.2.2 Sensor Data Preparation for Model Input

To decrease the computational error in the model, the input data were normalised to a range of [0,1] for each sensor [8]. The normalisation reduces the range of output from the sensors, which in raw output form would be in the range of 0 to 50,000 ppm for the CO_2 sensor and 0.7 to 1.0 V for the O_2 sensor. Providing the input data for each sensor to the model is approximately of the same range, the magnitude of the values themselves are less critical. However, the range of 0 to 1 was selected for ease of conversion, as each sensor output is compared to its maximum output value and normalised. The data are passed to the modelling script in matrix form, where a balance matrix is preferred with all values in a small range. The sensor test data was observed to be noisy, therefore a filter (such as low pass or moving average smoothing) is applied. The changes in the sensor outputs due to the gas concentration are greater than the magnitude of the noise, thus patterns for modelling were not greatly affected by the filtering process.

The required procedure performed to normalise the data is shown in Table 4.2; it is first assumed that the sensor outputs are converted to gas concentration using the calibration data provided by each manufacturer. Once the data have been processed by the model, the normalisation factor was removed, to return the value back to a concentration (the inverse of the normalisation process).

Table 4.2 – Normalisation process required for each sensor.

Sensor (output name)	Expected Range	Sensor Normalisation Factor
CO ₂ (c ₁)	0-50,000ppm	$c_1/50,000$
O ₂ (c ₂)	16-21%	$(c_2 - 16)/5$
RH (c ₃)	0-50%	$c_3/50$

4.2.3 Model Training and Testing Vectors

To form a model the algorithm needs to learn patterns and features from the input data – i.e. a ‘Training’ set of data is required. The ‘Testing’ set of data is the matrix that was classified, based on the information gained from the training dataset. The overall data set must carefully be split into two subsets. In the extreme case, where all samples are used for training, the model becomes a look-up table. In this approach, original samples of course were classified very accurately, however new cases are far less likely to be classified, with such an enormous number of possible combinations of features, there is little chance that an identical case will be found [3]. This problem is termed ‘overspecialisation’ or ‘over-fitting’.

The learning methods considered in this work are all ‘supervised’ learning, where the user informs the software of the desired output for each input data pattern, often achieving greater accuracy on smaller datasets, than ‘unsupervised’ learning [9]. Unsupervised learning is where no prior information about the data is known and training is based solely on the patterns in the data [10]; this method is less common in the literature [11].

A number of methods are available for splitting the data, in order to evaluate the error in the modelling system. The accuracy of the system is usually defined as the probability of correctly classifying a randomly selected instance [12]. The most common methods for testing the accuracy of a system are ‘cross-validation’ and ‘bootstrapping’ [13]. Another common method is called the hold out method, which splits the data into two mutually exclusive subsets; a training set and a hold out (test) set.

For the hold out procedure it is common to designate 2/3 of the data set for training and 1/3 for testing [12]. Using these typical ratios, the hold out true error estimate is relatively pessimistic; a resampling method provides better estimates of the true error rate [3]. The ‘leave-one-out’ method is a special (extreme) case of the cross validation system [14]. It is mathematically simple and provides an almost unbiased estimate of the ability of a classifier. It uses the complete sample population minus one ($N - 1$) as the training set, then tests it on the remaining sample [15]; this procedure is repeated N times. This method uses all of the data to classify one sample at a time, thus its bias is low, but it suffers from high variance [16]. However it is computationally intensive (with N classifiers required), but is recommended for small datasets with limited training data [14] (~100 sample sets with 50 cases each [3]).

The general cases of cross-validation are named ‘k-fold cross-validation’. The samples are divided up into k groups, in each trial one group is used for testing and the remaining $k - 1$ groups for training, so that every group is used as the test set once. This method makes good use of the available data, so is useful when the amount of available data is limited [14]. With the case of a low amount of data (relatively small, 72 samples), 2 fold cross validation was used; the data was split equally into two groups using a random selection method.

4.2.4 Partial Least Squares (PLS)

PLS is a regression procedure, in its simplest form, that specifies a linear model between a dependent response (y) and predictor variables (x 's), as shown in the section above [17]. The technique was originally reported by Wold in the 1960s forming an extension to the multiple linear regression (MLR) model [18]. It manages to extend the MLR model, without imposing the restrictions entailed with discriminant analysis, PCR (principal components regression) and canonical correlation [17]. As PLS is not limited by these restrictions, it is probably the most flexible of the various multivariate extensions of the MLR model.

As in MLR, PLS is used to form a linear model, i.e. PLS finds the linear combination of a predictor variable (X) that best explains a response variable (Y) [19]. Two algorithms have been documented for computing PLS regression; the standard algorithm is called NIPALS (nonlinear iterative PLS) or alternatively SIMPLS algorithm could be implemented [17]. The software package MatLab has a built-in

function for performing PLS regression which is based on the SIMPLS algorithm (although either could be implemented). A brief explanation of how PLS regression was reported by Wold is given below [20].

The target of the PLS algorithm is expressed in equations (4.2) and (4.3), where a set of scores (T) is calculated. T must be found so that the residual factors E and F are small, while also being a good descriptor of both sets of data.

$$X=TP'+E \quad (4.2)$$

$$Y=TC'+F \quad (4.3)$$

If the model has N factors, T is an $I \times N$ matrix of PLS scores, P is a $K \times N$ matrix of x -loadings and C is a $M \times N$ matrix of y -loadings. A graphical representation of the PLS analysis is shown in Fig. 4.8. Equation (4.4) shows the calculation of the scores matrix T, as the projection of the data X onto a $K \times N$ weights matrix W^* .

The relationship between the weights matrix and eigenvectors $X'YY'X$ is such that successive PLS factors form the largest covariance between Y and X. The solutions given by PLS are constrained so that the columns of the scores matrix T and weights matrix W^* are orthogonal and orthonormal respectively.

$$T=XW^* \quad (4.4)$$

The equations (4.2) to (4.4) can be rearranged to show the PLS solution to the regression. This is shown in equations (4.5) and (4.6), where B is a matrix of regression coefficients ($K \times M$ size).

$$Y=XW^*C'+F=XB+F \quad (4.2)$$

$$B=W^*C' \quad (4.3)$$

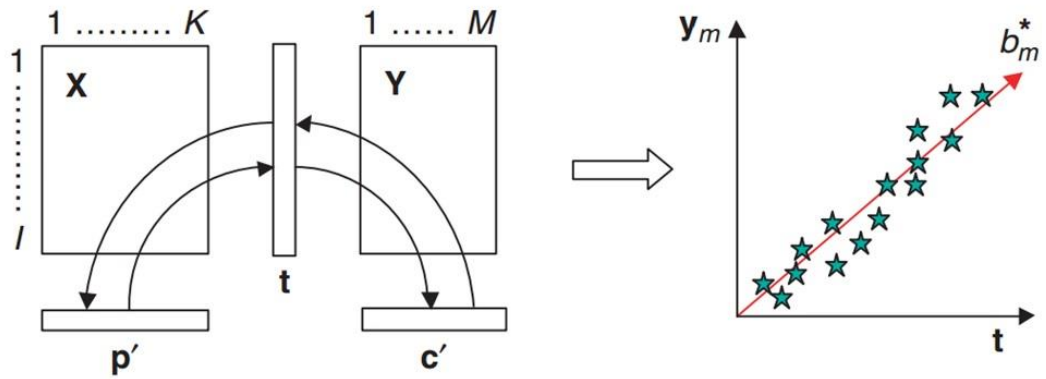


Fig. 4.8 – Schematic representation of PLS algorithm [20]. Left graphic shows factor decomposition is used to obtain scores t common to X and Y that reflects their covariance. Plot on right shows regression is applied to relate t to each of the response variances y_m via regression coefficient b_m^* .

4.3 Gas Rig Classification Experimentation

The O_2 and CO_2 sensors were tested using pulses of each gas. To test for any cross-sensitivity, one gas (either O_2 or CO_2) was kept at a constant concentration while the other was pulsed. The model was developed to classify the concentration of the target gas, without cross-sensitivity to the presence of another gas. The O_2 gas concentrations were generated between 16 % and 21 %, using synthetic air and N_2 . CO_2 gas concentrations were pulsed between 0 % and 5 % with a balance of synthetic air. The pulses for each gas were stepped at one minute time intervals.

The gas concentrations were pulsed in 1 % steps cylindrically, to simulate the cyclical nature of breathing. Fig. 4.9 shows the raw output data recorded from the O_2 and CO_2 gas sensors over one repetition. An example of the processed data (O_2 sensor raw output in Volts is converted to a percentage) is shown in Fig. 4.10. In the example test patterns shown, the CO_2 is pulsed to a constant concentration at 1 min intervals for a period of 10 minutes (first at 2 % then increased to 3 %). The O_2 gas concentration is pulsed from 20 % to 16 % at 1 min intervals (baseline of synthetic air, 21 % O_2).

The gas flow was kept constant at 1 SLPM (standard litre per minute). The outputs from the O_2 , CO_2 and RH sensors were normalised to a range of between 0 and 1, as shown in Fig. 4.11. The RH and temperature measurements were recorded using the GE Chipcap2, which verified that the environmental conditions were constant throughout the experiments.

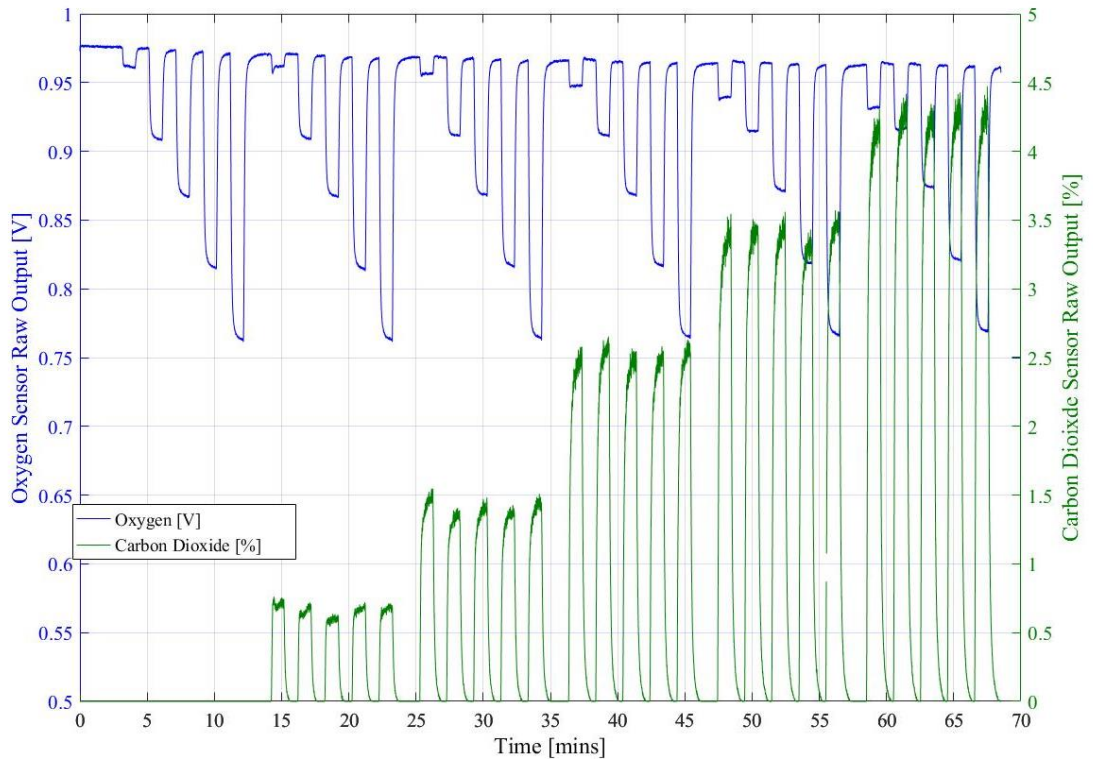


Fig. 4.9 – Raw sensor outputs from pulsing experiments, over a duration of 70 min.

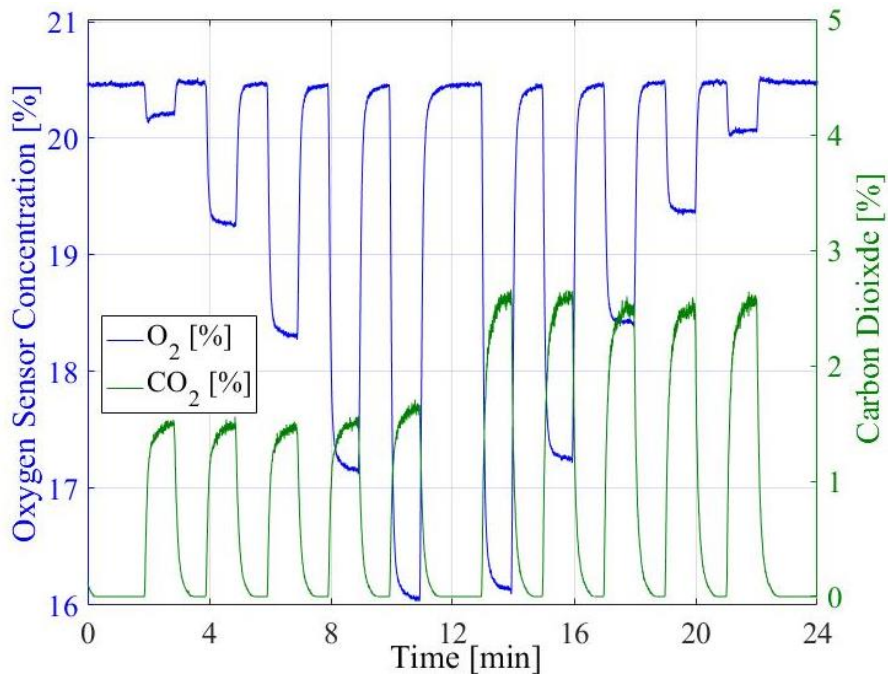


Fig. 4.10 – Section of test patterns used to generate the PLS regression model of the O₂ and CO₂ sensors converted to percentage concentrations.

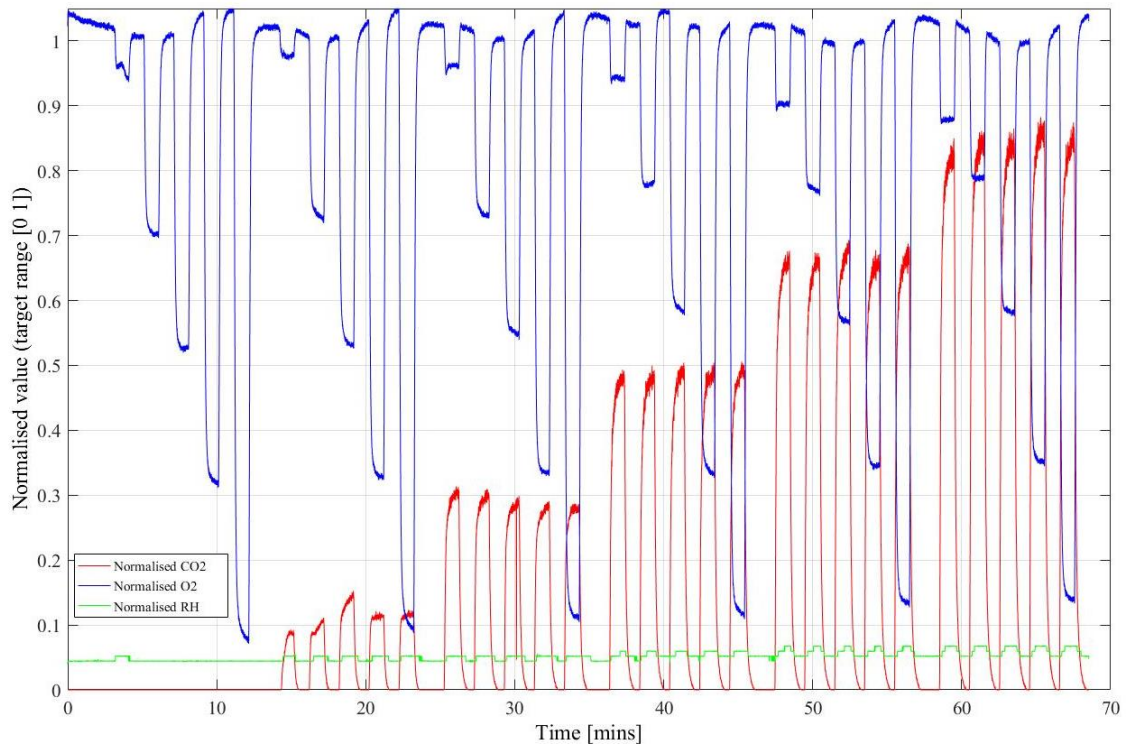


Fig. 4.11 – Normalised data for O₂, CO₂ and RH sensors shown for the 70 minute repetition.

The response times of the O₂ and CO₂ sensors were investigated by fitting bi-exponential curves, as of the form equation (4.2).

$$y = a \left(1 - e^{-\frac{t}{\tau_1}} \right) + b \left(1 - e^{-\frac{t}{\tau_2}} \right) + c \quad (4.2)$$

The values for each of the unknowns (i.e. a, b, t_1, t_2 etc.) were calculated using the MatLab curve fitting toolbox. A 20 s window was taken from the start of the response of each sensor, to which the bi-exponential curve was fitted.

4.3.1 Experimental Results for Gas Rig Classification

The raw sensor data, shown in Fig. 4.9, was analysed and post-processed using MatLab 2014. Example curve fit outputs for the O₂ and CO₂ sensors are shown in Fig. 4.12 a) and b) respectively. For the O₂ sensor a very close fit ($R^2=0.999$) was found (where R is the coefficient of determination). The bi-exponential curve was used to calculate the t_{90} response time for each of the sensors. For the O₂ sensor the response time was found to be 9.5 s on average. For the CO₂ sensor, the curve fitting process achieved a good fit ($R^2=0.998$); a slower response time of 14.1 s found on average.

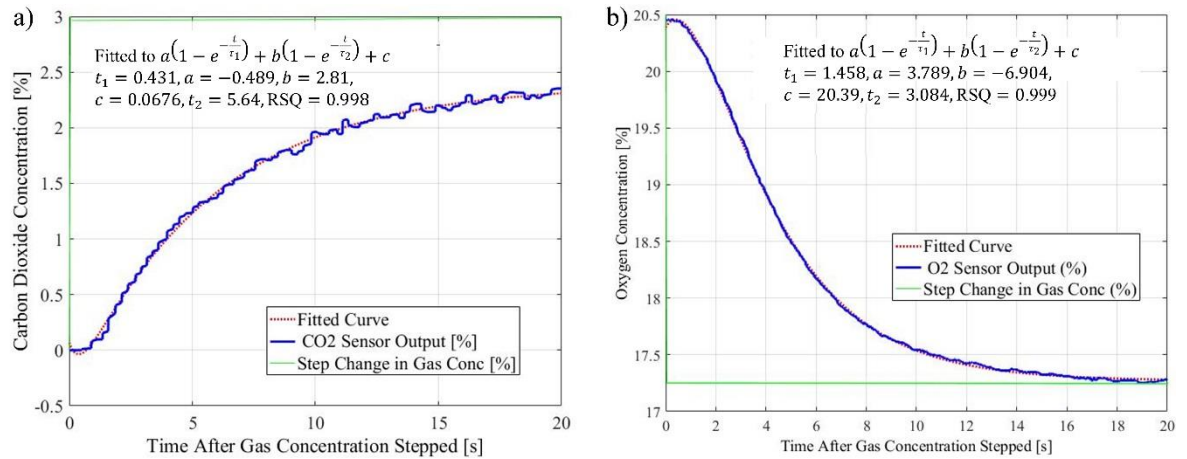


Fig. 4.12 a) First 20 s window from the O₂ sensor showing raw sensor output, bi-exponential fitted curve and step change in O₂ concentration; b) First 20 s window from the CO₂ sensor response to a step gas concentration change, with raw, fitted curve and input step change plotted.

The PLS model outputs for O₂ and CO₂ are shown in Fig. 4.13 a) and b), respectively. The O₂ sensor is shown to produce high accuracy, with a 95 % confidence interval (CI) that the sensor was close to the desired 0.52 % target accuracy. This target accuracy is required to make EE measurements to the desired 1 % accuracy. The repeatability of the O₂ measurements is acceptable, however results at 20 % O₂ level have greater variation of 0.3 % compared to the 0.1 % accuracy shown at lower concentrations.

The CO₂ sensor results demonstrate poorer performance, needing a 70 % CI to come close to the desired 1.20 % relative accuracy. The spread of these results is lower (mean 0.06 %), however given the lower range of CO₂ of interest, the accuracy of the CO₂ sensor is inferior. The CO₂ sensor in general underestimates the concentration of the gas present, as notably visible in the normalised plot (Fig. 4.11), where a value of 1 corresponds to a concentration of 5 %.

The maximum output from the sensor is in the range of 0.83 to 0.86 (normalised) when exposed to 5 % concentration of CO₂ (generated by the gas testing rig). The underestimation of the CO₂ concentration does not affect the PLS modelling stage, as the model tries to fit the normalised output to the specified normalised input. For example, the output at 4 % and 5 % CO₂ when normalised is ~0.67 and ~0.83 respectively, when values of 0.8 and 1.0 ideally would be expected. The difference

between the normalised values is 0.16, sufficient when only six values of CO₂ are configured in order to be able to distinguish the two concentrations.

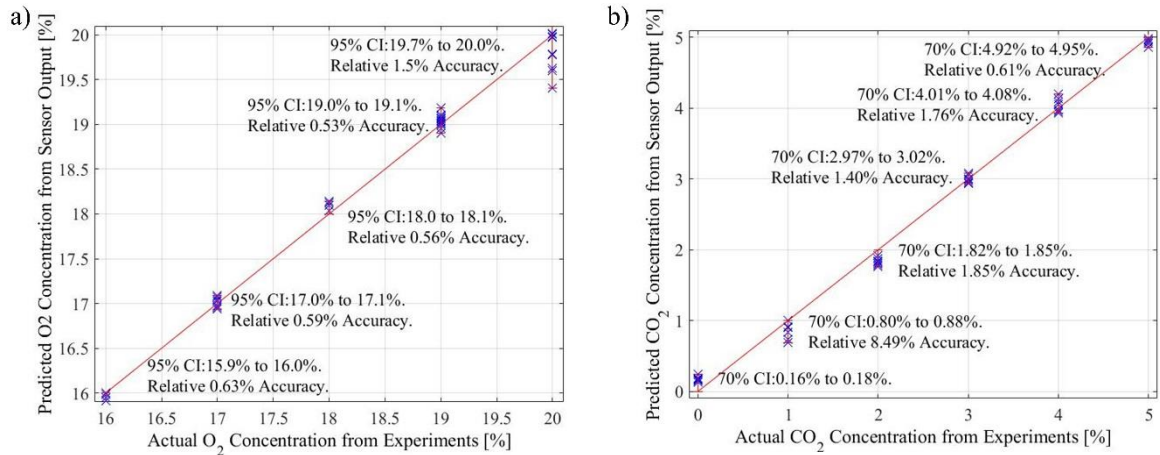


Fig. 4.13 a) Model output for O₂ sensor including 95 % CI calculations to assess performance, demonstrating that the sensor is operating close to the desired target 0.52 % accuracy; b) Model output for the CO₂ sensor, target relative accuracy of 1.20 %, 70 % CI demonstrates poor performance.

The digital output from the CO₂ sensor demonstrated a significant level of noise throughout the output range (~0.08 % broadband noise). To account for the slow response time measured (> 10 s) it was assumed a digital filter was integrated into the CO₂ sensor itself, which limited the performance of the device. The instruction manual with the SprintIR sensor discussed the possibility of activating an adjustable digital filter. For these experiments it was deactivated, according to the steps detailed in the manual.

The O₂ sensor provided a smooth output throughout the experiment, although it did not provide a sufficiently fast output to perform breath-by-breath measurements. It can be assumed the slow response time was due to the operation of the sensor, where the diffusion of O₂ molecules into the electrochemical cell accounts for the majority of the delayed response. According to the specification of the device, Alphasense do not include any filter into the construction of the O2G2 sensor. Therefore the output from the device will not be delayed by any processing stages. The electronic circuitry to amplify the micro-amp current output from the sensor is custom designed, and does not include any filtering elements. The circuit was optimised for response time, with any filtering required only possible in the final post data-logging stages.

4.3.2 Verification of CO₂ Sensor Performance

The performance of the SprintIR CO₂ sensor did not meet the specification declared on the datasheet provided by the manufacturer (GSS). The response time of the sensor was not sufficient for breath measurement (14.1 s measured compared to the 1.2 s specified [21]) and the accuracy was poor (70 % CI barely sufficient to meet 1.20 % target accuracy). To verify whether the design of the system (e.g. chamber, gas mixing profile) affected the performance, the affordable commercial device was tested against a relatively expensive reference sensor (Hummingbird IR3107 CO₂ sensor [22]).

The CO₂ sensors were exposed to CO₂ in the range of 0 to 4 %, generated using a gas testing rig and 5 % cylinder of CO₂, diluted with synthetic air where required. The total flow rate was kept constant at 0.5 SLPM to avoid damage to the expensive commercial sensor. The test pattern had 1 % steps of CO₂, for an interval of 1 minute each, returning to a baseline of synthetic air. The Hummingbird commercial sensor was connected downstream of the SprintIR sensor to ensure the response time comparison was altered only by the operation of the sensors and not by the gas mixing time. Fig. 4.14 shows the output from both the commercial devices, where a median filter was applied to each device at 5 sample points (data logged at 100 Hz).

The IR3107 sensor demonstrates that the level of CO₂ generated by the gas rig is likely to be accurate and only a minor delay in the response time shown by the SprintIR sensor can be attributed to the design of the sensor chamber. The spurious peaks shown at the switching points from synthetic air to low percentage concentrations of CO₂ for the Hummingbird output are due to the sudden switching of the MFCs, which cause a momentary increase in CO₂ concentration in the chamber (< 2 s). This effect could be reduced by reconfiguring the PID control setup in the MFCs, but was left constant so as not to disrupt the performance of the gas testing system for higher gas concentration mixtures.

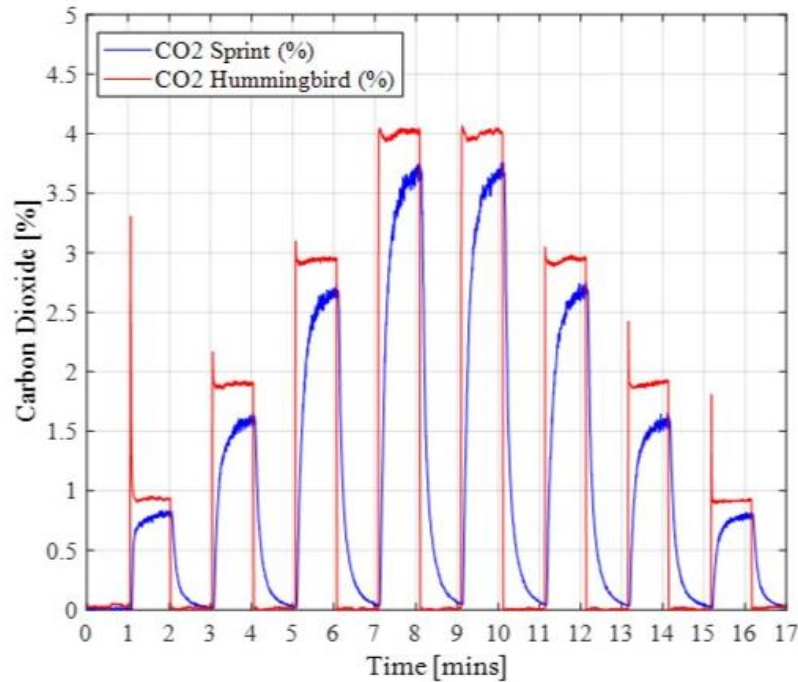


Fig. 4.14 – Comparison between the SprintIR and the IR3107 gas sensors for 1 minute pulses of CO₂ in the range of 0 to 4 %.

The SprintIR sensor underestimates the concentration of CO₂ present, by approx. 7.5 % in some measurements (e.g. peak values on average of 3.71 % were found when exposed to 4.0 % CO₂ concentration). In the parallel measurements, the Hummingbird sensor measures approximately 4.0 %, although some level of noise is present in the output (~0.05 % variance). The level of noise present in the SprintIR sensor output is ~0.1 % CO₂. The device was calibrated prior to the experiment, to 0 % CO₂ in air and nitrogen. The device produces consistent measurements, if the excessive level of noise is filtered. For example, the average output after 1 minute of exposure to 2 % CO₂ was 1.60 % for the first step and 1.59 % for the second step.

The main factor preventing the use of the SprintIR in a breath-by-breath analyser is the inadequate response time. To verify if any sampling techniques could be implemented to capture the end of an exhalation and hold it for a short period (e.g. sample alternate exhalations) the t_{90} response time was measured for both the GSS and Hummingbird sensors. To avoid the level of noise falsifying the 90 % of final value measurement point, bi-exponential curves, Figs. 4.11, were fitted to the output response from the instant the step change in gas concentration change occurred. A 20 s window was taken to enable the best exponential curve fitting, where it was assumed that the sensor would be likely reach its t_{90} value within 15 s. Fig. 4.15 a) and b) show

the output from the models for the GSS SprintIR and Hummingbird IR3107 sensors respectively, for the fifth pulse of CO₂ (as shown in Fig. 4.14), to a 4 % CO₂ input concentration. The calculated t_{10} to t_{90} times for each step (from Fig. 4.14) are shown in Table 4.3. This period indicates the time taken for the sensor output to alter from 10 % of the final output value to 90 % of the final output value.

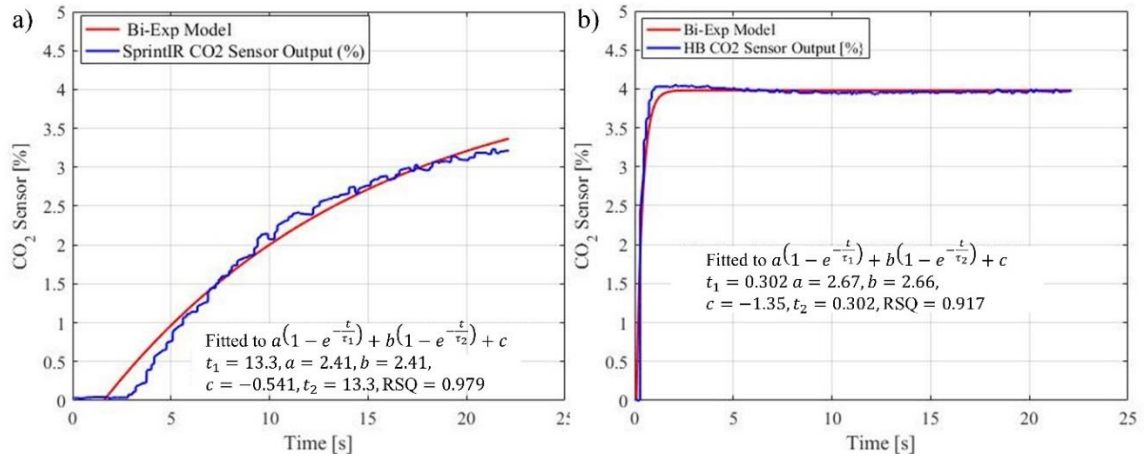


Fig. 4.15 – Bi-Exponential models fitted to 20 s output window of a) Affordable commercial SprintIR sensor and b) Relatively expensive commercial Hummingbird sensor.

Table 4.3 – Response times calculated for the turn-on phase for both commercial CO₂ devices.

Step	1 %	2 %	3 %	4 %	4 %	3 %	2 %	1 %
SprintIR								
t_{10} to t_{90} [s]	17.95	38.25	56.69	58.45	57.57	61.52	42.71	41.04
IR3107								
t_{10} to t_{90} [s]	0.55	1.00	1.11	1.33	1.84	2.43	0.96	1.33

The t_{10} to t_{90} response times were calculated to investigate the response time of the device, without considering the initial mixing time of the chamber and avoiding any baseline noise. The exponential fit for the SprintIR sensor required extending to a 60 s range, to allow response times above 20 s to be calculated. The disappointing performance of the SprintIR sensor was consistent throughout the measurements, where the response time improved for lower concentrations, but never approached the

quick response required for breath analysis. The Hummingbird device was slower (~1.5 s) than specified in the datasheet (0.1 s) [22], however the flow conditions were not optimised for this sensor (as previously detailed, the SprintIR sensor was connected in the chamber prior to the IR3107). Considering the flow rate (0.5 SLPM) and the volume (gas pipes and chambers) that delayed the mixing of the gas, the IR3107 responded with reasonable speed for breath-by-breath analysis. However, the relative expense of the device means that it cannot be included in a low-cost breath analyser.

The output sensor responses shown in Fig. 4.15 are both after exposure to 4 % CO₂; the SprintIR device only reaches ~3 % after the 20 s period (whereas the IR3107 reaches its final output ~4 % after < 2 s). The poor performance from the affordable sensor demonstrates the need for development of a reliable, affordable and fast CO₂ sensor for use in projects such as breath analysers, safety sensors and portable equipment. The design and construction of a prototype CO₂ sensor designed for breath-by-breath analysis is detailed in the chapter IV.

4.4 VOC Sensor Measurements

For breath analysis the measurement of VOCs is of great interest for disease detection [23]. In this work, metal oxide sensors was used (as discussed in chapter III), which can be sensitive to a number of VOCs. The initial experiments, performed with commercial MOX devices, tested the response of tin oxide sensors to carbon monoxide (CO). The experiments were designed to test the response of the sensors (in terms of time and stability) to a benchmark gas. CO was a gas of interest for human EE analysis, where sensors (e.g. NDIR CO₂) could exhibit cross-sensitivity, and also CO on the breath is associated with smoking cigarettes. Two devices were selected, that offered low power consumption (< 100 mW) and were physically small (< 15 x 15 x 10 mm). The SB-500-12 (FIS, Japan) was compared to the TGS-5342 (Figaro, Japan) in preliminary testing. The FIS device was chosen for its smaller physical size (10 mm cylindrical design, 15 mm high) and greater response to CO. A drawing of the device is shown in Fig. 4.16 a), with the equivalent circuit (usual principle for all MOX devices) shown in b).

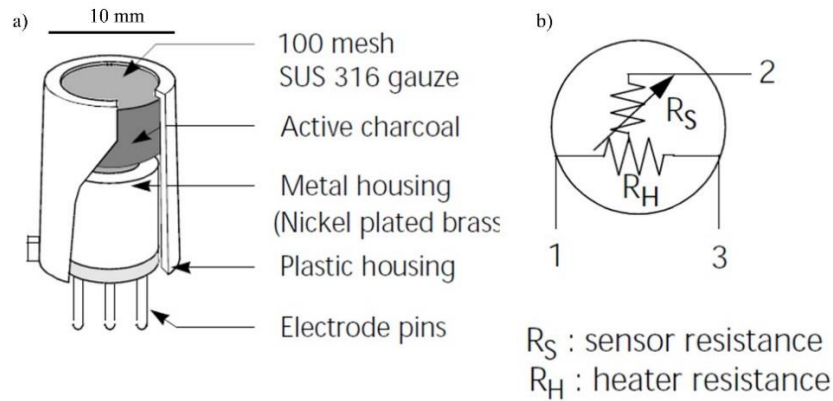


Fig. 4.16 a) Components shown inside FIS SB-500-12 sensor for CO detection; b) Equivalent circuit shown for the device, typically 2.8Ω heater resistance at room temperature and $4.5 \text{ k}\Omega$ to $40 \text{ k}\Omega$ sensor resistance in the presence of 100 ppm CO.

From FIS datasheet [24].

The CO sensor experiment involved pulsing a concentration of CO in the sensor chamber in a similar manner to Fig. 4.11. The CO concentration was varied between a ppm concentration and the baseline of synthetic air (0 ppm CO) in 1 minute steps. The sensor was tested at a concentration of 10, 20, 50, 100 and 150 ppm CO for five consecutive pulses each. The output is shown in Fig. 4.17, for the total experiment of 70 min duration.

The variance shown in the initial 14 minutes is due to the O_2 concentration being pulsed for the Alphasense sensor (output not shown). The O_2 sensor was exposed to O_2 concentrations identical to those shown in Fig. 4.11 (for the experiment in Fig. 4.17, CO is exchanged for CO_2).

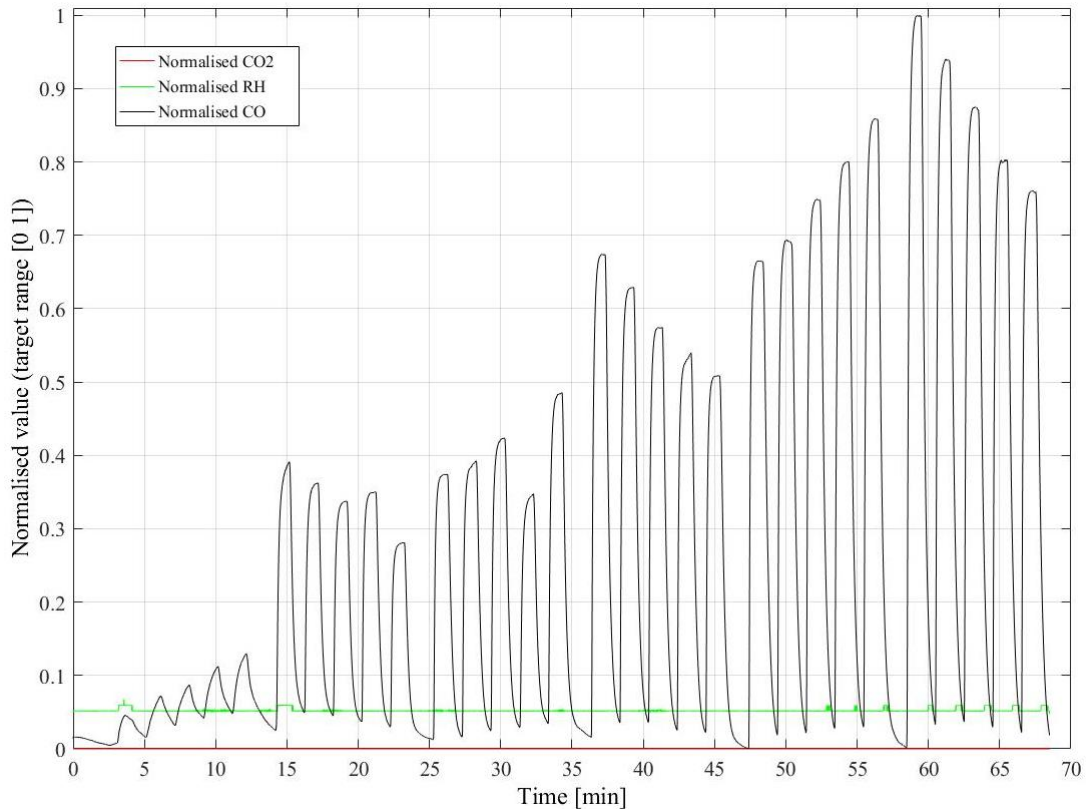


Fig. 4.17 – FIS CO sensor output when exposed to pulses of CO (0, 10, 20, 50, 100, 150 ppm) for five consecutive pulses of 1 min each.

The SB-500-12 demonstrated considerable cross-sensitivity to the concentration of O_2 , which was only varied by 5 % (21 % to 16 %). Therefore, this device would produce a response for an exhalation, due to the decrease in O_2 on exhalations, compared to ambient conditions; when low levels of CO (< 50 ppm) are expected in breath, a normalised response of ~ 10 % due to the change in O_2 is not acceptable for breath measurements. From this undesired trend, the concentrations of CO are not easily distinguishable, i.e. 10 ppm CO (15 to 25 min on the experimental timescale) cannot be separately classified from the 20 ppm pulses (25 to 35 min timescale). The peak normalised 10 ppm output (0.39) is within the range shown for 20 ppm CO (0.35 to 0.49). The modelling regression algorithm discussed above was applied to the four repetitions of the CO pulsing experiment. The output plot is shown in Fig. 4.18.

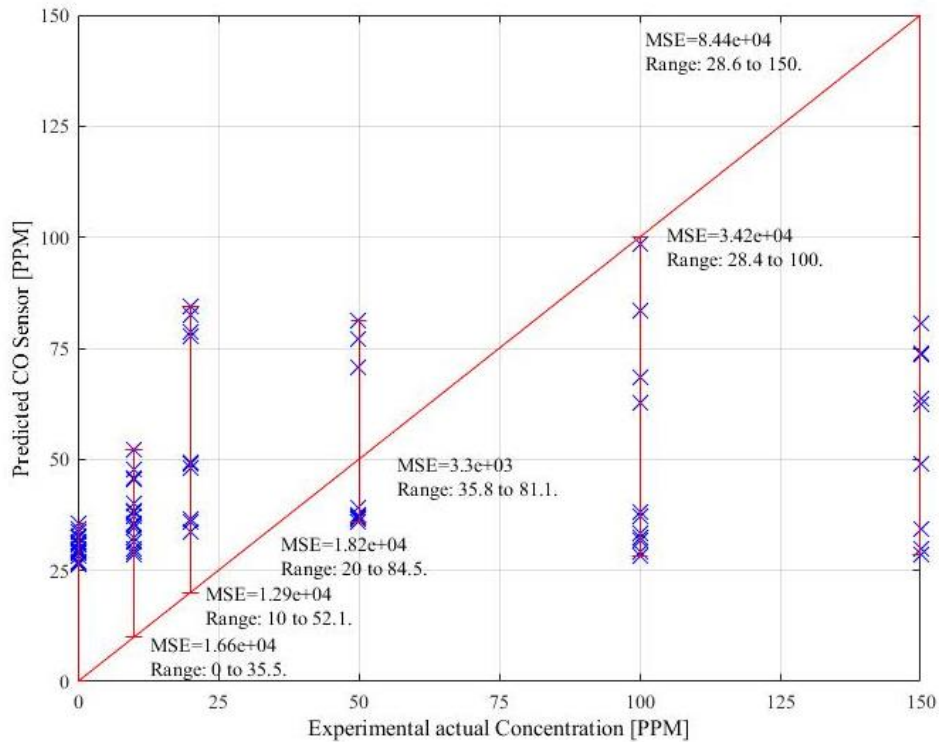


Fig. 4.18 – Model output from CO sensor data, showing predicted vs actual concentration for 50:50 split of training and test data.

In general, the model was not able to successfully match the test set of data to the correct gas concentration. The 70 minute experiment (four repetitions) demonstrated that the sensor did not produce a stable output, and had cross-sensitivity to O_2 concentration. The device had poor response time (~ 30 s) and did not return to a stable baseline.

The 10 ppm steps were incorrectly classified in the range of 0 to 35 ppm, similarly the 150 ppm range was incorrectly classified as low as 29 ppm. The level of RH was kept constant (dry conditions), as humidity is known to affect MOX sensor performance. The overall poor performance of the device, and other models (e.g. the Figaro TGS-5342) demonstrated there was a need to design a new MOX sensor for breath analysis. The development of a new MOX sensor is discussed in the further work section in chapter IV.

4.5 Conclusions

The mainstream chamber designed for breath analysis was found to be unsuitable for fast response measurements. The dead volume (~ 126 ml) of the chamber created a large delay between a change in gas mixture and sensor response. In the case of

exhaled breath measurements, the sample could become compromised with both inhaled and exhaled air mixing together continuously. The fast response (specified as 0.1 s) IR3107 CO₂ sensor had an increased (~1.2 s) response time after the gas was passed through the main-stream chamber. The mainstream design did not require any pump to extract a sample through the sensor chamber, but did not include any measures to prevent condensation rain-out from the humid exhaled breath.

The affordable commercial sensors selected for this work demonstrate the lack of availability of suitable commercial sensors for breath-by-breath analysis. The SprintIR CO₂ sensor had a poor response time (14.1 s) and poor stability (noise ~0.1 %). The device did not meet the 1.20 % tolerance required for accurate (± 1 %) EE measurements desired. The FIS CO sensor was unstable when the concentration of O₂ was varied (between 21 % and 16 %, the variance expected between exhaled and inhaled air). The performance was improved compared to devices from other manufacturers (e.g. Figaro), but the device was not suitable for breath measurements.

The O₂ sensor (Alphasense O2G2) demonstrated a stable performance of the electrochemical cells, with repeatable results across five repetitions of pulsed measurements. The regression modelling demonstrated that the sensor performed adequately to meet the 0.52 % target accuracy for EE measurement. However, the response time of the sensor (9.5 s) is too slow for breath-by-breath measurements. The device was replaced by an alternative model (City Technology MOX-20, chapter VII) for side-stream measurements, but with the disadvantage of a bulky design and the black-box nature of the sensor. The City Technology device offered a greatly improved response time (<1 s), required to monitor breath in real time. The lifetime of both types of sensor could be an issue for a breath analyser in use over a period of years, when both devices are only designed to last between 12 and 24 months. In the longer term (weeks) the drift of the sensor is considerable (e.g. ~10 % output voltage over a period of months), which means regular calibration is required.

The flow and temperature and RH sensors were not rigorously tested during mainstream sensor testing. The performance of the gas sensors in the system in a laboratory environment (with dry gases) was deemed inadequate for any fruitful measurements to be obtained from breath measurements. The output from the

temperature and RH sensor was recorded to show that the environmental conditions during testing were constant, in a laboratory gas bench rig.

The large variation in flow rate (i.e. inhale and exhale of the order of ± 20 SLPM) can affect sensor performance. The Hummingbird commercial CO₂ sensor, for example, is designed to operate at around 100 ml/min [22], with a small inlet of 1.6 mm internal diameter, and could be damaged at higher flow rates. A side-stream sampling system can be driven using a pump (or fan) which operates at a fixed flow rate. Although turbulent flow can be generated due to the operation of the pump, the flow rate is within a controlled range (e.g. 0.15 SLPM, with a variance of ~20 %).

It was therefore concluded a side-stream system would be required to measure EE using the available gas sensors. This type of system was not initially preferred, due to the additional chamber needed to house the sensors (separate from mainstream tubing). Also, a pump is required to extract a sample of gas, which increases the weight of the system and power consumption.

4.6 References

- [1] W.J. Malley, *Clinical Blood Gases: Assessment & Intervention*, Elsevier Health Sciences, London, U.K., 2013.
- [2] J. Villadsen, S.Y. Lee, J. Nielsen, G. Stephanopoulos, *Fundamental Bioengineering*, Wiley, Weinheim, Germany, 2016.
- [3] S.M. Weiss, C.A. Kulikowski, *Computer systems that learn: classification and prediction methods from statistics, neural nets, machine learning, and expert systems*, M. Kaufmann Publishers, San Mateo, U.S., 1991.
- [4] J.A. Covington, J.W. Gardner, S.-L. Tan, Velocity-optimized diffusion for ultra-fast polymer-based resistive gas sensors, *IEE Proc. - Sci. Meas. Technol.* 153 (2006) 94–100. doi:10.1049/ip-smt:20050035.
- [5] J. Haywood, P.T. Coverley, W.J. Staszewski, K. Worden, An automatic impact monitor for a composite panel employing smart sensor technology, *Smart Mater. Struct.* 14 (2005) 265–271. doi:10.1088/0964-1726/14/1/027.
- [6] S. Zhang, C. Xie, M. Hu, H. Li, Z. Bai, D. Zeng, An entire feature extraction method of metal oxide gas sensors, *Sensors Actuators B Chem.* 132 (2008) 81–89. doi:10.1016/j.snb.2008.01.015.
- [7] R. Gutierrez-Osuna, a. Gutierrez-Galvez, N. Powar, Transient response analysis for temperature-modulated chemoresistors, *Sensors Actuators B Chem.* 93 (2003) 57–66. doi:10.1016/S0925-4005(03)00248-X.
- [8] S. Suzuki, M. Ando, H. Hashimoto, H. Asama, Deliberation of value-sympathy model for adaptive service attendant system, in: *IECON 2011 - 37th Annu. Conf. IEEE Ind. Electron. Soc.*, IEEE, 2011: pp. 2112–2117. doi:10.1109/IECON.2011.6119634.
- [9] A. Clark, C. Fox, S. Lappin, *The Handbook of Computational Linguistics and Natural Language Processing*, John Wiley & Sons, Somerset, U.K., 2013.
- [10] E.M. Tzanakou, *Supervised and Unsupervised Pattern Recognition: Feature Extraction and Computational Intelligence*, CRC Press, Boca Raton, U.S., 1999.
- [11] T. Hastie, R. Tibshirani, J. Friedman, *The Elements of Statistical Learning*, Springer New York, New York, NY, 2009. doi:10.1007/978-0-387-84858-7.
- [12] R. Kohavi, A study of cross-validation and bootstrap for accuracy estimation and model selection, in: *Int. Jt. Conf. Artif. Intell.*, Morgan Kaufmann Publishers Inc., 1995: pp. 1137–1143.
- [13] Y. Hong, R. Barlett, *Routledge Handbook of Biomechanics and Human Movement Science*, Routledge, London, U.K., 2008.
- [14] S. Banik, R.M. Rangayyan, J.E.L. Desautels, *Computer-Aided Detection of Architectural Distortion in Prior Mammograms of Interval Cancer*, Morgan & Claypool Publishers, 2013.
- [15] D.M. Hawkins, S.C. Basak, D. Mills, Assessing model fit by cross-validation., *J. Chem. Inf. Comput. Sci.* 43 (2003) 579–86. doi:10.1021/ci025626i.

-
- [16] A.K. Jain, P.W. Duin, Statistical pattern recognition: a review, *IEEE Trans. Pattern Anal. Mach. Intell.* 22 (2000) 4–37. doi:10.1109/34.824819.
- [17] T. Hill, P. Lewicki, *Statistics: Methods and Applications : a Comprehensive Reference for Science, Industry, and Data Mining*, StatSoft, Inc., Tulsa, U.S., 2006.
- [18] J.W. Gardner, P.N. Bartlett, *Electronic noses: principles and applications*, Oxford University Press, Oxford, U.K., 1999.
- [19] S. Dua, R. Acharya U, *Data Mining in Biomedical Imaging, Signaling and Systems*, Taylor & Francis, Boca Raton, U.S., 2011.
- [20] J.L.S. Lee, I.S. Gilmore, The Application of Multivariate Data Analysis Techniques in Surface Analysis, in: *Surf. Anal. – Princ. Tech.*, 2nd Ed., John Wiley & Sons, Ltd, Chincester, U.K., 2009: pp. 563–612. doi:10.1002/9780470721582.ch10.
- [21] GSS, H. Speed, C. Dioxide, SprintIR Datasheet, *Gas Sens. Solut.* (2016). https://www.gassensing.co.uk/media/1091/sprintir_-datasheet_gss.pdf (accessed July 1, 2016).
- [22] Hummingbird Technologies, Hummingbird Ir3107, Hummingbird. (2013). <http://www.hummingbirdsensing.com/en/products/carbon-dioxide/ir3107> (accessed September 3, 2014).
- [23] R. Gasparri, M. Santonico, C. Valentini, G. Sedda, A. Borri, F. Petrella, et al., Volatile signature for the early diagnosis of lung cancer., *J. Breath Res.* 10 (2016) 16007. doi:10.1088/1752-7155/10/1/016007.
- [24] FIS, FIS Gas Sensor SB-500-12, *Gas Sensors.* (2006). <http://www.fisinc.co.jp/en/common/pdf/ESB50012.pdf> (accessed August 10, 2016).

CHAPTER V

Development of a Low-Cost NDIR Gas Sensor System for Breath CO₂ Analysis

Preface

As discussed in Chapter III, commercially available CO₂ gas sensors are not regarded as adequate for breath-by-breath measurements in a portable breath analyser. The principle of NDIR measurements, a physical absorption process that occurs almost instantaneously, although the response time of sensors to CO₂ is limited by IR emitter bandwidth and signal processing algorithms. To develop a fast response, affordable and low-power CO₂ a novel NDIR system has been designed and built. The system is based upon a miniature low-cost CMOS IR source, which has very good emission qualities at the wavelength CO₂ absorbs IR radiation. This chapter details the development of a low-noise, low-cost, low-power drive system for the emitter to enable the desired response to CO₂ to be extracted from the noisy signal recorded by the IR thermopile detector. The emitter can be driven with a constant DC voltage, however to enable better sensitivity and reliability, an AC drive is preferred. The IR path length affects the resolution of CO₂ that can be detected. The results of low (ppm level) CO₂ gas experiments are presented and discussed. The effects of varying the IR path length are also investigated with trials shown from lengths of 10 mm to 80 mm.

5 Carbon Dioxide Breath Sensing

CO₂ is an important gas to measure for EE analysis. The commercial EE analysers that are available, such as the Bodygem which only measure O₂ concentration, are widely criticised for neglecting CO₂ measurement and assuming a constant respiratory quotient (which varies between individuals) [1]. The current generation of affordable devices are not capable of breath-by-breath measurements, with poor stability and slow response times. In this chapter, the development of a miniature, fast response and low-cost NDIR CO₂ sensor is detailed.

NDIR affordable sensors are usually limited to detection in the range of 1 to 10 %; concentrations of 500 ppm cannot be distinguished from the background system noise. A new NDIR sensor was developed, with a Silicon-On-Insulator (SOI) IR emitter and commercial thermopile detector. What is required is a system that is capable of detecting the concentration of CO₂ as low as 10 ppm, but also in the range of interest (1 to 5 %) for use in breath analysis. The importance of accurate sensing, for ppm accuracy even at high percentage concentrations, stems from the Weir equation (2.4) used to calculate EE. In previous work (discussed section 3.1) it was found that the CO₂ concentration needs to be measured to a tolerance of 1.20 % (relative accuracy, i.e. 600 ppm accuracy at 5 % CO₂), to obtain a 1 % accurate EE measurement.

The general operation of NDIR sensors was discussed previously. In this chapter the components inside the sensors are discussed in detail. Traditionally, NDIR sensors use micro bulbs as sources of IR. Although readily available, bulbs provide a high power, less reliable (1000 hour life) and bulky radiation source compared to newer technology such as CMOS micro hotplates. In particular SOI IR emitter have greater reliability, faster response and smaller physical dimensions [2,3]. An SOI emitter is shown in Fig. 5.1 a), mounted in a TO46 header in Fig. 5.1 b). An early generation plasmonic emitter was used, with improved emission at the wavelength required for CO₂ detection. A Heimann commercial thermopile detector is shown in Fig. 5.1 c). It would be beneficial for the sensor developed to have a sufficiently fast response to detect an exhalation, which is likely to be a period of approximately 3 s [4]. Exhaled gas is difficult to store and transport [5] and the breath analyser developed in this project would ideally perform EE analysis without the assistance of a clinical practitioner.

In terms of cost, MEMS based IR emitters cannot yet compete with simple IR micro bulbs [6], but affordable CMOS based systems (with detectors) are possible, when the market volume increases. The field of NDIR detection is still open to development [7], in that there is a need for low cost, low power and precise instruments (under £20) which has yet to be realised. Silicon based CO₂ sensors have been studied for over a decade; in recent years the focus of development has been on improving the sensor design to enable greater sensitivity, faster response, improved reliability with lower power consumption [8].

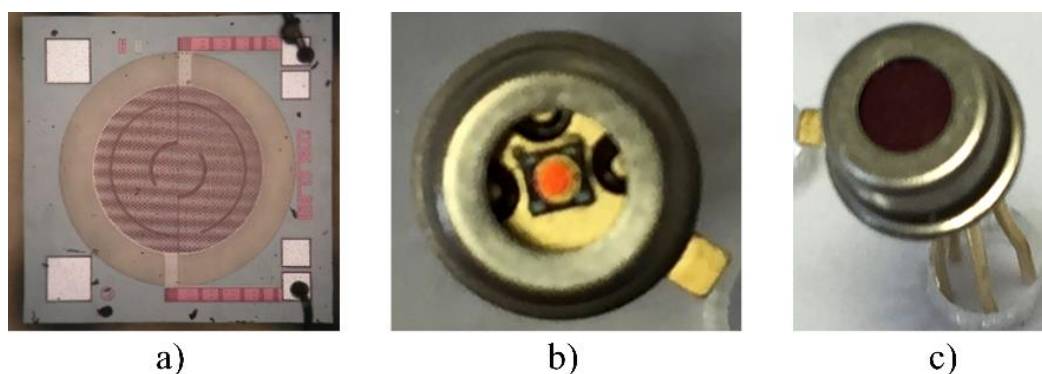


Fig 5.1 a) SOI emitter, provided by Cambridge CMOS Sensors Ltd (CCS), with 0.28 mm² heating area; b) Emitter mounted on a TO46 header for fitting into the NDIR system; c) Heimann commercial thermopile also mounted on a TO46 header.

5.1 NDIR Emitter Drive Signal

For a given NDIR hardware configuration, the emitter drive source is the most crucial component with respect to developing a system capable of accurate and reliable gas measurement. Careful amplification of the nano-amp signal received at the detector and the post-processing of the received signal are also required to retrieve information from the thermopile output data; however the bandwidth of the drive source of the IR emitter dictates the signal processing techniques that can be applied and their effectiveness. The need for a stable heater drive can be seen in Fig. 5.2, where a steep exponential increase in heater temperature is produced from a small change in input drive voltage (i.e. between 2 V and 2.2 V). Furthermore, the heater drive voltage should not usually exceed 2.3 V (particularly not for a prolonged period), else risk failure of the device (through over heating).

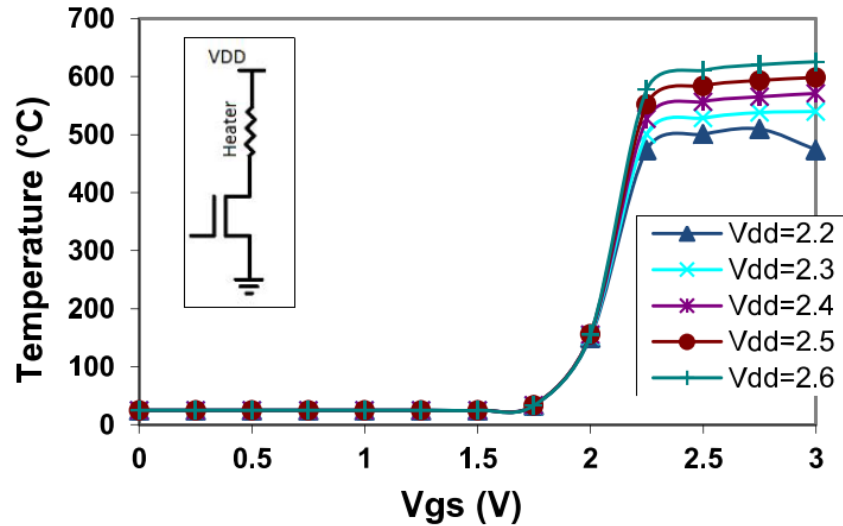


Fig. 5.2 – The temperature that a CMOS IR resistive heater produces compared to the transistor drive voltage [6].

The thermopile detector senses a change in temperature due to the IR radiation from the emitter. Ideally, for the sensor to be singularly sensitive to CO₂, only changes in CO₂ gas concentration along its IR path would change the level of radiation received by the detector. Noise, such as thermal Johnson noise, present in the thermopile output (discussed in detail in the following section) necessitate post-processing stages in NDIR systems. A heater emitting an unknown variable IR radiation can become a large source of noise, where a 10 °C shift in output temperature can occur from a change in drive signal of ~ 10 mV. A stable drive signal can prevent this source of noise from corrupting the output signal.

5.1.1 Emitter DC Drive

A DC drive voltage was used for initial testing with the NDIR system. A DC source requires less complex drive and receive circuitry – and stable generators of a DC voltage are readily available. The drive signal was generated using a data acquisition (DAQ) module (NI USB 6341) which also recorded the output data (at 100 Hz). The emitter was controlled using a current drive system. The device was specified as operating at 500 °C (recommended in unpublished datasheet) with a 70 mA drive current.

The optical path length dictates the detection range of the IR system. In the case of a metal tube forming the gas chamber, the material of the pipe (and finish) can affect the strength of the received IR radiation at the detector. A DC experiment was

performed to verify the range of detection possible with a 12 mm path length, and to demonstrate the benefit of a tube internally plated with gold compared to a non-plated (aluminium) tube. A photograph of the rapid prototyped holder for the two tubes is shown in Fig. 5.3 (the internal diameter of pipe is 3 mm). The output recorded from the sensor is shown in Fig. 5.4, a) with a gold tube and b) with an aluminium tube (of identical length). The sensor was tested against CO₂ concentration in the range of 1 to 5 %, for steps of 2 minutes each (returning to a baseline of synthetic air, 0 % CO₂, also for a period of 2 minutes).

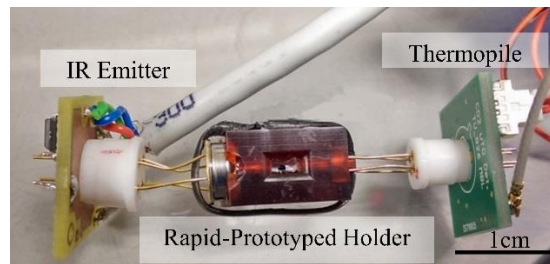


Fig. 5.3 – Photograph of the holder for the gold or aluminium tube (12 mm IR path length).

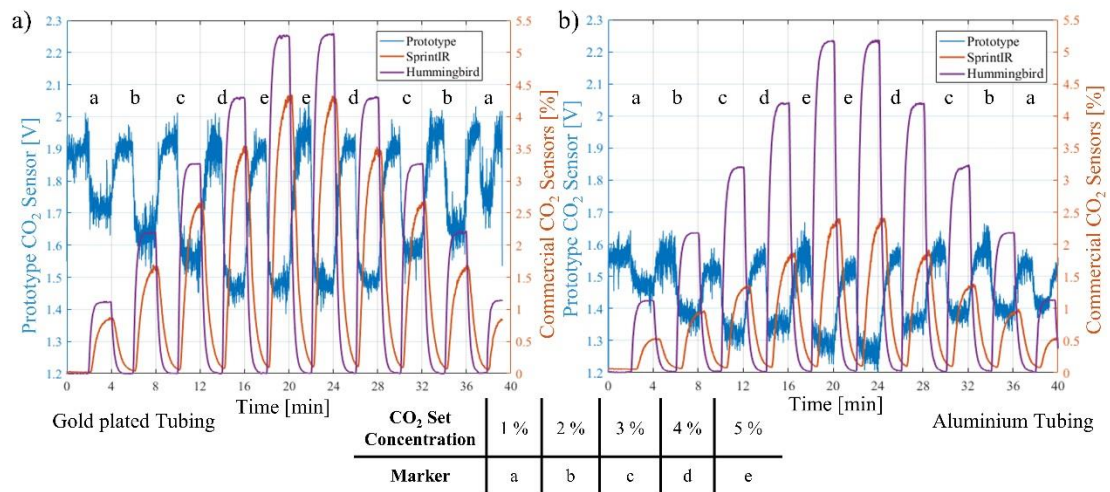


Fig. 5.4 – Prototype CO₂ sensor compared against two commercial reference devices with IR path a) of gold plated tube and b) of aluminium tube.

A 100 ml chamber was used to test the three sensors shown in Fig. 5.4. The tube holder (Fig. 5.3) had an inlet and outlet for the sample gas cut into a window in the side of the container and was placed inside the larger 100 ml chamber. The reference commercial devices were an affordable (€150) CO₂ sensor (GSS SprintIR) and an expensive (€1750) medical grade device (Hummingbird IR3107). The sensor outputs were filtered with a 99 point median filter, with a sampling rate of 100 Hz. The t_{90}

response of the commercial devices has been discussed previously. In this experiment, the prototype CO₂ sensor achieved a t_{90} of 15 s. A shorter response time would be likely with a smaller external chamber.

The noise encountered when operating an NDIR system with a DC drive is demonstrated in the output results (0.05 V noise level throughout). The baseline is not stable in Fig. 5.4 a) nor b), demonstrating that a minor fluctuation (~ 0.2 °C) in ambient temperature can cause unpredictable drift in the sensor output (variance in output temperature is continuous throughout the measurement, tested in a temperature controlled room, but only controlled to ~ 0.5 °C). Outside of a laboratory environment far larger temperature variations would be expected. The average baseline for the aluminium tube is 1.56 V, with a variance between 1.53 to 1.59 V (S.D. of 0.02 V). The experiment was performed in dry conditions (0 % RH) and at a constant flow rate of 0.5 SLPM. The DC drive prevents filtering through frequency band-pass filters. An additional RC- (or Sallen-Key) -filter could be implemented, but at the expense of decreased response time (and the low frequency drift due to ambient temperature, or humidity and pressure, would not be removed).

The gold plated tube resulted in a greater IR signal at the detector, although the limit of detection was not greatly improved. The level of noise was consistent for both experiments. The first (and final) steps were for 1 % CO₂ concentration, and could be distinguished from the synthetic air measurements. The 1 % increase in CO₂ concentration causes a decrease in raw output voltage (after amplification) by 0.18 V for the gold tube compared to 0.1 V for the aluminium counterpart. Increasing steps of CO₂ (1 % each step) caused an exponentially decreasing drop in output voltage. For the aluminium tube, a 1 to 2 % change in CO₂ caused a 0.08 V decrease in output voltage, for the change between step a and b in Fig. 5.4 b). A change in CO₂ from 4 % to 5 % caused a 0.04 V decrease in the output voltage (the difference between steps d and e).

The range of higher concentrations that can be distinguished with the prototype sensor is limited by the small difference in output response (i.e. concentrations above 5 % would be inseparable from a 5 % reading). In this way the sensor becomes saturated, and the level of the IR radiation absorbed by the CO₂ gas inside the chamber does not increase further. In other tests, it was found that the path length affects this saturation

limit (i.e. a shorter path permits higher concentrations to be detected, although lower concentrations become suppressed by the background noise level). The cause of the saturation of the sensor could be due to the spread of the IR radiation. CO₂ gas is heavier than air, so could sink to the bottom of the pipe, and only affect the beams of radiation that are reflected and that travel through the lower section of the pipe. It is assumed that the majority of the IR radiation is transmitted in parallel from the chip.

The performance of the commercial sensors demonstrated the superior performance of the IR3107 compared to the SprintIR. The SprintIR, as previously demonstrated, had a slower response time compared to the expensive IR3107, and did not output a close measurement to the set CO₂ concentration. The IR3107 overestimated the concentration of CO₂ presented to the sensor, (registering 5.2 % for 5 % CO₂ measurement), although the overestimation was consistent throughout. The sensor returned to a stable baseline (~ 0 %), compared to the SprintIR which returned to approximately 0.08 % between the steps for CO₂ concentrations.

The gold tube in general produced a marginal improvement in response which cannot justify the additional expense and manufacturing difficulty for the plated tube to be used instead of an aluminium alternative. The aluminium pipe produced a lower overall response (maximum step of 0.3 V, ~ 19 % of synthetic air baseline value) compared to the gold tube (0.4 V maximum step, 21 %). The decrease in signal output was not substantial (fall from 1.9 V to 1.6 V baseline), when a gain of 2,100 was required in the amplification circuitry in the post-thermopile processing stage.

5.1.2 Emitter AC Drive

It is advantageous to drive the IR emitter with an AC signal to enhance the methods of filtering available (which can be used to remove baseline drift), reduce power consumption and to increase the lifetime of the device. The precise input signal required to prevent undesired drift (caused by a noisy drive) should be created by a designated waveform generator. Preliminary testing included generating an AC signal using the digital to analogue (DAC) convertor on the NI USB DAQ and a DAC on an Arduino Uno microcontroller. Both the sources were able to generate a sinusoidal wave at the desired offset, amplitude and frequency, but added jitter to the drive signal and caused an unwanted temperature shift in the IR radiation from the output of the emitter. A dedicated IC (AD9837 [9]) was chosen from Analog Devices (USA), which can produce sinusoidal, triangular or square waves at a frequency programmable

through digital communication with a microcontroller. The precision frequency generation by such a chip is close the precision possible with an oscillator circuit. However, the IC chip can be programmed to any desired frequency (within the range of the chip, e.g. up to 5 MHz with 0.02 Hz resolution [9]). For development of a NDIR system, the unit can therefore be trialled in order to find the optimal frequency for CO₂ detection.

The output from the thermopile detector after excitation from the sinusoidal IR signal is in the micro-volt range. For the signal to be recorded by either a USB DAQ or microcontroller the raw output is amplified (perhaps by a factor of ~3000). The change in amplitude of the sinusoid signal output from the detector corresponds to the concentration of CO₂ to which the sensor is exposed. The results can be normalised to a baseline of synthetic air, to show the change in the received signal and to ease comparison between measurements. For the majority of measurements performed, a single detector is used, which reduces the size of the device and cost. A dual detector configuration can aid removal of the drift, discussed above, with a DC drive (i.e. environmental temperature shifts over time), but at the potential cost of additional noise (i.e. other noise factors detected by both thermopile detectors). The noise is often not in phase between the detectors, so the overall level of noise (if the reference signal is compared to the sensing signal) can increase.

The amplitude of the sinusoid is taken as the response to the presence of CO₂ gas to help mitigate the low frequency drift (e.g. environmental factors). For example, the sinusoidal signal is pulsed between two temperatures (e.g. 150 °C and 550 °C) a change in environmental temperature will increase both temperatures by a similar value (i.e. if temperature change by 3 °C, it can be assumed that the heater output will increase by 3 °C throughout the operating range). This technique is not as robust as employing a dual detector, however the trade-off is a reduction in complexity and cost.

5.1.2.1 Lock-in Amplifier

The use of a lock-in amplifier is an example of the improved signal processing available by using a known AC drive signal. The amplifier compares a received noisy signal to a given reference signal. Signals with the frequency of the reference wave are recovered from the combination of all other components of the noisy input signal [10]. For this technique to be effective, the operation of the NDIR system must avoid certain bands of noise, for instance 50 Hz noise from laboratory equipment or DC low

frequency noise. It is possible to implement the device using a microcontroller, however in this work the desire is to minimise the computational load (to avoid compromising the signal handling of other sensors in the breath analyser). A dedicated IC chip was preferred for extracting the desired signal. Lock-in amplifiers are commercially available. Previously it has been reported that lock-in amplifiers have been used for CO₂ detection in laboratory environments, however the bulky (benchtop) instruments used are unsuitable for a portable unit [11,12]. In this project the functionality of the benchtop lock-in amplifiers was replicated using a commercial IC chip (AD630, Analog Devices, USA). A block diagram of the setup is shown in Fig. 5.5.

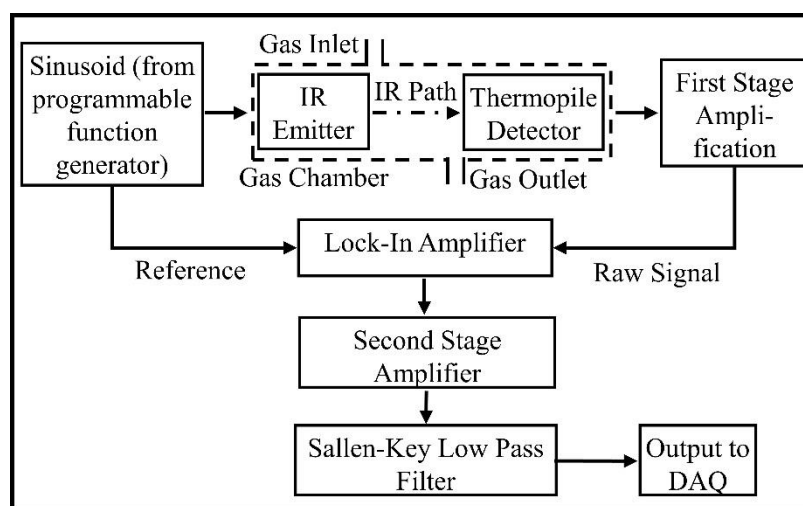


Fig. 5.5 – Functional block diagram of NDIR sensor system with lock-in amplifier.

The lock-in amplifier takes a major role in recovering the desired sinusoidal signal. The received signal from the thermopile circuitry is compared to the emitter drive signal and the original sinusoidal waveform is recovered. A simplified circuit schematic is shown in Fig. 5.6, where the lock-in amplifier requires a dual power supply (+5 V and –5 V). The operation of the lock-in amplifier is demonstrated in Fig. 5.7. The heater drive signal (i.e. the reference signal to the lock-in amplifier) is generated by a microcontroller (initially a dedicated device is used, the Arduino Pro Mini) paired with the AD9837 programmable function generator.

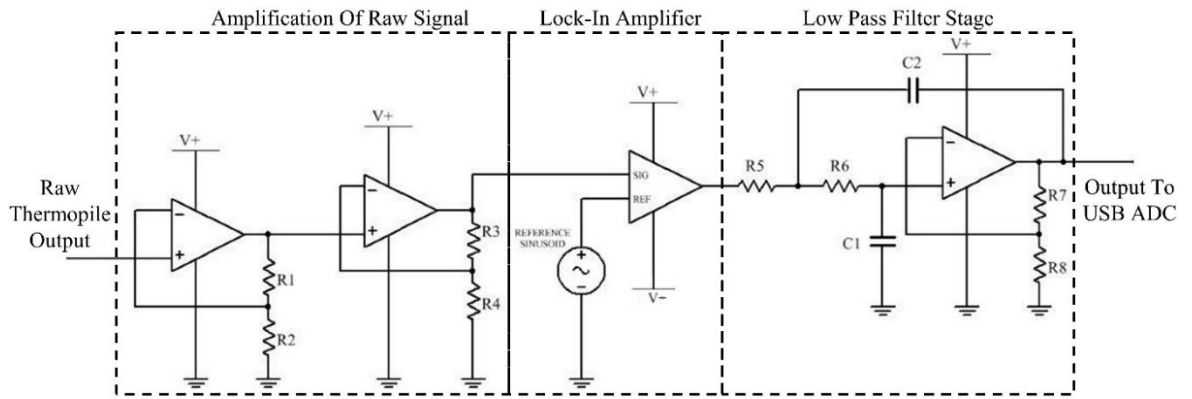


Fig. 5.6 – Simplified circuit schematic of NDIR lock-in system, showing initial amplification stage, lock-in IC chip and final filtering process.

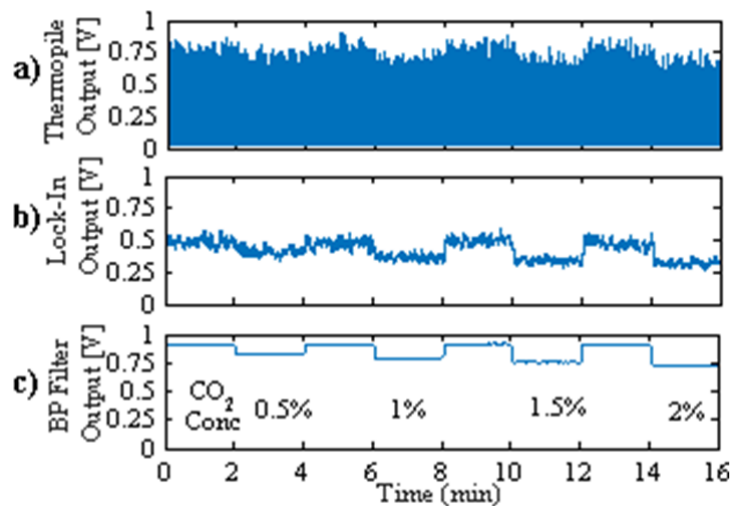


Fig. 5.7 – Operation of lock-in amplifier. Raw thermopile output (a) is compared to a reference sinusoid (from signal generator) with lock-in amplifier (b) and then the output is filtered (c).

5.1.2.2 Digital Filtering

An alternative method to using a lock-in amplifier to extract the desired AC signal from the thermopile raw output is to use digital filtering. If the expected form of the output signal is known, then a perfect digital filter can be designed to extract only the desired component. The method of digitally filtering the signal can reduce the response time of the sensor. Filters based on averaging samples to smooth signals (e.g. low pass, median or mean) can slow sensor response times, however filtering in the frequency domain is more effective without compromising performance. A fast response sensor is beneficial for breath-by-breath sensors as well as safety conscious devices [13].

It has been reported that thermopile detectors have at least three types of noise: temperature, thermal and signal [8]. The dominant noise source is thermal noise [14], which limits the detectors sensitivity. Temperature noise, generated by environmental fluctuates, can be reduced by the use of a dual thermopile detector. One channel is only sensitive to wavelength of the gas of interest, and the other configured to filter a different wavelength. Thermal noise, caused by the thermopiles resistance, is wide-band [15] and more challenging to overcome. By pulsing the emitter, with perhaps a sinusoidal signal, and extracting only the desired signal from the detector, much of this thermal noise can be eliminated.

In this section a fully CMOS-compatible tungsten IR emitter [6] is modelled. The heater includes a plasmonic layer and is based on tungsten metallisation. The device is miniature and stable up to 600 °c, but retains the low-cost, high volume advantages of CMOS manufacture. Characterisation of SOI tungsten heaters has previously been performed using 2D or 3D modelling techniques [16–21]. Ali et al. shows that heaters could be used up to 700 °c without damage, also noting very low power consumption at 600 °c (12 mW) [18,20,22]. However, this is the first time that the modelling of SOI heaters have been performed and analysed for the use of NDIR emitters (previous examples presented were for the design of resistive gas sensors).

The equations presented below model the IR emitted from the SOI hotplate in terms heat dissipation. This enables the heat transferred from the heated region to the ambient region to be considered. The heat losses from the hotplate consist of conduction, thermal radiation and convection [23,24]. Losses due to convection can dominate (69%) the heat losses from the device in the case of larger substrates (e.g. 1.8 mm² square) [25], whereas they have a lesser effect for smaller devices (e.g. 33% for 0.8 mm²). In the case of smaller devices, the heat loss due to conduction dominates [26].

The Beer-Lambert law (eqn. 3.2) expresses the intensity of light transmitted through an absorbing medium. The absorption index, constant k_g , for CO₂ was calculated from the High-Resolution Transmission Molecular Absorption Database (HITRAN) [27], via the HITRAN Application Programming Interface (HAPI) [28]. The frequency dependent cross section (σ) for CO₂ is shown in Fig. 5.8 over wavelengths from 4 to 5 μm .

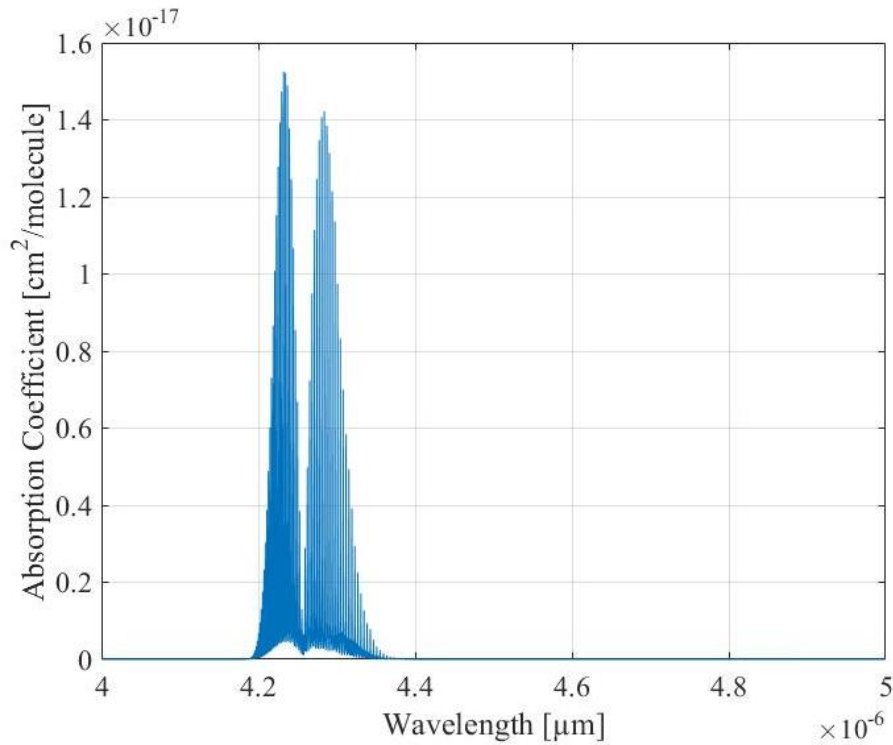


Fig. 5.8 – Absorption coefficient for CO₂ across the wavelength range of 4 to 5 μm .

The voltage applied to the SOI heater, i.e. Fig. 5.1 a), produces a current. The voltage (V_H) is related to the power consumed by the heater with equation (5.1), assuming it is in steady state and given an expected response time in the millisecond range, namely:

$$P = V_H^2 / R_H(t). \quad (5.1)$$

The resistance of the heater ($R_H(t)$) at a given temperature t can be represented by (5.2), where R_0 is the initial resistance at a reference temperature (t_0), and R_{tr} is the track resistance linking the heating element to the package header. A tungsten heater needs a quadratic term unlike a platinum heater.

$$R_H(T) \approx R_{tr} + R_0[1 + \alpha\Delta T + \beta\Delta T^2] \quad (5.2)$$

The power losses of the device can also be related to its temperature by (5.3) [29].

$$P(\Delta T) = a\Delta T + b\Delta T^2 + c\Delta T^4 \quad (5.3)$$

Where a , b and c represent the power consumed by conduction, convection and radiation, respectively. As the radiation losses account for < 5 % [25] of the total power loss, these will be assumed negligible, and thus (5.3) can be simplified to yield (5.4).

$$P \approx a\Delta T + b\Delta T^2 \quad (5.4)$$

Given that the power losses of the heater and its power consumption are equal when the heater is operating at a steady-state temperature, equations (5.1) and (5.4) can be reduced to eqn. (5.5).

$$a\Delta T + b\Delta T^2 \approx V_H^2/R_H(t) \quad (5.5)$$

Equation (5.2) can be substituted in eqn. (5.5) to relate the heater voltage to the resistance of the heater element and tracks:

$$V_H^2 = \{R_{tr} + R_0[1 + \alpha\Delta T + \beta\Delta T^2]\} \times (a\Delta T + b\Delta T^2) \quad (5.6)$$

Given eqn. (5.6), the heater voltage can be described by a quartic equation:

$$\begin{aligned} V_H^2 = & (R_{tr}a + R_0a)\Delta T + (R_{tr}b + R_0b + R_0a\alpha)\Delta T^2 \\ & + (R_0\alpha b + R_0\beta a)\Delta T^3 + R_0\beta b\Delta T^4 \end{aligned} \quad (5.7)$$

The relationship between the heater voltage and temperature rise (ΔT) can be expressed as a quadratic, because higher order ΔT terms are ignored. Orders of ΔT raised above squared power are shown to be negligible in eqn. (5.2) and eqn. (5.3).

$$(R_{tr}b + R_0b + R_0a\alpha)\Delta T^2 + (R_{tr}a + R_0a)\Delta T - V_H^2 \approx 0 \quad (5.8)$$

The solution to (5.8) can be found, then taking only the positive root (as ΔT must always be positive):

$$\Delta T \approx \frac{\sqrt{(R_{tr}a + R_0a)^2 + 4(R_{tr}b + R_0b + R_0a\alpha)(V_H^2)} - a(R_{tr} + R_0)}{2(R_{tr}b + R_0b + R_0a\alpha)} \quad (5.9)$$

The values of a and b are unknown, and have to be estimated from experimental data. Unpublished data provided by CCS showed that the applied voltage and current in relation to the ΔT were used to fit eqn. (5.4). A curve fitting toolbox in Matlab (2015a) was used to estimate the values for a and b , as shown in Fig. 5.9.

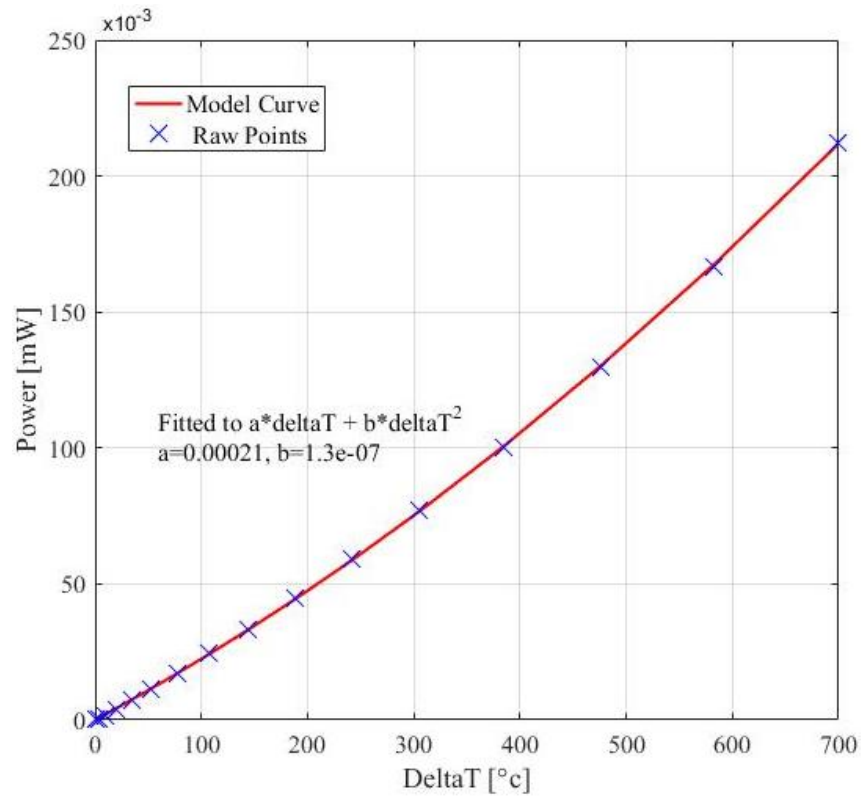


Fig. 5.9 – Model curve fitted to find the coefficients for power losses due to conduction and convection terms only.

The resistance of the hotplate, measured as a 1 Hz sinusoid, was provided as a voltage source input. The rise in temperature was plotted against the resistance measured in Fig. 5.10. Given the relationship (5.2), the values corresponding to the track resistance of the device and the heating element (at initial room temperature) can be obtained. R_{tr} was calculated as 3.78Ω and the initial resistance of the heater element, given an initial temperature of $25 \text{ }^\circ\text{C}$, was 13.90Ω (total resistance of 17.68Ω). This compares favourably with the measured baseline resistance of 17.90Ω .

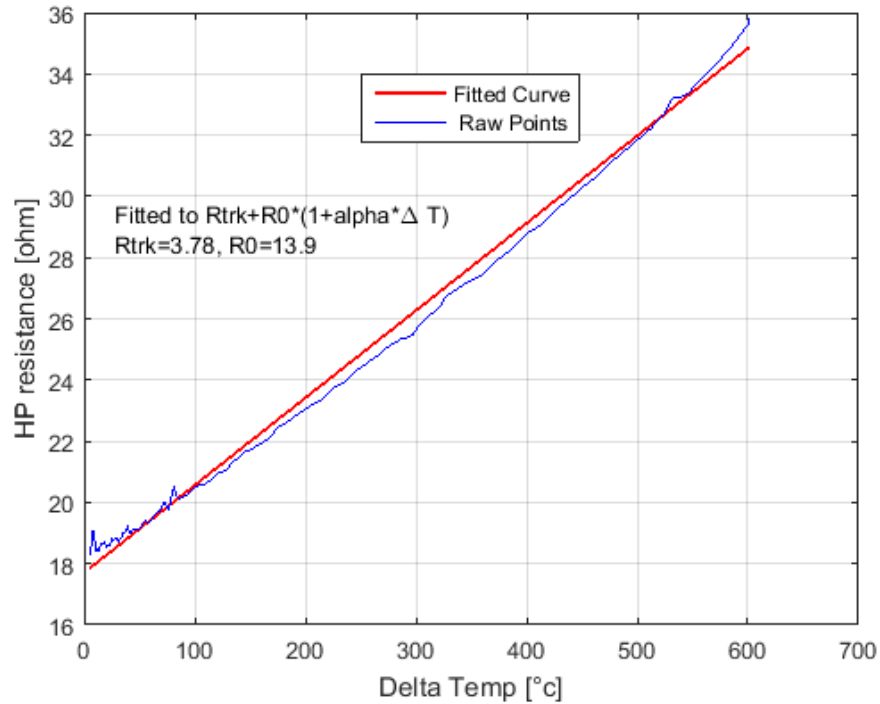


Fig. 5.10 – Measured hotplate resistance compared to ΔT .

The heater was driven with a sinusoid signal of the form (5.10), where angular frequency $\omega = 2\pi f$. Here c denotes the amplitude of the sinusoid (from centre point), d the offset and f the desired frequency (in Hz).

$$V_H(t) = c \times \sin(\omega t) + d \quad (5.10)$$

A sinusoidal input with amplitude of 1.15V, with a 1.15V offset, was used as the input to the model ($V_H(t)$) as shown in Fig. 5.11 a). The output of the model, using eqn. (5.9), is shown below in Fig. 5.11 b). The desired output temperature for a peak voltage input of 2.3V is ~ 600 °C ($\Delta T = 575$ °C). The output from the model peaks at 605.4 °C.

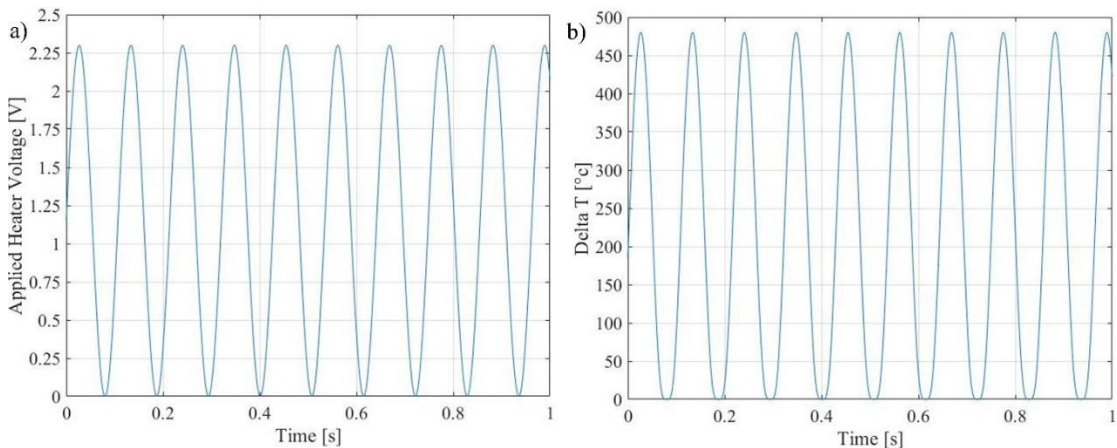


Fig. 5.11 a) Input sinusoid to the model over a 1 s period; b) Output from the model, showing $\Delta T(t)$ over a period of 1 s, the waveform is no longer perfectly sinusoidal.

The model output waveform was verified against the response detected by an IR detector (Heinmann J21). FFTs were taken from each for comparison, as shown in Fig. 5.12.

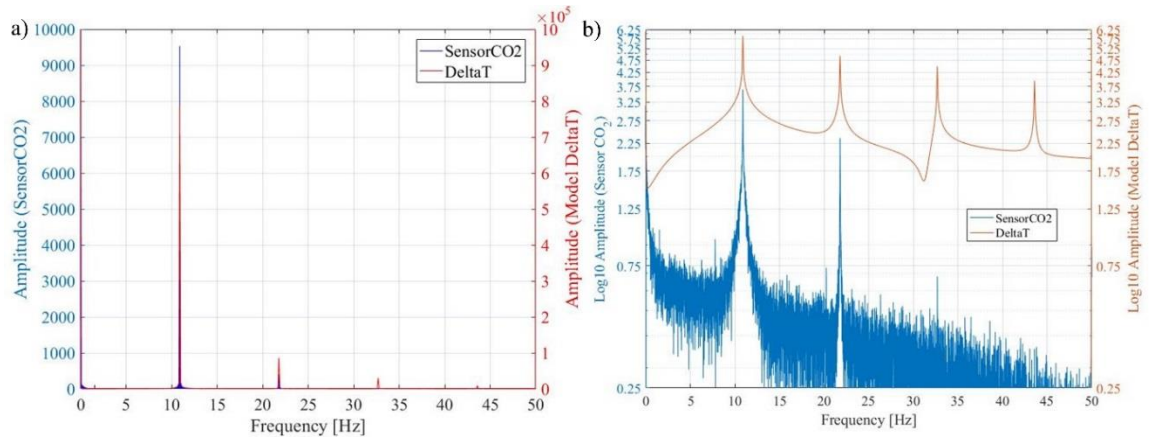


Fig. 5.12 a) FFT plot comparing the CO₂ detector data and model output waveform;
b) Corresponding plot on logarithmic scale.

The output from the model equations matches the response measured from the experimental setup. The Heinmann FFT peaks are visible at 10, 20 and 30 Hz, showing the signal received is no longer perfectly sinusoidal. A custom filter can be designed to extract only these peaks from the noisy signal in the frequency domain.

A block diagram of the signal processing is shown in Fig. 5.13. The left hand side of the diagram shows that the required peaks can be identified by using the model equations and the raw input (drive) waveform. The digital filter is designed using the output characteristics from the model and applied to the detector signal (right hand side of the diagram). The amplitude of the sinusoid is found (centre of diagram) and then the filtering is applied. The output is the filtered amplitude of the sinusoidal signal.

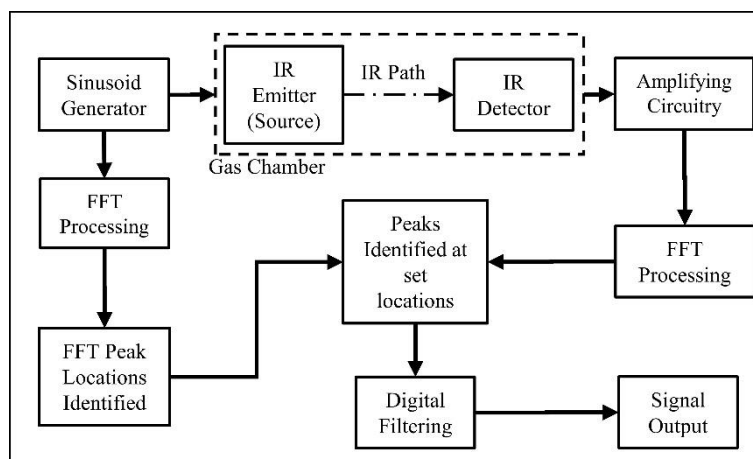


Fig. 5.13 – Block diagram of digital filtering process used to recover the response to CO_2 from the noisy detector signal.

5.2 Experimental Results

The experimental setup used a NI DAQ to record the output signals, as previously discussed for the DC drive measurement configuration. The NDIR system was trialled with two different configurations: an aluminium chamber (80 mm IR path length) is used as a benchmark system (Fig. 5.14) and a variable path length (10, 20 and 40 mm IR path lengths, Fig. 5.15).

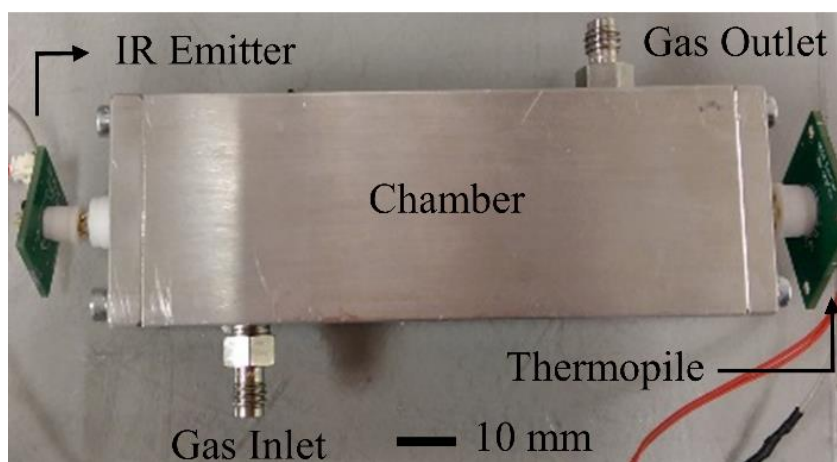


Fig. 5.14 – Photograph of the 80 mm aluminium bench top chamber showing the PCBs for the IR emitter and thermopile detector.

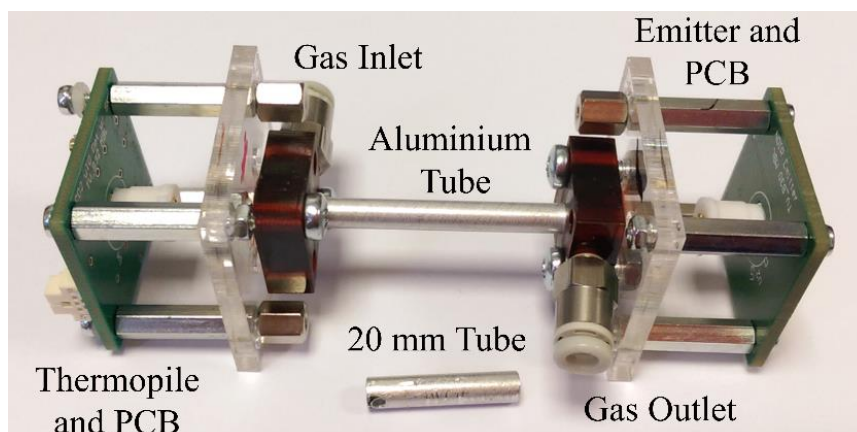


Fig. 5.15 – Photograph of the adjustable path length design of the IR emitter and detector housing. 40 mm aluminium tube is fitted with 20 mm tube as shown.

5.2.1 Lock-In Amplifier 80 mm Path Length

The first prototype bench-top unit was formed from an aluminium chamber (Fig. 5.14) with an IR path length of 80 mm between the IR emitter and the thermopile detector. The sensor was exposed to CO₂ concentrations from 50 ppm to 2.5 %, generated on a gas test bench, with a constant flow rate of 0.5 SLPM. Fig. 5.16 a) and (b) demonstrates the resilience of the system to humidity, where the system was tested in dry gas and 25 % RH.

The sensor outputs displayed excellent stability. The increased level of humidity decreases the number of reflections off the side-walls of the tube (particularly if water droplets were to collect at the lower side of the tube). The received signal is lower (voltage magnitude), but there is less noise received. The reflections contribute to the noise received, as the beams of IR light that are reflected do not travel the same distance as the light which travels in a straight line directly from the IR emitter to the detector.

Concentrations from 100 ppm to 2.5 % were repeated twice during the experiment, with average variations of ~0.23 % and 0.10 % between the repetitions for dry and 25 % RH, respectively. The addition of humidity increased the stability of the sensor output, but decreased the normalised reading by an average of 1.2 %.

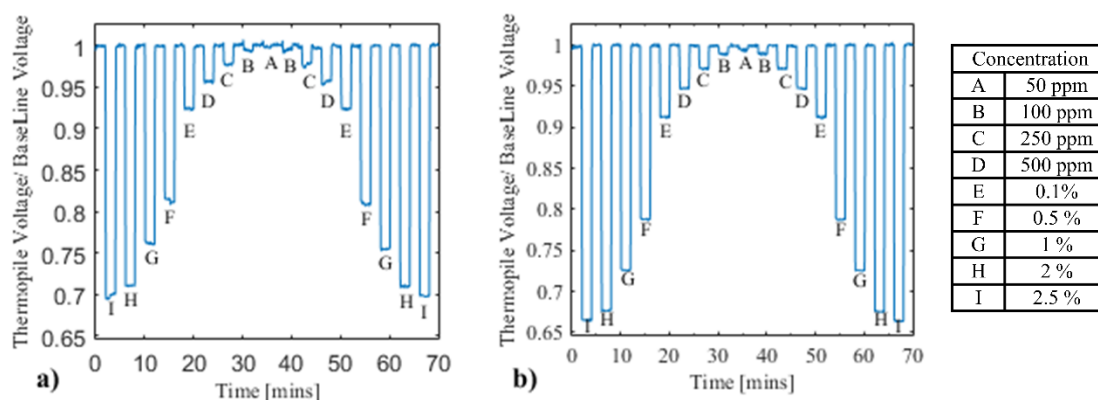


Fig. 5.16 – Sensor outputs (relative to baseline of synthetic air with 80 mm path length showing detection of CO₂ in the range of 50 ppm to 2.5 %, (a) with dry gases and (b) in a constant environment of 25 % relative humidity.

The lock-in amplifier maintains a frequency lock throughout the experiments, where no spurious spikes from other frequencies are generated. An average time of 2.4 s for the sensor to reach 90 % of final output (t_{90}) was calculated. In the case of a CO₂ sensor, an 80 mm path was found to be unsuitable for CO₂ breath analysis, where the sensor saturated with ~2.5 % CO₂. Although low ppm measurements of CO₂ are not necessary for breath analysis, other compounds, such as acetone, can be present in breath in such concentrations. Diabetic subjects can exhibit a strong level of acetone [30,31], which would be of interest for further breath analysis studies. Although not shown here, future work could involve trialling filter caps on the detector with bandwidth centred around perhaps 3.39 μm [32] in order to detect acetone in breath.

5.2.2 Lock-In Amplifier Path Length Optimisation

The preliminary experiments above proved that using an 80 mm path length CO₂ concentrations of interest in breath analysis (e.g. between 4 and 5 %) could not be distinguished. A prototype test unit was developed, including rapid prototyped parts, in order to trial different path lengths. The device, shown in Fig. 5.15, allowed large variation in path length, only restricted by the length of aluminium tube. Furthermore, the identical aluminium tubing is a suitable size for use in portable breath analyser. Any anomalies in tubing specification between a bench test rig and the final unit to include in a breath analyser will be removed by use of the same compact tubing. Preliminary work with a DC drive signal suggested that the finish of the tubing is of some importance to the strength of IR radiation transmitted between the emitter and detector, where a gold plated tube has a far greater reflectivity than an otherwise

identical aluminium counterpart. For this testing only aluminium tubing was used, due to ready availability allowing a wide variety of lengths to be tested without risk of damage to surface plating. In practice, stainless steel or nickel coated aluminium would be more reliable.

The length of tubing (optical path distance) in the NDIR assembly was varied between 10, 20 and 40 mm. The concentration of CO₂ was varied between 0.5, 1, 2, 3, 4 and 5 %. Each gas concentration was tested for 1 minute, returning to a baseline of synthetic air with no CO₂ present between each desired concentration. The gas flow rate was set at a constant 0.5 SLPM throughout the experiments. The processed time series data for a 40 mm path length are shown in Fig. 5.17. To ensure the reliability of the measurements, each path length was tested for five repetitions. The ability to adjust the length of the tube consequently entails the possibility of introducing alignment errors between the IR source and detector. This was mitigated by a visual inspection of the setup between repetitions, verification of the output voltage level of the thermopile detector on the gas test rig and constant monitoring of the gas flow rate out of the sensor (i.e. in a system with no leaks, the gas input will equal the gas output). The data recorded over the five repetitions for path length the average value for each gas concentration (with dry gases) are summarised in Fig. 5.18 and compared with each of the three selected path lengths.

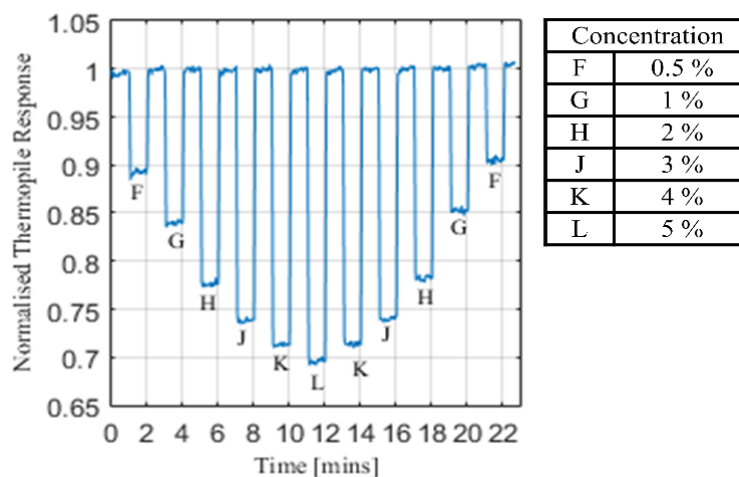


Fig. 5.17 – Response of the sensor to CO₂ concentrations in the range of 0.5 % to 5 % with a 40 mm IR path length.

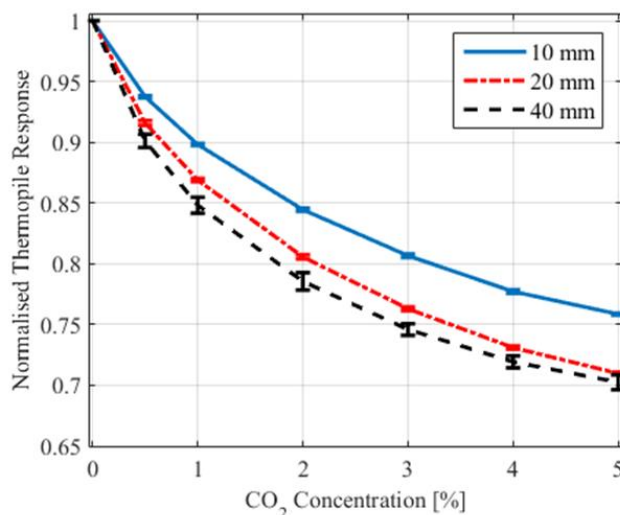


Fig. 5.18 – Comparison between 10, 20 and 40 mm path lengths for CO₂ detection in the range of 0.5 to 5 %.

Accurate detection of CO₂ concentrations in the region of 4 to 5 % is important for breath analysis. The response curves for 20 mm and 40 mm path lengths exhibit a similar trend to the higher concentrations shown for the initial experiment (80 mm path length), where the sensor output becomes saturated. The error bars on the graph represent the variation in average recorded value between repetitions. The error bars plotted for the 40 mm 4 % and 5 % measurement values are separated only by 0.007 (fractional change), thus the output response for 4 and 5 % cannot conclusively be determined. The 20 mm result demonstrates an improved result, where, including the error approximation, the 4 % and 5 % readings are separated by twice the fractional change of the 40 mm result (0.014). However this result is still barely a 1.4 % response change and therefore determining the accurate gas concentration is likely to become difficult, especially when measurements are taken with non-synthetic gases and with water vapour.

Although the sensor response is lower for a given concentration, the 10 mm path length results demonstrate promising responses to 4 and 5 % inputs of CO₂. The output response varies only by ~25 %, given a 5 % change in CO₂ concentration. Comparatively, ~29 % change in output response is observed with the 20 mm path configuration and ~30 % change for the 40 mm path length. However for the same change in CO₂ concentration, the output response varies by ~2.5 %, accounting for measurement errors. The dry results indicate the 10 mm path length is most suitable

for measuring CO₂ concentrations in the range of 0 to 5 %, with synthetic gases. Breath is almost completely saturated with water vapour, which absorbs IR radiation at certain wavelengths, and has been previously reported to have an effect on NDIR sensing [33].

The system with 10, 20 and 40 mm path lengths was tested at RH levels of 25 % and 50 %, over the same CO₂ concentrations (0, 0.5, 1, 2, 3, 4 and 5 %). For these experiments a constant ambient temperature of 25 °C was maintained throughout the test period. A time series plot for a 40 mm path length experiment is shown in Fig. 5.19. The experimental results are summarised in Fig. 5.20, at the same scale as the corresponding dry plot. Overall the response has been muted, regardless of path length. In dry conditions, 2% CO₂ produced output responses of ~16 %, ~18 % and ~22 % intensity change for 10, 20 and 40 mm path length, respectively. With a gas mixture containing 25 % RH, the responses have been decreased on average to 12 %, ~14% and ~15 %, respectively, for a 2 % step in CO₂ concentration. The presence of the water vapour also affected the measurement error, where additional noise was introduced into the system. For dry gases the standard deviations between all measurements for the 10, 20 and 40 mm path lengths were recorded as 0.1%, 0.1 % and 0.5 %, respectively. In conditions of 25 % RH these errors were calculated as 0.4 %, 0.1 % and 0.1%, respectively. The 10 mm path length demonstrates a quadrupling of error, however the 4 cm path length demonstrates a fifth of the error when comparing dry to 25 % humid conditions.

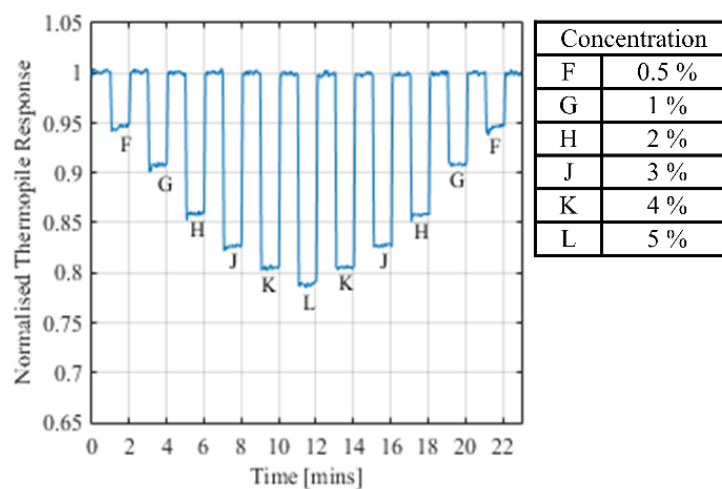


Fig. 5.19 – Time series data for 40 mm path length in 25 % RH conditions. CO₂ varied from 0.5 % to 5% with constant 0.5 SLPM flow.

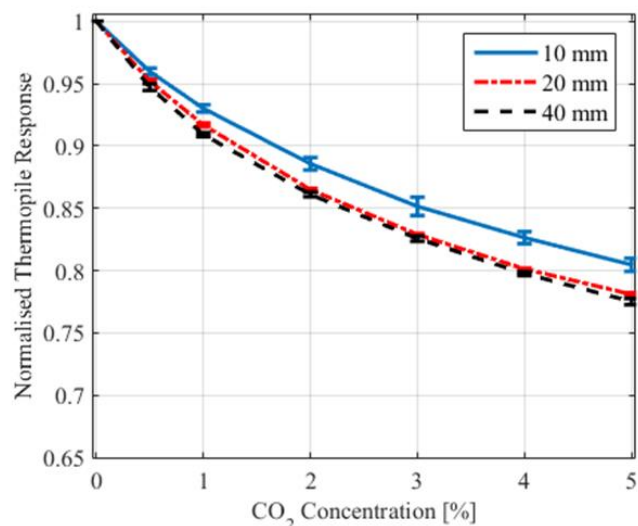


Fig. 5.20 – Data from 10, 20 and 40 mm path lengths summarised for 25 % RH conditions.

The most notable change from a dry to 25 % RH environment is the reduced separation between the 20 and 40 mm path length responses. In dry conditions the 40 mm path produced a higher response by on average 1.5 % (across all concentrations), but at 25 % RH the response was only 0.6 % greater. The 10 mm path length produces a lower response, but still maintains easy distinction between 4 % CO₂ and 5%. The 50 % RH condition response plot (Fig. 5.21) demonstrates an even smaller difference in intensity measured for the 20 mm and 40 mm path lengths, with just a 0.5 % greater response for the longer path. The results demonstrate that humidity decreases the response to CO₂, particularly with the smaller diameter tube (3.1 mm internal for the portable breath analyser tubing, compared to 10 mm for the aluminium chamber). It is a possibility that water droplets condensed inside the tube, and affected the IR radiation in a greater manner for the smaller diameter tubing.

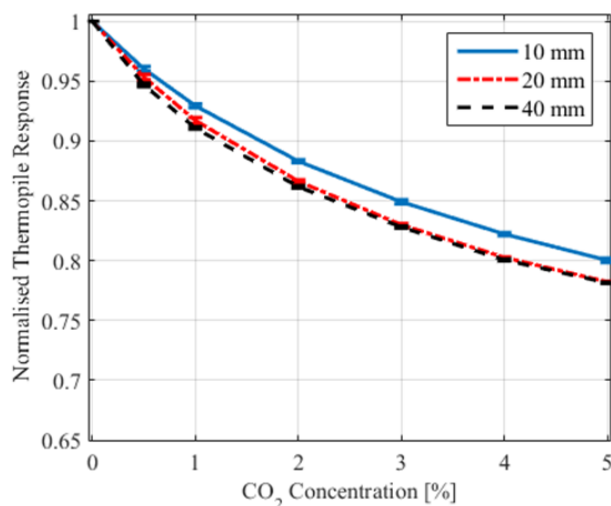


Fig. 5.21 – Data recorded at 50 % RH for path lengths of 10, 20 and 40 mm.

The measurements taken in 50 % RH demonstrate that the system is still able to function with humid gases and the sensor remains stable, despite a decrease in response. Overall the system is more stable with the higher level of humidity, where similar standard deviations were calculated as 0.1 %, 0.1 % and 0.08% for the 10, 20 and 40 mm experiments at 50 % RH, respectively. The response of the system becomes closer to a linear plot, with increasing levels of RH. The 10 mm path length was selected for the portable breath analyser, based on its physically compact design and ability to provide an adequate response in order to separate 4 % and 5 % concentrations of CO₂, in both dry and wet conditions.

5.3 Digital Filtering

The digital filtering approach was found to enable lower gas concentrations to be resolved, although the stability achieved with the lock-in amplifier configuration was compromised. The lock-in amplifier required a dual power supply, which is not convenient for a handheld unit (e.g. powered from a 5 V USB supply). The hotplate drive speed was trialled at 10 Hz and 5 Hz. The modulation frequency affects the output of the heater. A higher frequency is preferred for faster readout, and noise reduction, however a lower frequency offers higher modulation depth.

The sensor was exposed to the gas concentrations shown in Fig. 5.22, with 80 mm separation between the hotplate and thermopile (aluminium chamber, Fig. 5.14). The hotplate was driven with a 10 Hz sinusoidal wave, pulsing the heater temperature between 600 °C to 150 °C. The gas flow rate remained constant at 0.5 SLPM. The

heater drive voltage, shown in Fig. 5.11 a) was again used as the input to the model. The raw output signal, pre-processed, is shown in Fig. 5.22, where the changes in CO₂ concentration are not recognisable. The corresponding FFT peaks were taken from the output thermopile signal, as shown in Fig. 5.23 a). The signal output after FFT processing is shown in Fig. 5.23 b).

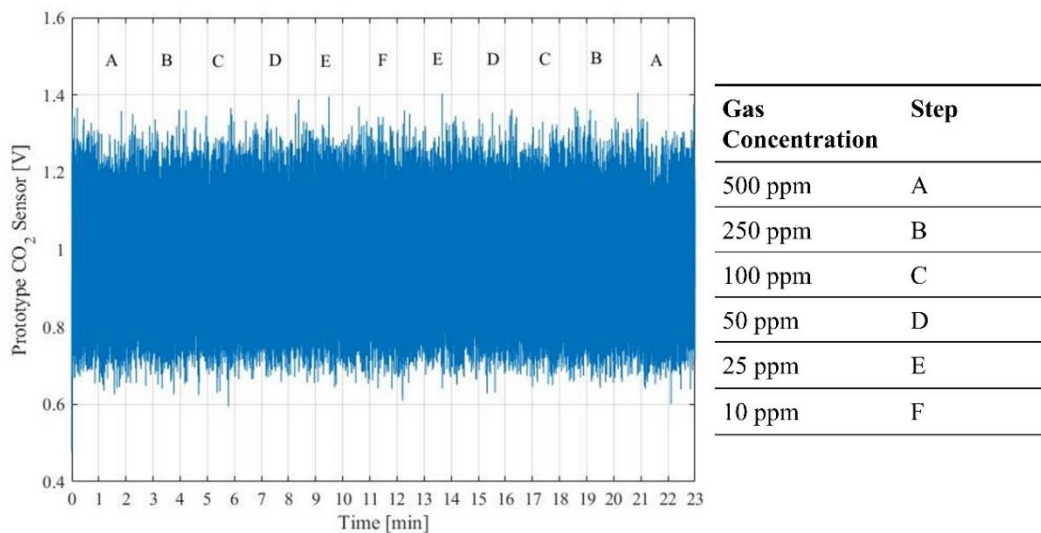


Fig. 5.22 – Raw amplified thermopile output from the CO₂ sensor system with concentrations shown in the table from 500 ppm to 10 ppm.

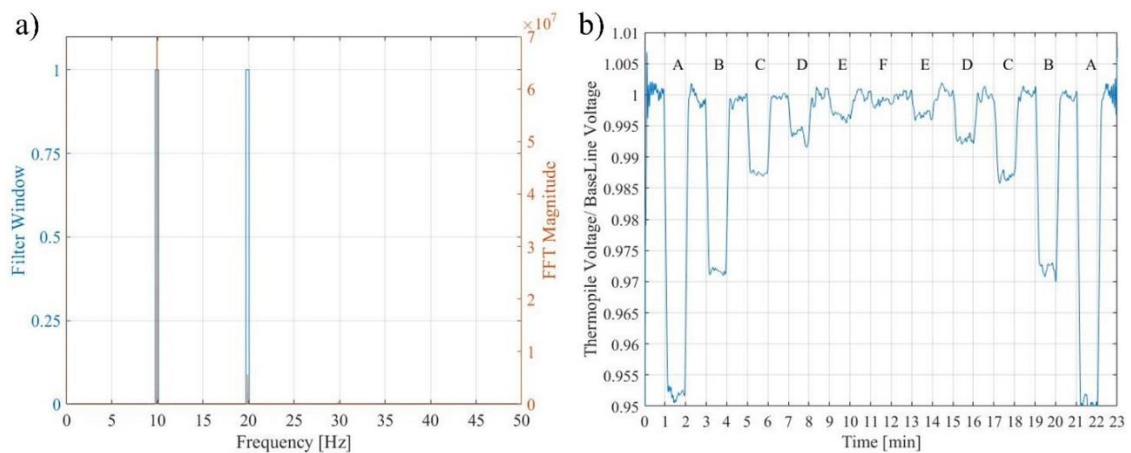


Fig. 5.23 – a) FFT filtering operation on the raw amplified thermopile signal produces b) FFT peak extraction data showing noise reduced output.

The post-processing of the signals was performed using code scripts written in MatLab 2015a. For the filtering process, a peak detection algorithm is used to detect the two dominant peaks from the FFT magnitude (i.e. the fundamental frequency and the first harmonic). A rectangular window is placed around the peaks, extending to 90% of

their maximum value, centred around the peak magnitude. The script to extract the peak automatically compares the output from the hotplate model equation and the output from the thermopile circuitry. The FFT has helped remove any high frequency noise, caused by other laboratory equipment or the 50 Hz power supply noise, and also any low frequency background noise.

The emitter source modulation depth decreases rapidly with frequencies above 10 Hz. Measurements performed at, for example 15 and 20 Hz, were found to be very unstable, thus it was not possible to distinguish 50 ppm or lower concentrations of CO₂. However, experiments were also performed at 5 Hz, to verify the principle of the processing technique. Fig. 5.24 shows the final, processed results, again tested with an 80 mm path length.

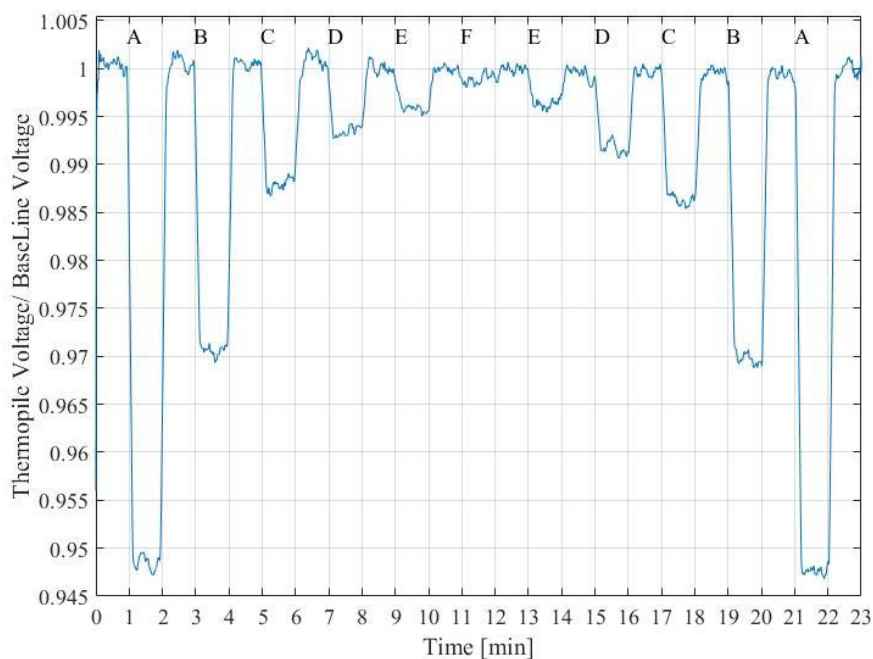


Fig. 5.24 – Measurements of CO₂ between 0.5 % and 5 % with a 5 Hz drive signal and 1 minute steps per concentration input.

5.4 Linearity of Response

The results presented above, for both the lock-in amplifier design and the FFT filtering procedure, demonstrate that the sensor offers repeatable measurements of CO₂ concentration. However, the results did not fit the simple Beer-Lambert law eq. (3.2). The response of the results is not linear, nor can a single exponential curve (i.e. the aforementioned law) fit to the output response. The raw output voltage from the lock-

in amplifier is shown in Fig. 5.25 for 50 % RH across the path lengths tested (10, 20 and 40 mm).

The Beer-Lambert law in the format eqn. (3.2) only accounts for the basic optical condition, with correlated light, where a single beam of light travels directly between the emitter and detector, is shown in Fig. 3.8. However, the emitter emits light with a 69° field of view, which will also generate reflections along the length of the aluminium tube.

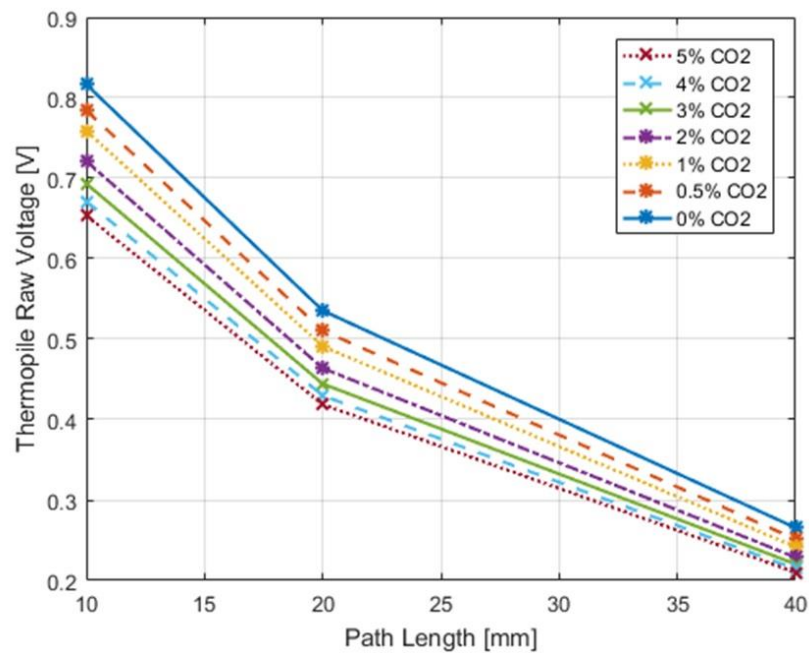


Fig. 5.25 – Thermopile raw output voltage compared to path lengths of 10, 20 and 40 mm across CO₂ gas concentrations from 0.5 to 5 %.

On the scale of this work, an in-depth model is not possible, but instead a simpler model is proposed to account for the highest intensity reflection (which reflects at the centre point of the tube). A modified version of the Beer-Lambert equation (5.11) is proposed which includes a term for the intensity lost due to reflections inside the tube and emitter itself (I_{int}), which do not reach the detector.

$$I(c) = I_{int} + I_0 [e^{-k_g l_1 c} + g e^{-k_g l_2 c}] \quad (5.11)$$

Also, the modified equation includes two path lengths l_1 (direct path length) and l_2 reflected path length (the highest intensity reflection, with only one bounce). l_2 is related to l_1 by $l_2 = \sqrt{l_1^2 + 4d^2}$, where d is the diameter of the tube, and g denotes the

reflections in all angles around the tube. The mass path (u) in (5.12) relates the number of molecules per area, given a known pressure (P), mixing ratio (q), distance (x) and temperature (T), where k is Boltzmann's constant [34].

$$u = \frac{qPx}{kT} \quad (5.12)$$

Equation (5.12) can be rearranged, and given the cross sectional area, can be used to calculate the coefficient k_g , and put into the correct form for substitution into the modified Beer's Law, as shown in (5.13).

$$k_g = \frac{P}{kT} \sigma \quad (5.13)$$

From the nature of the experimental setup, it can be assumed that the pressure is atmospheric and any fluctuations will be negligible. From the HITRAN database [27], the experimental temperature is reported as 296 °K (23 °C). The thermopile cap filter specified with a central frequency of 4.26 μm and a bandwidth of 0.18 μm . From the data shown in Fig. 5.8, the cross section was calculated $\sigma = 9.88 \times 10^{-19}$ $\text{cm}^2/\text{molecule}$. Therefore the constant $k_g = 241.9 \text{ cm}^{-1}$. The modified equation was used to model the 50 % RH data with a 10 mm path length. The modelling provided an excellent fit ($R^2=0.999$) to the 10 mm data shown in Fig. 5.25. The model demonstrates (Fig. 2.26) that the reflections contribute a large proportion of the light received by the detector. The values for I_{int} , I_0 and I_g were found to be 0.72, 0.26 and 0.059, respectively.

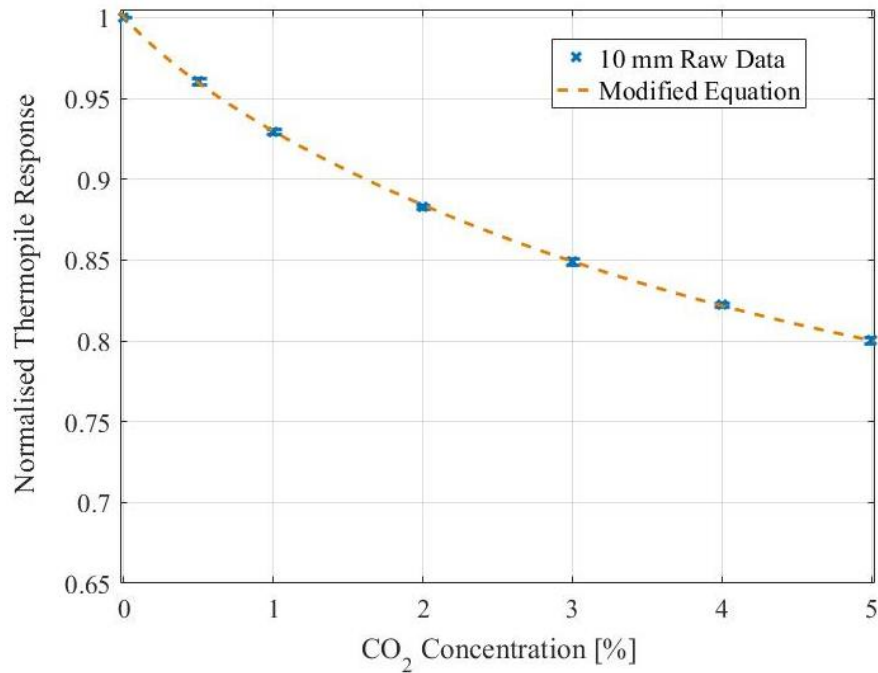


Fig. 5.26 – Modified Beer-Lambert law equation plotted against output data for 10 mm IR path length (50 % RH) for CO₂ concentration from 0 % to 5 %.

Equation (5.11) was fitted to the experimental data reported in Fig. 5.24, and values obtained for I_{int} , I_0 and g as 0.92, 0.077 and 0.018, respectively. The curve fit is shown in Figure 5.27, where the R^2 goodness of fit was 0.998. The curve fit demonstrates that both methods (the lock-in amplifier and FFT filtering) present similar results and the exponential curves fit the output produced by the sensor. The lower concentrations shown in the FFT model plot demonstrate that the effect is independent of path length and concentration.

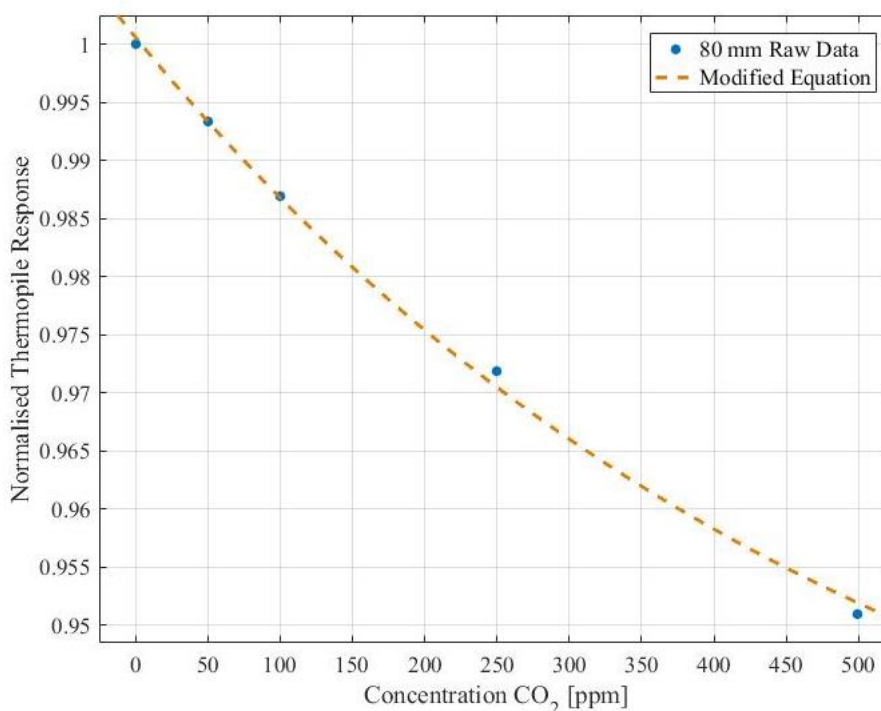


Fig. 5.27 – Modified Beer-Lambert law equation (3.2) plotted against output data for 80 mm IR path length for the FFT digital filtering method with concentrations of CO₂ from 0 to 500 ppm.

5.5 Conclusions

In this chapter the importance of the NDIR drive signal has been reported. The AC drive signal provides a considerable advantage over a DC approach; however the AC signals received at the thermopile require more complex analysis to enable the desired response to CO₂ to be extracted. The DC based system demonstrated the operation of the NDIR detector. The trials with both gold and aluminium plated tubing revealed the improved performance of gold plating did not justify the additional design complexity and cost. Although the received signal produced a lower output signal at the thermopile, the sensitivity to CO₂ changed only by 2 %.

The bench top lock-in amplifier design showed promising results for stable detection of high concentrations of CO₂. The system produced lower sensitivity than a digital filtering process, but an 80 mm path length was sufficient to detect CO₂ in the range of 50 ppm to 2.5 %. The dedicated lock-in amplifier chip reduced the processing load of the data logging system. The 80 mm path system was trialled at 25 % RH which decreased the normalised readings by, on average 2.3 %, (but increased stability by 0.13 %).

Experiments performed consider variation of the path length (10, 20 and 40 mm) demonstrated that a 10 mm path permitted concentrations up to 5 % to be detected. Besides the advantage of a smaller design, the 10 mm path length allowed for easier discrimination between concentrations of CO₂, where the 40 mm system became saturated at higher concentrations of CO₂. To verify the functionality of the system when the test gas contained water vapour, the system was exposed to dry, 25 % RH and 50 % RH conditions. The 10 mm path length was adversely affected, demonstrating an increase in noise. However, the longer path lengths performance, although marginally less affected by the presence of humidity, were not sufficiently sensitive to breath levels of CO₂. A humidity sensor will be included in the breath analyser system to allow the level of water vapour to be monitored and compensated for.

The model of the NDIR emitter developed through equations of the heat produced enabled digital filters to be designed specific for the waveforms expected to be received by the NDIR detector. Filtering the noisy thermopile output in the frequency domain avoided the need for high order analogue filtering, which extends the response time of the sensors. The output from the model produced a good response to CO₂ in the range of 10 to 500 ppm with an 80 mm path length. The response was less stable than using the lock-in amplifier technique, but can be easily integrated into a portable design (without the need for a dual power supply).

5.6 References

- [1] E.J. Anderson, L.G. Sylvia, M. Lynch, L. Sonnenberg, H. Lee, D.M. Nathan, Comparison of energy assessment methods in overweight individuals., *J. Acad. Nutr. Diet.* 114 (2014) 273–8. doi:10.1016/j.jand.2013.07.008.
- [2] A. De Luca, M.T. Cole, A. Fasoli, S.Z. Ali, F. Udrea, W.I. Milne, Enhanced infra-red emission from sub-millimeter microelectromechanical systems micro hotplates via inkjet deposited carbon nanoparticles and fullerenes, *J. Appl. Phys.* 113 (2013) 214907. doi:10.1063/1.4809546.
- [3] J. Spannhake, O. Schulz, A. Helwig, G. Muller, T. Doll, Design, Development and Operational Concept of an Advanced MEMS IR Source for Miniaturized Gas Sensor Systems, in: *IEEE Sensors, 2005.*, IEEE, n.d.: pp. 762–765. doi:10.1109/ICSENS.2005.1597811.
- [4] B. Hok, Hå. Pettersson, A. Kaisdotter Andersson, S. Haasl, P. Akerlund, B. Hök, et al., Breath analyzer for alcolocks and screening devices, *IEEE Sens. J.* 10 (2010) 10–15. doi:10.1109/JSEN.2009.2035204.
- [5] K.M. Dubowski, Breath analysis as a technique in clinical chemistry, *Clin. Chem.* 20 (1974) 966–972.
- [6] S.Z. Ali, A. De Luca, R. Hopper, S. Boual, J.W. Gardner, F. Udrea, et al., A low-power, low-Cost infra-red emitter in CMOS technology, *IEEE Sens. J.* 15 (2015) 6775–6782. doi:10.1109/JSEN.2015.2464693.
- [7] P. Barritault, M. Brun, O. Lartigue, J. Willemin, J.-L. Ouvrier-Bufferet, S. Pocas, et al., Low power CO₂ NDIR sensing using a micro-bolometer detector and a micro-hotplate IR-source, *Sensors Actuators B Chem.* 182 (2013) 565–570. doi:10.1016/j.snb.2013.03.048.
- [8] A. Graf, M. Arndt, M. Sauer, G. Gerlach, Review of micromachined thermopiles for infrared detection, *Meas. Sci. Technol.* 18 (2007) R59–R75. doi:10.1088/0957-0233/18/7/R01.
- [9] Analog Devices, AD9837 Programmable Waveform Generator, Analog Devices Tech. Doc. (2012). <http://www.analog.com/media/en/technical-documentation/data-sheets/AD9837.PDF> (accessed August 15, 2016).
- [10] G. de Graaf, R.F.F. Wolffenbuttel, Lock-in amplifier techniques for low-frequency modulated sensor applications, *Instrum. Meas. Technol. Conf. (I2MTC), 2012 IEEE Int.* (2012) 1745–1749. doi:10.1109/I2MTC.2012.6229510.
- [11] J. Hodgkinson, R. Smith, W.O. Ho, J.R. Saffell, R.P. Tatam, Non-dispersive infra-red (NDIR) measurement of carbon dioxide at 4.2 μ m in a compact and optically efficient sensor, *Sensors Actuators B Chem.* 186 (2013) 580–588. doi:http://dx.doi.org/10.1016/j.snb.2013.06.006.
- [12] A. Lambrecht, S. Hartwig, J. Herbst, J. Wöllenstein, J. Woellenstein, Hollow fibers for compact infrared gas sensors, *Proc. SPIE.* 6901 (2008) 69010V/1-69010V/11. doi:10.1117/12.761539.
- [13] M. Urbański, R. Szewczyk, Analysis of response time of carbon dioxide sensor in chemical sensor system for mobile robot, in: R. Szewczyk, C. Zieliński, M.

- Kaliczyńska (Eds.), Prog. Autom. Robot. Meas. Tech. Vol. 3 Meas. Tech. Syst., Springer International Publishing, Cham, Switzerland, 2015: pp. 277–284. doi:10.1007/978-3-319-15835-8_30.
- [14] E. Socher, O. Bochobza-Degani, Y. Nemirovsky, A novel spiral CMOS compatible micromachined thermoelectric IR microsensor, *J. Micromechanics Microengineering*. 11 (2001) 574–576. doi:10.1088/0960-1317/11/5/320.
- [15] S.M. Kashmiri, S. Xia, K.A.A. Makinwa, A temperature-to-digital converter based on an optimized electrothermal filter, *IEEE J. Solid-State Circuits*. 44 (2009) 2026–2035. doi:10.1109/JSSC.2009.2020248.
- [16] P. Guha, S.Z. Ali, C.C.. Lee, F. Udrea, W.I. Milne, T. Iwaki, et al., Novel design and characterisation of SOI CMOS micro-hotplates for high temperature gas sensors, *Sensors Actuators B Chem.* 127 (2007) 260–266. doi:10.1016/j.snb.2007.07.047.
- [17] C. Lu, D. Setiadi, F. Udrea, W.I. Milne, J.A. Covington, J.W. Gardner, 3D thermo-electro-mechanical simulations of gas sensors based on SOI membranes, 2000 Int. Conf. Model. Simul. Microsystems - MSM 2000. (2000) 297–300.
- [18] S.Z. Ai, W. Gonzalez, J.W. Gardner, F. Udrea, Analysis of high temperature SOI micro-hotplates, in: 2004 Int. Semicond. Conf. CAS 2004 Proc. (IEEE Cat. No.04TH8748), IEEE, 2004: pp. 351–354. doi:10.1109/SMICND.2004.1403015.
- [19] F. Udrea, J.W. Gardner, D. Setiadi, J.A. Covington, T. Dogaru, C.C. Lu, et al., Design and simulations of SOI CMOS micro-hotplate gas sensors, *Sensors Actuators B Chem.* 78 (2001) 180–190. doi:10.1016/S0925-4005(01)00810-3.
- [20] S.Z. Ali, F. Udrea, W.I. Milne, J.W. Gardner, Tungsten-Based SOI Microhotplates for Smart Gas Sensors, *J. Microelectromechanical Syst.* 17 (2008) 1408–1417. doi:10.1109/JMEMS.2008.2007228.
- [21] T. Iwaki, J.A. Covington, F. Udrea, S.Z. Ali, P.K. Guha, J.W. Gardner, Design and simulation of resistive SOI CMOS micro-heaters for high temperature gas sensors, *J. Phys. Conf. Ser.* 15 (2005) 27–32. doi:10.1088/1742-6596/15/1/005.
- [22] S. Ali, A. De Luca, Z. Racz, P. Tremlett, T. Wotherspoon, J.W. Gardner, et al., Low power NDIR CO₂ sensor based on CMOS IR emitter for boiler applications, *IEEE SENSORS 2014 Proc.* (2014) 934–937. doi:10.1109/ICSENS.2014.6985155.
- [23] X. Yi, J. Lai, H. Liang, X. Zhai, Fabrication of a MEMS micro-hotplate, *J. Phys. Conf. Ser.* 276 (2011) 12098. doi:10.1088/1742-6596/276/1/012098.
- [24] A. Pike, J.W. Gardner, Thermal modelling and characterisation of micropower chemoresistive silicon sensors, *Sensors Actuators B Chem.* 45 (1997) 19–26. doi:10.1016/S0925-4005(97)00261-X.
- [25] S. Astié, a. M. Gué, E. Scheid, L. Lescouzères, A. Cassagnes, Optimization of an integrated SnO₂ gas sensor using a FEM simulator, *Sensors Actuators A Phys.* 69 (1998) 205–211. doi:10.1016/S0924-4247(98)00096-X.
- [26] A. Götz, I. Gràcia, C. Cané, E. Lora-Tamayo, M.C. Horrillo, J. Getino, et al., A

- micromachined solid state integrated gas sensor for the detection of aromatic hydrocarbons, *Sensors Actuators B Chem.* 44 (1997) 483–487. doi:10.1016/S0925-4005(97)00171-8.
- [27] L.S.S. Rothman, I.E.E. Gordon, Y. Babikov, A. Barbe, D. Chris Benner, P.F.F. Bernath, et al., The HITRAN2012 molecular spectroscopic database, *J. Quant. Spectrosc. Radiat. Transf.* 130 (2013) 4–50. doi:10.1016/j.jqsrt.2013.07.002.
- [28] R. V Kochanov, Working with HITRAN database using HAPI: HITRAN Application Programming Interface, in: *Int. Symp. Mol. Spectrosc., International Symposium on Molecular Spectroscopy, 2015*: p. 2013. doi:10.15278/isms.2015.mh03.
- [29] J.W. Gardner, F. Udrea, W.I. Milne, Numerical simulation of a new generation of high-temperature micropower gas and odour sensors based on SOI technology, in: V.K. Varadan (Ed.), *1999 Symp. Smart Struct. Mater., International Society for Optics and Photonics, 1999*: pp. 104–112. doi:10.1117/12.354292.
- [30] M. Righettoni, A. Tricoli, S.E. Pratsinis, Si:WO₃ Sensors for highly selective detection of acetone for easy diagnosis of diabetes by breath analysis., *Anal. Chem.* 82 (2010) 3581–7. doi:10.1021/ac902695n.
- [31] K.-W. Kao, M.-C. Hsu, Y.-H. Chang, S. Gwo, J.A. Yeh, A sub-ppm acetone gas sensor for diabetes detection using 10 nm thick ultrathin InN FETs., *Sensors (Basel)*. 12 (2012) 7157–68. doi:10.3390/s120607157.
- [32] R. Li, Y. Xiong, Y. Wang, F. Wan, Research on Infrared Breath Alcohol Test Based on Differential Absorption, in: *2009 First Int. Conf. Inf. Sci. Eng., IEEE, 2009*: pp. 4086–4089. doi:10.1109/ICISE.2009.959.
- [33] D. Baschant, H. Stahl, Temperature resistant IR-gas sensor for CO₂ and H₂O, *Proc. IEEE Sensors, 2004*. 1 (2004) 142–145. doi:10.1109/ICSENS.2004.1426120.
- [34] C.H. Blake, M.M. Shaw, Measuring NIR atmospheric extinction using a global positioning system receiver, *Publ. Astron. Soc. Pacific*. 123 (2011) 1302–1312. doi:10.1086/662980.

CHAPTER VI

Development of Software for Laboratory and Handheld Data Acquisition

Preface

LabVIEW software was developed to acquire the data from the gas sensors tested. The interface extended to control of gas MFCs, which were used to generate a set of concentrations of various gases (CO₂, CO, NO₂, O₂ etc.) during the testing of the side-stream analyser. A further interface was written to communicate with a microcontroller used in the hand-held analyser, and record the data at 200 Hz, output in serial format. To facilitate mobile measurements, without a computer, an Android application was written to allow wireless communication (Bluetooth) with the analyser. The application was able to display the received data in real-time, and record the files to an SD card in the smartphone. A 1 minute breath sample could be taken using the application, and EE calculated immediately on the smartphone itself. The LabVIEW and Android applications developed in this work have enabled the testing and recording of a variety of gas sensors (MOX, NDIR, electrochemical) and the use of the hand-held analyser outside of a laboratory environment.

6 Control and Acquisition Software

The gas sensors in this work and the housing chamber are designed to enable a fast response time for breath-by-breath analysis. The data acquisition sub-system must be capable of recording the output from the sensors with a high bandwidth else risk comprising the sensor output. To verify the sensor response time and generate precise gas mixtures software was developed for a gas test rig. For portable sensing, a microcontroller was used to transmit wirelessly the sensor data to a smartphone or laptop computer.

6.1 Bench Gas Rig Control Software

A benchtop gas testing rig was constructed (Fig. 6.1), consisting of four mass flow controllers (MFCs, Alicat MC-5SLPM-D) and one mass flow meter (MFM, Alicat M-5SLPM-D). The monitor (A) displays the control systems for the gas mixture system and the output recorded from the gas sensors. A regulated power supply (B), TTI QL564TP, is used to provide controlled power levels (voltage and current limited) to the sensors. The MFCs (C) enable the generation of gas mixtures, with the current flow rates and selected gas shown on LCD screens at the front of each device. The DAQ (D), National Instruments (NI) USB 6343, is used to interface between the computer and analogue gas sensors (two-wired differential inputs). The sensor chamber (E) can be interchanged depending on the type of gas sensor under test. The exhaust is connected to the right of the chamber, with the output from the four MFCs mixed together to the left of the chamber. The heater block (F) allows heating of the humidity line, to prevent condensation forming along the line at high levels of humidity.

Flow charts showing the operation of the NI LabVIEW 2013 software and the code used to operate the gas testing rig are shown in Appendix C. Code for writing values to the MFCs and reading data from the data acquisition unit are shown.

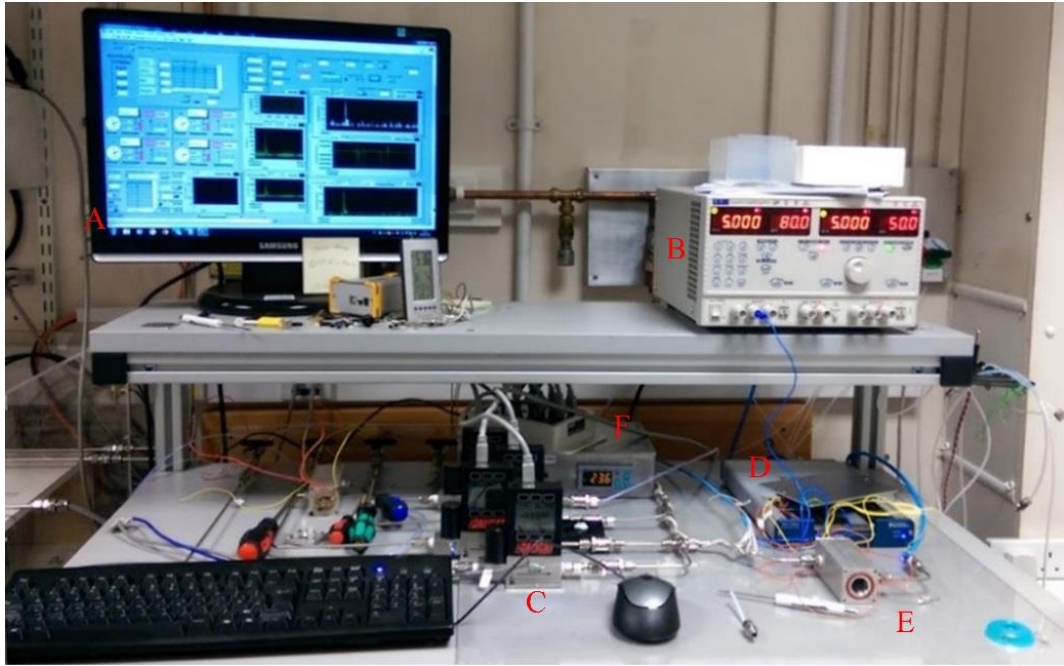


Fig. 6.1 – Photograph of gas testing rig in laboratory.

The gas testing rig enables a mixture of gases to be created and the RH in a gas chamber to be varied. The system also controlled a furnace (Memmert UNP 200), in which the gas sensor chamber could be fitted and the environmental temperature varied. A block diagram of the gas rig is shown in Fig. 6.2. The system is designed to generate gas mixtures with flow rates up to 5 SLPM (limit of MFCs). The minimum flow rate it is possible to produce with each individual MFC is 15 ml/min.

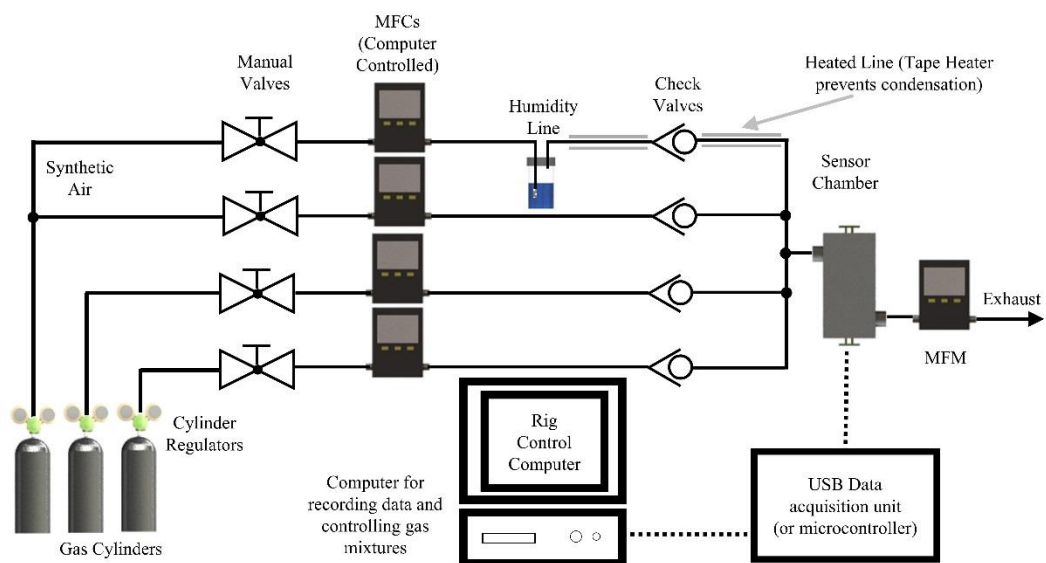
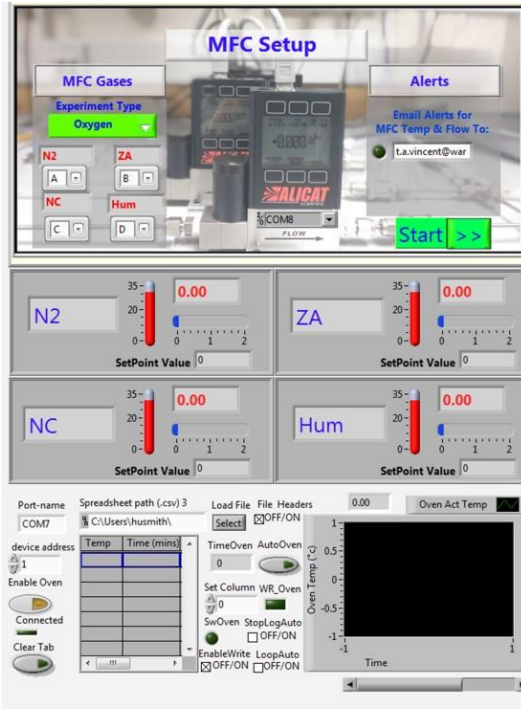


Fig. 6.2 – Block diagram of gas rig.

The data logging ability of the gas testing rig has been referred to in previous chapters. The software has interfaces for commercial sensors, which can be benchmarked against prototype research devices. The virtual front panel of the software is shown in Fig. 6.3. The software can be used independently of the data logging interface (where only gas mixtures are controlled); this allows for the rig to be used with external data logging software.

Located just outside of the photograph of the rig is a commercial safety sensor unit, which detects the presence of CO, CO₂ and NO₂ in the environment. This air quality sensor sounds an alarm immediately, if a safe threshold for a particular gas is exceeded. Risk assessments, safe systems of work (SSoW) and control of substances hazardous to health (COSHH) assessments were undertaken prior to any testing of gas.



MFC Setup

MFC Gases
Experiment Type: Oxygen

Alerts
Email Alerts for MFC Temp & Flow To: t.vincent@war

N2 **ZA** **NC** **Hum**

SetPoint Value: 0

Port-name: COM7
Spreadsheet path (.csv): C:\Users\husmith\...
Load File: Select
File Headers: OFF/OON

device address: 1
Enable Oven: Connected
Clear Tab

TimeOven: 0
AutoOven: OFF/OON
Set Column: WR_Oven
SwOven: OFF/OON
StopLogAuto: OFF/OON
EnableWrite: OFF/OON
LoopAuto: OFF/OON

Oven Temp (C): 0.00
Oven Act Temp: 0.00

Time

MFC Control

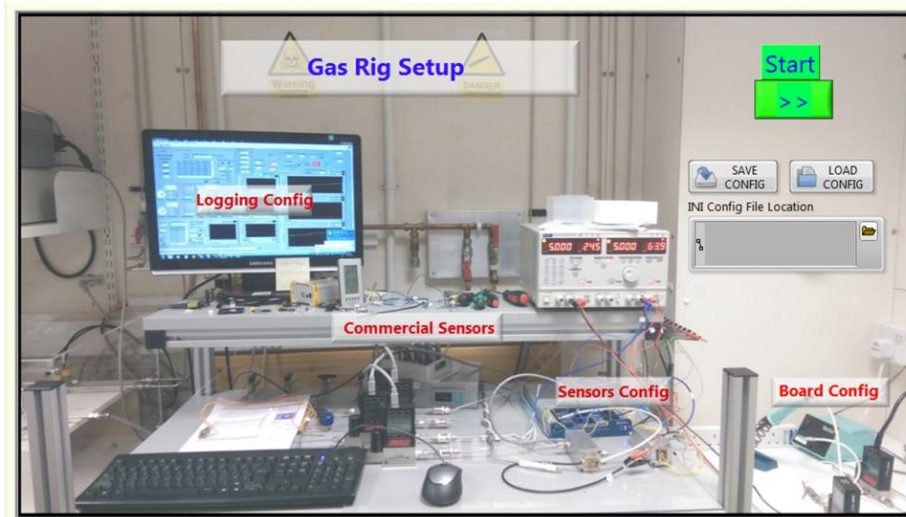
- Gas Configuration
- Manual Value Change
- Table of Flow Values
- Automatic Value Calculation

MFC Readouts

- Gas Configured
- Current Flow Rate
- Programmed Flow Rate
- Temperature of Controller

Furnace Control

- Temperature Input
- Current Temperature
- Device Configuration



Gas Rig Setup

Start >>

SAVE CONFIG LOAD CONFIG

INI Config File Location

Logging Config

Commercial Sensors

Sensors Config

Board Config

Gas Rig Setup Page

- Logging Setup
- Commercial Devices Configuration
 - Gas Sensor Port Selection
- Board Parameter Input
- Save or Load Configuration
- Start Data Acquisition

Fig. 6.3 – Screen-print of LabVIEW interface for gas rig control and layout diagram showing options in each sub-section of the interface.

6.1.1 Data Acquisition

Analogue data output from gas sensors connected to the benchtop rig are recorded by on a computer (Microsoft Windows 7 operating system). A NI USB-6343 DAQ unit permits up to 32 analogue inputs specified at 16 bit resolution (range ± 10 V) [1].

Additionally, 4 analogue outputs are available to the same specification. A LabVIEW virtual instrument (VI) was designed to efficiently display the DAQ measurements on-screen in real time. A screen-print of the data acquisition screen is shown in Fig. 6.4.

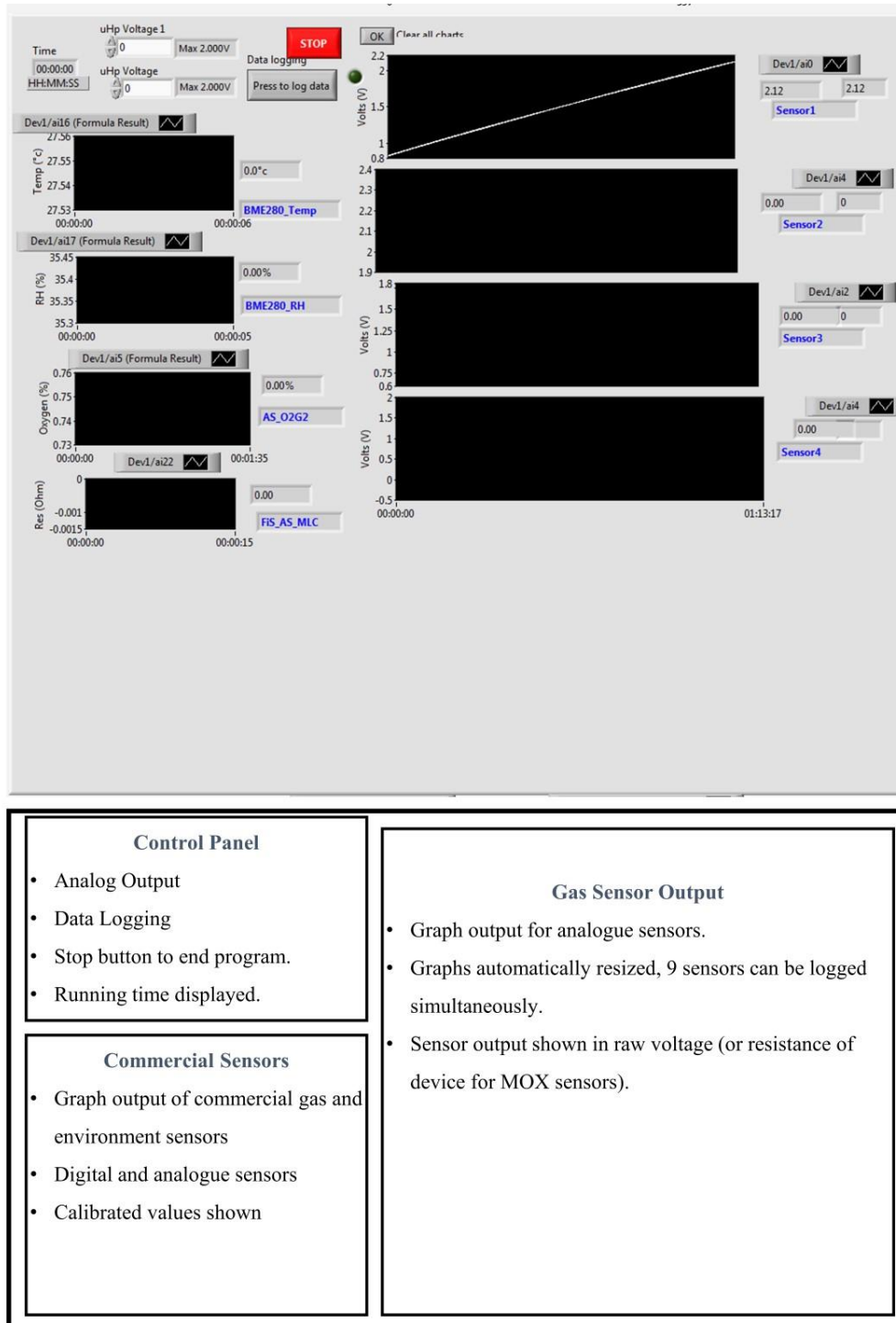


Fig. 6.4 – Screen-print of the data logging interface with graphs to show both prototype and commercial sensor outputs. The layout shown is of the control screen.

The data are recorded into a proprietary NI format (*.TDMS, technical data management streaming [2]), which allows a fast data stream to be recorded (required at high sampling rates). The resulting output files usually require converting from a binary format to a text format for further data processing. The additional post-processing effort is offset by the reliability and robustness achieved during the critical data logging phase. The data logging process also enables compression of the data, i.e. averaging of samples over a set period to reduce the file size (for long measurement periods of perhaps up to 24 hours). Limited real time signal processing can be performed on the signal. The board configuration screen (on the initial VI screen) enables parameters from the circuit boards to be entered. These allow the resistance of the sensor to be calculated and plotted, as opposed to only the raw output voltage being displayed. Additionally, either of these display modes can be filtered (a moving average filter is applied). The width of the moving average filter is set at 1 s, and can be adjusted in the program code.

Miniature commercial sensors can target the mobile device market, and often provide digital outputs (e.g. I²C, SPI, etc.). The output form of these devices is usually converted to a serial (COM port) standard, which can in turn be converted to a USB input. The VISA (virtual instrument software architecture) standard is used to obtain data from the serial devices and provides a string format output into a LabVIEW VI. The sampling rate of these devices does not always match the user selected sampling rate for the NI DAQ. To ensure that the commercial sensor outputs are logged at the same time intervals, the devices sampled at a lower rate are up-sampled to match the higher sampling rate. The default sampling rate is configured as 100 Hz.

An example commercial sensor included in the system is a Bosch BME280 sensor (used for temperature and humidity sensing). An Atmel ATtiny85 microcontroller is used to convert the digital I²C output from the BME280 to a serial output (converter board shown in Fig. 6.5). The microcontroller is powered and connected to the computer with a USB to serial adapter. The BME280 is a miniature device (for an enlarged photograph see the inset in Fig. 6.5) which is supplied with a 2.5 × 2.5 mm land pattern. The versatile device offers I²C and SPI outputs and requires a 3.3 V power supply [3]. The sensor can be placed into a gas sensor chamber. The interface board, located outside the chamber, is connected (via 4 pins) through a connector on the chamber lid. In turn, the board is connected to a computer via the cable shown.

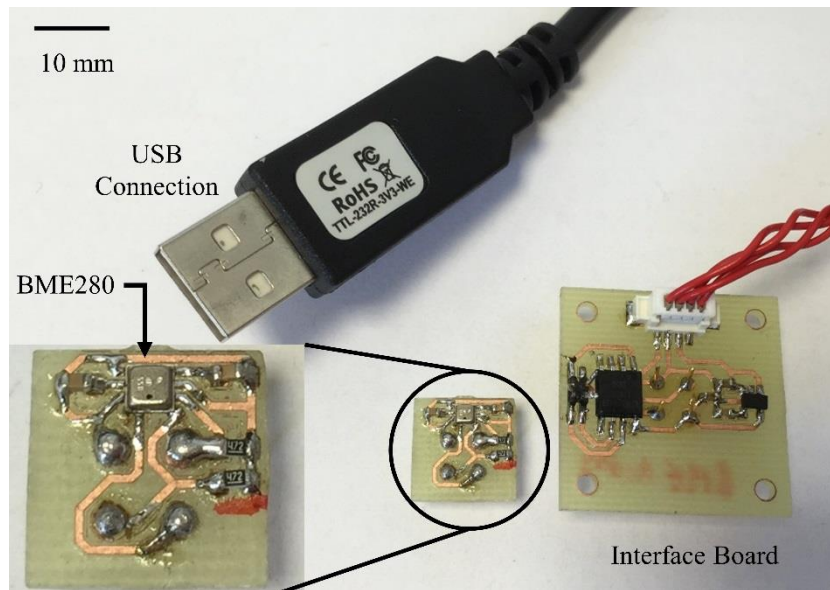


Fig. 6.5 – Photograph of a BME280 chip mounted on a circuit board. The interface board converts the sensor output to serial communication which is then converted to the USB inside the connector shown.

6.1.2 Heater and Emitter Control

The heater on a MOX sensor and IR emitter for CO₂ sensors can be controlled using a module within the LabVIEW VI. Although the IR emitter is best controlled using a dedicated chip, for improved stability, the gas rig system allows trial heater voltages to be tested, without chip reprogramming. The front panel control, shown in Fig. 6.6, allows either a sinusoid, DC, square or custom wave pattern to be generated using the NI DAQ analogue output.

The custom waveforms can be configured using a spreadsheet file. The output can be changed in real-time, using numerical controls. In the example shown in the figure, a sinusoidal waveform is generated, where the graph shows the output waveform, which is turned into a numerical list of data points and transmitted through the analogue output port.

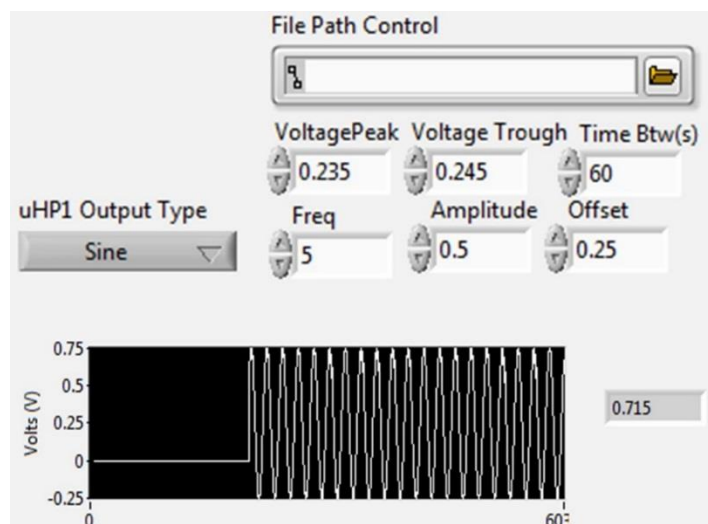


Fig. 6.6 – NI DAQ Analogue output system (IR emitter and MOX heater control).

The custom file output could be used to generate unique patterns for MOX sensors. As previously discussed, MOX films are sensitive to different compounds at different heater temperatures. By varying the heater temperature, different compounds can be distinguished in an unknown mixture of gases. The sinusoidal generator mode was designed for testing the effect of increasing frequency on the IR emitter output. A decline in output emission would be expected for an increase in frequency (unpublished datasheet).

The current consumption of the circuits can be monitored using the power supply shown in Fig. 6.1. In the case of the MOX sensors, the readout given on the display provides confirmation of the operation of the heater drive circuit. The serial output from the power supply is not yet utilised in the LabVIEW VI. The power supply has three output channels, which can be used to power MOX devices separately to observe current demand over time.

6.1.3 Furnace Control

The environmental temperature in which a sensor operates can often affect the operating mechanism. To experiment with temperatures in the range of ~ 5 °C above ambient to 300 °C a furnace (Mettler [4]) was used to vary both the ambient temperature of the gas sensor, and the gas itself. A photograph of the furnace located on the laboratory bench underneath the MFC setup is shown in Fig. 6.7. The large internal area of the oven ($400 \times 320 \times 250$ mm – width, height, depth) introduced a considerable warm up time (perhaps 45 mins to 180 °C), however this did not restrict the chambers that could be tested [4].



Fig. 6.7 – Photograph of the Memmert Furnace; temperature controlled environment from 5 °C above ambient to ~ 300 °C.

The slow time constant (i.e. caused by the large dead volume) inside the furnace provided a stable baseline temperature when testing the NDIR sensors in particular. A constant ambient temperature was desired to reduce drift over the duration of the experiment. In the case of other types of sensor, such as MOX or electrochemical, the sensor chamber can be placed inside a heater and the environmental temperature controlled to within ± 0.1 °C. Dry block heaters are commonly used, for their precise temperature control and laboratory grade construction. However, the temperature of these devices is regulated at a rate of ~ 2 Hz. The shift in temperature, even by 0.1 °C, is a large variation for a NDIR device, thus interferes with the signal received by the IR detector. It was therefore found that dry block heaters are not ideal for NDIR measurements – instead a larger environmental furnace was preferred.

The furnace control interface (shown in Fig. 6.3) enabled a set of temperatures to be programmed, i.e. step changes, over a desired period of time. The VI enabled the temperatures required to be entered in a table (or loaded from a spreadsheet format) along with the time for each step. The time taken to heat or cool the furnace was not incorporated into the program. The graph in the furnace module of the virtual front panel shows the current oven temperature (when connected).

6.1.4 MFC Module

The module to program the MFCs with gas flow rates and therefore generate the desired gas mixture is located in the upper left of the LabVIEW VI (Fig. 6.3). The interface is designed to be inherently adaptable to the wide range of gases and VOCs that can be tested with the rig. The initial configuration, displayed on the front panel immediately after executing the VI, requests the user selects the gas(es) or VOC to be tested. The drop down selection box lists 12 gases (or combinations of gases) which the software is currently configured to operate with. Once the gas type for the experiment is selected, the four connections for the four MFCs are displayed. The order of the MFCs is adjustable to allow for the different possible physical gas line connections to the rig.

The MFC configuration is a step only required at the start of each experiment. A ‘save config’ option is available on the front panel, which saves all the options (including those for data logging, sensor and board type) to a text file. The saved file can be loaded (‘load config’) when required, to restore all the settings for a specific gas experimental setup. The save file option also saves the limits and output data for the DAQ analogue output ports, which can prevent user errors occurring between setting the configuration for MOX and NDIR sensors.

The single value screen, shown in Fig. 6.8 a), appears once the user confirms the configuration for the MFCs. This screen is designed for leak testing the system. This screen allows the user to manually send gas flow rates to the controllers. An example leak test is to set a value of 0.5 SLPM of synthetic air and observe the output on the MFM (synthetic air is referred to as Zero Air in the screen prints).

The program does not automatically send the values when they are typed into the boxes (nor on the return key being pressed), instead the values are sent together, when the send button is pushed. When generating mixtures of gases, it is rare to require only one MFC value to be changed at only one time, thus the send button must be pushed before any values are modified at the MFC level. For instance, to change from a baseline of only synthetic air to a mixture of NO₂, two flow controller values must be changed (air and NO₂). If these two controllers are not changed instantaneously, a flow variation would occur, which could produce a pronounced effect on the sensor output.

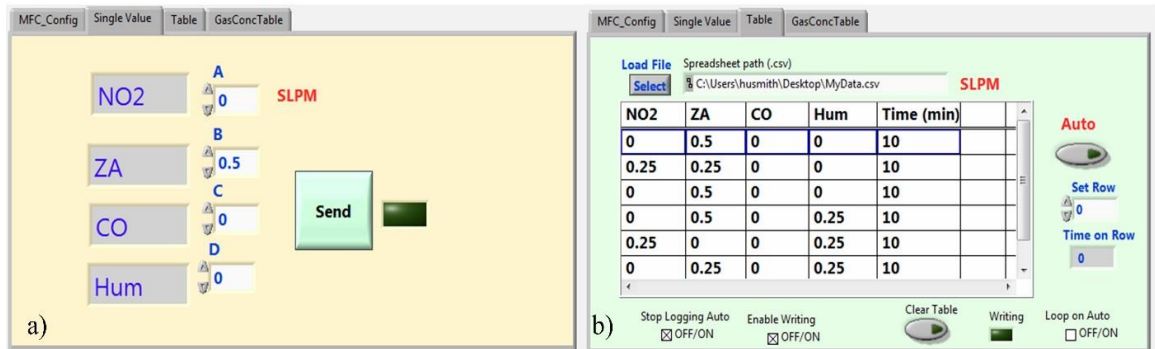


Fig. 6.8 – LabVIEW VI for basic programming of MFCs, a) One value sent to the controllers with manual button push; b) Table of flow values, rows written automatically to the flow controllers after a given time.

The flow values can be stepped automatically from a tablet format as shown in the screen print in Fig. 6.8 b). The flow values must be calculated manually, and can be typed directly into the table or loaded manually. The final tab, discussed below, automates the calculation of the desired gas concentration mixture into gas flow rates. The manual table is designed if the configuration cannot be programmed into the software or for other testing purposes.

The general operation of the gas rig is usually controlled using the automated gas flow calculation screen shown in Fig. 6.9. The user is required to only type (or load from a spreadsheet) the list of required gas concentrations, humidity levels and times for each concentration step. From this information, the flow rates required are calculated for the four MFCs in the system. The concentration of each gas cylinder (as connected to the gas rig) must be entered in the upper right corner of the screen. Default values are saved in the configuration.

The screenshot shows the MFC_Config software interface. At the top, there are tabs for 'MFC_Config', 'Single Value', 'Table', and 'GasConcTable'. Below the tabs, there is a 'Load File' section with a 'Select' button and a spreadsheet path: 'C:\Users\SOI-HITS\Desktop\Tim\'. To the right of the path are sliders for 'Chiller Temp °c' (set to -10), 'CO PPM' (set to 300), 'NO2 PPM' (set to 3), and 'CO2 %' (set to 5). An 'Auto' button is also present.

Below the sliders are two tables. The left table has columns: 'NO2 ppm', 'Hum (Fr)', 'CO PPM', and 'Flow To'. The right table has columns: 'NO2', 'ZA', 'CO', 'Hum', and 'Time (m)'. The right table has a blue highlight on the first row.

At the bottom of the interface, there are several control buttons: 'Zero Flow' (checked OFF/ON), 'Stop Logging' (checked OFF/ON), 'Loop' (unchecked OFF/ON), 'Enable Writing' (checked OFF/ON), 'Clear Table' (button), 'Writing' (button), 'Set Row' (button), and 'Time on Row' (button).

Below the interface is a diagram with three boxes:

- Concentration Input**
 - Concentration requirements typed or loaded from spreadsheet.
 - Total flow rate configured and length of time for each step.
 - Humidity can be controlled. Error reported if value not obtainable.
- Concentrations of gases supplied to the rig (cylinders). Auto button begins operation from selected line.**
- Calculated MFC Flow Rates**
 - Program calculates values required for the MFCs to create the desired input gas concentrations.
 - Flow rates are shown in table format, with blue box indicating current line written to MFCs.
- Flow Controller Advanced Section**
 - Parameters for advanced control of program operation.
- Time on current row and which row is selected.**

Fig. 6.9 – Screen print of an automated gas flow calculation (upper right table) given input of the desired gas concentrations (upper left table). The lower diagram indicates the function of each section of the VI.

The flexibility of the gas rig is demonstrated by the options available. The rig must be capable of a range of operations (e.g. 5 minute calibration phases to 24 hour stability experiments). Options are available to ‘loop’ the flow configuration (to repeat the table, until stopped by the user). At the end of the final row of the table, the flow is automatically zeroed and the data logging stopped (these options can be disabled as necessary).

6.2 Microcontroller Data Acquisition

The LabVIEW VI developed above formed the software component of a bench top benchmark system for gas sensor testing. The configuration is unsuitable for portable applications, requiring a computer and a bulky USB data acquisition unit. The DAQ itself is limited to analogue sensor inputs (i.e. measuring a voltage) and therefore cannot be used with digital sensors, such as the I^2C output from the breath flow meter. USB adaptors are available, although these add to the bulk of the system. High quality

analogue to digital converters (i.e. at least 12 bit or even 16 bit) are commonplace on microcontrollers. The ability to sample both analogue and digital outputs to a high degree of accuracy allows microcontrollers to replace the benchtop apparatus used for data acquisition.

A section of the microcontroller code is shown in Appendix D. The code shows how the signals are obtained at 200 Hz, and the transmission of the data over a serial (USB) connection.

The Teensy 3.2 (PJRC, USA [5]) was selected as the microcontroller to acquire the data from the gas sensors and transfer it in serial format to a computer or smartphone. A photograph of the microcontroller is shown in Fig. 6.10. A prototype PCB interface board was developed to interface the U.FL coaxial and power connections from the gas sensors. Table 6.1 shows the features of the microcontrollers used in this work. In the portable breath analyser, Teensy is the only microcontroller utilised, although the other listed devices were used in preliminary testing. The Uno [6] was used as an interface for commercial CO₂ sensors and the Sensirion flow sensor. The Pro Mini [7] was used as the microcontroller for the frequency generator chip. The ATtiny85 [8] was used to interface the digital temperature/humidity sensor (BME280), discussed above, to a serial USB connection. The KL25Z [9] was trialled in initial work, but the Teensy device range superseded its functionality and compatibility with other programming environments (i.e. LabVIEW etc.).

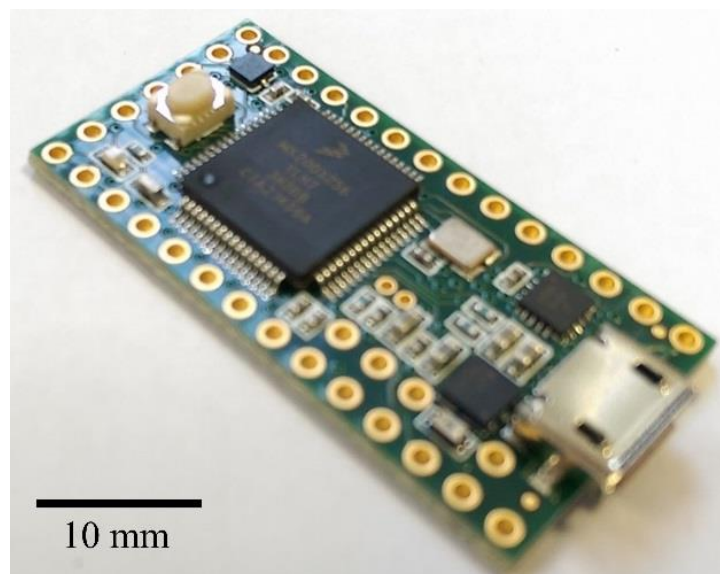


Fig. 6.10 – Photograph of PJRC Teensy 3.2 microcontroller with micro USB port.

Table 6.1 – List of microcontroller devices and specifications used in this work.

Specification	PJRC	Arduino	Arduino	Atmel	Freescale
	Teensy 3.2 [5]	Uno [6]	Pro Mini [7]	ATtiny85 [8]	KL25Z [9]
Microcontroller	Cortex M4	ATmega328P	ATmega328	ATtiny85	Cortex M0+
Voltage Supply [V]	3.3 to 5	5	3.3 or 5	1.8 to 5.5	5
Digital Pins	34	14	14	6	14
Analog Inputs (resolution [bits])	21 (16)	6 (10)	6 (10)	3 (10)	6 (16)
Analog Outputs	1 (12 bit)	0	0	0	1 (12 bit)
Flash Memory [kb]	128	32	32	8	128
Clock Speed [MHz]	72	16	8 or 16	20	48
Dimensions	17 × 36	69 × 53	17 × 33	5 × 5	84 × 53

The Teensy microcontroller offered excellent analogue to digital capabilities, a 16 bit interface (the same quality as the NI DAQ used in the laboratory setup). The bit accuracy reduced the error in the conversion from the raw sensor outputs to a digital format for onward transmission to a data logging device. The CO₂ NDIR thermopile, MOX VOC sensor, O₂ sensor and temperature and humidity sensor outputs were recorded in this manner. An I²C input was used to communicate with the SFM3000 flow sensor. An SPI link was used between the microcontroller and the frequency generator chip (AD9837 in the NDIR system).

6.2.1 Sample Rate

The output from the CO₂ detector is in sinusoidal format, at 5 Hz. The signal processing is performed using software algorithms, post data collection. The accurate recording of the AC signal is paramount in order to obtain accurate CO₂ concentrations. The Nyquist theorem for digital sampling states that for a sine wave

with temporal frequency f to be faithfully reproduced, it must be sampled at a minimum frequency of $2f$ [10]. However, to ensure the 5 Hz wave can be reproduced digitally to a very high accuracy the sampling rate of the microcontroller was set significantly higher than 10 Hz. A 200 Hz sampling rate was selected, as a balance between size of data collected (considering it must be transferred in real time to a data logger) and the ability to very accurately reproduce the 5 Hz signal.

Aliasing, the effect when a high frequency signal is sampled below the Nyquist rate and an artificial lower frequency is observed, is not usually observed at low frequencies using high sampling rates [11]. The variability in the amplitude of the low frequency 5 Hz sinusoid is difficult to measure if not sampled with sufficient precision. To select a sampling frequency data was collected at 100, 200 and 500 Hz. Aliasing was visible at 100 Hz (i.e. changes in a 0.01 V were not recorded). At 500 Hz a higher error rate was observed; the volume of data was too great for a real time plot to be displayed and the data to be saved to a file.

Fig. 6.11 demonstrates the aliasing effect observed with a 2 Hz sinusoid (solid line), sampled at four different sampling frequencies f_s . When sampled at 16 Hz in a) the wave can be reproduced by linear interpolation (dashed line), linking the sampled points (dots). The reliability of the interpolation method is not evaluated and the sinusoid does not vary in amplitude. The reduction in quality of the reproduced wave is apparent in b), where the sine wave sampled is compared to a saw tooth waveform. No aliasing occurs in the above two cases, as the original frequency can be recovered using linear interpolation.

In Fig. 6.11 c) aliasing does not occur, but the resampled wave noticeably deviates from the original curve (5 Hz is greater than the Nyquist rate of $2 \times 2 \text{ Hz} = 4 \text{ Hz}$). The original frequency is still present but the original waveform is difficult to visualise in the sampled format. Aliasing occurs in d), where the sampling frequency is only 0.5 Hz above the maximum sine wave frequency (constant 2 Hz). In this case a lower frequency wave is recorded after linear interpolation. The higher sampling frequency set in the microcontroller prevents any deviation between the re-sampled wave and the original sinusoid.

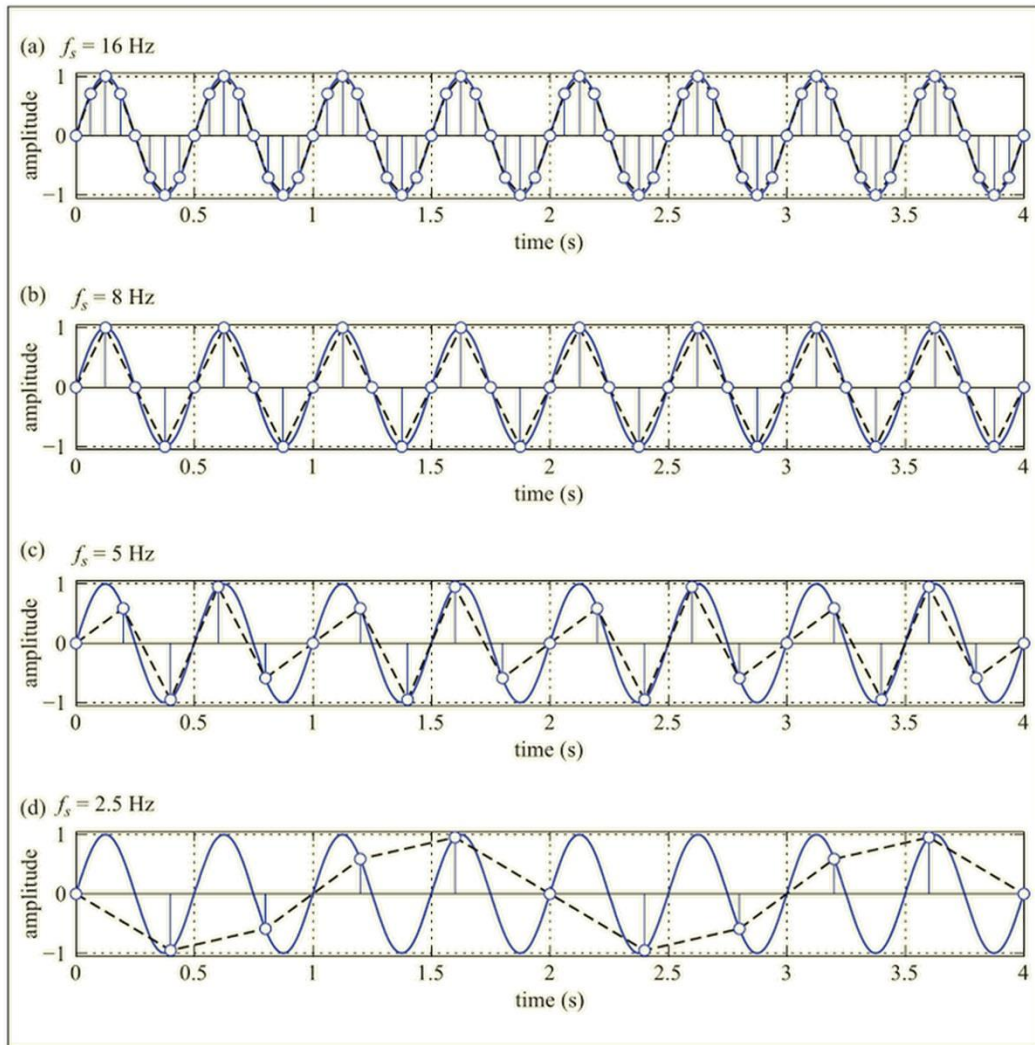


Fig. 6.11 – Effect of aliasing on a 2 Hz analogue sinusoidal waveform over a 4 s period, sampled at a) 16 Hz, b) 8 Hz, c) 5 Hz and d) 2.5 Hz. The original waveform is shown as solid line, dots indicate the sampling points and the dashed line shows the curve reproduced by linear interpolation [12].

The Teensy microcontroller has two ADCs and thus can allow two sensor inputs to be read simultaneously. To ensure that the FFT processing of the CO₂ sensor thermopile data can be accurately reproduced, the sampling rate must be constant. The microcontroller contains four interval timers. There are a total of 6 sensors to be recorded (including the digital flow meter). The sampling rate is set to enable sampling at 400 Hz, where two samples are averaged to produce a 200 Hz output. It is not possible to sample to digital sensor at a rate of 200 Hz; instead it is sampled using one timer at a rate of 50 Hz. One timer is used to ensure that the collected data are sent to a computer or smartphone at a rate of 200 Hz. The remaining two timers (and the two ADCs) are used to sample the five analogue sensors, with priority given to the O₂ and

CO₂ sensors. To enable sufficient speed to complete the analogue read operations, the bit accuracy was set to 12 bits. The data are transmitted to the data logging device in float format (3 decimal places).

6.2.2 Communication Link

A USB connection is the standard communication method integrated into all the microcontrollers listed in Table 6.1, except for the Pro Mini and ATtiny85 (which have only serial connection output, which must be converted to USB). A wired link provides a robust and reliable communication protocol between the end data logging device and the microcontroller. The USB port on a computer or micro port on a modern smartphone usually provides a power source for a slave device (5 V). Although the current output is limited (perhaps 500 mA on a USB 2.0 port or 200 mA for a smartphone [13]), it is sufficient to power the low-power miniature gas sensors. The majority of the current drawn from the system is due to the pump required to sample the gas through the side-stream chamber.

The breath analyser designed in this work aimed to provide a portable solution as an alternative to a benchtop based system. A wired USB connection to a smartphone adds complexity to the system, although the handheld unit would not require a separate power source (battery). Details of the USB link to a smartphone are given in the application section below. Bluetooth was found to offer a preferred means of connecting to both a laptop computer and a smartphone. The wire-free solution enabled comfortable measurements to take place and relies on a standardised connection method, often included in laptop computers and smartphones (i.e. no drivers required). Bluetooth is not integrated into the Teensy microcontroller, although an add-on module (generic HC-05, Hobbytronics [14]) can transmit serial data through Bluetooth. The module can operate at 3.3 or 5 V and requires a maximum of 40 mA. For both the Bluetooth and USB communications a standard 115,200 kbps rate was selected.

The breath analyser was tested with subjects inside whole room calorimeters. These rooms were sealed (air-tight) from the outside laboratory. The Bluetooth link enabled the breath analysers to be placed inside the room while the data logging process could be monitored from outside. For long experiments, where several hours of data logging was required, the data were recorded on a laptop computer.

6.3 LabVIEW Breath Analyser Interface

A LabVIEW VI (2013) was designed for the receiving and saving of the signals transmitted from the microcontroller via either Bluetooth or USB. The software was installed on both Microsoft Windows 10 and Windows 7 laptop computers. Providing that the breath analyser was paired and assigned a serial COM port, the VI could connect to the microcontroller via Bluetooth or USB without requiring any re-programming modification (except specifying the correct COM port). No additional software was required on the laptop computers (besides LabVIEW), where the Bluetooth pairing and management was performed using the software integrated into the Windows operating system or the bundled applications from the manufacturer of the laptop as appropriate.

The software developed in LabVIEW, shown in Fig. 6.12, does not perform any signal processing on the acquired data. Post-processing stages are performed in a separate script discussed in chapter VIII. The graphs displayed on the front panel display the data from the sensors. The flow sensor data are received in a digital format (float value of litres per minute). The device was not calibrated during testing, but relied on the pre-set factory settings from the manufacturer. The analogue sensors (O_2 , temperature and relative humidity) outputs are displayed in calibrated form. The O_2 sensor is calibrated pre- and post- each experiment, although the calibration data used in the VI are obtained from laboratory bench top experiments (i.e. the graphic display of data is for reference only). The VOC and CO_2 sensors are shown in raw voltage format (the VOC sensor is not connected in the screen print below). The data (raw data directly obtained from the microcontroller) are saved to a TDMS file type, as discussed above.

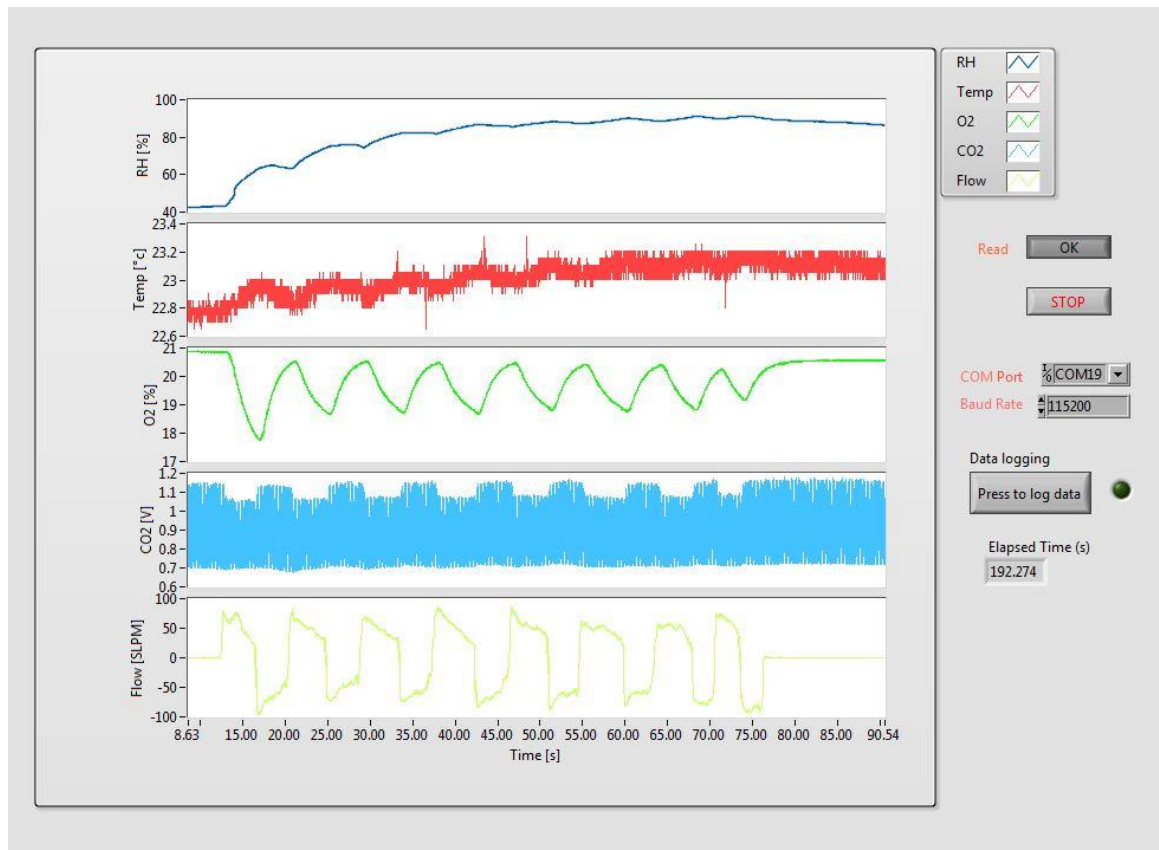


Fig. 6.12 – Screen print of LabVIEW VI showing data acquired from a breath analyser using a USB link with a microcontroller. Example breathing for a 1 minute period is shown.

The LabVIEW software was designed to allow robust data logging, without consuming computational resources. The lightweight application functioned on a range of laptops reliably and was tested for periods of up to 5 hours. The NI base software allowed compatibility across a range of versions of Windows operating systems. The block diagram LabVIEW code is given in Appendix E.

6.4 Android Application for Breath Analyser

Two android applications were developed for recording the data from the breath analyser which negated the need for a bulky computer. Android was chosen as the target mobile operating system, due to the capability to receive data from either USB or Bluetooth sources. Furthermore, there were few restrictions to saving the data and a flexible programming environment (Android Studio 1.5.1). Initially an application to link to the microcontroller via a micro USB link was developed. A second application was later developed to allow Bluetooth communication. The applications were both tested on a HTC M8 Smartphone running Android 5. As discussed above

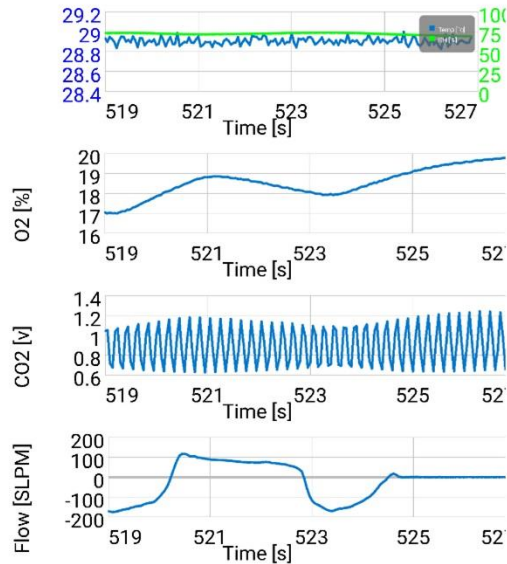
with the data acquisition interface written for a computer, the application to record the data would not attempt to perform in-depth post-processing, but instead focus on reliable and accurate recording of the sensor data.

6.4.1 Application for USB Microcontroller Link

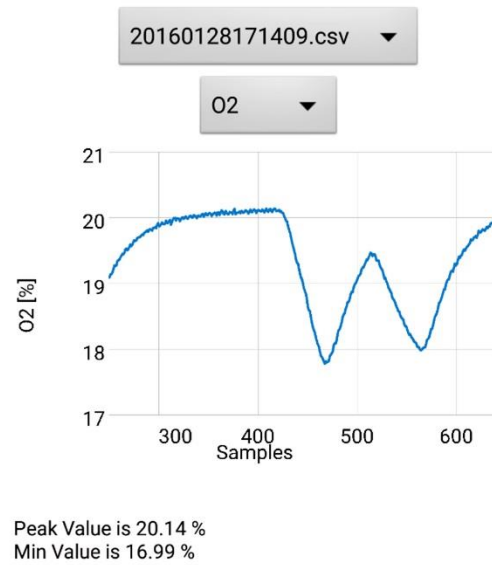
A USB link was initially trialled as a simple means of powering the microcontroller and receiving sensor data. The application was split into three parts; a first screen to select the USB serial connection; a screen to log the data from the sensors (the VOC sensor was not included when this application was developed) and a screen to perform basic analysis of the data (post-logging). The application was based around a USB-Serial library, designed for communication with USB devices plugged into the micro USB port on an Android smartphone.

The application was designed to allow continuous data logging during the period that it was open. The screen print in Fig. 6.13 a) shows the main data logging screen. As discussed above, the temperature, humidity, flow and O₂ sensors are calibrated, whereas the raw voltage is displayed for the CO₂ sensor. The screen print shown in Fig. 6.13 b) demonstrates the basic analysis of the data performed after the logging process. The features demonstrated only calculate the peak and minimum values across the experimental data. Further signal processing algorithms were not added to this version of the application, where the application developed to allow Bluetooth communication was preferred.

USB Data Logging in Progress



Data Analysis



a)



b)



Fig. 6.13 – Screen prints from the Android USB wired data logging application, a) Breath data are recorded and graphed in real time; b) Basic data analysis performed post-logging, showing the data recorded for the O₂ sensor during one experiment.

The data were recorded to comma separated value (CSV) files, which were stored on the memory card inside the mobile phone. The analysis of the data recorded with this Android application is transformed from raw quantities to EE and discussed in chapter VIII (the analysis performed on a computer). The breath analyser system was estimated to have a peak power consumption of 100 mW, however had a noticeable effect on the battery life of the smartphone (i.e. power taken through the micro USB port). The comfort of using the breath analyser was compromised by the cable link to the smartphone. The procedure of comfortably locating the face mask into position to form a seal around the face could cause the USB cable (to the smartphone) to become disconnected.

The application was able to successfully log data at 200 Hz. The amount of data appearing on the screen was reduced to ~ 8 s to prevent overloading of the device on updating the graphical interface (and leave insufficient computational overhead to

obtain data from the USB). The user interface was not developed for the application. The goal of targeting an easy to use application was not completed. Cosmetic changes to the layout of the application could visually improve its appeal and ease of use.

6.4.2 Application for Bluetooth Communication with Breath Analyser

In contrast to the application developed with LabVIEW for Windows computers, the Android application coded above for USB communication did not support Bluetooth. A second Android program was written to allow a wireless Bluetooth link between the breath analyser and smartphone. The convenience of a cable-free design enabled the user to take comfortable breath samples. Sections of the code programmed to the Android smartphone are shown in Appendix F.

A separate battery was required for the breath analyser, it was of similar capacity (~2800 mAh) to that inside a smartphone (but was the dedicated source of power) and thus extended the time that the breath analyser could be used without a mains power supply (perhaps over 2.5 hours usage). Additionally, as the micro USB port of the Android smartphone was not connected to the analyser, the phone could be charged while taking measurements (or connected to a computer for debugging purposes).

The application displayed graphs to show real-time data acquired from the microcontroller, in a similar format to the USB application above. A photograph of the data being recorded on a smartphone is shown in Fig. 6.14. The application shows the output from the O₂, temperature, RH and flow in calibrated units. The CO₂ sensor is analysed in real time, using an algorithm to extract the amplitude of the waveform, and this voltage is displayed in the graph (previous applications only showed sinusoidal output). The VOC sensor output is shown as a voltage. The application was designed to take 1 minute EE measurements. The calculation performed to obtain the value is discussed in a later chapter. The graphs on screen update every 10 samples (where an average value is shown). In the output CSV log file the 200 Hz sampled data are recorded. The application was found to reduce the performance of the smartphone if a higher update rate was configured.

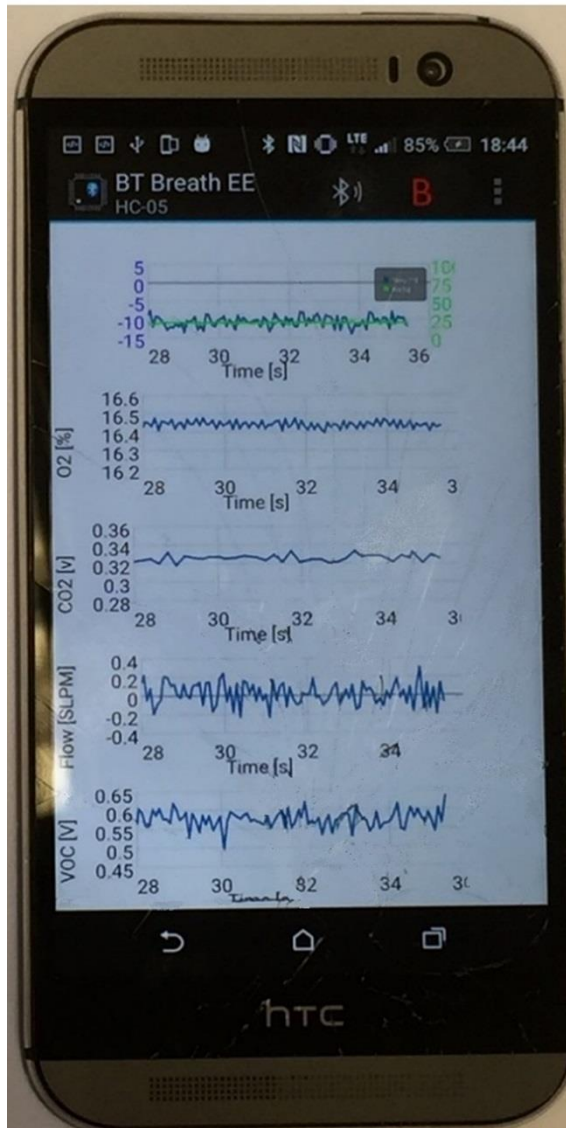


Fig. 6.14 – Photograph of a smartphone connected to breath analyser via a Bluetooth connection used for taking breath EE measurements and recording data.

The calibrated value for CO₂ is not presented in the application the value shown, e.g. a constant value ~ 0.33 V in the screen print in Fig. 6.14, provides an easier to read view of the CO₂ concentration (previous versions of the application showed only the raw sinusoidal signal). A variance of ~ 0.1 V would be expected for a 5 % change in CO₂, between inhaled and exhaled gas. The amplitude of the sinusoidal wave previously presented in other applications corresponds to the concentration of CO₂ to which the sensor is exposed. An algorithm to identify the peaks and troughs from the sinusoidal waveform is implemented every 120 samples (then the troughs are subtracted from the peaks to find the amplitude of the wave).

The script does not rely on prior knowledge of the frequency of the waveform (the frequency of the aforementioned 5 Hz sine wave can be varied without creating the need to modify the script). The code does not rely on a defined number of peaks/troughs. The program stores the peaks and troughs that are identified in the previous 120 samples. If the number of peaks does not equal the number of troughs, the corresponding values are taken from the previous data set. This ensures that there are the same number of peaks and troughs. Then the troughs are subtracted from the peaks to find the amplitude of the wave. This analysis is less detailed and accurate than that performed in the post-processing usually executed on a computer (e.g. FFT filtering). However the benefit of a presentable CO₂ readout is that the user can identify the approximate response from the NDIR sensor in real time.

The microcontroller is not instructed to send the value from the sensors to the smartphone. The timer inside the microcontroller is used, which enables consistent sampling of sensor outputs, without reliance on a software timer inside the smartphone. If the smartphone application was to close suddenly, or become accidentally disconnected, then the data logging could be resumed quickly. It was found that the high sampling rate required robust acquisition of the signal over Bluetooth. The serial data were transmitted from the microcontroller with a new line indicating a distinct sample from all the sensors (i.e. 200 lines transmitted per second). The receiving application did not rely on detecting a new line break with every transmission, as it could become lost. The pattern of the signal was identified, and checked against the expected pattern for the 6 sensors. A seventh field was added to the end of the serial line, to indicate the time (in ms) since the microcontroller started acquiring data. This provided a means of verifying the sampling rate and the data being received successfully by the smartphone.

The application was designed to take 1 minute breath samples from the user of the breath analyser. The user first started the application and paired to the Bluetooth module by pressing the Bluetooth icon at the top centre of Fig. 6.14. The application would then display the sensor data in the graphs (8 s view). Data logging would not occur until the user pressed the 'B' breath button (top right of the application). A countdown of 3 s would appear on the screen, after which the data logging would commence and the user should breathe into the device. A countdown (red) bar at the top of the application indicates the progression of the 1 minute breath sampling period.

At the end of the 1 minute period a message appears immediately, indicating the metabolic rate measured over the period. The logged data are stored in a CSV file, which can be analysed later (an option in the drop down menu, top right of the application).

The Bluetooth link was found to be a reliable means of communicating with the portable breath analyser. The link allowed a range of at least 5 metres without a loss in signal quality. The robustness of the connection was not specifically tested, nor was any mechanism to store the data at the transmitter implemented. The connection was used to test the analyser with subjects in whole body calorimeters, and it was found less than 10 samples were lost in a 3 hour experiment. One laptop (with integrated Bluetooth transceiver) was capable of connecting to two breath analysers simultaneously. To protect against data corruption or loss, in the unlikely event of a computer failing, experiments were performed with one analyser paired per laptop.

6.5 Conclusions

In this chapter the acquisition software for both computer and smartphone applications has been introduced. The LabVIEW VI for control of the bench gas rig has been detailed. The gas rig was a fundamental part of creating a breath analyser, where the performance of the sensors was assessed prior to their exclusion or inclusion in the project. The software for the control of the MFCs was designed for the purpose of sensor testing, and therefore included options for generating gas concentrations and step changes in environmental conditions as needed to comprehensively evaluate sensor performance.

The gas testing rig was based on 4 MFCs and 1 MFM. Inherently, testing of gases implies a low level of risk. The important health and safety criteria were met for every gas tested on the rig. A safety sensor was installed in close proximity to the rig. In the case of the alarm sounding the procedure detailed in the SSoW would be implemented and the rig and gas cylinders secured. The gas testing rig was used throughout the duration of this work with no failures.

A commercial NI DAQ unit was used to record the output response from the gas sensors. The unit provided 32 analogue inputs, allowing a range of sensors to be trialled simultaneously. The high quality ADC (16 bit) enabled accurate measurements to be taken and did not restrict the signal processing carried out post-logging. The VI

written to display and record the samples taken from the DAQ unit was designed to allow for up to 9 sensors (differential measurements) to be recorded together. Additionally, commercial sensors could also be connected and recorded, with the data aligned to a user selectable sampling frequency.

A LabVIEW VI was also used to connect to the breath analyser developed during this project. A Teensy microcontroller was used to acquire the data from the sensors, where the affordable device was of suitable size for a portable application (17 × 36 mm base dimensions). The microcontroller was selected for its digital and analogue inputs (16 bit possible) and the ready integration with a smartphone via USB or Bluetooth. The VI software allowed a laptop computer to communicate with a breath analyser device (wireless or wired). Data logging was performed at 200 Hz, offering consistent reliable performance, by either method.

Two Android applications were developed, where connection to a breath analyser unit was possible via Bluetooth or USB. The applications were at the proof-of-concept stage, where the user interface did not meet the goal of a pleasant experience, although functionality was demonstrated. The smartphone data logger was successfully used to record breath samples to a memory card in CSV format. The concept application offered a portable solution to breath analysis, where in previous generations a laptop computer was generally required.

6.6 References

- [1] National Instruments, NI 6343 Specifications, NI Manuals. (2015) 2. <http://www.ni.com/pdf/manuals/374567d.pdf> (accessed August 26, 2016).
- [2] National Instruments, The NI TDMS File Format, NI White Pap. (2015). <http://www.ni.com/white-paper/3727/en/> (accessed August 26, 2016).
- [3] Bosch, BME280 Datasheet, Bosch Sensortec. (2015) 1–54. https://ae-bst.resource.bosch.com/media/_tech/media/datasheets/BST-BME280_DS001-11.pdf (accessed August 26, 2016).
- [4] Memmert, UNB/UFB Operating Instructions, Univers. Ovens. (2009) 5. doi:10.1007/BF00980884.
- [5] PJRC, Teensy USB Development Board, Teensy. (2016) 2. <https://www.pjrc.com/store/teensy31.html> (accessed August 26, 2016).
- [6] Arduino, Arduino Uno, Arduino Genuin. Uno. 328 (2016) 2. <http://medcontent.metapress.com/index/A65RM03P4874243N.pdf> (accessed August 26, 2016).
- [7] Arduino, Arduino Pro Mini, Arduino Prod. (2016) 2. <https://www.arduino.cc/en/Main/ArduinoBoardProMini> (accessed August 26, 2016).
- [8] Atmel, ATtiny85, Microcontrollers AVR. (2015) 2. <http://www.atmel.com/devices/attiny85.aspx?tab=parameters> (accessed August 26, 2016).
- [9] NXP, FRDM-KL25Z, Free. Free. Boards. (2016). <http://www.nxp.com/products/software-and-tools/hardware-development-tools/freedom-development-boards/freedom-development-platform-for-kinetis-kl14-kl15-kl24-kl25-mcus:FRDM-KL25Z> (accessed August 26, 2016).
- [10] J. Pawley, Handbook of Biological Confocal Microscopy, Springer US, Boston, U.S., 2012.
- [11] B.K. Shepard, Refining Sound: A Practical Guide to Synthesis and Synthesizers, OUP USA, New York, U.S., 2013.
- [12] R. Kuc, Electrical Engineering in Context: Smart Devices, Robots & Communications, Cengage Learning, Boston, U.S., 2014.
- [13] E. Ogren, USB On-The-Go presents benefits, challenges to power designers, EE Times. (2003). http://www.eetimes.com/document.asp?doc_id=1226476 (accessed August 26, 2016).
- [14] Hobbytronics, HT Bluetooth Module V2, Wirel. Modul. (2012). <http://www.hobbytronics.co.uk/wireless/bluetooth/bluetooth-module-v2> (accessed August 26, 2016).

CHAPTER VII

Side-Stream Breath Analyser

Preface

The mainstream analyser presented in chapter IV was used to characterise gas sensors for their response time and sensitivity. In this chapter a side-stream sampling system has been designed, specifically for the measurement of human EE in real-time via breath analysis, which was not possible with the mainstream system. The chamber was designed to accommodate affordable and miniature gas sensors, and optimise their performance (e.g. constant flow rate, less variable levels of temperature and humidity). The housing was constructed from polyoxymethylene, a robust but easy to machine material. In part, various sub-assemblies were rapid-prototyped to create structures that would be impractical to machine using traditional methods. The gas sensors developed in this work were installed inside the housing and tested with gas concentrations similar to those found in an exhalation (16 % O₂ and 5 % CO₂). The response of the electrochemical O₂ sensor was analysed by comparing a 12 month old device to a new product. A time-delay model was constructed to explain the slow response of the cell. The calibration procedure for the side-stream system involves testing 4 concentrations of CO₂ (0 % to 5 %) and 3 concentrations of O₂ (21 % to 0 %). The performance of the prototype NDIR CO₂ sensor was found to be adequate for breath-by-breath sampling, although the O₂ sensor demonstrated a poor performance.

7 Side-Stream Sampling

There are two possible methods of measuring the gas contained in an exhalation in real-time; either main- or side-stream sampling. A breath analyser was developed utilising the main-stream sampling technique, detailed in chapter IV. However the fast flow rate of an exhalation, large dead volume of the main-stream chamber and large variance in temperature and humidity prevented an accurate measurement of gases contained in an exhalation. The volumetric flow rate in the mainstream can vary by up to ± 100 L/min typically [1]. The gas mixing time is increased with a large dead volume, which consequently can increase the time for the gas sensors to respond to a change in gas concentrations. Side-stream sampling offers a solution to many of these problems, whereby a sample is drawn off the main-stream flow. Thus the flow across the remote sensors, which can be located in a separate chamber, can be set at a constant rate (i.e. a pump can be used to continuously draw a sample).

The flow sensor (needed to calculate the volume of an exhalation) resides in the main-stream tubing (thus calculate the volume exhaled, not the volume through the side-stream). Assuming the gas exhaled is mixed, the sample taken through the side-stream will contain the same concentration of gases as the main-stream mixture.

The reduced flow rate given to the sensors allows a longer response time for a response to be produced. Also, if the flow rate is constant, there is reduced risk of turbulence (due to the lower Reynolds number), which would affect mixing time in the sensor chamber. It is common for gas sensors to present a level of flow dependence to their response (i.e. a baseline shift). High flow rates could damage the sensors (caution is advised in the gas sensor datasheets [2,3]), thus a low flow through the side-stream will benefit sensor lifetime. MOX and NDIR gas sensors have been reported to be sensitive to the flow rate across the devices [4,5]. The flow rate dependence of the electrochemical O₂ sensor is discussed in section 8.2. The level of humidity in the side-stream section can be reduced (i.e. by use of a filter). It is likely a decrease in temperature (from body to ambient) will cause the condensation to form in the main-stream tubing, but it will not affect the sensors located in the side-stream section. The temperature is likely to vary less in the side-stream, due to the gas having travelled sufficient distance to already have cooled from body temperature to ambient.

7.1 Side-Stream Chamber

The principal purpose of the side-stream chamber is to house the gas sensors for metabolic rate analysis. The housing must allow a sample of gas to be extracted from the main-stream exhalation. Secondly, the chamber must be lightweight (so the unit can be held in the hand) and robust (to withstand an environment outside of laboratory conditions). The main exhalation pathway must be low resistance, to reduce the chance of taking an EE measurement from affecting metabolic rate (i.e. if the subject has to breathe harder to exhale through the system then the consequence will be an increased metabolic rate).

7.1.1 Design of Sensor Housing

The chamber was designed in Dassault Systemes Solidworks 2015. The design layout is shown in Fig. 7.1. The housing was constructed from polyoxymethylene (POM, also known as polyacetal), which was selected for its excellent chemical resistance, low water absorption and light-weight properties [6]. The material is used in industry to machine precision parts, due to excellent dimensional stability. The side-stream section was extracted vertically from the main-stream, thus serving as a water drip-out area. Any water condensing in the initial section of side-stream tubing can exhaust from the device via the main-stream pathway. To provide a comfortable operating position, the mainstream flow was extracted horizontally. Significant angular change in flow direction can introduce turbulent flow, however it was important to avoid the main-stream flow rate and direction from influencing the flow volume through the side-stream section.

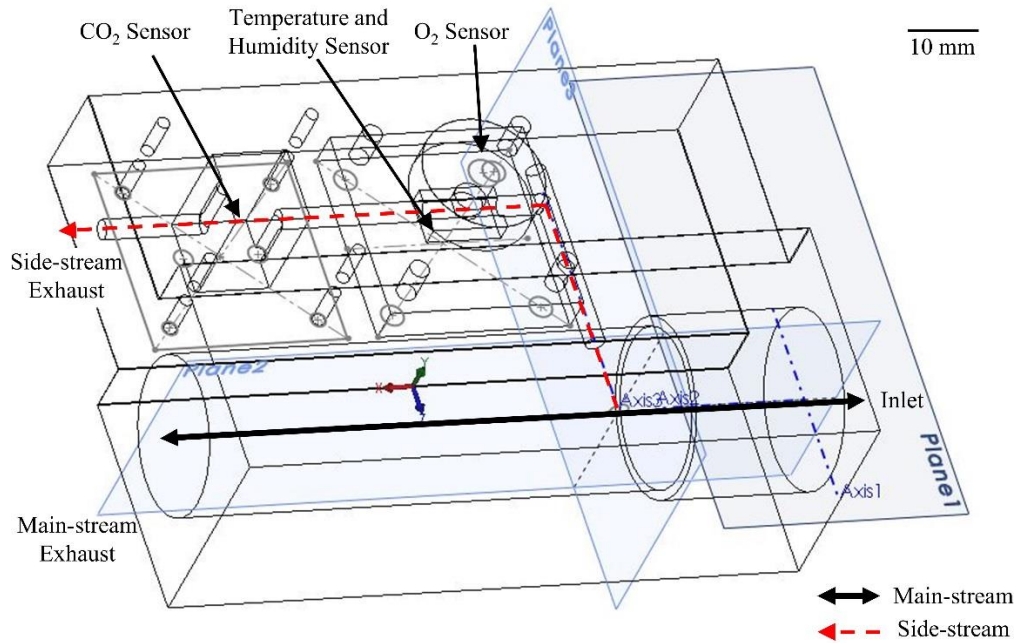


Fig. 7.1 – Diagram showing layout of side-stream chamber. Mainstream and side-stream flow paths identified for directions of inhalation and exhalation.

The diameter of the mainstream tubing was kept constant for both the masks and mouthpieces (20 mm). The enlarged diameter of the tubing shown on the right-hand side of Fig. 7.1 allowed the flow sensor (outer diameter 22 mm) to connect to the system. The width of the upper side-stream section was set to 12 mm, which allowed a path length of ~10 mm for the NDIR sensor (located at the left end of the diagram).

7.1.2 Flow Modelling

To ensure the flow through the device was not turbulent, the design was analysed in the Flow Simulation package within Solidworks. The input flow was entered as 30 L/min, the maximum flow rate of an exhalation (as shown in chapter III). The outlet through the side-stream was controlled by a pump (Micropumps D200) [7]. The pump was set to have a flow rate of 150 ml/min as a compromise between flow speed across the sensors and time for the sensors to respond. A range of 100-200 ml/min is recommended by Hummingbird for the commercial Pm1111E oxygen transducer [2] for similar applications. The flow velocity through the device is shown in Fig. 7.2 for an exhalation considering atmospheric pressure at the exhaust of the main-stream tubing.

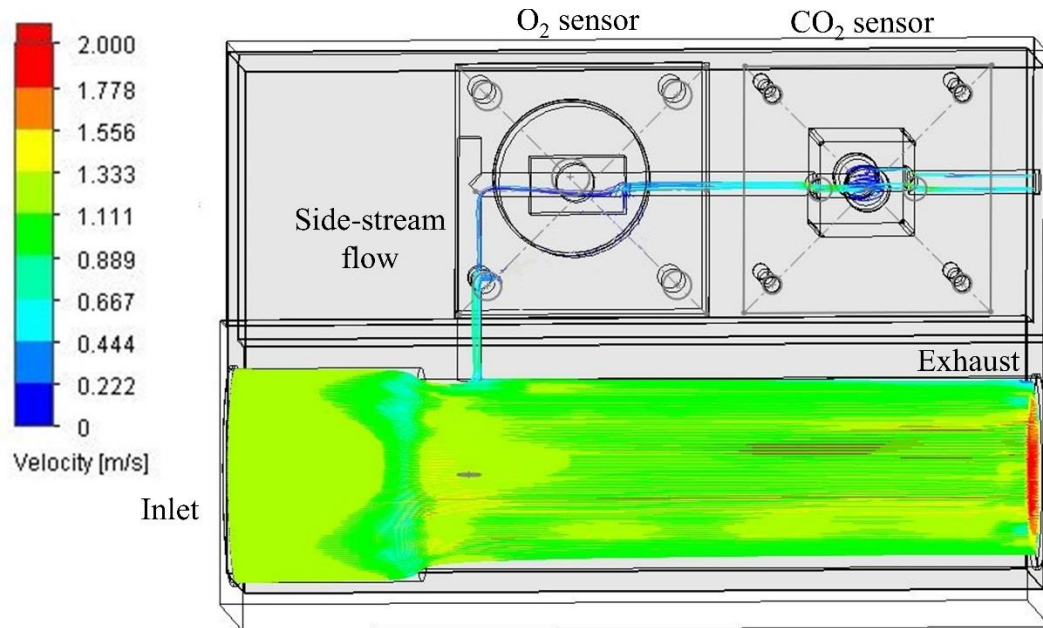


Fig. 7.2 – Flow simulated through the chamber for the peak flow rate of a resting exhalation.

The simulation demonstrates the need for some length of side-stream tubing prior to the sensors (~2 cm) from the main-stream and similarly after a sharp corner (i.e. 90 °) in the tubing. Initially, the sensors were placed 1 cm from the corner, but turbulent flow was found. Sufficient space was left in the side-stream tubing to reduce the risk of turbulent flow.

The high velocity (reaching 2 m/s in the centre of the main-stream tubing) demonstrates the advantage of a side-stream sampling system, where the constant flow rate is better suited for the current research generation of gas sensors. The side-stream tube is approximately 75 mm long (from join with mainstream tubing to exhaust). The diameter of the tube is 2.5 mm, giving a volume of 0.37 ml. At a flow rate of 150 ml/min, and assuming ideal flow, the volume of the cylinder is drawn through the system within 0.15 s (i.e. time delay before the sensors are exposed to the gas from the mainstream section).

The side-stream flow section was designed to house the sensors with a low dead-volume. The flow simulation shows there is minimal wasted volume between sampling from the main-stream and exposing the sensors to the gas. An alternative design would be to have a tube connecting a mouthpiece to a sensor chamber. This design would further increase the delay in sampling the exhaled gas. Furthermore, for a portable system, a fully integrated solution (without modular units) was essential.

The NDIR sensor was positioned further away from the turbulent section of the side-stream flow, as this sensor was noted as being flow sensitive.

7.1.3 Construction of Chamber

The finished chamber, constructed in the School of Engineering Workshops at the University of Warwick, is shown in Fig. 7.3. In total four chambers were manufactured, of which 3 were fully assembled to make the breath analysers.

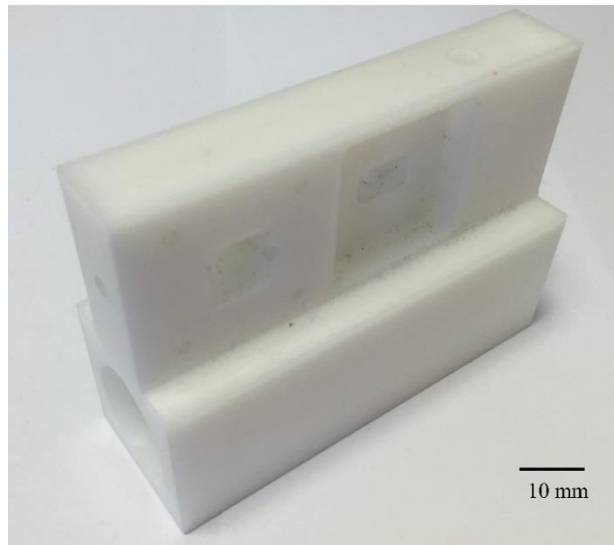


Fig. 7.3 – Manufactured chamber for the hand-held analyser, constructed from POM.

The side-stream tubing diameter was 2.5 mm, to prevent the tubing becoming blocked by small particles, but would not significantly increase the dead volume of the tubing (the section has a volume of ~ 0.4 ml). Particles in exhaled breath associated with a healthy human can be in the range of 0.3 to 10 μm [8]. For use in a free-living environment, the device has to be resilient against other particles found in an exhalation, such as food matter, discussed chapter III, or potentially medication (e.g. asthma medicines). Aerosol treatments have been noted to exhibit particle sizes up to 10 μm [9]. Particles of this dimension are unlikely to obstruct the side-stream path. Larger particles from foreign sources may be of similar size to the tubing diameter, although it is unlikely that they would be drawn into the side-stream section.

The NDIR sensor section of the unit was not constructed from the material used for the outer chamber. The sensor is designed with a direct path between the thermopile detector and IR emitter, through which the flow of the sample gas mixture (i.e. breath or air) must travel. A 3D printed module was designed to house the aluminium tubing for the sensor, while directing the side-stream flow from the POM chamber through

the tube and back into the POM chamber. A sketch of the module is shown in Fig. 7.4 a) and a photograph of the 3D printed part in b). The add-on part was inserted into the square section in the POM housing and sealed.

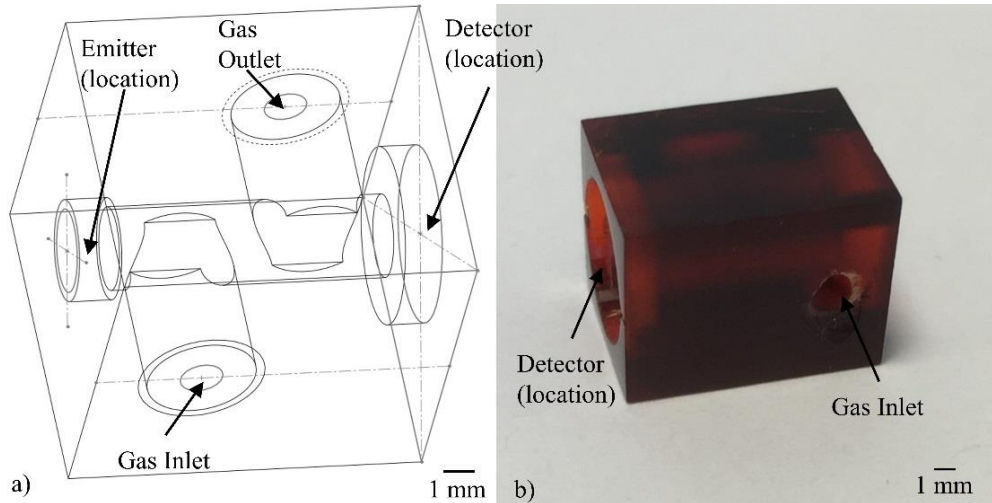


Fig. 7.4 – NDIR holder to fit inside POM chamber, a) Sketch in Solidworks; b) Photograph of 3D printed part.

7.1.4 VOC Sensor Holder

The chamber was designed to house the sensors for EE analysis. A sensor for VOC analysis was included as an add-on module. A sketch of the part in Solidworks is shown in Fig. 7.5 a) and a photograph of the 3D printed part in b).

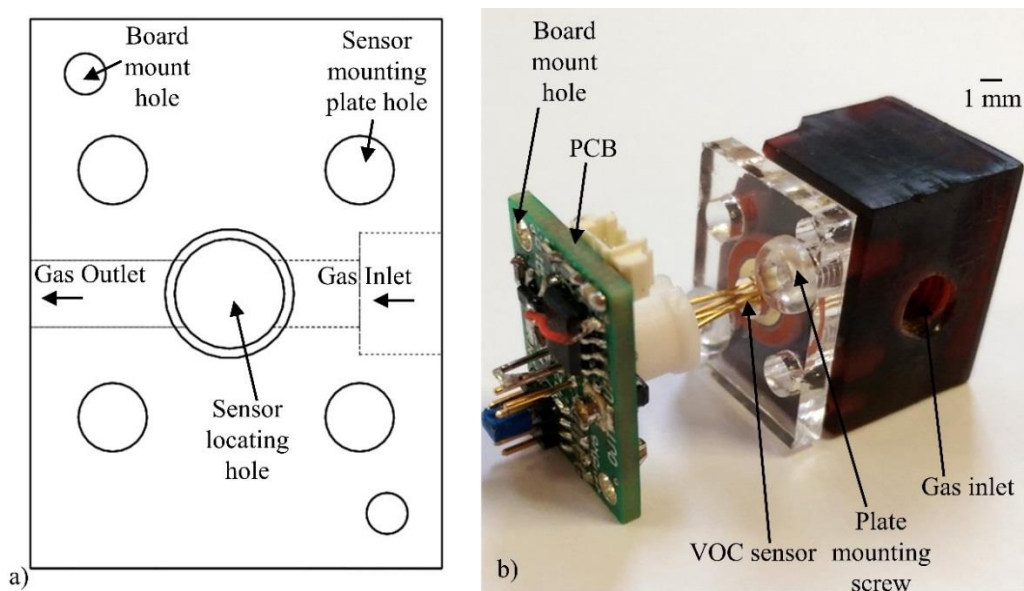


Fig. 7.5 – VOC sensor holder add-on module to the chamber, a) Sketch in Solidworks; b) 3D printed part with the VOC sensor on TO46 header inserted. Interface circuit board attached.

A 3D printer part was also designed to house the VOC sensor. To ensure a compact design, the add-on part was attached to the end of the POM chamber and directed the flow across a MOX sensor and then to the pump, via a 3 mm push fit connector. The interface board is shown with the VOC sensor in Fig. 7.5 b). The add-on module allowed different VOC sensors to be substituted, as necessary, for different thick film coatings. The interface board was designed to be compatible with a range of VOC sensors, with adjustable resistance via jumper selection (1 k Ω to 1 M Ω).

7.1.5 Main-stream and Side-stream Sensor Systems

The initial technical specification preferred a mainstream unit, which did not require the complexity of a side-stream system. The sensors available for the project, which remain affordable but accurate, prevent a main-stream system being a feasible breath analyser. The pump in particular is an undesirable component for a portable analyser. A 5 V pump can consume up to 0.48 W and adds audible noise to the sensor system (15 dba noise level) [7]. The pump can increase in temperature during a long period of operation, which can affect the sensor performance. The response time of the system is limited by the side-stream system, with a delay of up to 1 s is possible, from the flow requiring time to be extracted through the side-stream tubing.

In terms of sensor performance, the primary benefit of a side-stream system is the reduction in dead volume inside the chamber (in the case of the systems designed in this project, a factor of 10 lower). The smaller volume decreases mixing (and thus benefits sensor response times) and the size of the overall instrument. The conditions in the side-stream, i.e. temperature, flow rate, humidity and contaminants (dust/dirt), are stable compared to the variability in the main-stream section. The sensitivity of the sensors to abrupt changes in flow rate means their ability to detect changes in gas concentration would be compromised. The ideal sensor output would respond only to a change in the concentration of a specific gas, whereas a level of cross sensitivity to high variances in flow rate, temperature or humidity is expected.

7.2 Oxygen Sensor Response

The Alphasense O₂ (O2G2) sensor response was tested in the design of the main-stream chamber. The sensor was found to exhibit a slow response time (t_{90} of 9.5 s), the sensor output was sensitive to flow rate and the sensor was not stable (did not return to baseline) for the duration of a 70 minute experiment. For the side-stream

sensor unit a replacement O₂ sensor (City Technology MOX-20) was used. The manufacturer's specification for the device indicated a much faster t_{90} response time of 0.75 s and a stable lifetime of over 12 months [10]. To verify these claims the sensor was tested in the laboratory for its ability to withstand changes in temperature, humidity and flow rate.

To compare the 'aging' of the sensor (i.e. changes in response characteristics over the lifetime of the device), one sensor was purchased at the start of the side-stream development (utilised on the gas bench rig) and a second sensor was purchased 12 months later. A comparison was performed against the two units on the gas bench rig (the new sensor was not used prior to the measurements, whereas the older sensor had been used weekly over a 12 month period). The sensors were tested by a repeated step in O₂ concentration from synthetic air (20.9 %) to a 50:50 mixture with N₂ (10.45 % O₂). The list of experiments and the conditions varied are shown in Table 7.1, where each step had a duration of 2 minutes.

Table 7.1 – Experimental parameters for comparison of O₂ sensors.

Adjusted Parameter	Constant Conditions
Temperature [°C]: 25, 27, 29, 31, 33, 35	0.5 SLPM Flow, 0 % RH.
RH [%] 0, 10, 20, 30, 40, 50, 60, 70	Elevated 35 °C temperature, 0.5 SLPM flow.
Flow [SLPM]: 0.25, 0.5, 1, 2	Room Temperature (24 °C), 0 % RH.

A chamber was constructed for the testing of the gas sensors subject to varying environmental conditions. The aluminium chamber was designed to sit inside a dri-block® heater (Fig. 7.6). The gas tube inside the chamber spanned the length of the chamber twice, to expose the gas to the temperature of the chamber (total length 62.5 cm). The construction drawing is shown in Fig. 7.7, where the gas piping can be viewed. It was assumed that the gas would reach the temperature of the chamber after it had passed through the length of piping (a combined temperature and humidity sensor was installed in the chamber in close-proximity to the gas sensors to measure the properties of the gas received by the sensors).



Fig. 7.6 – Photograph of the aluminium chamber to house O_2 sensors for the experiments, with a temperature and humidity sensor fitted to measure environmental conditions.

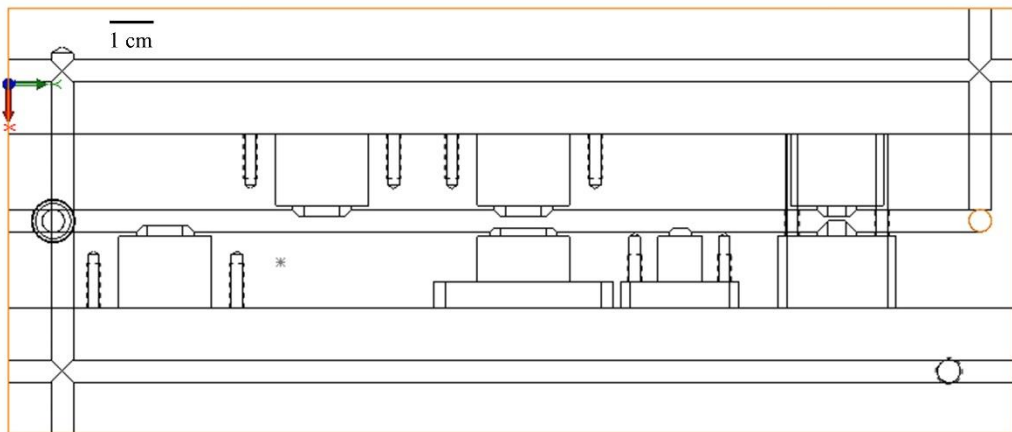


Fig. 7.7 – Drawing of the aluminium chamber in Solidworks, showing construction of the gas tubing and the location of the sensor mounting.

The total dead volume of the chamber (to the location of the O_2 sensors) was calculated as 12.3 ml. Assuming ideal plug flow, the gas flow supplied to the O_2 sensors would be varied as follows (time taken to fill chamber dead volume and reach sensors): 0.25 SLPM (2.9 s); 0.50 SLPM (1.5 s); 1.00 SLPM (0.7 s) and 2.00 SLPM (0.4 s).

7.2.1 Flow Dependence

The flow was varied according to the procedure in Table 7.1, over a range of flow rates from 0.25 to 2 SLPM. The un-used sensor is referred to as ‘new’ and the device purchased 12 months previously is called the ‘old’ sensor. The experiment was repeated for five repetitions (plots in Figs. 7.9 to 7.11 show mean output and standard deviation from these repetitions). The average output for both sensors at each flow rate is shown in Fig. 7.8.

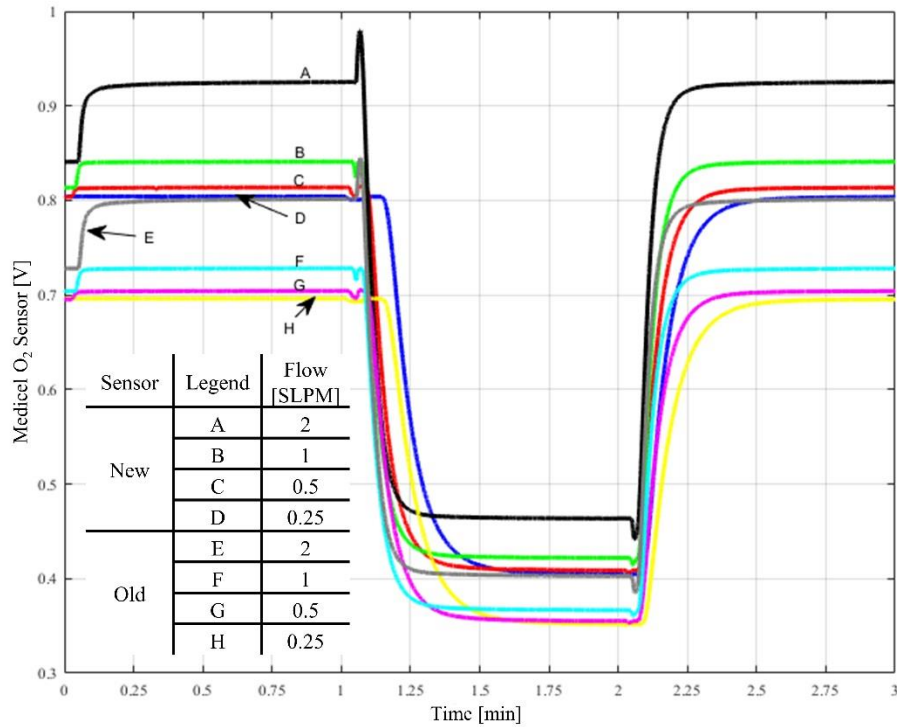


Fig. 7.8 – Response of new and old O_2 sensors to step a change in O_2 concentration at flow rates of 2, 1, 0.5 and 0.25 SLPM.

The output of the older sensor is visibly lower (i.e. the sensor was less sensitive) than the newer device, however the performance of the devices is otherwise qualitatively similar. Both devices exhibit a similar voltage decrease to the step decrease in O_2 concentration (~ 0.4 V).

The average responses are compared in Fig. 7.9, with error bars indicating the variance across the five repetitions. When the sensor is operated with a flow rate across the sensing area of 2 SLPM a significantly higher output voltage is found, shown in Fig. 7.9 a). The magnitude of the voltage increase is ~ 0.12 V for the older sensor and 0.15 V for the newer device, compared to the output voltages in 20.9 % O_2 at lower flow rates.

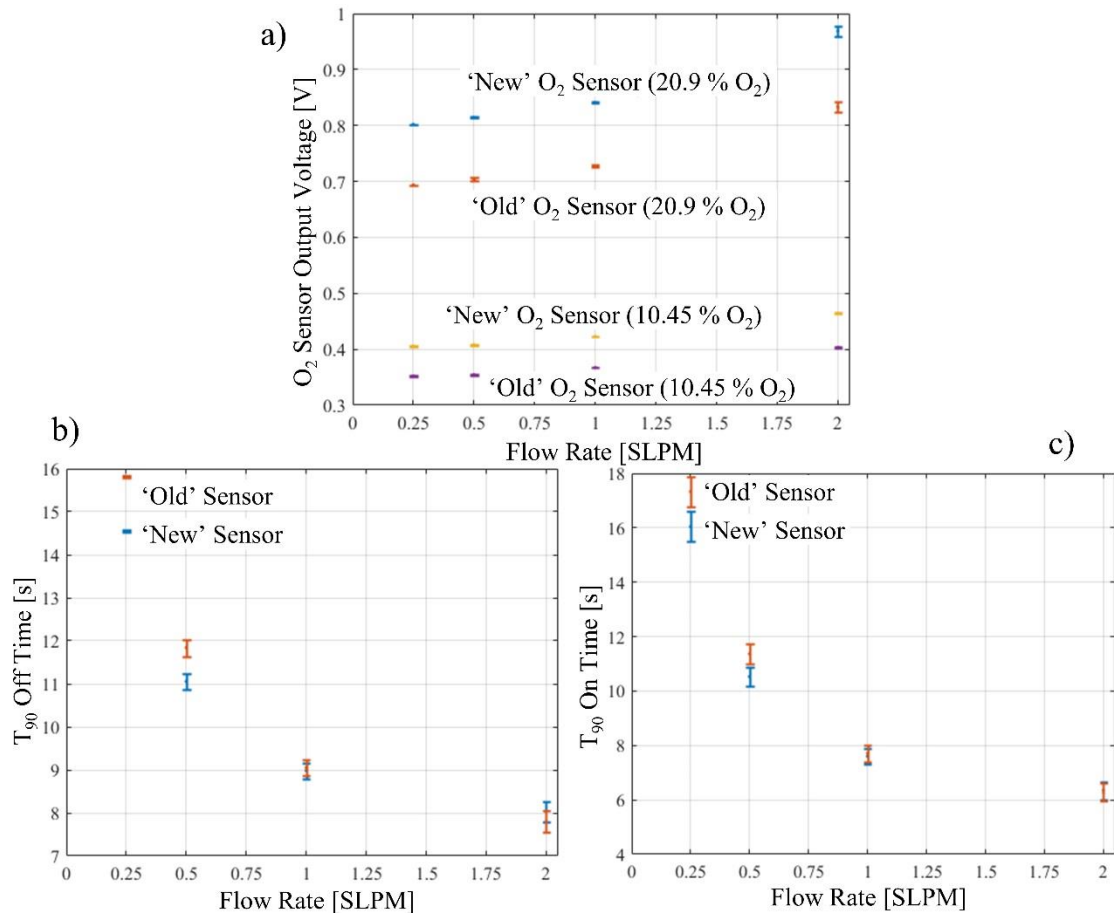


Fig. 7.9 – Comparison of old and new MOX-20 O₂ sensors, a) Voltage output at varying flow rates (O₂ concentration as specified); b) t_{90} response time for the sensor to recover to baseline from 10.45 % O₂; c) t_{90} response time for the sensor to reach final value for 10.45 % O₂ from a baseline of 20.9 % O₂.

The time response for the O₂ sensors is improved at higher flow rates, on average for the new device 6.2 s to reach 90 % final output voltage for a 50 % decrease in O₂ (at 2 SLPM), shown in Fig. 7.9 c). At 0.25 SLPM the response time is almost a factor of three longer (16.1 s); the time the mixture requires to reach the sensor is longer (considering the tube length, ideally 0.4 s for the higher flow rate and 2.9 s for the lower). When the sensor is used with a high flow rate the permeable membrane could become damaged. The quicker response times demonstrate the chemical reaction inside the sensors is also affected. The quicker reaction speed could indicate higher consumption of the electrolyte, which would increase the rate of aging of the sensor. Furthermore, the delicate internal structures of the sensor could become damaged with the high pressure experienced at higher flow rates.

The recovery time of the sensor when the concentration of O₂ concentration is increased is slower than the comparative response time for a decrease in O₂. This phenomenon is visible independent of flow rate. Fig. 7.9 b) shows that the response time for an increase in O₂ concentration is affected by flow rate in the same manner as the ‘turn on’ time. The 1 SLPM flow rate lowers the response time to ~ 9 s, in this case both sensors respond in the same time period, whereas a low flow rate (0.25 SLPM) decreases the response time to ~ 14.6 s for the new device and 15.9 s for the older sensor.

In the case of the side-stream chamber pump extraction system, a lower flow rate (0.15 SLPM) was selected. The tubing inside the hand-held chamber is smaller than the test chamber as demonstrated in Figs. 7.8 and 7.9. The mixing time for the side-stream chamber is less likely to have an impact on sensor response time, the reduced flow rate will prevent damage to the sensor membrane or the internal electrolyte barrier inside the cell.

Furthermore, if a pump were to draw a flow of, for example, 2 SLPM through the system, the rate of extraction could be similar to the rate of exhalation flow (towards the end of an expiration). The end-expiration gas, in pure form, is perhaps the main gas of interest for breath analysis, as discussed in section 2.4. In this scenario, the pump could force ambient air into the system (through the exhaust of the main-stream tubing), which would therefore cause an undesired mixture of end-of-expiration gases and ambient air to be created. Thus a low flow rate (0.15 SLPM) was selected, although a fast response time is advantageous, the sampling of solely end-expired gas is of higher importance. The increase in response time due to the flow rate is somewhat exaggerated in Fig. 7.9, considering the time necessary for the gas mixture to reach the O₂ sensor through the tubing in the chamber (range from 2.9 s to 0.4 s).

7.2.2 Temperature Dependence

Environmental (and sample gas) temperature variance produced less variance on the output signal from the O₂ sensors compared to flow rate. The devices were tested in a dri-block® heater, with temperature stepped from 25 °C to 35 °C in 2 °C steps. The experiment was repeated with three repetitions for each temperature. Fig. 7.10 a) shows the output voltage of the O₂ sensors in relationship to temperature and b) shows the corresponding ‘turn on’ and ‘turn off’ response times for both devices.

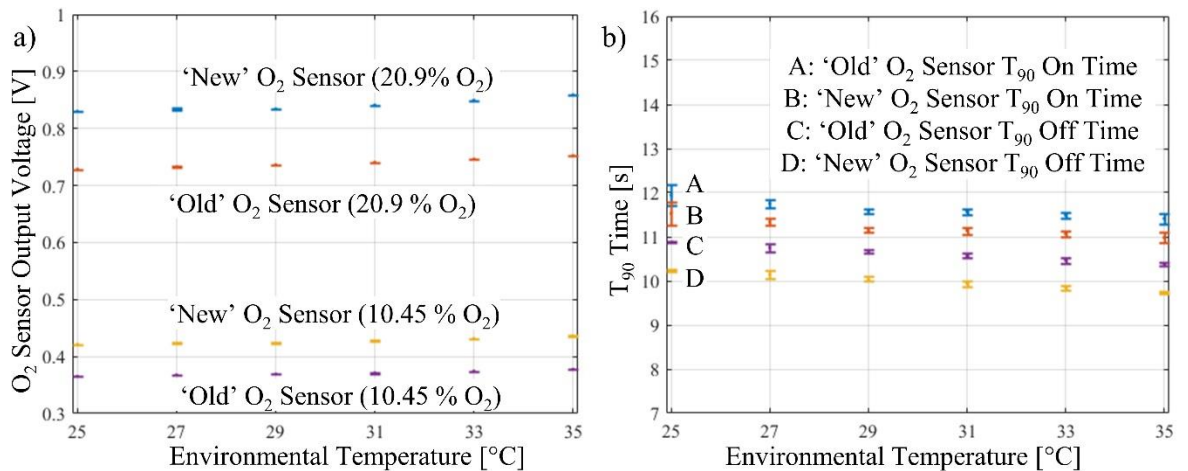


Fig. 7.10 – Response from two oxygen sensors for a change in environmental temperature, a) Voltage output from the devices; b) Response time for the devices to turn 'on' to a step concentration change from 20.9 % to 10.45 % O₂ and 'turn off' for the opposite increase in O₂ concentration.

The migration of the sensor output was minor for both the older and newer sensors, where the output for each device shifted ~ 0.02 V across the range of temperatures tested (independent of gas concentration). Exhaled breath temperature (body temperature, 36 °C) will cool to a temperature within the range tested once the sample of gas reaches the O₂ sensor. A temperature and humidity sensor is located immediately in front of the O₂ sensor to measure the conditions to which the sensors are exposed.

The response times for each sensor resembled the trend shown in Fig. 7.9. The new sensor is consistently faster (~ 0.6 s on average) to respond to a step decrease in O₂ concentration, and faster to recover to a baseline O₂ concentration (0.7 s). Fig 8.10 b) is plotted for comparison with Fig. 7.9 b) and c), and demonstrates that temperature does not affect response times. The temperature dependence of the O₂ sensor is somewhat limited by the design of the cell. Most O₂ commercial sensors have a capillary restrictor placed at the top of the cell (to which the membrane is attached). The capillary causes the temperature coefficient to be considerably reduced [11], as the physical gas phase diffusion results in a cell limiting current, where the output is related to the square root of the temperature [12].

7.2.3 Humidity Dependence

Humidity is known in MOX sensor development phase as producing a considerable effect for semiconductor sensors. Electrochemical sensors are usually more resilient

to humidity, where the membrane can act as a barrier to the water droplets. The sensor was tested over a humidity range of 0 % (dry) to 70 % RH in 10 % steps. The voltage output from each sensor is shown in Fig. 7.11 a) and the corresponding t_{90} response in Fig. 7.11 b).

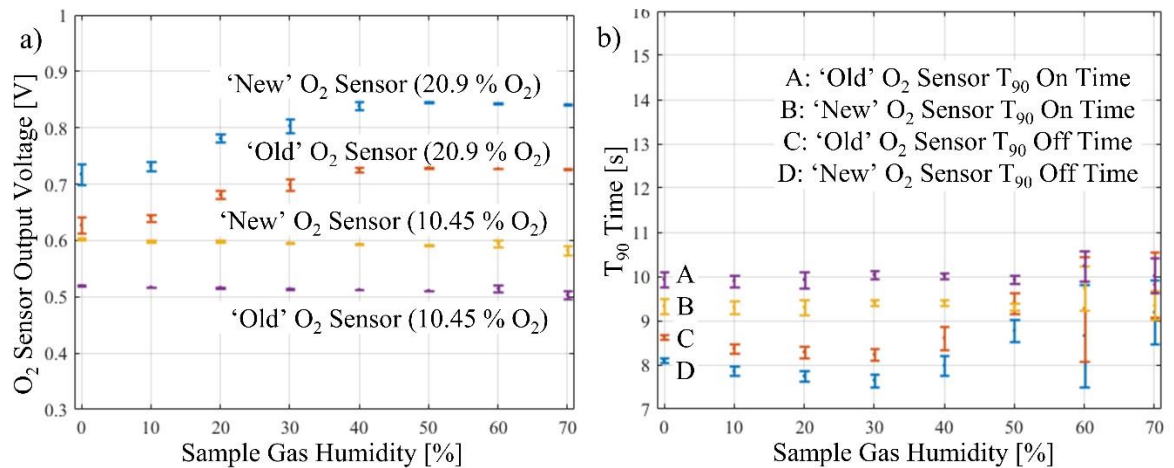


Fig. 7.11 – Response from the new and 12 month old O₂ sensors to a change in humidity condition, a) Voltage output from the sensors; b) Response time for the sensors to turn ‘on’ to a step decrease in O₂ concentration (20.9 % to 10.45 %) and to turn ‘off’ for a step in O₂ of opposite direction.

The voltage output from the gas sensors in a mixture of 10.45 % O₂ does not vary by a significant margin over the range of humidity from 0 % to 70 % RH. For both sensors an output change of ~ 0.03 V is observed. The output level in 20.9 % O₂ concentration is considerably higher when the level of RH exceeds ~ 40 % than the initial dry or 10 % RH condition. The new sensor outputs ~ 0.73 V in dry (~ 0.75 in 10 % RH) compared to an output of 0.86 V at 40 % RH. At 40 % and above RH (tested to a level of 70 % RH) the sensor output is stable.

The response and recovery times are less affected by the changes in humidity. The turn ‘on’ response times (to a decrease in O₂) vary only by ~ 5 % during the experiments. The turn ‘off’ recovery times vary by ~ 7 % below 40 % RH, but increase for both sensors by 50 and 70 % RH (> 10 % change). In general, the response times are stable, and the performance of the sensors is not adversely affected by the change in RH conditions.

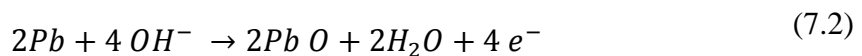
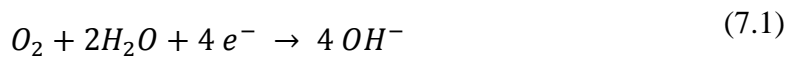
The variable conditions in RH are most prominent at low levels of RH (< 40 %). In the case of breath analysis, the sensors are likely to be operated in a normal room

environment (~ 40 or 50 % RH) and be exposed to breath (up to saturated, 100 % RH). The experiment in Fig. 7.11 a) demonstrates that the O₂ sensors are stable at high levels of humidity, and a decline in output occurs only in dry conditions.

7.2.4 Governing Equations of O₂ Sensor Reaction

A schematic of a low temperature electrochemical oxygen cell is given in a chapter III. To understand the delayed response of the O₂ sensors shown in the sections above, the chemical reaction equations governing the operation of the cell are investigated.

The reduction of oxygen occurs at the sensing electrode, equation (7.1), which is made of a material that complements this reaction (electrocatalysts) [12]. As a result of this reaction, electrons are released from the counter electrode, equation (7.2), which comprises an anode of readily corrodible metal (e.g. lead). The lead reacts with hydroxyl ions, which migrate from the cathode reaction through the electrolyte. The overall reaction occurring inside the cell is given by equation (7.3) [13].



The life-time of an electrochemical cell is limited by the mass of material in the anode electrode. For an O₂ sensor this can mean the life-time of the sensor is decreasing when the sensor is left in room conditions (with 20.9 % O₂), even if the sensor is not under test. Once all the material is consumed the sensor will no longer respond to a gas concentration change. The failure can occur rapidly, however the expected life-time of commercial sensors is usually 12 to 24 months [14]. The Cottrell equation (7.4) is used to describe the reduction of the electroactive species [15]. The equation relates the Faraday (charge on 1 mol of electrons in coulombs) F , the electrode area A_e (in m²), the diffusion coefficient D (in m²s⁻¹), the concentration of electroactive species C_∞ (in mol m⁻³) and the current time t (in s).

$$i_F(t) = nFA_eC_\infty \left(\frac{D}{\pi t}\right)^{1/2} \quad (7.4)$$

The response time of the oxygen sensor was found to be a limiting factor for breath-by-breath analysis. As demonstrated in the section 3.2.1 above, part of the delay is due to the time taken for the gas sample to reach the sensor, and penetrate through the sensor membrane. A flow diagram to demonstrate the functionality of the side-stream system is shown in Fig. 7.12. The delay in response was attributed to 3 factors: The time to fill the main-stream chamber ('tank'); the time to fill the side-stream chamber ('SensCham') and the time for the sensor to respond ('SensDev'). The delay mechanism can be represented as a resistor capacitor (RC) circuit, where three delay phases correspond to the above factors. The diagram for the equivalent is shown in Fig. 7.13, where the load at the end of the circuit represents the pump located at the end of the side-stream.

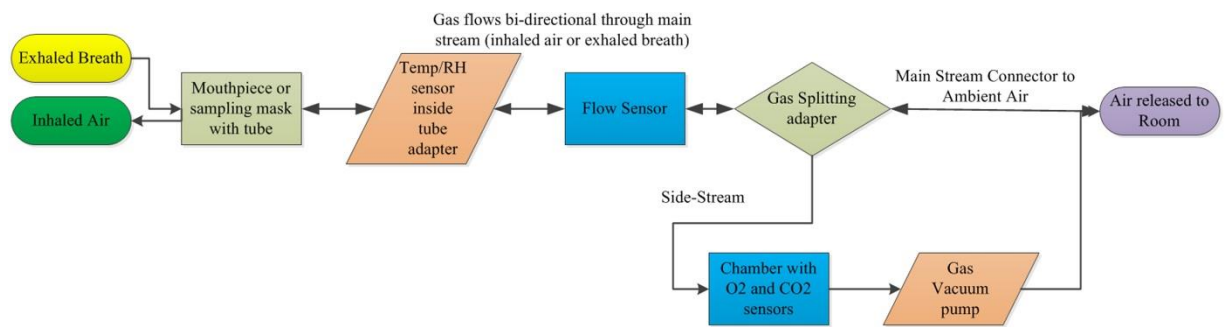


Fig. 7.12 – Flow diagram to show the side-stream system to be modelled.

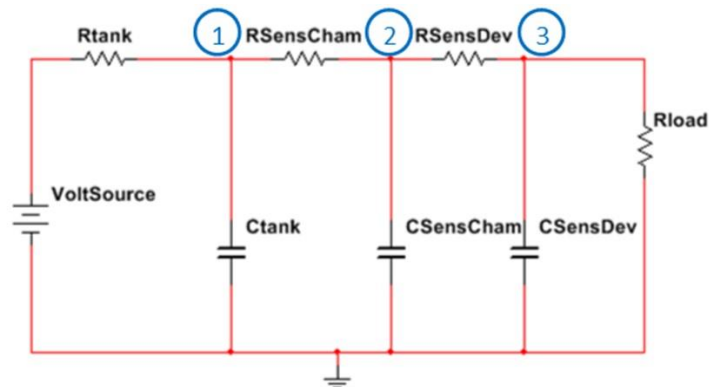


Fig. 7.13 – RC equivalent circuit diagram for the side-stream system.

Kirchoff's current law was applied to the three nodes of the circuit, as labelled in the circuit shown in Fig. 7.13. The resulting equations are shown in (7.5), (7.6) and (7.7), respectively.

$$C_1 \frac{dV_1}{dt} = \frac{V_{in} - V_1}{R_1} + \frac{V_1 - V_2}{R_2} \quad (7.5)$$

$$C_2 \frac{dV_2}{dt} = \frac{V_1 - V_2}{R_2} + \frac{V_2 - V_3}{R_3} \quad (7.6)$$

$$C_3 \frac{dV_3}{dt} = \frac{V_2 - V_3}{R_3} + \frac{V_3}{R_4} \quad (7.7)$$

The equations were solved numerically in the software package Berkeley Madonna 8.3.18. The equations were solved over a 6 second period. The circuit allows modelling of the first order lag to reflect the diffusion (Fick's Law) of the gas through the sensor membrane and gel electrolyte. The component values for the O₂ sensor curve shown in Fig. 7.14 are shown in Table 7.2. The output from the O₂ sensor was normalised to a 0 to 1 scale, to enable the modelling process. Simply, the data were scaled by subtracting the minimum sensor output from each output voltage, then dividing by the maximum sensor output value. Breath data was used to solve the equations, to represent a realistic scenario. The gas rig was unable to simulate a change in direction of flow nor a gradual change in gas concentration (only step changes were possible).

The exhalation data were provided by a subject who was requested to breathe at a fixed rate of 5 s exhale and 5 s inhale (shown in Figs. 7.14 and 7.15). The subject was allowed 1 minute of breathing in this manner to become familiar with the apparatus (a second minute was permitted in some cases to ensure the subject was comfortable). The data was recorded for a 1 minute period once the subject was accustomed to breathing for a cycle length of 10 s (this will be referred to as breathing at a 'fixed rate').

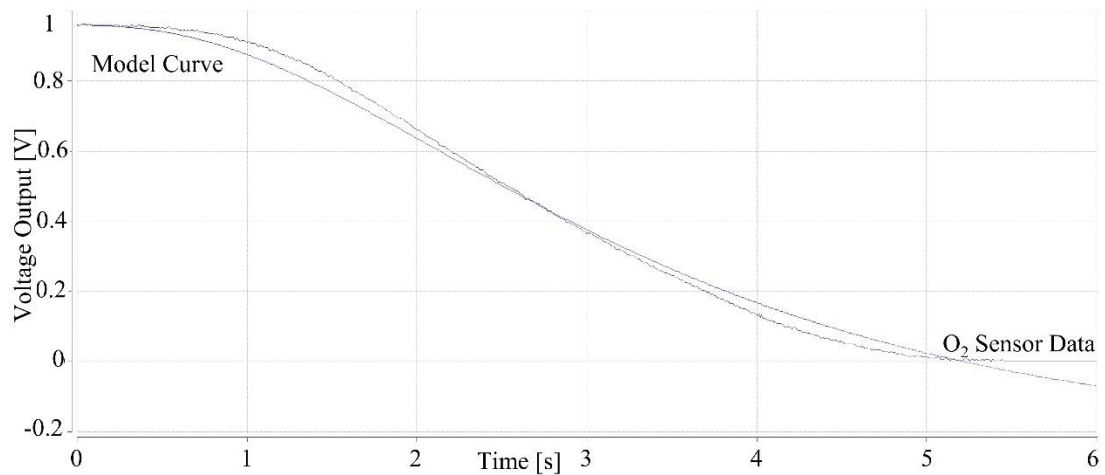


Fig. 7.14 – Model fit created within Berkeley Madonna compared against O₂ sensor data for an exhalation.

Table 7.2 – Component values estimated using Berkeley Madonna.

Component	Value	Time
		Constant [s]
R_{tank}	1.24 k Ω	1.06
C_{tank}	852 μ F	
$R_{SensCham}$	8.93 k Ω	1.14
$C_{SensCham}$	12.8 μ F	
$R_{SensDev}$	320 k Ω	1.01
$C_{SensDev}$	3.17 μ F	

The component values shown in Table 7.2 were calculated based on restrictions placed on the time constant values. The time to fill the mainstream chamber ('tank') was calculated based on a flow rate of 6.6 L/min and a volume of 96 ml (i.e. the time constant for R_{tank} and C_{tank} would be expected to be approximately 0.87 s). The time to fill the side-stream chamber ('sensCham') with a volume of 4 ml and flow 150 ml/min would be approximately 1.6 s. The model outputs suggest the mainstream chamber takes a longer time than expected to fill (1.06 s) and the side-stream chamber takes a shorter time (1.14 s). Based on these two time delay estimates, to fit the model to the sensor output response, the sensor would take 1.01 s to respond ('SensDev').

The exhalation data and modelled curve demonstrate a similar shape for the initial 5 s, although the final second is not represented accurately. The model data continues at

a steady gradient decrease, whereas the sensor output decays to a steady value. The modelling process was repeated, except without requesting the subject to breathe at a fixed rate (instead, breathing naturally, and calmly, with some time allowed for familiarisation). A commercial CO₂ sensor was included in the system (SprintIR) for comparison. The calibrated outputs from both the O₂ sensor (MOX-20) and the CO₂ sensor are shown in Fig. 7.15.

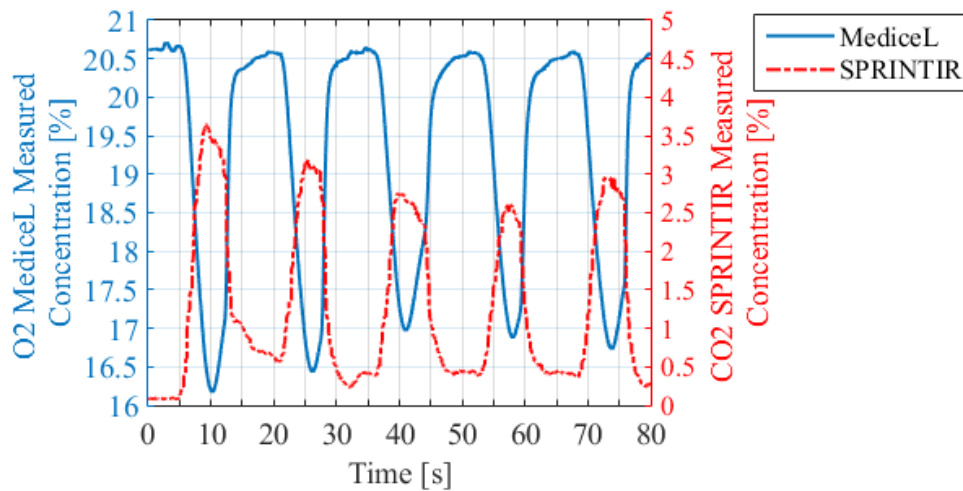


Fig. 7.15 – Subject breathing through the side-stream device, output from the O₂ and CO₂ sensors.

The sensors were found to respond to the breath cycles, with O₂ concentration varying from 20.6 % (ambient) to 16.63 %, and the CO₂ from 0 % (ambient) to 2.71 %. The measurements show considerable intra-subject variation, where concentrations in each breath differ. Using the RC model shown in Fig. 7.13, curves were fitted according to the response from each gas sensor. The fitted curves, Fig. 7.16, show reasonable approximations; regression coefficients R^2 of 0.990 and 0.991 with RMSEs (root mean square errors) of 0.029 and 0.032 for the O₂ and CO₂ sensors. The high R^2 values suggest a good model, but a poor fit to the shape of each response curve was noted. The final 0.5 s of the curve was poorly fitted, similar to the shape identified in Fig. 7.14.

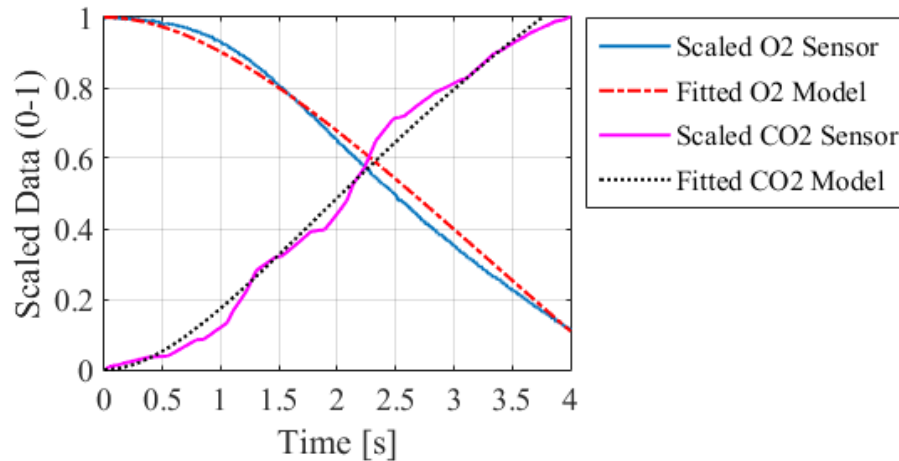


Fig. 7.16 – Scaled (0 to 1) responses from the O_2 and CO_2 sensors for an exhalation, with fitted delay model outputs.

A step-input was used to generate the exponential output from the model. It was noted that an input function better suited to the complex wave shape of exhaled gas flows would be more realistic. However, when the output from the flow sensor (which exhibited a fast response) was analysed the accuracy of the fits did not improve, but worsened considerably (RMSEs of 0.027 and 0.029 for the O_2 and CO_2 sensors, respectively). An example of the flow sensor output is shown in Fig. 2.7; an example of the normal flow cycle expected during breathing is shown in Fig. 2.10. A step input was used for the modelling process in general, as the additional noise associated with the flow sensor output was transferred to the model in cases of abnormal exhalation patterns.

7.2.5 Design Considerations

A slow response was found from both the MOX-20 O_2 sensors compared to the necessary fast response for breath-by-breath analysis. During the modelling phase of the project, a commercial rapid response medical O_2 sensor was not available for comparison. The models created from the RC circuit demonstrated that the sensor performance was largely due to a simple time delay, which occurred during the mixing of the gases in the sensing chamber and the transmission of the oxygen through the membrane on the sensor. The lowest time delay (Table 7.2) was noted to be from the O_2 sensor itself (1.01 s), compared to the time delay through the tubing (mainstream 1.06 s and side-stream 1.14 s). When a subject breathes through the device, the gas exhaled must propagate a considerable distance (perhaps 200 mm of tubing) to reach

the gas sensors. It is this delay which can be modelled as a simple time delay, where the exhaled gas is not presented to the sensors for perhaps 2.2 s.

The MOX-20 sensor was selected for further development in the hand-held breath analyser, for its considerable performance improvement over the Alphasense O2G2. The fundamental operation of electrochemical cells limits their application in fast-response equipment. The devices are widely available and affordable, which is not true of typical medical O₂ sensors, which operate on a paramagnetic basis [16].

The range of experiments performed with varying humidity, temperature and flow (Figs. 7.9, 7.10 and 7.11) demonstrate the electrochemical cells are flow dependent, but resilient to the temperature and humidity in a side-stream system. The constant flow rate, set by a pump, in a side-stream system combats the decline in performance, which would be exhibited in a main-stream system, with varying flow rates between an inhalation and an exhalation. The decrease in performance caused by the aging of the cell over a life-span of 12 months is not unexpected from the guidelines given by the manufacturer [10], where the cell typically drifts by < 10 % over a one-year period in ambient air. The experimental evidence comparing a sensor that has been used for 12 months and a new sensor are not dissimilar to the datasheet performance life-span.

The results from the experiments show that the oxygen sensor cannot be used in a breath analyser for longer than a 1 year period. The drift visible over a 12 month period highlights the need for a form of calibration to be undertaken, perhaps monthly (the linear drift visible in sensor performance indicates a calibration with room air could be sufficient to indicate the decrease in sensor performance). At the current stage of development, the performance of the oxygen sensor should be monitored, with the sensor calibrated regularly to analyse long-term usability. The membrane of the sensor could potentially become blocked over time (with matter from an exhalation) and should be monitored during the prototyping phase of the breath analyser.

The unit is easily powered from a single USB port, with a maximum current draw of 410 mA (average 370 mA). The pump contributes ~ 25 % of the total power consumption (100 mA). The Bluetooth wireless module was selected for miniature size and compatibility with the microcontroller, thus the power consumption was higher than devices compliant with the Bluetooth low energy standard. When the module is searching for a paired device current draw can peak at 50 mA.

7.3 Side-stream Gas Bench Rig Experiments

The POM chamber was tested against gas concentration mixtures of O₂ and CO₂ within the gas rig at the University of Warwick to assess the performance of the side-stream mechanism. Sensors for flow (Sensirion SFM3000), temperature and humidity (GE Chipcap 2), CO₂ (prototype NDIR device) and O₂ (City Technology MOX-20) were installed into the sensor chamber, shown in Fig. 7.17. The electronics and microcontroller used for data logging are not shown in the photograph. To test the chamber from a gas bench source (not a human breath) a cap was fitted onto the end of the flow sensor (to a Swagelok connector) and a push fit connector was connected to the end of the side-stream tube (pump removed).

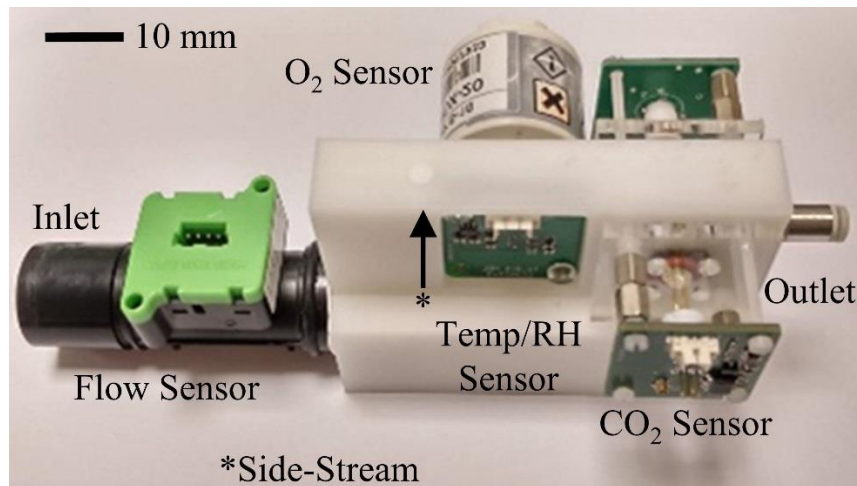


Fig. 7.17 - Photograph of the breath analyser with sensors for flow, temperature, humidity, CO₂ and O₂.

The exhaust from the main-stream was temporarily sealed, so the flow would only exhaust through the side-stream. A cap was fitted in the outlet of the mainstream section, thus the mixing in the tubing remained unchanged. To ensure that the gas from the rig did not vent into the laboratory, the exhaust from the side-stream section was connected to the MFM in the gas rig. The Teensy microcontroller was used to record the data, which was connected to a computer via a USB interface. The unit was powered solely from the USB connection.

The O₂ and CO₂ sensors were tested in the side-stream experiments as a calibration for breath measurements. The calibration procedure was repeated prior and post each breath experiment. The flow rate was set to 0.15 SLPM to equal the flow generated by

the pump. The O₂ sensor was calibrated to three concentrations (0 %, 16 %, and 21 %) for 5 min each. The CO₂ sensor was calibrated to four concentrations (0 %, 1 %, 2.5 % and 5 %) for 1 min each. A minimum of four points were necessary due to the exponential type calibration curve reducing in accuracy with a lower number of points (the curve is better defined). Fig. 7.18 shows one result for the O₂ sensor raw voltage output, from a 25 min calibration experiment. The result for one CO₂ calibration experiment is shown in Fig. 7.19. The amplitude of the sinusoidal (5 Hz) signal for the sensor has been extracted from the raw voltage output.

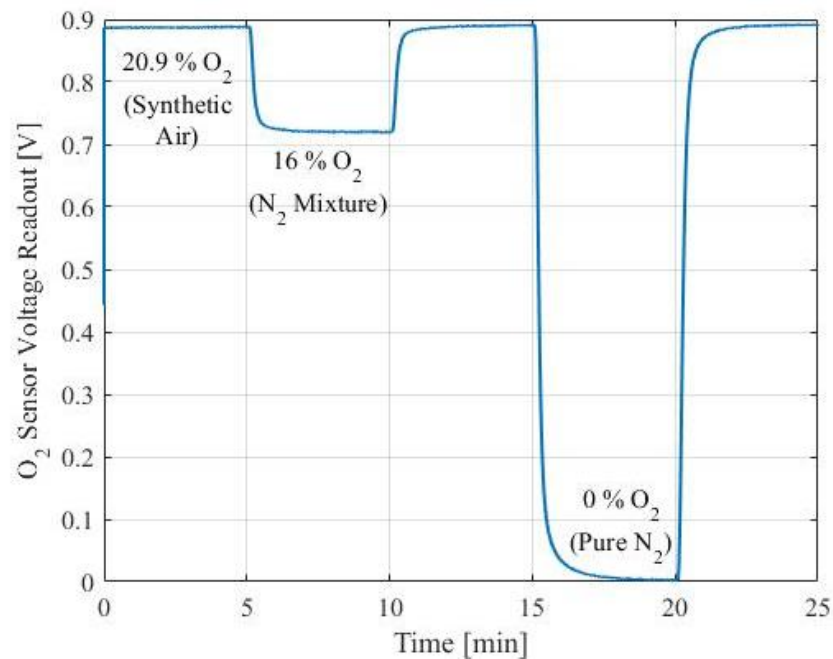


Fig. 7.18 – O₂ sensor calibrated with 3 gas concentrations.

The electrochemical O₂ sensor has been reported to drift over a period of months. The calibration experiment allows this drift to be compensated. The result shown in Fig. 7.18 (performed with a device 3 months old) demonstrates the sensor produces an output of 0.89 V in synthetic air and 0.002 V at 0 % N₂.

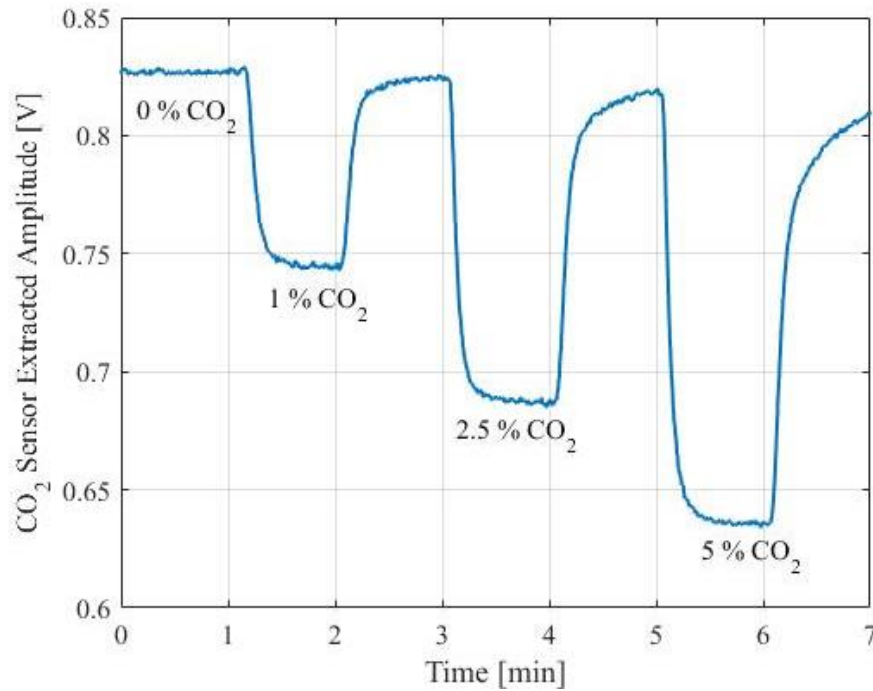


Fig. 7.19 – CO₂ sensor calibrated with 4 gas concentrations.

The sensor was left for a 5 min period to stabilise at each concentration. The t_{90} response time of the sensor was measured as 15.2 s for the step change input from 20.9 % to 0 % O₂. The average sensor voltage for the final 2 minutes of each concentration step was taken as a calibration reference. A linear fit was applied to the sensor output, as shown in Fig. 7.20 a). The raw sensor output shown in Fig. 7.18 was entered into the calibration equation to produce the output in terms of percentage O₂, as shown in Fig. 7.20 b). This procedure was repeated for each experiment and for each O₂ sensor.

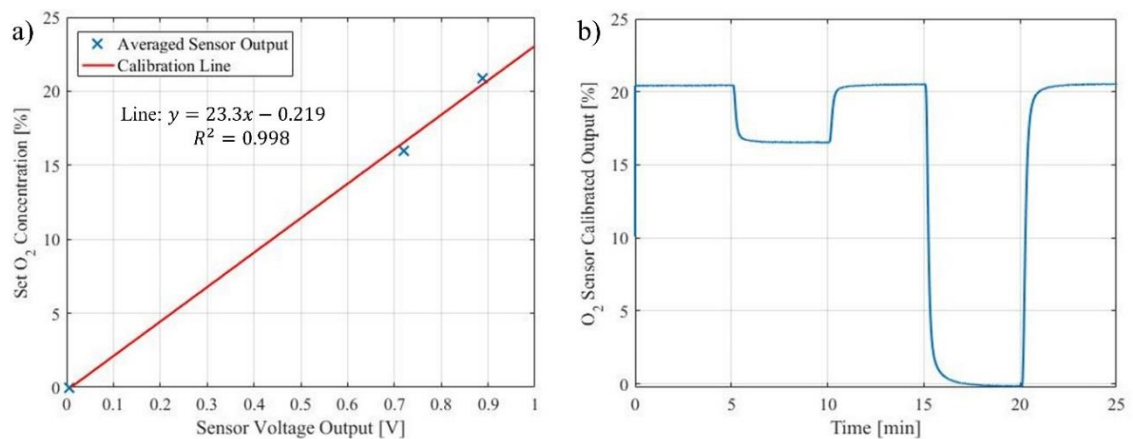


Fig. 7.20 – Oxygen sensor calibration procedure, a) Calibration line calculated for raw voltage data; b) Calibration equation applied to the raw sensor voltage output.

The CO₂ sensor was calibrated for the average output for the last 30 s of each concentration step. The prototype NDIR device had a t_{90} response time of 11.5 s for the 1 % step in CO₂ concentration. Both the O₂ and CO₂ sensors demonstrated longer response times (a significant increase of 5 s). The delay in the response time is in part due to the slow mixing that takes places in the tubing necessary to connect the hand-held unit to the gas testing rig MFCs (~20 cm length). The tube (1 mm inside diameter) was approximated to a pure time delay. An exponential calibration curve was calculated for the CO₂ raw voltage output, as shown in Fig. 7.21 a). The calibrated sensor output is shown in Fig. 7.21 b). The sensor demonstrates a reasonably noise-free output, although at the higher concentration steps (2.5 and 5 % CO₂) noise of magnitude 0.02 % is visible. The fluctuations are likely due to the measurement system rather than gas mixing, as they are particularly noticeably ~20 s after the start of each concentration step.

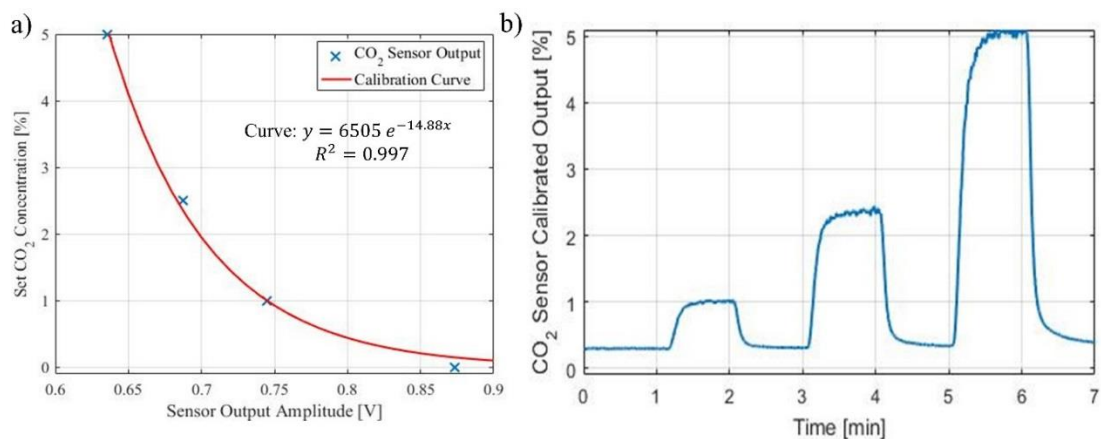


Fig. 7.21 – Carbon dioxide sensor calibration procedure, a) Calibration curve calculated for raw sensor voltage data; b) Calibration equation applied to raw sensor output.

7.4 Side-stream Laboratory Breath Tests

The necessary ethics approval for these breath tests was obtained prior to any experiments being performed. The submitted request forms and final letter granting permission for such experiments to be performed at the University of Warwick are shown in Appendix B.

The side-stream system was initially tested with a slower, fixed breathing rate; subjects were asked to breathe to a constant breathing pattern, with equal exhalation and inhalation time period. For the initial experiments, the data were recorded via a wired

connection to a computer. A smartphone connection was possible with a wired USB connection, shown in Fig. 7.22 a), or via wireless connection, Fig. 7.22 b). For short wireless measurements, total duration, under 30 minutes, the unit was powered with a small 500 mAh battery, which is visible on the right side of the photograph ($3.5 \times 3 \times 1$ cm). A larger battery (2800 mAh, $7.5 \times 2 \times 2$ cm) allowed for measurement durations up to 2.5 hours. The microcontroller was powered from the battery, which was used to power the sensors and pump. The 5 V output from the battery was passed through a 5 V regulator. The VOC sensor (in a 3D printed holder) is visible at the end of the side-stream section in Fig. 7.22 b).

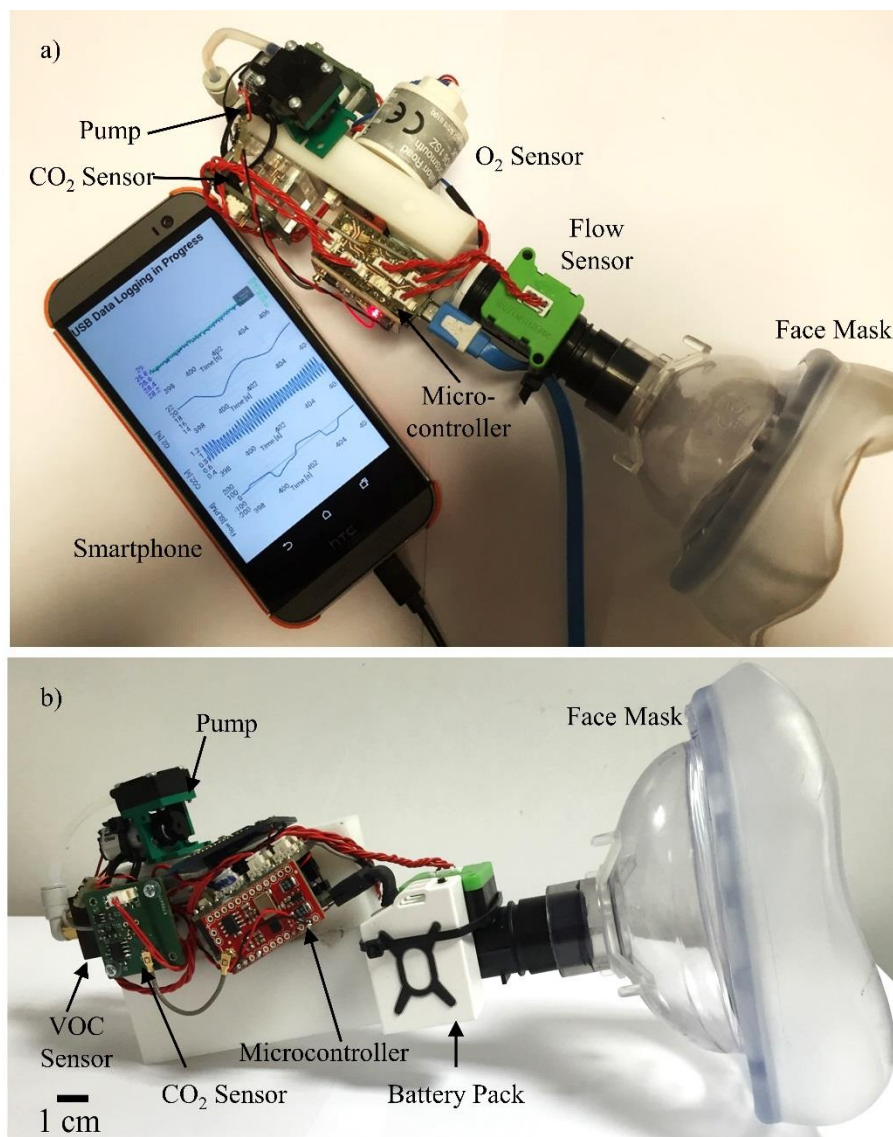


Fig. 7.22 – Photographs of the hand-held analyser when used, a) With wired connection to Smartphone; b) With wireless Bluetooth connection.

The subjects were not asked to perform any breath manoeuvres, only to maintain a 1:1 inhale:exhale ratio for a period of 1 minute. In the initial trials, subjects in the laboratory were asked to reduce their breathing ratio to 6 times per minute (i.e. 5 s exhale and 5 s inhale). After a one minute break, a second sample was taken at 10 breaths per minute (the value common for a normal adult per minute at rest), again with fixed cycle ratio. A mask, shown in the photographs above, was preferred to a mouthpiece/nose clip arrangement. The mouthpiece was found to encourage salivation, which increased the water content in the exhalation.

The masks were chosen as a comfortable means of breath sampling. The masks were sourced from SP Services Ltd. (Telford, U.K.) and two sizes, medium (RE/072) and large adult (RE/071), were offered to the subjects. The outlet from the mask was a 22 mm inner diameter tube, to which the flow meter was directly connected. The data were logged at 200 Hz for all of the sensors in the unit, as discussed in the chapter VI. The output from the O₂ and CO₂ sensors is shown in Fig. 7.23. Section a) of the figure shows the sensor responses when the subject was breathing at 6 breaths per minute and b) shows when the subject was asked to increase their breathing rate to 10 breaths per minute.

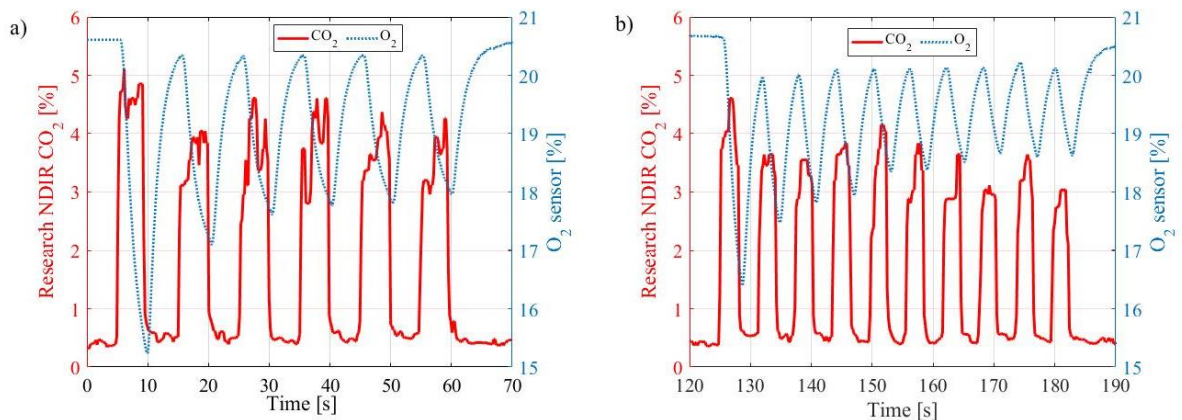


Fig. 7.23 – Subject breaths through the breath analyser for period of 1 minute, a) At a breathing rate of 6 cycles per minute; b) At a rate of 10 cycles per minute.

The O₂ sensor was not able to measure the change in oxygen content with high accuracy during a breath when the subject was exhaling at 6 breaths per minute. The sensor did not reach a plateau at the end of each exhalation, nor did the output return to the baseline value (ambient conditions expected of 20.6 %) during inhalation periods. During these periods the sensor measured 20.25 % O₂ on average for the six

inhalations shown in Fig. 7.23 a). The average value of the sensor output during exhalation was 17.27 %, compared to an expected decrease in O₂ concentration of between 4 and 5 % for a resting adult exhaling.

The O₂ sensor demonstrated a similar lack of accurate breath-by-breath performance when the subject was asked to exhale at a rate of 10 breaths per minute, shown in Fig. 7.23 b). The sensor averaged a final output of 18.1 % when the subject was inhaling, with no plateau. During inhalation, the sensor returned to an average value of 20.1 %, compared to the initial baseline of 20.6 %. The initial exhalation trough was 16.5 %, compared to the final three exhalations of ~ 18.6 % O₂. The exponential upward trend demonstrated for the O₂ sensor in both Fig. 7.23 a) and b) in exhaled O₂ content is due to the physiological and psychological effect of breathing into an apparatus. Although the main-stream tubing of the device was designed to add the least resistance, breathing into any mask causes an increase in respiratory resistance.

The psychological effect of the mask on the face also causes the first exhalations when using the device to be larger than found during normal breathing (perhaps ~1 min). The effect is prominent on the O₂ sensor, with a slow recovery time, as the user becomes accustomed to breathing through the device. The CO₂ demonstrates a ~ 0.7 % increase in exhaled concentration for the initial breath, although it recovers quickly to a normal exhaled value. The exponential trend notable in the O₂ sensor output is not visible. It is likely the level of CO₂ exhaled does not change as significantly as the O₂ exhaled when the user is breathing abnormally. To avoid the familiarisation effect (the user becoming accustomed to breathing through the mask) at least a 1 minute period was allowed prior to the start of exhalation measurements to ensure that the user is comfortable with breathing through the device.

The CO₂ sensor performed adequately with regard to the measurement of each breath, demonstrated in Fig. 7.23 a) for a subject exhaling at 6 breaths per minute. The sensor output returned to a baseline of approximately 0.4 % CO₂ during inhalation periods. The average concentration over the six exhalations was 3.88 %, compared to an expected increase of between 4 and 5 % for an adult. The noise level shown for the CO₂ sensor in Fig. 7.23 a) is on average ~0.4 %, in part due to a slow read-out rate. The sensor is only driven at 5 Hz, thus five readings of CO₂ concentration are taken per second. With a limited number of readings, digital filtering techniques (e.g.

moving average) are not effective; anomalies in the sensor response are therefore unlikely to be filtered out.

The noise level present in the CO₂ sensor when the subject was breathing at 6 breaths per minute is reduced (~ 0.15 % on average). The cleaner result could indicate that the natural breathing rate is more stable and comfortable for the subject (i.e. a regular breathing pattern promotes a smoother transition from inhaling to exhaling). The highest level of noise on the CO₂ sensor output in Fig. 7.23 a) often occurs after the exhalation stage begins. The concentration of CO₂ exhaled in Fig. 7.23 b) is lower on average (3.71 %) compared to a) due to the faster breathing rate. The baseline of 0.4 % CO₂ is maintained throughout the experiment (the initial value and during inhalation periods).

To verify the output from the CO₂ sensor it was tested against a commercial device (Hummingbird IR3107) IR sensor. A subject was asked to breathe with an equal inhale and exhale ratio and an overall period of 6 s. The O₂ sensor data were also recorded, but a commercial device for comparison was not available. The results obtained were consistent with the experiments in Fig. 7.23; the results from a second subject are shown in Fig. 7.24. The CO₂ comparison data are shown in a) and the O₂ sensor output in b).

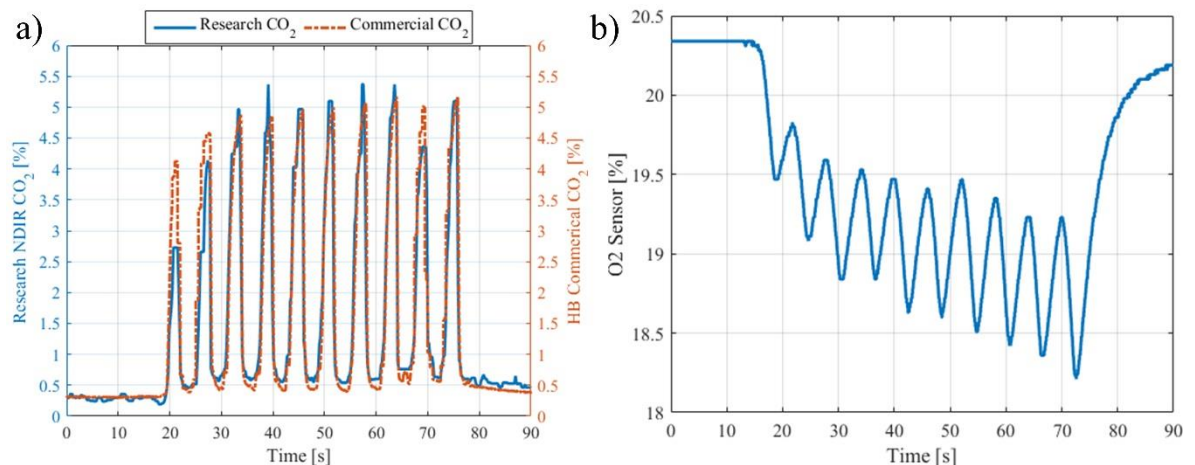


Fig. 7.24 – Side-stream analyser tested with subject exhaling at 10 breaths per minute, 90 s data shown, a) Comparison of the prototype NDIR sensor against a commercial device (Hummingbird IR3107); b) Corresponding O₂ sensor output.

The CO₂ sensor captures the exhalations well, demonstrating a similar performance to that of the commercial device. The t_{90} response time was on average 1.7 s for the

research device. The commercial device offers a t_{10} to t_{90} response time of around 100 ms [3]. Comparison between the commercial and research sensors yielded a variance of 0.29 % for a 95 % confidence interval. The mean recorded CO₂ value across the 10 breath samples was 4.70 %, which is in the expected range for a normal subject of between 4 and 5 %.

The research CO₂ sensor demonstrates similar performance to Fig. 7.23, where a plateau is not reached at the end of each exhalation. The sinusoidal drive rate is limited, as discussed previously. If the 5 Hz drive frequency was increased to 100 Hz there would be a far greater number of samples per breath. The dimensions of the SOI CMOS IR emitter are related to the response time of the device. The larger emitter size chosen in this work provides greater emissivity for higher detector response, but prevents the faster drive signals desired for a reduction in noise and greater measurement rate.

The O₂ sensor performance, Fig. 7.24 b), is similar when compared to the data for the previous subject in Fig. 7.23. The baseline concentration of O₂ is ~ 20.4 % in this experiment; the sensor does not return to this value during the inhalation period (when the sensors are exposed to ambient room air). The sensor could be affected by the elevated level of humidity of an exhalation (peak measured of ~ 80 % in side-stream chamber after an exhalation). Furthermore, the minimum O₂ concentration in normal subjects is expected to be in the range of 16 to 17 % in exhaled breath. In the case of the 10 exhalations shown in Fig. 7.24 b), the average exhaled O₂ content was 18.7 %.

The mean O₂ concentration measured during inhalation is 19.5 %. The cause of the inadequate response could perhaps be due to the detection principle of the sensor. The electrochemical device measures O₂ concentration through a reaction inside a gel solution. The reaction rate is slightly slower as the device ages. If the device is tested on a large number of subjects the sensor could require cleaning. It is possible that a filter could be installed in the side-stream tubing to prevent particulate matter from affecting sensor performance.

7.5 Conclusions

The side-stream chamber designed in this work was used to measure concentration of O₂ and CO₂ exhaled. The design of the chamber was optimised in computer aided design software, and the flow through the chamber analysed. For a resting exhalation,

the main-stream flow can reach 30 L/min (assuming the subject is relaxed, as per the requirements for resting EE measurement), compared to the side-stream extraction (controlled by a pump), which was specified at 150 ml/min. The vertical extraction tube was created to ensure the level of humidity in the side-stream section was not increased by condensing water vapour. Furthermore, the 90 ° pipe prevented large flow variation in the side-stream section, which would be detrimental to sensor performance.

The main body of the chamber was constructed from POM, which was noted as a light-weight but durable material. POM is convenient for prototype constructions, easy to machine and resilient to gases. The smooth finish to the chamber allowed subjects to hold the device comfortably and while in the development phase, no additional cover was used. The VOC sensor and NDIR sensor had rapid-prototyped components, which enabled integration into the POM chamber. The dimensions of the chamber were based upon the need to extract a laminar flow from breath and the 10 mm path length required by the NDIR device.

The electrochemical O₂ sensor was tested against varying flow rates (0.25, 0.5, 1.0, 2.0 SLPM), temperatures (25, 27, 29, 31, 33, 35 °C) and levels of humidity (0, 10, 20, 30, 40, 50, 60, 70 %). Humidity and temperature had little impact on performance, compared to flow rate. For a new (unused) sensor the output voltage was seen to increase from 0.8 V to 0.95 V when in conditions of 20.9 % O₂ with flow varied from 0.25 to 2 SLPM. The environmental parameter variance experiments demonstrated the need for the device to be used in only a constant flow rate situation, although temperature and humidity were less critical.

The t_{90} response time for the O₂ device was increased from ~9 s to 14.6 s (turn-on for 20.9 % O₂) when the flow rate was decreased from 2.0 SLPM to 0.25 SLPM. The slow response time (compared to < 2 s for the CO₂ sensor) promoted the need to model the output from the O₂ sensor. The output was compared to a resistor-capacitor circuit (3 stage). The 3 delay phase model exhibited similar characteristics to the O₂ sensor response (R^2 of 0.990), although the final stage of the response (given 6 s of data) was not well represented. The RC model did not start to plateau, whereas the exponential output from the O₂ sensor started to reach a final value. The O₂ sensor performance was not significantly affected by aging (although < 10 % drift is likely), the t_{90}

response time was similar (15.9 s at 0.25 SLPM). The device may not need regularly replacing, although calibration may be required in-frequently to monitor the level of drift.

Calibration was performed prior to each measurement with the hand-held analyser for levels of O₂ (20.9, 16, 0 %) and levels of CO₂ (0, 1, 2.5, 5 %). The O₂ sensor output followed a linear trend, whereas an exponential trend was found for the CO₂ sensor. The side-stream analyser was connected to the gas rig (without a pump) for calibration (due to the low 1 SLPM flow rate from the gas rig being insufficient to replace the main-stream flow from an exhalation). The t_{90} response times were noted to increase by 5 s due to this change in measurement technique.

One minute breath samples were taken from subjects in a laboratory environment to test the performance of the side-stream analyser. In this initial testing, the subjects were asked to inhale and exhale with a 1:1 time ratio of either 3 s or 5 s (i.e. 10 breaths or 6 breaths per minute). For the results presented for one subject breathing slowly, the average exhaled concentrations were 17.27 % and 3.88 % for the O₂ and CO₂ sensors respectively. The O₂ sensor output exponentially trended upwards over the duration of the 1 minute experiment. When the subject was asked to breathe at the faster rate the average O₂ and CO₂ concentrations were 18.1 % and 3.71 % respectively. The notable decrease in the O₂ sensor output (0.83 % compared to 0.17 % for the CO₂ sensor) demonstrates the slower performance of the O₂ sensor can prevent the final O₂ concentration from an exhalation being detected.

In the laboratory breath tests, the environmental temperature was controlled (to within 1 °C). In the post-processing of the EE results the data recorded from the temperature and humidity sensor can be used to compensate for environmental changes. The environmental temperature is unlikely to vary significantly over a 1 minute period, although measurements taken periodically (over a number of hours) would benefit from temperature normalisation.

The CO₂ sensor was compared to a commercial device (Hummingbird IR3107) when another subject was asked to breathe through the device for a 1 minute period (6 s breath cycle). The prototype device compared well to the commercial product, a variance of 0.29 % for a 95 % confidence interval was found. The O₂ sensor demonstrated a similar performance to previous tests, although an exponential

decrease was found for this subject. The trend was less prominent for the CO₂ sensors. The exponential trends in the sensor outputs are in part due to the user becoming familiar with breathing through a mask into an apparatus. In future measurements, the users will be allowed at least a 1 minute period to become accustomed to the equipment before the gas concentrations are sampled.

The performance of the hand-held analyser was in-part adequate for breath analysis of EE. The CO₂ sensor performed similarly to a commercial device, although the O₂ sensor was not satisfactory. Affordable O₂ cells are often based on an electrochemical principle. The reactions inside the electrolyte gel limit the response times of the sensors. In the next chapter the analyser is tested on subjects in respiratory chambers. Although the response of the O₂ sensor is limited, the performance was a significant improvement over similar commercially available electrochemical cells (e.g. Alphasense O2G2, tested previously).

7.6 References

- [1] A.M. Luks, R.W. Glenny, Clinical Exercise Testing, in: R.J. Mason, J.D. Ernst, T.E. King, S.C. Lazarus, J.F. Murray, J.A. Nadel, et al. (Eds.), Murray Nadel's Textb. Respir. Med., W.B. Saunders, Philadelphia, U.S., 2016: p. 445. doi:<http://dx.doi.org/10.1016/B978-1-4557-3383-5.00026-9>.
- [2] Hummingbird Technologies, Pm111e Instruction Manual, 7th Ed., Servomex, 2014.
- [3] Hummingbird Technologies, Hummingbird Ir3107, Hummingbird. (2013). <http://www.hummingbirdsensing.com/en/products/carbon-dioxide/ir3107> (accessed September 3, 2014).
- [4] M. Liess, A new low-cost hydrogen sensor build with a thermopile IR detector adapted to measure thermal conductivity, *J. Sensors Sens. Syst.* 4 (2015) 281–288. doi:10.5194/jsss-4-281-2015.
- [5] A. Rydosz, T.P.K.W. and S.G. Wojciech Maziarz, Deposition of Nanocrystalline WO₃ and CuO Thin Film in View of Gas Sensor Applications, (2014) 150–155.
- [6] U. Vaidya, Composites for Automotive, Truck and Mass Transit: Materials, Design, Manufacturing, DEStech Publications, Lancaster, U.S., 2011.
- [7] Micropumps, Diaphragm Pumps Datasheet, Pump Datasheets. (2015). <http://docs-europe.electrocomponents.com/webdocs/145e/0900766b8145ed36.pdf> (accessed August 26, 2016).
- [8] P. Fabian, J. Brain, E.A. Houseman, J. Gern, D.K. Milton, Origin of exhaled breath particles from healthy and human rhinovirus-infected subjects., *J. Aerosol Med. Pulm. Drug Deliv.* 24 (2011) 137–47. doi:10.1089/jamp.2010.0815.
- [9] D.S. Gardenhire, Rau's Respiratory Care Pharmacology, 8th Ed., Elsevier Health Sciences, St. Louis, U.S., 2013. doi:10.1017/CBO9781107415324.004.
- [10] City Technology, MOX-20 MediceL, 2013 (n.d.). <http://www.citytech.com/PDF-Datasheets/mox20.pdf>.
- [11] R. Kocache, The measurement of oxygen on gas mixtures, *J. Phys. E.* 19 (1986) 401–412. doi:10.1088/0022-3735/19/6/001.
- [12] R.L. Smith, B.S. Hobbs, J. Watson, D. Hall, J. Llinas, D. Young, et al., Reliability Engineering, in: Sensors, Nanosci. Biomed. Eng. Instruments, 3rd Ed., CRC Press, Boca Raton, U.S., 2006: pp. 1–13. doi:10.1201/9781420003161.sec1.
- [13] Alphasense, How Oxygen Sensors Work, 44 (2007) 7–10. http://www.alphasense.com/WEB1213/wp-content/uploads/2013/07/AAN_009.pdf.
- [14] P.R. Warburton, R.S. Sawtelle, A. Watson, A.Q. Wang, Failure prediction for a galvanic oxygen sensor, *Sensors Actuators B Chem.* 72 (2001) 197–203.

doi:10.1016/S0925-4005(00)00534-7.

- [15] A.J. van Stroe, L.J.J. Janssen, Determination of the diffusion coefficient of oxygen in sodium chloride solutions with a transient pulse technique, *Anal. Chim. Acta.* 279 (1993) 213–219. doi:10.1016/0003-2670(93)80320-K.
- [16] R. Chen, F. Formenti, A. Obeid, C.E.W. Hahn, A.D. Farmery, A fibre-optic oxygen sensor for monitoring human breathing, *Physiol. Meas.* 34 (2013) N71.

CHAPTER VIII

Energy Expenditure Analysis

Preface

Three hand-held analysers were developed to test subjects against a reference whole body calorimeter. Two measurements were performed simultaneously with two handheld units and two respiratory chambers. A unit comprising commercial O₂ and CO₂ sensors was also tested. The resting EE of 10 subjects was tested, with EE measurements taken on the hand-held units every 20 min (for a 3 min period). The prototype analysers were found to overestimate the EE of 9 subjects by +2.4 % (one subject was excluded due to discomfort). The Harris-Benedict equation was used to calculate the BMR for each subject, but was found to overestimate this by +41.5 % on average. The smartphone companion application is tested, when EE is measured outside of a laboratory environment. A large variance in EE (0.65 kcal/min) was found, demonstrating the need for strict measurement protocols to calculate resting EE. The side-stream analyser, developed in Chapter VII, provided good estimates for the energy requirements of the 10 subjects, although further work is required to investigate the individual components of total daily EE.

8 Resting Energy Expenditure Measurements

The portable EE analyser developed in this thesis was trialled against a whole body calorimeter, the current gold-standard for metabolism measurement [1]. The performance of the instrument was verified with 10 subjects tested inside respiratory rooms. The subjects remained seated and relaxed throughout the 3 hour experiment to assess resting EE. The breath data collected were recorded wirelessly using a laptop computer as the subjects were isolated inside the rooms.

The portability of the hand-held unit was utilised, when EE measurements were performed with a smartphone, outside of a laboratory environment. EE was assessed over the period of an office day (free-living), with measurements taken hourly. The increase in EE due to eating a meal and physical activity was observed during daily living. An example use of a portable and quick measurement system is for measurements of the DIT component of EE, notable after a meal is consumed. The period of a time that the DIT component influences total EE is dependent on the content of the meal consumed, as discussed in section 1.2.

Westerterp reported the postprandial rise in EE lasts for several hours and is completely terminated approximately 10 hours after the last meal, although there is disagreement regarding the length of the period [2]. The amount of carbohydrates, protein and fat in the meal effects the length of the period the DIT component is increased. It has been reported peaks in blood glucose levels occur after approximately 1 hour post-eating due to the consumption of carbohydrates, 2.5 hours due to protein consumption and 3.5 hours for fat consumption [3].

8.1 Resting EE Experiment Methodology

The side-stream analyser, detailed in the previous chapter, was tested against a respiratory room calorimeter at the Human Metabolism Research Unit (HMRU), University Hospitals Coventry and Warwickshire NHS Trust (UHCW). Two hand-held analysers were tested within two respiratory rooms simultaneously (one spare analyser was available). The side-stream analysers were cased in plastic housings to ensure that the sensors were not damaged during their use with volunteers (photograph Fig. 8.1). The enclosure was lightweight, but sturdy, and enabled the unit to be held easily in the hand. An exhaust, from the mainstream, was 3D printed with a 22 mm

outer diameter for additional tubing to be connected. A mask was connected directly to the flow meter inlet. A micro USB port on the end of the device was used to power the device (via a USB power supply) and, when desired, to communicate with the device via a wired connection.

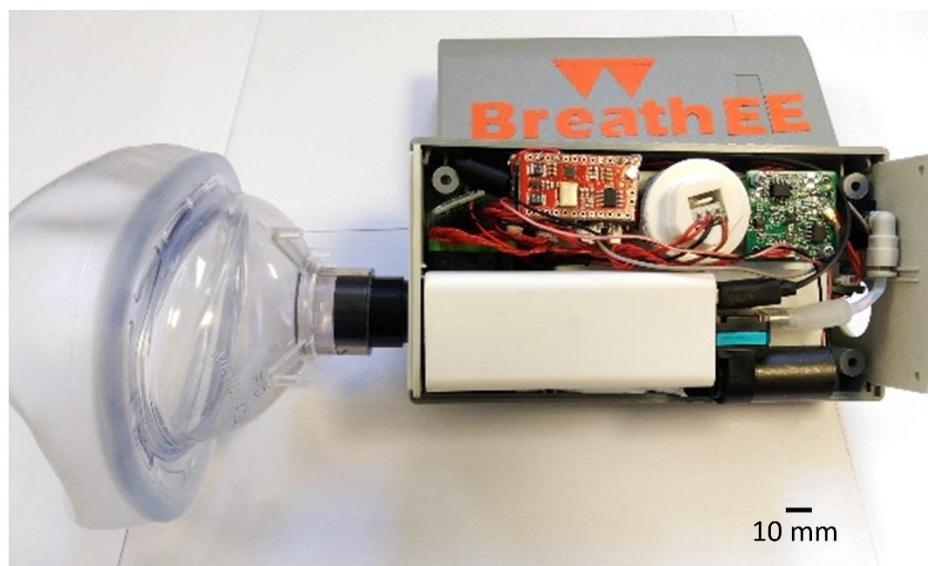


Fig. 8.1 – Photograph of hand-held breath analyser, installed in a robust enclosure for monitoring of EE inside respiratory chambers. Battery power available for portable measurements.

8.1.1 Commercial Sensors in Comparative Side-Stream Unit

To assess the breath-by-breath sampling of the hand-held units, a side-stream analyser was constructed, containing commercial sensors. A photograph of the unit is shown in Fig. 8.2, with a commercial O_2 sensor (Hummingbird Pm1111E), commercial CO_2 sensor (Hummingbird IR3107), microcontroller (Teensy 3.2) and 150 ml/min pump (Micropumps D200). The unit connected was to a computer via a wired USB connection. The LabVIEW VI developed for the hand-held analyser recorded the data from the microcontroller (200 Hz). A 3D printed adaptor (shown on the right of Fig. 8.2) enabled a side-stream sample to be taken from the exhaust of the hand-held analyser. The O_2 sensor functioned via the paramagnetic principle, thus had to be kept on a stable surface during operation.

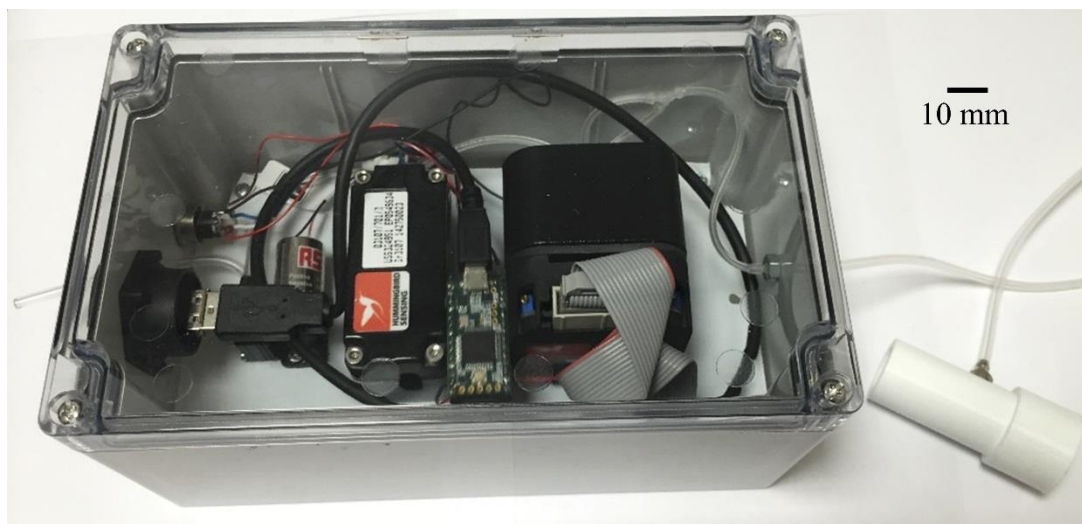


Fig. 8.2 – Photograph of additional side-stream analyser, consisting of commercial sensors for comparison against the prototype hand-held breath analyser.

8.1.2 Measurement Protocol

Ten volunteers were recruited for measurements inside the respiratory rooms. The measurement protocol allowed drinks of water, but asked subjects to fast for a minimum of 6 hours prior to the start of measurements. The subjects entered the chambers and were seated comfortably in chairs (without caster wheels). The aim of the experiments was to assess resting EE, as a baseline comparison between the respiratory rooms and the side-stream instruments. The volunteers were asked to relax and remain awake, but remain still and make minimum movement; reading or watching television were suggested activities.

The subjects, once comfortable inside the rooms, were instructed on how to use the measurement apparatus. In one room, assigned at random, the side-stream instrument with commercial sensors was connected in parallel to a hand-held analyser. In the other room, the side-stream analyser was separate to the hand-held analyser. In this room measurements were taken twice, alternately the hand-held unit followed by the analyser with the commercial sensors. The rationale for the experiments was explained, emphasising the need for the subjects to remain relaxed and still for a resting EE measurement. The subjects were asked to practice breathing through the hand-held analyser and the need for the mask to be sealed against the face was explained. The subjects were asked to breathe in a normal manner, without or increasing their breathing rate or tidal volume. Subjects were asked to remove glasses if they obstructed the seal of the mask around their nose.

The experiments were performed over a 3 hour period, with 30 minutes prior to this to allow for the chambers to stabilise. Every 20 minutes the subjects were instructed via an intercom to breathe through the analysers. A 3 minute measurement was taken (although data were recorded continuously throughout the experiment). At the end of the measurement period the subjects were told to stop breathing through the apparatus. In the room where the hand-held analyser and side-stream commercial sensor system were tested separately, the subject was also instructed which device to use first. After the 3 minute period, the users were instructed to switch apparatus and breathe through the other device. After a second 3 minute period the subject was told to return the apparatus to the desk.

8.1.3 Collection of Data

The LabVIEW VI, discussed in chapter VI, was used to capture the data from the hand-held units. A wireless Bluetooth link was used to communicate with the analysers, which were isolated inside the chambers. The devices were powered by mains power USB supplies. A laptop was used to record the data from each unit, where the storage capacity of a computer was preferred over a smartphone for the 3 hour long experiments. Table 8.1 summarises the sensors incorporated into each breath analyser.

Table 8.1 – List of sensors included in the respective breath analysers.

Hand-Held Analysers Unit 1 and Unit 2 (Side-stream sensors)	Commercial Sensors Unit 1	Commercial Sensors Unit 2 (Side-stream sensors)
<ul style="list-style-type: none"> • O₂ (City Technology, MOX-20) • CO₂ (novel research) • VOC (novel research) • Temperature and RH (GE, ChipCap2) • Flow sensor in mainstream (Sensirion, SFM3000) • Data captured with Teensy Microcontroller 	<ul style="list-style-type: none"> • O₂ (Hummingbird, Pm1111E) • CO₂ (Hummingbird, IR3107) • Temperature and RH sensor in mainstream. • Flow sensor in mainstream (Sensirion, SFM3000) • Data captured with Arduino Uno Microcontroller 	<ul style="list-style-type: none"> • O₂ (Hummingbird, Pm1111E) • CO₂ (Hummingbird, IR3107) • Data captured with Teensy Microcontroller

The data collected were shown on the computer screen in real-time and monitored by the experiment coordinator. If the subjects were using the devices incorrectly (i.e. not holding the mask firmly to their face etc.), an abnormal sensor output would indicate that a fault had occurred. The intercom in the rooms was used to communicate with the subject and instruct how to correct the error. The unit containing the commercial sensors was not wirelessly connected (i.e. data logging was performed on a laptop computer inside the chamber via a wired USB link). If a fault occurred with the device this could not be identified from outside the chamber. The sensor systems with commercial sensors were not available for the first two subjects.

8.1.4 Subjects

A total of 10 subjects were recruited from the University of Warwick and the UHCW. In order to view assess the EE variation between genders and age, four male volunteers were requested to participate and six female, with a range of ages, as possible with the sample size. Ethics approval was granted for experiments to be performed at the University of Warwick (to allow for preliminary testing). The breath experiments performed at the HMRU were granted ethics approval from a committee at the UHCW.

The sample size of 10 subjects was considered sufficient for the distribution of the sample mean to be approximately that of a normally distributed population [4]. In general according to the central limit theorem, a sample size of > 30 would be required for a population (regardless of normal distribution or not), however given a normal distribution a lower sample size can be used [5,6]. For example, a sample size of 50 is likely to include $\sim 95\%$ of a normally distributed population which is reduced to 92% for a sample size of 10 (reduced again to 90% for a sample size of 8) [7]. The distribution of the EE of the general population is not widely reported in the literature. The height of adults is widely reported as being close to normally distributed across the population (of the UK, considering genders separately) [8–10]. The BMI of the UK population was also noted as having an approximately normal distribution [11,12].

The subjects were asked to sign a study consent document prior to their participation in the study. Photographs or videos of the subjects while they participated in the experiment were not permitted. Data for their height, weight, age, gender and ethnicity were collected. The subjects in this work had an average age of 36.3 years (range 23

to 63 years, standard deviation (STD) of 10.4 years). The average height of the sample group was 1.69 m (range 1.6 to 1.8 m, STD 0.06 m). The average weight for the group was 70.2 kg (range 52.2 to 100.8 kg, STD 12.8 kg). The BMI average for the group was 24.5 kg/m² (range 18.9 to 35.3 kg/m², STD 4.24 kg/m²). For analysis, the subjects were grouped by gender, BMI and age. In general, the population is classified as underweight, normal, overweight or obese with BMIs of < 18.5, 18.5 to 24, 25 to 29 and > 30 kg/m² respectively [13]. By age, the adult subjects were grouped from 18 to 34 years, 35 to 49 years and > 50 years.

8.2 Experimental Results

The commercial sensor units and the hand-held analysers were calibrated to dry gas mixtures of O₂ and CO₂ (procedure discussed in chapter VII) for each subject both pre- and post- measurement. The volumes of O₂ consumed and CO₂ produced were converted to standard pressure, temperature, dry (STPD) readings during post-logging data processing to compensate for the high humidity level and elevated temperature found in exhaled breath. Pressure compensation was required, as the rooms are kept below atmospheric pressure, which induces a notable effect on sensor output when the rooms are sealed.

8.2.1 Measured Gas Concentrations and Sensor Response

The sensor data were continuously recorded throughout the duration of the 3 hour experiments, including the additional period prior to the measurement for the gases inside the rooms to stabilise. During this period the use of the apparatus was demonstrated to the subjects and they were asked to practice breathing through the devices for approximately 30 s to ensure that they understood the operation of the instruments. The data obtained from the sensors (after calibration) were in the form shown in Fig. 8.3, with O₂ sensor data shown in a) and CO₂ data in b).

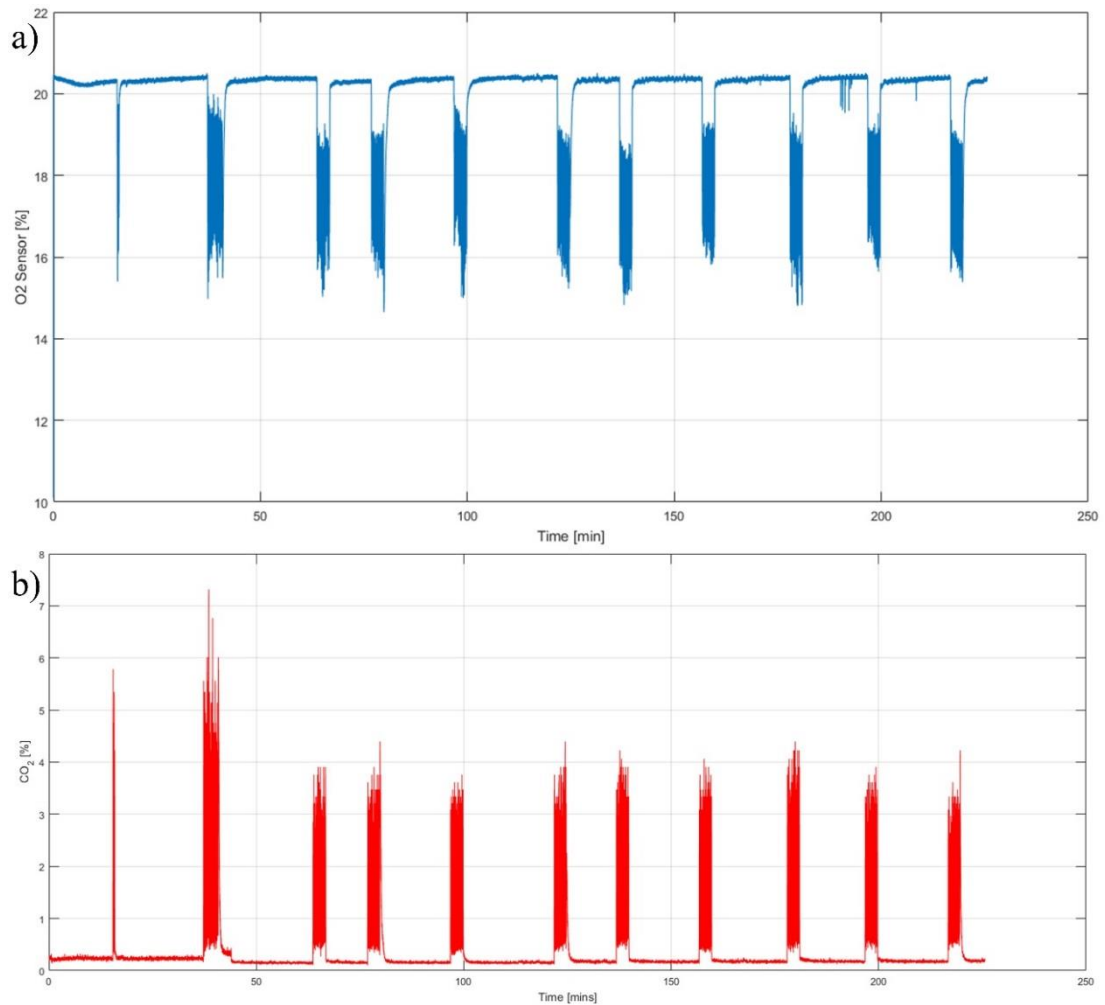


Fig. 8.3 – Output data plots for one subject for the duration of the 3 hour experiment for a) The O₂ concentration measured (MOX-20 sensor) and b) The CO₂ concentration measured (prototype NDIR sensor).

The data show the subject breathing through the device at 20 min intervals. The peaks at ~10 min into the experiment were due to the subject being shown how to use the equipment (each subject was asked to breathe through the device for approximately 30 s). The initial repetition produces a higher level of CO₂ (exhale average peak 5.2 % CO₂) compared to the subsequent 9 sample periods (average peak 3.7 %). The elevated CO₂ level was due to the subject becoming further accustomed to breathing through the device; heavier breathing was noted initially, before a normal level was established once the subject became relaxed as the experiment progressed. The effect is prominent on the CO₂ sensor, where the O₂ sensor is less affected (peak exhalation output average 15.8 %). The third period where the subject was breathing through the device is shown enlarged in Fig. 8.4. The exhaled concentrations of O₂ and CO₂ are shown in a), the flow rate and tidal volume in b) and the temperature and RH in c).

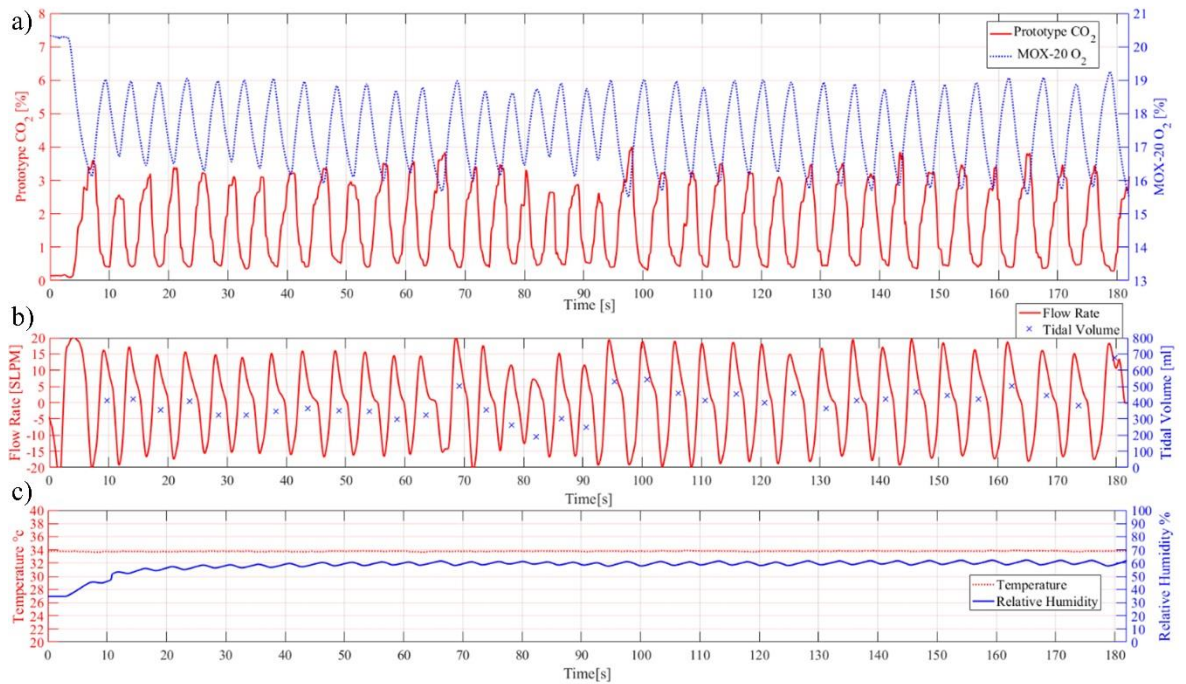


Fig. 8.4 – Sensor data for a 3 min period when the subject was breathing through a hand-held analyser, a) O₂ and CO₂ sensor data (MOX-20 and prototype NDIR sensor, respectively); b) Flow sensor data (SFM3000 sensor) with tidal volume; c) Temperature and RH sensor data (ChipCap2 sensor).

The O₂ and CO₂ sensor performance observed with ‘natural’ breathing were similar to those shown for fixed cycle period breathing, demonstrated in the initial laboratory trials (section 8.4). The O₂ sensor did not return to a baseline ambient O₂ concentration reading (20.2 % O₂); the response time of the sensor limited its response to the exhaled and inhaled gases, when the subject was breathing at a rate of 12 breaths per min. The O₂ sensor demonstrated typical performance for a device limited by a response time barely sufficient to monitor gas concentration which varies at a comparable time period.

The CO₂ sensor returned to a reading close to the baseline ambient value (0.15 %) when the subject was exhaling (on average 0.35 %). The gas mixture in the side-stream tubing was likely to return to baseline during inhalation periods. The CO₂ sensor demonstrated good performance for the exhalations, where a plateau was reached for the majority of the breaths shown in Fig. 8.4 (on 9 occasions from the 36 breaths the sensor output does not plateau).

The temperature was significantly elevated inside the unit, a constant 33.8 °C was measured (ambient 23 °C), and the sensor did not produce a response to the higher temperature (36°C body temperature) of the exhaled gas. The decrease in temperature was in part due to cooling in the upper airways, mouth and nose. The pump was inside the sealed hand-held unit, causing an increase in temperature, over the 3 hour period of operation. The temperature of the side-stream was constant and did vary the response of the sensors. As the temperature was similar to body temperature, water droplets did not condense inside the unit. The level of relative humidity measured was less than previously measured for an exhalation (nearly 100 % saturated), and varied between 58 % and 61 % on average (inhalation to exhalation). The reduced level of humidity benefited the O₂ and CO₂ sensor responses, which were shown to be cross-sensitive to water vapour in chapter VII.

The tidal volume (volume exhaled) by the subject was calculated for the period of positive flow rate readings (i.e. air flow direction was from the mouth of the subject through the device). The value is marked on the graph in Fig. 8.4 b). The tidal volume can be used to indicate if the subject is operating the device correctly. The tidal volume can be approximated at between 6 and 8 ml/kg body weight [14,15]. A reduced tidal volume can indicate that the subject is not holding the device correctly (i.e. gas is leaking around the edges of the mask) or they are struggling to breath naturally through the device. An increase in tidal volume (e.g. 1048 ml for the initial breath shown in Fig. 8.4) indicates that the subject is breathing heavily through the device. The volume exhaled (i.e. of O₂ and CO₂) directly affects the metabolic rate calculation, using the Weir equation (2.4).

The subject demonstrated a regular breathing pattern (Fig. 8.4) for the duration of the 3 minute experiment. A tidal volume of ~ 400 ml could be approximated for the subject, calculated from body weight. The average value measured, excluding the initial breath, was 398 ml (STD 91.6 ml). In this particular session the subject provided data suitable for resting EE calculations.

8.2.2 Sensor Performance and Comparison to Respiratory Chambers

The data provided from the respiratory chamber were formatted in ml/min O₂ consumption and CO₂ production suitable for calculation of EE from the Weir equation (2.4). To find the corresponding volume of each gas (O₂/CO₂) measured

using the hand-held analysers, the flow rate data collected from the hand-held analysers were integrated. The trapezium rule was used to find the volume of gas exhaled (ml/sample). A simplified data processing block diagram (performed using a Matlab script) is shown in Fig. 8.5.

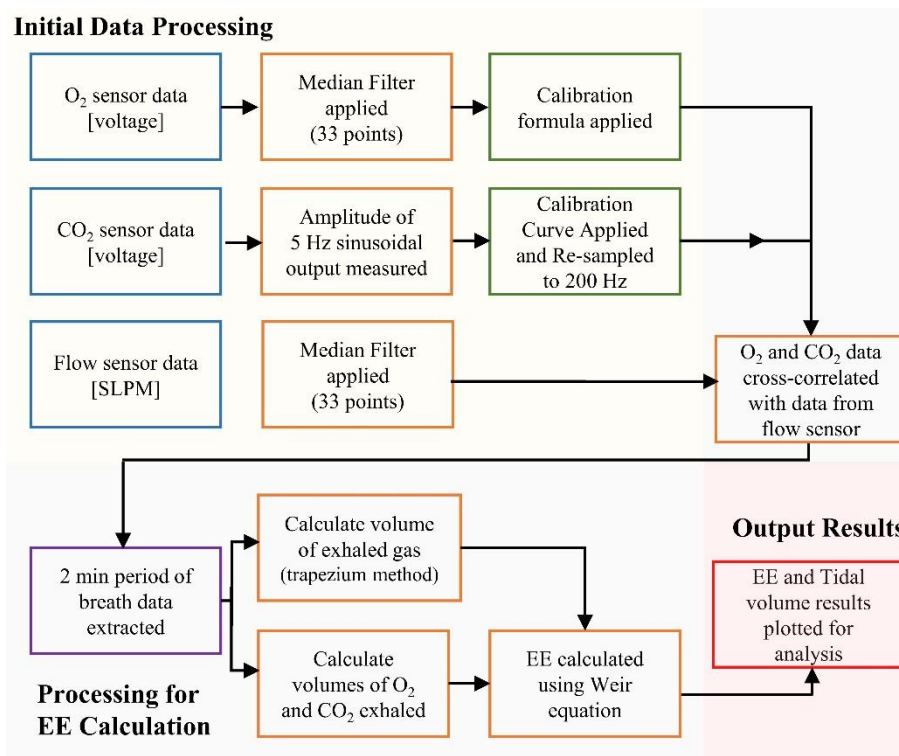


Fig. 8.5 – Simplified block diagram showing the data processing stages from calculating human EE from the raw data collected from the O₂, CO₂ and flow sensors.

A 2 minute period was extracted from each 3 minute sampling period and the volume of each gas exhaled calculated (given 1 sample was taken every 200 Hz). The CO₂ data was re-sampled to match the 200 Hz read-out rate of the flow and O₂ sensors (the CO₂ concentration could only be calculated at 5 Hz intervals). The gas concentration data were cross-correlated with the flow data to ensure accurate calculation of the volume of each gas (O₂/CO₂) exhaled per breath (given the flow sensor was in the mainstream tubing and the gas sensors located in the side-stream chamber). The cross-correlation step also allowed the slow response times of the sensors to be mitigated (i.e. typically a total delay of 2 s was found for the O₂ sensor and 0.7 s for the CO₂ sensor). The data were compared based on 5 min averages from the respiratory rooms and the 2 min averages from the hand-held analysers (extracted from the breath samples provided every 20 min).

The O₂ and CO₂ volumes consumed and produced are shown for the hand-held analysers and whole body calorimeters in Fig. 8.6. The data from two subjects are shown, a) and b) for a male subject and c) and d) for a female subject. Plots a) and c) show the O₂ sensor data and b) and d) show the CO₂ sensor data. The subjects were classified in the same age group (35 to 49 years age), but different BMI groups (male had BMI of 23.5 kg/m² compared to female 25.6 kg/m²). The 180 min experiment includes only the duration for which measurements were taken with the hand-held analyser.

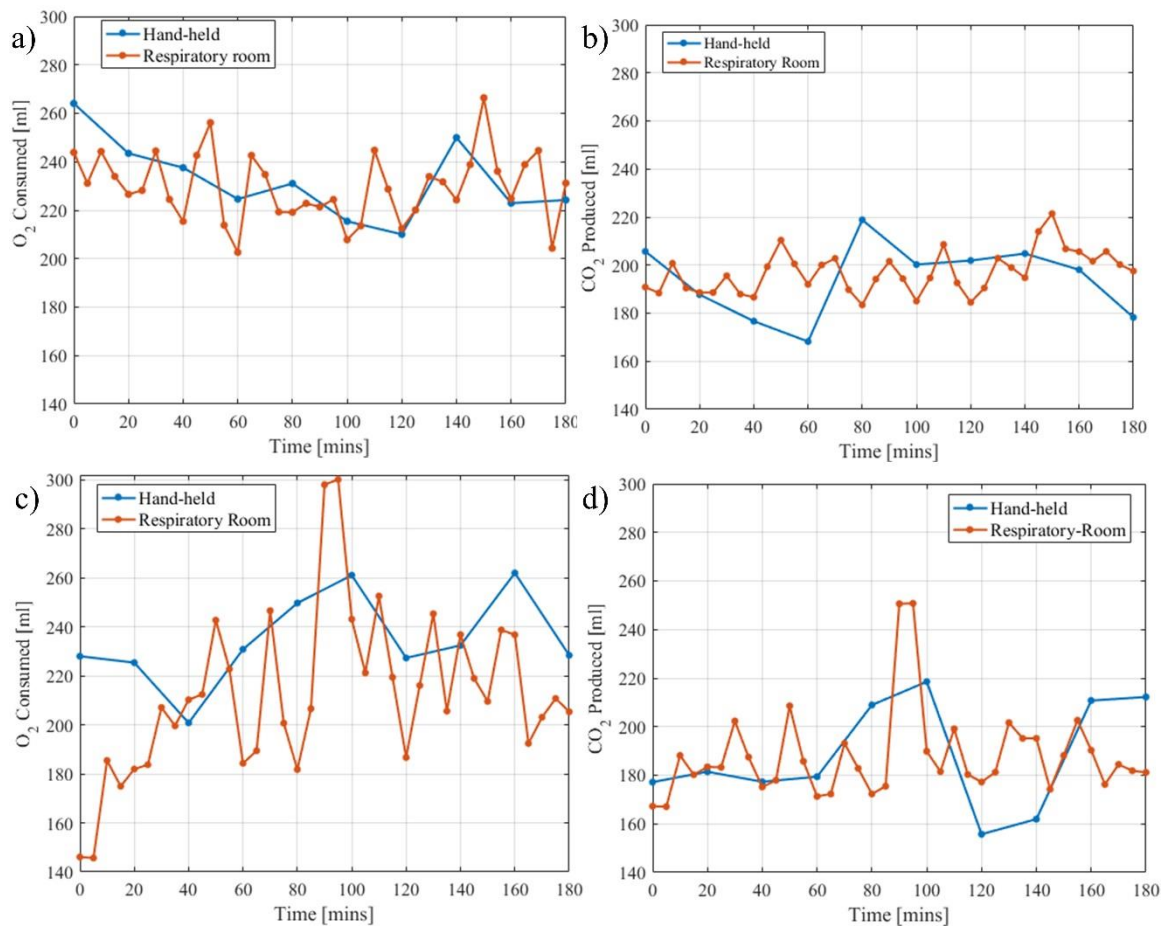


Fig. 8.6 – Subject data comparison between the hand-held analysers and respiratory rooms, a) O₂ consumed by one female subject; b) Corresponding CO₂ produced; c) O₂ consumed by one male subject; d) Corresponding CO₂ produced.

The male subject shown in Fig. 8.6 expended more energy than the female subject (average 1112 cal/min compared to 1036 cal/min). Considering the male and female population in general, the EE of men is ~10 % for the given age range (shown in Fig. 1.1). In the case of the two subjects shown above, the female has a comparatively higher EE, which is likely due to a higher BMI.

The volumes of O₂ and CO₂ measured with the hand-held analyser demonstrate similar characteristics to the reference values recorded from the respiratory chambers. It is noted with both measurement instruments, the elevated level of O₂ consumed and CO₂ produced during the initial breathing session with the hand-held analysers (i.e. $t = 0$ min). The data shown in Fig. 8.6 a) show O₂ consumption of 264 ml/min for the initial period decreasing to 244 ml/min for the second period (at $t = 20$ min). Although a familiarisation period is allowed, the subjects were found not to be accustomed to breathing through the hand-held unit during the first sampling session.

The O₂ consumption for the subject in Fig. 8.6 c) peaked at 300 ml/min during a 5 min period from $t = 90$ min. In this case the subject did not remain in a seated position, and thus increased their EE. This period was not recorded on the hand-held analyser (i.e. the subject returned to a sedentary position when using the device). An increased EE level (1263 cal/min) is recorded on the hand-held device at $t = 100$ min.

The O₂ measurements inside the respiratory room were more variable than those for CO₂, shown in Fig. 8.6; O₂ STD of 13.9 ml/min for a) and 32.7 ml/min for c) compared to CO₂ STD of 8.6 ml/min for b) and 17.2 ml/min for d). The effect was less visible for the hand-held device. The device was likely more affected by the breathing rate of the subjects compared to the O₂ sensor. As shown in Fig. 8.6, the STD of the O₂ sensor in the hand-held device for a) was 16.3 ml/min and 17.5 for c) compared to 14.9 ml/min for b) and 21.3 ml/min for d). The additional variance for the second subject was due to a period of unforeseen activity.

The data collected for the O₂ and CO₂ volumes exhaled from the respiratory rooms, hand-held devices and analysers with commercial sensors are summarised in Fig. 8.7 a) and b) respectively for the complete sample group of 10 subjects. The error bars indicate the STD and the centre point indicates the average EE for the 3 hour experiment. For the first 3 subjects, some individual breath samples were discarded due to low tidal volume (outside of 80 % of the 6 ml/kg value), proving that the mask was not sealed correctly. The volumes of O₂ and CO₂ measured had a range of 185.2 to 307.7 ml/min and 155.2 to 249.6 ml/min respectively.

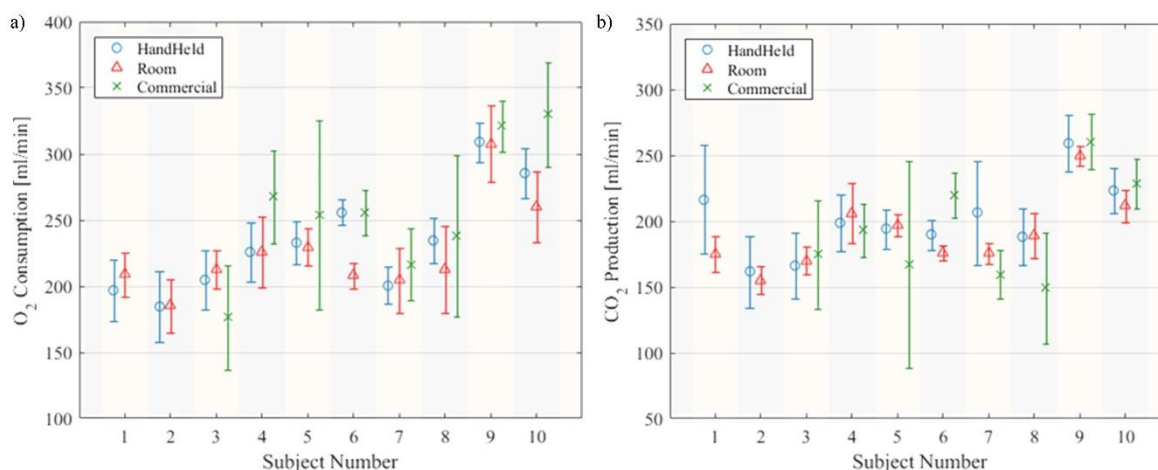


Fig. 8.7 – Data collected from 10 subjects with hand-held analysers, respiratory rooms and analysers with commercial sensors, a) O₂ consumed and b) CO₂ produced.

On average the O₂ consumption was overestimated by +3.4 % (-11.9 to +48.2 ml/min) and the CO₂ production by 5.4 % (-7.4 to 41.3 ml/min) for the hand-held devices when compared with the calorimeter chambers. The slow electrochemical O₂ sensor output was cross-correlated with the flow sensor data (on average the sensor exhibited an approximately 2 s delay). The O₂ consumption was measured reliably with the hand-held devices, the cell produced a stable output.

The commercial paramagnetic cell overestimated O₂ volume by on average +9.0 %. The technology used inside the cell was noted to be sensitive to movement, pressure and flow rate. Although precautions were taken to reduce the variance of these variables (room pressure was constant, constant flow rate and the equipment was not moved during the experiment) the sensor was not inherently resilient to breath measurements. Due to their large volume, the respiratory rooms tend to average the measurements of exhaled gas, and the sampling technique is not affected by the tidal volume or breathing rate of the subject.

When the average value recorded using the commercial NDIR sensor is considered, the device performed well compared to the respiratory room measurements (average error of -0.50 %). However, the sensor did not produce a stable output with an average STD of 32.2 ml/min. The hand-held sensor demonstrated higher stability with an average STD of 24.0 ml/min. The lower average error of the commercial product demonstrates the reproducibility of the device was higher, but with reduced precision compared to the prototype device. The stability of the commercial device is dependent

on flow rate, temperature and humidity. The fast response of the commercial product allowed the sensor to display breath-by-breath measurements, although with the compromise of a lower level of stability.

The limiting factor of the developed CO₂ sensor is the data processing, which is itself limited by the slow drive rate. The slow read-out rate (5 Hz) implies a slower response time and inherently noisy output. Furthermore the output response (voltage amplitude change of sinusoid) is small (~0.1 V per 1 % CO₂) which limits the accuracy to which the CO₂ concentration can be determined. Housing the sensors in close proximity can contribute to the noise factor, which affected the ability to read-out accurate CO₂ data. With prolonged use, housing components, such as pump, which can generate heat, can cause drift over the experimental period.

8.2.3 Energy Expenditure Measurements

The Weir equation (2.4) was used to calculate EE on a minute by minute basis for all three measurement instruments. The accuracy of the O₂ sensor measurements had a greater influence (i.e. multiple of 3.91 volume of O₂ consumed compared to 1.1 for volume of CO₂ produced) on the EE calculations. The EE for each subject across the 3 hour period was calculated for each instrument, shown in Fig. 8.8. In this section, the following abbreviations are used to distinguish the 3 instruments: Hand-Held (HH), Respiratory Room (RR) and Commercial Sensor (CS).

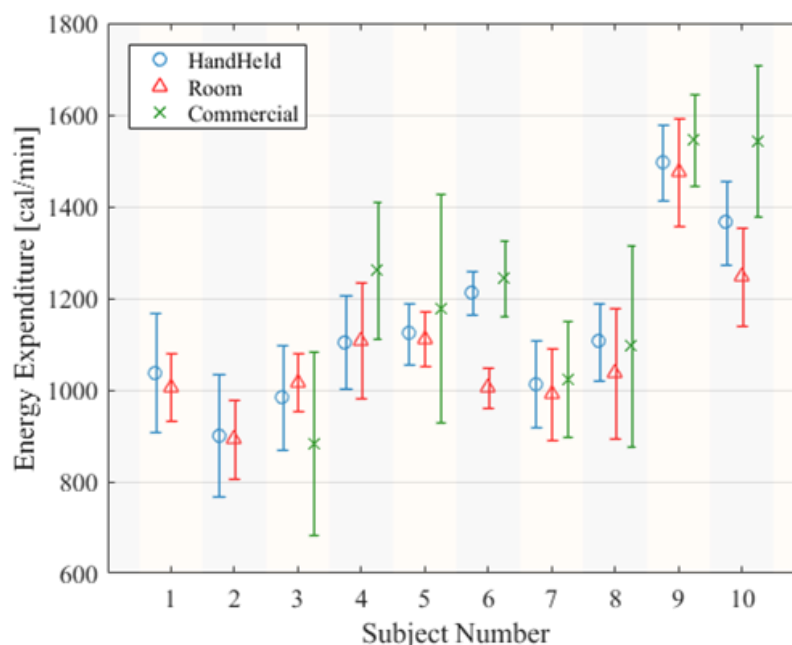


Fig. 8.8 – EE calculated for 10 subjects using HH devices, RR systems and the CS analyser.

The EE measurements taken with the HH analysers show good performance in comparison to the RR measurements (EE error range from -31.5 to +207 cal/min, average + 4.2 %). The lowest EE measured by the HH and RR systems was subject 2 (no analyser with CS was available); EE was measured as 893 and 901 cal/min for the RR and HH systems respectively. The highest EE was measured for subject 9 for all three instruments; 1474, 1495 and 1545 cal/min for the HH, RR and CS systems respectively. The greatest difference (with the HH and CS devices) was for subject 6, who was noted to feel less comfortable with the apparatus. The exclusion of the subject reduced the average overall error to +2.4 %.

The systems developed with the CS demonstrated disappointing results, considering the expense of the components. On average EE was overestimated by +9.6 % (range - 133 to +296 cal/min). The cause of the large error was attributed to the sensitivity of the O₂ sensor to its environment. The O₂ sensor overestimated the consumption of O₂ by on average 10.5 % across the 10 subjects; the CO₂ sensor underestimated the CO₂ production by -1.48 %. A disadvantage of the purchase of sensors separately from a commercial side-stream breath sampling unit is the devices are not optimised for breath sampling, with regards to calibration format and data processing techniques. The sensors were calibrated rigorously prior to each chamber measurement, however internal firmware adjustments were not possible.

The STD of the RR measurements was on average 92.3 cal/min. This value is ~10 % of the EE measured for the subjects. The variability is likely to come not from the measurement equipment, but from the subjects inside the room, making sub-conscious movements over the period of the experiment. The EE on average measured across the group from the RRs (0.9 to 1.5 kcal/min) was lower than average values reported by Knab et al. (1.3 to 2.5 kcal/min) [16]. The lower value likely demonstrates the willingness of the subjects to follow the measurement protocol (i.e. to make minimal movement throughout the 3 hour experiment duration).

The dependence of human EE on BMI, age and gender was discussed in chapter I (Fig. 1.1). A sample size of 10 limited the potential to investigate these relationships, with 4 subjects in the aged 18 to 34 year group, 4 in the 35 to 50 year group and 2 in the 50+ group. In terms of BMI, 6 subjects were classed as ‘Normal’, 3 as ‘Overweight’ and 1 as ‘obese’ (none ‘underweight’). The relationship between the EE

measured by the HH device and subject age is shown in Fig. 8.9 a). The subjects are listed according to their BMI in Fig. 8.9 b) with their gender shown and EE measured by the HH device.

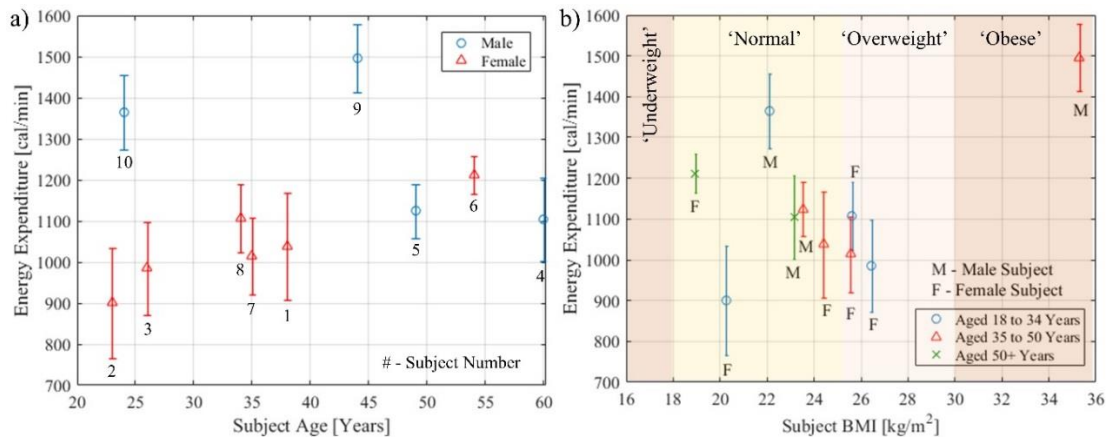


Fig. 8.9 – EE measured with HH instrument in relation to a) Subject age and gender; b) Subject BMI, age and gender.

An exponential decrease is expected in BMR (basal metabolic rate) with age, normally decreasing by 1 or 2 % per decade. The decrease is less visible in adults compared to children. The measurement protocol was not designed to measure BMR, however measurement of resting EE was desired. It is assumed, given two subjects of the same BMI and gender, that EE will decrease according to age, in the same manner as BMR. The exponential trend is visible for three male subjects (numbers 10, 5, 4 with a BMI of $\sim 23 \text{ kg/m}^2$) in Fig. 8.9 a), excluding one male subject with a higher BMI (subject 9, 35 kg/m^2).

The trend is less visible for the female population in the study. Subjects 3, 7 and 8 have a BMI $\sim 26 \text{ kg/m}^2$ (subject 1, BMI $\sim 24 \text{ kg/m}^2$). The subjects 8, 7 and 1 are of the same age group and a trend cannot be established over the small age range of 5 years. Subject 3 was ~ 10 years younger, but had a 6.4 % lower EE (measured using the HH device). The RR measurements for subject 3 indicated an EE similar to that of the female subjects 1, 7 and 8 (average 1012 cal/min, range 990 to 1031 cal/min). Considering the reported trend in EE decline with age, the results demonstrate the need for individual measurement of human metabolism. Subject 3 has a lower EE than that which would be predicted using guidance from the literature. The comparison with the Harris-Benedict equations is presented below, from which it was noted subject 3 had the highest calculated BMR from the female study group.

The outlier noted in Fig. 8.8 (subject 6) is again visible in Fig. 8.9, with a high energy expenditure (1211 cal/min), but low BMI (18.9 kg/m²). The majority of the subjects are grouped in the centre of Fig. 8.9 b), with 6 subjects classified in the range of 23 to 26 kg/m². The EE for this sub-group of participants (4 female) is ~1060 cal/min ($\pm 6\%$). Three of the female group are categorised as ‘overweight’ although no male subject is in the overweight category. From this small sample group a conclusive outcome cannot be determined. The higher BMI of the females could be caused by excessive food consumption relative to their calorific need. If the 6 subjects were to eat an identical diet, the female subjects would be more likely to gain weight, given a similar lifestyle, as their resting EE is lower in general.

8.2.4 Harris-Benedict BMR

Equations (2.11) and (2.12) are used to calculate the BMR for men and women, given measurements of height and weight and the age of the subject. In chapter II, the use of the HB equation was discussed, with predictive equations common in ICUs where indirect calorimetry is traditionally difficult to deploy. The EE was calculated for each subject using the appropriate HB equation; the results are compared in Fig. 8.10 to the EE measurement generated with the HH analysers. The complete dataset of EE calculations (from HH, CS and HB) are compared to the RR measurements in Table 8.2.

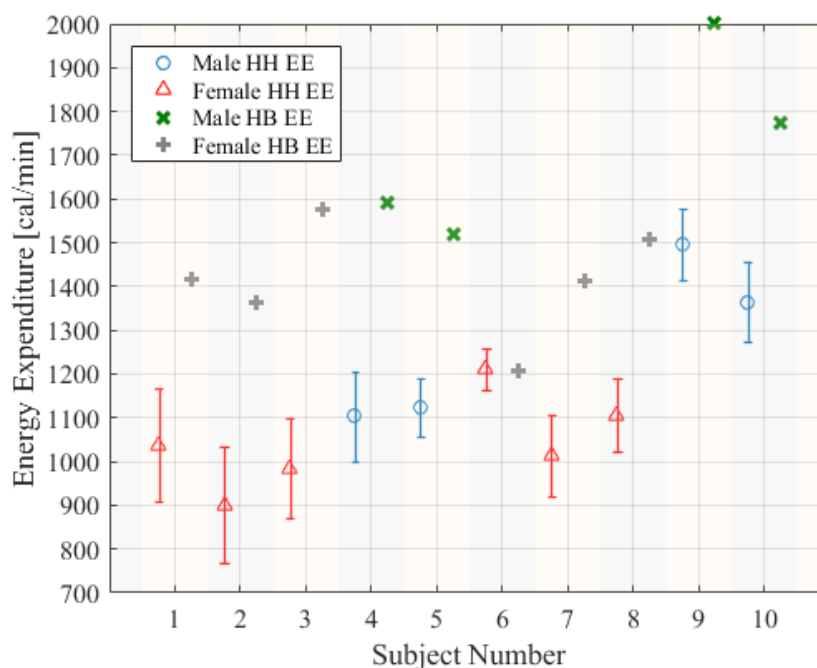


Fig. 8.10 – EE measured on HH instrument compared to calculated BMR using HB equation.

Table 8.2 – Summary of the EE data from the 10 subjects compared to the reference standard of the RR measurement.

Subject Number	EE RR [cal/min]	EE HH [cal/min] (% Error)	EE CS [cal/min] (% Error)	BMR HB [cal/min] (% Error)
1	1007	1038 (+3.1)	NA	1416 (+40.7)
2	893	901 (+0.9)	NA	1362 (+52.6)
3	1017	985 (-3.1)	883 (-13.2)	1577 (+55.1)
4	1108	1104 (-0.4)	1261 (+17.1)	1592 (+43.7)
5	1112	1123 (+1.1)	1178 (+6.5)	1520 (+36.7)
6	1005	1212 (+20.6)	1243 (+21.5)	1207 (+20.2)
7	990	1014 (+2.4)	1024 (+3.0)	1411 (+42.6)
8	1037	1106 (+6.7)	1097 (+6.0)	1507 (+45.4)
9	1475	1495 (+1.4)	1545 (+7.2)	2000 (+35.6)
10	1247	1365 (+9.4)	1543 (+28.6)	1773 (+42.2)
Overall Average	1089	1134 (+4.2)	1222 (+9.6)	1536 (+41.4)

The data presented in Fig. 8.10 demonstrate that the HB equation overestimates the energy need for each and every subject. The percentage error is expressed in Table 8.2 (average 41.5 %, range +20.2 to +55.1 %). The female cohort is overestimated by an average of +42.7 % compared to the male group +31.6 %. The HB equation thus does not provide a suitable means of determining the energy needs for the subjects tested in the experiment. The HH device provides a greatly improved estimated for EE.

The largest error in the HB calculations was found for subject 3, with an overestimation of +55.1 %. The failure to predict BMR demonstrates the use of EE measurement in the general population. The BMR for the subject is predicted to be higher than an older subject, with lower BMI (e.g. subject 1). The RR and HH measurements demonstrate the EE of subject 3 is lower than subject 1 and supports the need for a greater understanding of what affects calorific requirements, in cases where height, weight and age and are not the only factors.

The HB equations were developed almost 100 years ago. Although other predictive equations have been developed since the Harris and Benedict's report in 1918, the HB equation is still one of the most widely used [17]. It has been reported the HB equation can produce significant variance compared to measured EE [18]. Furthermore, it has been reported that the r^2 value reported in the Harris Benedict article (and other articles reporting novel predictive equations) did not exceed 0.70 [19]. Overestimates in the range of +30 % have previously been reported [20]. It has been suggested that body composition has changed a great deal since 1919, when the HB equation was first derived.

8.3 Smartphone EE Measurement

The principle of EE measurement in a free-living environment was tested using the hand-held breath analyser and the associated application on a smartphone. A block diagram for the measurement procedure is shown in Fig. 8.11. Subjects were asked to breathe normally through the hand-held instrument, wearing a face mask. The application provided EE measurements for each 1 minute sample provided. Two measurements were taken for each use of the device, with the first discarded to allow the user to become familiar with breathing through the apparatus.

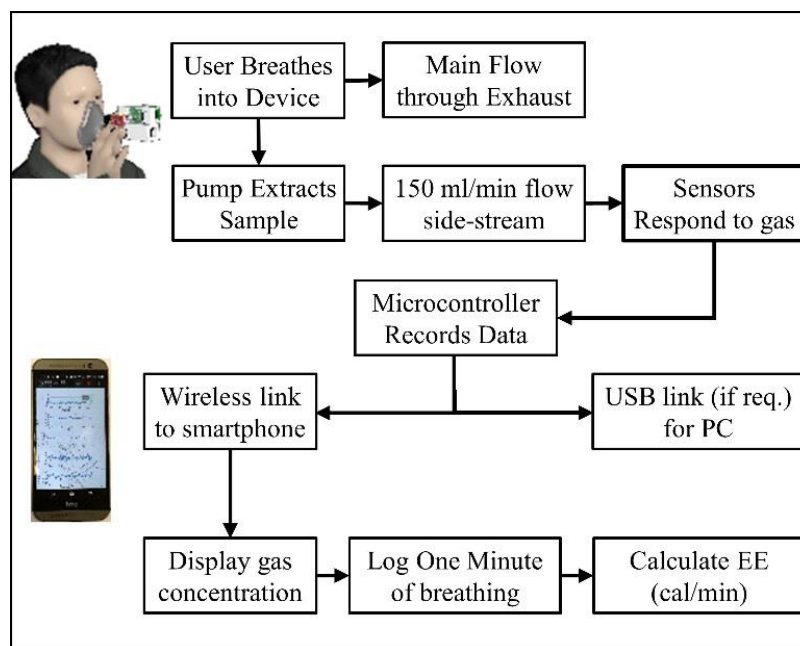


Fig. 8.11 – Block diagram for operation of the hand-held measurement device with a smartphone application.

The O_2 and CO_2 sensor calibrated outputs are shown for two subjects in Fig. 8.12 a) and b). The O_2 sensor is shown again to provide a larger response (trough of 15 % compared to 17.2 %) when a subject breathes slower through the instrument.

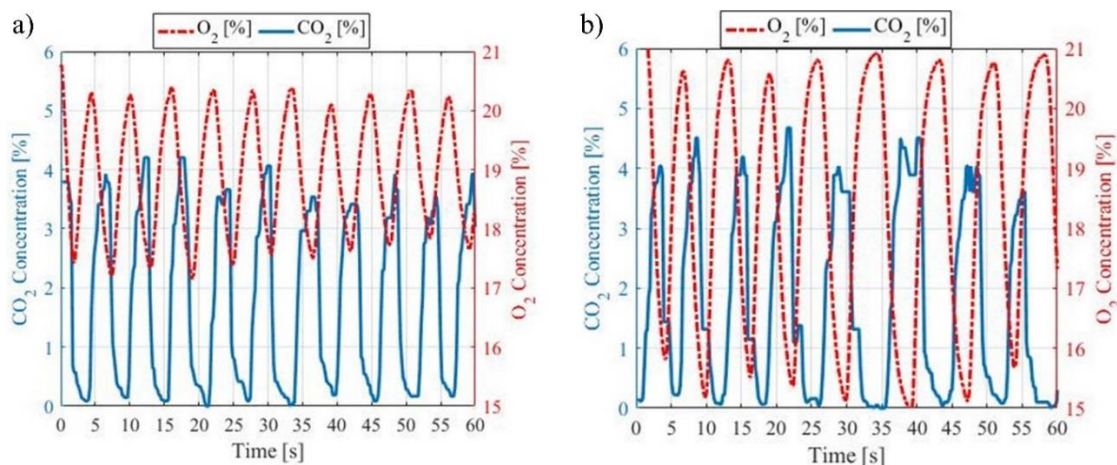


Fig. 8.12 – Concentrations of O_2 and CO_2 recorded over a 1 minute period for a) One subject with a respiratory rate of 10 breaths per minute; b) Second subject with a respiratory rate of 8 breaths per minute.

The data logging process (200 Hz) on the smartphone application does not affect the operation of the portable unit. The application records the outputs for the CO_2 , O_2 , temperature and RH, VOC and flow sensors. The CO_2 sensor is less affected by the breathing rate of the subject; a similar level ($\sim 4\%$ peak in exhaled CO_2 concentration)

is reached in the case of both subjects. The initial laboratory tests of the side-stream analyser demonstrated additional noise ($\sim 0.2\%$) with a slower breathing rate, as again visible in Fig. 8.12 b).

The data logging screen on the smartphone is shown in Fig. 8.13 a). A countdown of 5 s is initiated when the user presses the red ‘B’ icon. During the breath sampling period a red bar across the top of the screen indicates the progression towards the end of the period. After 60 s, the data logging stops and a message is shown on the screen, Fig. 8.13 b), to inform the user of their EE measured during the one minute period.

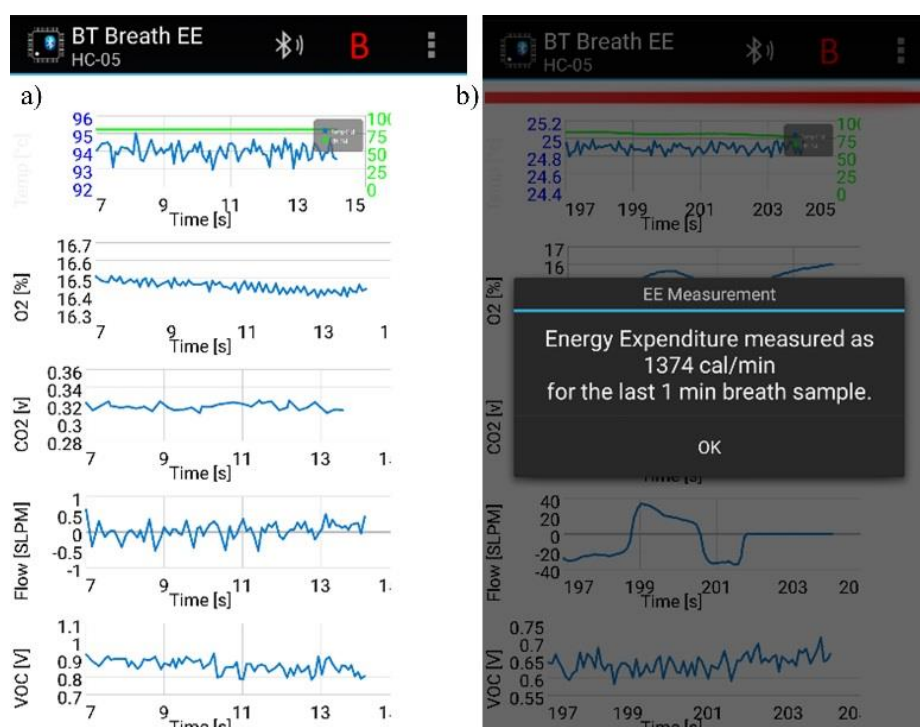


Fig. 8.13 – Screen prints from Android smartphone showing the companion EE measurement application for the hand-held analyser, a) Data logging screen; b) EE measurements performed over a 1 minute period.

The data recorded over a 6 hour period (10 am to 4 pm) for one subject is shown in Fig. 8.14. The subject used the device during a sedentary office day (desk-based work), with a meal indicated in the plot. A light form of exercise is indicated in the activity period, where the subject walked for approximately a 1 hour period, including climbing several flights of stairs.

The output from the smartphone application in Fig. 8.14 demonstrates the challenge of performing EE measurements in a free-living environment. The two lowest

measurement points (11:00 and 16:00) are most likely to be close to sedentary EE. The peak EE is measured after the activity phase (15:00). There are two peaks in EE prior to eating (12:00 and 13:00) which would not be expected for the routine noted. The office-based work involves a higher level of activity than was requested of subjects in the respiratory chamber measurements above.

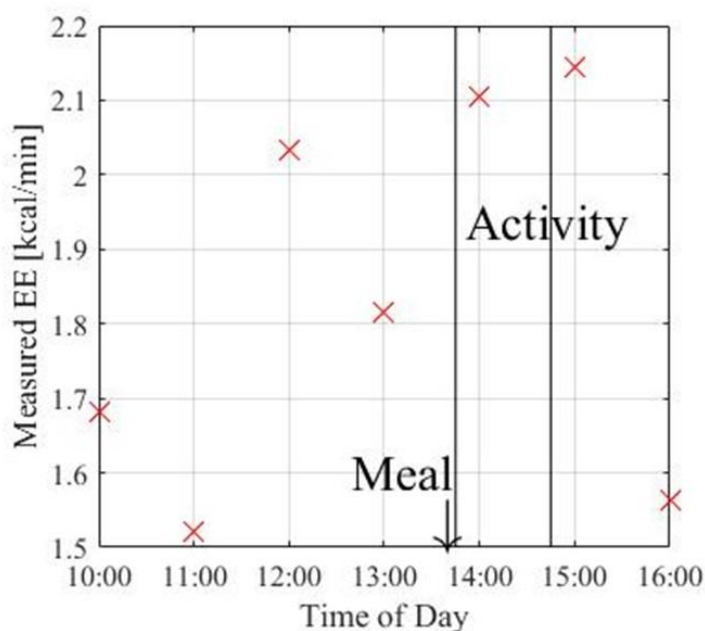


Fig. 8.14 – EE recorded over a 6 hour period for one subject. Measurements taken at 1 hr intervals during an office-based day. One period of activity shown between the vertical time lines and the meal time is indicated with arrow.

The spuriously high EE measurements could be caused by a burst of activity (such as moving from a sitting position to standing). The subject was requested to remain seated while taking the EE measurements, but also it was requested that the measurements be taken hourly. The large variance in EE (0.65 kcal/min) between the readings is likely due to the lack of a strict protocol. For these measurements, the subject was allowed to perform their daily activities, without compromising on food/drink consumption or being asked to remain seated for a fixed time (e.g. 10 min) before commencing a measurement.

The one day experiment demonstrates the possibility of the hand-held device to research EE within a free-living environment. Such measurements are only possible with a portable, quick and robust device. The flexible measurement protocol did not allow the individual components of EE to be tested. Of particular interest is diet

induced thermogenesis (DIT), which is shown as a small increase in EE after consumption of a meal. The energy cost of the activity period was also not assessed for the short measurement period.

8.4 Conclusions

The EE measurement capability of the hand-held devices was assessed against a whole body calorimeter and a breath analyser with commercial sensors. One hand-held portable device was also tested in a free-living environment using a smartphone to record the EE from one subject. Ten subjects (6 female) were tested inside whole body calorimeters for a 3 hour period. At 20 min intervals the subjects were asked to breathe through the portable analysers for a 3 min period.

The measurements of EE were found to be unreliable initially for the first 3 subjects, with some samples discarded due to the subject not holding the mask to their face correctly. An improved training procedure for later subjects mitigated this problem. The subjects were asked to remain in a seated position, with minimal movement for the duration of the experiment. The subjects adhered to this protocol, although a variation in O₂ and CO₂ measurements was recorded overall for the chamber sensors. The variance is due to the subjects occasionally moving inside the chamber.

The volumes of O₂ and CO₂ measured with the hand-held units had a range of 185.2 to 307.7 ml/min and 155.2 to 249.6 ml/min, respectively. The hand-held device on average overestimated the O₂ consumption of the subjects by 3.4 % compared to 5.4 % for the CO₂ production. The electrochemical O₂ sensor produced a stable and reliable output, but required cross-correlation to the flow sensor data (2 s delay found) for the volume of gas exhaled to be calculated.

The commercial paramagnetic O₂ sensor produced an inaccurate and unreliable response (O₂ consumption overestimated by +9.0 % on average). The STD for the sensor was found to be on average 32.2 ml/min. The commercial NDIR CO₂ sensor performed well, with an average error of -0.50 % (but had a higher variance, STD of 24.0 ml/min). The poorer performance of the hand-held sensor was due to the slow drive signal (5 Hz), which limited the signal processing that could be performed on the sensor output.

The hand-held units produced good results for EE calculations compared to the reference standard respiratory rooms. The EE error range (-31.5 to +207 cal/min) was superior to the error found with the analyser using commercial sensors (-133 to +296 cal/min). One subject was excluded, due to not feeling comfortable with the apparatus; on average, for the remaining 9 subjects, the EE was overestimated by +2.4 %. The results were compared to the Harris-Benedict equation, which overestimated energy need (BMR on average was overestimated by 41.5 %, with no improvement for the male or female groups).

The portability of the device was utilised when EE measurements were performed in a free-living environment over a 6 hour period. Hourly measurements of EE were taken for a subject in an office-based job. A large variance in EE was found (0.65 kcal/min), which could not be explained by meal consumption or by a conscious increase in activity. The measurement protocol needs to be revised for future work, to allow the daily energy needs of subjects to be assessed.

Future work needed involves investigating the components which contribute to total daily EE. The component of DIT is of particular interest, to view the energy cost of digesting food. The wealth of experiments possible with a quick and easy to use portable device has yet to be realised.

8.5 References

- [1] R.C. Schulman, J.I. Mechanick, Metabolic and nutrition support in the chronic critical illness syndrome., *Respir. Care.* 57 (2012) 958-77–8. doi:10.4187/respcare.01620.
- [2] K.R. Westerterp, Diet induced thermogenesis., *Nutr. Metab. (Lond).* 1 (2004) 5. doi:10.1186/1743-7075-1-5.
- [3] Montana State University, Food Processing Takes Time, *Sport. Nutr.* (1998). <https://web.archive.org/web/20160225083056/http://btc.montana.edu/olympics/nutrition/eat09.html> (accessed February 25, 2016).
- [4] S.A. Haslam, C. McGarty, *Research Methods and Statistics in Psychology*, 2nd Ed., SAGE Publications, Los Angeles, U.S., 2014.
- [5] L.M. Sullivan, *Essentials of Biostatistics*, Jones and Bartlett Publishers, Sudbury, U.S., 2008. doi:10.1017/CBO9781107415324.004.
- [6] H.M. Bush, *Biostatistics: An Applied Introduction for the Public Health Practitioner*, Cengage Learning, New York, U.S., 2011. doi:10.1017/CBO9781107415324.004.
- [7] R.C. Elston, W. Johnson, *Basic Biostatistics for Geneticists and Epidemiologists: A Practical Approach*, Wiley, Chincester, U.K., 2008.
- [8] A. Bryman, D. Cramer, *Quantitative Data Analysis with Minitab: A Guide for Social Scientists*, Taylor & Francis, London, U.K., 2003.
- [9] D. Shaw, *One Stop Doc Metabolism & Nutrition*, CRC Press, London, U.K., 2012.
- [10] R. Gomm, *Social Research Methodology: A Critical Introduction*, 2nd Ed., Palgrave Macmillan, London, U.K., 2008. doi:10.1017/CBO9781107415324.004.
- [11] M. Ng, P. Liu, B. Thomson, C.J.L. Murray, A novel method for estimating distributions of body mass index, *Popul. Health Metr.* 14 (2016) 6. doi:10.1186/s12963-016-0076-2.
- [12] R. Lustig, *Obesity Before Birth: Maternal and prenatal influences on the offspring*, Springer US, New York, U.S., 2010.
- [13] J.K. Ehrman, *Clinical Exercise Physiology*, Human Kinetics, Champaign, U.S., 2009.
- [14] P. Barash, *Clinical Anesthesia*, 6th Ed., Lippincott Williams & Wilkins, Philadelphia, U.S., 2009.
- [15] G.C. White, I.F. Rate, *Basic Clinical Lab Competencies for Respiratory Care: An Integrated Approach*, Cengage Learning, New York, U.S., 2012.
- [16] A.M. Knab, R.A. Shanely, K.D. Corbin, F. Jin, W. Sha, D.C. Nieman, A 45-minute vigorous exercise bout increases metabolic rate for 14 hours, *Med. Sci. Sport. Exerc.* 43 (2011) 1643–1648. doi:10.1249/MSS.0b013e3182118891.
- [17] S.A. McClave, H.L. Snider, Use of indirect calorimetry in clinical nutrition,

-
- Nutr. Clin. Pract. 7 (1992) 207–221. doi:10.1177/0115426592007005207.
- [18] X. Xian, A. Quach, D. Bridgeman, F. Tsow, E. Forzani, N. Tao, et al., Personalized Indirect Calorimeter for Energy Expenditure (EE) Measurement, *Glob. J. Obesity, Diabetes Metab. Syndr.* 2 (2015) 4–8.
- [19] M.M. Gottschlich, *The Science and Practice of Nutrition Support: A Case-based Core Curriculum*, Kendall Hunt, 2001.
- [20] J. Sharlin, S. Edelstein, *Essentials of Life Cycle Nutrition*, Jones & Bartlett, Sudbury, U.S., 2011.

CHAPTER IX

Conclusions and Further Work

Preface

A hand-held unit capable of EE measurement both in a laboratory environment and free-living has been developed. The device, comprising affordable and miniature gas sensors, meets the project aims to create a robust system for wide-spread adoption. The unit was already successfully tested with 10 subjects, who were able to use the unit with only minimal training. The hand-held unit samples breath through a side-stream system, developed after preliminary testing showed that accurate measurements of gas concentration could not be made in the mainstream tubing. A VOC sensor was developed as an add-on module for the system, although this has not undergone testing with exhaled breath. The VOC sensor was tested on a laboratory gas testing rig, to low ppm and ppb concentrations of acetone and NO₂ respectively. Further work involves increasing the capability of the breath analyser and investigating the component of EE associated with digestion, to meet the aim of detecting a 1 % change in EE.

9 Project Conclusions

A hand-held analyser capable of determining human EE has been developed through the measurement of exhaled breath samples. The device was trialled on 9 subjects and measured EE to an accuracy of 2.4 % compared to reference respiratory room data (1 subject excluded due to discomfort). The device included sensors for CO₂, O₂, temperature and relative humidity, flow and a semiconductor VOC sensor, which was not utilised during the EE measurement tests.

In the prototyping phase of the project, a mainstream analyser was constructed (see chapter IV). The unit was used to investigate the capability as of selected CO, CO₂, O₂ and temperature and humidity sensors. The analyser was not developed into an instrument capable of human EE due to the available sensors being unsuitable for direct mainstream sampling (excessive peak 30 L/min flow rate, extreme temperature and humidity change (ambient to ~36 °c and almost 100 % saturated). The development of a hand-held measurement tool continued in the form of a side-stream design analyser.

Sensors considered for VOCs and CO₂ were found to be incapable of sampling breath in real time (chapter III). The commercial MOX sensors tested offered poor performance (not capable of ppb measurements) for the compounds of interest on an exhalation. The affordable CO₂ NDIR commercial sensors were found to have poor response times (>20 s for SprintIR) and a high level of noise (0.1 % CO₂ readout). Novel sensors for VOCs and CO₂ were therefore developed to meet the needs of this project.

9.1 Human Energy Expenditure

The hand-held device was developed in part to help increase the awareness of calorific intake. The information provided by the NHS in the UK, discussed in chapter I, advises that the daily calorie intake for men should not exceed 2,500 kcal and 2,000 kcal for women [1]. These guideline figures are representative for the population included in our test cohort. The average EE for 5 female subjects, measured using the hand-held analyser, was 1,009 cal/min (excluding one subject due to discomfort). The average EE for 3 male subjects was 1,241 cal/min (excluding one subject, with high BMI above the normal and overweight ranges).

In basic terms, to maintain a certain body weight, calorific intake must equal calorific need, i.e. total daily EE must equal total calorific intake [2] (details in chapter I). The resting metabolic rate component of total daily EE contributes approximately 60 to 70 % of the overall daily expenditure [3–5]. For the measurement protocol adopted inside the respiratory room, a value of 70 % can be assumed, given the subjects were sedentary in a seated position (i.e. not resting on a bed in a supine position). The values of EE measured for male and female subjects can be extrapolated for a 24 hour period to give an average energy requirement of 2,553 kcal and 2,075 kcal per day (to maintain the same body weight), respectively. The values calculated are similar to the recommendations from the NHS UK, with a variance of +53 kcal for men and +75 kcal for women. A larger sample size, with a greater range of ages (particularly for the age group over 50 years old) would improve the potential of EE recommendations that could be drawn from the work.

The range of EE found for the male and female subjects in the human experiments demonstrated the need to assess energy requirements on an individual basis. The range of EE values across 5 female subjects (901 cal/min to 1106 cal/min) could not be explained by BMI and age. The Harris-Benedict equation was used as a benchmark comparison, as it is reported that the equation is used in clinical situations, where indirect calorimeters are rarely available [6]. The EE of one subject was overestimated by 55.1 % by the equation. This error was likely introduced as the subject had a BMI classified as ‘overweight’ but a low EE (1017 cal/min reference respiratory room value, 985 cal/min measured by the hand-held analyser and 1577 calculated with the equation).

9.2 Portable EE Measurements

The smartphone application developed in this work enabled the use of the hand-held analyser outside of the laboratory environment (chapter VI). A wireless (Bluetooth) link negated the need for a wired (USB) connection and increased the compatibility with almost any Android Bluetooth enabled smartphone. The technology was suitable for this application, where the data transfer speeds enabled a high rate of sampling (200 Hz) and with a useful range (~10 m) for taking measurements when subjects were isolated in the respiratory rooms.

In chapter II, alternative techniques of measuring EE using portable equipment were investigated. Methods, such as activity and heart rate monitoring, were noted as being suitable for quantifying if vigorous activity was performed during a given day, however did not provide clinically acceptable EE information. The doubly-labelled water technique offers EE tracking without the need for any equipment while the experiments are being performed in a free-living environment. The technique is expensive and invasive, so cannot be considered for use in the general population.

The portable EE measurement unit developed in this thesis was subjected to testing outside of a laboratory setting. The results for one subject were presented over a one day period in an office-based environment. The subject was asked to take hourly measurements for a duration of 6 hours. The lowest level (perhaps resting) EE was measured as 1.53 kcal/min. A large EE variance was notable in the output from the device (0.65 kcal), caused by the lack of a strict measurement protocol. The subject was asked to maintain their normal daily routine, but return to a seated position to make the EE measurements. The subject was not asked to rest (e.g. sit still for a period of 10 min) prior to making the measurements. The activity, if any, performed immediately before taking the measurements would have a significant influence on the outcome.

The affect of eating and activity on a daily routine are less visible, due to the variance in the EE readout during the sedentary periods of the day. Furthermore, a meal was consumed within 15 min of the activity (walking and climbing stairs), thus the effect of each individual component cannot be identified. The peak EE calculated was 2.15 kcal/min following the activity period, with a high value recorded (2.1 kcal/min) after consuming the meal and ~10 min after starting the activity session.

9.3 Achievements

The aims of this work were detailed in chapter I. A device was successfully developed that was capable of human EE measurements. The measurement period was reduced to 1 min for the mobile measurements (although 1 min was allowed prior to each measurement for familiarisation). The unit did not require any storage of gases, and was able to measure the O₂ and CO₂ concentrations on a breath-by-breath basis.

The robustness of the unit over a long term period was not assessed, however the robust ABS housing protected the internal sensor components during the subject

testing phase (construction details in chapter VII). The unit can be held comfortably in one hand ($150 \times 75 \times 60$ mm) but cannot be classified as miniature. The internal housing for the gas sensors ($85 \times 55 \times 30$ mm) is the major component inside the unit. The width of the main-stream tubing (20 mm) prevents a small chamber being developed. The side-stream extraction tube was positioned 70 mm from the main-stream exhaust, to prevent any undesired mixing of ambient and exhaled gases. A smaller length of main-stream tubing would reduce the size of the hand-held unit, but with the increased risk of a pure sample of exhaled gas not being extracted.

The sensors inside the unit did not require regular replacement and one set of sensors was used for the testing of 5 subjects (per device) in the respiratory chambers. The sensors were calibrated both pre- and post-measurement. The O₂ sensors (City technology MOX-20) did not exhibit a high level of drift (< 0.05 V, average output 0.7 V) that can be associated with aging electrochemical cells, although the test period (< 1 month) was shorter than the life-span of the devices (> 12 months). The prototype CO₂ sensor was susceptible to a higher level of drift between experiments (~ 0.5 % CO₂). The effect of the drift was mitigated by calibration. The baseline shift could be illuminated by considering the initial sensor output as being in ambient conditions (0 % CO₂).

The device was easy to use, and most subjects inside the chambers could be left unattended to make their own EE measurements. The improved training for the final 7 subjects enabled every breath sample to be validated (> 80 % of 6 ml/kg tidal volume), where some breath samples were discarded for the first 3 subjects. The critical element was to ensure that the subjects understood the volume of each exhalation was important for EE calculations. Unfortunately, users with glasses had to remove them in some situations, where the mask could not be sealed around their nose and mouth.

The smartphone application was only used under supervision. Once the Bluetooth connection was established, the user needs only to push one button to begin an EE measurement. Instruction material, such as a demonstration video explaining the use of the equipment, would have benefited the user of the instrument. However, the need to breathe naturally and without forcing an exhalation can initially be problematic for some subjects. The data logging applications were not personalised to individuals. To

help take accurate resting EE measurements, the application could take user data (e.g. weight) to calculate the expected tidal volume per breath. In post-data collection analysis, for the first two subjects where heavy breathing occurred occasionally, the periods of breathing outside of the expected range (e.g. between 6 and 8 ml/kg body weight) were removed. This prevented distortion of the calculated EE due to erroneous measurements.

The device was in general easy to use, although as discussed above in the smartphone section, the need for a consistent environment between measurements is difficult to enforce with the user in a free-living environment.

The prototype testing in this project only consisted of resting EE comparison experiments. The potential to measure a 1 % change in EE was not assessed. Further work is needed to attempt to measure the DIT component (energy cost of food digestion). DIT only contributes a small percentage (~8 %) of total daily EE and, dependent on the food consumed, can only be measured for a few hours (~ 4 to 8 hours) after consuming a meal [7].

The units developed in this project were compared to a reference respiratory room configuration and analysers consisting of commercial O₂ and CO₂ sensors (10 subjects tested). Considering an average of 10 measurements taken over a 3 hour period, the EE was overestimated by +4.2 %. The unit with commercial sensors overestimated EE by +9.6 % on average. The Harris-Benedict equation was found to perform poorly, and overestimated EE by +41.4 % on average. The overestimation could in part be due to the subjects breathing too heavily into the device, as EE was found to fall during the experiments for some subjects. The overall average EE measured by the respiratory rooms was 1089 cal/min. The range of EE measured (0.9 to 1.5 kcal/min) was lower than average values previously reported by Knab et al. (1.3 to 2.5 kcal/min), although the subjects in the experiments in this project were asked to refrain from making extensive movements during the experiment [8].

The RMR measured by the handheld devices compared favourably to the typical values of reported in the literature. Men are expected to have a basal energy need of slightly >1 kcal/min (1.1 to 1.3 kcal/min range) and women slightly <1 kcal/min (0.8 to 1.0 kcal/min) [9]. The 10 measurements limit the analysis of different groups of the population (e.g. age, gender, ethnicity etc.) but demonstrate the excellent

reproducibility of the handheld units, both in terms of biological and sensor performance.

The sensor system was designed on a modular basis. Some parts (e.g. connectors, exhaust, CO₂ holder and VOC holder) were rapid prototyped to enable unique structures to be formed, which it was not possible to create using the base material of POM.

9.4 Further Work

The sensors developed during this work are part of an ongoing process to develop sensors capable of mobile sensing. There is growing need in the sensor industry for sensors that can be used in mobile phones, remote locations and portable applications. The miniaturisation of sensors, with reduction in power consumption and cost, enables the use of devices outside of a laboratory. The novel NDIR sensor discussed previously forms a base for expanding into detecting lower concentration gases and a wider range of compounds with a miniature sensor system.

9.4.1 MOX VOC Sensor

The development of a MOX VOC sensor offers the possibility to detect various diseases (e.g. asthma, COPD) from a breath sample. Furthermore, VOCs on the breath could help further understand the metabolism processes that occur in humans (discussed in chapter III). In general, the response times of MOX sensors (> 30 s) limits their use in breath-by-breath work. The importance of a fast response time is useful for breath-by-breath analysis, as well as being able to provide instantaneous results, without the need to store gas.

9.4.1.1 MOX Hotplate Temperature

The temperature at which the hotplate on a MOX sensor operates defines the sensitivity of the device and the response time. It is usual to operate the hotplate at constant temperature, although further work could investigate pulsing the heater between two temperatures. This would reduce power consumption and could potentially reduce response times (with additional signal processing of the transition periods between the two temperatures).

A trade-off has to be made between the sensitivity of the sensor, which is usually higher at lower operating temperatures, and the response time (which is usually lower

at higher operating temperatures) [10], stability of the sensor can also vary depending on the configured temperature. Preliminary work was performed to view the effect of varying operating temperature on the sensitivity of the sensor. The sensor was exposed to 50 ppb NO₂ and the sensitivity calculated at different hotplate temperatures, as shown in Fig. 9.1 a). The corresponding plot with response and recovery times plotted for operating the sensor at 250, 300, 350, 400 and 450 °C is shown in Fig. 9.1 b).

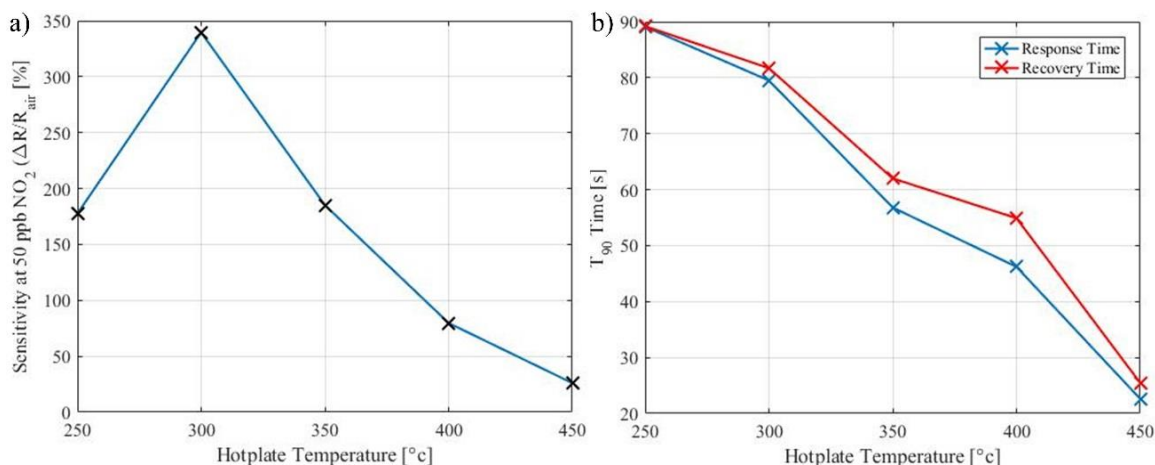


Fig. 9.1 a) Average sensor response time as a function of temperature for 50 ppb of NO₂ in 50 % RH diluted with synthetic air; b) Corresponding response and recovery times in the same conditions.

The temperature at which a MOX sensor operates must be tailored to the application requirements. In the case of NO₂ sensing the device shown in Fig. 9.1 has highest sensitivity at 300 °C, however slow response and recovery times (~ 80 s). The recovery time is longer than the response time regardless of constant hotplate temperature. For the application of breath sampling the hotplate temperature was fixed at 350 °C, with reasonable sensitivity (~180 %) and acceptable response and recovery times (< 60 s). The response and recovery times are shown as the time taken for the response output to reach 90 % of its final value. The operating temperature of 350 °C has previously been reported for WO₃ MOX sensors, although a slower recovery time (2 min) was specified [11].

The sensor must be annealed at a temperature higher than the desired operating temperature, to ensure high stability. It is suggested that the reason for the sensitivity of devices varying with temperature is due to the grain size of the oxide material [12]. Fine particles have been reported as offering increased sensitivity (at temperatures in the range of 250 to 350 °C) [13]. The temperature dependent sensor response is

affected by other factors, both chemical and physical. Adsorption and desorption are temperature-activated processes, thus dynamic properties of the sensor depend exponentially on the temperature (recovery and response times) [14]. Temperature also has an effect on the surface coverage, co-adsorption and chemical decomposition which result in different static characteristics at different temperatures. The true relationship between the surface temperature of a MOX sensor in the presence of reducing gases and the conductance of the device make a very complex relationship [15].

9.4.1.2 MOX Sensor Coating

SnO₂ has been a material of interest for many years, but recently the interest in other compounds such as WO₃, Ln₂O₃ and TiO₂ (titanium dioxide) has been growing [16]. A number of factors have been identified as contributing towards the response of MOX sensors: grain size, surface morphology, microstructure, defect density and distribution, porosity, crystallinity and chemical composition [17]. It has been found the conductivity varies inversely with the charge density. The presence of oxygen vacancies, which act as electron donors in n-type semiconductors, determines the electronic properties of the film.

Further work is required to investigate MOX sensor coatings. Preliminary tests were performed with WO₃ (New Metals and Chemicals Ltd) coated sensors (without additional doping). The coating was mixed and deposited by Dr. B. Urasinska-Wojcik, University of Warwick. Results are presented below for the sensors. Further investigation is required to verify if the sensitivity of the sensor can be increased by mixing of small quantities of noble metal dopants with the WO₃ layer [17]. The dopant functions as a catalysis to the electrochemical reactions occurring in the film. The stability of the film can also be improved. In some cases two metal oxides can be combined to enhance the benefits of multiple sensing materials. For example, Pt and calcium oxide (CaO) have been added to SnO₂ sputtered films to increase both the sensitivity and stability (consequently reducing the recovery time) [18]. A Scanning Electron Microscope (SEM) photograph of the WO₃ material deposited on the MEMS sensor is shown in Fig. 9.2.

The SEM photograph demonstrates the porous nature of the thick film covering. In porous layers each grain possesses a surface depleted area and current has to pass

through the intergranular contacts [19]. The sensor will only operate at the best possible performance for a given MOX material if the layer is correctly deposited. The thickness of the layer depends on the viscosity of the paste and the subsequent annealing process [16]. In the case of the sensors presented in Fig. 9.6, the film was left to dry for 12 hours post-deposition and then the sensor was set to be annealed at 450 °C for 1 hour, followed by 23 hours at 350 °C.

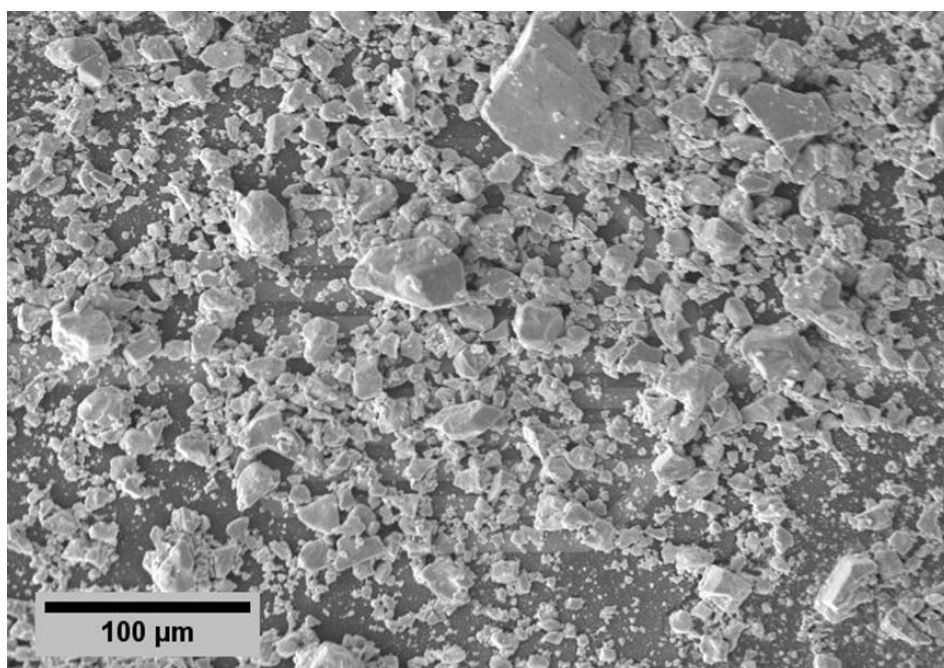


Fig. 9.2 – SEM photograph of surface deposition of WO₃ material onto the sensor surface at 250× magnification. Coating manufactured and deposited courtesy of Dr. B. Urasinska-Wojcik, University of Warwick.

9.4.1.3 NO₂ Experimental Results

Results are presented here for the detection of low concentrations of NO₂, thus allowing the improvement upon the commercially available devices to be demonstrated (which target NO₂ measurement applications). Further work involves testing the sensor to other VOCs found on breath. The WO₃ coating used in the sensors discussed in this section provided excellent stability and has great, but not fully explored, potential to detect biomarkers on exhaled breath.

The gas testing experiments were performed on a gas testing rig – operation described in chapter VI. The rig allowed for gas mixtures of NO₂ and CO to be generated, diluted with synthetic air in both dry and humid conditions. The flow rate was kept constant

at 1 SLPM throughout each experiment. The sensor was housed in an aluminium chamber for the experiments, with a dead volume of 6 ml. For presentation of the results, the sensor response (S) is defined as the ratio of the sensor resistance R_{NO_2}/R_{air} , where the subscript denotes the gas exposed to the sensor (i.e. a mixture of NO_2 or pure synthetic air). The sensor resistance is the resistance of the device coated with the tungsten oxide film, calculated from the potential divider relationship show in Fig. 3.20. The measurements were all performed at ambient room temperature (24 °C) and the micro hotplate heater set to 350 °C.

The sensor was compared to a reference commercial sensor (SGX Sensortech MICS-2714), designed for NO_2 sensing (range specified in the range of 0.05 to 10 ppm) [20]. The commercial device was tested in the same conditions as the prototype NO_2 sensor. The heater temperature was not specified by the manufacturer, but the instructions of its operation were followed from the datasheet (unpublished document). The sensor was tested with the NO_2 prototype sensor in both dry and 25 % RH conditions, with gas concentrations ranging from 10 ppb to 250 ppb (5 min steps for each concentration, as shown in Table 9.1, returning to a baseline of synthetic air for the same period). The sensor has been reported on in the following publication [21]. The time-dependent response of the sensor is shown in Fig. 9.3 a), in dry conditions, and the sensitivity as a function of the concentration shown in b).

Table 9.1 – Gas Concentration steps of NO_2 tested with the MOX sensor.

Step	NO_2
	Concentration [ppb]
A	250
B	100
C	50
D	25
E	10

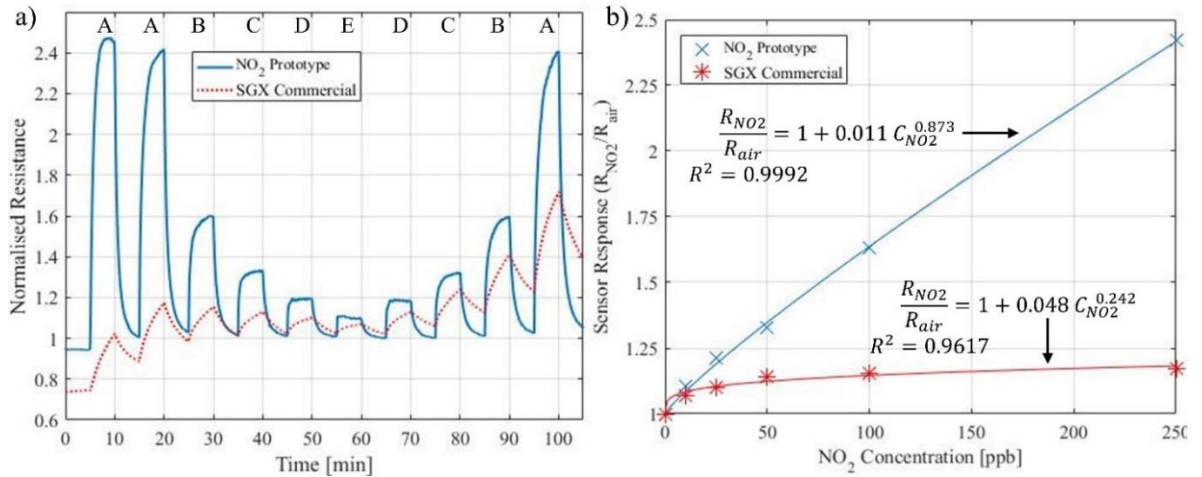


Fig. 9.3 – Response of the sensor to NO₂ in dry conditions, a) plotted as a function of time and b) sensitivity against concentration.

The initial concentration step (250 ppb) is repeated twice at the start of the experiment. This is to allow the sensor to stabilise. The baseline resistance is initially lower prior to the first concentration step. Post the initial step the baseline stabilises, which is an affect expected of MOX devices. The phenomenon is visible on both the commercial reference and prototype NO₂ sensors. The sensor was also tested in conditions of 25 % RH and 50 % RH, as shown in Figs. 9.4 and 9.5.

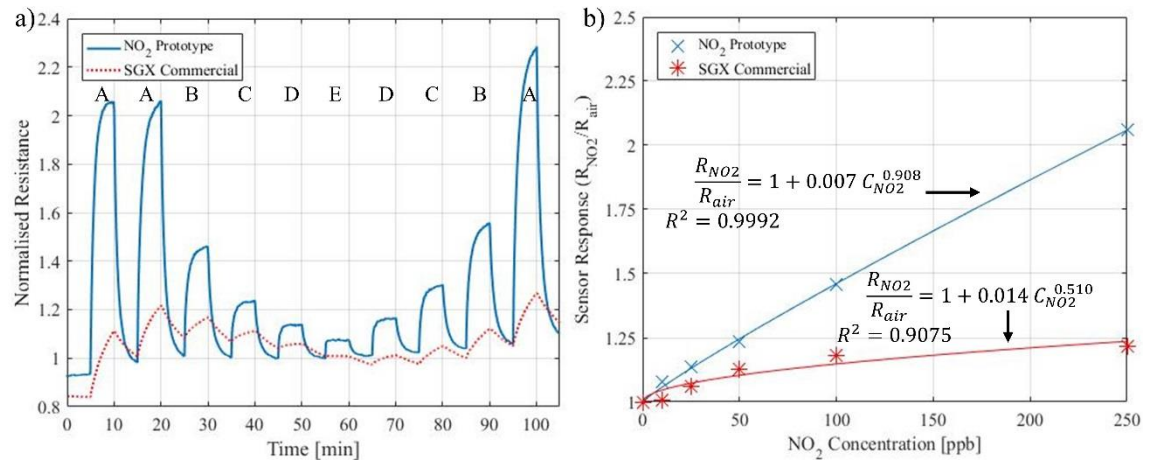


Fig. 9.4 - Sensors tested in 25 % RH conditions, a) response time plot shown and b) sensitivity.

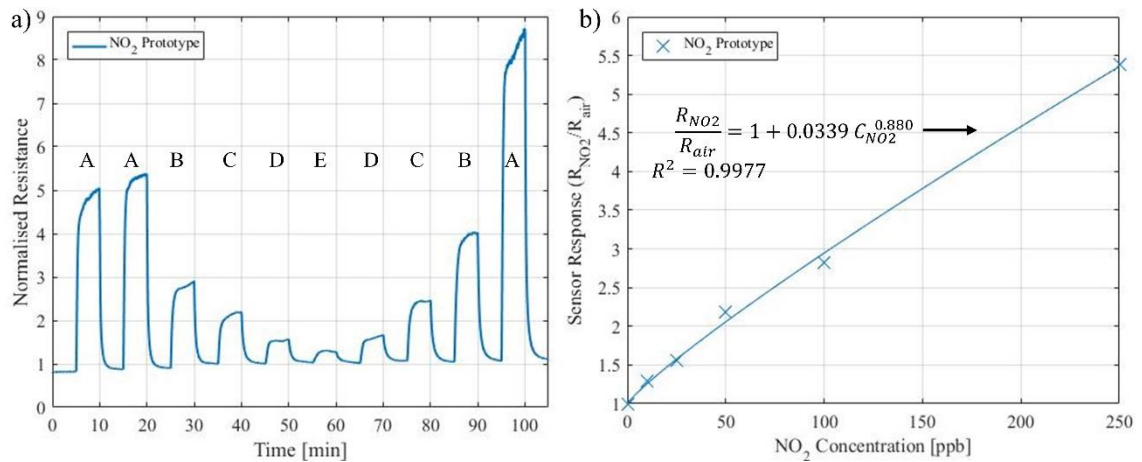


Fig. 9.5 - Sensor tested in 50 % RH conditions, a) response time plot shown and b) sensitivity.

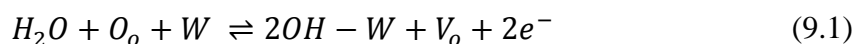
The resistance increases for both sensors in the presence of NO₂. This is the expected response for an n-type device (for an oxidising gas). For each experiment shown in Figs. 9.3 b), 9.4 b) and 9.5 b) the law expressed in (3.7) is fitted to the response. The value of exponent β is close to 1 in all cases, suggesting that the chemisorbed surface oxygen species are in a negatively charged state. The power law was found to produce an excellent comparison to the prototype sensor output (R^2 goodness of fit test equalling 0.992 in dry and 25 % RH conditions and 0.9977 in 50 % RH).

The response of the prototype sensor improves at higher humidity, with a response of magnitude 2.4 and 2.06 in dry and 25 % RH conditions compared to a magnitude of 5.4 (normalised response) in 50 % RH. Although dry conditions are often used as a benchmark for comparing sensor performance, MOX sensors are not particularly suited to 0 % RH. The lack of any water vapour in the air can cause the sensing layer to dry out, and then the sensor can become damaged and unresponsive. The common recommended minimum level is 5 % RH [20], although in the case of the sensor developed in this work, the device was found to operate with good sensitivity even in dry conditions. In the case of breath analysis, the level of humidity is extremely high, although for some applications (combustion sensing) low humidity operation could be advantageous.

The SGX Commercial sensor performs poorly in all of the trials performed against the prototype device. The device is specified as being capable of detecting 100 ppb NO₂, however although a step change in resistance is visible, it does not produce a distinct response during the 5 min steps of 250 ppb or 100 ppb NO₂ gas (250 ppb and 100 ppb

cannot be distinguished). The MICS-2714 does not produce a stable response throughout the duration of the experiment, regardless of RH condition. The large baseline drift and slow response to the presence of NO₂ prevented detection of concentrations less than 100 ppb. The output response does not wholly accurately follow the empirical law (eqn. 9.4), with goodness of fits calculated as 0.9617 in a dry environment and 0.9075 in 25 % RH.

In the experiments presented in Figs. 9.3 to 9.6 there is a decrease in the resistance of the sensor due to the presence of water vapour. The interaction of the water molecules with the WO₃ surface takes place via the electron donating adsorption. The dissociative chemisorption process results in the formation of hydroxyl groups on the thick film surface, a two stage process [22]. The first step is shown in equations (9.1) and (9.2) and the second step in eqn. (9.3). First, the water molecules adsorbed on the surface react with the lattice sites (W). Equation (9.2) demonstrates the relationship between the lattice oxygen at the oxygen site (O_o) and the vacancy created at the oxygen site (V_o). H^+ (from the dissociation of water molecules) reacts with the ionised oxygen (displaced from the lattice) to form the hydroxyl group given in (9.3). Thus, as stated earlier, the resistance of the film decreases, due to the electrons accumulating on the surface [23].



The performance of the prototype sensor is significantly better than both the commercial device and others reported in the literature. The level of NO₂ concentration detected and the response time of the device are superior to previous reports. Su and Peng reported on the fabrication of a room-temperature NO₂ sensor based on WO₃ and reduced graphene oxide nanocomposite films [24]. It was noted that the device exhibited a strong response to low concentrations of NO₂ gas at room temperature and had satisfactory linearity and favourable long-term stability. A micrograph of the film, formed by a metal organic decomposition process at 500 °C, is shown in Fig. 9.6.

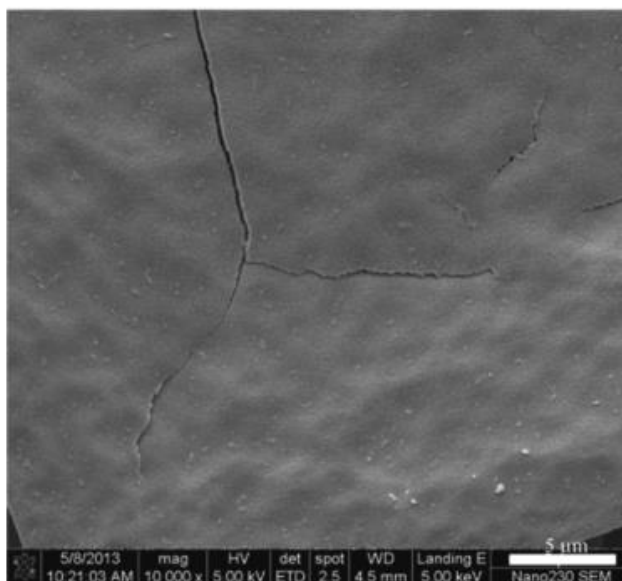


Fig. 9.6 – SEM micrograph of WO_3 film sensor by Su and Peng, fabricated by one-pot polyol process [24].

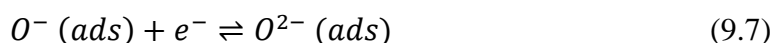
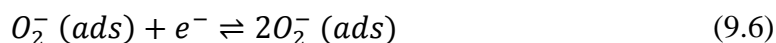
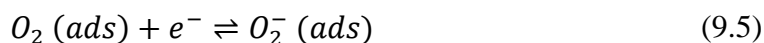
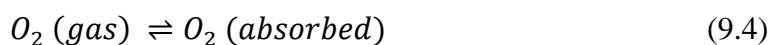
The sensor reported by Su and Peng was tested in NO_2 environments from 0.5 to 20 ppm. The response at 500 ppb was ~ 0.2 , rising to ~ 1700 at 20 ppm. The exposure time was set to a maximum of 10 min, but the sensor did not saturate during that period (10 min was therefore defined as the response time). The recovery time took 18 min at an exposure of 5 ppm. It was suggested that the sensor may be suitable for measuring nitrogen oxides generated by combustion facilities (which are known to be harmful to the human body), although the performance was not exceptional compared to the commercially available devices.

To detect VOCs in breath, the sensor must be able to detect concentration in the ppb range. The improvement made with the prototype gas sensor compared to previous MOX sensors reported in the literature is a high sensitivity for low ppb measurements. Chung et al. reported a maximum sensitivity of 12 to an environment of 100 ppm NO_2 using a thick film WO_3 based sensor [25]. The sensor was fabricated by a screen printing method. The thick film was fired at 700°C and operated at 100°C , from which Chung et al. noted excellent sensor properties (response and recovery characteristics). The response and recovery times were of the order of 100 s, fast considering the low operating temperature. Films fired at 600°C and 800°C were also trialled. The size of the grains and macro pores were found to gradually increase with an increase in firing temperature. Experimental data demonstrates similar response

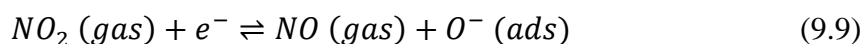
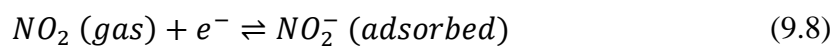
after firing at 700 and 800 °C (and poorer response characteristics at 600 °C), although higher stability was visible for the 700 °C fired films.

The effect of the grain size in WO₃ films on the ability of the sensor to respond to nitrogen oxides gases was reported by Tamaki et al. [26]. The mean crystallite sizes of WO₃ were varied in the range of 16 to 57 nm. Grain sizes between 33 and 57 nm were found not to affect sensitivity significantly. A sharp increase in sensitivity was observed for grains smaller than 33 nm, where the sensitivity more than doubled for a grain size of 25 nm to 5 ppm NO₂ (*S* of 18 compared to 46). Crystalline sizes below 25 nm were found to be of comparable sensitivity to those of 33 nm size. In the sensors developed in this work, these remarkable characteristics were likely achieved due to comparatively small grain sizes. The reduced size allows for greater surface area, and increases the likelihood of the grains to absorb oxygen to form ionised species. The sensing WO₃ layer is several μm thick, which has a porous structure. The diffusion of NO₂ into the sensing body enables the process to reach the inner film, where the interdigitated electrons are located.

Xia et al. reported on NO₂ sensor powders fabricated by a colloidal chemical method. The crystalline particles constructed from WO₃ doped with gold were formed at around 28 nm size [27]. The doping weight was investigated (0.25, 0.5, 1.0 and 1.5 wt%) to NO₂ gas at 10 ppm concentration. The maximum response was found at 150 °C for 1.0 wt% doped WO₃ (400 %). The optimal response to acetone was noted as being at 200 °C. The intrinsic conductance of WO₃ increases with increasing temperature. The adsorbed oxygen molecules transform into oxygen ions by capturing free electrons from the oxide. This process causes a decrease in the conductance of the oxide. The equations (9.4 – 9.7) express this reaction [27][28].



With an oxidising gas, such as NO₂, the gas molecules are adsorbed through weak van der Waals forces (physisorption) and covalent bonding (chemisorption) [28]. The adsorption of NO₂ causes a decrease in conductivity, which can be explained by the reactions expressed in (9.8) and (9.9) [27].



Blo et al. studied WO₃ nano-powders doped with manganese, tantalum and zirconium [29]. The response of the printed thick film sensor was optimal again at 150 °C, regardless of doping material. The grain size varied, depending on doping and annealing temperature; the smallest grains were produced for manganese doped WO₃ (44 to 72 nm). The sensor was almost in-sensitive to CO; the lack of CO response was attributed to the chemisorption sensing mechanism, which is different than for tin oxide sensors. Blo et al. demonstrated the sensor was sensitive to 500 ppb NO₂ and noted the sensors were suited for low temperature operation; the samples were more conductive than tin oxide films by three orders of magnitude at their low operating temperature.

9.4.1.4 Acetone Experimental Measurement

The prototype sensor developed in this work was found to produce a remarkable response to NO₂. The sensor was not rigorously optimised to sense acetone (in terms of hotplate temperature). Elevated concentrations of acetone on breath (> 1800 ppb compared to 300 – 900 ppb, shown in Table 3.7) can be used as a biomarker for type-I diabetes [30]. Breath measurements of acetone could provide a non-invasive means of diabetes diagnosis. WO₃ based sensors have been reported to offer good sensitivity to acetone and the potential to detect acetone in the low ppm (< 2 ppm) range [31].

It has been suggested that an acetone breath sensing unit could be used as a tool to screen patients for diabetes in an economically viable and reliable manner [32]. Real time analysis would allow a quick diagnoses and thus a large numbers of subjects could be tested. It has been reported that the subjects need not fast prior to the measurements, where higher acetone levels were still prevalent in diabetic compared to non-diabetic subjects in conditions of only 2 hours post feeding [32]. The MOX sensor developed in this chapter, demonstrated a stable response to acetone in the range of 100 to 300 ppm (Table 9.2). The normalised resistance response is shown in Fig. 9.7 a) and the sensitivity in b). The experiments were again performed in dry conditions, with 5 min steps for each concentration (returning to baseline of dry synthetic air).

Table 9.2 – Gas Concentration steps of acetone tested with the MOX sensor.

Step	Acetone Concentration [ppm]
F	300
G	250
H	200
I	150
J	100

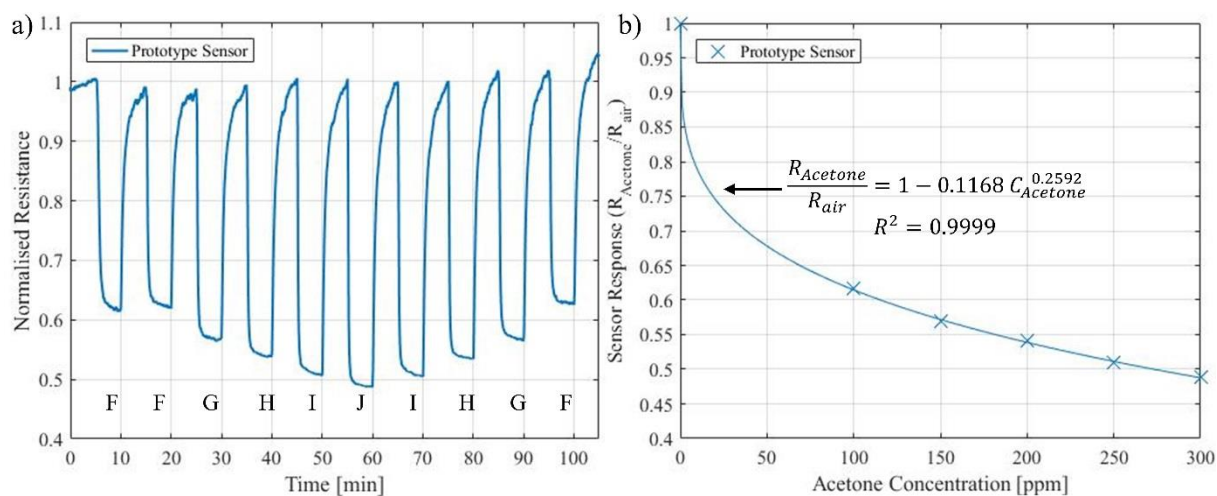


Fig. 9.7 – Sensor tested in acetone 100 to 300 ppm, with a) Normalised resistance plot and b) response plot.

The response to acetone is the opposite to that shown for NO_2 ; when the sensor is exposed to an increase in acetone concentration its resistance decreases. For acetone, $\text{C}_3\text{H}_6\text{O}$, the reducing hydrogen species are bound to carbon. Therefore it is more difficult for the acetone vapour to dissociate into the reactive reducing components in the thick film surface. An electron is released back to the conduction band when acetone vapour reacts with the chemisorbed oxygen (which causes the resistance of the sensing layer to decrease) [28]. The process is very temperature dependent. At temperatures above $300\text{ }^\circ\text{C}$ (i.e. the sensor in this work was operated at $350\text{ }^\circ\text{C}$) the amount of absorbed oxygen ion species insufficient to react with the acetone vapour molecules. It is noted by Khadayate et al. highest sensitivity is achieved at $300\text{ }^\circ\text{C}$, falling to half the maximum value of 450 % at temperatures of $250\text{ }^\circ\text{C}$ and $350\text{ }^\circ\text{C}$ [33].

The prototype sensor demonstrated a clear response to acetone, although the sensitivity was significantly lower compared to NO₂. A maximum response of 0.48 was observed for 300 ppm acetone. Righettoni et al. report detection of acetone in the range of 20 to 80 ppb (steps of 20 ppb distinguishable) using nanoparticle WO₃ film, doped with 10 % Silica SiO₂, directly deposited onto interdigital electrodes [34]. The sensor operated at a temperature of 325 °C for the optimum response to acetone. The diameter of the nanoparticles was between 14 and 16 nm. The sensor response was found to be ~ 6 to detect 1 ppm acetone, and the development of the device was noted as a key development towards a breath acetone sensor. The response and recovery times however were in the range of 10 min, considering an experiment with a 50 ppb acetone concentration step.

9.4.1.5 Response Processing

Although the response and recovery times recorded for the prototype MOX sensor are a great improvement on those reported in the literature (< 1 min compared to 10s of minutes) the requirement of a fast response sensor for breath analysis (<10 s response time) is not met. The excellent stability recorded with the developed MOX sensor and the repeatable response produced in variable conditions allows further signal processing to be performed on the raw sensor output. Preliminary methods of signal processing are presented here, although further work is required to refine these algorithms.

The speed of the response to a gas is dependent on the reactions occurring inside the thick film on the MOX sensor. Although these reactions can take a significant time (e.g. 1 minute) to stabilise (i.e. when the final resistance of the sensor is reached) the initial reactions can be used to predict the final response of the sensor. For the experiment shown in Fig. 9.9 a), with NO₂ gas tested at 50 % RH, the response time at 250 ppb is 40.2 s on average, which decreases to 72.1 s for 50 ppb. This decrease in response time is in-part due to the decreased speed of the reactions on the surface and inside the thick film. The final resistance response is not visible, until the output stabilises, however the initial response period can be used to identify the type of gas that the sensor is exposed to and its concentration.

An example is shown in Fig. 9.8. The sensor is exposed to gas concentrations of CO and NO₂, Fig. 9.8 a). The heater is pulsed on and off (room temperature to 350 °C) at

1 minute intervals. The data are sampled at 100 Hz, the first 80 differentiated samples are shown in b), taken from the second pulse during the cycle of each gas concentration. The sensor has a high response to exposure to NO₂ (i.e. 50 or 100 ppb). The magnitude of the peak indicates concentration, where 100 ppb has a greater peak (5.85×10^5 compared to the 50 ppb peak of 5.7×10^5). The sensor demonstrates a low response to CO, although the response is not identical to that in synthetic air.

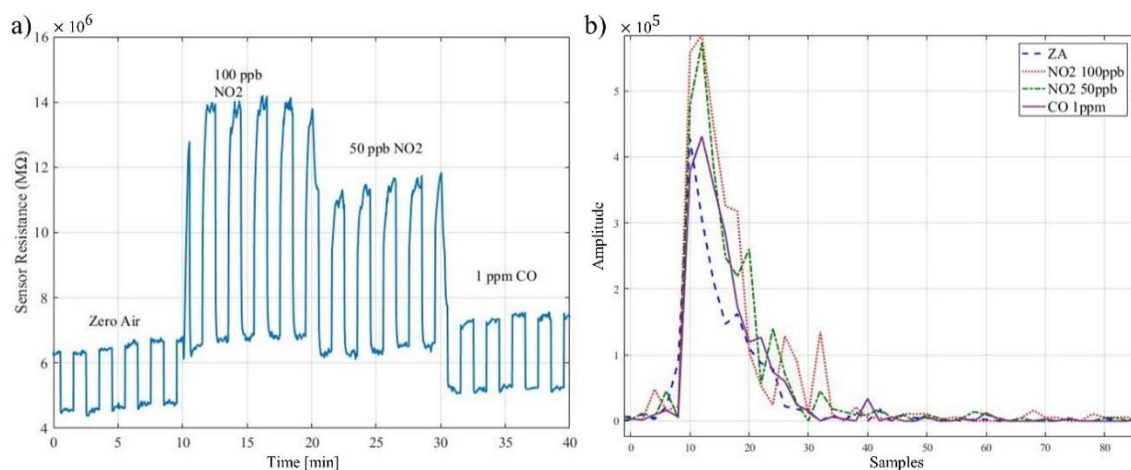
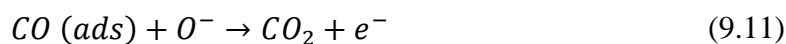


Fig. 9.8 - a) Resistance response plot for the prototype sensor to concentrations of NO₂ and CO; b) Differentiated initial responses to each gas concentration.

The differentiated pulse signal can help to determine the gas and concentration from less than 1 second of the sensor response. This technique can help reduce the response time of the sensor, although it is not well reported in the literature. The heater is pulsed on and off to allow the gas to be sampled at 1 minute intervals (i.e. the differential of the sensor response is only taken when the heater temperature is changed). The stable response from the sensor lessens the need for high order filtering, thus the differential can be taken without compromising the response time due to signal processing need.

The response to CO involves different reaction mechanisms, as specified in equations (9.10) and (9.11) when a CO molecule comes into contact with the surface of the sensor [35,36]. Typically at temperatures above 300 °C the dominant species on the oxide surface is O^- . The reaction increases the conductivity of the tungsten oxide, through donation of an electron to the WO₃ conduction band.



A notable MOX sensor has been developed, capable of sensing NO₂ down to 10 ppb limit of detection. The thick film device is also capable of detecting acetone in the same configuration, although the operating temperature and film doping do not provide optimal performance.

The sensor has been tested in conditions of dry, 25 % and 50 % RH. The sensitivity of the sensor has been proven to be far superior to the commercially available MOX sensors (response of a magnitude 5, compared to 1.25 for 250 ppb NO₂). The development of research NO₂ sensors are widely reported in the literature, although few demonstrate the response times or resilience to humidity required to operate as a breath-by-breath sensor.

9.4.2 O₂ and CO₂ Sensors

The The NDIR CO₂ sensor (development details in chapter V) provided a good response time (< 2 s), but was not resilient to temperature or humidity variance. A reference channel would improve its robustness, but at the cost of size and complexity. Further work is needed to develop an efficient NDIR emitter, to reduce the power consumption of the unit and improve the response time of the chip. The limited read-out speed of 5 Hz can be improved to improve the accuracy of the CO₂ measured during inhalation and exhalation periods.

The hand-held unit developed was comfortable and easy to use, however it did not offer the portability desired in the project. The size of the sensors, and battery required to power the pump were limiting factors. The general purpose pump was not designed for quiet operation, which provided some discomfort to the subjects while confined in the chamber environment. The sensors developed in this work to measure CO₂ and VOCs are of miniature size, which could be considered a step towards the target goal of a miniature sensing unit.

The electrochemical O₂ sensor provided an output sufficient to calculate EE, but its bulky size was not ideal for a portable instrument. The slow performance, caused in part by a thick membrane, limited the response time. Electrochemical cells are not commonly used in breath analysers, for this problem, although the reliability of the cell and robustness to exhaled breath, proved the cells did not need replacing throughout the testing phase with subjects.

The current work confined the measurement of human gases to monitoring exhaled breath. Non-invasive techniques for O₂ and CO₂ monitoring are possible. Transcutaneous sensors (that measure gas concentrations by being attached to the skin) are commonly used for monitoring of O₂ levels in neonatal care [37]. CO₂ sensing can be performed in a similar manner. Transcutaneous CO₂ monitors heat the skin (to ~40 °c) to induce vasodilation of the capillary bed. The heated area increases the blood flow and facilitates the diffusion of O₂ and CO₂ from the capillary to the sensor [38]. An electrochemical principle is used to measure the concentration of O₂ and CO₂. No reports have currently been found in the literature to suggest these sensors based on transcutaneous principles have been used to measure EE.

The power consumption of the unit overall was not optimised for low-power applications (and long battery life). The maximum current draw (at 5 V) was 410 mA (of which ~ 25 % was needed by the pump). The Bluetooth wireless module was not Low Energy ready (50 mA needed) which also contributed to the high power consumption. The sensor components were low-power (i.e. NDIR, MOX and O₂ sensors), and required a total of ~ 70 mA. The power requirements of the NDIR sensor could be further reduced via the use of a smaller IR emitter (there is great interest in plasmonic IR emitters which optimise the IR emission at desired wavelengths). A USB battery pack (suitable for mobile phone charging) provided a portable power source for the hand-held analysers. The 2800 mAh battery (shown in Fig. 8.1) provided a measurement lifetime of 2.5 hours (continuous operation).

9.4.3 Software

The applications developed enabled measurements to be performed on either an Android smartphone or a Windows computer. To target a wider audience, an application for other mobile platforms would be required. Besides the portability of using a smartphone to make measurements, the additional capability of such a device was not used. For example, the sensors included in most smartphones (e.g. accelerometers, GPS) are already used to monitor the activity of the user. These provide information that is of interest to the user, although as discussed previously, do not provide a clinically accurate reading. However, such information could be used to establish if the user was ready to make a resting EE measurement (i.e. the application could ask the user to remain sedentary for a fixed period, prior to making a measurement).

The application did not provide an intuitive interface. Although simple to use, no guidance (e.g. video material or screen prompts) were given to the user, to aid their operation of the EE measurement device. In future work, the application could be developed to give the user prompts of which buttons to press, as well as an interactive demonstration on the operation of the graphical interface.

9.4.4 Experimental

The experiments performed in this work do not tackle the wealth of possible measurements that can only be performed with a hand-held device that is quick and easy to use.

The experimental comparison with respiratory rooms measured only resting EE. The other components of EE (DIT, physical activity etc.) are not measured and are still not understood in the literature. The experiments most commonly reported are related to weight loss and specific subject groups (e.g. elderly [39], pregnant [40] etc.). In order to fully investigate the nature of the intra-individual variable components of EE, it is necessary to provide an affordable hand-held device for ready distribution to the general population.

The VOCs in the exhaled breath of subjects have not been rigorously tested in this work. The detection of compounds suggested in chapter III (e.g. acetone, NO₂, NO, CO etc.) could potentially aid disease diagnostics. A wealth of other compounds have been detected in breath, although the usefulness of some is less clear. A fingerprinting approach is often taken to identify a specific disease, without the need to identify the individual compounds.

The reproducibility between the three produced hand-held analysers was not comprehensively evaluated. The three analysers were connected in series to allow one breath to be sampled by all the devices. The outputs from the O₂ and CO₂ sensors are shown in Fig. 9.9 a) and b), respectively.

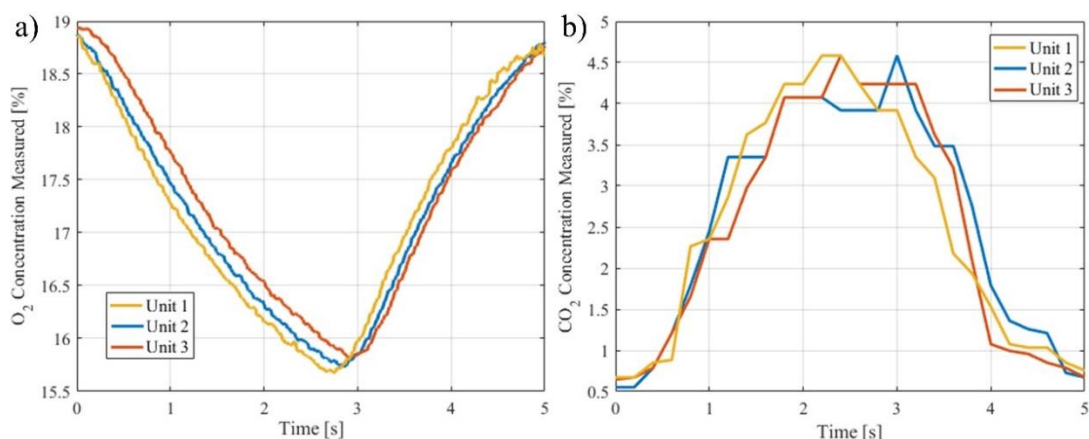


Fig. 9.9 – A single breath sampled through three analysers, a) O₂ sensor response; b) CO₂ sensor response.

The O₂ and CO₂ sensor results are similar across all three devices. The O₂ sensor responds quicker in the first unit, closest to subject providing the breath sample. Fig. 9.9 a) and b) show calibrated plots, where each unit was separately calibrated. The parameter values used in the calibration curves varied between units. The time between requiring calibration was not assessed, nor the amount of drift that occurred between calibrations. The calibration required for the CO₂ sensor was noted to vary partially from unit 1 compared to units 2 and 3. The mounting for the IR emitter effects the IR emission received by the IR detector (i.e. the angle of which IR is emitted is varied). Although identical mechanisms were used between the units, it is possible the performance of the IR emitter could be compromised by poor installation. Further work needed involves testing the reproducibility of the hand-held units to several breath tests and thus the ability for accurate EE calculation.

The current generation of EE measurement uses urine samples to measure protein metabolism [41]. Outside of a laboratory environment, this method is cumbersome and inconvenient. There is great potential to use a nitrogen-based VOC sensor to measure protein metabolism. In this current work, nitrogen metabolism was not measured, as it was found only to contribute < 2 % (chapter III) to the total daily EE. This value could vary in the wider population, and the lack of measurement of this component of metabolism should not be ignored.

The use of a mask to collect breath samples caused minor discomfort for 2 subjects during the EE measurements in the trial reported in this work (chapter VIII). This discomfort is not uncommon and it has been reported the discomfort of using EE

apparatus can affect measurements [42]. With the current generation breath analyser system, the volume of an exhalation must be captured. The volume exhaled is required to calculate the amount of O₂ consumed and CO₂ produced. Wearing of mask may not be socially acceptable and could hinder the use of a portable breath analyser in the community. If the volume of breath exhaled could be calculated by an alternative means, it would open the possibility for mask-free analyser systems.

9.5 Concluding Remarks

The hand-held breath analyser developed in this work have provided proof-of-concept level devices for EE measurement in a free-living environment. The awareness of the issues caused by a population becoming obese is still a global problem. The variability in the EE measured in the 10 subjects in the respiratory rooms proves the need for the measurement of energy need on an individual basis, where the current factors used in mathematical equations (height, weight, age) are not sufficient to allow useful values to be determined.

The technology included in everyday devices (smartphones, wearable technology) does not often include gas sensors. The ongoing development of miniature devices for detection of compounds in the ambient air and breath are growing research fields. The potential to include sensors in consumer technology means the development of accurate, fast and affordable sensors will be of interest to sensor companies in the coming years.

9.6 References

- [1] NHS, What should my daily intake of calories be? - Health questions - NHS Choices, NHS Choices. (2013) 2014. <http://www.nhs.uk/chq/pages/1126.aspx?categoryid=51> (accessed April 30, 2014).
- [2] S.G. Dudek, *Nutrition Essentials for Nursing Practice*, Wolters Kluwer Health, Philadelphia, U.S., 2013.
- [3] J.S. Ruud, *Nutrition and the Female Athlete*, Taylor & Francis, Boca Raton, U.S., 1996.
- [4] P.G. Kopelman, I.D. Caterson, W.H. Dietz, *Clinical Obesity in Adults and Children*, 3rd Ed., Wiley, Chincester, U.K., 2009.
- [5] J.S. Skinner, *Exercise Testing and Exercise Prescription for Special Cases: Theoretical Basis and Clinical Application*, 3rd Ed., Lippincott Williams & Wilkins, Philadelphia, U.S., 2005.
- [6] A. Subramaniam, M. McPhee, R. Nagappan, Predicting energy expenditure in sepsis: Harris-Benedict and Schofield equations versus the Weir derivation., *Crit. Care Resusc.* 14 (2012) 202–10.
- [7] L. Jonge, G.A. Bray, The thermic effect of food and obesity: a critical review., *Obes. Res.* 5 (1997) 622–31. doi:10.1002/j.1550-8528.1997.tb00584.x.
- [8] A.M. Knab, R.A. Shanely, K.D. Corbin, F. Jin, W. Sha, D.C. Nieman, A 45-minute vigorous exercise bout increases metabolic rate for 14 hours, *Med. Sci. Sport. Exerc.* 43 (2011) 1643–1648. doi:10.1249/MSS.0b013e3182118891.
- [9] E. Whitney, S.R. Rolfes, *Understanding Nutrition*, Cengage Learning, Belmont, U.S., 2007.
- [10] G. Pacchioni, S. Valeri, *Oxide ultrathin films: science and technology*, Wiley, Weinheim, Germany, 2012. doi:10.1017/CBO9781107415324.004.
- [11] W. Qu, R. Green, M. Austin, C. Lee, G. Lee, M. Fleischer, et al., Development of multi-functional sensors in thick-film and thin-film technology, *Meas. Sci. Technol.* 11 (2000) 1111.
- [12] G. Korotcenkov, Gas response control through structural and chemical modification of metal oxide films: state of the art and approaches, *Sensors Actuators B Chem.* 107 (2005) 209–232. doi:10.1016/j.snb.2004.10.006.
- [13] J. Haeng Yu, G. Man Choi, Electrical and CO gas sensing properties of ZnO–SnO₂ composites, *Sensors Actuators B Chem.* 52 (1998) 251–256. doi:10.1016/S0925-4005(98)00275-5.
- [14] J. Mizsei, A.D. Brailsford, M. Yussouff, E.M. Logothetis, Theory of gas sensors, *Sensors Actuators B Chem.* 23 (1993) 135–138. doi:10.1016/0925-4005(94)01269-N.
- [15] A.P. Lee, B.J. Reedy, Temperature modulation in semiconductor gas sensing, *Sensors Actuators B Chem.* 60 (1999) 35–42. doi:10.1016/S0925-4005(99)00241-5.

- [16] V. Guidi, M.A. Butturi, M.C. Carotta, B. Cavicchi, M. Ferroni, C. Malagù, et al., Gas sensing through thick film technology, *Sensors Actuators B Chem.* 84 (2002) 72–77. doi:10.1016/S0925-4005(01)01077-2.
- [17] D. Rickerby, Metal Oxides: Nanostructured Metal Oxides for Gas Sensing Applications, in: *CRC Concise Encycl. Nanotechnol.*, CRC Press, Boca Raton, U.S., 2015: pp. 525–540. doi:10.1201/b19457-44.
- [18] T.-R. Ling, C.-M. Tsai, Influence of nano-scale dopants of Pt, CaO and SiO₂, on the alcohol sensing of SnO₂ thin films, *Sensors Actuators B Chem.* 119 (2006) 497–503. doi:10.1016/j.snb.2006.01.017.
- [19] I. Simon, N. Bârsan, M. Bauer, U. Weimar, Micromachined metal oxide gas sensors: opportunities to improve sensor performance, *Sensors Actuators B Chem.* 73 (2001) 1–26. doi:10.1016/S0925-4005(00)00639-0.
- [20] SGX SensorTech, Gas Sensors: Metaloxide (MICS): MICS-4514, SGX. (n.d.). <https://www.cdiweb.com/ProductDetail/MICS4514-SGX-Sensortech-Limited-formerly-e2v/333417/> (accessed July 1, 2016).
- [21] B. Urasinska-Wojcik, T.A. Vincent, M.F. Chowdhury, J.W. Gardner, Ultrasensitive WO₃ gas sensors for NO₂ detection in air and low oxygen environment, *Sensors Actuators, B Chem.* 239 (2017) 1051–1059. doi:10.1016/j.snb.2016.08.080.
- [22] D. Patil, Y.-K. Seo, Y.K. Hwang, J.-S. Chang, P. Patil, Humidity sensing properties of poly(o-anisidine)/WO₃ composites, *Sensors Actuators B Chem.* 128 (2008) 374–382. doi:10.1016/j.snb.2007.06.026.
- [23] D. Chen, X. Hou, H. Wen, Y. Wang, H. Wang, X. Li, et al., The enhanced alcohol-sensing response of ultrathin WO₃ nanoplates, *Nanotechnology.* 21 (2010) 35501.
- [24] P.-G. Su, S.-L. Peng, Fabrication and NO₂ gas-sensing properties of reduced graphene oxide/WO₃ nanocomposite films, *Talanta.* 132 (2015) 398–405. doi:10.1016/j.talanta.2014.09.034.
- [25] Y.-K. Chung, M.-H. Kim, W.-S. Um, H.-S. Lee, J.-K. Song, S.-C. Choi, et al., Gas sensing properties of WO₃ thick film for NO₂ gas dependent on process condition, *Sensors Actuators B Chem.* 60 (1999) 49–56. doi:10.1016/S0925-4005(99)00243-9.
- [26] J. Tamaki, Z. Zhang, K. Fujimori, M. Akiyama, T. Harada, N. Miura, et al., Grain-Size Effects in Tungsten Oxide-Based Sensor for Nitrogen Oxides, *J. Electrochem. Soc.* 141 (1994) 2207–2210. doi:10.1149/1.2055088.
- [27] H. Xia, Y. Wang, F. Kong, S. Wang, B. Zhu, X. Guo, et al., Au-doped WO₃-based sensor for NO₂ detection at low operating temperature, *Sensors Actuators B Chem.* 134 (2008) 133–139. doi:10.1016/j.snb.2008.04.018.
- [28] L. Wang, P. Gouma, Selective Crystal Structure Synthesis and Sensing Dependencies, in: A.M. Carpenter, S. Mathur, A. Kolmakov (Eds.), *Met. Oxide Nanomater. Chem. Sensors*, Springer, New York, U.S., 2013: pp. 167–188. doi:10.1007/978-1-4614-5395-6_5.
- [29] M. Blo, M.C. Carotta, S. Galliera, S. Gherardi, A. Giberti, V. Guidi, et al.,

- Synthesis of pure and loaded powders of WO₃ for NO₂ detection through thick film technology, *Sensors Actuators B Chem.* 103 (2004) 213–218. doi:10.1016/j.snb.2004.04.053.
- [30] M. Righettoni, A. Tricoli, S.E. Pratsinis, Si:WO₃ Sensors for highly selective detection of acetone for easy diagnosis of diabetes by breath analysis., *Anal. Chem.* 82 (2010) 3581–7. doi:10.1021/ac902695n.
- [31] L. Wang, K. Kalyanasundaram, M. Stanacevic, P. Gouma, Nanosensor Device for Breath Acetone Detection, *Sens. Lett.* 8 (2010) 709–712. doi:10.1166/sl.2010.1334.
- [32] C. Jiang, M. Sun, Z. Wang, Z. Chen, X. Zhao, Y. Yuan, et al., A portable real-time ringdown breath acetone analyzer: toward potential diabetic screening and management, *Sensors.* 16 (2016).
- [33] R.S. Khadayate, J.V. Sali, P.P. Patil, Acetone vapor sensing properties of screen printed WO₃ thick films, *Talanta.* 72 (2007) 1077–1081. doi:10.1016/j.talanta.2006.12.043.
- [34] M. Righettoni, A. Tricoli, S.E. Pratsinis, Thermally stable, silica-doped ε-WO₃ for sensing of acetone in the human breath, *Chem. Mater.* 22 (2010) 3152–3157. doi:10.1021/cm1001576.
- [35] D. Patil, P. Patil, V. Subramanian, P.A. Joy, H.S. Potdar, Highly sensitive and fast responding CO sensor based on Co₃O₄ nanorods, *Talanta.* 81 (2010) 37–43. doi:10.1016/j.talanta.2009.11.034.
- [36] C. Academy, G. Shao, J. Guo, J. Xie, X. Duan, B. Wu, et al., The preparation of CoWO₄/WO₃ nanocomposite powder, *J. Wuhan Univ. Technol. Sci. Ed.* 19 (2004) 1–3. doi:10.1007/BF03000154.
- [37] J.M. Adams, Blood Gas and Pulmonary Function Monitoring, in: *Man. Neonatal Care*, Wolters Kluwer Health/Lippincott Williams & Wilkins, Philadelphia, U.S., 2008: p. 343.
- [38] I.M. Cheifetz, J. Salyer, G. Schmalisch, J.D. Tobias, Classical Respiratory Monitoring, in: P.C. Rimensberger (Ed.), *Pediatr. Neonatal Mech. Vent. From Basics to Clin. Pract.*, Springer Berlin Heidelberg, Berlin, Heidelberg, 2015: pp. 375–419. doi:10.1007/978-3-642-01219-8_12.
- [39] S. Heiermann, K. Khalaj Hedayati, M.J. Müller, M. Dittmar, Accuracy of a Portable Multisensor Body Monitor for Predicting Resting Energy Expenditure in Older People: A Comparison with Indirect Calorimetry, *Gerontology.* 57 (2011) 473–479. doi:10.1159/000322109.
- [40] M. Blackburn, D. Calloway, Heart rate and energy expenditure of pregnant and lactating women, *Am. J. Clin. Nutr.* 42 (1985) 1161–1169.
- [41] N. V Bhagavan, E. Metabolism, *Medical Biochemistry*, 4th Ed., Elsevier Science, San Diego, U.S., 2001.
- [42] J.L. Miles-Chan, D. Sarafian, J.P. Montani, Y. Schutz, A.G. Dulloo, Sitting comfortably versus lying down: is there really a difference in energy expenditure?, *Clin. Nutr.* 33 (2014) 175–8. doi:10.1016/j.clnu.2013.11.009.

CHAPTER X

Appendices

Preface

This final section documents two papers submitted for a book chapter and journal article. Also, the assessment submitted to the Biomedical and Scientific Research Ethics Committee is included. A portion of the code written to communicate with the sensors system developed in this project is detailed. The development of microcontroller and smartphone code, as well as their counterparts on data logging computers has formed an important part of the successful breath analysis experiments.

10.2 Appendix B – Ethics Approval for Laboratory Breath Testing

Prior to any testing with human volunteers at the University of Warwick, a Biomedical and Scientific Research Ethics Committee (BSREC) application was filed. The committee approval the studies. The attached pages show the BSREC application and final granted approval letter.

10.2.1 B.1 - BSREC Application Form



Biomedical and Scientific Research Ethics Committee (BSREC):
Application Form for Ethical Approval

SECTION 1. APPLICANT DETAILS	
1.1 RESEARCHER	
Researcher's Title:	Mr
Researcher's Forename:	Timothy
Researcher's Surname:	Vincent
Researcher's Faculty/School and Department: School of Engineering	
<u>Researcher's Status:</u>	
Undergraduate Student	<input type="checkbox"/>
Taught Postgraduate Student	<input type="checkbox"/>
Research Postgraduate Student	<input checked="" type="checkbox"/>
Staff	<input type="checkbox"/>
Other	<input type="checkbox"/>
Please specify:	
<u>If Student:</u>	
Name of course/qualification:	MEng Electronics Engineer
<u>If Staff:</u>	
Researcher's Post:	
1.2 RESEARCHER'S CONTACT DETAILS	
Warwick e-mail address:	t.a.vincent@warwick.ac.uk
Daytime telephone number:	024 7652 8168
Postal address:	School of Engineering, University of Warwick, Coventry, CV4 7AL
1.3 SUPERVISOR - COMPLETE FOR ALL STUDENT PROJECTS	
Supervisor's Title:	Prof
Supervisor's Forename:	Julian
Supervisor's Surname:	Gardner
Supervisor's Post: Head of Microsensors and Bioelectronics Laboratory	
Supervisor's Faculty/School and Department:	School of Engineering
Supervisor's Warwick e-mail address:	j.w.gardner@warwick.ac.uk
Supervisor's daytime telephone number:	024 7652 3695

SECTION 2. PROJECT DETAILS	
2.1 Project Title:	Handheld Breath Analyser
2.2 Estimated Start Date of Project:	01/09/2013
2.3 Estimated Completion Date of Project:	31/08/2017
2.4 Sponsoring Organisation: (for University of Warwick staff and students, undertaking non-commercial projects, this will be the University of Warwick)	Jointly organised between University of Warwick and University Hospitals Coventry and Warwickshire NHS Trust.
2.5 Funder: (e.g. unfunded student project, unfunded Departmental project, Medical Research Council (MRC), Economic & Social Research Council (ESRC), EU)	Jointly funded between University of Warwick and University Hospitals Coventry and Warwickshire NHS Trust.
2.6 TYPE OF PROJECT	
Is the project:	
Primary Research	<input checked="" type="checkbox"/>
Research limited to the use of previously collected <i>identifiable</i> data	<input type="checkbox"/>
Research limited to the use of previously collected <i>anonymised</i> data	<input type="checkbox"/>
Service Evaluation and/or Development	<input type="checkbox"/>
Clinical Audit	<input type="checkbox"/>
Other	<input type="checkbox"/>
Please specify:	
2.7 LINKS WITH OTHER BSREC APPLICATIONS	
Is the project linked to any other BSREC application? Yes	
If yes, detail:	
Project title:	HMRU Experiments
Chief Investigator:	Dr John Hattersley
BSREC Reference (if known):	
Nature of linkage: Dr. Hattersley coordinates breath analysis experiments at the University Coventry Hospital, requesting patients to provide similar samples to the ones required for this study. Dr Hattersley is part of the team for this breath analysis project.	

	other activities that represent a threat to themselves or others (e.g. sexual activity, drug use, or professional misconduct)?		
D	Could the study induce psychological distress or anxiety , or produce humiliation , or cause harm , or lead to negative consequences beyond the risks encountered in normal life ?	<input type="checkbox"/>	<input checked="" type="checkbox"/>
E	Does the study involve substantial physical exertion ?	<input type="checkbox"/>	<input checked="" type="checkbox"/>
F	Does the study involve the administration of any substance?	<input type="checkbox"/>	<input checked="" type="checkbox"/>
G	Does the study involve physically intrusive procedures , use of bodily materials or human tissue , or DNA/RNA analysis ?	<input type="checkbox"/>	<input checked="" type="checkbox"/>
H	Is any reward , apart from travelling and other expenses, to be given to participants?	<input type="checkbox"/>	<input checked="" type="checkbox"/>
I	Does the study involve collaboration with any company or organisation external to the University of Warwick?	<input checked="" type="checkbox"/>	<input type="checkbox"/>
J	Could the proposal give rise to researchers having any conflicts of interest ?	<input type="checkbox"/>	<input checked="" type="checkbox"/>
K	Will the researchers go to any areas where their safety may be compromised ?	<input type="checkbox"/>	<input checked="" type="checkbox"/>
L	Will pregnant women be participants in the study?	<input type="checkbox"/>	<input checked="" type="checkbox"/>

SECTION 4. SIGNATURES AND DECLARATIONS

4.1 RESEARCHER/APPLICANT

I undertake to abide by the University of Warwick's Research Code of Practice in undertaking this study.

I understand that BSREC grants ethical approval for projects, and that the seeking and obtaining of all other necessary approvals and permissions prior to starting the project is my responsibility.

I understand that I must not begin research and related projects with human participants until I have received full approval from the relevant Research Ethics Committee of the University of Warwick.

I understand that any changes that I would like to make to this study after receiving approval from BSREC must follow BSREC procedures as detailed on the BSREC web pages.

Name of Researcher: Timothy Vincent

Signature:

Date:

NB: The applicant must post a wet ink signature copy of this form to: BSREC Administrator, B032, Medical School Building, Warwick Medical School, University of Warwick, Coventry, CV4 7AL

4.2 SUPERVISOR AUTHORISATION FOR STUDENT PROJECTS

I confirm that I have read this application and will be acting as the student researcher's supervisor for this project.

The proposal is viable and the student has the appropriate skills to undertake the research. Participant recruitment procedures, including the Information Leaflet(s) to be provided and the process for obtaining informed consent, are appropriate, and the ethical issues arising from the project have been addressed in the protocol.

I understand that BSREC grants ethical approval for projects, and that the seeking and obtaining of all other necessary approvals and permissions prior to starting the project is the responsibility of the student.

I understand that research and related projects with human participants must not commence without full approval from the relevant research ethics committee of the University of Warwick.

Name of Supervisor: Prof. Julian Gardner

Signature:

Date:

NB: An e-mail from the Academic Supervisor that states the above, in lieu of a wet ink signature on this form, may be sent to: bsrec@warwick.ac.uk

10.2.2 B.2 - BSREC Protocol



BIOMEDICAL & SCIENTIFIC RESEARCH ETHICS COMMITTEE (BSREC) Application – Protocol/Proposal

Metabolic Rate Breath Analysis

Summary

This project aims to create a novel portable breath analyser capable of determining a patient's resting metabolic rate (RMR). RMR provides an indication of how much energy the body needs to perform vital functions (breathing, circulation etc.) and can be used to help provide metabolic requirement advice. The subjects will need to breathe normally into a sampling collecting chamber (via a tube) for a short period of time. Results measured via the portable device will be compared to those obtained from the respiratory rooms or a metabolic cart.

The research involved in this project complements research being carried out in the NHS Trust University Hospitals Coventry and Warwickshire, where energy expenditure is measured in respiratory rooms. The project aims to help increase medical knowledge into breath analysis and provide a prototype device that can be used quickly by subjects but still provide an accurate RMR reading. The participants will only need to give short breath samples, for a number of repetitions, exact details of which have yet to be determined. Every possible experiment has already been performed, using laboratory gases, to verify the functionality of the device, but the breath contents of humans cannot be reproduced, thus volunteers are required to provide real breath samples.

Background

Obesity is a growing problem in the UK, costing the NHS increasing amounts of money. RMR values provide a valuable insight into a person's dietary demands and by obtaining accurate and specific values for a patient's true RMR can make people aware of their body's requirements.

The current method of obtaining RMR (at the University Hospital Coventry) is to take a 24 hour measurement with the patient inside an environmentally controlled and monitored respiratory room. This 'gold standard' is inconvenient for healthy subjects, where their daily routine cannot be followed, but also impossible to implement when subjects are undergoing other treatments. For instance, the metabolic intake for patients in ICU (Intensive Care Units) is vital to their recovery, which could be predicted with much greater accuracy if an estimate of their RMR could be obtained.

The main components needed to calculate a patient's metabolic rate for a subject are the volumes of carbon dioxide produced and oxygen consumed. The oxygen and carbon dioxide content in exhaled breath can be measured using appropriate gas sensors, whilst flow, temperature and relative humidity sensors are also required to calculate volume of gas exhaled. An extensive range of experiments have been performed to test the prototype analyser, using laboratory gases, although to further the testing procedure the device must now be tested with exhaled breath.

Substantial research has been undertaken to investigate RMR of subjects through respiratory chamber measurements. In these experimental conditions, there is considerable information on how a person's metabolic rate varies over the course of a day, for instance after a meal or just prior to going to sleep. However, research into metabolic rate determination from a portable breath analyser is limited and further research into measuring a person's metabolic rate over a longer period than one day is a relatively unexplored field. The device developed in this project aims to complement the knowledge gained from the respiratory chambers at the HMRU and attempt to provide information about a person's RMR based on breath samples taken over a much shorter period, than the common one day (24 hour) experiment duration.

This project aims to initially start by investigating metabolic rate analysis, starting by measuring Oxygen (O₂) and Carbon Dioxide (CO₂) breath concentrations, before investigating other elements that can be discovered from breath samples. This project focuses upon developing a novel portable device that can operate with the required accuracy as to support clinical diagnosis. Whilst research in this area is promising; a portable device with sufficient accuracy for use in clinical diagnostics has yet to be produced, including devices capable of monitoring resting metabolic rates.

Aims/Objectives

The overall aim of this project is to develop a novel portable, handheld breath analyser capable of outputting detailed results of the gas concentrations in a sample. Initially the device will only analyse a small number of gases (O₂, CO₂ & CO), but future revisions could analyse a wider range of gases to improve measurements (from cross sensitivity) or aid further care by diagnosing diseases.

This study aims to verify if the device is capable of measuring the concentrations of gases inhaled and exhaled, while being exposed to the abnormal conditions of breathing, when compared to the ideal gas sensor testing conditions found in the current laboratory testing rig. The study participants will not be asked to perform any task other than breathe normally into our device. The gas concentrations of exhaled breath should be within a standard range, however the purpose of the study is to test for human variation, as due to a number of factors, such as the health of the patient, their recent food intake or alcohol consumption (among a large number of other parameters) the contents of their individual exhaled breath is predicted to vary widely. Due to these unique factors, breath samples cannot be reproduced in a laboratory, and therefore must be taken from real human volunteers.

The first objective is to get a prototype portable device to produce comparative RMR results to the 'gold standard' respiratory chamber, such as the rooms in the HMRU (Human Metabolism Research Unit) at Coventry University Hospital. Respiratory chambers are specially designed rooms, capable of monitoring the gases exhaled on the breath of a subject placed inside for a period of up to 36 hours. The gases going into and coming out the room are measured enabling the change in gas concentrations due to the subject's presence to be observed. The next milestone will be to complete this first device, for instance housing it in a handheld package, and integrate the necessary calculations to convert gas concentrations to an understandable metabolic readout. The final objective would be to design a device that can be taken home by a patient and used outside of laboratory conditions, without support from the hospital staff.

This project will not be able to proceed without human breath samples. The device functionality must be verified on volunteers' breath, testing if the prototype is capable of coping with the

different conditions of exhaled breath, compared to the near perfect gas testing conditions, upon which the device has currently been trialled, on a gas testing rig. Using the available equipment in the gas testing laboratory, a large number of experiments have already been performed, without human subjects, meaning almost every possible combination of gases expected in exhaled breath has been tested. Therefore the next step is to prove our device is also capable of performing similarly when measuring gases exhaled from human participants. It is hoped that even a small number of volunteers will produce dynamic results, as a subject's individual breath can be affected by the time of day, what they have recently consumed, their oral hygiene and if they have smoked recently or exercised in the past 12 hours.

Design/Methodology

The purpose of this investigation is to collect breath data from volunteers, which will provide a quantitative means of assessing the functionality of the portable breath analyser. The tests will be performed on subjects who are all either staff or students from the University of Warwick, all over the age of eighteen.

The subjects will be required to blow into either a sample collecting bag, or directly through the device. For analysis of metabolic rate, a breath which mimics free living would be preferred (not forced, as natural as possible). However, it is noted that asking a patient to breath through any sort of device will alter their breathing pattern. After a short period of time the participant should become accustomed to breathing through the device. A number of different breathing patterns may be simulated, some examples are listed below, which will be adapted as the experiments progress, depending on quality of results generated and period of time taken to perform each procedure. The results of the experiment will be observed in real time. If for any reason, data collection fails, or erroneous results are recorded, then the patient will be asked to repeat the measurements. As this study progresses the experiments will be repeated to help mitigate inter-individual variation and to obtain further data for analysis, or to allow the patient again to be used to breathing through the device, if they are struggling to become accustomed to the apparatus.

- Example Experiment 1: Breathe normally through the device for a period of no more than 2 minutes. This period needs to be flexible, as the volunteers individually adapt to the sensation of breathing into a mouthpiece (while wearing nose-clip). The system has been designed to add as little resistance to the respiratory system as possible; however it is inevitable to add a small amount, which should not cause any discomfort.
- Example 2: Three respiratory cycles will be recorded for each patient. This is consistent with measurements taken at the HMRU, where three cycles was found to be sufficient to sample the gases present in exhaled breath. Again, these will be normal breathing patterns, and ideally as close to breathing in free-living, without being involved in a laboratory experiment.
- Example 3: The participants will be asked to inhale deeply and then exhale through the device for a period of up to 10 seconds (as long as the participant feels comfortable). This will allow the sensors response to extreme levels of flow rate to be observed in the experiments results, compared to normal breathing.
- Example 4: If willing, the participant may be asked to hold their breath for a short period and then exhaled through the device. This is to observe how the concentrations of gases change in the lungs, due to breath holding.

The subjects will never become breathless nor oxygen deprived, as they will be observed continuously while providing the breath samples, and the experiment will be halted immediately if they show any signs of distress. No respiratory manoeuvres, other than normal breathing, will be required from the subjects, except holding their breath for a few seconds. It is hoped that as the subject is breathing normally, they will be able to provide repeat measurements to allow analysis of intra-subject variability. At the current stage of planning the study, it is not known how many repetitions will be required per subject; however these will become clear as the study progresses. Sufficient repetitions will be taken to attempt a 95% confidence interval for the gas concentrations in exhaled breath for each volunteer.

The availability of participants for the study will be based upon volunteers. The breath variation between different groups of humans is noted, as part of the HMRU's past experiments, where fitness and age, for example, can play a large role in the patient's metabolic rate. The results produced from the initial measurements performed for this study will require extensive data processing. This will help refine and adapt later experiments, to produce best results, from a well optimised and efficient test procedure.

A sample size of 40 volunteers will be selected, allowing sufficient data to perform analysis if the data is found not to follow a uniform distribution. Volunteers (staff or students from the university) will be recruited via an advertisement placed on the University of Warwick's Research Participation webpage (<http://www2.warwick.ac.uk/insite/topic/research/research>).

The participants will be under no obligation to contribute to this portable breath analysis study, and can leave at any time, as the samples collection methods are non-invasive and require voluntary patient cooperation. The subjects will have to approve for their breath to be sampled and monitored, but the breath sampling device will not present any further obstruction to their normal daily living, besides having to wear a nose clip and breathe through a mouthpiece.

Before any measurements are attempted using the portable breath analyser, the volunteers will be informed of the purpose of the study and asked to read the participate leaflet and give their written consent. It will be explained the device only measures the gases they inhale and exhale, and does not affect their breathing patterns, and should not prove difficult to breathe through. Again, they will be informed the study will not be carried out over a long period of time, and each measurement will take less than two minutes. For the sample collection the subject should be as at ease as possible (natural free living ideally), therefore should not feel uncomfortable at any point, but will be informed they can stop and leave the experiment instantaneously whenever they wish.

The data will be collected and stored using a laptop computer, running logging software. The data does not contain any personal information about the participant, only the gas concentrations in their breath. The purpose of this initial study is to test the functionality of the portable breath analyser, comparing its response to that of the HMRU's chambers. Therefore no further information is required about the patient to analyse the data, only the raw gas sensor responses.

The sensors have previously been tested in sterile perfect conditions (for the sensors) and these experiments aim to trial the devices in a clinical environment, as breath gas content varies drastically from the mixtures of gas that have been trialed previously.

Ethical Considerations

Informed Consent

Before each subject is asked to take part in any experimentation, the purpose of the experiment will be explained clearly verbally to them, allowing any questions to be answered, in addition to being provided with an information leaflet again reiterating the details of the test. Furthermore the participant will be shown the test equipment, and be reassured the conditions during the experiment should mimic free living as much as possible. If the subject is satisfied about the experiment details, they will be asked if they are willing to take part. If willing, they asked to give written indication via a consent form.

Participant Confidentiality

The data collected during the portable breath analysis study will not contain information that could be used to identify an individual, only raw gas sensor outputs from a breath sample. The patient will be randomly assigned an experiment number, which will not be linked to any data which could be used to identify the participant. No photographs of the volunteers will be taken while they are in the laboratory, nor will any identifying features be recorded.

Data Security

The data collected during the measurements will be stored electronically, on a password protected computer, provided by the University of Warwick. It will be stored on a hard drive in a locked PhD office at the University of Warwick. The drive itself will again be password protected. The consent forms, along with any other administrative records, will be stored in the same location, but as paper copies, will be locked in cabinets. The data recorded will be stored for a sufficient period to allow analysis of the data and for comparison between experiments and future studies. If they desire, their records will be permanently deleted from the project data store at any point during after the study.

Other Considerations

As detailed above, the volunteers will be able to withdraw from the experiments whenever they wish. The data will be stored for a as secure manner as possible, however the volunteers can request at any time the data be permanently deleted. If any of the data should be published, this will be impossible, however the data published will lack any way of identifying the participant. The patient's will be informed of this (via the information leaflet) before signing the consent form. Any patient suggesting they wish to withdraw during the experiment can do so, with the data deleted immediately. After the study, the data will be stored by experiment and can be deleted immediately upon the request of the participant. If there is any way of tracing back the patient's data, it will be sourced and deleted (permanently).

The participates are providing breath samples, only to test the functionality of the portable metabolic rate analyser. The only gases sampled are Carbon Dioxide, Oxygen and Carbon Monoxide. The experiment will not require disclosure of any sensitive information (such as criminal or professional misconduct).

The aim of this study is to aid development of a portable breath analyser. By taking part, the subjects help further research, by comparing the functionality of the prototype device, to the proven HMRU calorimeter chambers. Only short measurements will be performed, but these can be related to those obtained over a much longer period (24 hours) in the HMRU's respiratory rooms. In the future,

metabolic rate analysis may not require the patient to remain in the chamber for 24 hours, but instead provide only a short breath sample, which may aid treatment of diseases etc. If any publications are created as a result of these experiments, the participants will be able to read a copy of the report.

There is no risk of any adverse effects for the subject taking part in the study. The data obtained will be anonymised and kept only for short periods of time. The study aims to be performed in conditions which as near replicate free (normal) living as possible, therefore should not provide any discomfort to the participant. The participants will not be asked to do anything more than normal breathing, therefore should not feel uncomfortable at any point during the experiments. There are no conceivable major risks to any participant.

Appendices

- Advert for participant recruitment website.
- Participant consent form.
- Invitation email for potential participants.
- Participant information leaflet.

10.2.3 B.3 - BSREC Participant Information Leaflet



PARTICIPANT INFORMATION LEAFLET

Study Title:	Metabolic Rate Breath Analysis
Investigator(s):	Timothy Vincent, Prof. Julian Gardner, Prof. Adrian Wilson, Dr. John Hattersley and Dr. Mike Chappell.

Introduction

You are invited to take part in a Research study. Before you decide, you need to understand why the research is being done and what it would involve for you. Please take the time to read the following information carefully. Talk to others about the study if you wish.

(Part 1 tells you the purpose of the study and what will happen to you if you take part. Part 2 gives you more detailed information about the conduct of the study)

Please ask us if there is anything that is not clear or if you would like more information. Take time to decide whether or not you wish to take part.

PART 1

What is the study about?

This experiment is about investigating gases present in exhaled breath and their relation to the body's metabolic rate (MR). An individual's MR is the amount of energy expended by the body over a given period of time, which includes basic functions necessary for life (breathing, circulation etc.), energy used during physical activity and energy used processing food consumed. Knowledge of MR is important for health individuals to aid understanding of daily energy requirements and food/dietary guidance. Of particular interest in our experiments, is to test if a person's MR can be determined quickly, using a breath analyser to measure breath samples given directly into a portable device. This project aims to develop a handheld, portable analyser that is capable of determining the users' MR from a short breath sample.

A well-proven method of finding a patient's MR requires a full 24 hour measurement inside a whole body calorimeter, which is a specially designed room to monitor inhaled and exhaled gases from a subject who remains inside the chamber for a period of up to 36 hours. The aim of developing a compact device is to shorten the time taken to determine MR by directly sampling breath. As a person's MR is effected by their activity (eating or exercising etc.), obtaining an immediate measurement allows this effect to be quantified, and improves the accuracy of a daily MR value.

To obtain a benchmark MR to trial the accuracy of our prototype system the participant will only be asked to breathe normally into the device and at no point will the participant become breathless. A number of sample breaths will be required, but each sample will take no longer than a few minutes to record. Approximately forty volunteers are needed for this study.

Do I have to take part?

It is entirely up to you to decide. We will describe the study and go through this information sheet, which we will give you to keep. If you choose to participate, we will ask you to sign a consent form to confirm that you have agreed to take part You will be free to withdraw at any time, without giving a reason and this will not affect you or your circumstances in any way.

What will happen to me if I take part?

You will be asked to provide a breath sample into a portable device for analysis. The measurement will be analysed using a prototype device, containing gas sensors used to assess the contents of your breath sample. The sample will be taken using a handheld breath analyser, with disposable mouthpiece and nose clip.

What are the possible disadvantages, side effects, risks, and/or discomforts of taking part in this study?

The experiments require only breathing to be sampled. Please be aware the measurements may take place soon after eating or after light exercise. These are factors that can affect MR readings, and are of interest to our study. As only breathing is required there is no real risk to the participant. The nose-clip required may be slightly uncomfortable, but any real discomfort and the experiment will be stopped immediately.

What are the possible benefits of taking part in this study?

At the end of the experiment, it is hoped an estimate for the participant's MR for the experimental period should be determined, which can provide useful dietary advice. There are no other direct benefits for participating, however the study aims to help future health care, by contributing to the knowledge that can be obtained from short breath samples.

Expenses and payments

Participants will not receive any reimbursement for taking part in this study.

What will happen when the study ends?

The study should not involve any activity outside of your normal daily routine. Breath samples should be provided in a relaxed manner, with no after effects. The data collected during the experiment will not contain sufficient information to be able to trace any measurements back to you as a participant. The information captured from breath samples given will be stored for use in further analysis after the study.

Will my taking part be kept confidential?

Yes. We will follow strict ethical and legal practice and all information about you will be handled in confidence. Further details are included in Part 2.

What if there is a problem?

Any complaint about the way you have been dealt with during the study or any possible harm that you might suffer will be addressed. Detailed information is given in Part 2.

This concludes Part 1.

If the information in Part 1 has interested you and you are considering participation, please read the additional information in Part 2 before making any decision.

PART 2

Who is organising and funding the study?

This study is part of a PhD project which is jointly funded by the NHS Trust Coventry and Warwickshire University Hospitals and the University of Warwick.

What will happen if I don't want to carry on being part of the study?

Participation in this study is entirely voluntary. Refusal to participate will not affect you in any way. If you decide to take part in the study, you will need to sign a consent form, which states that you have given your consent to participate.

If you agree to participate, you may nevertheless withdraw from the study at any time without affecting you in any way.

You have the right to withdraw from the study completely and decline any further contact by study staff after you withdraw.

Study participants are free to withdraw at any point and any data provided will be deleted. There will be no consequences to withdrawing.

What if there is a problem?

This study is covered by the University of Warwick's insurance and indemnity cover. If you have an issue, please contact Jo Horsburgh (details below).

Who should I contact if I wish to make a complaint?

Any complaint about the way you have been dealt with during the study or any possible harm you might have suffered will be addressed. Please address your complaint to the person below, who is a Senior University of Warwick official entirely independent of this study:

Jo Horsburgh
Deputy Registrar
Deputy Registrar's Office
University of Warwick
Coventry, UK, CV4 8UW.
T: +00 44 (0) 2476 522 713 E: J.Horsburgh@warwick.ac.uk

Will my taking part be kept confidential?

The data collected during the experiment will not contain sufficient information to be able to trace any measurements back to you as a participant. Taking part in the experiment will be kept confidential. The data stored will be assigned randomly generated experiment number, which will be the only method used to identify the measurement records provided. Any electronic data stored will be kept on a password protected computer on password protected media, stored in a secure location at the University of Warwick.

What will happen to the results of the study?

The data from this study will be used to develop the portable breath analyser unit. The findings of the study will be available to patients upon request. The results may be used in publications, where the functionality of the portable analyser may be explained and the results from this experiment may be discussed to aid the device's proven functionality.

Who has reviewed the study?

This study has been reviewed and given favourable opinion by the University of Warwick's Biomedical and Scientific Research Ethics Committee (BSREC): Insert your BSREC number here (given to you when your study is approved) and include the date on your approval letter from BSREC.

What if I want more information about the study?

If you have any questions about any aspect of the study or your participation in it not answered by this participant information leaflet, please contact:

Timothy Vincent,
T.A.Vincent@warwick.ac.uk,
024 7652 8168

Prof. Julian Gardner (Academic Supervisor),
J.W.Gardner@warwick.ac.uk,
024 7652 3695

Thank you for taking the time to read this participant information leaflet.

10.2.4 B.4 - BSREC Participant Consent Form



CONSENT FORM

(Biomedical and Scientific Research Ethics Committee) Study Number:

Patient Identification Number for this study:

Title of Project: Metabolic Rate Breath Analysis

Name of Researcher(s): Timothy Vincent, Prof. Julian Gardner, Dr. John Hattersley, Prof. Adrian Wilson and Dr. Mike Chappell..

Please initial all boxes

1. I confirm that I have read and understand the information sheet dated May 2014 (version 1.0) for the above study. I have had the opportunity to consider the information, ask questions and have had these answered satisfactorily.
2. I understand that my participation is voluntary and that I am free to withdraw at any time without giving any reason, without my medical or legal rights being affected.
3. I understand that relevant sections of my medical notes and data collected during the study, may be looked at by individuals from The University of Warwick, from regulatory authorities (or from a relevant NHS Trust), where it is relevant to my taking part in this research. I give permission for these individuals to have access to my records.
4. I agree to take part in the above study.

Name of Participant

Date

Signature

Name of Person
taking consent

Date

Signature

10.2.5 B.5 - BSREC Participant Recruitment Email Template

April 2014



**BIOMEDICAL & SCIENTIFIC RESEARCH ETHICS COMMITTEE (BSREC)
Application – Protocol/Proposal**

Metabolic Rate Breath Analysis – Invitation Letter for Research Participants

Metabolic Rate Breath Analysis Research

Hello,

We are looking for volunteers to take part in a breath sampling study to help develop a portable analyser. Participants will not have to perform any activities outside of their daily activities, perhaps including a form of light exercise; measurements involve simply breathing through a mouthpiece into the device.

What are we trying to achieve?

- Develop a portable device, able to estimate the amount of calories required by a human body per day.
- Estimate the metabolic rate (amount of energy expended) of a participant during a short measurement period of a few minutes.

How will participant's breath samples be taken?

- The volunteer will be asked to remain in a comfortable position for a few minutes, while breathing normally through a mouthpiece into our breath analyser.
- If the volunteer is comfortable, experiments involving breath holding of short periods (~10 seconds), may be undertaken, to expose the device to a range of exhalation flow rates.
- Exercise increases metabolic rate, some measurements may involve a period of exercise before taking a measurement.

If you choose to volunteer you will be asked to attend a short session in which you will be asked to provide a number of breath samples into the device.

The experiments will all take place on campus, at the University of Warwick.

Thank you for your interest!

Tim Vincent

T.A.Vincent@warwick.ac.uk

10.2.6 B.6 - BSREC Recruitment Advert for Research Webpage

April 2014



**BIOMEDICAL & SCIENTIFIC RESEARCH ETHICS COMMITTEE (BSREC)
Application – Protocol/Proposal**

**Metabolic Rate Breath Analysis –
Advertisement for Research Participants**

<http://www2.warwick.ac.uk/insite/topic/research/research>

**Metabolic Rate Breath Analysis Research via a Novel Portable
Analyser**

A unique portable breath analyser has been developed at the University and we need volunteers to test the device, simply by providing a number of breath samples. The analyser will allow a participant's metabolic rate (energy expended) during the measurement to be calculated, and the amount of calories needed per day to be estimated.

A single measurement should take only a few minutes of breathing through a mouthpiece into the device. Every volunteer's breath samples will be unique. Participation will help further the development of the device and research into the area of metabolism and breath analysis.

Please contact Tim Vincent at T.A.Vincent@warwick.ac.uk for more information or to volunteer for the study.

10.2.7 B.7- BSREC Full Approval Letter

23rd May 2014

Warwick
Medical School

PRIVATE
Mr Timothy Vincent
C/O Prof Julian Gardner
School of Engineering
University of Warwick
CV4 7AL

Dear Timothy

Study Title and BSREC Reference: *Handheld Breath Analyser* REGO-2014-738

Thank you for submitting the above-named project to the University of Warwick Biomedical and Scientific Research Ethics Committee for research ethical review.

I am pleased to advise that research ethical approval is granted.

May I take this opportunity to wish you success with the study, and to remind you that any substantial amendments require approval from the Committee before they can be implemented. Please keep a copy of the original signed version of this letter with your study documentation.

Yours sincerely



Dr David Davies
Chair
Biomedical and Scientific
Research Ethics Sub-Committee

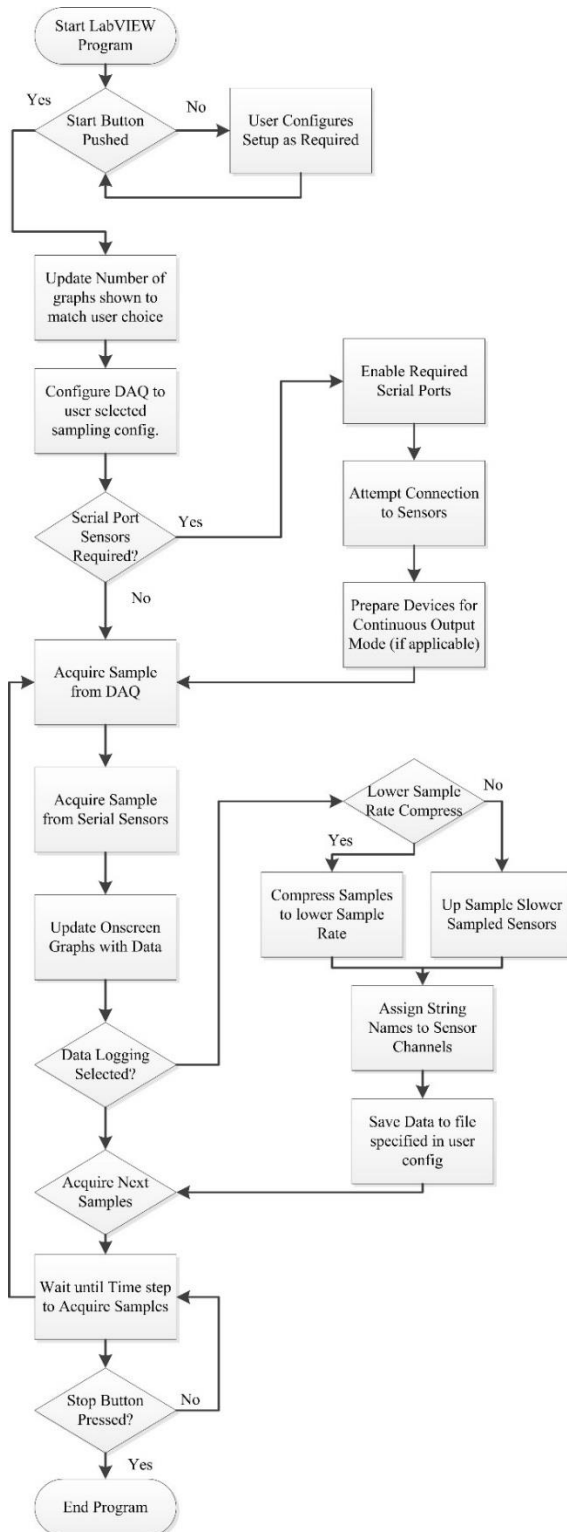
**Biomedical and Scientific
Research Ethics Sub-Committee**
A010 Medical School Building
Warwick Medical School,
Coventry, CV4 7AL.
Tel: 02476-151875
Email: BSREC@Warwick.ac.uk

Medical School Building
The University of Warwick
Coventry CV4 7AL, United Kingdom
Tel: +44 (0)24 7657 4880
Fax: +44 (0)24 7652 8375

10.3 Appendix C – Gas Testing Rig LabVIEW Software

Interface software for the gas testing rig was written using National Instruments LabVIEW 2013. The operation is described in Chapter 7. Flow charts and code screen prints are displayed in this section.

10.3.1 C.1 - Gas Rig Data Logging Flow Chart



10.3.2 C.2 - Gas Rig Data Logging Code

A screen print of the LabVIEW code is shown in the figures below. Only a sample of the code is displayed, where the entire program cannot be displayed in printed format.

Fig. C.1 shows the initial phase of the data logging process. The user selects the number of sensors connected to the rig in a preliminary configuration screen. This code displays the corresponding number of graphs (i.e. 1 per sensor), and hides the remaining (maximum of 9 sensors possible).

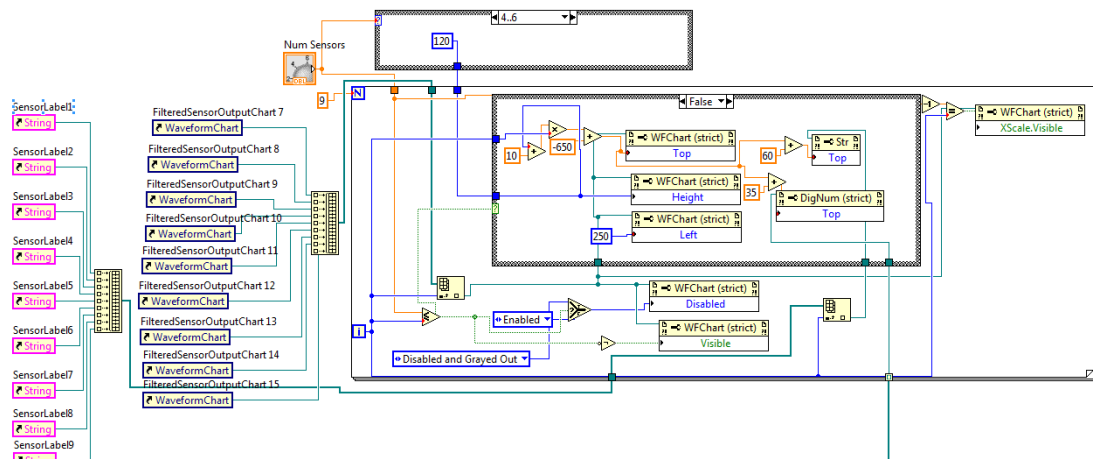


Fig. C.1 – Screen print of interface screen layout preparation code.

Fig. C.2 shows the acquisition of the data, from the USB data collection unit to the graphical display and collection into an array. The array is prepared for writing to a log file. A filter is optionally enabled, which can be displayed on the front panel interface.

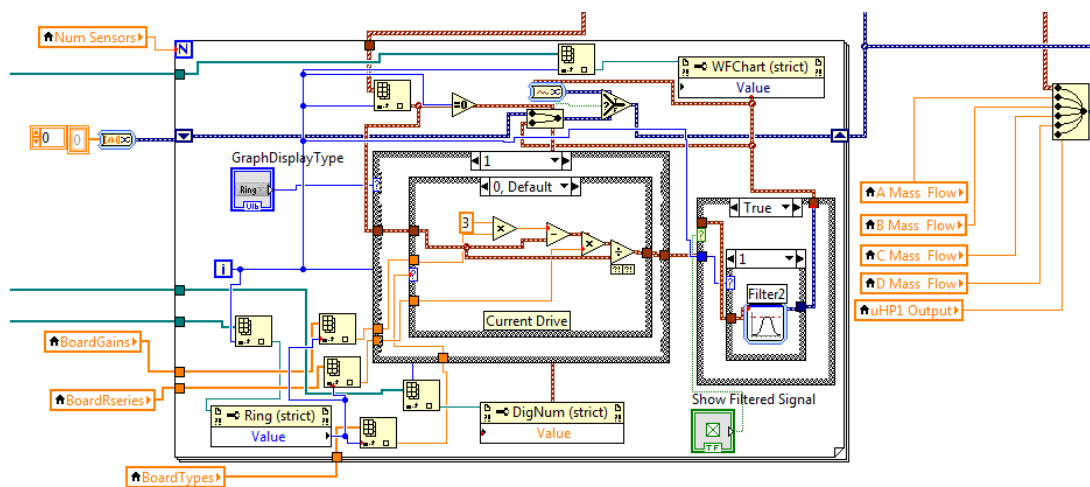


Fig. C.2 – Screen print of acquisition of data from USB unit to front panel display.

The data array is written to a .TDMS (proprietary format for National Instruments' software). This binary format is used to ensure that the data is written efficiently to a file, with no delay in logging, which could cause data to be lost. A screen print showing how the columns are labelled in the file (given a string input of the sensor names) is shown in Fig. C.3.

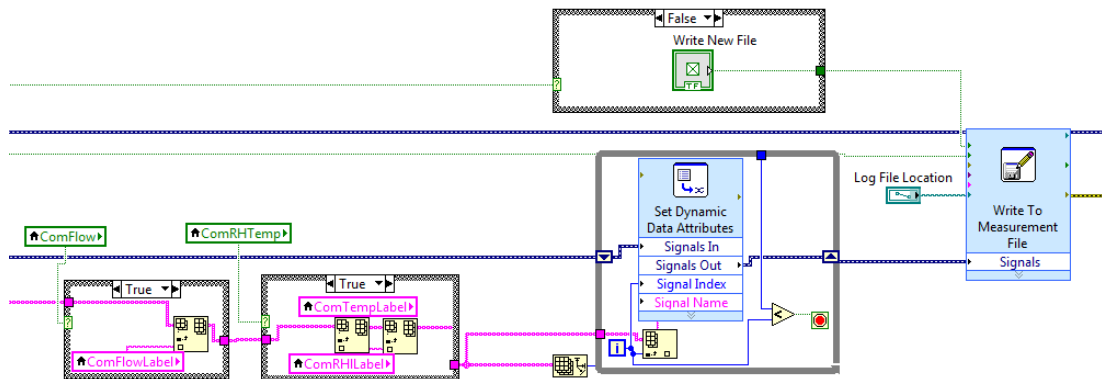


Fig. C.3 – Screen print of saving data to file with column labels.

The oven section of the control panel was designed to allow the gas sensor environments to be varied in temperature. A table input allows for step changes in temperature, after a given desired period has elapsed. The temperature measurement recorded from the oven is visually displayed and logged to the main file, with the gas sensor data. The code for controlling the oven is shown in Fig. C.4.

A section of code was developed to allow accurate generation of waveforms (sinusoid, square etc.) from the analogue output of a USB unit. The code was executed at a fixed frequency (1 kHz) to enable known frequencies to be generated, without using a USB data acquisition unit with a built in frequency generator. This enabled low frequency waves to be generated, using standard equipment, with high accuracy. The range of parameter inputs possible through the front panel enabled centre voltage and offsets to be created. A file, containing output voltages and desired time step for each row could be loaded, to enable custom cycles of output voltage to be deployed. This is of particular use for temperature modulating sensors. The code section is shown in Fig. C.5.

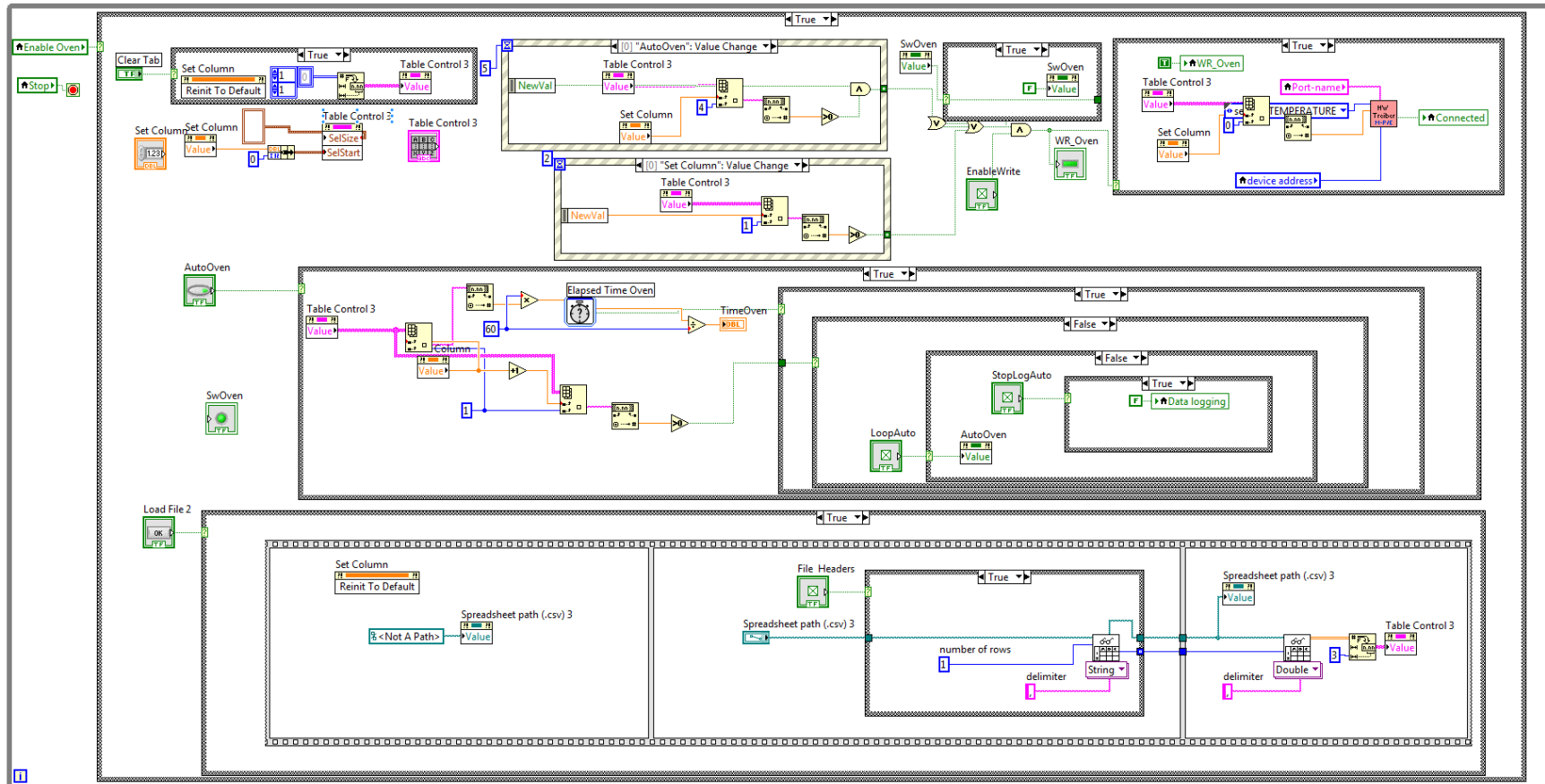


Fig. C.4 – Screen print of control software for Memmert Oven used in the gas testing rig. Temperature values set in a table can be sent to the oven after the passage of a set period of time, to enable step changes in the environment of the gas sensor chamber (inside the oven).

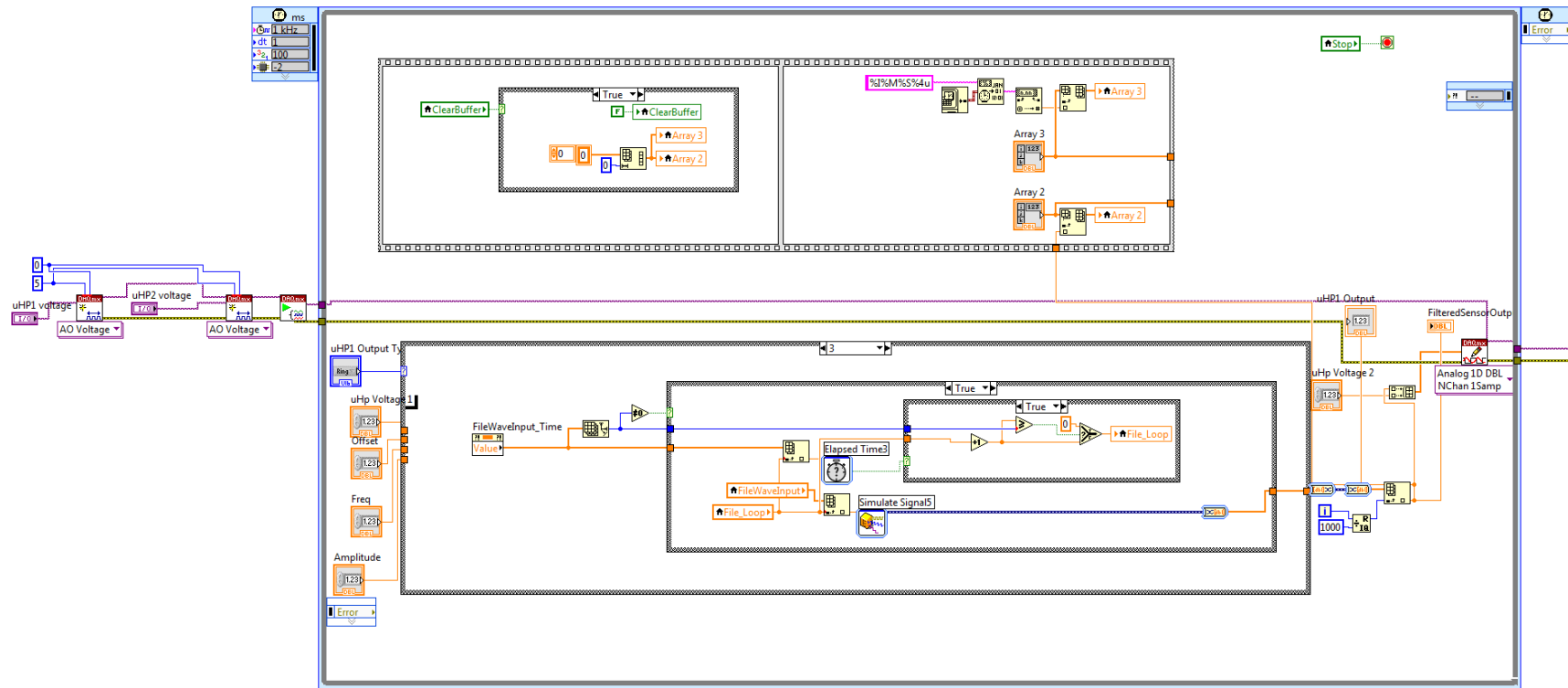
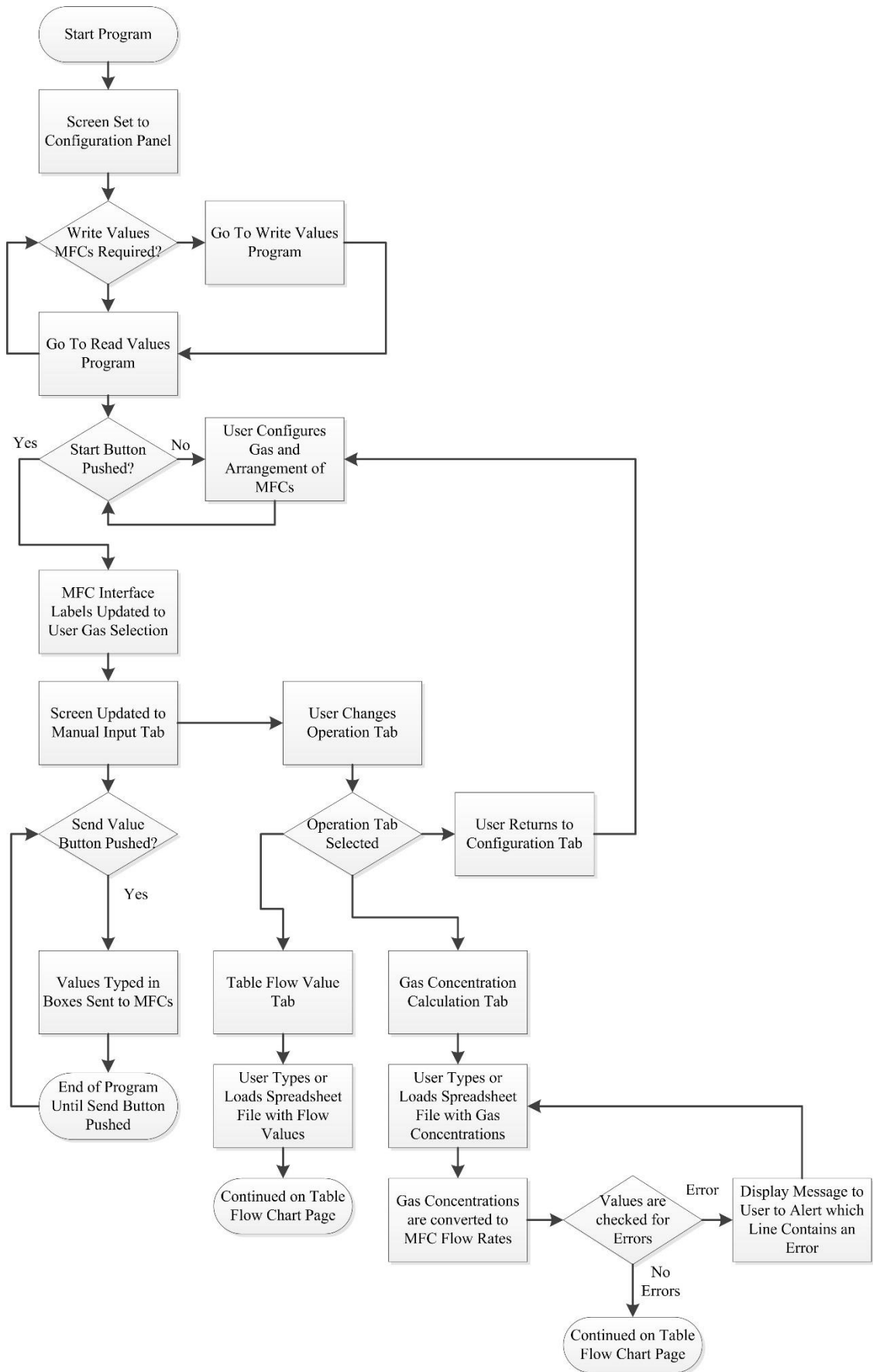
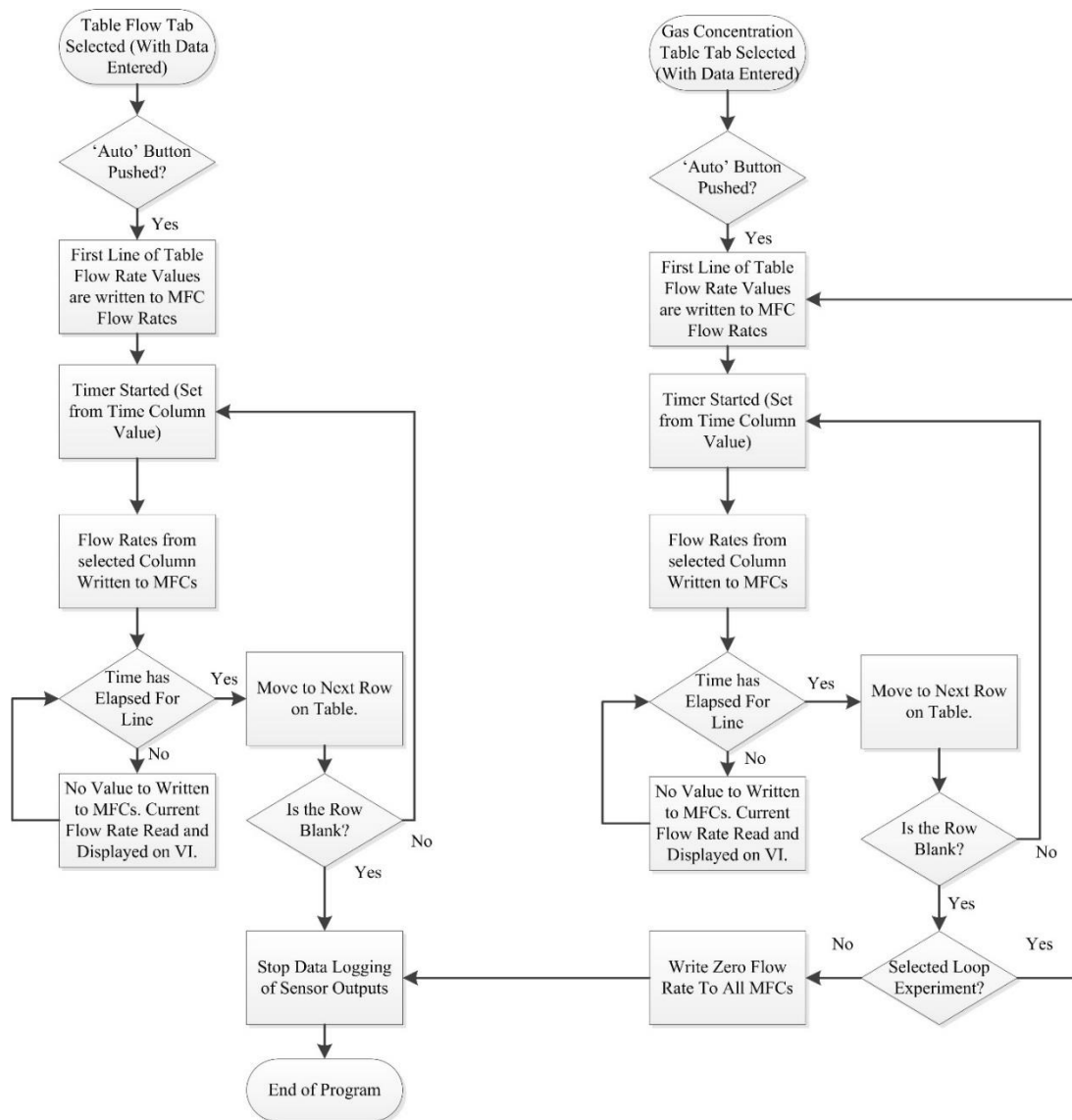


Fig. C.5 – Screen print of code to output various waveform shapes from a file or from set parameters to the analogue output from a USB unit (National Instruments Data Acquisition Unit). The code allows for a sinusoid, square wave or DC voltage to be applied to the analogue output. A file can be loaded with custom points (voltages) and a time period (s) which will be output through the analogue port. The loop is executed at a fixed rate (1 kHz) to ensure accurate frequency generation.

10.3.3 C.3 - Gas Rig Mass Flow Controller Operation Flow Chart





The testing rig is designed to test a range of gases, where concentrations can be varied using the mass flow controllers. There are four tabs on the MFC software front panel; first one to configure which gas will be tested, a second to manually send a single value to the four MFCs on the rig, a third to send a row of flow values from a table and a fourth page to automatically calculated necessary flow rate from a given desired gas concentration. A screen print of the code used for the automatic flow calculation is shown in Fig. B.6.

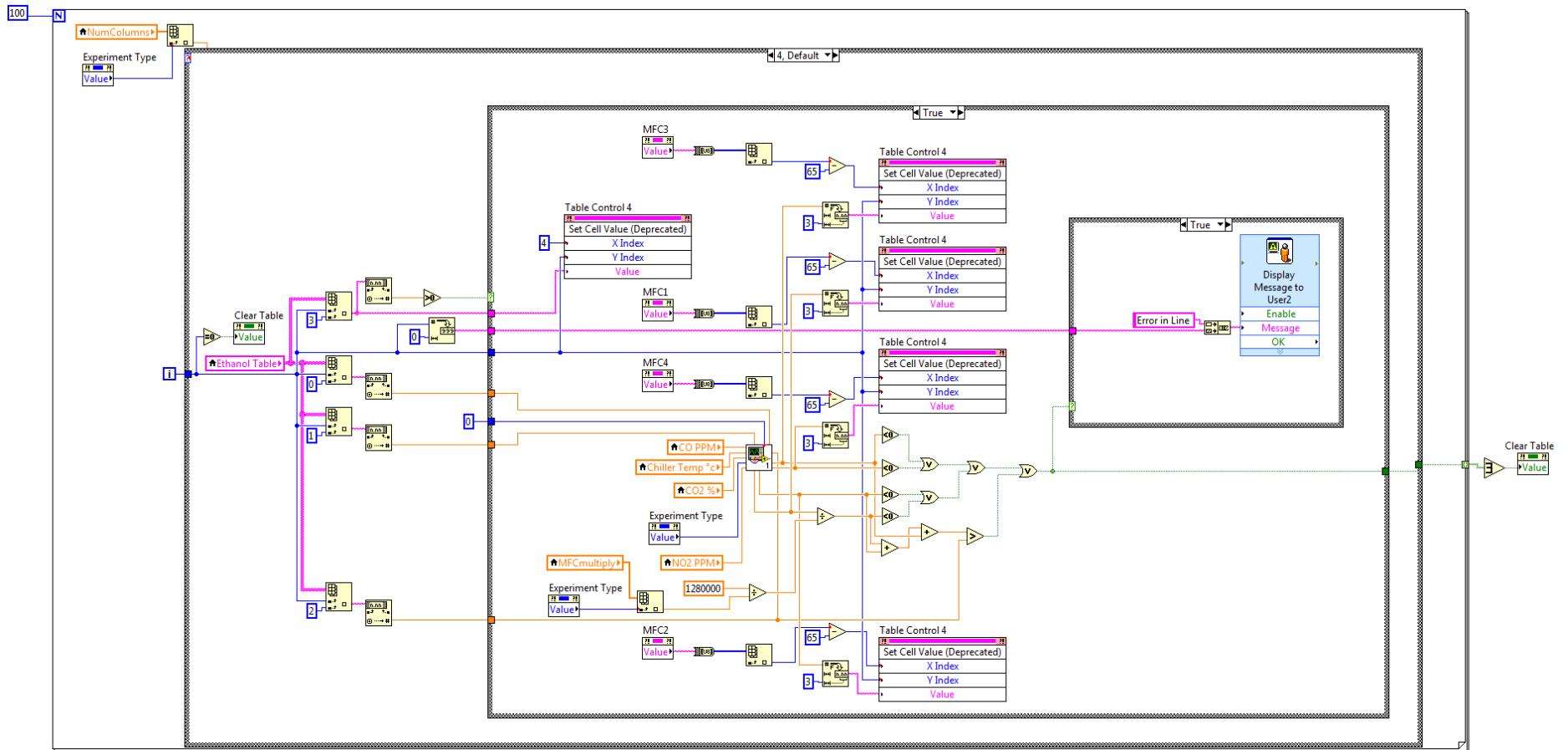


Fig. C.6 – Screen print of code to send flow values to MFCs on gas testing rig. Sub-VI is used to calculate flow rates from desired gas concentrations.

The sub-VI takes the gas concentrations available in the gas cylinders and calculates the flow rate required to create the desired gas concentration (given a balance gas). A screen print of the code is shown in Fig. C.7. The code includes compensation for the addition of humidity, which is created through the introduction of saturated synthetic air.

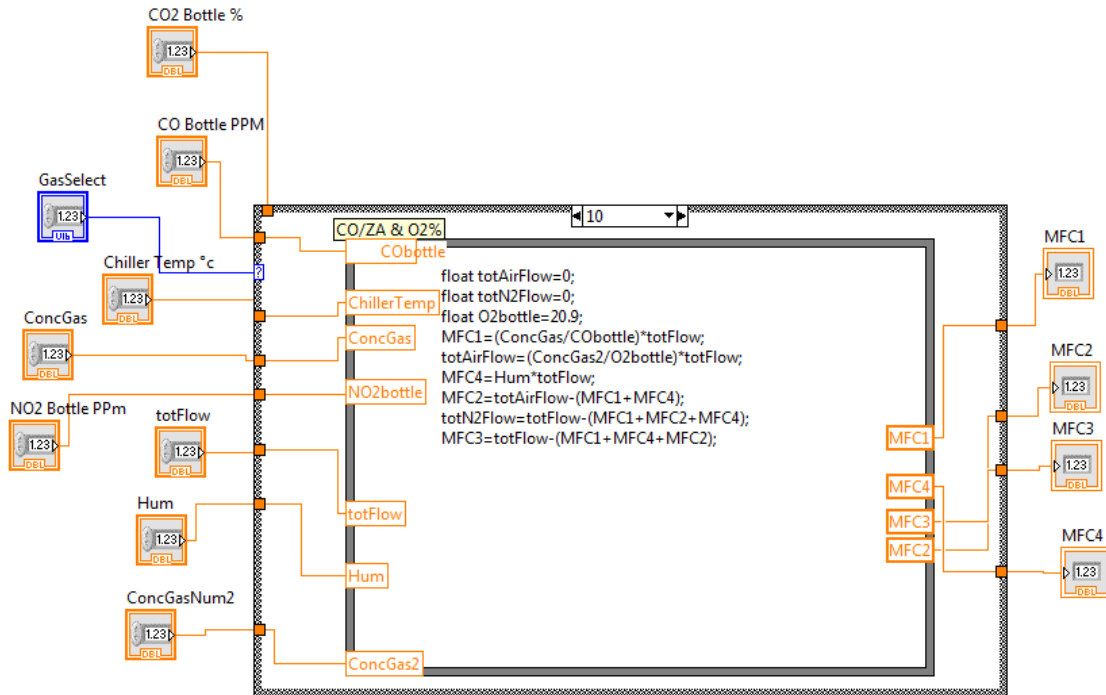


Fig. C.7 – Screen print of sub-VI code to calculate flow rates for MFCs, given a desired gas concentration and the concentration available from the gas cylinders.

10.4 Appendix D – Microcontroller code for Acquiring Sensor Signals

The Teensy microcontroller code was written in the Arduino (C/C++) programming language. The microcontroller is designed for use with Arduino software, and many libraries to ease acquisition of signals from digital (I²C) and analogue inputs are included with the programming package.

The software was written to log the signal received from all the sensors at 200 Hz. The commercial flow sensors (Sensirion SFM3000) was found to be capable of providing an output at 10 Hz rate, and thus was extrapolated, so values could be reported back to the LabVIEW VI (Appendix C) at the desired frequency. There are 3 timers available on the microcontroller. The values are read from each analogue input pin (NDIR, MOX, temperature, humidity and O₂ sensors) at a rate of 400 Hz, and 2 values are averaged, in a buffer, to get the value reported at the baseline 200 Hz. A section of the code to print the values to the serial port is shown in Fig. D.1.

```
// This function will be called with the desired frequency
// start the measurement
void timer1_callback(void) {

    adc->startSingleRead(readPin2, ADC_0);
    adc->startSingleRead(readPin3, ADC_0);
}

void timer2_callback(void) { // Print values to serial (200 Hz)
    if(!buffer0->isEmpty() &&!buffer1->isEmpty() &&!buffer2->isEmpty()) { // read the values in the buffer
        Serial.print(buffer0->read()*3.3/adc->getMaxValue(),3); //O2 sensor
        Serial.print(",");
        Serial.print(buffer1->read()*3.3/adc->getMaxValue(),3); //MOX sensor
        Serial.print(",");
        Serial.print(buffer2->read()*3.3/adc->getMaxValue(),3); //NDIR sensor
        Serial.print(",");
        Serial.print(buffer3->read()*3.3/adc->getMaxValue(),3); //temperature and RH sensors
        Serial.print(",");
        Serial.print(flowrate,3); //Flow rate sensor
        Serial.print(",");
        Serial.println(millis());
    }
}

void timer3_callback(void) { //Flow Sensor Read
//   Wire.begin(0x40); // start the I2C interface
    Wire.beginTransaction(0x40);
    // Wire.write(0);
    Wire.write(0x10);
    Wire.write(0x00);
    Wire.requestFrom(0x40, 3);
    for(int i = 0; i<3; i++){
        while(!Wire.available()) { } // do nothing until data arrives
        val[i] = Wire.read();
    }
    flowmeasure=word(val[0],val[1]); //calculate flow rate, based on calibration data.
    flowrate=((float)flowmeasure-(float)offsetflow)/((float)scalefactorflow);
    Wire.endTransmission();
}
}
```

Fig. D.1 – Screen print of a section of the microcontroller code written to acquire the signals from the sensors in the hand-held unit.

10.5 Appendix E – Handheld Breath Analyser Data Logging LabVIEW Software

The software required to acquire the data from the handheld analysers contains only part of feature set available from the gas testing rig interface shown in Appendix B. Data are recorded from a serial port connection with the Teensy microcontroller. The data is logged to a file, with column labels providing corresponding to the data string received from the microcontroller. A timestamp is affixed to the end of each serial string transmitted from the microcontroller, thus it does not rely on the data being received and processed on the data logging computer. The complete code for the VI is shown in Fig. E.1.

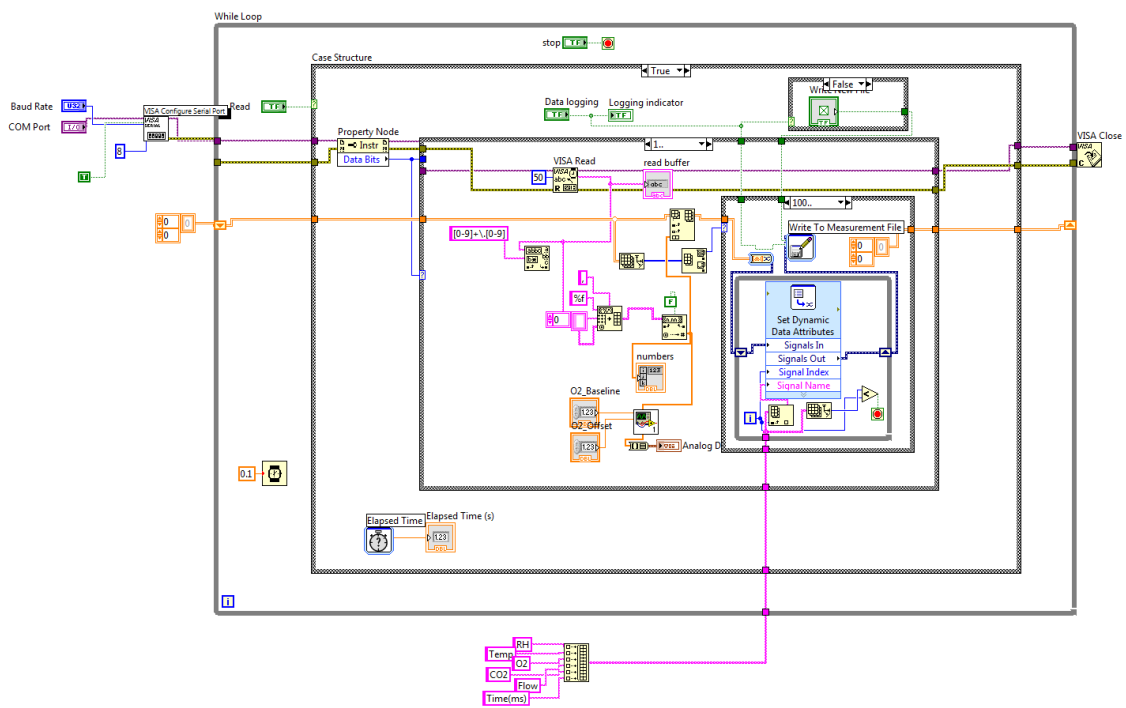


Fig. E.1 – Screen print of LabVIEW code for recording data from the Teensy microcontroller for the handheld analysers.

10.6 Appendix F – Android code for Data Analysis from Hand-Held Unit

An Android application was written in Java using Android Studio (V1.5.1) to communicate wirelessly with the hand-held breath analysers. The basic user interface displayed graphs of the sensor outputs and allowed EE to be calculated from a 1 min breath sample (immediately after the sample was given). A screen print of the layout design of the application is shown in Fig. F.1, with the graph controls highlighted.

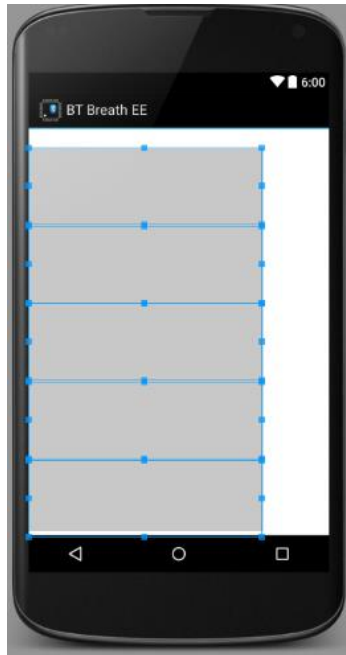


Fig. F.1 – Screen print of Android layout designer in Android Studio, with the graph elements on the main-screen of the application selected.

A message string is received over a Bluetooth serial link. The string is passed to a function to save the data to a log file. The data are received at 200 Hz, thus a number of lines are stored in a buffer, prior to being written to a comma separated value file. A section of the code used to perform this task is shown in Fig. F.2.

```

StringBuilder msg = new StringBuilder();
if (show_timings) msg.append("[").append(timeformat.format(new Date())).append("]");
if (show_direction) {
    final String arrow = (outgoing ? " << " : " >> ");
    msg.append(arrow);
} else msg.append(""); //mod TAV

msg.append(hexMode ? Utils.printHex(message) : message);
if (outgoing) msg.append('\n');
tempHolder+=msg;
String tempsplit[]=tempHolder.split("\r\n");
if(tempsplit.length!=0){
    for(int i=0;i<tempsplit.length-1;i++){
        tempsplit[i]=tempsplit[i].replace("[", "");
        tempsplit[i]=tempsplit[i].replace("]", "");
        //Log.d("tempsplitis",String.valueOf(tempsplit[i].toCharArray()));
        String fields[]=tempsplit[i].split(",");
        if(fields.length==7){
            //Log.d("Got", fields[0]+"_" +fields[1]+"_" +fields[2]+"_" +fields[3]+"_" +fields[4]+"_" +fields[5]);
            countReads+=1;
            tempVal+=((Double.parseDouble(fields[1])/3.3)-0.2424)*165;
            rhVal+=Double.parseDouble(fields[0])*30.3;
            O2Val+=Double.parseDouble(fields[2])*27.24-0.2724; //calibrate HERE for O2 sensor
            CO2Val+=Double.parseDouble(fields[3]);
            FlowVal+= Double.parseDouble(fields[4]);
            VOCVal+=Double.parseDouble(fields[5]);
            measTime+=Double.parseDouble(fields[6])/1000;
            CO2special.add(Double.parseDouble(fields[3]));
            CO2time.add(Double.parseDouble(fields[6])/1000);
            filebuffer.add(tempsplit[i]);
            filebuffer.add("\r\n");
            if(storeFull){
                TempDataFull.add((Double.parseDouble(fields[1])/3.3)-0.2424)*165;
                RHDataFull.add(Double.parseDouble(fields[0]) * 30.3);
                O2DataFull.add(Double.parseDouble(fields[2]) * 34.056 - 0.8155); //calibrate HERE for O2 sensor
                CO2DataFull.add(Double.parseDouble(fields[3]));
                FlowDataFull.add(Double.parseDouble(fields[4]));
                TimeDataFull.add(Double.parseDouble(fields[6]));
            }
        }
    }
}

```

Fig. F.2 – Screen print of code section showing data being received from a serial link and being stored in a buffer.

The CO₂ sensor output is a sinusoidal waveform. The amplitude of the wave is determined in the application, in real time and displayed on a graph in the main-screen. The code finds the peaks and troughs in the received waveform (where a buffer of 120 samples is given). The function is shown in Fig. F.3.

```

maxtab.clear();
mintab.clear();
maxtabPos.clear();
mintabPos.clear();
deltatab.clear();
deltapos.clear();
double thisVal=0;
double delta=0.05;//0.025; //0.05
double[] x = new double[timevals.size()];
for(int k = 0; k < x.length; k++)
    x[k] = timevals.get(k);

double mn = Double.POSITIVE_INFINITY;
double mx= Double.NEGATIVE_INFINITY;
//mn=Inf;mx = Inf, -Inf
double mxpos = 0;
double mnpos=0;

boolean lookformax = true;

for (int m=0;m<x.length;m++) {
    thisVal = v[m];
    if (thisVal > mx) {
        mx = thisVal;
        mxpos = x[m];
    }
    if (thisVal < mn) {
        mn = thisVal;
        mnpos = x[m];
    }
    if (lookformax) {
        if (thisVal < mx - delta) {
            maxtab.add(mx);
            maxtabPos.add(mxpos);
            mn = thisVal;
            mnpos = x[m];
            lookformax = false;
        }
    }else {
        if (thisVal > mn + delta) {
            mintab.add(mn);
            mintabPos.add(mnpos);
            mx = thisVal;
            mxpos = x[m];
            lookformax = true;
        }
    }
}
}

```

Fig. F.3 – Screen print of code section to calculate the amplitude of a sinusoidal signal.

After 1 minute of breath data is collected, the program can calculate the EE for the given period. The calculated value is displayed to the user as a pop-up message. The code used to display the message is shown in Fig. F.4.

```

double CO2calculated=0;
CO2calculated=calcTrapz(CO2withFlowExFull, deltaspos, 0.001 / 60);

for(int icomb=0;icomb<FlowDataFull.size();icomb++){
    O2DataInvFull.add(((O2DataFull.get(icomb)-O2DataFull.get(maxO2cal))/100)*flowO2ExFull.get(icomb));
}
double O2calculated=0;
O2calculated=calcTrapz(O2DataInvFull,TimeDataFull,0.001/60);
double EE=0;
EE=((O2calculated*-1000)*3.941+((CO2calculated*1000)*1.1));
Log.d("EE calculated as:",String.valueOf(EE));
TextView title = new TextView(this);
title.setText("EE Measurement");
title.setPadding(10, 10, 10, 10);
title.setGravity(Gravity.CENTER);

AlertDialog.Builder builder = new AlertDialog.Builder(this);
builder.setCustomTitle(title);
builder.setMessage("Energy Expenditure measured as\n" + String.valueOf(Math.round(EE)) + " cal/min\nfor the last 1 min breath sample.");
builder.setCancelable(false);
builder.setNegativeButton("OK", (dialog, id) -> { dialog.cancel(); });
AlertDialog alert = builder.show();
TextView messageText = (TextView)alert.findViewById(android.R.id.message);
messageText.setGravity(Gravity.CENTER);

```

Fig. F.4 – Screen print of code used to display the EE calculated from a 1 minute breath sample.